

Proteomic Characterisation of the *mdx-4cv* mouse model of Duchenne Muscular Dystrophy



**Maynooth
University**

National University
of Ireland Maynooth

Submitted to Maynooth University for the degree of
Doctor of Philosophy

Sandra Murphy, B.Sc

July 2018

Supervisor

Professor Kay Ohlendieck
Department of Biology
Maynooth University
NUI Maynooth
Co. Kildare
Ireland

Head of Department

Professor Paul Moynagh
Department of Biology
Maynooth University
NUI Maynooth
Co. Kildare
Ireland

Table of Contents

Table of contents	ii
List of figures	viii
List of tables	xiv
Publications	xviii
Presentations	xxi
Acknowledgments	xxiv
Declaration	xxvi
Abbreviations	xxvii
Abstract	xxxiii
Chapter 1 Introduction	1
1.1 Muscle biology	2
1.1.1 Muscle structure	2
1.1.2 Muscle fibre types	5
1.1.3 Muscle excitation-contraction coupling	7
1.1.4 Muscle development	8
1.1.5 Muscle regeneration	9
1.1.6 Muscle aging and sarcopenia	11
1.2 Duchenne Muscular Dystrophy	13
1.2.1 Dystrophin and its isoforms	16
1.2.2 Dystrophin and the dystrophin-glycoprotein complex	19
1.2.3 Structural roles of the DGC	22
1.2.4 Signalling roles of the DGC	22
1.2.5 The mechanical and calcium hypotheses of Duchenne Muscular Dystrophy	25
1.2.6 The role of inflammation in the progression of dystrophinopathy	27
1.2.7 Current and emerging therapies for Duchenne Muscular Dystrophy	29
1.2.8 Animal models of Duchenne Muscular Dystrophy	33
1.3 Proteomics	37
1.3.1 Gel electrophoresis	39
1.3.2 Label-free liquid chromatography mass spectrometry	40

1.3.3	Skeletal muscle proteomics	43
1.4	Biomarkers	44
1.4.1	Biomarkers for neuromuscular disease	46
1.5	Aims of the project	49
Chapter 2	Materials and Methods	52
2.1	Materials	53
2.1.1	General chemicals and reagents	53
2.1.2	1D gel electrophoresis	53
2.1.3	Mass spectrometry	53
2.1.4	Immunoblotting	53
2.1.5	ELISA	54
2.1.6	Immunofluorescence microscopy	54
2.2	Methods	56
2.2.1	<i>mdx</i> and <i>mdx-4cv</i> mouse models of Duchenne Muscular Dystrophy, and wobbler mouse model of Amyotrophic lateral sclerosis	56
2.2.2	Sample preparation of crude tissue extracts	57
2.2.3	Sample preparation for the isolation of crude microsomes	58
2.2.4	Wheat germ agglutination for the purification of sarcolemma vesicles from crude microsomes	58
2.2.5	Chemical cross-linking of wild-type versus <i>mdx-4cv</i> crude microsomes	59
2.2.6	Sample preparation and immuno-depletion of murine serum	60
2.2.7	Acetone precipitation	60
2.2.8	2D CleanUp (BioRad)	61
2.2.9	Protein quantification using the Bradford assay system	61
2.2.10	1D gel electrophoresis	61
2.2.11	Gel staining techniques	63
2.2.11.1	Colloidal Coomassie stain	63
2.2.11.2	Silver stain	64
2.2.12	Sample preparation for label-free liquid chromatography mass spectrometry	64

2.2.13	Filter Aided Sample Preparation	65
2.2.14	On-membrane digestion	65
2.2.15	In-gel digestion	66
2.2.16	Label-free liquid chromatography mass spectrometry	67
2.2.16.1	LC-MS/MS using a Q-Exactive mass spectrometer	67
2.2.16.2	LC-MS/MS using an LTQ Orbitrap XL mass spectrometer	67
2.2.17	Qualitative proteomic profiling of mass spectrometric data	68
2.2.18	Quantitative proteomic profiling of mass spectrometric data using Progenesis QI for Proteomics Software	68
2.2.19	Quantitative proteomic profiling of mass spectrometric data using MaxQuant and Perseus Software	69
2.2.20	Generation of heat maps using Perseus	70
2.2.21	Bioinformatics analysis of proteomic data	70
2.2.22	Comparative immunoblot analysis	71
2.2.23	Enzyme linked immunosorbent assay	72
2.2.24	Immunofluorescence microscopy	72
Chapter 3	Proteomic evaluation of alterations in protein abundance and protein interactions in hind limb extracts from the <i>mdx-4cv</i> mouse model of Duchenne muscular dystrophy	74
3.1	Introduction	75
3.1.1	Experimental Design	77
3.2	Results	79
3.2.1	Label-free LC-MS/MS analysis of dystrophin-deficient hind-limb muscle	79
3.2.2	Distribution of protein changes in <i>mdx-4cv</i> hind-limb	86
3.2.3	Verification of proteomic findings by comparative immunoblotting	91
3.2.4	Gel electrophoretic analysis of chemically cross-linked muscle microsomes	98
3.2.5	Mass spectrometric identification of proteins with altered electrophoretic mobility	99
3.2.6	Mass spectrometric identification and bioinformatics	

	analysis of altered protein interactions in muscular dystrophy in gel zone A	101
3.2.7	Mass spectrometric identification and bioinformatics analysis of altered protein interactions in muscular dystrophy in gel zone B	105
3.2.8	Mass spectrometric identification and bioinformatics analysis of altered protein interactions in muscular dystrophy in gel zone C	111
3.3	Discussion	116
3.3.1	Conclusion	127
Chapter 4	In-depth proteomic analysis of the dystrophin-associated glycoprotein complex and the sarcolemma-enriched fraction from normal and dystrophic muscle	129
4.1	Introduction	130
4.1.1	Experimental Design	134
4.2	Results	136
4.2.1	Proteomic characterisation of the dystrophin complex enriched fraction	136
4.2.2	Mass spectrometric identification of dystrophin co-purifying proteins	140
4.2.3	Comparative immunoblotting of desmoglein-1 in wild-type and <i>mdx quadriceps femoris</i> and <i>longissimus dorsi</i>	145
4.2.4	Qualitative analysis of wild-type versus <i>mdx-4cv</i> enriched sarcolemma	148
4.2.5	Quantitative analysis of wild-type versus <i>mdx-4cv</i> enriched sarcolemma	150
4.2.6	Bioinformatics of differential proteins in wild-type versus <i>mdx-4cv</i> enriched sarcolemma	156
4.2.7	Comparative immunoblotting of differential proteins in wild-type versus <i>mdx-4cv</i> enriched sarcolemma	162
4.3	Discussion	168

4.3.1	Conclusion	180
Chapter 5	Proteomic profiling of the aged <i>mdx-4cv</i> heart; implications for dystrophinopathy-related cardiomyopathy	181
5.1	Introduction	182
5.1.1	Experimental Design	184
5.2	Results	185
5.2.1	Qualitative analysis of wild-type versus <i>mdx-4cv</i> senescent heart	185
5.2.2	Quantitative analysis of cardiac dystrophin and members of the dystrophin-glycoprotein complex	186
5.2.3	Label-free LC/MS-MS analysis of protein species with reduced expression in <i>mdx-4cv</i> crude heart extracts	188
5.2.4	Label-free LC/MS-MS analysis of protein species with increased expression in <i>mdx-4cv</i> crude heart extracts	191
5.2.5	Distribution of protein changes in dystrophic <i>mdx-4cv</i> cardiac tissue	195
5.2.6	Comparative immunoblot analysis of wild-type versus <i>mdx-4cv</i> 20-month heart	200
5.3	Discussion	205
5.3.1	Conclusion	210
Chapter 6	Glial fibrillary acidic protein as a marker of neurotoxicity in the <i>mdx-4cv</i> model of dystrophinopathy	212
6.1	Introduction	213
6.1.1	Experimental Design	215
6.2	Results	217
6.2.1	Label-free LC/MS-MS analysis of altered protein species in total <i>mdx-4cv</i> brain extracts	217
6.2.2	Distribution of protein changes in dystrophic <i>mdx-4cv</i> brain tissue	222
6.2.3	Verification of proteomic alterations in dystrophin-	

	deficient brain tissue by immunoblotting	225
6.2.4	Immunoblot and immunofluorescence microscopy analysis of GFAP as a marker of reactive gliosis	229
6.3	Discussion	237
6.3.1	Conclusion	245
Chapter 7	Proteomic profiling of serum and saliva in the <i>mdx-4cv</i> model of dystrophinopathy	246
7.1	Introduction	247
7.1.1	Experimental Design	250
7.2	Results	252
7.2.1	Gel electrophoretic and immunoblot analysis of immunodepleted serum samples	252
7.2.2	Qualitative analysis of the serum proteome	255
7.2.3	Quantitative label-free LC-MS/MS analysis of wild-type versus <i>mdx-4cv</i> serum	255
7.2.4	Distribution of protein alterations in dystrophic serum	261
7.2.5	Independent verification of differentially abundant proteins by immunoblotting	265
7.2.6	Immunoblot analysis of the increased abundance of haptoglobin in <i>mdx-4cv</i> serum	269
7.2.7	ELISA analysis of the increased abundance of FABP-1 and haptoglobin in <i>mdx-4cv</i> serum	273
7.2.8	Protein identification in wild-type and <i>mdx-4cv</i> saliva	276
7.2.9	Comparison of the wild-type saliva core proteome with the wild-type serum proteome	277
7.2.10	Quantitative analysis of wild-type versus <i>mdx-4cv</i> saliva	282
7.3	Discussion	287
7.3.1	Conclusion	301
Chapter 8	General Discussion	302
8.1	Discussion	303
8.1.1	Concluding Remarks	323

List of Figures

Chapter 1

Figure 1.1	Structure of skeletal muscle	4
Figure 1.2	Protein markers of skeletal muscle fibre types	6
Figure 1.3	Different promoter regions for dystrophin isoforms	17
Figure 1.4	Structural characteristics of full-length dystrophin and its isoforms	18
Figure 1.5	The dystrophin-glycoprotein complex	21
Figure 1.6	Overview of gel versus gel-free mass spectrometric approaches	42
Figure 1.7	Overview of potential protein biomarker candidates in Duchenne muscular dystrophy	48
Figure 1.8	Histological and immunofluorescence microscopical analysis of dystrophic <i>mdx-4cv</i> skeletal muscle	51

Chapter 3

Figure 3.1	Label-free quantitative proteomic analysis of wild-type versus <i>mdx-4cv</i> crude hind-limb extracts	85
Figure 3.2	PANTHER analysis of the 156 proteins with increased abundance in <i>mdx-4cv</i> skeletal muscle	87
Figure 3.3	PANTHER analysis of the 43 proteins with decreased abundance in <i>mdx-4cv</i> skeletal muscle	88
Figure 3.4	Bioinformatics analysis of altered protein expression in dystrophic skeletal muscle	90
Figure 3.5	Electrophoretic and immunoblot analysis of wild-type and <i>mdx-4cv</i> muscle	92
Figure 3.6	Comparative immunoblot analysis of proteins with an increased abundance in dystrophic <i>mdx-4cv</i> hind-limb skeletal muscle	93
Figure 3.7	Comparative immunoblot analysis of proteins with an increased abundance in dystrophic <i>mdx-4cv</i> hind-limb skeletal muscle	94

Figure 3.8	Comparative immunoblot analysis of proteins with a decreased abundance in dystrophic <i>mdx-4cv</i> hind-limb skeletal muscle	95
Figure 3.9	Immunofluorescence and immunoblot analysis of collagen in normal versus dystrophic <i>mdx-4cv</i> muscle	97
Figure 3.10	Gel based chemical cross-linking analysis of skeletal muscle microsomes	98
Figure 3.11	Mass spectrometric identification of cross-linked muscle proteins with an altered electrophoretic mobility	100
Figure 3.12	Bioinformatics analysis of proteomic changes detected in gel zone A in the microsomal fraction from dystrophic muscle	104
Figure 3.13	Bioinformatics analysis of proteomic changes detected in gel zone B in the microsomal fraction from dystrophic muscle	110
Figure 3.14	Bioinformatics analysis of proteomic changes detected in gel zone C in the microsomal fraction from dystrophic muscle	115
Figure 3.15	Schematic illustrating the fibrotic process in Duchenne muscular dystrophy	119
 Chapter 4		
Figure 4.1	Flowchart illustrating the bio-analytical procedure for the proteomic characterisation of dystrophin and its associated glycoprotein complex and for the sarcolemma enriched fraction	133
Figure 4.2	Cellular component enrichment analysis of the DGC fraction	138
Figure 4.3	STRING analysis of DGC proteins	139
Figure 4.4	Immunoblot analysis of the cytolinker desmoglein-1 in dystrophic <i>quadriceps femoris</i> skeletal muscle	146
Figure 4.5	Immunoblot analysis of the cytolinker desmoglein-1 in dystrophic <i>longissimus dorsi</i> skeletal muscle	147
Figure 4.6	Cellular component analysis of wild-type versus <i>mdx-4cv</i>	

	sarcolemma data	149
Figure 4.7	PANTHER analysis of proteins with increased abundance in <i>mdx-4cv</i> muscle sarcolemma	157
Figure 4.8	PANTHER analysis of proteins with decreased abundance in <i>mdx-4cv</i> muscle sarcolemma	158
Figure 4.9	STRING analysis of proteins with increased abundance in <i>mdx-4cv</i> muscle sarcolemma	159
Figure 4.10	STRING analysis of proteins with decreased abundance in <i>mdx-4cv</i> muscle sarcolemma	160
Figure 4.11	Enriched KEGG pathways of proteins with altered abundance in <i>mdx-4cv</i> muscle sarcolemma	161
Figure 4.12	Electrophoretic and immunoblot analysis of wild-type and <i>mdx-4cv</i> muscle	163
Figure 4.13	Comparative immunoblot analysis of proteins with decreased abundance in dystrophic <i>mdx-4cv</i> enriched sarcolemma	164
Figure 4.14	Comparative immunoblot analysis of myelin protein zero in dystrophic <i>mdx-4cv</i> enriched sarcolemma	165
Figure 4.15	Comparative immunoblot analysis of proteins with increased abundance in dystrophic <i>mdx-4cv</i> enriched sarcolemma	166
Figure 4.16	Comparative immunoblot analysis of proteins with increased abundance in dystrophic <i>mdx-4cv</i> enriched sarcolemma	167
Figure 4.17	Localisation of desmosomes in cardiac tissue	171
Figure 4.18	Impaired sarcolemmal integrity in the <i>mdx-4cv</i> model of Duchenne muscular dystrophy	176
 Chapter 5		
Figure 5.1	Reduction in the expression of DGC proteins as identified by LC-MS/MS	187
Figure 5.2	PANTHER analysis of altered protein species in dystrophic heart	195
Figure 5.3	STRING analysis of the 54 proteins with increased	

	expression in <i>mdx-4cv</i> heart	197
Figure 5.4	STRING analysis of the 44 proteins with diminished expression in <i>mdx-4cv</i> cardiac tissue	198
Figure 5.5	Enriched KEGG terms in proteins with increased abundance in the aged dystrophic heart	199
Figure 5.6	Enriched KEGG terms in proteins with decreased abundance in the aged dystrophic heart	198
Figure 5.7	Electrophoretic and immunoblot analysis of wild-type and <i>mdx-4cv</i> heart	201
Figure 5.8	Comparative immunoblot analysis of proteins with decreased abundance in dystrophic <i>mdx-4cv</i> cardiac tissue	202
Figure 5.9	Comparative immunoblot analysis of proteins with increased abundance in dystrophic <i>mdx-4cv</i> cardiac tissue	203
Figure 5.10	Comparative immunoblot analysis of proteins with increased abundance in dystrophic <i>mdx-4cv</i> cardiac tissue	204
Chapter 6		
Figure 6.1	Graphical representation of changed protein classes with altered abundance in <i>mdx-4cv</i> brain tissue	223
Figure 6.2	Interaction map of altered proteins from <i>mdx-4cv</i> brain tissue	224
Figure 6.3	Electrophoretic and immunoblot analysis of wild-type and <i>mdx-4cv</i> brain	226
Figure 6.4	Comparative immunoblot analysis of proteins with increased abundance in dystrophic <i>mdx-4cv</i> brain tissue	227
Figure 6.5	Comparative immunoblot analysis of proteins with decreased abundance in dystrophic <i>mdx-4cv</i> brain tissue	228
Figure 6.6	Immunoblot analysis of the specificity of the GFAP antibody	231
Figure 6.7	Dilution series of the GFAP antibody	232

Figure 6.8	Comparative immunoblot analysis of the glial fibrillary acidic protein GFAP in wild-type versus <i>mdx-4cv</i> brain specimens	233
Figure 6.9	Comparative immunoblot analysis of the glial fibrillary acidic protein GFAP in wild-type versus <i>mdx-4cv</i> brain specimens from 2-12 months	234
Figure 6.10	Comparative immunoblot analysis of the glial fibrillary acidic protein GFAP in wild-type versus wobbler brain specimens	235
Figure 6.11	Immunofluorescence microscopy of GFAP in wild-type versus <i>mdx-4cv</i> brain sections	236
Figure 6.12	A potential role for astrogliosis in the pathophysiology of mental impairment in the dystrophin-deficient brain	241
 Chapter 7		
Figure 7.1	Gel electrophoretic and immunoblot analysis of albumin depletion in wild-type and <i>mdx-4cv</i> serum	253
Figure 7.2	Immunoblot analysis of immunoglobulin depletion in wild-type and <i>mdx-4cv</i> serum	254
Figure 7.3	PANTHER analysis of proteins with increased abundance in <i>mdx-4cv</i> serum	262
Figure 7.4	PANTHER analysis of proteins with decreased abundance in <i>mdx-4cv</i> serum	263
Figure 7.5	ClueGO analysis of proteins with increased abundance in <i>mdx-4cv</i> serum	264
Figure 7.6	Electrophoretic and immunoblot analysis of wild-type and <i>mdx-4cv</i> serum	266
Figure 7.7	Comparative immunoblot analysis of proteins with increased abundance in dystrophic <i>mdx-4cv</i> serum	267
Figure 7.8	Comparative immunoblot analysis of proteins with decreased abundance in dystrophic <i>mdx-4cv</i> serum	268
Figure 7.9	Mass spectrometric fingerprint of haptoglobin	269
Figure 7.10	Comparative immunoblot analysis of haptoglobin in dystrophic 6-month <i>mdx-4cv</i> serum	270

Figure 7.11	Electrophoretic and immunoblot analysis of wild-type and <i>mdx-4cv</i> 12-month old serum	271
Figure 7.12	Comparative immunoblot analysis of haptoglobin in dystrophic 12-month <i>mdx-4cv</i> serum	272
Figure 7.13	Comparative immunoblot analysis of FABP-1 in dystrophic 12-month <i>mdx-4cv</i> serum	272
Figure 7.14	Box and whisker plots and ROC curve for FABP-1	274
Figure 7.15	Box and whisker plots and ROC curve for haptoglobin in 6-month serum	274
Figure 7.16	Box and whisker plots and ROC curve for haptoglobin in 12-month serum	275
Figure 7.17	Protein class of salivary proteins	276
Figure 7.18	Biological process analysis of the serum versus saliva proteome	278
Figure 7.19	Cellular component analysis of the serum versus saliva proteome	279
Figure 7.20	Molecular function analysis of the serum versus saliva proteome	280
Figure 7.21	Mass spectrometric fingerprint of kallikrein-1	283
Figure 7.22	Proteomic identification of kallikrein isoform Klk1 in saliva from the <i>mdx-4cv</i> mouse model of Duchenne muscular dystrophy	284
Figure 7.23	Volcano plots of all identified proteins based on relative abundance differences between wild-type and <i>mdx-4cv</i> saliva	286
Figure 7.24	The role of the immune system in dystrophinopathy	289
Figure 7.25	Complement and coagulation cascades in <i>Mus musculus</i>	296
Chapter 8		
Figure 8.1	Overview of muscular dystrophy-induced changes in dystrophic tissue	311
Figure 8.2	Cross-comparison of differentially abundant proteins in tissue proteomic studies	317

List of Tables

Chapter 2

Table 2.1	Antibodies	55
Table 2.2	Composition of buffers used for protein extraction	58
Table 2.3	SDS-PAGE gel components for 10% resolving gels	63
Table 2.4	SDS-PAGE gel components for 5% stacking gels	63

Chapter 3

Table 3.1	List of identified proteins with ≥ 3.5 -fold increased abundance in 6-month old <i>mdx-4cv</i> hind-limb versus age-matched wild-type hind-limb as determined by label-free LC-MS/MS	80
Table 3.2	List of identified proteins with a significantly decreased abundance in <i>mdx-4cv</i> hind-limb versus age-matched wild-type hind limb as determined by label-free LC-MS/MS	83
Table 3.3	Mass spectrometric identification of proteins with a reduced electrophoretic mobility detected in gel zone A following chemical cross-linking of the microsomal fraction from wild-type mouse skeletal muscle	102
Table 3.4	Mass spectrometric identification of proteins with a reduced gel electrophoretic mobility detected in gel zone A following chemical cross-linking of the microsomal fraction from <i>mdx-4cv</i> mouse skeletal muscle	103
Table 3.5	Mass spectrometric identification of proteins with a reduced gel electrophoretic mobility in gel zone A following chemical cross-linking of the microsomal fraction from both wild-type and <i>mdx-4cv</i> mouse skeletal muscle	103
Table 3.6	Mass spectrometric identification of proteins with a reduced gel electrophoretic mobility detected in gel zone B following chemical cross-linking of the microsomal fraction from wild-type mouse skeletal muscle	106
Table 3.7	Mass spectrometric identification of proteins with a	

	reduced gel electrophoretic mobility detected in gel zone B following chemical cross-linking of the microsomal fraction from <i>mdx-4cv</i> mouse skeletal muscle	107
Table 3.8	Mass spectrometric identification of proteins with a reduced gel electrophoretic mobility in gel zone B following chemical cross-linking of the microsomal fraction from both wild-type and <i>mdx-4cv</i> mouse skeletal muscle	109
Table 3.9	Mass spectrometric identification of proteins with a reduced gel electrophoretic mobility detected in gel zone C following chemical cross-linking of the microsomal fraction from wild-type mouse skeletal muscle	112
Table 3.10	Mass spectrometric identification of proteins with a reduced gel electrophoretic mobility detected in gel zone C following chemical cross-linking of the microsomal fraction from <i>mdx-4cv</i> mouse skeletal muscle	113
Table 3.11	Mass spectrometric identification of proteins with a reduced gel electrophoretic mobility in gel zone C following chemical cross-linking of the microsomal fraction from both wild-type and <i>mdx-4cv</i> mouse skeletal muscle	114
Chapter 4		
Table 4.1a	Mass spectrometric identification of protein components of the dystrophin complex enriched fraction from rabbit skeletal muscle	142
Table 4.1b	Mass spectrometric identification of 8 additional protein components of the dystrophin complex enriched fraction from rabbit skeletal muscle, identified by a <i>Mammalia</i> database	144
Table 4.2	List of proteins with ≥ 4 -fold increased abundance in 5-month old <i>mdx-4cv</i> enriched sarcolemma versus age-matched wild-type enriched sarcolemma as determined by label-free LC-MS/MS	151

Table 4.3	List of identified proteins with a significantly decreased abundance in 5-month old <i>mdx-4cv</i> enriched sarcolemma versus age-matched wild-type enriched sarcolemma as determined by label-free LC-MS/MS	154
 Chapter 5		
Table 5.1	Components of the DGC with reduced expression in 20-month <i>mdx-4cv</i> heart	186
Table 5.2	List of identified proteins with a significantly reduced abundance in 20-month old <i>mdx-4cv</i> heart versus age-matched wild-type heart as determined by label-free LC-MS/MS	189
Table 5.3	List of identified proteins with a significantly increased abundance in 20-month old <i>mdx-4cv</i> heart versus age-matched wild-type heart as determined by label-free LC-MS/MS	192
 Chapter 6		
Table 6.1	List of identified proteins with a significantly reduced abundance in 12-month old <i>mdx-4cv</i> brain versus age-matched wild-type brain as determined by label-free LC-MS/MS	219
Table 6.2	List of identified proteins with a significantly increased abundance in 12-month old <i>mdx-4cv</i> brain versus age-matched wild-type brain as determined by label-free LC-MS/MS	220
 Chapter 7		
Table 7.1	List of identified proteins with ≥ 12.7 -fold increased abundance in 6-month old <i>mdx-4cv</i> serum versus age-matched wild-type serum as determined by label-free LC-MS/MS	256
Table 7.2	List of identified proteins with a significantly decreased abundance in 6-month old <i>mdx-4cv</i> serum versus age-	

	matched wild-type serum as determined by label-free LC-MS/MS	259
Table 7.3	Identification of kallikrein 1 and kallikrein 1-related peptidases in wild-type serum and saliva	281
Table 7.4	List of identified proteins with a significantly increased abundance in 6-month old <i>mdx-4cv</i> saliva versus age-matched wild-type saliva as determined by label-free LC-MS/MS	285
Table 7.5	List of identified proteins with a significantly decreased abundance in 6-month old <i>mdx-4cv</i> saliva versus age-matched wild-type saliva as determined by label-free LC-MS/MS	285
Table 7.6	Major circulating protein biomarkers of dystrophinopathy common to our LC-MS/MS data and the literature	292
Chapter 8		
Table 8.1	Shown are the 12 proteins detected by label-free mass spectrometric analysis to have altered abundance in three of four dystrophic proteomes; 6-month old crude skeletal muscle, 5-month old sarcolemma, 20-month old heart, and 12-month old brain	318

Publications

Research Papers

Sandra Murphy, Margit Zweyer, Rustam R. Mundegar, Dieter Swandulla and Kay Ohlendieck. 2018. Proteomic identification of elevated saliva kallikrein levels in the *mdx-4cv* mouse model of Duchenne muscular dystrophy. *Biochemistry and Biophysics Reports*. In press. <https://doi.org/10.1016/j.bbrep.2018.05.006>

Sandra Murphy, Margit Zweyer, Rustam R. Mundegar, Dieter Swandulla and Kay Ohlendieck. 2018. Comparative gel-based proteomic analysis of chemically crosslinked complexes in dystrophic skeletal muscle. *Electrophoresis*. In press. <https://doi.org/10.1002/elps.201800028>

Sandra Murphy, Margit Zweyer, Michael Henry, Paula Meleady, Rustam R. Mundegar, Dieter Swandulla and Kay Ohlendieck. 2018. Proteomic analysis of the sarcolemma-enriched fraction from dystrophic *mdx-4cv* skeletal muscle. *Journal of Proteomics*. In press. <https://doi.org/10.1016/j.jprot.2018.01.015>

Sandra Murphy and Kay Ohlendieck. 2018. Proteomic profiling of large myofibrillar proteins from dried and long-term stored polyacrylamide gels. *Analytical Biochemistry* **543**: 8-11

Sandra Murphy, Heinrich Brinkmeier, Mirjam Krautwald, Michael Henry, Paula Meleady and Kay Ohlendieck. 2017. Proteomic profiling of the dystrophin complex and membrane fraction from dystrophic mdx muscle reveals decreases in the cytolinker desmoglein and increases in the extracellular matrix stabilizers biglycan and fibronectin. *J Muscle Res Cell Motil.* **38(2)**: 251-268

Sandra Murphy and Kay Ohlendieck. 2017. Mass spectrometric identification of dystrophin, the protein product of the Duchenne muscular dystrophy gene, in distinct muscle surface membranes. *Int J Mol Med.* **40(4)**: 1078-1088.

Sandra Murphy, Paul Dowling, Margit Zweyer, Michael Henry, Paula Meleady, Rustam R. Mundegar, Dieter Swandulla and Kay Ohlendieck. 2017. Proteomic

profiling of *mdx-4cv* serum reveals highly elevated levels of the inflammation-induced plasma marker haptoglobin in muscular dystrophy. *Int J Mol Med.* **39(6)**: 1357–1370.

Sandra Murphy, Paul Dowling, Margit Zweyer, Rustam R. Mundegar, Michael Henry, Paula Meleady, Dieter Swandulla and Kay Ohlendieck. 2016. Proteomic analysis of dystrophin deficiency and associated changes in the aged *mdx-4cv* heart model of dystrophinopathy-related cardiomyopathy. *J Proteomics* **11(145)**:24-36.

Sandra Murphy, Margit Zweyer, Michael Henry, Paula Meleady, Rustam Mundegar, Dieter Swandulla and Kay Ohlendieck. 2015. Label-free mass spectrometric analysis reveals complex changes in the brain proteome from the *mdx-4cv* mouse model of Duchenne muscular dystrophy. *Clin Proteomics* **12**:27.

Sandra Murphy, Margit Zweyer, Rustam Mundegar, Michael Henry, Paula Meleady, Dieter Swandulla and Kay Ohlendieck. 2015. Concurrent Label-Free Mass Spectrometric Analysis of Dystrophin Isoform Dp427 and the Myofibrosis Marker Collagen in Crude Extracts from *mdx-4cv* Skeletal Muscles. *Proteomes* **3(3)**: 298-327.

Sandra Murphy, Michael Henry, Paula Meleady, Margit Zweyer, Rustam R. Mundegar, Dieter Swandulla and Kay Ohlendieck. 2015. Simultaneous pathoproteomic evaluation of the dystrophin-glycoprotein complex and secondary changes in the *mdx-4cv* mouse model of Duchenne muscular dystrophy. *Biology* **4(2)**: 397-423.

Review Papers

Sandra Murphy, Margit Zweyer, Rustam R. Mundegar, Dieter Swandulla & Kay Ohlendieck. 2018. Proteomic serum biomarkers for neuromuscular diseases. *Expert Review of Proteomics.* **15(3)**: 277-291

Sandra Murphy, Paul Dowling and Kay Ohlendieck. 2016. Comparative Skeletal Muscle Proteomics Using Two-Dimensional Gel Electrophoresis. *Proteomes* **4(3)**: 27

Paul Dowling, **Sandra Murphy** and Kay Ohlendieck. 2016. Proteomic profiling of muscle fibre type shifting in neuromuscular diseases. *Expert Review of Proteomics* **13(8)**: 783-99

Sandra Murphy and Kay Ohlendieck. 2015. Proteomic profiling of the HSPB chaperonome: Mass spectrometric identification of small heat shock proteins in stressed skeletal muscles. *JOMICS* **5(1)**: 17-29

Ashling Holland, **Sandra Murphy**, Paul Dowling and Kay Ohlendieck. 2015. Pathoproteomic profiling of the skeletal muscle matrisome in dystrophinopathy-associated myofibrosis. *PROTEOMICS* **16(2)**: 345-66

Sandra Murphy and Kay Ohlendieck. 2015. The biochemical and mass spectrometric profiling of the dystrophin complexome from skeletal muscle. *Computational and Structural Biotechnology Journal* **14**: 20-27

Book Chapters

Sandra Murphy and Kay Ohlendieck. 2018. Proteomic Profiling of the Dystrophin-Deficient Brain. In: Bernardini C. (eds) Duchenne Muscular Dystrophy. Methods in Molecular Biology, vol 1687. Humana Press, New York, NY

Sandra Murphy and Kay Ohlendieck. 2018. Protein Digestion for DIGE Analysis. In: Ohlendieck K. (eds) Difference Gel Electrophoresis. Methods in Molecular Biology, vol 1664. Humana Press, New York, NY

Sandra Murphy. 2018. Subcellular Fractionation for DIGE-Based Proteomics. In: Ohlendieck K. (eds) Difference Gel Electrophoresis. Methods in Molecular Biology, vol 1664. Humana Press, New York, NY

Sandra Murphy and Paul Dowling. 2018. DIGE Analysis of ProteoMinerTM Fractionated Serum/Plasma Samples. In: Ohlendieck K. (eds) Difference Gel Electrophoresis. Methods in Molecular Biology, vol 1664. Humana Press, New York, NY

Sandra Murphy and Kay Ohlendieck. 2016. The Extracellular Matrix Complexome from Skeletal Muscle, Composition and Function of the Extracellular Matrix in the Human Body, Dr. Francesco Travascio (Ed.), InTech, Available from: <http://www.intechopen.com/books/composition-and-function-of-the-extracellular-matrix-in-the-human-body/the-extracellular-matrix-complexome-from-skeletal-muscle>

Presentations

Poster Presentations

Proteomic identification of novel brain and serum biomarkers linked to the pathophysiology of Duchenne muscular dystrophy. **Sandra Murphy**, Margit Zweyer, Paul Dowling, Michael Henry, Paula Meleady, Dieter Swandulla and Kay Ohlendieck. World Muscle Society Congress, October 2017. St. Malo, France.

Proteomic identification of elevated serum haptoglobin levels in dystrophinopathy. **Sandra Murphy**, Paul Dowling, Margit Zweyer, Michael Henry, Paula Meleady, Dieter Swandulla and Kay Ohlendieck. HUPO 2017: 16th Human Proteome Organization World Congress, September 2017. Convention Centre, Dublin.

Proteomic profiling of the *mdx-4cv* mouse model of Duchenne muscular dystrophy reveals reactive gliosis in the dystrophin-deficient brain. **Sandra Murphy**, Margit Zweyer, Michael Henry, Paula Meleady, Rustam R. Mundegar, Dieter Swandulla and Kay Ohlendieck. Brain research in Ireland: Investing in all our futures, March 2017. Science gallery, Trinity College Dublin.

Comparative proteomic profiling of dystrophin deficiency and its concomitant secondary abnormalities in the senescent *mdx-4cv* cardiac model of muscular dystrophy-associated cardiomyopathy. **Sandra Murphy**, Paul Dowling, Margit Zweyer, Rustam R. Mundegar, Michael Henry, Paula Meleady, Dieter Swandulla and Kay Ohlendieck. ProteoMMX Strictly Quantitative 4.0, April 2016. Chester, UK.

Simultaneous pathoproteomic evaluation of the dystrophin-glycoprotein complex and secondary changes in the *mdx-4cv* mouse model of Duchenne muscular dystrophy.

Sandra Murphy, Michael Henry, Paula Meleady, Margit Zweyer, Rustam R. Mundegar, Dieter Swandulla and Kay Ohlendieck. Biology Research Day 2015. Maynooth University.

Departmental Seminars

Defeating the deadly Duchenne: A proteomics approach. June 2018. Maynooth University Annual Biology Research Day.

Saliva proteome analysis in the *mdx-4cv* model of Duchenne muscular dystrophy. May 2018. Maynooth University Seminar Series.

Proteomic profiling of the dystrophin complex, and membrane fraction from the dystrophic *mdx quadriceps femoris*; involvement of desmoglein-1, fibronectin and biglycan in disease pathophysiology. June 2017. Maynooth University Annual Biology Research Day.

The search for serum biomarkers in Duchenne muscular dystrophy. April 2017. Maynooth University Seminar Series.

The roles of myofibrosis and astrogliosis in the pathophysiology of Duchenne muscular dystrophy. June 2016. Maynooth University Annual Biology Research Day.

This old heart; The role of fibrosis in the aged dystrophic heart. April 2016. Maynooth University Seminar Series.

Glial fibrillary acidic protein as a marker of neuro-toxicity in Duchenne muscular dystrophy. September 2015. Maynooth University Seminar Series.

Oral Presentations

Serum haptoglobin as a marker of sterile inflammation in dystrophinopathy. November 2016. Inflammatory Diseases- Mechanisms and Clinical Perspectives Conference, Maynooth, Co. Kildare.

Label-free mass spectrometric analysis of the membrane-associated protein dystrophin and secondary changes in the senescent *mdx-4cv* model of dystrophinopathy-related cardiomyopathy. May 2016. Irish Mass Spectrometry Annual Conference, Dublin.

Conferences

- 2018 Irish Mass Spectrometry Society Annual Conference. Dublin, Ireland. **Attended.**
- 2018 Analysis and Integration of Transcriptome and Proteome Data. EMBL Heidelberg, Germany. **Participation in EMBL training course.**
- 2017 World Muscle Society Congress. St. Malo, France. **Poster Presentation.**
- 2017 HUPO 2017: 16th Human Proteome Organization World Congress. Convention Centre, Dublin, Ireland. **Poster Presentation.**
- 2017 Irish Mass Spectrometry Society Annual Conference. Dublin, Ireland. **Attended.**
- 2017 Brain research in Ireland: Investing in all our future. Trinity College Dublin, Ireland. **Poster Presentation.**
- 2016 Inflammatory Diseases- Mechanisms and Clinical Perspectives Conference. Maynooth, Ireland. **Oral and Poster Presentation.**
- 2016 Irish Mass Spectrometry Annual Conference. Dublin, Ireland. **Oral Presentation.**
- 2016 ProteoMMX Strictly Quantitative 4.0. Chester, UK. **Poster Presentation.**
- 2015 Irish Mass Spectrometry Society Annual Conference. Dublin, Ireland. **Attended.**
- 2015 Join Our Boys Trust International Conference. Dublin, Ireland. **Attended.**

Acknowledgements

Firstly, I would like to sincerely thank my supervisor Professor Kay Ohlendieck. I really appreciate all your advice, support, guidance and encouragement over the past four years. It has been a pleasure to work as an undergraduate and postgraduate student in the Muscle Biology lab, and I owe that to your dedication and passion for research. I have enjoyed our many chats, from science to politics and of course football, and I will miss working with you. I will be always grateful for the many papers we achieved and for your unwavering support, thank you for everything!

To Dr. Paul Dowling, thank you so much for your wisdom with all things proteomics. I'm sure at times it felt like I was your adopted student with my endless questions! I am so grateful for your patience and kindness, and for helping me with job-hunting and interview preparation.

I would like to acknowledge the MU Hume scholarship, the Health Research Board, Muscular Dystrophy Ireland and Deutsche Duchenne Stiftung - Aktion Benni und Co for generously funding my research.

To Dr. Paula Meleady (DCU) for your continuous collaboration, and a special thank you to Mick Henry for teaching me all I know about Progenesis software. I always learned so much from you on my trips to DCU, you truly are a proteomics wizard. Thanks also for letting me run samples on your "beast" of a mass spec!

Thank you to Professor Heinrich Brinkmeier (University of Greifswald, Germany) for your collaboration on the *mdx* project, and for providing us with tissue samples.

A huge thank you to Professor Dieter Swandulla and Margit Zweyer (University of Bonn, Germany) for providing us with so many samples over the years. Thank you, Margit, for all your microscopy work and help with optimising the saliva collection protocol.

To all members of the Biology Department at Maynooth University who keep the place running, and who have made Maynooth such a great place to work. A special

thanks to Michelle for your ability to fix any problem, and to Caroline for all your help with mass spectrometry!

Thank you to Ashling, a former member of the Muscle Biology lab. Thanks for showing me the ropes as a fourth-year student in the lab, and for your continuous advice even after you moved to Paul's lab and then to England. A massive thank you to all the other labs, for lending me chemicals, and most importantly for all the laughs at tea, lunch and nights out! To Dearbhlaith, Dean, Felipe, Rose and Rachel (even though you left us for New Zealand!), thanks for the adventures and for being the best group of people to do a PhD with. Please come visit in Newcastle!

To all of the young boys and families battling Duchenne muscular dystrophy everyday, you are an inspiration. I hope that one day our efforts can help you. Keep hoping and never give up.

Finally, I owe so much to my amazing family. A massive thank you to Shane, for always being there to cheer me up. I'm sure you are sick to death of hearing about mass spec and western blots, but you never failed to make me smile and kept me going on those days when nothing worked in the lab. Thank you for all the lovely dinners; I promise I'll cook more now. Thanks for the many amazing holidays, and for turning conferences into trips abroad! The last seven years have been the most fun, and I am so excited for our move to Newcastle! To Serena, for being so supportive in everything I do. Ever since I was little, you have always been my inspiration! Even though you did leave us for the beauty of the Caribbean and continually make us jealous with your boat parties and festivals. Hopefully now that I have a "real job" I can come visit! To Mom and Dad for being fantastic parents. You have always encouraged Serena and I, and your guidance, support and love has helped me achieve my goals. Thank you for always listening to my science woes and for being my audience for practising presentations. And Dad, after 25 years I will finally leave home! I am eternally grateful to you both for all you have done and continue to do for me. Thank you!

DECLARATION

This thesis has not been submitted in whole or part to this or any other university for any degree and is the original work of the author except where stated.

Signed _____

Sandra Murphy, B.Sc

Date _____

Abbreviations

1D	One-dimensional
2D	Two-dimensional
2D-DIGE	Two-dimensional difference in-gel electrophoresis
2D-GE	Two-dimensional gel electrophoresis
AAV	Adeno-associated viral
Ab	Antibody
ACh	Acetylcholine
AChR	Acetylcholine receptor
ACN	Acetonitrile
ADP	Adenosine diphosphate
Akt	Protein kinase B
ALS	Amyotrophic lateral sclerosis
ANOVA	Analysis of variance
AON	Anti-sense oligonucleotides
APS	Ammonium persulphate
ATP	Adenosine triphosphate
AUC	Area under the curve
BMD	Becker muscular dystrophy
BS ³	Bis(sulfosuccinimidyl)suberate
Bromophenol Blue	3',3'',5',5'' tetrabromophenolsulfonphthalien
Chk	Chicken
CID	Collision-induced dissociation
CRISPR	Clustered regularly interspaced short palindromic repeat
CTGF	Connective tissue growth factor
CV	Coefficient of variation
DAMPS	Danger-associated molecular patterns
DAVID	Database for annotation, visualization and integrated discovery
DDA	Data-dependent acquisition
DG	Dystroglycan
DGC	Dystrophin-associated glycoprotein complex

DHPR	Dihydropyridine receptor
dH ₂ O	Distilled water
DIA	Data-independent acquisition
<i>dko</i>	Double knock-out
DMD	Duchenne muscular dystrophy
DTT	Dithiothreitol
DYB	Dystrobrevin
ECM	Extracellular matrix
EDL	Extensor digitorum longus
EDTA	Ethylenediaminetetraacetic acid
ELISA	Enzyme linked immunosorbent assay
ER	Endoplasmic reticulum
ERK	Extracellular signal-regulated kinase
FABP	Fatty acid binding protein
FASP	Filter aided sample preparation
FDR	False discovery rate
g	Grams
<i>g</i>	<i>g</i> force
GABA _A	Gamma-aminobutyric acid
GAS	Gastrocnemius
GFAP	Glial fibrillary acidic protein
GO	Gene ontology
Grb2	Growth factor receptor-bound protein 2
Grb2-Sos1	Growth factor receptor-bound protein 2-son of sevenless
GRMD	Golden retriever muscular dystrophy
Gt	Goat
h	Hour(s)
HCl	Hydrochloric acid
HDR	Homology-directed repair
HEPES	4-(2-Hydroxyethyl)piperazine-1-ethanesulfonic acid
hnRNPs	Heterogeneous nuclear ribonucleoproteins
HSC	Hepatic stellate cells
HSP	Heat shock protein

HRP	Horse radish peroxidase
HyperLOPIT	hyper-plexed localization of organelle proteins by isotope tagging
IAA	Iodoacetamide
IB	Immunoblot
ICAT	Isotope-coded affinity tag
iNOS	Inducible nitric oxide synthase
iPSCs	Induced pluripotent stem cells
iTRAQ	Isobaric tags for relative and absolute quantitation
IQ	Intelligence quotients
JNK	c-Jun NH2-terminal kinase
kb	Kilobase
kDa	Kilo Daltons
KEGG	Kyoto encyclopaedia of genes and genomes
KLK	Kallikrein
LC-MS	Liquid chromatography mass spectrometry
LC-MS/MS	Liquid chromatography tandem mass spectrometry
LDH	Lactate dehydrogenase
LFQ	Label-free quantification
LV	Left ventricle
M	Molar
Mb	Megabase
mAb	Monoclonal antibody
MAP	Mitogen-activated protein
MAPKAPK2	MAP kinase-activated protein kinase 2
<i>mdx</i>	X-linked muscular dystrophy mouse model
<i>mdx-4cv</i>	X-linked muscular dystrophy mouse model-4cv
MEK	Mitogen-activated protein kinase kinase
mgf	Mascot generic file
MyHC	Myosin heavy chain
min	Minute(s)
ml	Millilitre
MLC	Myosin light chain
mm	Millimetre

mM	Millimolar
MMP-9	Matrix metalloprotease 9
MS	Mass spectrometry
Ms	Mouse
MRM	Multiple reaction monitoring
MRFs	Myogenic regulatory factors
MRI	Magnetic resonance imaging
MW	Molecular weight
m/z	Mass/charge ratio
NCAM	Neuronal cell adhesion molecule
NHEJ	Non-homologous end joining
nm	Nanometre
nNOS	Neuronal nitric oxide synthase
NSAA	North star ambulatory assessment
pAb	Polyclonal antibody
PANTHER	Protein analysis through evolutionary relationships
PBS	Phosphate buffered saline
PDZ	Post Synaptic Density protein-95, Drosophila discs large protein, and the Zona occludens protein 1
PEG3	Paternally expressed gene 3
PH	Pleckstrin homology
pI	Isoelectric point
PICs	Positive interstitial cells
PIC	Protease inhibitor cocktail
PMCA	Plasma membrane calcium-ATPase
ppm	Parts per million
PRM	Parallel reaction monitoring
PVP-40	Polyvinylpyrrolidone-40
Rac1	Ras-related C3 botulinum toxin substrate 1
Rb	Rabbit
ROC	Receiver operating characteristic
RyR	Ryanodine receptor
s	Second(s)
SDS	Sodium dodecyl sulphate

SDS-PAGE	Sodium dodecyl sulphate polyacrylamide gel electrophoresis
SILAC	Stable isotope labelling with amino acids in cell culture
SEM	Standard error of the mean
SERCA	Sarcoplasmic endoplasmic reticulum calcium ATPase
SG	Sarcoglycan
SH2	Src homology 2
Shp	Sheep
SLR	Spectrin-like repeat
SMA	Spinal muscular atrophy
SSPN	Sarcospan
SR	Sarcoplasmic reticulum
STRING	Search tool for the retrieval of interacting genes/proteins
SWATH	Sequential window acquisition of all theoretical fragment ion spectra
SYN	Syntrophin
T-tubules	Transverse tubules
TEMED	N,N,N',N'-tetramethylethylenediamine
TFA	Trifluoroacetic acid
TGF- β	Transforming growth factor beta
TnC	Troponin C
TNF- α	Tumour necrosis factor alpha
TnI	Troponin I
TnT	Troponin T
V	Volts
VDAC	Voltage-dependent anion-selective channel
WebGestalt	Web-based gene set analysis toolkit
wr	Wobbler
<i>wt</i>	Wild-type
XCorr	Cross correlation
XL	Cross-linker
XLDCM	X-linked dilated cardiomyopathy

μg	Microgram
μl	Microlitre
μm	Micrometre

Abstract

Duchenne muscular dystrophy is a highly complex multi-system disorder caused by primary abnormalities in the *Dmd* gene encoding the membrane cytoskeletal protein dystrophin. The resulting loss of the dystrophin protein triggers a concomitant disintegration of the dystrophin-associated glycoprotein complex at the sarcolemma. This complex links intracellular actin to components of the extracellular matrix and serves as a stabilising support network during normal muscle excitation-contraction-relaxation cycles. In Duchenne muscular dystrophy, the loss of dystrophin and its associated protein complex leads to membrane instability and micro-rupturing, the influx of excessive levels of calcium ions, the activation of proteases, sterile inflammation and eventually muscle degeneration and infiltration of adipose and connective tissue. Affected children suffer from severe and progressive skeletal muscle wasting with a loss of independent ambulation occurring during the early teenage years. In addition to muscle wasting, other manifestations of the disease include cardiomyopathy, respiratory insufficiency and scoliosis, along with non-progressive cognitive impairments in a subset of patients. Proteomics represents an ideal bioanalytical tool for the elucidation of the molecular mechanisms that underlie muscular dystrophy and for the identification of novel biomarker candidates. The research presented here has employed label-free liquid chromatography mass spectrometry along with chemical cross-linking mass spectrometry to characterise alterations in protein abundance and protein interaction patterns, respectively, in the *mdx-4cv* animal model of Duchenne muscular dystrophy. Proteins of particular interest have been further verified by biochemical assays including comparative immunoblotting and enzyme-linked immunosorbent assays. In-depth analyses have been performed on skeletal muscle, the aged heart, and brain tissue to investigate proteome-wide changes in the skeletal musculature, the cardiorespiratory system and the central nervous system. In addition, proteomic profiling of serum and saliva samples from dystrophic *mdx-4cv* mice has been conducted to identify potential minimally invasive biomarker candidates for the improved diagnosis, prognosis and therapy-monitoring of X-linked muscular dystrophy.

Chapter One

Introduction

1.1 Muscle Biology

Representing one of the most dynamic and plastic tissues in the human body, muscle accounts for approximately 40% of the total body mass. Composed of myofibres, nerves, blood vessels and connective tissue, the body musculature is highly complex and has a range of integral functions; primarily related to posture, locomotion, heat homeostasis and metabolism (Ohlendieck, 2011b). Four main types of muscle exist; skeletal muscle, cardiac muscle, smooth muscle and myoepithelial cells. Skeletal muscle contains 50-75% of all proteins in the body, and it is primarily involved in metabolism and mechanical support (Frontera and Ochala, 2015). From a mechanical perspective skeletal muscle converts chemical energy to mechanical energy, provides support to the whole body and enables movement. From a metabolic point of view, skeletal muscle contributes to the basal metabolic rate, is responsible for the production of heat to maintain core body temperature and acts as a reservoir for amino acids and carbohydrates for intra-muscular utilisation (Wolfe, 2006). Skeletal muscle is multi-nucleated, striated (due to the organisation of the sarcomeres) and under voluntary control. Cardiac muscle is found only in the heart, is under the control of the autonomic nervous system, and while also striated differs from skeletal muscle by the presence of intercalated discs (Kostetskii et al., 2005), which support synchronised cardiac muscle contraction. The high concentration of mitochondria make cardiac muscle resistant to fatigue (Dorn, 2013). Smooth muscle is an involuntary, non-striated muscle type found in the lining of blood vessels and in internal organs. Myoepithelial cells are typically found in glandular epithelia. They exist as a thin layer between the basement membrane and the luminal cells, and their contractile ability enables them to expel glandular secretions. Given muscle tissue is under extreme stress due to high energy demands and the strain of excitation-contraction-relaxation cycles, muscle is highly adaptable, plastic, and has efficient molecular chaperones and cellular repair mechanisms (Murphy and Ohlendieck, 2016).

1.1.1 Muscle Structure

Skeletal muscle has a highly organised architecture of muscle fibres and associated connective tissue. Individual muscles are surrounded by a layer of connective tissue called the epimysium. Groups of fibres within an individual muscle are surrounded by a second layer of connective tissue called the perimysium, while individual muscle fibres are surrounded by the endomysium and the sarcolemma (Gillies and Lieber,

2011). Each muscle fibre contains thousands of myofibrils and individual myofibrils are composed of a series of sarcomeres; the basic contractile unit of muscle. Figure 1.1 illustrates a single myofibril containing the typical A-bands and I-bands of skeletal muscle and an enlarged view of an individual sarcomere with its associated protein constellation. The arrangement of the filament systems of the sarcomere give skeletal muscle its distinctive striated appearance. Four principal filament systems exist in skeletal muscle; actin-containing thin filaments, myosin-containing thick filaments, titin-containing filaments which span half the sarcomere and the giant protein nebulin which spans the length of the actin filaments (Clark et al., 2002). The sarcomeres are delineated by the Z-discs which is also the site at which the thin filaments, titin filaments and nebulin filaments are anchored. The thin filaments, which also contain the regulatory proteins tropomyosin and troponin, and the thick filaments are responsible for muscle contraction, the large elastic protein titin acts as a “molecular spring” and is responsible for stabilising and aligning the thick filament and may help generate force (Fukuda et al., 2008) while nebulin is suggested to regulate the length of the thin filaments (Kruger et al., 1991).

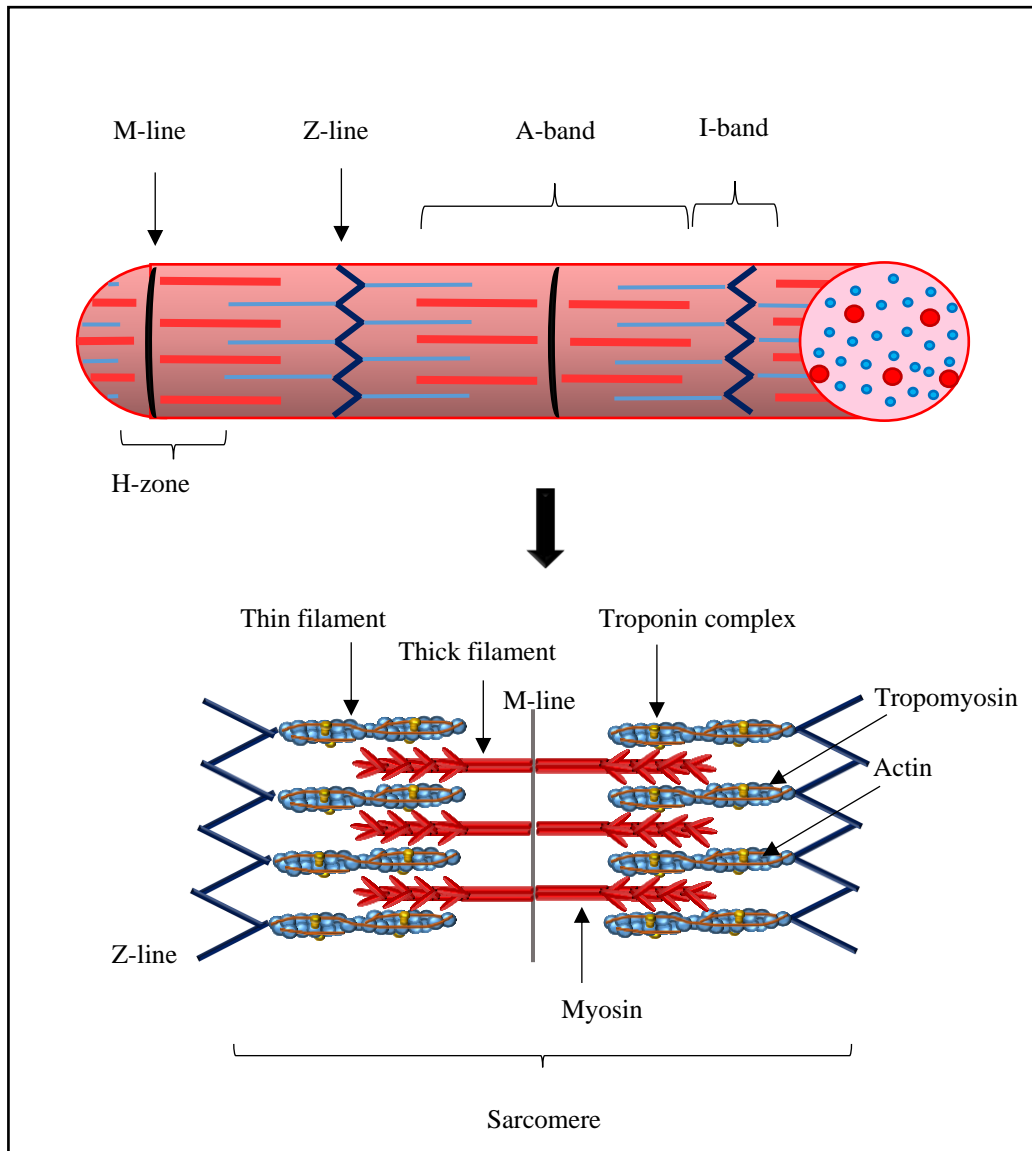


Figure 1.1: Structure of skeletal muscle

Shown in the upper part of the image is a portion of a muscle myofibril depicting some of its key features; the M-line, Z-line, A-band, I-band and H-zone. Depicted underneath is an enlarged image of a sarcomere, which contains the thin and thick filaments that are responsible for skeletal muscle contraction. The thin filaments are composed of actin, tropomyosin and a troponin complex (consisting of troponin I, troponin T and troponin C), while the thick filaments are composed of myosin.

*Image adapted from Frontera and Ochala, 2015

1.1.2 Muscle Fibre Types

Skeletal muscle is highly plastic and dynamic, and its adaptability to changed functional demands is largely due to enormous diversity in contractile proteins and bioenergetic enzymes. In human skeletal muscle, skeletal muscle fibres are classified as slow oxidative (type I), moderately fast oxidative glycolytic (type IIa) and fast glycolytic (type IIb) (Ohlendieck, 2011c). The majority of adult skeletal muscles are characterised by a complex arrangement of fast-twitching fibres, slow-twitching fibres, and hybrid fibres, whereby the ratio of slow-to-fast-to-hybrid fibres is related to the functional status of the individual muscle (Dowling et al., 2016b). Skeletal muscle fibres can be typically classified by colour, fibre diameter, resistance to fatigue, metabolism, capillary density, triglyceride concentration, levels of myoglobin and glycogen, and the density, ultrastructure and enzyme activity of mitochondria (Schiaffino and Reggiani, 2011). Muscle proteins can also be used as markers to determine general trends in fibre-type distributions. As illustrated in Figure 1.2 below, although the overall protein banding pattern is similar between the predominantly slow *soleus* muscle, and the predominantly fast *gastrocnemius* and *extensor digitorum longus* muscles from 12-month old C57/BL10 mice, the intensity of immuno-labelled bands for the slow myosin heavy chain (MyHC)-I(β), and the fast SERCA1 and slow SERCA2 isoforms of the sarcoplasmic reticulum Ca^{2+} -ATPase clearly shows differences in the expression of fibre-type-specific protein isoforms.

A number of neuromuscular disorders and muscle co-morbidities can induce fibre-type transitions in skeletal muscle, either directly as a result of active fibre conversions or indirectly through a heightened susceptibility of certain fibre types to cellular degeneration and muscle atrophy. Slow-to-fast fibre transitions are evident in response to muscular atrophy (denervation, disuse, immobilisation), diabetes and obesity. Fast-to-slow transitions are detected in cancer cachexia, inflammatory myopathies and sarcopenia of old age (Dowling et al., 2016b).

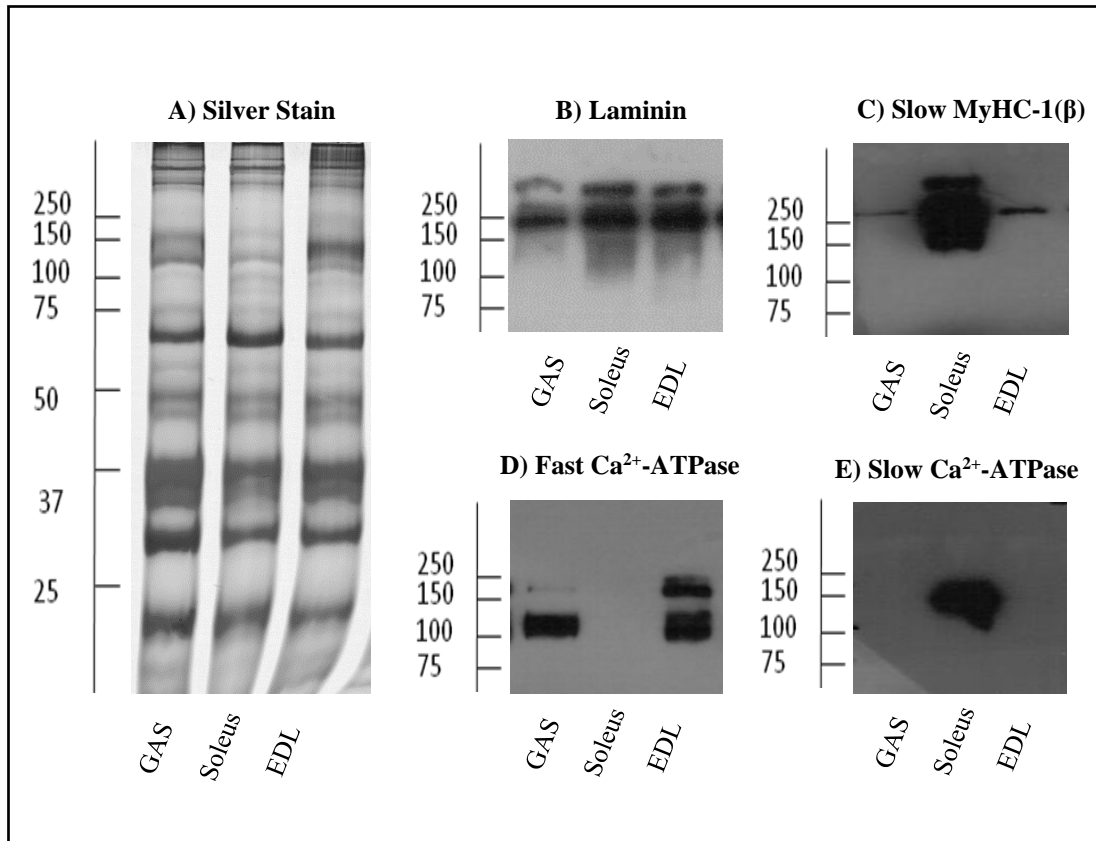


Figure 1.2: Protein markers of skeletal muscle fibre types

Shown is a silver stained gel (A) of tissue homogenates from the individual muscle types *gastrocnemius* (GAS), *soleus* and *extensor digitorum longus* (EDL) from 12-month old C57/BL10 mice. Illustrated also are immunoblots to the equal loading protein laminin (B), the slow myosin heavy chain MyHC-I(β) isoform (C), and the fast SERCA-1 (D) and the slow SERCA-2 (E) isoforms of the sarcoplasmic reticulum Ca^{2+} -ATPase.

*Image adapted from Dowling et al., 2016b

1.1.3 Muscle Excitation-Contraction Coupling

During skeletal muscle development, skeletal muscle fibres are innervated to form a motor unit. The motor unit is the basic functional component of the neuro-motor system and is defined as a motor neuron and all the skeletal muscle fibres that it innervates. The innervation ratio can range from a few fibres in some extraocular muscles to thousands of fibres per motor neuron in some limb muscles (Monti et al., 2001). Muscle contraction is therefore linked to the motor neuron system in which an action potential travels along a motor neuron until it reaches the axon terminal where it activates calcium voltage gated channels. The subsequent release of calcium ions, Ca^{2+} , causes the release of the neurotransmitter acetylcholine (ACh) from nerve terminals where it enters the synaptic cleft and acts as the stimulus for muscle contraction. ACh binds to the post-synaptic acetylcholine receptors (AChR) located within the motor end plate at the muscle sarcolemma, which facilitates the opening of voltage-gated sodium channels and the influx of sodium ions, Na^+ , into the cell (Stephenson et al., 1998). This event results in membrane depolarisation and the propagation of the action potential along the muscle sarcolemma until it is detected by the α_{1s} -subunit of the dihydropyridine receptor (DHPR) in sarcolemmal invaginations known as the transverse tubules (T-tubules). This induces a conformational change in the DHPR, in which the cytoplasmic loop between repeats II and III in the α_{1s} -subunit has been found to be crucial for the propagation of the action potential to the sarcoplasmic reticulum (SR) (Stephenson et al., 1998). The conformational change in the DHPR enables it to interact directly with the ryanodine receptor (RyR1), a high molecular weight (~550 kDa per monomer) homo-tetramer resident in the SR membrane. This binding facilitates the opening of the RyR1 calcium channels, enabling an influx of Ca^{2+} from the lumen of the SR into the cytoplasm of the muscle cell (Calderón et al., 2014).

However, not all RyRs are coupled to DHPR receptors. These single receptors are likely activated by excess Ca^{2+} released by neighbouring RyRs. This amplification of the Ca^{2+} signal is referred to as calcium-induced-calcium-release and is dominant in cardiac tissue (Froemming and Ohlendieck, 2001). The released Ca^{2+} ions bind to regulatory Ca^{2+} -specific binding sites on the calcium-binding troponin C (TnC), which exposes a series of hydrophobic residues in its N-terminus. This facilitates the interaction of TnC with inhibitory troponin I (TnI) and tropomyosin-binding troponin T (TnT). This structural change in the troponin complex promotes the translocation of

the troponin-tropomyosin complex away from the outer domain of actin filaments (Gomes et al., 2002). In the presence of ATP, the myosin head of the thick filament can then interact with the myosin-binding site on actin. As the actin filaments and the myosin heads couple they cause sliding of the thin filaments past the thick filaments, creating a cross-bridge and muscle contraction. Removal of Ca^{2+} from the N-terminal Ca^{2+} -binding site of TnC inhibits the interaction of myosin heads and actin filaments. The removal of Ca^{2+} from the cytoplasm is first mediated by calcium-buffering proteins such as the 12 kDa protein parvalbumin and later by sarcoplasmic reticulum calcium transport ATPase (SERCA), which mediate the pumping of Ca^{2+} from the cytoplasm back to the SR (Calderón et al., 2014). The sarcolemma returns to its resting potential, the interaction between the DHPR and RyR1 dissociates and the muscle relaxes.

Mutations in genes that encode proteins directly involved in the excitation-contraction-relaxation cycle are responsible for a number of hereditary myopathies. Mutations in the calcium release RyR1 are largely responsible for malignant hyperthermia and central core disease. Hypokalemic periodic paralysis is associated with genetic abnormalities in the voltage-sensing α_{1s} -subunit of the DHPR, which may affect interactions with RyR1, and thus interfere with normal excitation-contraction coupling (Froemming and Ohlendieck, 2001). Brody disease is characterised by muscle cramping and exercise-induced impairment of muscle contraction and has been linked to reduced activity of SERCA1, resulting in delayed muscle relaxation. Reduced SERCA1 activity is accompanied by mutations in the ATP2A1 gene in some but not all patients, indicating that Brody disease is genetically heterogeneous (Voermans et al., 2012).

1.1.4 Muscle Development

Myogenesis is the process by which muscle is generated during embryonic development. During gastrulation a mesodermal layer is created between the endoderm and the ectoderm and this mesoderm gives rise to muscle, along with blood vessels, connective tissue and bone (Grefte et al., 2007). Muscle originates from distinct mesodermal tissues; the trunk and limb skeletal muscles are formed from the dermomyotome and the dermomyotome-derived myotome, whereas muscles of the head are formed from the cranial mesoderm. Transcription factors are key players in the development of skeletal muscle. This network of signalling molecules includes the

myogenic regulatory factors (MRFs) MyoD, Myf5, MRF4 and myogenin, which influence myogenic determination and differentiation, and the paired-box transcription factors Pax3 and Pax7 involved in myogenic specification (Endo, 2015). Muscle progenitor cells delaminate from the dermomyotome and also migrate into limb buds, where through the activation of the MRFs they become myoblasts. Myogenin, MyoD and MRF4 then cause the differentiation of myoblasts into myocytes, where they eventually fuse and mature into multinucleated myotubes (Grefte et al., 2007). Innervation and the expression of muscle specific proteins such as the full-length Dp427 dystrophin isoform, muscle myosin heavy and light chains, and the nicotinic acetylcholine receptor, are involved in the transition to an innervated mature myofibre which can then form a functional motor unit (Holland and Ohlendieck, 2013). The adult motor unit is composed of numerous muscle fibres and is highly plastic, resulting in an ability of skeletal muscle to adapt to a variety of stimuli, including but not limited to alterations in neuromuscular activity levels, endurance exercise, denervation, disuse, trauma and the natural aging process.

1.1.5 Muscle Regeneration

Since myonuclei are post-mitotic, muscle repair and regeneration require *de novo* myotube formation, which is facilitated by satellite cells. Satellite cells initially provide myoblasts for muscle growth before becoming mitotically quiescent during muscle maturation (Relaix and Zammit, 2012). They are located between the basal lamina and the sarcolemma of myofibres, and express Pax7 and M-cadherin. While normally in a dormant state, satellite cells are activated upon injury to facilitate muscle regeneration. The exit from quiescence into a proliferative state is mediated by various extracellular signalling factors released from damaged muscle fibres which bind to receptors on quiescent satellite cells to stimulate their activation. These include fibroblast growth factor 2, hepatocyte growth factor, insulin-like growth factor 1 and TNF- α (Dumont et al., 2015). The activation process is similar to embryonic development, in which the activated satellite cells upregulate the expression of MyoD and Myf5 to become proliferative. Down-regulation of Pax3 and Pax7 and up-regulation of myogenin and MRF4 lead to the terminal differentiation of these myoblasts, which then either fuse to one another to generate new muscle fibres or attach to damaged muscle fibres to aid muscle repair (Grefte et al., 2007).

Satellite cells also demonstrate a capacity for self-renewal, where satellite cell division results in one progeny which becomes a myonucleus and the other remains as a satellite cell to maintain the satellite cell population (Moss and Leblond, 1971) in a process known as asymmetrical cell division. While this ability to self-renew earned them the status of stem cell, there is little evidence to suggest that satellite cells can give rise to other cell lineages and so they can be considered as a monopotent myogenic stem cell (Relaix and Zammit, 2012). While satellite cells represent the principal myogenic precursor cell and their ablation severely impairs the regenerative capacity of skeletal muscle, other non-satellite cells exist which can support myogenesis. Positive interstitial cells (PICs) are a population of Pax7 negative, PEG3 (paternally expressed gene 3) positive cells which reside in mature skeletal muscle. They can acquire Pax7 and MyoD expression, which enables them to contribute to myogenesis and skeletal muscle regeneration *in vivo*. Unlike satellite cells, PICs are bipotent with an ability to give rise to both smooth and skeletal muscle (Mitchell et al., 2010). While Pax7 expression is a requirement for myogenic specification of PICs, it is not necessary for the smooth muscle fate of PICs. In addition, a contractile cell population named pericytes have been shown to fuse to myofibres and contribute to myogenesis (Dumont et al., 2015).

The natural aging process and muscle disease have an impact on the regenerative capacity of satellite cells. In senescence there is a decrease in both satellite cell numbers and the myogenic capacity of individual satellite cells, which is postulated to be influenced by both intrinsic and extrinsic factors (Dumont et al., 2015). Duchenne muscular dystrophy is a chronic disease of muscle degeneration, where continuous cycles of muscle damage result in the constant activation of satellite cells, leading to premature exhaustion of the satellite stem cell pool. However, the observation that satellite cell numbers in dystrophic muscle are equal to or higher than the number found in age-matched healthy muscle, led to the hypothesis that intrinsic defects in satellite cells may contribute to the severity of muscular dystrophy. Dystrophin and other members of the dystrophin-glycoprotein complex (DGC) are expressed in activated satellite cells. In the absence of dystrophin, cell polarity and asymmetric cell division (the process by which two cells with different cellular fates are generated) is lost, resulting in a reduction in the number of myogenic progenitor cells (Dumont and Rudnicki, 2016). Impaired cell polarity of dystrophin-deficient satellite cells also increases the proportion of abnormal cell divisions and satellite cells

may be targeted for senescence or apoptosis, as seen in satellite cells from the *mdx* mouse model of Duchenne muscular dystrophy (Chang et al., 2016). Thus, future therapeutic strategies for Duchenne muscular dystrophy should take into account the need to restore cell polarity and satellite cell function.

1.1.6 Muscle Aging and Sarcopenia

During the natural aging process, the majority of individuals will experience an age-dependent decline in muscle mass accompanied by a loss of strength and/or physical performance. This loss of muscle mass termed sarcopenia (sarx=flesh and penia=loss) occurs in both sexes with advanced age, and is complicated by sedentary lifestyle, poor nutrition and co-morbidities such as cancer and diabetes (Ohlendieck, 2011a). Sarcopenia is strongly suggested to be a result of a multi-factorial pathology. There is an age-dependent decrease in the number of motor neurons due to apoptosis, which is accompanied by cycles of denervation and re-innervation. Sprouting of nearby surviving motor neurons results in the re-innervation of some but not all denervated muscle fibres, and results in the formation of very large motor units and a concomitant decrease in fine motor skills (Aagaard et al., 2010). This axonal sprouting is proposed to compensate for the loss of motor neurons until approximately 50% of them have died (McNeil et al., 2005). After this stage, and/or when axonal sprouting becomes inadequate or absent a drastic reduction in muscle fibre numbers and size can be seen in skeletal muscle. Other contributing factors to muscle aging include a decline in muscle protein synthesis, uncoupling between excitation and contraction, impaired regenerative capacity and a decline in the number of satellite cells, altered metabolic pathways, increased oxidative stress, and perturbed levels of growth factors and cytokines (Aagaard et al., 2010, Edström et al., 2007).

Mass spectrometry-based proteomics is an unbiased analytical tool for identifying alterations in protein expression patterns and such an approach has detected altered abundance and post-translational modifications for numerous proteins in aged muscle. Proteomic surveys of muscle extracts from aged human and animal muscle has identified a fast-to-slow fibre type transition, as indicated by increased abundance of slow isoforms of myosin heavy chains, myosin light chains, actin and tropomyosin (Gelfi et al., 2006, Gannon et al., 2009). This muscle transformation is accompanied by a decrease in certain glycolytic enzymes including enolase and pyruvate kinase and increases in mitochondrial enzymes such as malate

dehydrogenase, prohibitin, and succinate dehydrogenase, indicating a glycolytic to oxidative shift in senescent muscle (Gelfi et al., 2006, O'Connell and Ohlendieck, 2009). However, variances do exist in the expression of certain glycolytic enzymes, indicating that complex metabolic alterations occur in aged muscle (O'Connell et al., 2007). In addition to fibre type transitions, alterations in the cellular stress response are also found to occur in senescent skeletal muscle. The family of heat shock proteins (HSP) are involved in molecular chaperoning by preventing protein mis-folding, helping to keep proteins in their native conformation, and counter-acting the development of inactive protein aggregates (Doran et al., 2009a). Many muscle associated HSPs are increased in abundance in response to stress and disease. Twenty-four hours following a period of non-damaging isometric contractions, *gastrocnemius* muscle from adult rats showed a significant increase in the abundance of HSP70 as determined by western blot analysis but no difference in HSP70 abundance was detected in aged rats. Since the initial resting level of HSP70 was comparable between adult and aged rats, this suggests a potential diminished cellular stress response in aged muscle fibres (Vasilaki et al., 2002). This is supported by the observation that transgenic overexpression of HSP70 in adult and aged mice helps protect against contraction-induced damage and aids a more rapid and complete recovery following muscle damage (McArdle et al., 2004). While these studies reveal a potential deficit in HSP70 in aged muscle, other proteomic studies have identified elevated levels of the 'α-crystallin' domain containing HSPs in senescent rat fibres. Increased abundance of the small HSPs αB-crystallin, cardiovascular HSP/HSPB7 and HSP20, but reduced levels of the high molecular mass stress proteins HSP60 and HSP70 were identified in 30-month old rat skeletal muscle (Doran et al., 2007). The co-appearance of ubiquitin conjugate and αB-crystallin immunoreactivity at the onset of myotome development in early chicken embryos, a time of intense morphological rearrangement, suggests that these proteins may be involved in cytoskeletal reorganisation (Scotting et al., 1991). Thus, the elevated abundance of the αB-crystallin in aged muscle may be linked to the major cellular re-structuring involved in the fast-to-slow transition process in senescent muscle.

Proteomic surveys of aged skeletal muscle have identified fast-to-slow muscle transitions, glycolytic-to-oxidative metabolic shifts and changes in molecular chaperoning. Such studies are beneficial in elucidating the molecular mechanisms of muscle aging and it is hoped that this would translate into improved diagnostic

procedures and treatment strategies to promote healthy aging in the face of extended human longevity.

1.2 Duchenne Muscular Dystrophy

Duchenne muscular dystrophy (DMD) is the most frequently inherited neuromuscular disease of childhood, affecting approximately 1 in every 3,500 live male births (Falzarano et al., 2015). This X-linked disorder is the result of primary abnormalities in the *Dmd* gene encoding the membrane cytoskeletal protein dystrophin. Mutations include deletions (~65%), duplications (~10%) and other small mutations, including nonsense and missense point mutations (~25%) (Ferlini et al., 2013). Mutations which change the open reading frame of the *Dmd* gene result in DMD while mutations which do not alter the reading frame result in the milder allelic disorder Becker muscular dystrophy (BMD), which is characterised by a later onset and a milder myopathy.

As reviewed in detail by Tyler, early cases of DMD were likely first described by Richard Partridge, Edward Meryon and William Little who examined male patients who exhibited muscle weakness (particularly affecting the proximal muscles of the arms and legs), enlarged muscles associated with muscle hypertrophy, curvature of the spine, delayed motor milestones and histological signs of fatty deposition (Tyler, 2003, Meryon, 1852). Importantly, histological analyses of the brain and spinal cord by Meryon and Little showed no detectable abnormalities leading to the hypothesis that it was primarily a disease of the musculature (Meryon, 1852). Characterisation of the disease is most classically associated with Duchenne, who identified six main pathological features of “pseudohypertrophic paralysis”; i) decrease in muscle strength, ii) inward curvature of the spine, iii) increased volume of affected muscles, iv) progressive nature, v) diminished electromuscular contractility in advanced stages and vi) no sign of fever, sensory abnormalities nor impaired function of the bladder nor intestine (Duchenne, 1867, Tyler, 2003). The English clinician Sir William Richard Gowers is most associated with describing the unusual way in which afflicted patients rise from the floor, termed Gowers’ sign and for observing i) that it primarily affected males, with males also exhibiting more severe symptoms than affected females, ii) that it was heritable based on observations that the disease affected multiple members of the same family and iii) that the disease seemed to always come from the mother’s side of the family; observations now known to be due to the X-linked nature of DMD (Clarke and Gowers, 1874, Tyler, 2003).

Despite these very early descriptions of DMD, it was not until 1987 that the defective gene and the protein it encodes were identified. Initially, while there were no clues regarding the identity of the defective gene, it was known to be located on the X chromosome because the disease primarily affected boys, and studies involving a small number of females with balanced X-autosome translocations with breakpoints at Xp21, who manifested signs of muscular dystrophy, suggested that the gene may be located at Xp21 (Boyd et al., 1986, Verellen-Dumoulin et al., 1984, Zatz et al., 1981). Restriction fragment length polymorphisms analysis was used to confirm that the *Dmd* gene was localised to the short arm of the X chromosome (Davies et al., 1983). The gene was identified through analysis of a patient with a deletion of part of band Xp21 that resulted in four X-linked disorders; DMD, chronic granulomatous disease, retinitis pigmentosa and the McLeod red cell phenotype (Francke et al., 1985, Guiraud et al., 2015). Subsequently, in 1987 the Kunkel lab cloned the complete cDNA of the *Dmd* gene and identified the protein product dystrophin (Koenig et al., 1987, Hoffman et al., 1987), which paved the way for a new era in muscular dystrophy research.

Clinical manifestations of the disease are undetectable at birth, although serum creatine kinase levels are already elevated, and so DMD is usually diagnosed in children around 2-5 years of age when the first symptoms appear (Blake et al., 2002). Initial signs of DMD include a delay in achieving motor milestones, delay in walking, waddling gait, unsteadiness and difficulty running and jumping. Subsequent symptoms include hypertrophy of proximal limb muscles (particularly the calf muscles), limb muscle weakness and Gowers' sign (Emery, 2002). The disease is highly progressive, with a loss of independent ambulation in the early teenage years. This is accompanied by curvature of the spine and weakness of the muscles of the arm. The disease is ultimately fatal, with death occurring in the early twenties often due to respiratory complications (Blake et al., 2002). However, given improvements in respiratory care in afflicted patients (Simonds et al., 1998), cardiomyopathy is increasingly becoming a significant source of mortality (Falzarano et al., 2015).

The effects of dystrophin deficiency are most clearly observed in the skeletal muscle as illustrated by difficulties with motor development. This is also seen in histological analyses of dystrophic skeletal muscle, where muscle fibre necrosis, infiltration of immune cells, alterations in fibre size, central nucleation (indicating muscle regeneration), deposition of adipose and connective tissue and reduced blood supply are evident (Haslett et al., 2002). However, not all skeletal muscles are affected

equally by dystrophin deficiency, with intrinsic laryngeal muscles, certain distal muscles and extraocular muscle spared from X-linked muscular dystrophy (Marques et al., 2007). Proteomic analyses of these spared muscle groups reveal increased abundance of the dystrophin homolog utrophin and a concomitant rescue of β -dystroglycan and calcium-buffering proteins such as calsequestrin (Lewis and Ohlendieck, 2010b, Dowling et al., 2003). Understanding the molecular basis behind these protected phenotypes may facilitate the development of new treatment strategies for DMD. In addition to severe and progressive skeletal muscle wasting, cardiomyopathy is a major clinical feature of X-linked muscular dystrophy. The absence of dystrophin triggers a loss of membrane integrity and affects L-type calcium channels and mechanical stretch activated receptors in the heart (Woolf et al., 2006). In a similar process to that seen in skeletal muscle, this then leads to altered calcium fluxes and the activation of calpain proteases which degrade contractile proteins, ultimately culminating in cell death, inflammation and fibrosis (Spurney, 2011). The cardiomyocyte degeneration and infiltration of connective tissue particularly affects the posterobasal segment of the left ventricle (LV), where an increase in wall stress and susceptibility to pressure overload is seen. Systolic LV function decreases, oxygen consumption increases and this leads to LV dilation and dysfunction (Fayssoil et al., 2010).

One of the principal extra-muscular manifestations of DMD is mild, non-progressive cognitive impairment which is seen in approximately one-third of patients. On average the intelligence quotient of DMD patients is one standard deviation below the population mean (Emery and Muntoni, 2003), with cognitive deficits particularly affecting verbal intelligence, attention span and memory (Marsh and Munsat, 1974, Wicksell et al., 2004). Interestingly, a number of groups have suggested that the specific dystrophin mutation may have an effect on the severity of cognitive defects. Patients with mutations located in the distal portion of the *Dmd* gene (involving the Dp140 brain isoform) are generally more severely affected than patients with mutations located in the proximal portion of the gene (not affecting Dp140) (D'Angelo et al., 2011). Daoud and colleagues found a similar correlation between mental impairments and mutation location, whereby patients with mutations affecting all dystrophin isoforms including the Dp71 brain isoform displayed cognitive performances significantly below average (clinically regarded as mentally retarded) while patients with mutations affecting all dystrophin isoforms except Dp71 had either

normal or borderline cognitive performances (Daoud et al., 2009). Dystrophin deficiency thus induces a range of pathological secondary defects affecting skeletal muscle, the heart and cognition.

1.2.1 Dystrophin and its isoforms

The *Dmd* gene spanning 2.5 Mb and 79 exons, which represents the largest identified gene in the human genome, encodes the membrane cytoskeletal protein dystrophin. The gene is located at the Xp21 locus. Expression of the dystrophin protein is under the control of 7 promoters, which produce three full-length Dp427 isoforms of dystrophin and four shorter isoforms named Dp260, Dp140, Dp116 and Dp71 (Muntoni et al., 2003), as shown in Figure 1.3. Expression of dystrophin is tissue specific; the independent muscle (M), brain (B) and Purkinje (P) promoters are responsible for Dp427 expression in striated skeletal and cardiac muscle, the brain and Purkinje neurons respectively. The four shorter isoforms of 260 kDa, 140 kDa and 116 kDa are expressed in the retina (Pillers et al., 1993), brain and kidney (Lidov et al., 1995), and Schwann cells respectively (Saito et al., 1999), while the 71 kDa isoform is found ubiquitously with particularly high levels in the central nervous system (Garcia-Tovar et al., 2001). These shorter isoforms lack the actin binding terminus associated with full-length dystrophin but retain the cysteine rich and carboxy terminus domains responsible for dystrophin's interaction with β -dystroglycan, dystrobrevin and syntrophin, as depicted in Figure 1.4.

Pioneering work by the Kunkel lab using positional cloning for the genetic analysis of X-linked muscular dystrophy led to the discovery of the dystrophin gene (Koenig et al., 1987). The 427 kDa isoform of dystrophin was identified as a member of the β -spectrin/ α -actinin family (Koenig et al., 1988), leading to the establishment of dystrophin as a stabilising linker at the sarcolemma capable of connecting the actin cytoskeleton to the extracellular matrix (Ervasti and Campbell, 1993). This membrane cytoskeletal protein is divided into four main domains; i) the amino terminal domain with a pair of calponin homology units capable of binding filamentous actin (Norwood et al., 2000), ii) a central rod domain containing 24 spectrin-like repeats interspersed by four proline-rich hinge domains (SLR 1-3, SRL 4-19 and SLR 20-24) (Koenig and Kunkel, 1990), iii) a tryptophan (WW) domain, and iv) a unique carboxy terminus which contains a syntrophin binding site in exon 74 (Ahn and Kunkel, 1995) and binds dystrobrevin through its two α -helical coiled coils (Sadoulet-Puccio et al., 1997). The

WW domain is a short conserved region which folds as a triple-stranded β -sheet and is usually involved in signalling through interactions with proline-rich or phosphorylated peptide sequences, and which is proposed to be responsible for binding to a Pro-Pro-x-Tyr core motif in the carboxy terminus of β -dystroglycan (Huang et al., 2000, Rentschler et al., 1999). A cysteine-rich domain, containing a ZZ module, which contains a second binding site for β -dystroglycan (Vulin et al., 2014) and two EF-hand motifs responsible for binding to calmodulin in a calcium-dependent manner, follow the WW domain.

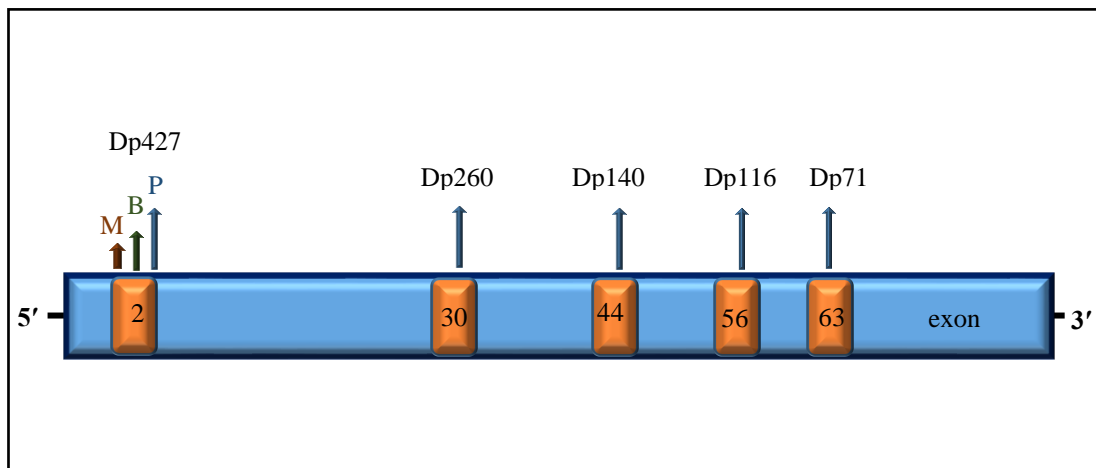


Figure 1.3: Different promoter regions for dystrophin isoforms

Dystrophin, located on Xp21, has multiple gene promoters giving rise to alternatively spliced isoforms. Expression of full-length dystrophin isoforms is controlled by three distinct promoters upstream of exon 2. This generates three Dp427 isoforms; Dp427-M (expressed in muscle), Dp427-B (expressed in brain tissue) and Dp427-P (expressed in cerebellar Purkinje fibres). Internal tissue-specific promoters transcribe smaller dystrophin isoforms; Dp260, Dp140, Dp116 and Dp71. Alternative dystrophin isoforms can also be generated through alternative splicing events or by using an alternative poly-(A) addition site in intron 70 (Dp40 isoform).

*Image modified from Blake et al., 2002.

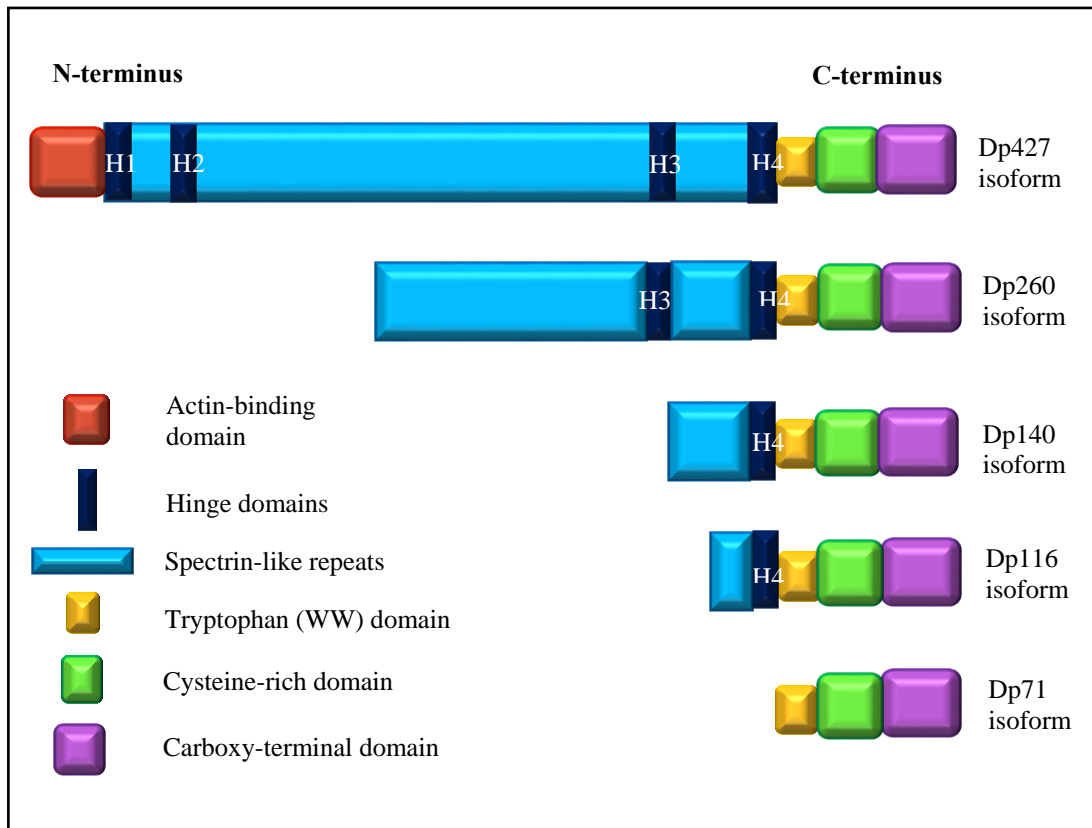


Figure 1.4: Structural characteristics of full-length dystrophin and its isoforms
 Schematic illustrating the various isoforms of dystrophin which exist; Dp427 is the full-length isoform, while Dp260, Dp140, Dp116 and Dp71 are shorter in size and lack some of the features seen in full-length dystrophin. Expression of dystrophin isoforms is tissue specific; Dp427-M in muscles, Dp427-B in the brain, Dp427-P in cerebellar Purkinje cells, Dp260-R in the retina, Dp140-B/K in the brain and kidney, Dp116-S in Schwann cells and Dp71 in brain and non-muscle tissues.

*Image adapted from McGreevy et al., 2015

1.2.2 Dystrophin and the dystrophin-glycoprotein complex

The identification of the dystrophin gene on the X chromosome and the subsequent discovery of its encoded protein dystrophin heralded the beginning of a new era in muscular dystrophy research (Hoffman et al., 1987). Shortly afterwards, work by the Campbell lab demonstrated that dystrophin could be enriched from detergent solubilised muscle membranes using wheat germ agglutination, despite not being glycosylated itself, due to interactions with wheat germ agglutinin binding glycoproteins (Campbell and Kahl, 1989). Serial anion exchange chromatography and sucrose gradient centrifugation of this dystrophin-enriched fraction resulted in the identification of several interacting proteins of 156 kDa, 50 kDa, 35 kDa and 25 kDa along with a triplet of 59 kDa and a doublet of 43 kDa (Ervasti et al., 1990). Since these proteins co-purified with dystrophin, co-localised with dystrophin at the sarcolemma and the 156 kDa protein was found to be significantly reduced in muscle samples from the dystrophic *mdx* mouse and from biopsy samples from DMD patients, the authors suggested that dystrophin existed as a hetero-oligomeric complex consisting of dystrophin, a 59 kDa triplet and four sarcolemmal proteins (156 kDa, 50 kDa, 43 kDa and 35 kDa) (Ervasti et al., 1990). These proteins have since been identified as α -dystroglycan (156 kDa), β -dystroglycan (one of the 43 kDa proteins) (Ibraghimov-Beskrovnaya et al., 1992), syntrophin (59 kDa) (Adams et al., 1993), the sarcoglycans; α -sarcoglycan (50 kDa), β -sarcoglycan (the other 43 kDa protein), δ -sarcoglycan (35 kDa) and γ -sarcoglycan (35 kDa) (Yoshida et al., 1994), and sarcospan (25 kDa) (Crosbie et al., 1997).

The structural organisation of the DGC has been debated and refined over a number of years, and is now considered to consist of dystrophin, the sarcolemmal proteins β -dystroglycan, α -sarcoglycan, β -sarcoglycan, δ -sarcoglycan, γ -sarcoglycan and sarcospan, the cytosolic proteins nNOS (neuronal nitric oxide synthase), syntrophins and dystrobrevins and the extracellular matrix proteins α -dystroglycan and laminin. The findings that i) α -dystroglycan and β -dystroglycan exist in a complex (Yoshida et al., 1994), ii) that α -dystroglycan had the capacity to bind to extracellular laminin (Ibraghimov-Beskrovnaya et al., 1992), iii) that β -dystroglycan could directly interact with dystrophin at its cysteine rich and C-terminal domains and iv) that dystrophin contained actin-binding domains (Levine et al., 1992), strengthened the initial hypothesis that in striated muscle the DGC plays a pivotal role in linking the actin cytoskeleton to the extracellular matrix (Ervasti and Campbell, 1993). The

current working model depicts dystrophin as a long rod-shaped cytoskeletal protein on the cytoplasmic side of the sarcolemma, which binds to actin at its N-terminus and at a second site within its rod domain, and which interacts with β -dystroglycan at binding sites on its cysteine-rich domain. β -dystroglycan in turn binds to α -dystroglycan, oligosaccharides on which are responsible for binding to laminin-2 of the extracellular matrix. α -dystroglycan can also bind the proteoglycans agrin, perlecan and biglycan (Durbeej and Campbell, 2002). The sarcolemmal sarcoglycan-sarcospan complex serves to strengthen the non-covalent interactions of dystrophin and α -dystroglycan with β -dystroglycan. α -dystrobrevin couples the sarcoglycan-sarcospan complex with dystrophin while the syntrophins serve as adaptor molecules, responsible for the recruitment of signalling molecules to the sarcolemma (Blake et al., 2002), as illustrated in Figure 1.5.

Whilst the core DGC is largely similar in skeletal and cardiac muscle, some differences in protein composition and subcellular localisation do exist (Lapidos et al., 2004). The cardiac DGC has an altered composition of syntrophin and dystrobrevin proteins, with reduced levels of β 1 syntrophin and α 1 dystrobrevin associated with the cardiac DGC and a stronger association between α 3 dystrobrevin and the cardiac DGC than that of the skeletal muscle (Johnson et al., 2012). In addition, the cardiac DGC has a number of different binding partners, including cavin-1, ahnak-1, α B-crystallin and cypher (Johnson et al., 2012). Additional complexes which exist solely in the DGC in skeletal muscle include caveolin-3 and the signalling molecule nNOS. Similar to other caveolin isoforms, caveolin-3 can form small membrane invaginations, named caveolae, which can act as a scaffold for signalling molecules. Indeed, caveolin-3 has been shown to directly bind to nNOS (Venema et al., 1997), which plays a role in vasoconstriction. In contrast, in the cardiac DGC it is endothelial NOS that is recruited, where it interacts with γ -sarcoglycan and δ -sarcoglycan (Heydemann et al., 2004). In terms of localisation differences, the skeletal DGC is restricted to the sarcolemma, whereas the cardiac DGC is also found in T-tubule invaginations (Klietsch et al., 1993).

Given the primary role of the DGC in linking the sub-sarcolemmal cytoskeleton to the extracellular matrix and thus acting as a stabilising support network during normal muscle excitation-contraction-relaxation cycles, mutations in its protein components lead to neuromuscular disease. Specifically, mutations in the genes encoding dystrophin, α -, β -, δ - and γ -sarcoglycans, caveolin-3 and laminin- α 2 lead to

Duchenne muscular dystrophy/Becker muscular dystrophy/X-linked dilated cardiomyopathy, limb-girdle muscular dystrophy types 2C-F, limb girdle muscular dystrophy type 1C and congenital muscular dystrophy respectively (Rahimov and Kunkel, 2013).

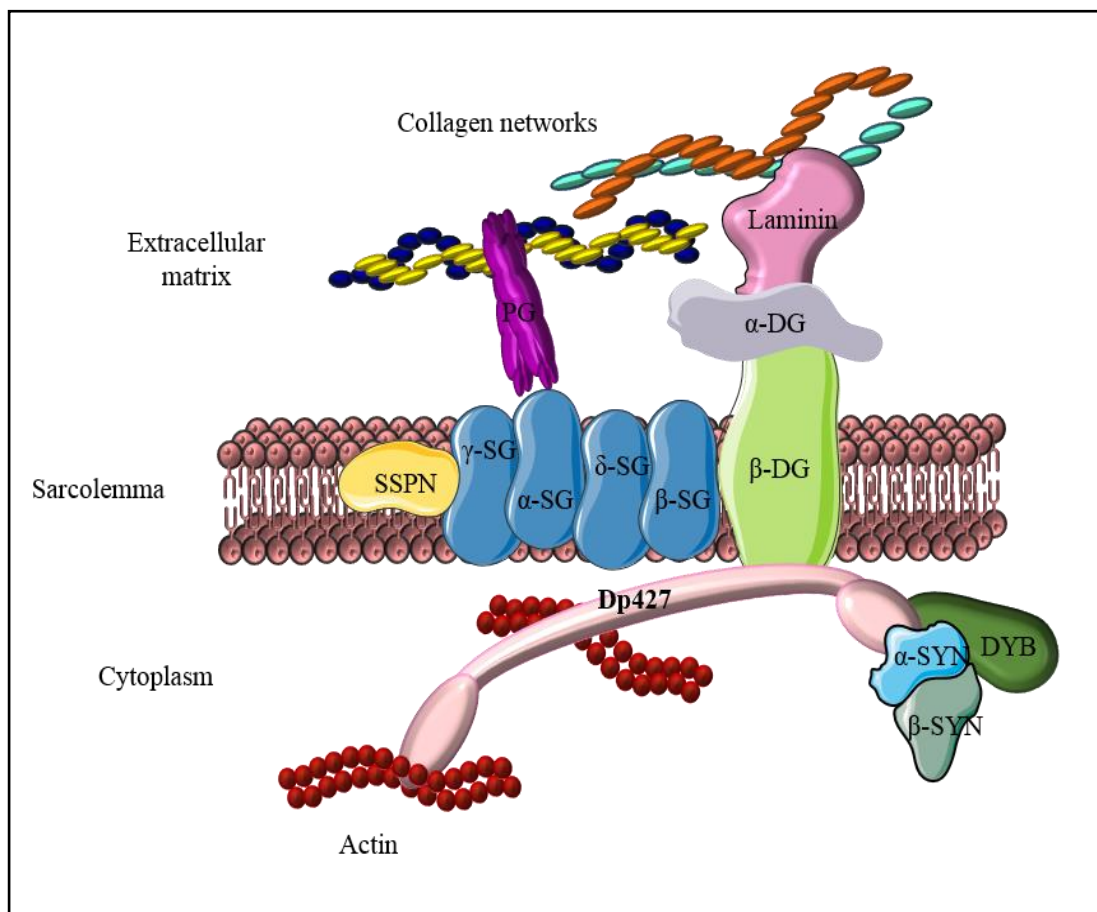


Figure 1.5: The dystrophin-glycoprotein complex

Pictured is the DGC in skeletal muscle, consisting of the full-length Dp427 dystrophin isoform (Dp427), linked to the sarcoglycan-sarcospan complex (α -SG, β -SG, γ -SG, δ -SG and SSPN), and the dystroglycan complex (β -DG and α -DG). α -dystroglycan binds to laminin, which links with collagen fibrils in the extracellular matrix. Other extracellular matrix proteins such as proteoglycans (PG) also interact with the complex. Cytoplasmic proteins include α -syntrophin (α -SYN), β -syntrophin (β -SYN), dystrobrevin (DYB) and actin. Overall this tight interaction of proteins lends stability to the sarcolemma during normal muscle excitation-contraction-relaxation cycles.

1.2.3 Structural roles of the DGC

A large body of evidence supports a structural role for the DGC. Firstly the similarities between dystrophin and spectrin, such as the presence of 24 spectrin-like repeats in the full-length dystrophin isoform, and dystrophin's links with the sub-sarcolemmal actin cytoskeleton, led to the hypothesis of dystrophin as a stabilising structure capable of resisting or decreasing mechanical strain on striated muscle during muscle contraction, similar to the role of the spectrin network in acting as a shock absorber in the red blood cell cytoskeleton (McGough, 1999). Later studies utilising yeast two-hybrid screens, illustrated linkage of the DGC with the desmin intermediate filaments through the proteins syncoilin (which binds to α -dystrobrevin) and dysbindin (which interacts with α -dystrobrevin and β -dystrobrevin), which added further weight to a mechanical role of the DGC (Newey et al., 2001, Benson et al., 2001). In addition, dystrophin is enriched at costameres, protein assemblies that are likely responsible for the lateral transmission of contractile forces from the sarcomeres to the sarcolemma to the extracellular matrix and finally to neighbouring cells (Danowski et al., 1992). A mechanical role for the DGC is also implied by the fact that the dystrophin-deficient sarcolemma is extremely fragile and permeable, with physical exercise aggravating this sarcolemmal permeability (Vilquin et al., 1998), and immobilisation of dystrophin-deficient muscle reduces signs of muscle pathology and muscle degeneration (Mokhtarian et al., 1999). Collectively, the data suggests that dystrophin, and its associated glycoprotein network, is involved in protection against mechanical stress, which has important implications for dystrophin-deficient muscle (Deconinck and Dan, 2007).

1.2.4 Signalling roles of the DGC

While initial studies focused primarily on the structural role of the DGC, the presence of multiple binding sites within the DGC suggests it may act as a scaffold for the recruitment of signalling molecules, and thus the DGC may regulate such signalling cascades. The dystroglycans and syntrophins have been particularly implicated for a role in cellular signalling. The interaction of β -dystroglycan with MEK (mitogen-activated protein kinase kinase) and ERK (extracellular signal-regulated kinase) suggests a role for the DGC in ERK-MAP signalling. While β -dystroglycan associates with active ERK1, it itself is not phosphorylated by ERK nor does it have any effect on the ability of ERK to phosphorylate its substrate myelin basic protein (Spence et

al., 2004). In addition, β -dystroglycan has no effect on MEK activity, and within its cytoplasmic tail it contains a motif previously identified as a conserved docking motif for MAP (mitogen-activated protein) kinases (Tanoue et al., 2000). Taken together this data therefore suggests that β -dystroglycan acts as a membrane anchor for signalling components of the ERK-MAP pathway. Tyrosine phosphorylation of the PPxY motif within β -dystroglycan results in the recruitment of a number of SH2 (Src homology 2) domain containing proteins including c-Src, Fyn, Csk, NCK, and SHC (Sotgia et al., 2001). β -dystroglycan has also been shown to interact with the adaptor molecule growth factor receptor-bound protein 2, Grb2, (Yang et al., 1995). This interaction between the proline-rich domain in β -dystroglycan's C-terminus and the SH3 domain of Grb2 may be involved in extracellular matrix-mediated signal transduction and/or cytoskeletal organisation. Further studies have demonstrated that laminin binding by dystroglycan recruits a Grb2-Sos1 (growth factor receptor-bound protein 2-son of sevenless) complex to the DGC via syntrophin and β -dystroglycan, resulting in activation of the downstream adaptor Rac1 (Ras-related C3 botulinum toxin substrate 1) which, through the Cdc42-Race effector p21 activated kinase 1, activates the JNK-p46 isoform of JNK (c-Jun NH2-terminal kinase), while laminin depletion results in the activation of JNK-p54 (Oak et al., 2003). The role of this laminin signalling could be to promote cell proliferation, an effect observed in C2C12 myoblasts (Oak et al., 2003). Collectively these studies indicate that the DGC has a key function in the recruitment of signalling molecules and thus may have a role in modulating a variety of signalling cascades.

The syntrophins are a class of scaffold proteins characterised by the presence of two pleckstrin homology (PH) domains, a PDZ domain (Post Synaptic Density protein-95, Drosophila discs large protein, and the Zona occludens protein 1), and a C-terminal domain exclusive to the syntrophins. The ability of the PH and PDZ domains to bind to a variety of proteins indicates a role for the syntrophins in cellular signalling (Constantin, 2014). For instance the PDZ domain of α 1-syntrophin binds to nNOS, which produces nitric oxide which exerts multiple effects on skeletal muscle including mitochondrial respiration, contractile ability, glucose metabolism and neuromuscular transmission (Grozdanovic and Baumgarten, 1999). In addition, various signalling molecules have been shown to associate with different syntrophin isoforms, leading to the proposal that the primary role of the syntrophins is to link signalling molecules to the DGC. These signalling molecules include phosphatidyl

inositol-4,5-bisphosphate (Chockalingam et al., 1999), stress-activated protein kinase-3 (Hasegawa et al., 1999), microtubule associated serine/threonine kinase (Lumeng et al., 1999) and diacylglycerol kinase ζ (Hogan et al., 2001). The presence of the integral membrane protein aquaporin-4 at the sarcolemma has also been shown to be dependent on interactions with the PDZ domain of α -syntrophin (Adams et al., 2001). More recent studies have identified that α 1-syntrophin also interacts with a number of heterotrimeric G protein α subunits in the brain, suggesting that it could possibly be involved in signalling pathways which utilise G-protein-coupled receptors (Okumura et al., 2008). In agreement with a role for the syntrophins in G-protein-coupled receptor signalling, Chen and colleagues identified an interaction between the PDZ domain of syntrophin (α -syntrophin, β 1-syntrophin and β 2-syntrophin) and the C-terminal domain of α 1-adrenergic receptors (Chen et al., 2006), G-protein-coupled receptors which operate in the cardiovascular system. A later study demonstrated that in mouse aortic smooth muscle cells α -syntrophin and β 2-syntrophin associate with α 1D-adrenergic receptor to form a signalling complex (in the proposed model the syntrophins anchor the α 1D-adrenergic receptor at the sarcolemma through interactions with dystrophin-utrophin and dystrobrevin), with this complex shown to be involved in vascular smooth muscle contraction and regulation of blood pressure (Lyssand et al., 2008). Such studies provide further support for a role for the syntrophins in regulating G-protein-coupled receptor signalling.

The sarcoglycan complex in cardiac and striated skeletal muscle consists of four sarcoglycan isoforms; α -sarcoglycan, β -sarcoglycan, γ -sarcoglycan and δ -sarcoglycan, and the 25 kDa transmembrane protein sarcospan (Crosbie et al., 1997). The primary role of the sarcoglycan complex appears to be to strengthen the interaction of β -dystroglycan with α -dystroglycan and dystrophin, with mutations in any of the four sarcoglycan isoforms leading to autosomal recessive limb girdle muscular dystrophy type 2 C-F. Aside from providing structural integrity, the sarcoglycan complex may be involved in signalling cascades, through the ability of α -sarcoglycan and γ -sarcoglycan to bind to the small leucine rich repeat proteoglycan biglycan (Rafii et al., 2006), an extracellular matrix protein involved in signalling pathways pertaining to muscle regeneration (Casar et al., 2004), tissue remodelling and stress fibre formation (Tufvesson and Westergren-Thorsson, 2003). γ -sarcoglycan has also been implicated in membrane signalling pathways affecting cell contractile ability, apoptosis and MAP kinase activation as γ -sarcoglycan deficiency in primary

skeletal myoblasts and in mice is associated with increased apoptosis, increased contractile pre-stress and alterations in the phosphorylation and activation of MAP kinase-pathway proteins. Hyper-activation was particularly seen for p38 MAP kinase and MAPKAPK2 (MAP kinase-activated protein kinase 2) in stretched γ -sarcoglycan null *tibialis anterior* muscle, suggesting a role for p38 MAPK pathway in stretch-induced mechano-transduction (Griffin et al., 2005).

Sarcospan, the last of the core dystrophin-interacting proteins to be identified, is also involved in cellular signalling. Sarcospan is suggested to influence muscle regeneration through activation of the Akt (protein kinase B) signalling cascade. Such a role for sarcospan is supported by studies indicating that over-expression of sarcospan (by two-three fold) helps to ameliorate the dystrophic phenotype in *mdx* mice by increasing protein abundance of utrophin, α -dystroglycan, β -dystroglycan, α -sarcoglycan, β -sarcoglycan and γ -sarcoglycan and stabilising a utrophin-glycoprotein complex at the sarcolemma (Peter et al., 2008), and that sarcospan-null muscle shows decreased Akt signalling, decreased utrophin expression and is incapable of efficient muscle regeneration following cardiotoxin injury (Marshall et al., 2012). Since pre-treatment of sarcospan-null muscle with adenovirus expressing constitutively active Akt results in normal utrophin abundance and improved regeneration following cardiotoxin injury, the authors proposed a molecular mechanism in which sarcospan regulates utrophin levels in an Akt-dependent manner, and this pathway may prove necessary for efficient muscle regeneration following injury (Marshall et al., 2012).

Since the discovery of dystrophin and its interacting proteins, the importance of the DGC as a stabilising structure for the muscle plasma membrane has been highlighted. However, newer lines of evidence such as those described above, have shown that in addition to its role in the mechano-protection of the sarcolemma, the DGC also plays a crucial role in a variety of signalling cascades.

1.2.5 The mechanical and calcium hypotheses of Duchenne Muscular Dystrophy

The mechanical hypothesis and the calcium hypothesis are the two main theories regarding how the loss of a single protein dystrophin results in the range and severity of symptoms seen in afflicted patients. As described in 1.2.1, dystrophin is a structural protein. The discovery of dystrophin and subsequent identification of a DGC (Hoffman et al., 1987), members of which also show reduced abundance in dystrophin-deficient muscle (Ohlendieck and Campbell, 1991a, Ohlendieck et al.,

1993), supports a role for structural deficits in the pathogenesis of DMD. The DGC interacts with a range of stabilising structural proteins such as desmin, spectrin and vinculin to form costameres, lattice structures located on the cytoplasmic side of the sarcolemma which are responsible for the lateral transmission of force from the sarcolemma to the basal lamina (Danowski et al., 1992). Along with disrupting the DGC, dystrophin deficiency affects this costameric lattice causing destabilisation of costameric actin's interaction with the sarcolemma (Rybakova et al., 2000), resulting in sarcolemmal instability and frailty. This increase in membrane permeability is evident by the infiltration of proteins, such as albumin and immunoglobulins, and the incorporation of dyes, such as Evans Blue Dye, into muscle fibres (Deconinck and Dan, 2007). In addition, dystrophic muscle demonstrates reduced capacity to sustain eccentric contraction (Moens et al., 1993), and sarcolemmal permeability, muscle weakness and necrosis are worsened following mechanical stress (Petrof et al., 1993, Ervasti, 2007), which is alleviated following transgenic full-length dystrophin expression in *mdx* mice (Cox et al., 1993b). Thus, dystrophin appears to provide mechanical support and stabilisation to the sarcolemma during normal muscle excitation-contraction-relaxation cycles, and so dystrophin deficiency has a negative impact on the ability of the sarcolemma to withstand mechanical stress (Ervasti, 2007).

Calcium has also been implicated in the pathophysiology of DMD, initially based on the observations that i) total calcium content is increased in muscle biopsies from Duchenne patients (Bodensteiner and Engel, 1978) and ii) the influx of Ca^{2+} through the sarcolemma is increased in dystrophic muscle (Tutdibi et al., 1999). This elevated Ca^{2+} influx through the dystrophin deficient membrane appears to occur through micro-lesions in the sarcolemma induced by mechanical stress and through mechano-sensitive calcium independent channels (Vandebrouck et al., 2002, Tutdibi et al., 1999, Deconinck and Dan, 2007). Micro-rupturing of the destabilised DGC-deficient sarcolemma triggers a Ca^{2+} -dependent membrane re-sealing process at leaky sites in the membrane. With increasing rounds of sarcolemmal wounding and re-sealing, localised Ca^{2+} influx results in calcium-mediated proteolytic alterations leading to the activation of Ca^{2+} leak channels near these sarcolemmal patches, which further increases the inflow of Ca^{2+} (Alderton and Steinhardt, 2000, Fong et al., 1990). Increased intracellular Ca^{2+} concentrations activate proteases called calpains which degrade contractile proteins and destroy membrane constituents thus further increasing Ca^{2+} influx into muscle fibres, eventually leading to cell death (Spencer et

al., 1995). A role for calcium in the disease pathology is further supported by the observations that *mdx* mice display reduced abundance of a range of calcium buffering proteins (Culligan et al., 2002, Doran et al., 2006a, Dowling et al., 2004), thus aggravating the Ca^{2+} overload in muscle fibres, and that inhibition of calpain (through over-expression of calpastatin or administration of leupeptin) reduces muscle necrosis in the *mdx* mouse model (Badalamente and Stracher, 2000, Spencer and Mellgren, 2002). However, the use of calpain inhibitors has been refuted by others (Briguet et al., 2008, Selsby et al., 2010), and a role for calpains in disrupting specific regulatory mechanisms rather than non-specific proteolysis in dystrophic muscle has been suggested (Tidball and Spencer, 2000).

1.2.6 The role of sterile inflammation in the progression of dystrophinopathy

A body of evidence exists which implicates the role of the immune system in the progression of dystrophic pathophysiology; mainly the observation that the onset of muscle histopathology coincides with the onset of inflammation and the suggestion that the beneficial effects of corticosteroids, such as Prednisone (Beenakker et al., 2005, Merlini et al., 2003), are due to the immunosuppressant activity of this class of drugs (Hussein et al., 2006). The absence of the full-length Dp427 isoform of dystrophin triggers sarcolemmal micro-rupturing, the influx of excessive Ca^{2+} , altered ion homeostasis, increased proteolysis and increased extracellular ATP levels (Deconinck and Dan, 2007). Such alterations in muscle homeostasis may act as DAMPS (danger-associated molecular patterns) resulting in the activation of the immune system. The role of the innate immune response in this sterile inflammation in DMD has been reviewed extensively (Spencer and Tidball, 2001, Villalta et al., 2015). The initial response is a classical Th1 mediated immune response, with the infiltration of neutrophils and M1 macrophages with a pro-inflammatory phenotype. These macrophages play a crucial role in the phagocytosis of myofibre debris and also secrete cytokines to promote myoblast proliferation (Madaró and Bouché, 2014). However, they also secrete pro-inflammatory cytokines such as IL-6, IL-1 β and TNF- α which can further propagate the inflammatory response leading to acute inflammation in the early stages of the disease. In particular, the pro-inflammatory environment in dystrophic muscle can result in the transcriptional activation of NF- κ B, which further promotes inflammation, and which can inhibit myogenesis by preventing myoblast differentiation (Bakkar et al., 2008). Indeed, the pharmacologic

inhibition of NF- κ B reduces inflammation, promotes muscle regeneration and can rescue contractile dysfunction in the dystrophic diaphragm (Kornegay et al., 2014, Peterson et al., 2011). In dystrophic muscle there is a transition from a Th1-mediated immune response to a Th2 response. This results in the infiltration of the alternatively activated M2 macrophages, largely associated with tissue repair and regeneration. Three subsets of M2 macrophages exist; M2a, M2b and M2c. M2a macrophages are associated with advanced stages of tissue repair and regeneration while both M2b and M2c macrophage subsets are associated with anti-inflammatory activity (Kharraz et al., 2013). In general M2 macrophages secrete IL-4 and IL-10, which have two main roles; they reduce the population of M1 macrophages (Villalta et al., 2011) and they promote myoblast differentiation and fusion. Thus, while the Th1 response is associated with muscle necrosis, the Th2 response is involved in muscle regeneration (Tidball and Villalta, 2010).

M1 macrophages contain iNOS (inducible nitric oxide synthase) which utilises the substrate arginine to produce nitric oxide which is responsible for nitric oxide-mediated muscle cell lysis in dystrophinopathy (Nguyen and Tidball, 2003). Unlike in acute tissue injury, a population of M2a macrophages accompany the influx of M1 macrophages in dystrophic tissue (Tidball and Villalta, 2010). These M2a macrophages contain arginase-1, which shares the common substrate arginine. Therefore, the infiltration of this macrophage population may reduce muscle lysis through competition for arginine. However, arginase may also be involved in promoting tissue fibrosis as illustrated by Wehling-Henricks and colleagues (Wehling-Henricks et al., 2010).

While the innate immune response has been extensively reviewed, the role of the adaptive immune response requires further investigation. While muscle regeneration in healthy skeletal muscle is not thought to involve an adaptive immune response, T cells are present in degenerating muscle fibres following injury (Madaro and Bouché, 2014). Depletion of either CD4⁺ or CD8⁺ T-cells results in a significant reduction in muscle pathology (Spencer et al., 2001). The crossing of T-cell null mice with *mdx* mice generates a dystrophin-deficient/T-cell null mouse model which displays reduced fibrosis and decreased/delayed collagen deposition in the diaphragm (Morrison et al., 2000) suggesting a role for the adaptive immune response in fibrosis. Others have suggested a role for autoimmunity in the disease aetiology. Dystrophic muscle, due to its leaky nature, releases a number of proteins into the bloodstream that

would normally be sequestered from the immune response. Thus, their release may trigger an immune response as they may be recognised as “foreign” and taken up by antigen-presenting cells to activate a T-cell mediated immune response.

Although gene therapy to restore dystrophin expression to all muscles of the body represents the ideal treatment for dystrophinopathy, it is currently hindered by a number of biological and technical difficulties. Researchers and clinicians have instead focused some of their attention to methods of ameliorating the secondary pathologies of fibrosis and inflammation (Mah, 2016). However, immunomodulation may prove to be a double-edged sword in DMD with a number of suggested mechanisms proposed to have beneficial effects on muscle necrosis and acute inflammation but detrimental impacts on tissue repair and regeneration. For example the inhibition of TNF- α , a major pro-inflammatory cytokine, by pharmacological means reduces muscle lysis and fibrosis (Hodgetts et al., 2006). However, TNF- α also acts as a chemoattractant for satellite cells and mesangioblasts (Lolmede et al., 2009), cells responsible for muscle regeneration, and thus TNF- α inhibition may hinder their recruitment to dystrophic muscle.

1.2.7 Current and Emerging Therapies for Duchenne Muscular Dystrophy

At present there is no cure for the genetic disorder DMD. However, intensive research into both dystrophin-dependent and dystrophin-independent strategies is currently underway. First suggested in 1974 (Drachman et al., 1974), administration of corticosteroids has become the gold standard treatment for slowing the progression of DMD, particularly by reducing inflammation (Wehling-Henricks et al., 2004) and influencing muscle regeneration and differentiation (Anderson et al., 1996, Anderson and Vargas, 2003). Duchenne patients treated with corticosteroids display improved muscle strength and function, a delay in respiratory dysfunction, scoliosis and loss of ambulation, improved cardiac function and a general improved quality of life (Balaban et al., 2005, Markham et al., 2005, Bushby et al., 2010). However, several side effects are associated with prolonged corticosteroid use, in particular weight gain, metabolic dysfunction, cushingoid appearance and osteoporosis (Angelini and Peterle, 2012, Bushby et al., 2010). The two main corticosteroids in use are Prednisone/Prednisolone and Deflazacort, an oxazoline derivative of prednisolone, which is associated with less side effects than prednisone (Bonifati et al., 2000).

While dystrophin gene therapy may represent the most logical of choices for the treatment of DMD, the large size of dystrophin cDNA (11 kb) prevents its insertion into most viral vectors, and with the exception of the small adeno-associated viral (AAV) vectors (which are too small to accommodate full-length dystrophin cDNA), the uptake of most viral vectors into skeletal muscle has been limited (Guiraud et al., 2015). Observations that patients with BMD who produce truncated dystrophin isoforms display a much milder phenotype than Duchenne patients led to the emergence of mini- and micro-dystrophins (Fairclough et al., 2013). The smaller cDNAs associated with these dystrophin isoforms can be packaged into recombinant AAV vectors, and have shown promise in animal models of the disease (Harper et al., 2002). However, their potential in humans is still uncertain with issues regarding immune responses to the AAV vector still to be resolved, given relatively high titres of virus are necessary to induce effective dystrophin expression (van Westering et al., 2015). A chimeric vector named rAAV2/8 has been described, and lower titres of this viral vector containing codon optimised micro-dystrophin was capable of restoring dystrophin expression in the heart and skeletal muscle of *mdx* mice without eliciting an immune response (Foster et al., 2008).

An alternative approach, also based on BMD, is that of exon skipping. This approach takes advantage of the smaller size of complementary RNA or DNA anti-sense oligonucleotides (AONs) which are easier to deliver than full-length dystrophin. These AONs target exons in the pre-mRNA preventing their inclusion into mRNA, thus restoring the reading frame, enabling the production of truncated dystrophin isoforms and converting DMD to the milder BMD (Aartsma-Rus and van Ommen, 2007). Initial beneficial effects in the *mdx* mouse (Aoki et al., 2010, Lu et al., 2003) led to subsequent clinical trials using 2-*O*-methyl-phosphothioate chemistry (drisapersen) and orpholino-phosphorodiamidate oligomer chemistry (eteplirsen), which demonstrated an increase in dystrophin-positive fibres, restoration of the sarcoglycans and nNOS to the sarcolemma and an improvement in the six minute walk test in treated patients compared to placebo controls (Mendell et al., 2013, Guiraud et al., 2015, Voit et al., 2014). While the FDA declined approval for drisapersen, eteplirsen (brand name Exondys 51) was granted accelerated FDA approval in September 2016, making it the first FDA approved drug specifically for the treatment of DMD (Lim et al., 2017). While this was welcomed by patients and advocacy groups, the approval was controversial given clinical trial results have shown only a

marginal improvement in DMD symptoms. In addition, exon skipping as a strategy is intrinsically specific, with eteplirsen and its associated skipping of exon 51 beneficial for only 13% of patients (Guiraud et al., 2015), and so in future other exons will need to be targeted in order for this type of therapy to be applicable to a greater number of patients.

Approximately 10-15% of patients have a non-sense mutation resulting in a premature stop codon and abrogation of dystrophin synthesis (van Westering et al., 2015). Aminoglycosides, traditionally a class of antibacterial drugs, have been exploited for their ability to “read-through” premature stop codons without affecting normal stop codons, thus restoring functional dystrophin production (Falzarano et al., 2015). Gentamicin was initially tested in Duchenne patients and its use resulted in significantly lower serum levels of creatine kinase and dystrophin restoration in a subset of patients (Malik et al., 2010). However, side effects render its chronic use unfeasible and a second compound PTC124 (ataluren or Translarna) was investigated instead. A phase 2b clinical study of ataluren in ambulatory Duchenne patients demonstrated that ataluren at 40 mg/kg/day slowed the rate of decline of walking ability and achieved a mean 30-meter difference between placebo and treated patients in the six minute walk test over 48 weeks (Bushby et al., 2014). This drug has since been granted orphan drug status by the European Medicines Agency and the FDA (Falzarano et al., 2015).

Mutations may also be corrected by gene editing through the cell’s own repair machinery and this forms the basis of the novel CRISPR-Cas9 system (clustered regularly interspaced short palindromic repeat-CRISPR-associated protein 9). In this method the nuclease Cas9 is guided by a single-guide RNA to a specific targeted genomic locus where it generates a double-stranded break. This is either repaired by non-homologous end joining (NHEJ), which generates insertion/deletion mutations and can lead to exon skipping, or by homology-directed repair (HDR), where an exogenous template is included and used to precisely modify a target locus (Mali et al., 2013, Long et al., 2014). Initially CRISPR-Cas9 methodologies were used to edit germline DNA in the *mdx* mouse model where the point mutation was corrected during embryonic development, which produced mosaic *mdx*-corrected mice displaying between 2-100% correction of the *Dmd* gene. Importantly, correction of just 17% of mutant *Dmd* alleles by HDR was sufficient to induce dystrophin expression in the majority of myofibres and at levels comparable to wild-type mice (Long et al., 2014).

Since genomic editing within the germ line is not possible in humans, the CRISPR-Cas9 system has been tested in post-natal *mdx-4cv* mice using the AAV delivery system. Work by Bengtsson and colleagues used two main approaches; i) use of NHEJ to excise exons 52 and 53, thus restoring the dystrophin opening reading frame and producing a dystrophin isoform missing 110 amino acids and ii) direct targeting of the mutation in exon 53 by including a “mutation-corrected” DNA template to enable possible HDR following Cas9-induced excision, thus facilitating the production of full-length dystrophin (Bengtsson et al., 2017). Both strategies enabled dystrophin production, which in turn led to localisation of nNOS to the sarcolemma and increases in specific force generating capacity. Excision of exons 52 and 53 (strategy i above) also induced dystrophin expression in the heart (Bengtsson et al., 2017). Since post-mitotic cells are only modestly amenable to HDR, Long and colleagues focused on exon skipping mediated by NHEJ to remove the disease-causing mutation in *mdx* mice. Similar results were achieved by this work, whereby dystrophin levels increased in the heart and skeletal muscle but not the brain (due to an inability of AAV to cross the blood-brain barrier) and serum creatine kinase levels and grip strength tests revealed an improvement in muscle function (Long et al., 2016). While CRISPR-Cas 9 is a promising strategy for the treatment of DMD, further research is required to determine the possibility of and risk associated with potential off-target effects.

Dystrophin-independent methods are also under investigation, principally involving modulation of the dystrophin homolog utrophin. The potential of utrophin as a therapy for dystrophin-deficiency in DMD is suggested by the fact that i) it shares significant homology with dystrophin, ii) significant increases in the abundance of utrophin are seen in a number of myopathies including DMD, iii) initial muscle necrosis in *mdx* mice only commences when the high levels of perinatal utrophin decline to levels seen in adult tissue suggesting a protective role for utrophin in the absence of dystrophin (Khurana et al., 1991) and iv) utrophin null-*mdx dko* (double-knockout) mice display an extremely severe myopathy (Deconinck et al., 1997, Perkins and Davies, 2002). The potential of utrophin as a disease modulator was first investigated in 1996 where transgenic *mdx* mice expressing a utrophin transgene under the control of a constitutive muscle promoter displayed a drastic improvement in the dystrophic phenotype characterised by a reduction in serum creatine kinase levels, reduced fibrosis, necrosis and central nucleation, and restoration of components of the DGC to the sarcolemma (Tinsley et al., 1996). More recently, AAV mediated mini-

utrophin gene transfer into the golden retriever model of muscular dystrophy (GRMD) has been achieved and shown to reduce fibrosis and increase abundance of β -dystroglycan and β -sarcoglycan, although immunosuppression was required to prevent an immune response to viral antigens and to achieve transgene persistence (Cerletti et al., 2003). Aside from transgenic expression of utrophin, an alternative therapeutic approach is to induce increased expression of the endogenous utrophin gene (Perkins and Davies, 2002). Based on this a utrophin modulator named SMT C1100/Ezutromid has recently undergone a phase 1 clinical trial to test safety, tolerability and pharmacokinetics (Ricotti et al., 2016) and a phase 2 clinical trial to test efficacy is currently underway.

A range of other strategies exist including decreasing the inflammatory response, reducing proteolysis by inhibiting calcium-dependent proteases (Tidball and Wehling-Henricks, 2004), increasing muscle mass by modulating the activity of myostatin (a negative regulator of muscle mass) (Bogdanovich et al., 2002) and increasing the expression levels of a number of genes; most notably nNOS (Lai et al., 2014), laminin and α 7-integrin (Rooney et al., 2009). The identification of the dystrophin gene has led to much improved insight into the pathophysiology of DMD and paved the way for the discovery of novel therapeutic approaches. Ultimately whilst genetic manipulations may be the only “cure” for DMD, these approaches are still in their infancy and at present modulation of the downstream abnormalities may provide the best opportunity for improving the quality of life of patients with DMD.

1.2.8 Animal Models of Duchenne Muscular Dystrophy

Both naturally occurring and engineered animal models exist for the comprehensive study of the pathophysiology of DMD, and which can be utilised for the development of novel therapeutics. While the available models also include non-mammalian models, such as *Drosophila melanogaster* and *Caenorhabditis elegans*, the most frequently used models in research are the mouse and canine models. Some newly developed models include the rat and pig DMD models.

The most widely used animal model in muscular dystrophy research is the *mdx* mouse. Identified in a colony of C57BL/10ScSn mice in the early 1980s (Bulfield et al., 1984), it displays elevated creatine kinase and pyruvate kinase levels and histological features of muscular dystrophy. The molecular basis of this dystrophic phenotype was subsequently identified as a nonsense point mutation (C-T transition)

in exon 23, resulting in a stop codon instead of a glutamine codon, which prevents expression of full-length dystrophin (Sicinski et al., 1989). Despite extensive rounds of muscle necrosis between 3-6 weeks of age (McGreevy et al., 2015), this mouse model represents a relatively mild phenotype in comparison to the human condition; the majority of skeletal muscle enters a stable phase due to a high regenerative capacity (Turk et al., 2005), mice have a reduced lifespan of approximately 19% as opposed to 75% reduction in humans (murine lifespan reduced from approximately 26.5 months to 21.5 months) (Chamberlain et al., 2007), and severe clinical features of dystrophinopathy such as muscle wasting, fibrosis and cardiac failure only appear to come into play in aged *mdx* mice (Van Erp et al., 2010, Pastoret and Sebille, 1995). The only exception is the *mdx* diaphragm, which like in human patients, shows severe and progressive deterioration (Stedman et al., 1991, Holland et al., 2015a, Doran et al., 2006b).

Four chemical variants of the *mdx* mouse were described in 1989 (Chapman et al., 1989). These mice were generated on the C57/BL6 background by chemical mutagenesis using N-ethyl-nitrosourea, and are referred to as *mdx-2cv*, *mdx-3cv*, *mdx-4cv* and *mdx-5cv* strains. These mice harbour different point mutations and have different characteristics. The mutation in *mdx-2cv* mice is a single base change in intron 42 (Im et al., 1996). The *mdx-3cv* mice is a result of a mutant splice acceptor site in intron 65 (Cox et al., 1993a). A C to T transition in exon 53 generates a premature stop codon and results in the *mdx-4cv* mouse (Im et al., 1996). An A to T transition in exon 10, which doesn't alter the encoded amino acid but which generates a new splice donor site resulting in a frameshift in the processed mRNA, is responsible for the *mdx-5cv* mouse (Im et al., 1996). Low levels of a dystrophin protein missing cysteine rich domain sequences are found to accumulate in the *mdx-3cv* model, due to alternative splicing events (Rafael et al., 1996). However, this dystrophin protein is non-functional and thus the *mdx-3cv* mice displays the same muscle phenotype as the other chemical variant *mdx* mice. In addition, the *mdx-3cv* mouse fails to express the 71 kDa isoform of dystrophin normally found in the brain and other non-muscle tissue, but this Dp71 isoform of dystrophin is expressed in the other *mdx* chemical variant strains (Im et al., 1996). The *mdx-4cv* and *mdx-5cv* mouse models contain 10-fold fewer dystrophin-positive revertant fibres than the *mdx* mouse (Danko et al., 1992), and so are particularly suited for the evaluation of novel therapeutics for DMD.

Given the relatively mild disease phenotype in *mdx* and *mdx* chemical variant mouse models, several double-knockout mice which show a more severe myopathy have been developed. Since increased abundance of the dystrophin homologue utrophin in *mdx* mice appears to ameliorate the dystrophic phenotype (Tinsley et al., 1998), dystrophin/utrophin *dko* mice have been generated. This *dko* strain displays a far greater clinical pathology, characterised by reduced weight, progressive curvature of the spine, early onset of muscle pathology (necrotic fibres and connective tissue evident in the diaphragm of *dko* mice at six days old), a reduction in force generation by the sternomastoid muscle, a significant reduction in membrane folding at the myotendinous junction which may affect force transmission between the muscle fibre and the tendon, histological evidence of myocyte damage in cardiac tissue of older mice reminiscent of that seen in DMD patients, and premature death (20 weeks compared to 21.5 months for *mdx* mice) (Deconinck et al., 1997, Grady et al., 1997). However, while these mice may more closely mirror the severity of clinical symptoms seen in patients with DMD, it is important to take into consideration that these mice carry mutations in genes other than the dystrophin gene, which is not the case for the human counterparts they attempt to mimic.

Another factor thought to be involved in the slowly progressive nature of dystrophinopathy in *mdx* mice is robust regeneration. Two *dko* strains have thus been produced to hamper this regenerative capacity in order to produce a model with severe myopathy. MyoD/dystrophin *dko* strains demonstrate severe and progressive cardiomyopathy, with cardiac fibrosis particularly affecting the left ventricle. The severe disease phenotype in this strain, which leads to premature death at approximately 12-months, is due to impaired muscle regeneration (Megency et al., 1999), where in the absence of MyoD there is a 2-fold increase in the number of satellite cells which self-renew instead of entering myogenesis (Megency et al., 1996). Crucial to muscle regeneration is the ability of cells to undergo repeated rounds of cell division, a process linked to telomere length, with telomere shortening associated with replicative senescence of somatic cells (Allsopp et al., 1992). Increased telomere length in laboratory mice compared to humans (5-15 kb in humans versus >40 kb in mice) (Kipling and Cooke, 1990) likely plays a role in the greater regenerative capacity and milder dystrophic phenotype of *mdx* mice compared to DMD patients. To investigate this Blau and colleagues have crossed *mdx-4cv* mice with mice lacking the RNA component of telomerase, and these *dko* mice have shortened telomeres and

a progressive muscular dystrophy phenotype leading to premature death (Sacco et al., 2010). These mice display elevated serum creatine kinase levels, reduced muscle performance, increased myofiber permeability as assessed by Evans Blue Dye uptake, infiltration of immune cells and muscle necrosis and fibrosis (Sacco et al., 2010). In particular these *dko* mice show extensive fibrosis and tissue scarring in cardiac tissue particularly localised to the left ventricle, impairment of left ventricular contractility and elevated markers of cardiac failure (atrial natriuretic peptide and brain natriuretic peptide); features reminiscent of the cardiac abnormalities seen in DMD patients (Mourkioti et al., 2013). In addition, telomerase dysfunction in this dystrophin deficient mouse strain appears to induce mitochondrial abnormalities and increased oxidative stress which is suggested to be responsible for lethal cardiomyopathy, since anti-oxidant treatment helps ameliorate the cardiac dystrophic phenotype (Mourkioti et al., 2013). Thus, these studies indicate that i) while initiated by dystrophin deficiency, the exhaustion of the muscle stem cell pool may be at least partly responsible for the progressive nature of DMD and ii) that the telomerase deficient *mdx* mouse represents an improved model, with potential applications in the testing of therapeutic options.

Canine X-linked muscular dystrophy is the result of a spontaneous mutation and is best characterised in the Golden Retriever breed (GRMD), in which the genetic basis of the disease is a single base change (A-G transition) in the 3' splice site of intron 6, which causes exon 7 to be deleted from the dystrophin transcript (but not the gene), and the ensuing frameshift results in the production of a truncated dystrophin protein (Sharp et al., 1992). This model possesses a number of clinical hallmarks of muscular dystrophy including elevated serum creatine kinase levels, muscular atrophy, curvature of the spine, fibrosis and histological evidence of muscle necrosis and regeneration (Valentine et al., 1992). Since the GRMD model more closely mirrors DMD patients than other animal models particularly in terms of size and disease pathophysiology, it has become especially useful for the evaluation of therapeutic approaches. In recent years the GRMD model has been used to assess the ability of mesangioblast stem cells (Sampaolesi et al., 2006), oligonucleotide therapy (Bartlett et al., 2000), adenovirus mediated utrophin transfer (Cerletti et al., 2003) and exon skipping (Vulin et al., 2012) to ameliorate the dystrophic phenotype.

The rationale behind the development of a porcine model of DMD was that given its larger size it could be useful for determining the logistics for the scale up of

novel therapeutics, such as dosing regime, titres and injection sites (Selsby et al., 2015). This model could therefore enable thorough pre-clinical trials which may be more predictive of the outcome in human counterparts, a major issue at present given that a number of potential therapies which showed promise in mouse models have been largely unsuccessful in human patients. Such a porcine model was generated in 2013 in which the exon corresponding to exon 52 in humans was replaced with a neomycin resistance cassette. This results in a +1 frameshift after the splicing of exon 51 to 53 (Klymiuk et al., 2013). This transgenic porcine model shows some of the main features of dystrophinopathy including a complete loss of dystrophin and compensatory increases in utrophin, elevated serum creatine kinase levels and muscle weakness. Histological analysis revealed alterations in fibre size, hypertrophic fibres, centrally nucleated fibres indicative of muscle regeneration, fibrosis and immune cell infiltration consistent with myopathy. The DMD pig also reflects the human pathology on a molecular level, with muscle proteome and transcriptome changes in 3-month old dystrophic pigs very similar to those reported in human patients (Fröhlich et al., 2016, Klymiuk et al., 2013). However, disease progression is significantly accelerated in the DMD pig compared to DMD patients, which is possibly due to accelerated growth after birth in pigs which may aggravate the dystrophin-deficient phenotype (Klymiuk et al., 2013).

While there is currently no one model which perfectly mirrors the dystrophic phenotype seen in afflicted patients, the large (and increasing) variety of animal models available offers enormous opportunity for the pathobiochemical characterisation of DMD and the testing of emerging treatment options.

1.3 Proteomics

Proteomics is the large-scale analysis of proteins from an organism, cell, tissue or biofluid and encompasses protein identification, expression, structure, post-translational modifications and protein interactions. The emergence of proteomics as a key technology was driven in part by the observations that i) in the human genome the approximately 20,700 genes present can be translated into more than 100,000 different protein isoforms (Lander, 2011), ii) proteins are the direct functional molecules in a living organism and iii) that while genomics has been incredibly important in understanding health and disease, the genome is relatively static whereas

proteomics offers the opportunity to study the response of an organism and its cells and tissues to stimuli, stress, changing environments and disease.

Proteomic workflows typically involve the separation of proteins, by gel or gel-free methods, followed by mass spectrometry analysis of protein/peptide fragments. Mass spectrometry data can be searched against the Uniprot database of protein sequences to identify proteins, and a variety of analytical software tools can then be used to measure protein abundance and protein modifications, such as phosphorylation. Two principal strategies exist for the mass spectrometric identification of proteins; top-down and bottom-up approaches. In the bottom-up approach proteins are first enzymatically digested to peptides and subjected to liquid chromatography mass spectrometry (LC-MS/MS). The peptides are identified by comparing the tandem mass spectra determined by LC-MS/MS with theoretical tandem mass spectra generated from *in silico* digestion of a protein database. The identified peptides are then assigned to a protein to give the protein components of the original sample (Zhang et al., 2013). This method has been more universally adopted as peptides are more easily fractionated, ionized and fragmented than intact proteins. The alternative approach of top-down proteomics analyses intact proteins which generally gives improved sequence coverage and better characterisation of post-translational modifications (Catherman et al., 2014). While the technical challenge of achieving proteome-wide analysis at the intact protein level has slowed the progress of this technique, improvements in protein separation, mass spectrometry instrumentation and bioinformatics tools may enable top-down proteomics to become a powerful approach. Indeed in 2011 Tran and colleagues used a novel four dimensional separation system to identify a total of 1,043 intact proteins of up to 105 kDa from nuclear and cytosolic extracts from HeLa S3 cells (Tran et al., 2011).

The field of proteomics in human biology has been aided substantially by the establishment of the Human Proteome Organization (HUPO) in 2001. Of particular importance has been the development of the human proteome project, a collaborative effort which aims to map the entire human proteome, which would be instrumental in enhancing understanding of human biology in health and disease. In particular, proteomic profiling of urine and serum has been extensively pursued given the perceived benefit of these biofluids as a source of minimally invasive protein biomarkers (Farrah et al., 2014). The development of the Cell Atlas has also been important in enhancing knowledge of the spatial distribution of the human proteome

at the subcellular level (Thul et al., 2017). While organelle proteomics can also be used to map proteins to particular cellular compartments, the immunofluorescence imaging approach used by Cell Atlas is advantageous in the identification of proteins found in compartments which are difficult to purify, and/or which possess distinct sub-structures. The approach therefore provides complementary data to that obtained by transcriptomics and proteomics. An alternative mass spectrometry-based approach to studying protein localisation is that of hyper-plexed localization of organelle proteins by isotope tagging (hyperLOPIT), which has been successfully used to unambiguously assign over 50% of detected proteins in a mouse pluripotent stem cell population to 14 distinct organellar and sub-organellar compartments including the plasma membrane, endosome, lysosome, mitochondrion, actin cytoskeleton, peroxisome and extracellular matrix (Christoforou et al., 2016). The remaining proteins were found to be localised to more than one compartment. Thus, the use of spatial proteomics has also highlighted the presence of “moonlighting” proteins, whereby proteins can localise to more than one cellular compartment where they may have context specific functions (Min et al., 2016). This increases the overall functional diversity of the proteome and illustrates the need for proteomics to not only identify proteins but to also understand their localisation, temporal expression and interaction patterns.

1.3.1 Gel electrophoresis

Gel electrophoresis is an analytical tool used for protein separation which became synonymous with mass spectrometry-based analyses in the early days of proteomics. One dimensional-gel electrophoresis (1D-GE) separates proteins based on their molecular mass, whereas two-dimensional gel electrophoresis (2D-GE) offers enhanced protein resolution by combining isoelectric focusing with gel electrophoresis to separate proteins first by their isoelectric point and second by their molecular mass (O'Farrell, 1975). In the first dimension protein samples are passively loaded onto thin strips of polyacrylamide gel with a fixed pH gradient during strip rehydration. The strips are then subjected to isoelectric focusing, during which proteins migrate through the gel until they reach their pI value, the pH at which the protein has no net charge. The focused strips are reduced and alkylated and loaded onto a polyacrylamide slab gel for further separation based on their molecular mass (Rabilloud and Lelong, 2011). Smaller proteins migrate through the gel more quickly than larger proteins, thus giving separation in the second dimension. A staining

process is required to visualise the proteins, which can be done pre- or post-electrophoresis, depending on the protein concentration used and the downstream applications. Protein spots of interest, for example those with differential abundance in different conditions as determined by software, can then be excised, digested into their constituent peptides and identified by mass spectrometry.

One major disadvantage of the 2D-GE approach is that of gel-to-gel variation, which was addressed in 1997 by the development of fluorescence difference in-gel electrophoresis (DIGE) (Unlü et al., 1997). In this approach the samples of interest are fluorescently tagged prior to isoelectric focusing with two different cyanine CyDye DIGE fluor dyes so that they can be run on the same 2D gel, thus circumventing the reproducibility issues associated with traditional 2D-GE. In addition, the inclusion of an internal standard, formed from equal amounts of every sample in the experiment and labelled with a third CyDye, enables assessment of biological and experimental variation and accurate quantification of changes in protein expression (Tannu and Hemby, 2006). 2D-DIGE has been used in various applications ranging from investigations into skeletal muscle biology (Staunton et al., 2012), cancer metastasis (Linge et al., 2012) and the efficiency of Chinese hamster ovary cell lines in bioprocessing (Meleady et al., 2011).

1.3.2 Label-free liquid chromatography mass spectrometry

In contrast to gel-based methods, LC-MS/MS uses “in-solution” digestion whereby the proteins of interest are extracted, precipitated to remove contaminating agents and digested to peptides prior to being separated by liquid chromatography and analysed by tandem mass spectrometry. This technique can identify a broader range of proteins; including low abundance proteins, integral membrane proteins, high molecular mass proteins and those proteins with extreme isoelectric points, thus circumventing some of the inherent caveats of 2D-GE (Murphy et al., 2016a). While gel-free quantitative proteomics can often incorporate metabolic and chemical labelling of proteins or peptides prior to mass spectrometric analysis, such as SILAC (Stable Isotope Labelling with Amino acids in Cell culture), iTRAQ (isobaric Tags for Relative and Absolute Quantitation) and ICAT (Isotope-Coded Affinity Tag), label-free quantitative proteomics can also be achieved (Xie et al., 2011). In metabolic and chemical labelling analyses, quantitation is determined by the mass increase provided by the labels and the relative signal intensities between labelled and unlabelled

samples. In a label-free experiment, quantitation is based on direct comparison of the mass spectrometry peptide ion intensities or spectral counts between the different samples (Ramasamy et al., 2014). An overview of the different proteomic methods is given in Figure 1.6. Sophisticated bioinformatics technologies are used to identify and quantify the peptides, to assign the identified peptides to proteins, and perform statistical analysis to generate lists of differentially abundant proteins. Label-free LC-MS/MS has been adopted by a number of researchers and used in diverse applications, such as generating proteomic maps of organs (Doll et al., 2017), understanding disease mechanisms (Holland et al., 2013) and identifying potential protein biomarkers for disease diagnosis and prognosis (Dowling et al., 2014b).

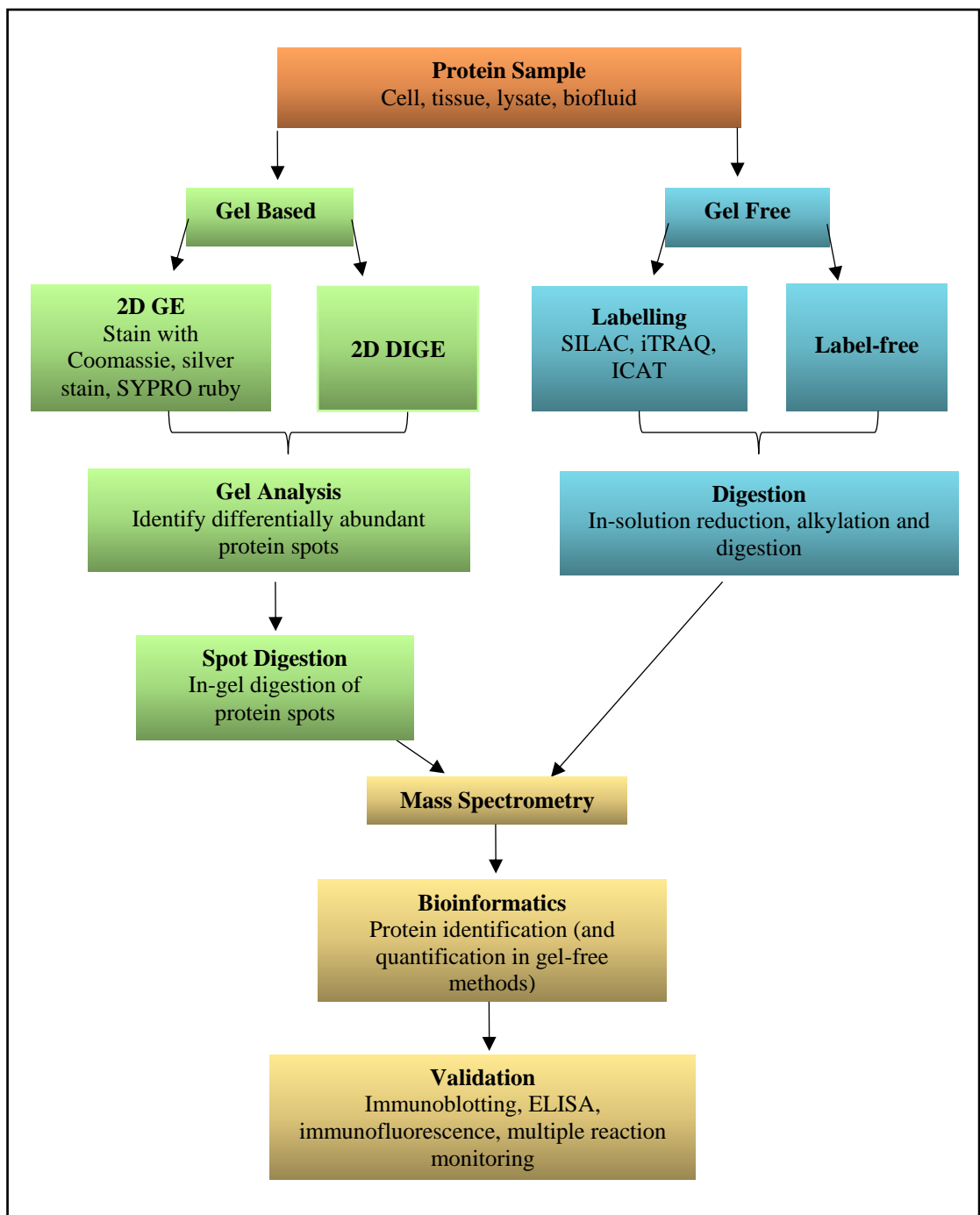


Figure 1.6: Overview of gel versus gel-free mass spectrometric approaches

Depicted above is a flow-chart showing the main steps involved in proteomic analyses of a protein sample of interest, using either a gel-based or gel-free approach. In a gel-free approach, samples can either be labelled, metabolically or chemically, or analysed in a label-free fashion.

1.3.3 Skeletal muscle proteomics

Skeletal muscle proteomics attempts to characterise the entire protein complement of the skeletal musculature. Such analyses have been paramount in understanding skeletal muscle maturation and aging (Murgia et al., 2017), in profiling physiological adaptations such as those seen in disuse atrophy and intense exercise (Holloway et al., 2009), and in identifying the molecular mechanisms involved in primary neuromuscular disorders, such as DMD and facioscapulohumeral muscular dystrophy (Fuller et al., 2016). Despite the importance of profiling the skeletal muscle proteome in health and disease, progress has been limited by the complexity and heterogeneity of skeletal muscle. Muscle is highly heterogeneous, composed of muscle fibres of varying contractile abilities (slow oxidative type I fibres, intermediate fast glycolytic/oxidative type IIa fibres and fast glycolytic type IIb fibres), and containing layers of connective tissue, capillaries and nerve cells (Murphy et al., 2016a). Thus homogenised muscle, which is used as the starting material for most comparative surveys, contains a highly varied mix of muscle, along with cells derived from the tendon, epimysium, endomysium, perimysium, blood vessels, motor neurons and satellite cells (Murphy et al., 2016a). This contamination of muscle fibres by other cell types must be taken into account when interpreting data from proteomic surveys of skeletal muscle. For this reason, it is also of utmost importance to verify proteomic data using independent bioanalytical techniques such as immunoblotting, biochemical assays, enzyme linked immunosorbent assays and/or microscopy.

In addition, contractile tissue contains a number of large protein complexes, including the DGC of the sarcolemma, the voltage-sensing DHPR of the transverse tubules, the RyR Ca^{2+} -release channel of the triad junctions, and the highly abundant actomyosin machinery (Ohlendieck, 2011c). The presence of these supramolecular protein complexes can represent a technical difficulty in muscle proteomics. Deep proteome analysis of mouse skeletal muscle suggests that the protein dynamic range in skeletal muscle spans over eight orders of magnitude from very high abundance proteins such as myosin to low abundance proteins including transcription factors. The top twelve most abundant proteins in muscle make up 50% of the total protein mass (Deshmukh et al., 2015). This renders mass spectrometry analyses quite challenging, whereby low abundance peptides are suppressed by high abundance peptides and thus are not selected for fragmentation. The contractile proteins titin and nebulin, which represent two of the top three most abundant proteins in muscle, are giant proteins

with molecular masses of 3,400 kDa and 800 kDa respectively (Murphy et al., 2016a). This represents a problem particularly for 2D-GE proteomic approaches where extremely large proteins can suffer from poor resolution and under-estimation of abundance. Analysis of the skeletal muscle proteome is further complicated by the plasticity of muscle, which is nonetheless crucial for its ability to adapt to changed functional demands. In particular, a number of genes may be differentially spliced, resulting in the production of a large number of protein isoforms, which may be then post-translationally modified, thus vastly increasing the number of proteins present in the muscle proteome. For instance, although the family of sarcoendoplasmic reticulum Ca^{2+} -ATPase pumps are encoded by three genes, alternative splicing and various post-translational modifications result in the production of more than ten different protein isoforms (Ohlendieck, 2011c).

Urea or detergent based protein extractions of total muscle tissue are the predominant methods used for the extraction of the near-to-complete muscle proteome. However, issues relating to protein dynamic range, sample complexity and the under-representation of integral membrane proteins have been addressed by i) the use of subcellular fractionation, as seen in organelle proteomics (Ohlendieck, 2011c), ii) protein or peptide fractionation such as ion exchange chromatography for proteins and strong cation or ion exchange chromatography for peptides (Deshmukh, 2016) and iii) affinity purification of target protein complexes (Turk et al., 2016).

1.4 Biomarkers

A biomarker is a naturally occurring molecule, gene or characteristic, which can be quantified accurately and reproducibly, and which can be evaluated objectively as an indicator of normal biological processes, pathological processes and/or pharmacologic responses to therapy (Strimbu and Tavel, 2010). Since proteins are the effector molecules in the body, and proteomics offers a large-scale, unbiased, bioanalytical approach to detect and quantify proteins, protein biomarkers are of particular interest in modern medicine. Such protein biomarkers could have potential uses in i) disease screening, ii) disease diagnosis and monitoring, iii) monitoring response to therapy, iv) guiding personalised medicine, and v) serving as surrogate clinical end-points in drug trials (Rifai et al., 2006). While both tissue samples and biofluids may be used for the identification of proteomic biomarkers, biofluids such as plasma, urine, and saliva are preferred given they can be obtained non- or minimally invasively. Proximal

fluids, fluid located in close proximity to the tissue of interest, may offer some advantages over the use of serum samples, whereby the discovery of biomarkers may be facilitated by the estimated high abundance of proteins in proximal fluid that may otherwise be highly diluted in peripheral circulation (Teng et al., 2010). While proteomic biomarkers have held much promise, a number of challenges exist in proteomic biomarker discovery: i) the complexity and dynamic range of plasma and other biofluids, ii) the predicted relative low abundance of disease-specific biomarkers and iii) variation in the human population (Rifai et al., 2006). The biomarker pipeline generally involves four key stages; i) the discovery stage, where candidate biomarkers are identified, often by comparative mass spectrometry approaches, ii) qualification stage where the differential abundance of a select number of candidate biomarkers of interest are confirmed in a larger number of samples and using alternative targeted methods, iii) verification, where the specificity of the candidate markers is examined, usually in population-derived human samples and iv) validation and clinical assay development, where the specificity and sensitivity of the marker/s is determined and a clinical assay is optimised (Paulovich et al., 2008, Rifai et al., 2006). While the initial discovery phase is generally successful in generating large lists of candidate proteins, very few proteins successfully pass the subsequent stages of the pipeline, with a major bottleneck occurring at the verification stage, during which the variation that occurs naturally in the human population, but which was minimised in the discovery phase, is re-introduced (Rifai et al., 2006).

Another compounding factor is limited resources (such as high-quality antibody assays) and access to clinical samples, which may prevent all putative biomarkers from being evaluated. Instead the most likely candidates are chosen based upon the availability of ELISA assays and knowledge of how the potential biomarker may relate to the disease, although biological understanding of many diseases is often too limited to rely on this. An alternative approach which may aid the current bottlenecks in the biomarker pipeline is the use of multiple reaction monitoring to quantitatively evaluate 100s of biomarker candidates simultaneously (Makawita and Diamandis, 2010). Ideally a reliable protein biomarker should be i) highly specific for the disease, ii) sensitive, iii) minimally invasive, iv) easy and cost effective to assay, v) expressed at high levels, and vi) minimally influenced by patient age, gender, ethnicity and lifestyle (Murphy et al., 2018b). The key characteristics will also be determined by the purpose of the biomarker. For example, a biomarker for screening

purposes of a healthy population must be highly sensitive to detect early symptoms, while a biomarker for evaluating patients will require a high degree of specificity (Ohlendieck, 2013). A cautionary tale comes from the paediatric plasma proteome, where a comprehensive longitudinal study illustrated that it varies extensively from neonate to adolescence, and thus proper age-matched controls in biomarker studies involving childhood disease are warranted (Liu et al., 2017). Despite the numerous issues associated with biomarkers and their poor transition into the clinic, with only one to two protein biomarkers being approved each year by the FDA across all diseases, proteomics is only in its infancy and still holds much promise for improving disease diagnosis, prognosis and therapeutic evaluation.

1.4.1 Biomarkers for neuromuscular disease

In the conventional diagnosis of neuromuscular disease histological, histochemical and immunohistochemical analysis of muscle biopsies are of crucial importance. Small angular atrophic fibres indicate denervation, small rounded atrophic and hypertrophic fibres along with increased central nucleation, replacement of muscle with adipose and connective tissue, and scattered pockets of de- and re-innervation reflect primary muscle disease, while special staining techniques are capable of detecting glycogen storage and lipid accumulation, nemaline bodies and the ragged red fibres of mitochondrial myopathies (Murphy et al., 2018b). However, while tissue biopsy can yield important information, its invasive nature precludes the possibility of repeat sampling and thus alternative methods of monitoring disease progression have been sought. Imaging technologies have been considered as they represent a safe and non-invasive means of monitoring neuromuscular disease (Scotton et al., 2014). Magnetic resonance imaging (MRI) has recently been shown to be useful in evaluating the progression of disease pathology in individual muscles in DMD patients, and it has thus been suggested that MRI represents an attractive option for guiding the selection of sufficiently well-preserved muscles for the evaluation of induced dystrophin production, which is a primary outcome assessed in many early stage clinical trials (Kinali et al., 2011). Proteomic biomarkers have also gained much interest, particularly for the monitoring of disease progression and response to therapy, as proteins can provide direct information regarding cellular pathways, and they can be identified and quantified in accessible bodily fluids, such as serum, saliva and urine (Scotton et al., 2014). In neuromuscular disease, protein markers of interest may

originate from degenerating muscle fibres and their surrounding tissues in addition to signalling factors from other organs in response to inflammation and systemic alterations (Murphy et al., 2018b). Increased abundance of creatine kinase is currently used in the diagnosis of DMD and in carrier detection. However, its levels are also increased in response to vigorous exercise and muscle damage in general and so is not specific for DMD. Additionally, its levels decrease over time as muscle is replaced by fibrous and adipose tissue and so it has limited utility in evaluating disease progression and response to therapy (Hathout et al., 2016). Numerous proteomic studies have been undertaken to find alternative protein biomarker candidates. Both targeted immunochemical analyses and large-scale mass spectrometry-based proteomic surveys of blood samples from Duchenne patients and from animal models of the disease have identified a variety of new biomarker candidates. They include fibronectin (Cynthia Martin et al., 2014); the myofibrillar proteins titin, myomesin 3, and filamin C, the glycolytic enzymes aldolase and glycogen phosphorylase and the transport proteins myoglobin and fatty acid binding protein-3 (Hathout et al., 2014); troponin I (fast skeletal muscle and cardiac), fibrinogen, osteomodulin, and disintegrin & metalloproteinase domain-containing protein 9 (Hathout et al., 2015); the acute phase protein haptoglobin (Murphy et al., 2017b); as well as titin fragments in urine (Rouillon et al., 2014).

An overview of some potential protein biomarkers of neuromuscular disease is illustrated in Figure 1.7. While comparative biofluid proteomics has been recognised as a swift and reliable screening approach in biomarker discovery, for a biomarker to give effective readouts of therapy effects and to act as predictors of benefit a good correlation between therapy-induced changes in the biomarker abundance and clinical benefit needs to be established (Hathout et al., 2016). A number of recent studies have attempted to identify such markers in animal models. Using wild-type, *mdx* and Fiona mice (transgenic *mdx* mice over-expressing utrophin), a panel of potential protein biomarkers to evaluate utrophin-based therapies has been identified. 80 proteins were detected as being highly differentiated in serum obtained from wild-type, *mdx* and Fiona animals and of these 80 proteins 60 of them were partially or fully rescued towards a wild-type level in the Fiona mice due to the increased abundance of utrophin (Guiraud et al., 2017). Similarly, myomesin-3, a marker of membrane leakage, has been shown to decrease towards normal levels in *mdx* mice treated with AON-mediated exon skipping therapy, and this correlated well

to restoration of dystrophin levels (Rouillon et al., 2015). Overall the use of protein biomarkers in neuromuscular disease diagnosis, prognosis, and therapy monitoring is extremely promising and may be useful in i) monitoring disease progression, ii) evaluating patient response to therapy, and iii) serving as surrogate endpoints in clinical trials. While large-scale proteomic approaches have been successful in identifying putative biomarkers in tissue samples and biofluids, more work is still needed to bridge the gap between identifying candidate protein markers and validating them for translation to clinical applications.

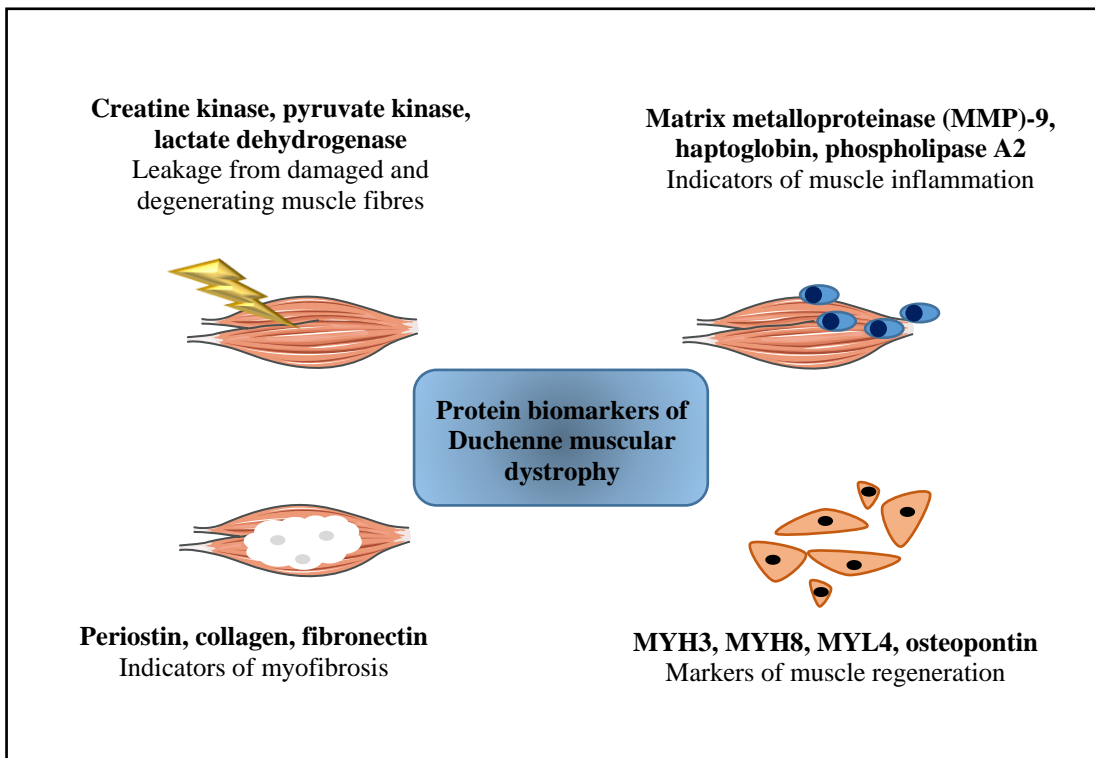


Figure 1.7: Overview of potential protein biomarker candidates in Duchenne muscular dystrophy

Depicted above are some of the major classes of protein biomarker candidates which reflect many of the main abnormalities seen in dystrophic skeletal muscle, primarily sarcolemmal instability and leakage of cytosolic proteins, sterile inflammation and the invasion of immune cells, muscle regeneration and the replacement of muscle with connective tissue in myofibrosis.

*Image adapted from <https://atlasofscience.org/serum-osteopontin-as-a-novel-biomarker-for-muscle-regeneration-in-duchenne-muscular-dystrophy/>

1.5 Aims of the project

DMD is a devastating neuromuscular disorder characterised by severe and progressive skeletal muscle wasting, cardiorespiratory complications and premature death. Since the discovery of genetic mutation in the dystrophin gene as the cause of DMD in 1986, intensive research has aimed to improve understanding of the disease pathogenesis on one hand and to identify potential therapies on the other. Mass spectrometry-based proteomics offers a large-scale, unbiased, technology-driven approach for the identification of alterations in the dynamic proteome. This research aimed to use new advances in mass spectrometry-based analyses to characterise proteomic alterations in the *mdx-4cv* animal model of DMD. Dystrophin deficiency and its associated histopathological features in the *mdx-4cv* mouse model used in this research were established by immunofluorescence microscopy and haematoxylin and eosin staining, which is illustrated in Figure 1.8.

Since dystrophin deficiency severely affects skeletal muscle, it was of interest to obtain a global overview of alterations in the skeletal muscle proteome. In order to determine such changes in muscle-derived proteins in the skeletal muscle, crude homogenates from the hind leg were analysed by LC-MS/MS. However, alterations in the dystrophic proteome consist not only of changes in protein abundance but also differences in protein oligomerisation. Thus, a chemical cross-linking study of tissue homogenates from skeletal muscle was undertaken with the purpose of elucidating changes in protein interaction patterns as a result of dystrophin deficiency.

One major challenge with the proteomic analysis of skeletal muscle is that its complexity and the high abundance of the contractile proteins can mask the mass spectrometric identification of other muscle proteins, which may otherwise provide novel insights into the disease pathophysiology and/or identify new protein biomarkers. Therefore, a focused subcellular proteomic study was performed on an enriched sarcolemma fraction using a lectin agglutination affinity procedure. This study was useful in providing a deeper understanding of proteomic alterations at the muscle sarcolemma, the site at which the DGC is located. Following this, an on-membrane digestion study of a dystrophin complex enriched fraction was carried out to identify new proteins which may exist in close proximity and/or interact with the DGC.

Cardiac dysfunction is a hallmark of DMD, particularly evident in patients 18 years and older, and which frequently contributes to mortality. For this reason,

proteome profiling of the senescent heart of 20-month old mice was carried out in an attempt to facilitate enhanced understanding of the molecular mechanisms underlying cardiomyopathy.

Approximately one-third of patients with DMD display non-progressive mild cognitive impairments, yet despite the large incident rate few molecular studies have been performed. To counteract this gap in the literature, a label-free LC-MS/MS study was conducted on whole brain homogenates from 12-month old mice.

There is an urgent requirement for new circulatory protein biomarkers of DMD for disease diagnosis, prognosis and therapy monitoring. At present, disease progression and response to therapeutic intervention are largely monitored by physical examination, including the six-minute walk test and the North Star Ambulatory Assessment. However, these tests are limited to ambulatory patients. To circumvent this issue, label-free proteomic profiling was employed to identify disease biomarkers in serum and saliva samples from the *mdx-4cv* mouse.

Thus, the overall aim of this body of research is to use mass spectrometry-based proteomics to generate an in-depth characterisation of alterations in the proteome of a variety of tissues and biofluids to comprehensively characterise the *mdx-4cv* animal model of DMD. Such a proteomic profile can enhance our understanding of the molecular mechanisms involved in the progression of disease in the skeletal muscle, the heart and the brain, establish altered protein oligomerisation patterns, identify novel interaction partners of the DGC and identify potential circulating protein biomarker candidates in serum and saliva which may be useful for monitoring disease progression and response to treatment.

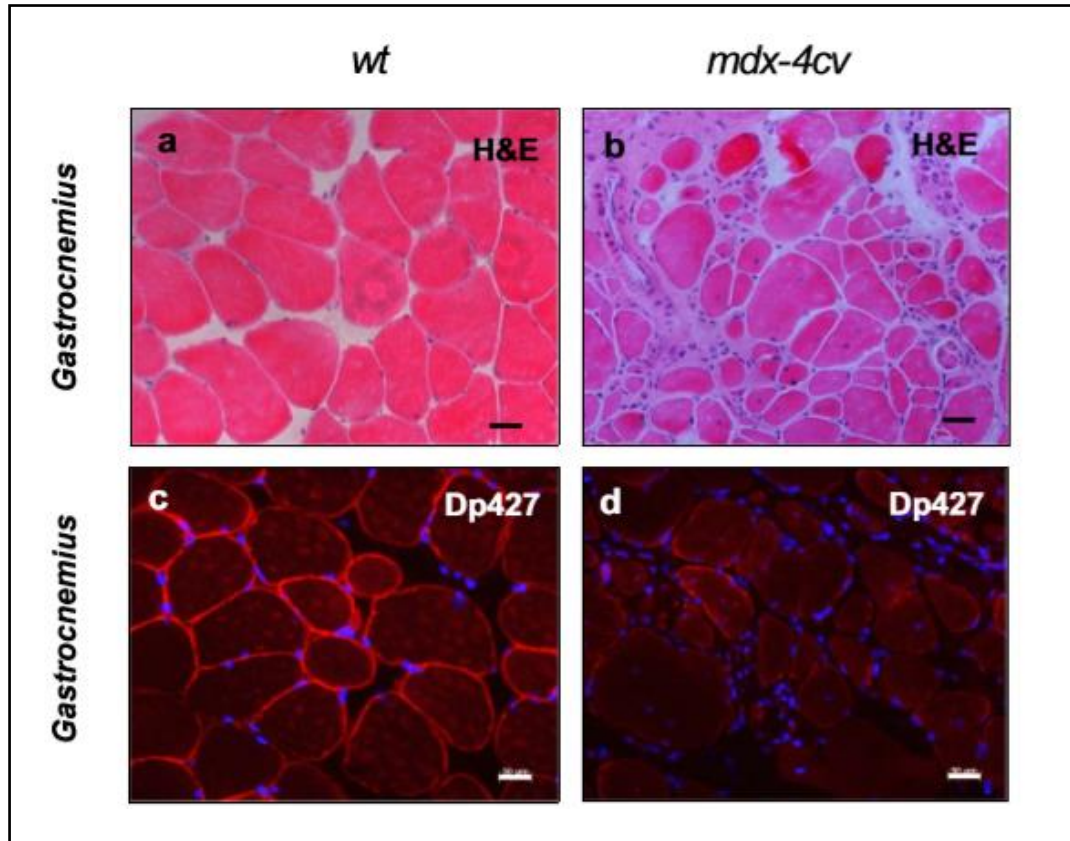


Figure 1.8: Histological and immunofluorescence microscopical analysis of dystrophic *mdx-4cv* skeletal muscle

Shown are transverse sections of gastrocnemius muscle from 6-month old wild-type (a, c; *wt*) and dystrophic (b, d; *mdx-4cv*) mice. Cryosections were stained with hematoxylin and eosin (a, b), and were immuno-labelled with an antibody to the full-length dystrophin isoform Dp427 (c, d). Bar equals 50µm.

*Image from Murphy et al., 2018a

Chapter Two

Materials and Methods

2.1 Materials

2.1.1 General chemicals and reagents

Distilled H₂O was purified using a Millipore Milli-Q apparatus to obtain milli-Q water 18MΩ. Complete mini tablets containing protease inhibitors were supplied by Roche Diagnostics (Mannheim, Germany). Bradford reagent for protein quantification and PrepReady™ 2D clean-up kit were obtained from Biorad Laboratories (Hemel-Hempstead, Hertfordshire, UK). Thermo Fisher Scientific provided the cross-linker BS³ (bis(sulfosuccinimidyl)suberate). All other general chemicals used were of analytical/electrophoretic/proteomic grade and were purchased from Sigma Chemical Company (Dorset, UK).

2.1.2 1D Gel Electrophoresis

Protein molecular mass markers and Laemmli-type buffer were purchased from Biorad Laboratories (Hemel-Hempstead, Hertfordshire, UK). Ultrapure Protogel acrylamide stock and 4X Protogel Resolving Buffer stock solutions were obtained from National Diagnostics (Atlanta, GA, USA). Protein staining of SDS-PAGE gels was performed using either silver nitrate from Sigma Chemical Company (Dorset, UK) or Coomassie Brilliant Blue G250 from Thermo Fisher Scientific (UK).

2.1.3 Mass Spectrometry

Sequencing grade modified trypsin and LysC were from Promega (Madison, WI, USA). Formic acid and acetonitrile were obtained from Fluka (Dorset, UK). C18 spin filters were purchased from Thermo Fisher Scientific (UK) and FASP vivacon 500 spin filters were obtained from Sartorius (Göttingen, Germany). LC-MS/MS vials and vial caps were purchased from VWR (PA, USA). All other analytical grade chemicals used for mass spectrometry were obtained from Thermo Fisher Scientific (UK), BioRad Laboratories (Hemel-Hempstead, Hertfordshire, UK) and Sigma Chemical Company (Dorset, UK).

2.1.4 Immunoblotting

Whatman nitrocellulose transfer membrane was obtained from Invitrogen (Carlsbad, CA, USA). Chemiluminescence substrate was from Roche Diagnostics (Mannheim, Germany). X-ray film was purchased from Santa Cruz Biotechnology (Santa Cruz, CA, USA). GBX Developer/Replenisher, GBX Fixer/Replenisher and Ponceau S-Red

Staining Solution were from Sigma Chemical Company (Dorset, UK). Commercially available antibodies used in this research were obtained from Abcam (Cambridge, UK), Novus Biologicals (Cambridge, UK), Sigma Chemical Company (Dorset, UK), EMD Millipore (Schwalbach am Taunus, Germany), BD Transduction Laboratories (Heidelberg, Germany), and Santa Cruz Biotechnology (Santa Cruz, CA, USA). All antibodies used are listed in Table 2.1. Peroxidase-conjugated secondary antibodies were from Merck (Kenilworth, NJ, USA).

2.1.5 ELISA

ELISA kits were purchased from Abcam (ab157714 to haptoglobin) and R&D Systems (FABP-1/L-FABP).

2.1.6 Immunofluorescence Microscopy

For immunofluorescence microscopy, normal goat serum, goat anti-rabbit Alexa Fluor 488 and goat anti-mouse IgG RRX (Rhodamine Red-X) antibodies were purchased from Molecular Probes, Life Technologies (Darmstadt, Germany). Cy3-conjugated goat anti-rabbit antibodies were from Jackson ImmunoResearch (West Grove, PA, USA). NovoCastra, Leica Biosystems (Newcastle Upon Tyne, UK) provided the NCL-Dys2 antibody to the carboxy terminus of dystrophin isoform Dp427 and Agilent Technologies (Hamburg, Germany) provided the Z033429 antibody to glial fibrillary acidic protein. The embedding medium Fluoromount G was from Southern Biotech (Birmingham, AL, USA). The DNA binding dye bis-benzimide Hoechst-33342 was obtained from Sigma Chemical Company (Dorset, UK).

Table 2.1: Antibodies

List of all commercially available antibodies used for this project including company and catalogue number, antibody specificity and host species.

Antibody	Species	Specificity	Company	Catalogue
Albumin	Chk	pAb	Abcam	ab14225-200
Annexin A2	Ms	mAb	BD Transduction Laboratories	A14020
Annexin A2	Rb	pAb	Abcam	ab41803
Annexin A5	Rb	pAb	Abcam	ab14196
Asporin	Rb	pAb	Novus Biologicals	NBP2-15492
β -dystroglycan	Rb	pAb	Abcam	ab43125
Biglycan	Gt	pAb	Abcam	ab58562
Cardiac myosin light chain 2	Rb	mAb	Abcam	ab92721
Calcium pump ATPase 2	Rb	pAb	Abcam	ab3529
Collagen VI	Rb	pAb	Abcam	ab6588
Desmin	Rb	pAb	Abcam	ab8592
Desmoglein isoform DSG1	Rb	mAb	Abcam	ab124798
Dysferlin	Rb	mAb	Abcam	ab124684
Fatty acid binding protein 1	Rb	mAb	Abcam	ab129203
Fibronectin	Rb	pAb	Abcam	ab2413
Glial fibrillary acidic protein	Rb	pAb	Abcam	ab7260
Haptoglobin	Rb	mAb	Abcam	ab131236
Lactate dehydrogenase	Rb	mAb	Abcam	ab52488
Lamin-B1	Rb	pAb	Abcam	ab16048
Laminin	Rb	pAb	Sigma Chemical Company	L9393
Lumican	Rb	mAb	Abcam	ab168348
Myelin PO protein	Rb	pAb	EMD Millipore	ABN363
Myoglobin	Rb	pAb	Santa Cruz	sc-25607
Parvalbumin	Rb	pAb	Abcam	ab11427
Periostin	Rb	pAb	Novus Biologicals	NBP1-30042
Transferrin	Shp	pAb	Abcam	ab9033-1
Tubulin, β -V subunit	Ms	pAb	Abcam	ab21754
Voltage-dependent anion channel VDAC-1	Ms	mAb	Abcam	ab14734

2.2 Methods

2.2.1 *mdx* and *mdx-4cv* mouse models of Duchenne Muscular Dystrophy, and wobbler mouse model of Amyotrophic lateral sclerosis

The *mdx* mouse is an established animal model which displays signs of dystrophinopathy due to a point mutation in exon 23 and loss of the full-length Dp427 dystrophin isoform (Sicinski et al., 1989). The *mdx* mouse and control wild-type mice used in experimental procedures described here were bred on a C57/BL10 background. *Quadriceps femoris* and *longissimus dorsi* from 100-day old *mdx* mice and control C57/BL10 mice were obtained from the Animal Facility of the University of Greifswald, Germany, and were used for the immunoblot analysis of desmoglein-1 abundance in Chapter 4.

The *mdx-4cv* mouse is an alternative animal model of DMD. First described in 1989, the *mdx-4cv* mouse model was generated by chemical mutagenesis using N-ethyl-nitrosourea (Chapman et al., 1989). The induced C to T transition at base 7916 in exon 53 of the dystrophin gene generates a premature stop codon, thus abrogating dystrophin synthesis. These mice demonstrate a number of histopathological features of dystrophinopathy and have the added advantage of possessing 10-fold fewer dystrophin-positive revertant fibres than the conventionally used *mdx* mouse model (Danko et al., 1992). The *mdx-4cv* mouse and control wild-type mice used in experimental procedures described here were bred on a C57/BL6 background. Skeletal muscle (Chapters 3 and 4), senescent cardiac tissue (Chapter 5), brain tissue (Chapter 6), and serum and saliva samples (Chapter 7) from *mdx-4cv* mice and control C57/BL6 mice were obtained from the Animal Facility of the University of Bonn, Germany.

The wobbler mouse is an animal model for human motor neuron disease, including amyotrophic lateral sclerosis. The spontaneous, recessive wobbler mutation has been identified as a mis-sense mutation in the ubiquitously expressed *Vps54* gene, which codes for a component of the Golgi-associated retrograde protein complex (Schmitt-John, 2015). The wobbler mouse and control wild-type mice used in this research were bred on a C57/BL6 background. Brain samples from two-month old wobbler and age-matched C57/BL6 mice, used in Chapter 6, were obtained from the Animal Facility of University of Bielefeld, Germany.

All mice (*mdx*, *mdx-4cv*, wobbler and their control counterparts) were kept under standard conditions and all procedures were carried out according to German

and Irish legislation on the use of animals in scientific research. Mice were sacrificed by cervical dislocation and tissue samples were removed and snap-frozen in liquid nitrogen. Samples were transported to Maynooth University, Ireland on dry ice and stored at -80°C prior to experimental use.

2.2.2 Sample preparation of crude tissue extracts

Optimised protocols were used for the extraction of the accessible protein constellation from tissues from control and dystrophic mice (Murphy et al., 2015b, Holland et al., 2013). All of the following procedures were performed on ice to minimise the degradation of muscle-derived proteins. For the same purpose all buffers used for tissue homogenisation were supplemented with a protease inhibitor cocktail. 100 mg of tissue (heart, brain, and various muscles of the hind leg) were finely chopped and homogenised in 10 volumes of buffer. A description of the various buffers and the tissue for which they were used is listed in Table 2.2. Tissues were homogenised using a hand-held IKA T10 Basic Homogeniser (IKA Labortechnik, Staufen, Germany). Following homogenisation, crude homogenates were incubated at 4°C for between 1.5 to 2 h with gentle shaking using a Thermomixer from Eppendorf (Hamburg, Germany). Homogenates were then centrifuged at 14,000 x *g* for 20 min using an Eppendorf 5417 R centrifuge (Eppendorf, Hamburg, Germany). The resulting supernatant was isolated taking care to disturb neither the uppermost fatty layer nor the pellet. Protein extracts were then stored at -20°C until required for further analysis.

Table 2.2 Composition of buffers used for protein extraction

Study	Buffer	Buffer Composition
Crude hind limb extracts	Homogenisation buffer	20 mM sodium pyrophosphate, 20 mM sodium phosphate, 1 mM MgCl ₂ , 0.303 M sucrose, 0.5 mM EDTA, pH 7.0
Crude microsomes	Homogenisation buffer	20 mM sodium pyrophosphate, 20 mM sodium phosphate, 1 mM MgCl ₂ , 0.303 M sucrose, 0.5 mM EDTA, pH 7.0
Aged cardiac samples	Lysis buffer	7 M urea, 2 M thiourea, 4% CHAPS, 2% DTT, 2% IPG buffer pH 3-10
Brain tissue extracts	Brain lysis buffer	8 M urea, 50 mM Tris-HCl pH 8.0, 1 mM EDTA

2.2.3 Sample preparation for the isolation of crude microsomes

A larger volume of starting material was required for this type of sub-cellular fractionation procedure than for crude tissue preparations. For this reason crude microsomes were isolated from combined muscles of the whole mouse hind leg (Carberry et al., 2014). 750 mg of tissue was finely chopped and homogenised as described in section 2.2.2. Following the isolation of the protein containing middle layer, this supernatant then underwent differential centrifugation using an Optima L-100 XP ultracentrifuge from Beckman Coulter, Inc. (Fullerton, CA, USA). Supernatants were centrifuged at 100,000 x g for 1 h at 4°C. Following ultracentrifugation the resulting supernatant was isolated and the pellet containing crude microsomes was re-suspended in an appropriate volume of homogenisation buffer (Murphy et al., 2015a). The crude microsomal fractions were then stored at -20°C.

2.2.4 Wheat germ agglutination for the purification of sarcolemma vesicles from crude microsomes

Wheat germ agglutination was employed to purify sarcolemma vesicles from crude microsomes, as described in detail by Ohlendieck and co-workers (Ohlendieck et al., 1991). Crude microsomes were prepared as described in 2.2.3 with the exception that

4 g tissue was initially homogenised and re-suspended in 7.5 volumes of homogenisation buffer and that microsomal pellets were re-suspended in 50 mM sodium phosphate, 0.16 M NaCl, pH 7.4 (buffer C) to give a final protein concentration of 1 mg/ml. An equal volume of 1 mg/ml wheat germ lectin (in buffer C) was added to the crude microsomes and mixed gently. Following a 10 min incubation on ice, the mixture was pelleted at 14,000 x g for 90 s. The supernatant from this centrifugation contained non-agglutinated vesicles, referred to as WGA void. The pellet was re-suspended in 20 mM Tris-HCl, pH 7.4, 0.303 M sucrose (buffer D), and centrifuged again at 14,000 x g for 90 s. This step was repeated once more to wash the pellet. The pellet was re-suspended in buffer D and de-agglutinated by incubation with 0.2 M N-acetyl-D-glucosamine in buffer D for 20 min at room temperature. The de-agglutinated suspension was centrifuged at 14,000 x g for 90 s, and the resulting supernatant was pelleted at 150,000 x g for 20 min at 4°C in an Optima L-100 XP ultracentrifuge from Beckman Coulter, Inc. (Fullerton, CA, USA). The pellet from this centrifugation step was re-suspended in buffer D and centrifuged again at 150,000 x g for 20 min at 4°C. This pellet, corresponding to purified sarcolemma vesicles, was re-suspended in an appropriate volume of label-free solubilisation buffer (6 M urea, 2 M thiourea, 10 mM Tris, pH 8.0 in LC-MS grade water) for subsequent label-free liquid chromatography mass spectrometry.

2.2.5 Chemical cross-linking of wild-type versus *mdx-4cv* crude microsomes

For the chemical cross-linking analysis described in Chapter 3, crude microsomes from wild-type and *mdx-4cv* skeletal muscle were diluted to a concentration of 2 mg/ml with 50 mM HEPES, pH 8.0. The water-soluble cross-linker BS³ [bis(sulfosuccinimidyl)suberate] was dissolved in 50 mM citrate buffer, pH 5.0, to minimise hydrolysis, at a concentration of 1 mg/ml (Murray and Ohlendieck, 2000). Initial optimisation studies tested various concentrations of BS³, including 0.1, 0.5, 1, 2, 5, 7.5, and 10 µg cross-linker per mg protein. 10 µg BS³ per mg protein was selected for the main study. Following the addition of BS³, samples were incubated at 25°C for 30 min. The cross-linking reaction was quenched by the addition of 50 µl 1 M ammonium acetate per ml reaction mixture (Murray and Ohlendieck, 1997). An equal volume of reducing sample buffer was added and the samples were subsequently heated at 50°C for 10 min. Cross-linked samples were then electrophoresed alongside

their non-cross-linked counterparts on 1D SDS-PAGE gels. For silver stain analysis total loading was 10 µg protein per well, while 30 µg protein was loaded per well for Coomassie staining and subsequent in-gel digestion.

2.2.6 Sample preparation and immuno-depletion of murine serum

The large dynamic range of serum and plasma is a major stumbling block for the effective proteomic profiling of biofluids as the high abundance of proteins such as albumin and immunoglobulins can mask the detection of lower abundance proteins in a data-dependent mass spectrometry experiment (Anderson and Anderson, 2002). The Proteome Purify Mouse Serum Protein Immunodepletion Resin from R&D Systems was used in this experiment to remove albumin and IgG from murine serum samples. 10 µl of serum was added to a micro-centrifuge tube containing 1 ml of immunodepletion resin. The tubes were mixed on a rotary shaker for 1 h at room temperature. Following the incubation period, the mixture of serum and resin was added to the upper chamber of a Spin-X filter unit (centrifuge tube with a 0.22 µm cellulose acetate membrane) and centrifuged for 2 min at 2,000 x g. The filtrate (immuno-depleted serum) was retained and stored at -20°C before further analysis.

2.2.7 Acetone Precipitation

Prior to mass spectrometric analysis immuno-depleted serum samples were purified by acetone precipitation. 4 volumes of cold 100% acetone was added to each sample and stored overnight at -20°C. Samples were centrifuged at 15,000 x g for 30 min at 4°C. The supernatant was decanted and replaced with 4 volumes of cold 50% acetone. The pellet was re-suspended by vortexing for 1 min. Samples were centrifuged again at 15,000 x g for 30 min at 4°C. The supernatant was once again decanted and replaced by 4 volumes of cold 50% acetone. Samples were vortexed and centrifuged once more at 15,000 x g for 30 min at 4°C. The supernatant was discarded, and the resulting pellet was allowed to air-dry for 10 min. Pellets were re-suspended in an appropriate volume of label-free solubilisation buffer (6 M urea, 2 M thiourea, 10 mM Tris, pH 8.0 in LC-MS grade water), and vortexed and sonicated, using a Sonoplus HD 2200, Bandelin (Berlin, Germany), to ensure full re-suspension.

2.2.8 2D CleanUp (BioRad)

The commercially available Ready Prep 2D clean up kit from Bio-Rad Laboratories (Hemel-Hempstead, Hertfordshire, UK) was used as an alternative to acetone precipitation for crude tissue extracts and sub-cellular fractions. The kit removes contaminants from protein extracts which may otherwise interfere with downstream mass spectrometric analysis. The purification was carried out as per the manufacturer's guidelines.

2.2.9 Protein quantification using the Bradford assay system

Protein quantification was carried out using the method of Bradford (Bradford, 1976). A standard curve was generated using a 1:1 serial dilution of a stock solution of 2 mg/ml BSA to give the following standards: 2 mg/ml, 1 mg/ml, 0.5 mg/ml, 0.25 mg/ml, 0.125 mg/ml and 0 mg/ml. Protein samples were appropriately diluted prior to quantification. Both standards and samples were constituted in the protein buffer. 5 μ l of sample and standards were added to a 96-well plate. 250 μ l of diluted Bradford reagent (diluted 1:4) was added to each well. The plate was left to incubate for 10 min at room temperature in the dark to allow for complete binding and the associated colour development. Absorbance of standards and samples was read at $\lambda=595$ nm using a Synergy HT BIO-TEK unit and KC4 software from Mason Technology Ltd. (Dublin, Ireland). Protein concentrations were determined using the standard curve, whilst multiplying by the dilution factor. Standards were analysed in duplicate while protein samples were analysed in triplicate.

2.2.10 1D Gel Electrophoresis

One dimensional sodium dodecyl sulphate polyacrylamide gel electrophoresis, 1D SDS-PAGE, was employed for examining protein banding patterns, to help confirm equal protein loading and for transfer to nitrocellulose membranes for comparative immunoblotting. 1D SDS-PAGE was conducted with a BioRad Mini-Protean III gel system (Biorad Laboratories, Hemel-Hempstead, Hertfordshire, UK). In general, 10% resolving gels with a 5% stacking gel were used. The APS and TEMED cause the gel to polymerise quite quickly so these were added to the resolving and stacking gel solutions just prior to use. The gels were made as listed in Tables 2.3 and 2.4. The resolving gel was poured into 1.0 mm glass plates, 1 ml of 100% methanol was pipetted along the top of the gel, and the gel was allowed to polymerise for

approximately 30 min at room temperature. The methanol overlay was removed with filter paper and the stacking gel was poured on top of the polymerised resolving gel. A 10 well comb was inserted before polymerisation of the stacking gel. Gels were either used after polymerisation was complete or were stored in damp tissue at 4°C for up to one week. Samples for electrophoresis were diluted 1:1 with Laemmli buffer supplemented with 350 mM DTT, boiled at 97°C for 7 min and then cooled on ice prior to loading (Laemmli, 1970). Alternatively, some gels were run under non-reducing conditions (where indicated). In this case samples were diluted 1:1 with Laemmli buffer which had not been supplemented with DTT nor any other reducing agent. Samples were then incubated at 37°C for 10 min prior to loading onto the gel. Typically, between 5-25 µg protein was loaded per well, with lower amounts for silver staining and higher concentrations for subsequent transfer to nitrocellulose membranes for immunoblot analysis. Molecular weight markers (Biorad Laboratories, Hemel-Hempstead, Hertfordshire, UK) ranging in molecular weight from 10-250 kDa were also ran on each gel. The gel rig was filled with SDS running buffer (25 mM tris base, 192 mM glycine, 0.1% (w/v) SDS) and electrophoresis was carried out at 60 V until protein samples entered the resolving gel at which stage voltage was increased to 120 V. Electrophoresis was terminated once the bromophenol blue tracking dye reached the end of the gel. Gels were carefully removed from the glass plates and were either placed in fixing solution (10% (v/v) acetic acid, 30% (v/v) ethanol) for protein staining or were transferred onto nitrocellulose membranes.

Table 2.3: SDS-PAGE gel components for 10% resolving gels

Reagent	10% Resolving Gel
Protogel (30% (w/v) Acrylamide/bis)	7.5 ml
4X Protogel Resolving Buffer	6 ml
Deionised water	10.25 ml
10% (w/v) APS	225 µl
TEMED	22.5 µl

Table 2.4: SDS-PAGE gel components for 5% stacking gels

Reagent	5% Stacking Gel
Protogel (30% (w/v) Acrylamide/bis)	2.25 ml
0.5 M Tris, pH 6.8	1.35 ml
Deionised water	7.5 ml
20% (w/v) SDS	135 µl
10% (w/v) APS	135 µl
TEMED	13.5 µl

2.2.11 Gel staining techniques

Gel staining techniques enable the visualisation of separated protein bands. Post-electrophoretic stains include Coomassie staining and silver staining. While silver staining is more sensitive than Coomassie staining, Coomassie staining is more compatible with subsequent mass spectrometric analysis of gel plugs of interest. Thus, a combination of staining techniques was used, depending on the downstream application.

2.2.11.1 Colloidal Coomassie Stain

The method of Neuhoff was used to perform colloidal Coomassie staining of polyacrylamide gels (Neuhoff et al., 1988). Following gel electrophoresis gels were briefly washed in MilliQ water and then were incubated overnight in colloidal Coomassie staining solution (1 part stock staining solution A [10% (w/v) ammonium sulphate, 2% (v/v) phosphoric acid], 40 parts stock staining solution B (5% Coomassie brilliant blue G-250, and 10 parts methanol). Gels were transferred to neutralisation

buffer (0.1 M tris, pH 6.5) for 1-3 min and then washed with 25% methanol for 1 min. This step could be repeated to remove any excess staining solution. Gels were then placed in fixation solution (20% (w/v) ammonium sulphate) until ready to scan. Colloidal Coomassie stained gels were scanned using a GE heathcare image scanner III (Little Chalfont, UK).

2.2.11.2 Silver Stain

Silver staining was the predominant staining technique used and the method of Chevallet was followed (Chevallet et al., 2006). Once gel electrophoresis was terminated, gels were placed in fixer (30% (v/v) ethanol, 10% (v/v) acetic acid) for a minimum of 30 min to fix proteins within the polyacrylamide gel. Gels were rinsed twice in 20% (v/v) ethanol for 10 min each time and rinsed twice in 100% MilliQ for 10 min each time. Gels were placed in sensitiser (0.8 mM sodium thiosulphate) for 1 min and then were rinsed again with 100% MilliQ for 10 min. Gels were transferred to silver staining solution (12 mM silver nitrate) for 30 min – 2 h. Following staining gels were briefly rinsed in 100% MilliQ, and then developed (15 g sodium carbonate, 125 µl formaldehyde, 62.5 µl of 10% (w/v) sodium thiosulphate, brought up to 500 ml with MilliQ) until distinct protein bands were visible. The staining was stopped upon the addition of stopper solution (20 g tris, 10 ml acetic acid, brought up to 500 ml with MilliQ). Gels were then scanned using a GE heath care image scanner III (Little Chalfont, UK).

2.2.12 Sample preparation for label-free liquid chromatography mass spectrometry

Following the determination of protein concentration using the Bradford assay system, sample volumes were equalised with label-free solubilisation buffer. Protein samples were reduced with 10 mM DTT for 30 min at room temperature with gentle shaking and alkylated with 25 mM IAA in 50 mM ammonium bicarbonate for 20 min at room temperature in the dark (Dowling et al., 2014a). To quench any unreacted IAA and thus prevent the alkylation of trypsin, a further 10 mM DTT was added to each sample and samples were incubated for 15 min at room temperature in the dark. Proteolytic digestion was achieved using a combination of the enzymes Lys-C and trypsin. Samples were initially digested with sequencing grade Lys-C at a ratio of 1:100 (protease: protein) and incubated at 37°C for 4 h. Samples were then diluted with four

times the initial sample volume using 50 mM ammonium bicarbonate to dilute the urea molarity to a range at which trypsin is active (Proc et al., 2010). Samples were then incubated with sequencing grade modified trypsin at a ratio of 1:25 (protease: protein) overnight at 37°C. The proteolytic digestion was halted by the addition of 2% trifluoroacetic acid (TFA) in 20% acetonitrile (ACN) (3:1 (v/v) dilution). The peptides were purified using Pierce C18 spin columns from Thermo Fisher Scientific (Dublin, Ireland), dried through vacuum centrifugation and re-suspended in loading buffer (2% ACN, 0.05% TFA in LC-MS grade water) (Murphy et al., 2015a). Peptide suspensions were vortexed and sonicated to aid full re-suspension. Samples were centrifuged briefly at 14,000 x g and the supernatant transferred to mass spectrometry vials. Any remaining peptide suspension was stored at -80°C.

2.2.13 Filter Aided Sample Preparation

Protein concentrations were equalised with label-free solubilisation buffer and 30 µg of protein was processed by the filter aided sample preparation (FASP) method (Wiśniewski et al., 2009) using a trypsin to protein ratio of 1:25 (protease: protein). Following overnight digestion and elution of peptides from the spin filter, 2% TFA in 20% ACN was added to the filtrates (3:1 (v/v) dilution). The peptides were then purified using Pierce C18 spin columns from Thermo Fisher Scientific (Dublin, Ireland), dried through vacuum centrifugation and re-suspended in mass spectrometry loading buffer (2% ACN, 0.05% TFA in LC-MS grade water). Peptides were vortexed, sonicated and briefly centrifuged at 14,000 x g and the supernatant transferred to mass spectrometry vials for label-free LC-MS/MS.

2.2.14 On-membrane digestion

For on-membrane digestion analysis, protein fractions underwent gel electrophoresis and transfer to nitrocellulose membranes prior to trypsin digestion, for which nitrocellulose membrane strips corresponding to the entire lane of proteins was used. Membrane strips were placed in 15 ml falcon tubes, de-stained with PBS and washed five times with dH₂O. The strips were subsequently blocked with 0.5% PVP-40 (polyvinylpyrrolidone) for 40 min at 37°C with agitation (Luque-Garcia and Neubert, 2009) to prevent non-specific binding of trypsin to the membrane. Since PVP-40 would have a negative impact on mass spectrometric analysis, excess PVP-40 was

removed by extensive washing with dH₂O and transfer of membrane strips to new 15 ml falcon tubes. 4 ml of reconstituted sequencing grade trypsin in digestion buffer (100 mM ammonium bicarbonate/10% ACN [1:1, v/v]) was added to each nitrocellulose strip; corresponding to a 1:20 ratio of trypsin to protein. The strips were digested overnight at 37°C with agitation. 4 ml of extraction buffer (5% formic acid/ACN [1:2, v/v]) was added to trypsin-digested membrane strips and incubated at 37°C for 15 min with agitation (Luque-Garcia and Neubert, 2009, Shevchenko et al., 2006). The supernatant was subsequently transferred to 1.5 ml micro-centrifuge tubes and dried by vacuum centrifugation. Dried peptides were re-suspended in 0.5% TFA/5% ACN and centrifuged in 22- μ m acetate cellulose spin filter tubes for 20 min to remove any membrane particles (Lewis and Ohlendieck, 2010a). Peptides were purified using C18 spin columns and dried by vacuum centrifugation. Dried peptides were stored at -80°C until ready for mass spectrometric analysis.

2.2.15 In-gel digestion

In-gel digestion for mass spectrometric analysis was performed as per the method of Shevchenko (Shevchenko et al., 2006). Coomassie-stained 1D gels were washed twice in dH₂O for 10 min. Gel bands of interest were excised and placed in Eppendorf micro-centrifuge tubes. Individual Coomassie-stained gel zones were de-stained by the addition of 100 μ l of 100 mM ammonium bicarbonate: neat acetonitrile (1:1) solution and incubated at 37°C for 30 min with gentle agitation. The solution was removed and 500 μ l neat acetonitrile was added to each gel zone and incubated at room temperature for 10 min with gentle agitation. The solution was removed, and gel pieces were then subjected to in-gel trypsin digestion. 50-100 μ l of re-suspended trypsin was added to each gel zone and incubated at 4°C for 30 min to allow slow diffusion of trypsin into the gel. A further 20 μ l of trypsin buffer was added, and gel zones were incubated for 90 mins at 4°C. 40 μ l of a 50 mM ammonium bicarbonate solution was added and left to incubate overnight at 37°C. 100 μ l extraction buffer [5% formic acid/neat acetonitrile (1:2)] was added to gel pieces and incubated at 37°C for 15 min with agitation. The supernatant, containing peptides, was transferred to fresh tubes, and dried down by vacuum centrifugation. Dried peptides were re-suspended in 0.5% TFA/5% ACN, purified by C18 spin columns and dried by vacuum centrifugation. Dried peptides were stored at -80°C prior to mass spectrometric analysis.

2.2.16 Label-free liquid chromatography mass spectrometry

LC-MS/MS was achieved using two different mass spectrometers. An Ultimate 3000 NanoLC system (Dionex Corporation, Sunnyvale, CA, USA) coupled to a Q-Exactive mass spectrometer (Thermo Fisher Scientific) in the Proteomics Suite at Maynooth University was used for studies involving proteins derived from hind-limb tissue (crude extracts and sarcolemma-enriched), cardiac tissue, serum and saliva. An Ultimate 3000 nanoLC system (Dionex Corporation, Sunnyvale, CA, USA) coupled to an LTQ Orbitrap XL mass spectrometer (Thermo Fisher Scientific) in the Proteomics Facility of the National Institute for Cellular Biotechnology, Dublin City University was used for the analysis of brain-derived proteins.

2.2.16.1 LC-MS/MS using a Q-Exactive mass spectrometer

Re-suspended peptide mixtures (a maximum load of the equivalent 1 μ g pre-digested protein) were loaded by an autosampler onto a C18 trap column (C18 PepMap, 300 μ m id \times 5 mm, 5 μ m particle size, 100 \AA pore size; Thermo Fisher Scientific). The trap column was switched on-line with an analytical Biobasic C18 Picofrit column (C18 PepMap, 75 μ m id \times 500 mm, 2 μ m particle size, 100 \AA pore size; Dionex). The peptides generated were eluted over either 65 min or 180 min using the following binary gradients: solvent A [2% (v/v) ACN and 0.1% (v/v) formic acid in LC-MS grade water] and 0-90% solvent B [80% (v/v) ACN and 0.1% (v/v) formic acid in LC-MS grade water]. The column flow rate was set to between 0.25 – 0.3 μ L/min (Murphy et al., 2015a, Murphy et al., 2016b). The Q-Exactive was operated in positive, data-dependent mode and was externally calibrated. Survey MS scans were conducted in the 300-1700 m/z range with a resolution of 140,000 (m/z 200) and lock mass set to 445.12003. CID (collision-induced dissociation) fragmentation was carried out with the fifteen most intense ions per scan and at a resolution of 17,500. A dynamic exclusion window was applied within 30 s. An isolation window of 2 m/z and one micro-scan were used to collect suitable tandem mass spectra.

2.2.16.2 LC-MS/MS using an LTQ Orbitrap XL mass spectrometer

Digested peptide samples (a maximum of 1 μ g) were loaded onto a C18 trap column (C18 PepMap, 300 μ m id \times 5 mm, 5 μ m particle size, 100 \AA pore size; Dionex). The first step in the LC-MS/MS protocol involved desalting, which was performed at a flow rate of 25 μ l/min in 0.1% TFA / 2% ACN for 10 min (Holland et al., 2015a). The

trap column was then switched on-line with an analytical PepMap C18 column (75 μm id \times 500 mm, 3 μm particle and 100 \AA pore size; Dionex). Peptides were eluted with the following binary gradients: solvent A [2% (v/v) ACN and 0.1% (v/v) formic acid in LC–MS grade water] and 0–25% solvent B [80% ACN and 0.08% (v/v) formic acid in LC–MS grade water] for 240 min and 25–50% solvent B for a further 60 min, with a column flow rate set to 0.35 $\mu\text{l}/\text{min}$ (Meleady et al., 2012a). Data were acquired with Xcalibur software, version 2.0.7 (Thermo Fisher Scientific). The LTQ Orbitrap XL mass spectrometer was operated in positive, data-dependent mode and was externally calibrated. Survey MS scans were carried out in the 400–1200 m/z range with the resolution set to a value of 30,000 (m/z 400) and lock mass set to 445.120025. CID fragmentation was carried out with the three most intense ions per scan (Holland et al., 2014). Within 60 s a dynamic exclusion window was applied. A normalized collision energy of 35%, an isolation window of 3 m/z and one micro-scan were used to gather suitable tandem mass spectra.

2.2.17 Qualitative proteomic profiling of mass spectrometric data

Qualitative data analysis was used for protein identification. Mass spectrometry raw files were processed using the Proteome Discoverer 1.4 (Thermo Fisher Scientific) software with Sequest HT as the search engine and the UniProt sequence database. The following search parameters were used for protein identification: (i) peptide mass tolerance set to 10 ppm, (ii) MS/MS mass tolerance set to 0.02 Da, (iii) up to two missed cleavages, (iv) carbamidomethylation set as a fixed modification and (v) methionine oxidation set as a variable modification. Mass spectrometry raw files were searched against the *Mus musculus* database (Chapters 3, 4, 5, 6 and 7) or the *Oryctolagus cuniculus* database and the *Mammalia* database (Chapter 4) (Liu et al., 2016). Peptides were filtered using a minimum XCorr score of 1.5 for +1, 2.0 for +2, 2.25 for +3 and 2.5 for +4 charge states, with peptide probability set to high confidence.

2.2.18 Quantitative proteomic profiling of mass spectrometric data using Progenesis QI for Proteomics Software

Irrespective of the mass spectrometer used, all raw data generated from LC-MS/MS was analysed using Progenesis QI for Proteomics software (versions 2.0 and 3.1; Non-Linear Dynamics, a Waters Company, Newcastle upon Tyne, UK). In order to account

for any drift in retention time between samples, a reference run was selected and the retention times of all other runs were aligned to this run (Holland et al., 2015b). The reference run selected was that which contained the highest number of peptide ions. The data was filtered using set criteria prior to exportation to Proteome Discoverer 2.0 (Thermo Scientific) as a mascot generic file (mgf). The following criteria was used: (i) peptide features with ANOVA ≤ 0.05 between experimental groups, (ii) mass peaks with charge states from +1 to +5 and (iii) greater than one isotope per peptide (Meleady et al., 2012b). This exported mgf file containing MS/MS spectra was used for peptide identification using Proteome Discoverer 2.0 against the search engines Mascot (version 2.3, Matrix Science, Boston, MA, USA) and Sequest HT (SEQUENT HT algorithm, licence Thermo Scientific, registered trademark University of Washington, USA) (Murphy et al., 2015b). The data was searched against the UniProtKB-SwissProt database (taxonomy: *Mus musculus*). A number of search parameters were used for proper protein identification: (i) peptide mass tolerance set to 10 ppm, (ii) MS/MS mass tolerance set to 0.02 Da, (iii) an allowance of up to two missed cleavages, (iv) carbamidomethylation set as a fixed modification and (v) methionine oxidation set as a variable modification (Murphy et al., 2017b). For re-importation back into Progenesis LC-MS software for further analysis, only high confidence peptides and those peptides with ion scores of 40.00 or more (from Mascot) and/or XCorr scores of 1.5 or more (from Sequest HT) were selected. The following criteria were applied to designate a protein as properly identified and with differential abundance: (i) an ANOVA score between experimental groups of ≤ 0.05 , and (ii) proteins with ≥ 2 peptides matched (Dowling et al., 2016a).

2.2.19 Quantitative proteomic profiling of mass spectrometric data using MaxQuant and Perseus Software

For quantitative analysis mass spectrometry files were analysed in MaxQuant (version 1.6.1.0), with the Andromeda search engine used to search the detected features against the UniProtKB-SwissProt database for *Mus musculus*. The following search parameters were used: i) first search peptide tolerance of 20 ppm, ii) main search peptide tolerance of 4.5 ppm, iii) cysteine carbamidomethylation set as a fixed modification, iv) methionine oxidation set as a variable modification, v) a maximum of two missed cleavage sites and vi) a minimum peptide length of seven amino acids. The FDR was set to 1% for both peptides and proteins using a target-decoy approach

(Grassl et al., 2016). Relative quantification was performed using the MaxLFQ algorithm (Cox et al., 2014). The “proteinGroups.txt” file produced by MaxQuant was further analysed in Perseus (version 1.5.1.6). Proteins that matched to the reverse database or a contaminants database or that were only identified by site were removed. The label-free quantification (LFQ) intensities were \log_2 transformed, and only proteins found in all replicates in at least one group were used for further analysis. Data imputation was performed to replace missing values with values that simulate signals from peptides with low abundance chosen from a normal distribution specified by a downshift of 1.8 times the mean standard deviation of all measured values and a width of 0.3 times this standard deviation (Deslyper et al., 2016). A two sample t-test was performed using $p \leq 0.05$ on the post imputed data to identify statistically significant differentially abundant proteins.

2.2.20 Generation of heat maps using Perseus

Heat maps illustrating protein abundances for statistically significant differentially abundant proteins were designed using Perseus software. The normalised abundances of differentially abundant proteins determined using Progenesis QI for Proteomics were loaded as a txt file into Perseus and the data was \log_2 transformed. Hierarchical clustering was then performed on Z-score normalised intensity values by clustering both samples and proteins using Euclidean distance and average linkage.

2.2.21 Bioinformatics analysis of proteomic data

A number of bioinformatics software packages were used to give comprehensive analyses of identified proteins with differential abundance. Such bioinformatics tools were used to i) classify the types of proteins identified, ii) give meaningful insights into the potential roles of identified proteins in disease pathophysiology and iii) identify potential associations between identified proteins. The PANTHER database of protein families (<http://pantherdb.org>; version 10.0) was used to group proteins based on their protein class (Mi et al., 2013). Differentially abundant proteins were also analysed by version 10.5 of the STRING database (<http://string-db.org/>) for medium (0.4) or high confidence (>0.7) interactions using the evidence view. STRING analysis clusters proteins based on known and predicted protein interactions that include direct physical and indirect functional protein associations (Szkarczyk et al., 2017). The DAVID bioinformatics resource (<https://david.ncifcrf.gov/>) was used

to identify enriched functionally related protein groups and KEGG pathway (<http://www.genome.jp/kegg/pathway.html>) was employed to map proteomic data onto pathway maps to enable biological interpretation of large proteomic datasets. The web-based gene set analysis toolkit (<http://www.webgestalt.org/>) was also used to interrogate proteomic datasets. Over-representation enrichment analysis was performed, with genome_protein-coding as the reference list, non-redundant gene ontology terms, a minimum of 2 genes for a category, an FDR \leq 0.05 and with the Benjamini & Hochberg method used for multiple test adjustment. The ClueGO app in the Cytoscape bioinformatics package was used to identify enriched GO categories, using a two-sided hypergeometric test and a Benjamini-Hochberg p value correction.

2.2.22 Comparative immunoblot analysis

Comparative immunoblot analysis was carried out for the independent verification of a number of important protein hits identified by LC-MS/MS. Immunoblotting was performed under routine conditions (Holland et al., 2013), typically using 25 μ g protein per lane. Proteins were first separated on hand-cast 10% polyacrylamide gels by SDS-PAGE and were subsequently transferred by the method of Towbin (Towbin et al., 1979) to Whatman nitrocellulose membranes in a Trans-Blot cell from Bio-Rad laboratories by wet transfer (transfer buffer: 25 mM tris, 192 mM glycine, 20% methanol) at 100 V for 70 min at 4°C. Transfer efficiency was assessed using Ponceau reversible stain (0.1% PonceauS, 5% acetic acid). To prevent non-specific binding, membranes were blocked for 1 h at room temperature using a milk protein solution (2.5% (w/v) fat-free milk powder in 10% PBS), and then incubated with appropriately diluted primary antibodies overnight at 4°C with gentle agitation. The following day membranes were washed twice in the milk protein solution for 10 min, and then incubated with appropriately diluted peroxidase-conjugated secondary antibodies for 1.5 h at room temperature with gentle agitation (Murphy et al., 2015a). Membranes were washed with the milk protein solution for 10 min twice and with 10% PBS for 10 min twice, and enhanced chemiluminescence was used for the visualisation of immuno-decorated protein bands (O'Connell and Ohlendieck, 2009). Densitometric scanning and statistical analysis of immunoblots was performed using a HP PSC-2355 scanner and ImageJ software (NIH, Bethesda, MD, USA) along with Graph-Pad Prism

software (San Diego, CA, USA), in which a p value ≤ 0.05 was deemed to be statistically significant.

2.2.23 Enzyme linked immunosorbent assay

ELISA assays were employed to independently verify some potential circulatory protein markers as identified by label-free LC-MS/MS. Crude serum samples were screened using quantitative sandwich enzyme immunoassays to haptoglobin and fatty acid binding protein 1. Serum samples were diluted appropriately (1:1,000 for haptoglobin assay and 1:400 for FABP-1) and were added to antibody-coated microtiter wells and incubated at room temperature as directed by the manufacturers' recommendations (20 min for haptoglobin and 2 h for FABP-1). After the incubation period wells were washed and a HRP labelled secondary detector antibody was added. After incubation at room temperature for 20 min in the dark, TMB chromogen substrate was added. The reaction was stopped after exactly 10 min (for haptoglobin) or 30 min (for FABP-1) and absorbance was measured at 450 nm on a microplate reader (Cynthia Martin et al., 2014). The quantity of protein in the test samples was interpolated from a generated standard curve and was corrected for sample dilution. All test samples were assayed in triplicate. The intra-plate % coefficient of variation (CV) was calculated and was found to be less than 10% for all assays (Murphy et al., 2017b).

2.2.24 Immunofluorescence microscopy

All immunofluorescence microscopy was performed by Margit Zweyer at the University of Bonn, Germany. Freshly dissected tissue specimens were quick-frozen in liquid nitrogen-cooled isopentane and 10 μ m sections cut in a cryostat. For collagen VI immuno-staining tissue sections were fixed in a 1:1 (v/v) mixture of methanol and acetone for 10 min at room temperature. For GFAP immuno-staining sagittal brain sections were fixed for 5 min in ice-cold 4 % (v/v) paraformaldehyde in PBS. For dystrophin immuno-staining, unfixed cryosections were boiled in PBS for 5 min. Tissue sections were permeabilised in 0.1% (v/v) Triton X-100 for 10 min (collagen VI and dystrophin) or 30 min (GFAP), and then blocked with 1:20 diluted normal goat serum for 30 min at room temperature. Primary antibodies to dystrophin, collagen VI and GFAP were diluted 1:20, 1:20 and 1:300, respectively, in PBS for overnight incubation at 4 °C. Specimens were carefully washed and then incubated with

fluorescently-labelled secondary antibodies, using 1:200 diluted anti-rabbit Alexa Fluor 488 antibody (collagen VI), 1:200 diluted anti-mouse RRX antibody (dystrophin) or 1:300 diluted anti-rabbit Cy3-conjugated antibody (GFAP) for 30 min (GFAP) or 45 min (collagen VI and dystrophin) at room temperature. Nuclei were counter-stained with 1 µg/ml bis-benzimide Hoechst 33342. Following antibody labelling, tissue sections were embedded in Fluoromount G medium and viewed under a Zeiss Axioskop 2 epifluorescence microscope equipped with a digital Zeiss AxioCam HRc camera (Carl Zeiss Jena GmbH, Jena, Germany).

Chapter Three

Proteomic evaluation of alterations in protein abundance and protein interactions in hind limb extracts from the *mdx-4cv* mouse model of Duchenne muscular dystrophy

3.1 Introduction

DMD is a highly progressive and ultimately lethal neuromuscular disorder characterised by deficiency of dystrophin, a 427 kDa cytoskeletal protein encoded by the *Dmd* gene on chromosome Xp21 (Nallamilli et al., 2014, Koenig et al., 1987) . This rod-shaped protein is located on the inner side of the cell membrane of muscle fibres, where it provides an anchor between cytoskeletal actin and the extracellular matrix. This is achieved through interactions with a variety of binding partners (Ibraghimov-Beskrovnaya et al., 1992), to form a highly organised dystrophin-glycoprotein complex (DGC). One of the primary roles of the DGC is the maintenance of sarcolemmal integrity, but it is also suggested to have regulatory roles through its interactions with signalling molecules such as nNOS (Ramachandran et al., 2013). In the absence of dystrophin the DGC is compromised. This results in a fragile sarcolemma which is prone to micro-rupturing during mechanical stress (Ohlendieck and Campbell, 1991a). This in turn leads to excessive influx of calcium ions and elevated intracellular calcium concentrations (Batchelor and Winder, 2006). This calcium hypothesis of DMD postulates that high intracellular calcium levels are responsible for the activation of proteases which lead to cell death, altered ion homeostasis and altered cell signalling (Deconinck and Dan, 2007).

Gel-based techniques for large-scale protein separation prior to mass spectrometric identification has been a mainstay of proteomics for many years. The power of gel-based techniques for comparative proteomics was greatly enhanced by the introduction of 2D-DIGE. The capacity to run multiple samples on the same gel removed the issue of gel-to-gel variation and thus improved the reproducibility of results (Marouga et al., 2005). However, gel electrophoresis is restricted by its limited resolving power for very large proteins, very small proteins, highly acidic proteins, highly basic proteins and hydrophobic proteins (Issaq and Veenstra, 2008, Vélez et al., 2015). Liquid-chromatography coupled to mass spectrometry has helped to improve this bioanalytical issue, but many comparative proteomic surveys have still failed to identify the membrane-associated protein dystrophin in total skeletal tissue extracts. The application of organelle proteomics to reduce sample complexity in skeletal muscle and enrich for membrane proteins has proved successful in identifying a number of components of the DGC including the full-length Dp427 isoform of dystrophin, dystroglycan, α 1-syntrophin, γ -sarcoglycan and δ -sarcoglycan (Murphy et al., 2015a). However, while this optimised methodology used minimal centrifugation

steps, subcellular fractionation may introduce artefacts in comparative proteomic studies. Thus, the identification of dystrophin deficiency and its associated secondary abnormalities by highly sensitive mass spectrometry in total skeletal tissue extracts from the *mdx-4cv* animal model of X-linked dystrophinopathy was attempted. The use of crude muscle extracts to identify potential muscle-associated biomarker candidates represents a more promising avenue for the establishment of a superior marker signature. In addition, the findings from this new study, using whole tissue proteomics, are important verification results in relation to previous sub-proteomic investigations. Since the *mdx-4cv* animal model used in this proteomic survey exhibits substantial myofibrosis (Danko et al., 1992), similar to that seen in the human condition, this proteomic study aimed to simultaneously study dystrophin deficiency and secondary fibrotic changes within the same tissue sample and the same analytical run.

While comparative proteomics can reveal significant insights into the molecular basis of neuromuscular disease, also of critical importance is the establishment of altered protein interactions in response to disease. The assembly of protein complexes and dynamic interactions between proteins are instrumental in many developmental, metabolic and physiological processes, and impaired protein complex formation can underlie many pathological processes (Murphy and Ohlendieck, 2016). This occurs in the case of DMD whereby the loss of the Dp427 full-length isoform of dystrophin results in a collapsed DGC and ultimately leads to membrane instability, abnormal Ca^{2+} influx and progressive skeletal muscle wasting. To investigate potential alterations in protein oligomerisation in dystrophic skeletal muscle membranes, chemical cross-linking using the agent bis[sulfosuccinimidyl]suberate (BS^3) was coupled with mass spectrometry. The BS^3 cross-linker (XL) used in this study is a member of the amine-reactive group of cross-linkers. Containing an *N*-hydroxysulfosuccinimide ester at each end of an 8-carbon spacer arm, BS^3 is a water-soluble, homo-bifunctional, non-cleavable and amine-reactive cross-linker, thus rendering it particularly useful for the stabilisation of protein complexes (Sinz, 2006). Additionally, the protein-XL conjugation reaction can be performed under experimental conditions which are relatively close to normal physiological conditions. The analytical workflow consisted of i) the subcellular enrichment of microsomal membranes from wild-type versus dystrophic skeletal muscle, ii) the stabilization of protein-protein interactions via the 11.4-Å cross-linker BS^3 , iii) the comparative one-dimensional gel electrophoretic separation of cross-

linked versus control microsomes for the detection of cross-linked protein complexes, iv) in-gel digestion to generate distinct peptide populations, and v) mass spectrometric identification of proteins that exist in apparent supramolecular complexes, and thus demonstrate a reduced electrophoretic mobility. The altered electrophoretic mobility of protein species in wild-type versus dystrophic muscle membranes in the presence of an XL agent was investigated in relation to specific high molecular mass ranges in polyacrylamide gels. Overall this analytical approach identified a variety of proteins with an enhanced tendency for oligomerisation in the dystrophic microsomal fraction, which are mostly involved in membrane repair, cytoskeletal remodelling, fibre regeneration, molecular chaperoning and oxidative metabolism. These findings suggest that distinct adaptations in critical protein-protein interaction patterns exist that may help counter-act progressive fibre wasting in muscular dystrophy.

3.1.1 Experimental Design

Skeletal muscle is severely affected in DMD, with muscle weakness and atrophy first evident in the proximal muscles, with later involvement of lower legs, forearms, neck and trunk. A loss of ambulation usually occurs around the early teenage years. Given the severity of skeletal muscle degeneration, it was of interest to obtain a global overview of proteomic alterations in skeletal muscle which may give novel insights into the disease pathology. To achieve this, label-free LC-MS/MS was performed on crude homogenates from the entire hind-leg of 6-month old wild-type and age-matched *mdx-4cv* mice (n=4). Proteomic profiling was performed using an Ultimate 3000 NanoLC system (Dionex Corporation, Sunnyvale, CA, USA) coupled to a Q-Exactive mass spectrometer (Thermo Fisher Scientific). Skeletal muscle-derived peptides were eluted using the following binary gradient: solvent A [2% (v/v) ACN and 0.1% (v/v) formic acid in LC-MS grade water] and 0-90% solvent B [80% (v/v) ACN and 0.1% (v/v) formic acid in LC-MS grade water]: 2% solvent B for 10.5 min, 2-40% solvent B for 110 min, 40-90% solvent B for 2.5 min, 90% solvent B for 9 min and 2% solvent B for 43 min. Relative quantification and identification was performed with Progenesis QI for Proteomics software, using Sequest HT and MASCOT search engines and the UniProtKB-SwissProt database. Bioinformatics analysis was conducted using the PANTHER database of protein families, and STRING software. Heatmaps of differentially abundant proteins were generated using Perseus software.

Using a panel of select antibodies, the abundance changes of number of proteins were independently verified by comparative immunoblotting.

In addition to alterations in protein abundance, it is likely that dystrophin deficiency and concomitant secondary abnormalities also affect protein interaction patterns. In order to investigate this possibility chemical cross-linking was combined with mass spectrometric analysis. For this study crude microsomes were prepared by ultracentrifugation of homogenates from 5-month old wild-type and age-matched *mdx-4cv* entire hind legs (n=4). The biochemical stabilisation of protein interactions was carried out with 10 µg of the homo-bifunctional and amine-reactive agent bis[sulfosuccinimidyl]suberate per mg protein, followed by protein shift analysis in one-dimensional gels. In-gel digestion was performed, and peptides were analysed by mass spectrometry using an Ultimate 3000 NanoLC system (Dionex Corporation, Sunnyvale, CA, USA) coupled to a Q-Exactive mass spectrometer (Thermo Fisher Scientific). Peptides were eluted using a 65 min method over the following binary gradient [solvent A: (2% (v/v) ACN and 0.1% (v/v) formic acid in LC-MS grade water and solvent B: 80% (v/v) ACN and 0.1% (v/v) formic acid in LC-MS grade water]: 3% solvent B for 5 min, 10-40% solvent B for 30 min, 40-90% solvent B for 5 min, 90% solvent B for 5 min and 3% solvent B for 10 min. Protein identification was achieved using Proteome Discoverer 1.4 against Sequest HT and the UniProtKB-SwissProt database. Venny 2.1 software was used to generate Venn diagrams to identify common and unique proteins between wild-type control, wild-type cross-linked, *mdx-4cv* control and *mdx-4cv* cross-linked proteins. Potential protein interactions amongst unique cross-linked proteins in *mdx-4cv* samples were analysed by version 10.5 of the STRING database for medium confidence (0.4) interactions using the evidence view.

3.2 Results

3.2.1 Label-free LC-MS/MS analysis of dystrophin-deficient hind-limb muscle

A label-free LC-MS/MS approach was used to identify potential changes in protein expression in the hind-limb muscle of the *mdx-4cv* animal model of X-linked muscular dystrophy. Since skeletal muscle is highly heterogeneous many comparative proteomic surveys have focused their efforts on identifying proteomic changes within individual muscles (Carberry et al., 2013). This approach has revealed that disease severity is also highly heterogeneous, with different muscle displaying varying degrees of neuromuscular damage. The heart and diaphragm are severely dystrophic and fibrotic in comparison to the leg, but the extent of muscle damage also varies greatly even within the skeletal muscles of the leg; *soleus* and *extensor digitorum longus* muscles are moderately affected, while *interosseus* and *flexor digitorum brevis* muscles are more mildly affected (Holland et al., 2015b). Hence this proteomic survey utilised tissue extracts from whole hind-limb muscle to attain a global analysis of proteomic alterations within the dystrophic leg.

The comparative proteomic study revealed major protein alterations in the dystrophic hind-leg. A total of 199 proteins were identified as having altered abundance of 2-fold or greater in *mdx-4cv* muscle preparations, and the abundance profile of these proteins is illustrated in Figure 3.1. Of these proteins, 156 proteins were increased in abundance (Table 3.1 and Table A3.1), while 43 proteins displayed decreased levels (Table 3.2). Proteins with drastically increased abundance include fibronectin, collagen α -2 (VI) chain, fibrinogen- γ chain and fibrinogen- β chain. Elevated levels of such proteins are indicative of fibrosis in *mdx-4cv* muscle. A number of tubulin isoforms also displayed increased expression which suggests compensatory up-regulation of cytoskeletal components to counter-act mechanical weakness in dystrophin-deficient cells. This study was also successful in identifying dystrophin as the protein with the highest reduction in dystrophic skeletal muscle, along with identifying reduced levels of α -1 syntrophin, another constituent of the DGC. Thus, this global proteomic analysis of hind-leg can unequivocally correlate the decrease in components of the DGC with the massive infiltration of connective tissue in dystrophic muscle.

Table 3.1: List of identified proteins with ≥ 3.5 -fold increased abundance in 6-month old *mdx-4cv* hind-limb versus age-matched wild-type hind-limb as determined by label-free LC-MS/MS

Accession	Gene Name	Protein Name	Unique peptides	Confidence score	Anova (p)	Max fold change
Q61879	Myh10	Myosin-10	2	89.20	4.14E-06	Infinity
P11276	Fn1	Fibronectin	2	133.42	2.67E-03	271.96
Q00898	Serpina1e	Alpha-1-antitrypsin 1-5	5	571.06	4.00E-06	187.00
Q922F4	Tubb6	Tubulin beta-6 chain	1	187.33	5.12E-04	59.01
Q02788	Col6a2	Collagen alpha-2(VI) chain	2	102.60	9.94E-04	44.37
P28653	Bgn	Biglycan	4	232.44	4.17E-03	17.82
Q8R5J9	Arl6ip5	PRA1 family protein 3	2	45.72	2.12E-04	16.11
Q9ESD7	Dysf	Dysferlin	2	62.55	4.13E-03	16.08
Q8VDD5	Myh9	Myosin-9	4	267.70	9.13E-03	15.76
Q9D154	Serpinb1a	Leukocyte elastase inhibitor A	9	608.03	1.20E-04	12.59
P09541	Myl4	Myosin light chain 4	7	467.03	1.70E-07	12.04
Q8VCM7	Fgg	Fibrinogen gamma chain	3	75.57	3.42E-04	11.00
Q8K0E8	Fgb	Fibrinogen beta chain	11	586.97	2.03E-04	10.97
P62835	Rap1a	Ras-related protein Rap-1A	2	111.67	4.82E-03	10.62
P99024	Tubb5	Tubulin beta-5 chain	4	211.97	1.02E-03	9.81
Q3TMP8	Tmem38a	Trimeric intracellular cation channel type A	2	192.70	4.05E-03	8.94
P21981	Tgm2	Protein-glutamine gamma-glutamyltransferase 2	2	98.65	2.33E-02	8.77
P13542	Myh8	Myosin-8	1	499.88	1.39E-02	8.63
O89053	Coro1a	Coronin-1A	2	83.25	4.52E-03	8.10
P51881	Slc25a5	ADP/ATP translocase 2	2	56.47	4.10E-03	8.06
P97449	Anpep	Aminopeptidase N	2	60.65	2.56E-03	7.80
Q9D1G3	Hhat1	Protein-cysteine N-palmitoyltransferase HHAT-like protein	5	363.57	9.73E-03	6.55
P28665	Mug1	Murinoglobulin-1	15	759.77	2.46E-03	6.51
P03921	Mtnd5	NADH-ubiquinone oxidoreductase chain 5	3	200.00	1.89E-02	6.28

Q8VDN2	Atp1a1	Sodium/potassium-transporting ATPase subunit alpha-1	5	274.26	1.51E-02	6.07
P68433	Hist1h3a	Histone H3.1	3	261.41	1.17E-02	5.98
P11087	Coll1a1	Collagen alpha-1(I) chain	4	205.30	1.65E-02	5.92
Q99JY9	Actr3	Actin-related protein 3	3	152.92	8.37E-05	5.59
Q7TSH2	Phkb	Phosphorylase b kinase regulatory subunit beta	2	72.79	3.58E-02	5.50
Q99MQ4	Aspn	Asporin	5	354.06	5.47E-04	5.43
Q61233	Lcp1	Plastin-2	6	251.30	1.09E-04	5.39
P41216	Acs11	Long-chain-fatty-acid-CoA ligase 1	5	242.74	2.00E-02	5.19
Q91V79	Fitm1	Fat storage-inducing transmembrane protein 1	2	114.05	1.23E-02	5.15
Q6PIE5	Atp1a2	Sodium/potassium-transporting ATPase subunit alpha-2	6	279.16	1.10E-02	5.02
P10107	Anxa1	Annexin A1	5	349.43	7.52E-04	4.99
Q68FD5	Cltc	Clathrin heavy chain 1	10	600.25	4.17E-04	4.82
Q00623	Apoa1	Apolipoprotein A-I	14	959.82	3.86E-04	4.63
A2AMM0	Murc	Muscle-related coiled-coil protein	4	173.61	1.74E-04	4.60
Q9CR62	Slc25a11	Mitochondrial 2-oxoglutarate/malate carrier protein	2	61.54	3.21E-02	4.60
P14094	Atp1b1	Sodium/potassium-transporting ATPase subunit beta-1	2	99.15	1.07E-02	4.39
Q9DBG6	Rpn2	Dolichyl-diphosphooligosaccharide--protein glycosyltransferase subunit 2	2	123.21	1.78E-02	4.26
P13020	Gsn	Gelsolin	10	696.42	1.54E-06	4.18
P62908	Rps3	40S ribosomal protein S3	3	191.57	1.56E-02	4.16
Q6Z WV3	Rpl10	60S ribosomal protein L10	2	130.31	3.57E-02	4.12
Q01339	Apoh	Beta-2-glycoprotein 1	3	76.33	1.62E-02	4.11
Q61147	Cp	Ceruloplasmin	2	104.55	5.98E-03	4.09
Q60854	Serpinb6	Serpin B6	13	834.53	1.05E-04	4.00
Q99P72	Rtn4	Reticulon-4	2	145.75	7.71E-03	3.96

Q8BH59; Q9QXX4	Slc25a12	Calcium-binding mitochondrial carrier protein Aralar1	7	511.83	1.41E- 02	3.91
P20918	Plg	Plasminogen	2	160.21	1.84E- 02	3.89
O09161	Casq2	Calsequestrin-2	3	162.35	4.14E- 04	3.87
Q61838	A2m	Alpha-2- macroglobulin	27	1386.61	4.62E- 03	3.79
P16546	Sptan1	Spectrin alpha chain, non-erythrocytic 1	5	348.06	6.92E- 03	3.75
O89104	Syp12	Synaptophysin-like protein 2	2	236.00	9.84E- 03	3.73
E9PZQ0	Ryr1	Ryanodine receptor 1	27	1821.46	9.26E- 03	3.72
Q71LX4	Tln2	Talin-2	2	46.72	2.45E- 02	3.69
P68369	Tuba1a	Tubulin alpha-1A chain	12	719.04	6.41E- 03	3.68
P22752	Hist1h2ab	Histone H2A type 1	4	199.02	1.92E- 03	3.67
P29621	Serpina3c	Serine protease inhibitor A3C	2	240.90	2.56E- 03	3.66
P01872	Ighm	Ig mu chain C region	3	242.28	4.58E- 03	3.65
Q9EQK5	Mvp	Major vault protein	2	108.45	2.87E- 03	3.59
P07356	Anxa2	Annexin A2	9	662.88	9.17E- 04	3.55
P00405	Mtco2	Cytochrome c oxidase subunit 2	3	118.86	1.54E- 02	3.52

Table 3.2: List of identified proteins with a significantly decreased abundance in *mdx-4cv* hind-limb versus age-matched wild-type hind limb as determined by label-free LC-MS/MS

Accession	Gene Name	Protein Name	Unique peptides	Confidence score	Anova (p)	Max fold change
P11531	Dmd	Dystrophin, Dp427	9	457.77	5.25E-05	14.61
Q8VCT4	Ces1d	Carboxylesterase 1D	4	175.05	1.94E-03	5.85
O55137	Acot1	Acyl-coenzyme A thioesterase 1	2	139.31	2.28E-03	4.35
P19096	Fasn	Fatty acid synthase	3	198.37	6.24E-03	4.00
Q9JJW5	Myoz2	Myozenin-2	2	67.37	1.66E-02	3.98
Q8C0M9	Asrg1l	Isoaspartyl peptidase/L-asparaginase	3	202.68	8.71E-04	3.98
P97823	Lypla1	Acyl-protein thioesterase 1	2	115.76	1.73E-02	3.96
P32848	Pvalb	Parvalbumin alpha	4	262.00	4.00E-02	3.95
Q61234	Snta1	Alpha-1-syntrophin	3	101.64	8.73E-04	3.69
P51667	Myl2	Myosin regulatory light chain 2, ventricular/cardiac muscle isoform	6	319.15	2.95E-02	3.64
Q08642	Padi2	Protein-arginine deiminase type-2	10	498.35	3.33E-03	3.55
P09542	Myl3	Myosin light chain 3	8	548.51	1.60E-02	3.51
P16015	Ca3	Carbonic anhydrase 3	21	1652.17	1.54E-03	3.44
Q8QZS1	Hibch	3-hydroxyisobutyryl-CoA hydrolase, mitochondrial	3	202.77	2.45E-03	3.15
Q64105	Spr	Sepiapterin reductase	7	515.05	2.04E-03	3.14
P70695	Fbp2	Fructose-1,6-bisphosphatase isozyme 2	9	592.73	3.22E-03	3.09
Q9DAK9	Phpt1	14 kDa phosphohistidine phosphatase	2	208.62	2.64E-04	3.02
P04247	Mb	Myoglobin	16	1768.39	6.53E-04	2.93
Q8BVI4	Qdpr	Dihydropteridine reductase	5	336.05	3.15E-04	2.91
Q9DBB8	Dhdh	Trans-1,2-dihydrobenzene-1,2-diol dehydrogenase	2	119.58	2.63E-02	2.90
Q9D358	Acp1	Low molecular weight phosphotyrosine protein phosphatase	2	115.63	2.47E-03	2.89
P06801	Me1	NADP-dependent malic enzyme	8	348.26	5.72E-03	2.85

P21107	Tpm3	Tropomyosin alpha-3 chain	3	113.68	2.45E-02	2.72
O55103	Prx	Periaxin	2	5.10	1.46E-02	2.67
Q8R1G2	Cmbl	Carboxymethylenebutenolide homologue	4	418.47	5.83E-03	2.64
Q9D0K2	Oxct1	Succinyl-CoA:3-ketoacid coenzyme A transferase 1, mitochondrial	2	143.49	9.92E-03	2.61
Q9WUZ5	Tnni1	Troponin I, slow skeletal muscle	2	114.05	3.34E-02	2.50
P56375	Acyp2	Acylphosphatase-2	3	227.82	5.51E-04	2.40
P17563	Selenbp1	Selenium-binding protein 1	7	398.91	7.34E-04	2.36
P14152	Mdh1	Malate dehydrogenase, cytoplasmic	8	588.67	4.42E-04	2.33
Q9CRB9	Chchd3	Coiled-coil-helix-coiled-coil-helix domain-containing protein 3, mitochondrial	2	191.91	8.31E-03	2.28
P70349	Hint1	Histidine triad nucleotide-binding protein 1	6	504.12	4.70E-03	2.27
P11404	Fabp3	Fatty acid-binding protein, heart	5	407.23	1.14E-02	2.21
Q01768	Nme2	Nucleoside diphosphate kinase B	3	216.20	2.94E-02	2.21
Q9D0S9	Hint2	Histidine triad nucleotide-binding protein 2, mitochondrial	2	88.74	7.99E-03	2.15
Q9CQR4	Acot13	Acyl-coenzyme A thioesterase 13	2	155.36	9.68E-03	2.14
P15626	Gstm2	Glutathione S-transferase Mu 2	5	300.40	1.95E-02	2.13
P08228	Sod1	Superoxide dismutase [Cu-Zn]	5	206.00	4.58E-03	2.09
Q8BZA9	Tigar	Fructose-2,6-bisphosphatase TIGAR	2	106.59	4.00E-03	2.08
Q91ZJ5	Ugp2	UTP--glucose-1-phosphate uridylyltransferase	15	949.23	2.70E-03	2.08
P63017	Hspa8	Heat shock cognate 71 kDa protein	4	465.80	3.12E-03	2.03
P15327	Bpgm	Bisphosphoglycerate mutase	3	213.38	1.34E-02	2.02
Q60864	Stip1	Stress-induced-phosphoprotein 1	3	175.87	1.85E-03	2.01

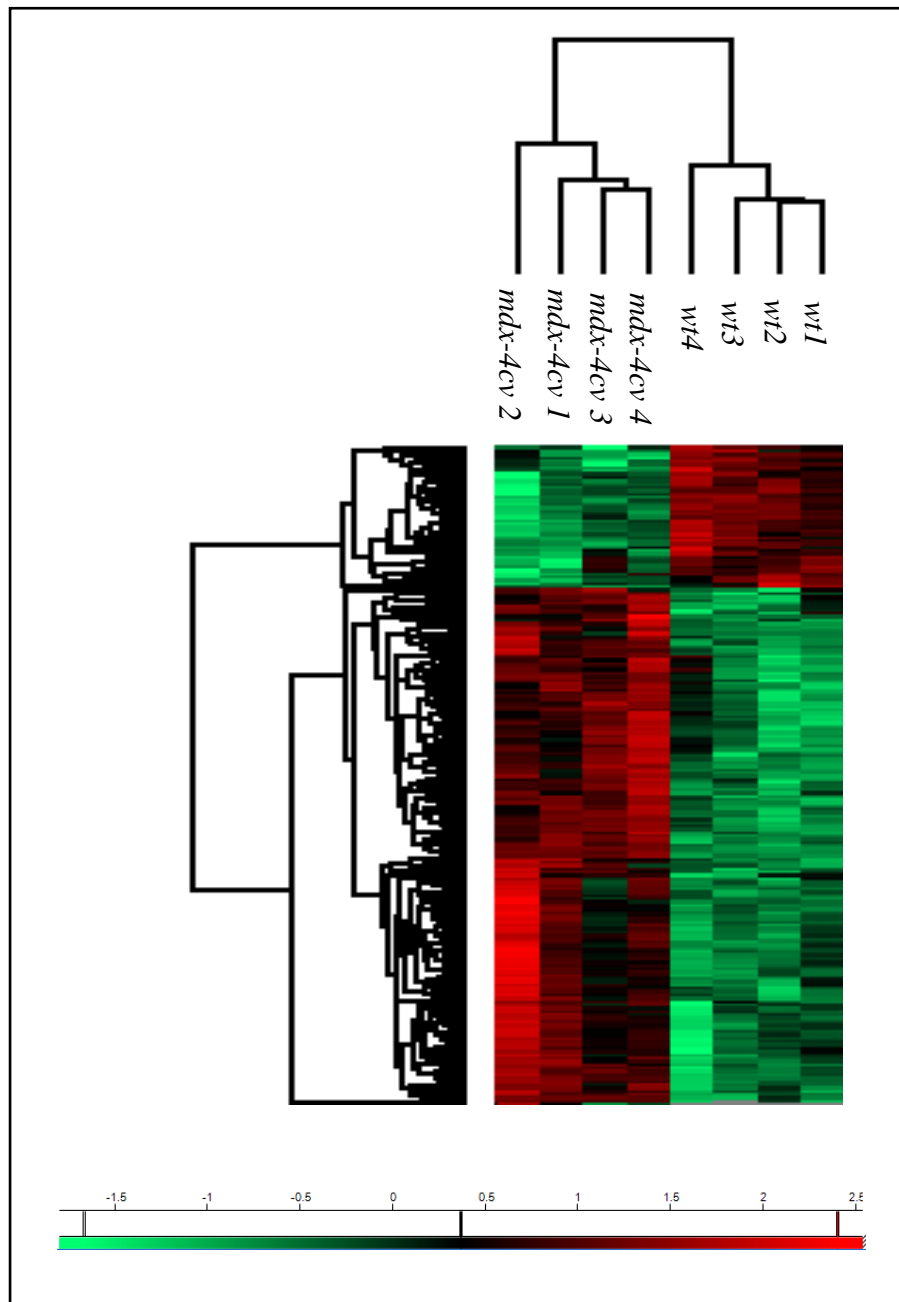


Figure 3.1: Label-free quantitative proteomic analysis of wild-type versus *mdx-4cv* crude hind-limb extracts

Depicted is the result from hierarchical clustering of the median protein expression values of all 199 statistically significant differentially abundant proteins, performed using Perseus software. Hierarchical clustering of z-score normalised intensity values resolved the four replicates of each sample group and illustrates diagrammatically the alterations in protein abundance between wild-type and *mdx-4cv* skeletal muscle.

3.2.2 Distribution of protein changes in *mdx-4cv* hind-limb

To explore the biological significance of the proteins displaying altered expression in dystrophic hind-leg, bioinformatics was employed. Both proteins with increased abundance (Figure 3.2) and proteins with reduced abundance (Figure 3.3) were grouped based on their protein class. The fact the class of cytoskeletal proteins is observed in both proteins with increased and decreased expression suggests that i) X-linked dystrophinopathy is primarily a cytoskeletal disease whereby dystrophin deficiency results in a concomitant decrease in other structural components of the DGC and ii) in dystrophic muscle there is a compensatory up-regulation of other cytoskeletal proteins to rescue the load-bearing capacity of the dystrophic hind-leg. Enzymatic activity also appears to be significantly affected in *mdx-4cv* muscle, with just over half (56%) of decreased proteins belonging to the class of hydrolases, oxidoreductases, transferases and phosphatases.

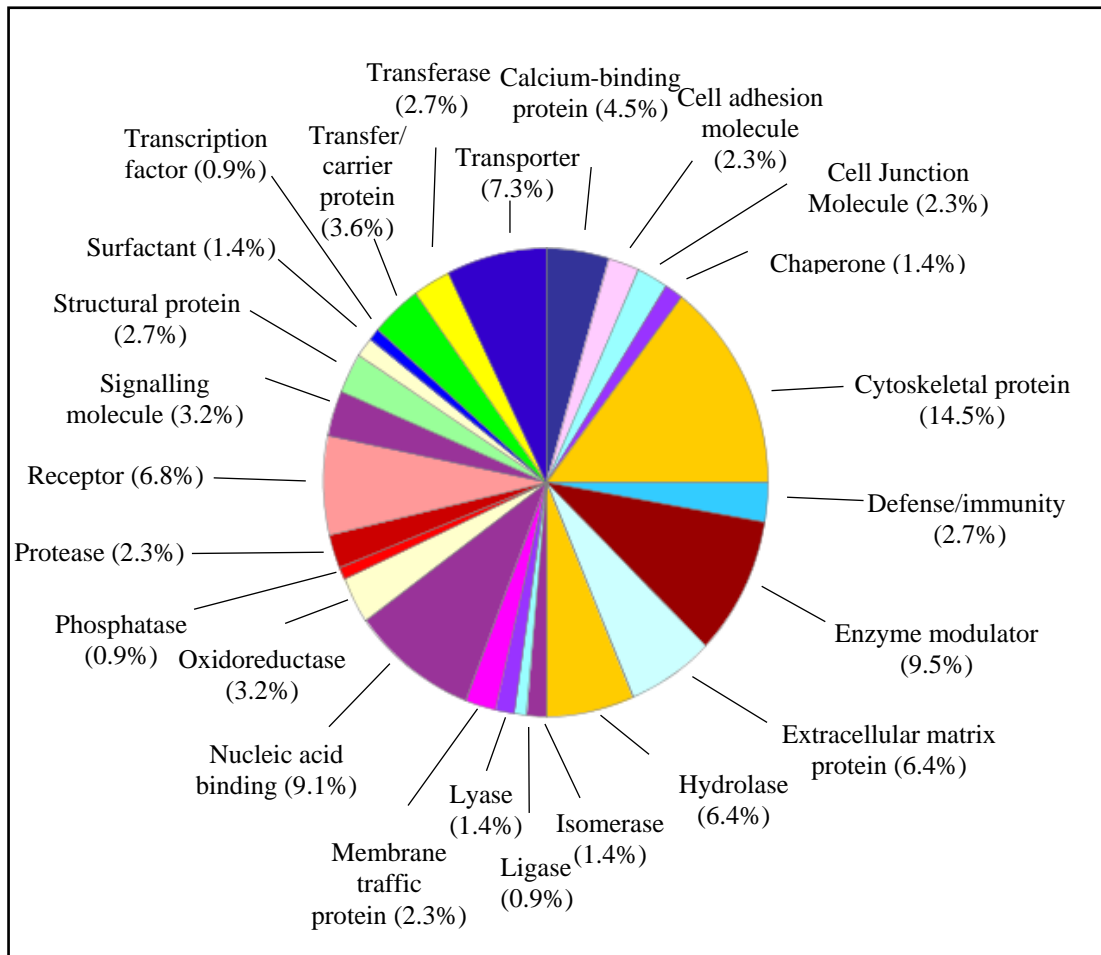


Figure 3.2: PANTHER analysis of the 156 proteins with increased abundance in *mdx-4cv* skeletal muscle

Proteins with elevated abundance in total tissue extracts from *mdx-4cv* hind-limb, as identified by label-free LC-MS/MS, were grouped into protein class using the bioinformatics package PANTHER.

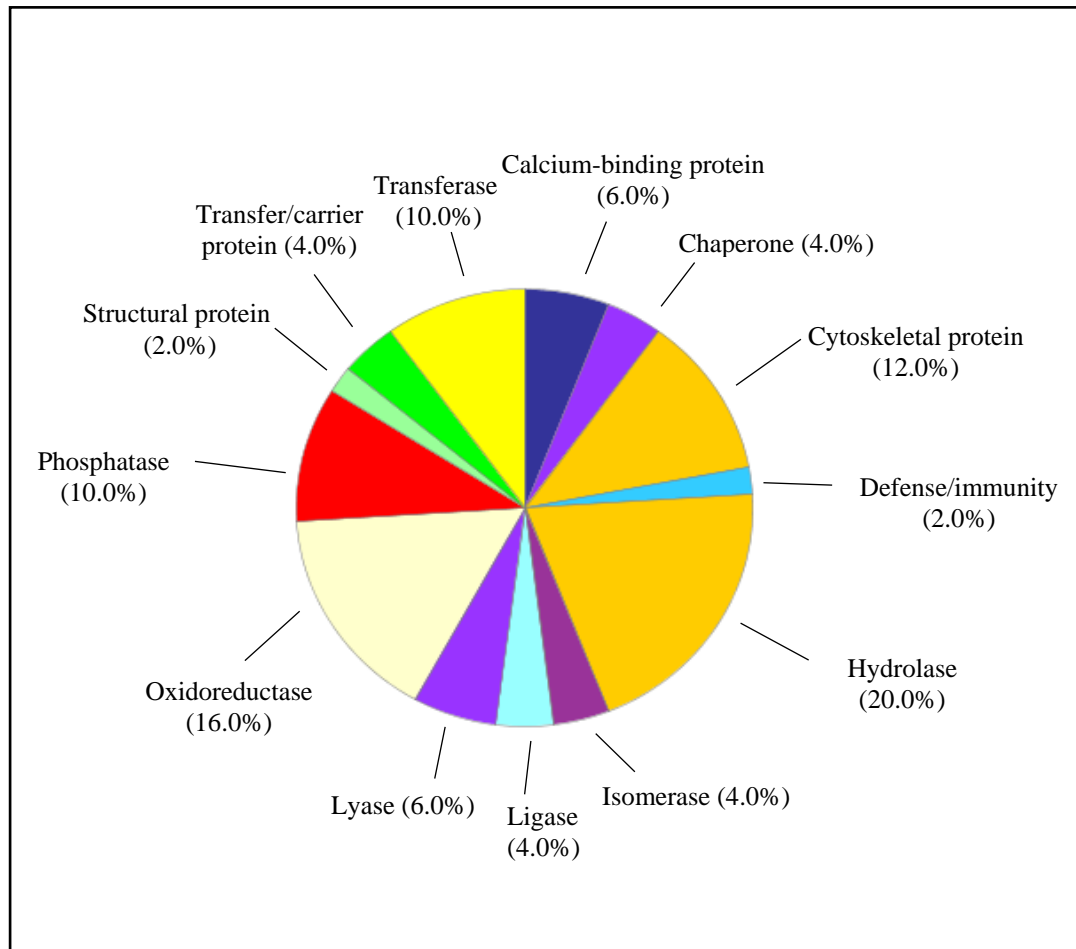


Figure 3.3: PANTHER analysis of the 43 proteins with decreased abundance in *mdx-4cv* skeletal muscle

Summary of proteins with reduced levels in total tissue extracts from *mdx-4cv* hind-limb as identified by label-free LC-MS/MS. Proteins with reduced abundance were classified by protein class using the bioinformatics software PANTHER.

Potential protein interactions were also examined using STRING analysis, which generates interaction maps based on direct physical and indirect functional protein linkages. Figure 3.4 depicts the global analysis of the 199 proteins with altered abundance in crude extracts from the dystrophic hind-limb. In analogy to the PANTHER bioinformatics analysis, a major protein cluster was identified for the cytoskeletal proteins, including vimentin, desmin, obscurin, filamin A, filamin C and various isoforms of myosin heavy chains and myosin light chains, indicating that the deficiency in dystrophin in X-linked dystrophinopathy has major implications for the cytoskeletal structure of cells. Other interesting protein clusters include the mitochondria and the ribosome, suggesting bioenergetic adaptations and increased protein synthesis respectively. Fibrotic pathways, a major hallmark of DMD, and wound healing were also detected, as indicated in Figure 3.4.

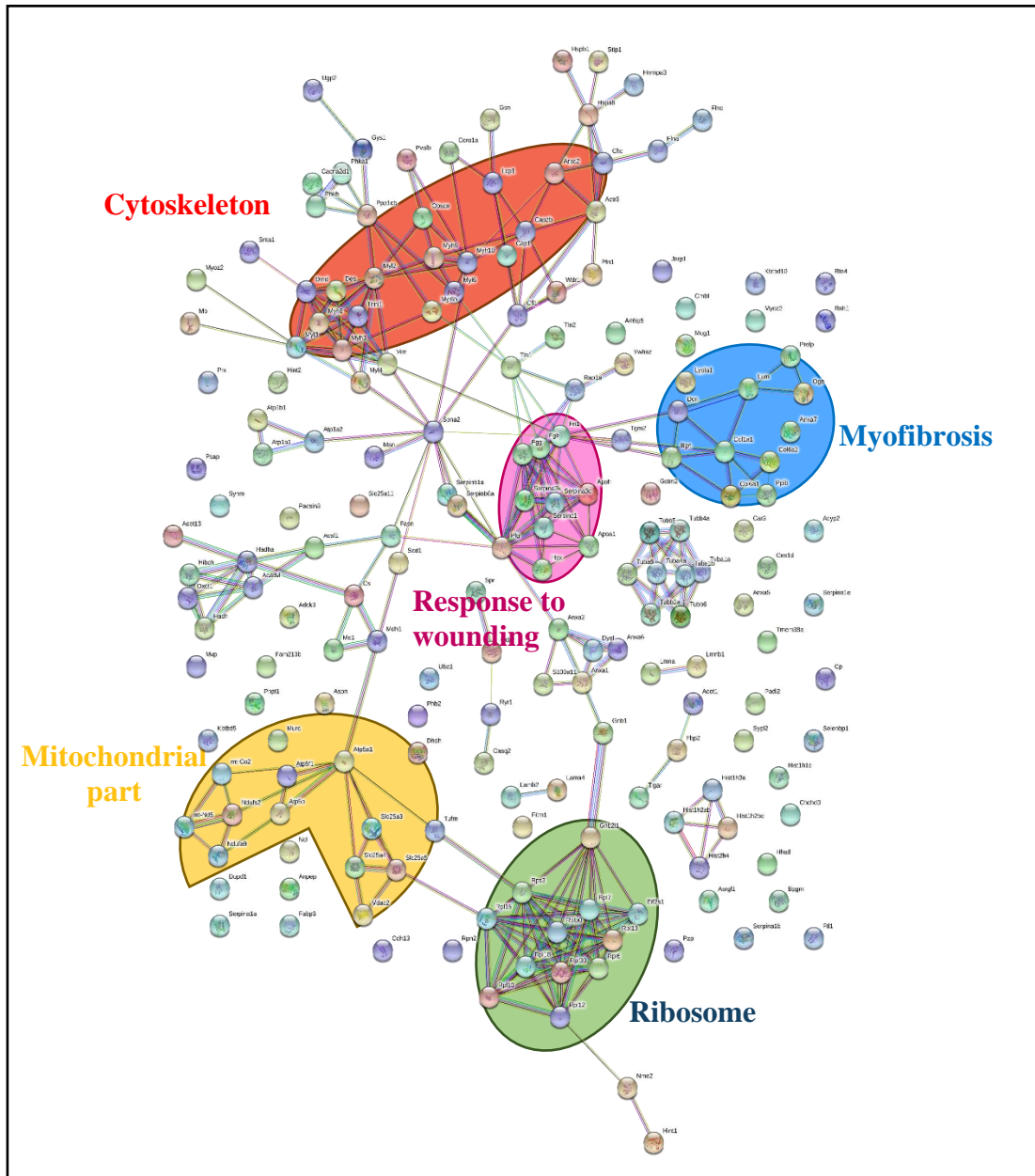


Figure 3.4: Bioinformatics analysis of altered protein expression in dystrophic skeletal muscle

The bioinformatics STRING database identified a number of interesting protein clusters, including the ribosome, the cytoskeleton, mitochondrial part, wound healing and myofibrils.

3.2.3 Verification of proteomic findings by comparative immunoblotting

Comparative immunoblotting using a panel of antibodies against select muscle-derived proteins was employed to independently verify some of the key proteomic hits that have been identified by label-free LC-MS/MS. Figure 3.5 shows a silver-stained gel of wild-type versus *mdx-4cv* muscle preparations, which indicates comparable protein banding patterns between control and dystrophic hind-leg. Immunoblotting with an antibody against the equal loading protein laminin, demonstrated comparable levels of this protein between wild-type and *mdx-4cv* samples (Figure 3.5). This, in conjunction with the silver stain analysis, illustrates equal protein loading. In contrast, altered abundance was detected for a range of proteins. Elevated levels of the cytoskeletal proteins β -tubulin and desmin was also determined (Figures 3.6 and 3.7), indicating the loss of dystrophin has a major impact on the cytoskeletal lattice. Increased annexin A2 abundance is indicative of membrane perturbations (Figure 3.6), while massive increases in the abundance of the extracellular matrix glycoprotein fibronectin was also detected by immunoblotting (Figure 3.7). Parvalbumin displays reduced abundance in *mdx-4cv* preparations, suggesting a reduction in the cytosolic calcium-buffering capacity of dystrophic muscle fibres (Figure 3.8). Taken together the comparative immunoblot analysis verifies the proteomic data in this report and illustrates the secondary abnormalities evident in dystrophic skeletal muscle.

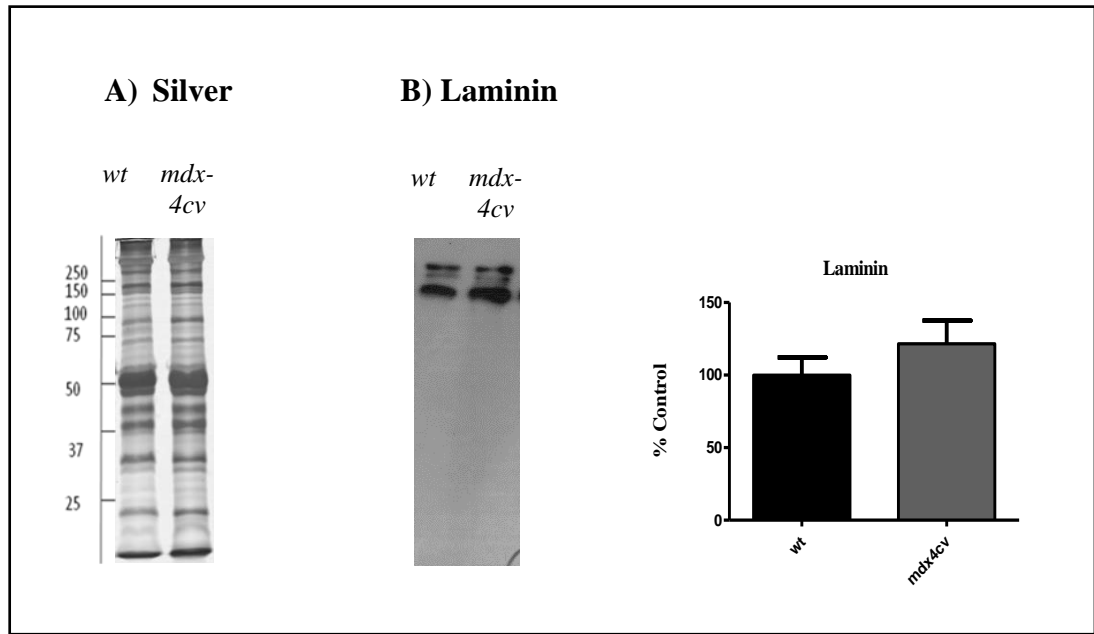


Figure 3.5: Electrophoretic and immunoblot analysis of wild-type and *mdx-4cv* muscle

Shown is a silver stained 1D gel (A) and immunoblot and statistical analysis of bands labelled with laminin (B). The silver stained gel shows comparable protein banding patterns for wild-type and *mdx-4cv* muscle preparations. Molecular weight marker is given on the left-hand-side of the image in kDa. Laminin immunoblotting did not show significant changes in concentration between wild-type and *mdx-4cv* samples and so it serves as a loading control for comparative immunoblotting. Graphical representation of the immuno-decoration level for laminin is shown (mean values \pm SEM, Student's *t*-test; unpaired; n=4).

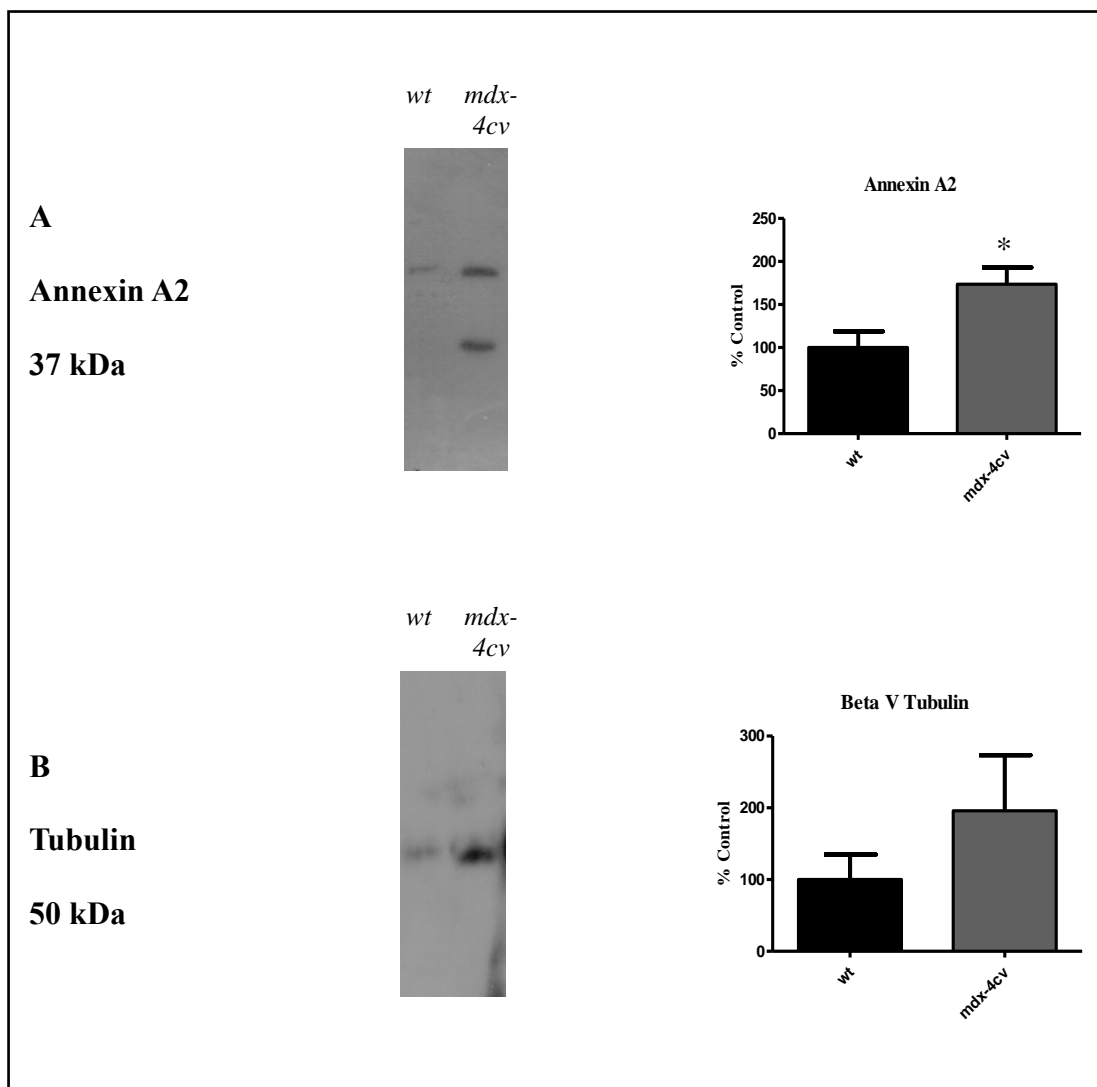


Figure 3.6: Comparative immunoblot analysis of proteins with an increased abundance in dystrophic *mdx-4cv* hind-limb skeletal muscle

Shown are representative immunoblots with immuno-decorated bands labelled with antibodies to the A2 isoform of annexin (A) and the microtubular protein β -tubulin (B). Statistical analysis of immuno-decoration was performed with Student's *t*-test (mean values \pm SEM; unpaired; $n=4$, $*p \leq 0.05$).

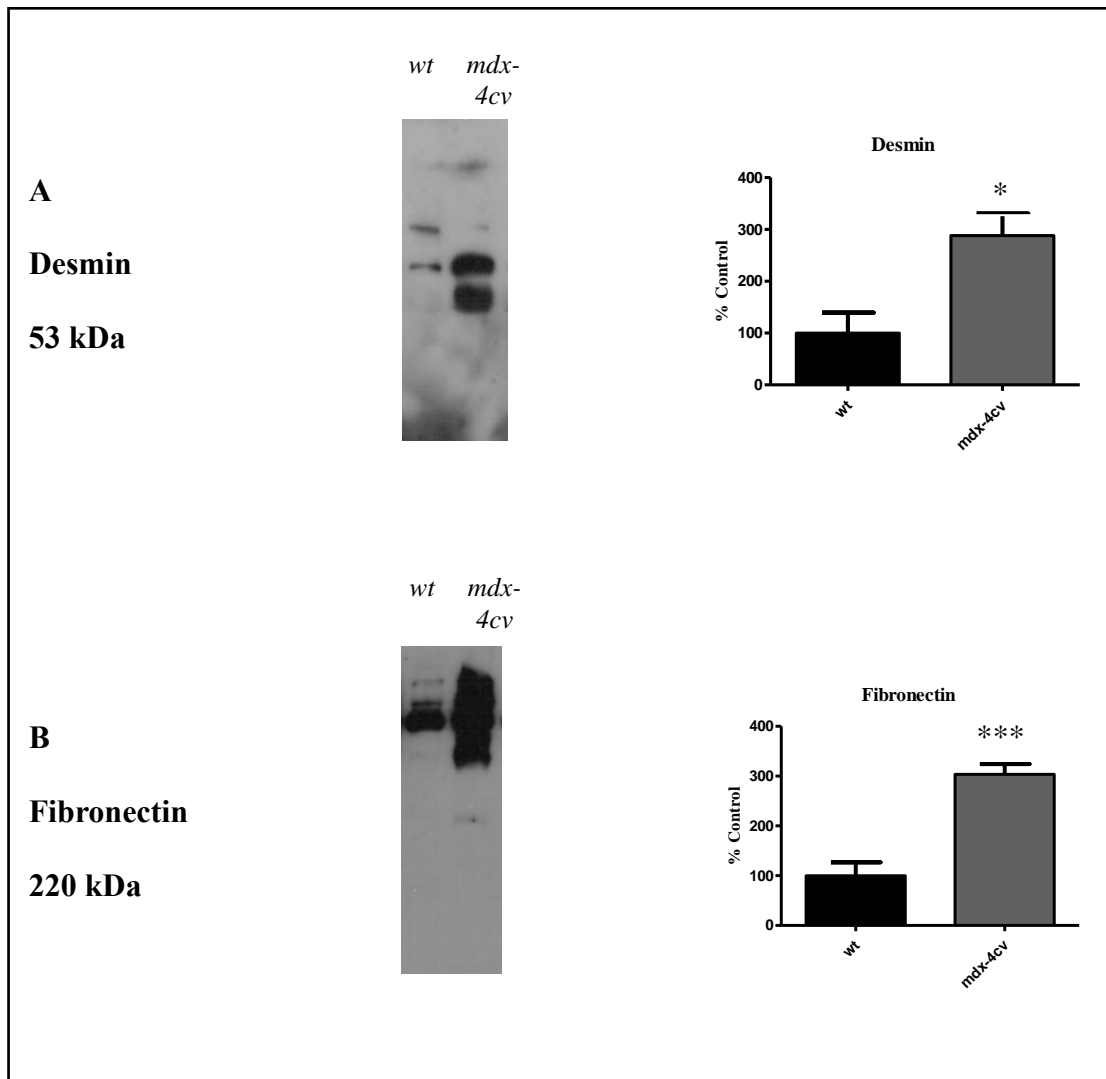


Figure 3.7: Comparative immunoblot analysis of proteins with an increased abundance in dystrophic *mdx-4cv* hind-limb skeletal muscle

Shown are representative immunoblots with immuno-decorated bands labelled with antibodies to the intermediate filament protein desmin (A) and the extracellular matrix protein fibronectin (B). Statistical analysis of immuno-decoration was performed with Student's *t*-test (mean values \pm SEM; unpaired; $n=4$, * $p \leq 0.05$, *** $p \leq 0.001$).

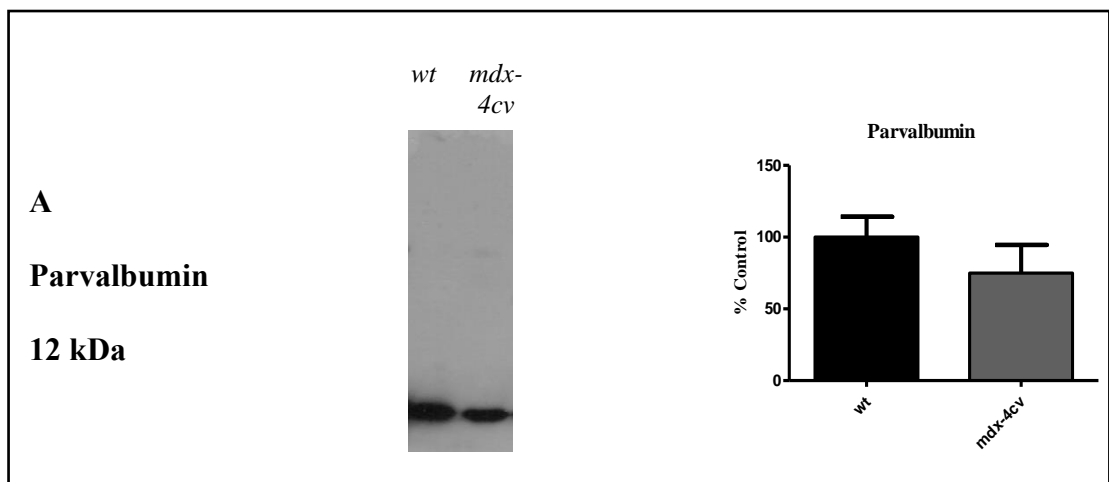


Figure 3.8: Comparative immunoblot analysis of proteins with a decreased abundance in dystrophic *mdx-4cv* hind-limb skeletal muscle

Shown is a representative immunoblot with immuno-decorated bands labelled with an antibody to parvalbumin (A). Statistical analysis of immuno-decoration was performed with Student's *t*-test (mean values \pm SEM; unpaired; $n=4$).

While the pathogenesis of DMD is largely attributed to two main processes; mechanical stress in dystrophin-deficient muscle fibres and elevated cytoplasmic calcium levels, fibrosis is also a major contributing factor to the pathology. Since this proteomic survey has for the first time identified dystrophin as the main down-regulated protein in total tissue extracts from skeletal muscle, we aimed to investigate myofibrosis in the same samples to place dystrophin deficiency in its proper pathophysiological context. Fibrosis was examined by a combination of immunofluorescence and immunoblotting of the collagen isoform COL-VI, as shown in Figure 3.9. In contrast to comparable levels of overall protein and laminin, collagen levels were found to be significantly increased in *mdx-4cv* skeletal muscle. Immunofluorescence microscopy verified this finding, with clearly elevated levels of collagen evident in Dp427-deficient muscle preparations.

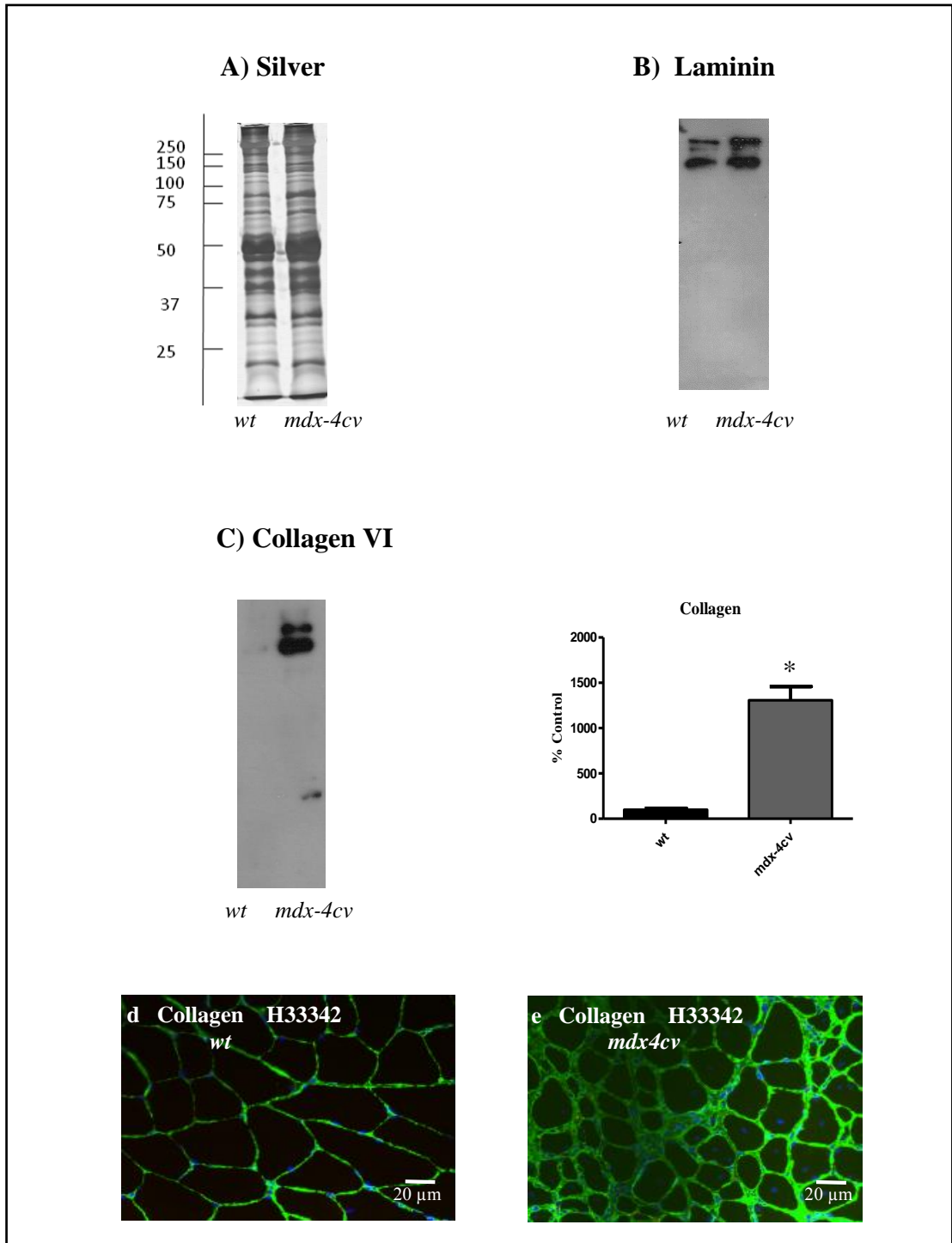


Figure 3.9: Immunofluorescence and immunoblot analysis of collagen in normal versus dystrophic *mdx-4cv* muscle

Shown is a representative silver stained gel (A), the unchanged abundance of laminin (B) and the increased abundance in collagen VI (C, D, E). Statistical analysis of immuno-decoration was performed with Student's *t*-test (mean values \pm SEM; unpaired; $n=4$, $*p\leq 0.05$). The immunofluorescence microscopy shows the labelling of the extracellular matrix in wild-type and *mdx-4cv* *gastrocnemius* muscle using antibodies to collagen VI (D, E). Nuclei were counter-stained with the DNA binding dye bis-benzimide Hoechst 33342.

*Image from Murphy et al., 2015b

3.2.4 Gel electrophoretic analysis of chemically cross-linked muscle microsomes

In order to optimise the ratio of protein to XL, microsomal fractions were treated with increasing amounts of XL from 0.1 μg XL per mg protein up to 10 μg XL per mg protein. Increasing amounts of XL induced the appearance of a band at approximately 150 kDa as determined by silver stain analysis of one-dimensional gels in both wild-type and dystrophic membranes. In addition, more intense protein staining was evident at high molecular masses with increasing amounts of XL, especially at 5 μg , 7.5 μg and 10 μg XL per mg protein, suggesting a potential shift of protein complexes to higher molecular masses, as depicted in Figure 3.10. Based upon these results 10 μg XL per mg protein was chosen for the main study.

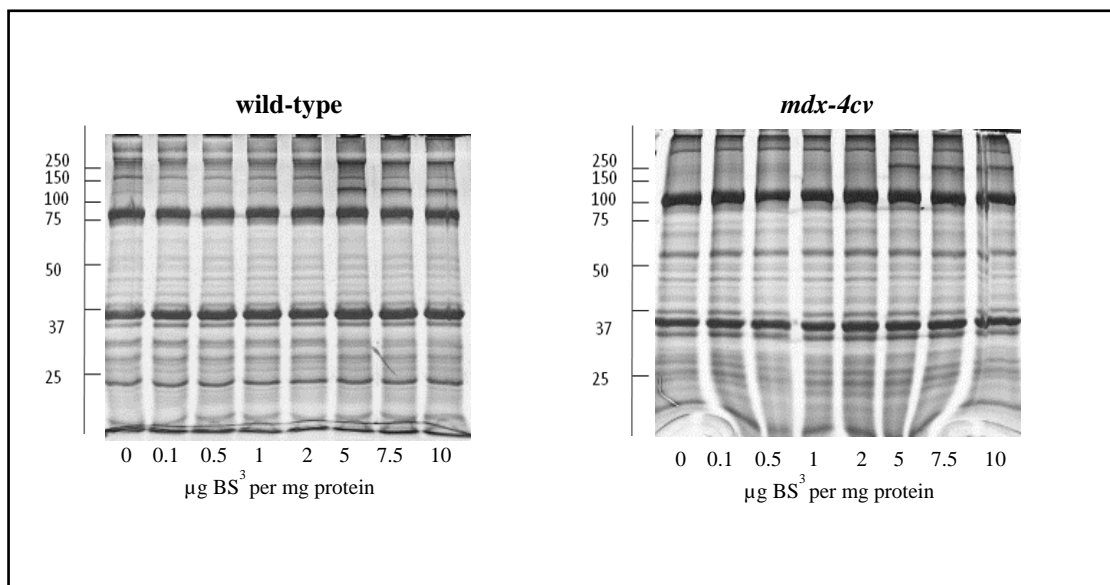


Figure 3.10: Gel based chemical cross-linking analysis of skeletal muscle microsomes

Shown are silver stained SDS-PAGE gels which represent the analysis of wild-type and *mdx-4cv* microsomes that were incubated with 0, 0.1, 0.5, 1, 2, 5, 7.5 and 10 μg BS³ XL per mg protein. Molecular mass standards (kDa) are indicated on the left-hand-side of the gel image.

3.2.5 Mass spectrometric identification of proteins with altered electrophoretic mobility

Based on the initial optimisation study, wild-type and *mdx-4cv* microsomes were incubated with either 0 μg XL per mg protein (control) or 10 μg XL per mg protein (cross-linked) (n=4 for each condition) and separated on one-dimensional SDS-PAGE gels. As illustrated in Figure 3.11, each lane was divided into five sections, labelled A-E, and trypsin-digested, and the resulting peptide populations were analysed by mass spectrometry. Qualitative data analysis identified a total of 346 proteins in wild-type samples (A-E inclusive) and a total of 370 proteins in *mdx-4cv* samples (A-E inclusive). Venn diagrams were used to identify common and unique proteins for wild-type control versus cross-linked samples for each gel zone A-E, and for *mdx-4cv* control versus cross-linked samples for each gel zone A-E. Only proteins identified by two or more unique peptides were used in the analysis. For the identification of common versus unique proteins, proteins were only considered to be unique if they were detected in all four replicates of one condition and in none of the four replicates in the other condition. Proteins which are considered common or shared between control and cross-linked lanes are those which are detected in all four of the control replicates and all four of the cross-linked replicates for a given gel piece. Figure 3.11 summarises these results and suggests that a considerable number of proteins exhibit tight protein-protein interaction patterns that can be stabilized by incubation with an XL agent. Although the majority of microsomal proteins did not undergo a drastic alteration in electrophoretic mobility following XL treatment, distinct cohorts of protein species do exhibit a BS³-dependent shift to higher molecular masses. The focus of this proteomic investigation was on the class of very high-molecular-mass complexes, denoted A-C, where the most visible changes in protein banding patterns is seen and where the highest number of proteins uniquely found in cross-linked samples is evident.

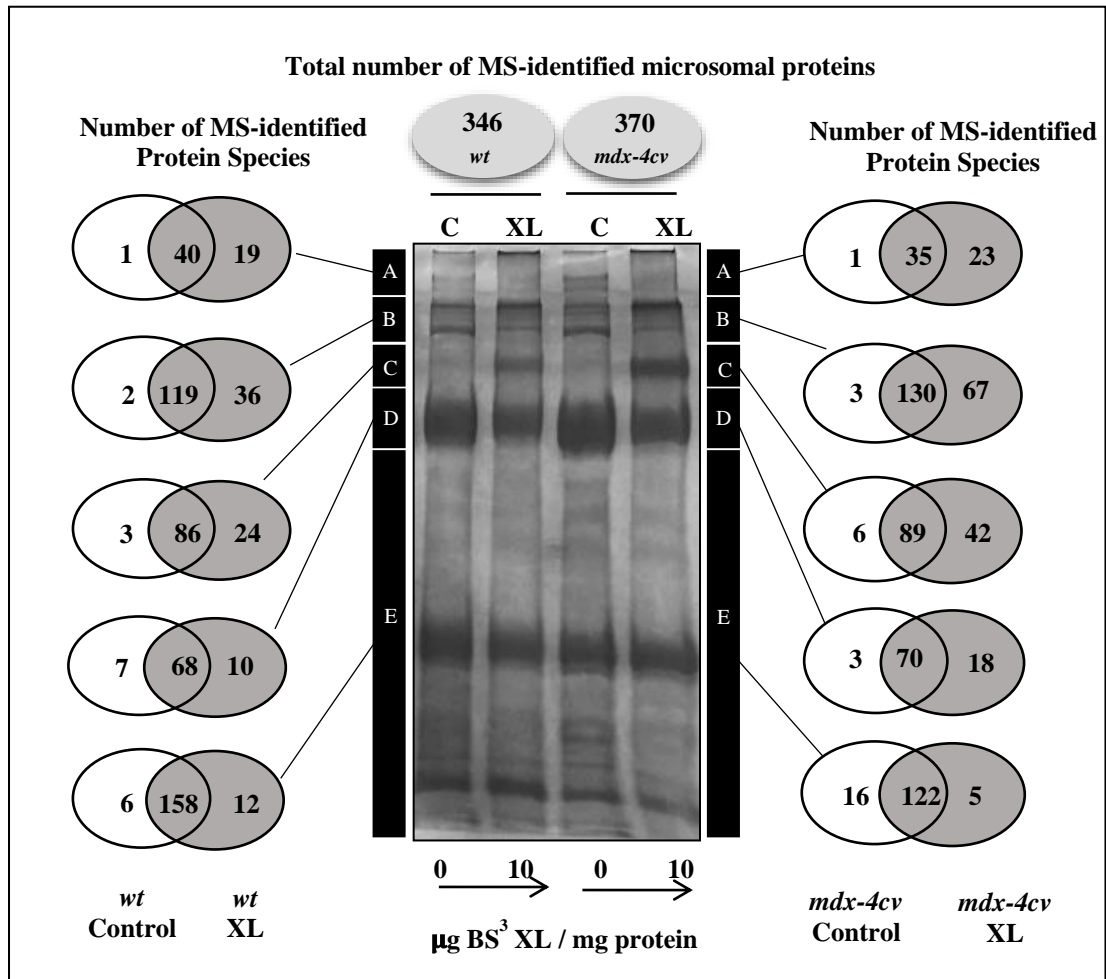


Figure 3.11: Mass spectrometric identification of cross-linked muscle proteins with an altered electrophoretic mobility

Shown is a Coomassie-stained SDS-PAGE gel with chemically cross-linked microsomes from wild-type versus dystrophic *mdx-4cv* skeletal muscle. Lanes 1 to 4 are non-treated wild-type muscle versus 10 $\mu\text{g BS}^3/\text{mg}$ protein-incubated wild-type muscle versus non-treated *mdx-4cv* muscle versus 10 $\mu\text{g BS}^3/\text{mg}$ protein-incubated *mdx-4cv* muscle preparations, respectively. The number of common and unique MS-identified proteins in the high to low molecular mass zones A-E of the analysed gel lanes is illustrated by Venn diagrams.

3.2.6 Mass spectrometric identification and bioinformatics analysis of altered protein interactions in muscular dystrophy in gel zone A

The comparison of proteins found exclusively in wild-type cross-linked samples in gel zone A with the proteins found exclusively in *mdx-4cv* cross-linked samples in gel zone A identified 11 proteins unique to wild-type samples, 15 proteins unique to *mdx-4cv* samples and 8 proteins in common as shown in Tables 3.3, 3.4 and 3.5 respectively. The detection of the Dp427 full-length isoform of dystrophin solely in wild-type samples confirmed the mutant status of the *mdx-4cv* mouse used. Other proteins of the DGC which were expected to cross-link with dystrophin were not detected. However, this is most likely due to their relatively low abundance and hydrophobicity, which are particular issues for gel electrophoretic analyses. However, delta-sarcoglycan was detected in gel zone B in both wild-type and *mdx-4cv* cross-linked microsomes (Table 3.8). Perilipin-4, a member of the perilipin family of proteins which associate with the surface of lipid droplets, was also detected in the wild-type cross-linked samples. This finding is consistent with previous immunofluorescence microscopy which revealed that perilipin-4 was located at or close to the muscle sarcolemma (Pourteymour et al., 2015). Additional proteins with a tendency to form large protein clusters in healthy skeletal muscle include molecular chaperones (HSP-90), metabolic enzymes (adenylate kinase isoenzyme 1), structural proteins (myosin-11) and transporters (myoglobin). The 15 proteins exclusively detected in *mdx-4cv* cross-linked microsomes suggest potential alterations in protein interactions in muscular dystrophy. As shown in Figure 3.12, STRING analysis of these proteins identifies two major protein clusters; one of the structural proteins myosin-3, myosin-9, vimentin, tubulin-beta-5, actin and the scaffolding protein caveolin-1, and another of mitochondrial enzymes including trifunctional enzyme subunit alpha, isoform 2 of 2-oxoglutarate dehydrogenase, elongation factor Tu, trifunctional enzyme subunit beta and dihydrolipoyllysine-residue succinyltransferase component of 2-oxoglutarate dehydrogenase complex. Also of interest is the identification of the membrane repair protein myoferlin.

Table 3.3: Mass spectrometric identification of proteins with a reduced electrophoretic mobility detected in gel zone A following chemical cross-linking of the microsomal fraction from wild-type mouse skeletal muscle

Accession	Protein Name	% Coverage	Unique peptides
P11531	Dystrophin, Dp427	5.98	17
Q3V1D3	AMP deaminase 1	19.06	9
P11499	Heat shock protein HSP 90-beta	8.98	6
O08638-2	Isoform 2 of Myosin-11	5.83	6
Q9Z1E4	Glycogen [starch] synthase, muscle	8.27	5
Q91YQ5	Dolichyl-diphosphooligosaccharide--protein glycosyltransferase subunit 1	9.05	4
Q9R0Y5	Adenylate kinase isoenzyme 1	23.2	3
P97447	Four and a half LIM domains protein 1	11.07	3
P43274	Histone H1.4	15.53	2
P04247	Myoglobin	21.43	2
O88492	Perilipin-4	12.83	2

Table 3.4: Mass spectrometric identification of proteins with a reduced gel electrophoretic mobility detected in gel zone A following chemical cross-linking of the microsomal fraction from *mdx-4cv* mouse skeletal muscle

Accession	Protein Name	% Coverage	Unique peptides
Q8BMS1	Trifunctional enzyme subunit alpha, mitochondrial	19.92	13
Q8VDD5	Myosin-9	7.4	13
Q7TQ48	Sarcalumenin	17.25	12
Q60597-2	Isoform 2 of 2-oxoglutarate dehydrogenase, mitochondrial	14.71	12
Q60847-4	Isoform 4 of Collagen alpha-1(XII) chain	5.1	7
Q8BFR5	Elongation factor Tu, mitochondrial	16.81	6
Q99JY0	Trifunctional enzyme subunit beta, mitochondrial	12.84	6
Q9D2G2	Dihydrolipoyllysine-residue succinyltransferase component of 2-oxoglutarate dehydrogenase complex, mitochondrial	8.37	4
Q7TSH2	Phosphorylase b kinase regulatory subunit beta	5.25	4
P13541	Myosin-3	19.38	3
P49817-2	Isoform 2 of Caveolin-1	19.05	3
Q69ZN7-4	Isoform 4 of Myoferlin	1.92	3
P60710	Actin, cytoplasmic 1	26.4	2
P99024	Tubulin beta-5 chain	15.32	2
P20152	Vimentin	9.23	2

Table 3.5: Mass spectrometric identification of proteins with a reduced gel electrophoretic mobility in gel zone A following chemical cross-linking of the microsomal fraction from both wild-type and *mdx-4cv* mouse skeletal muscle

Accession	Protein Name	% Coverage <i>wt</i>	Unique peptides <i>wt</i>	% Coverage <i>mdx-4cv</i>	Unique peptides <i>mdx-4cv</i>
Q91Z83	Myosin-7	32.87	25	25.68	17
Q8CAQ8-2	Isoform 2 of MICOS complex subunit Mic60	14.75	8	24.4	13
Q9D6R2	Isocitrate dehydrogenase [NAD] subunit alpha, mitochondrial	21.58	6	13.11	4
P13542	Myosin-8	45.07	6	38.26	4
Q02788	Collagen alpha-2(VI) chain	5.13	5	8.03	7
P10493	Nidogen-1	3.05	3	1.77	2
P0CG49	Polyubiquitin-B	32.79	2	32.79	2
P68372	Tubulin beta-4B chain	17.3	2	15.28	2

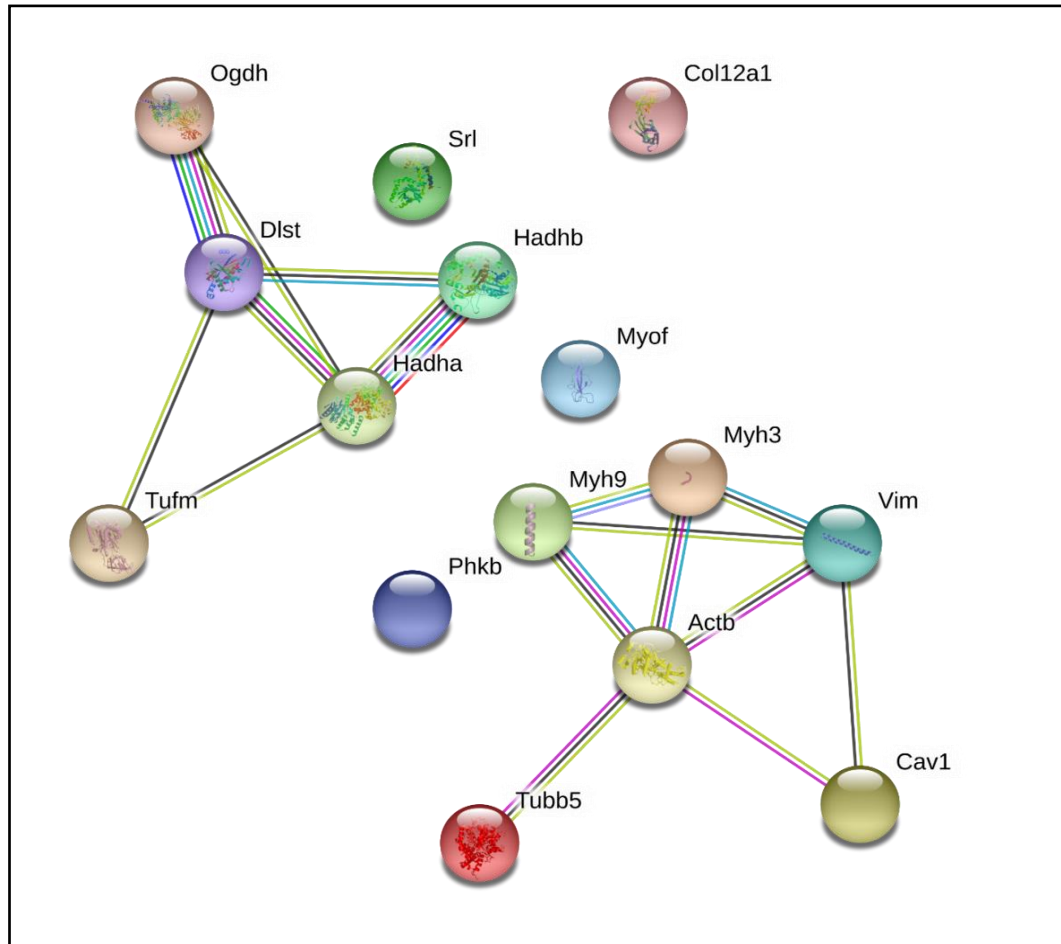


Figure 3.12: Bioinformatics analysis of proteomic changes detected in gel zone A in the microsomal fraction from dystrophic muscle

Shown are the findings from the bioinformatics analysis of protein interactions using STRING software program.

3.2.7 Mass spectrometric identification and bioinformatics analysis of altered protein interactions in muscular dystrophy in gel zone B

The comparison of proteins found exclusively in wild-type cross-linked samples in gel zone B with the proteins found exclusively in *mdx-4cv* cross-linked samples in gel zone B identified 17 proteins unique to wild-type samples, 48 proteins unique to *mdx-4cv* samples and 19 proteins in common as shown in Tables 3.6, 3.7 and 3.8 respectively. Similar to gel zone A, the proteins detected in wild-type microsomes include transporters (long-chain fatty acid transport protein 1), molecular chaperones (60 kDa heat shock protein) and the sarcolemma-associated protein perilipin-4. Other proteins with a reduced electrophoretic mobility pattern include the cellular adhesion proteins membrane primary amine oxidase and integrin beta-1, the adaptor protein LIM domain-binding protein 3, and the mitochondrial proteins apoptosis-inducing factor 1, ATP synthase F(0) complex subunit B1, atypical kinase COQ8A, and succinate--CoA ligase [ADP/GDP-forming] subunit alpha. The largest number of proteins unique to *mdx-4cv* cross-linked microsomes was detected in gel zone B. Augmented tendency for oligomerisation was seen for proteins associated with the mitochondria, including succinate-Coenzyme A ligase, electron transfer flavoprotein beta polypeptide, CDGSH iron-sulfur domain-containing protein 1, acyl-Coenzyme A dehydrogenase, and glycerol-3-phosphate dehydrogenase 1, which may indicate metabolic alterations in the dystrophic skeletal muscle. STRING analysis, as depicted in Figure 3.13, identified enriched levels of proteins associated with the proteasome and with protein processing in the endoplasmic reticulum, including 26S proteasome non-ATPase regulatory subunit 1, 26S proteasome non-ATPase regulatory subunit 2, 26S proteasome regulatory subunit 8, ATP-binding cassette sub-family B member 8, calnexin, UDP-glucose glycoprotein glucosyltransferase 1 and hypoxia up-regulated protein 1, indicating a potential increase in molecular chaperoning activity to limit proteotoxic effects in the dystrophin deficient muscle. Another interesting protein cluster is that of the integrins integrin alpha-7, integrin beta-2 and isoform 2 of integrin alpha-M with alpha-actinin-2 and vimentin.

Table 3.6: Mass spectrometric identification of proteins with a reduced gel electrophoretic mobility detected in gel zone B following chemical cross-linking of the microsomal fraction from wild-type mouse skeletal muscle

Accession	Protein Name	% Coverage	Unique peptides
O70423	Membrane primary amine oxidase	13.2	8
P63038	60 kDa heat shock protein, mitochondrial	13.26	5
Q6PA06	Atlastin-2	11.66	5
Q91ZJ5-2	Isoform 2 of UTP--glucose-1-phosphate uridylyltransferase	13.68	5
P61027	Ras-related protein Rab-10	27.5	5
Q9Z0X1	Apoptosis-inducing factor 1, mitochondrial	10.62	4
P43274	Histone H1.4	15.07	4
Q9CQQ7	ATP synthase F(0) complex subunit B1, mitochondrial	11.72	3
Q60936	Atypical kinase COQ8A, mitochondrial	5.43	3
P09055	Integrin beta-1	5.76	3
P18572-2	Isoform 2 of Basigin	11.72	3
O88492	Perilipin-4	16.75	3
Q9WUM5	Succinate--CoA ligase [ADP/GDP-forming] subunit alpha, mitochondrial	12.43	3
Q02053	Ubiquitin-like modifier-activating enzyme 1	3.69	3
Q8CGC7	Bifunctional glutamate/proline--tRNA ligase	1.85	2
Q9JKS4-4	Isoform 4 of LIM domain-binding protein 3	4.18	2
Q60714	Long-chain fatty acid transport protein 1	3.87	2

Table 3.7: Mass spectrometric identification of proteins with a reduced gel electrophoretic mobility detected in gel zone B following chemical cross-linking of the microsomal fraction from *mdx-4cv* mouse skeletal muscle

Accession	Protein Name	% Coverage	Unique peptides
Q6P5E4	UDP-glucose: glycoprotein glucosyltransferase 1	16.63	21
Q9JI91	Alpha-actinin-2	27.4	14
O35129	Prohibitin-2	44.15	11
P20152	Vimentin	31.76	10
O08749	Dihydrolipoyl dehydrogenase, mitochondrial	22	9
P70170-3	Isoform SUR2C of ATP-binding cassette sub-family C member 9	8.6	9
Q9DCN2-2	Isoform 2 of NADH-cytochrome b5 reductase 3	38.49	8
Q9D024	Coiled-coil domain-containing protein 47	20.08	7
Q9DBG6	Dolichyl-diphosphooligosaccharide--protein glycosyltransferase subunit 2	20.29	7
Q3U7R1	Extended synaptotagmin-1	9.25	7
Q3MI48-2	Isoform 2 of Junctional sarcoplasmic reticulum protein 1	42.81	7
Q8BMK4	Cytoskeleton-associated protein 4	14.26	6
P11835	Integrin beta-2	12.06	6
Q61738-4	Isoform Alpha-7X2A of Integrin alpha-7	7.53	6
P51174	Long-chain specific acyl-CoA dehydrogenase, mitochondrial	16.74	6
Q8JZQ2	AFG3-like protein 2	6.61	5
Q61102	ATP-binding cassette sub-family B member 7, mitochondrial	7.31	5
P35564	Calnexin	14.21	5
Q6PA06-2	Isoform 2 of Atlastin-2	18.04	5
P18826-2	Isoform 2 of Phosphorylase b kinase regulatory subunit alpha, skeletal muscle isoform	5.15	5
Q91WC3	Long-chain-fatty-acid--CoA ligase 6	8.75	5
Q921I1	Serotransferrin	8.61	5
Q3TXS7	26S proteasome non-ATPase regulatory subunit 1	6.4	4
P62908	40S ribosomal protein S3	18.11	4
P16015	Carbonic anhydrase 3	21.15	4
O54724	Caveolae-associated protein 1	14.54	4
Q8CHS7	Dehydrogenase/reductase SDR family member 7C	15.76	4
Q9DCW4	Electron transfer flavoprotein subunit beta	20	4
P13707	Glycerol-3-phosphate dehydrogenase [NAD(+)], cytoplasmic	12.03	4
Q9JKR6	Hypoxia up-regulated protein 1	5.61	4
P05555-2	Isoform 2 of Integrin alpha-M	5.89	4
Q9Z2I9	Succinate--CoA ligase [ADP-forming] subunit beta, mitochondrial	7.56	4
P68369	Tubulin alpha-1A chain	27.49	4
P68368	Tubulin alpha-4A chain	25.45	4
Q8VDM4	26S proteasome non-ATPase regulatory subunit 2	4.74	3
P17182	Alpha-enolase	16.13	3

Q9DCX2	ATP synthase subunit d, mitochondrial	25.47	3
Q9CXJ4	ATP-binding cassette sub-family B member 8, mitochondrial	5.44	3
P58252	Elongation factor 2	4.31	3
Q923T9-3	Isoform 3 of Calcium/calmodulin-dependent protein kinase type II subunit gamma	8.69	3
Q8BI84-3	Isoform 3 of Melanoma inhibitory activity protein 3	5.51	3
P51150	Ras-related protein Rab-7a	18.36	3
P62196	26S proteasome regulatory subunit 8	10.84	2
P62702	40S ribosomal protein S4, X isoform	8.37	2
Q91WS0	CDGSH iron-sulfur domain-containing protein 1	22.22	2
Q9CQC9	GTP-binding protein SAR1b	11.11	2
Q922Q8	Leucine-rich repeat-containing protein 59	8.14	2
Q9D1G1	Ras-related protein Rab-1B	28.86	2

Table 3.8: Mass spectrometric identification of proteins with a reduced gel electrophoretic mobility in gel zone B following chemical cross-linking of the microsomal fraction from both wild-type and *mdx-4cv* mouse skeletal muscle

Accession	Protein Name	% Coverage <i>wt</i>	Unique peptides <i>wt</i>	% Coverage <i>mdx-4cv</i>	Unique peptides <i>mdx-4cv</i>
Q8BW75	Amine oxidase [flavin-containing] B	23.27	11	36.15	15
G5E829	Plasma membrane calcium-transporting ATPase 1	12.79	10	12.7	13
P97807-2	Isoform Cytoplasmic of Fumarate hydratase, mitochondrial	31.05	9	32.98	15
Q8BRK9	Alpha-mannosidase 2x	9.55	8	9.55	8
Q9DB73	NADH-cytochrome b5 reductase 1	30.16	7	28.85	8
Q6GQT9	Nodal modulator 1	6.43	7	9.64	10
P05201	Aspartate aminotransferase, cytoplasmic	17.19	6	18.16	7
Q8C7X2-2	Isoform 2 of ER membrane protein complex subunit 1	7.75	6	12.47	9
P48678-2	Isoform C of Prelamin-A/C	13.07	6	28.05	13
Q99MR8	Methylcrotonoyl-CoA carboxylase subunit alpha, mitochondrial	8.79	5	9.62	5
Q9CQF9	Prenylcysteine oxidase	15.05	5	17.03	6
P67778	Prohibitin	24.63	5	21.69	5
Q62351	Transferrin receptor protein 1	7.86	5	18.22	11
Q9CRD2	ER membrane protein complex subunit 2	17.51	4	11.78	3
P28665	Murinoglobulin-1	3.32	4	5.01	6
P82347	Delta-sarcoglycan	9	2	9	2
Q3TDQ1	Dolichyl-diphosphooligosaccharide--protein glycosyltransferase subunit STT3B	2.55	2	5.35	3
Q9QYG0-2	Isoform 2 of Protein NDRG2	8.96	2	8.96	2
Q9CRB9	MIC complex subunit Mic19	8.37	2	21.59	6

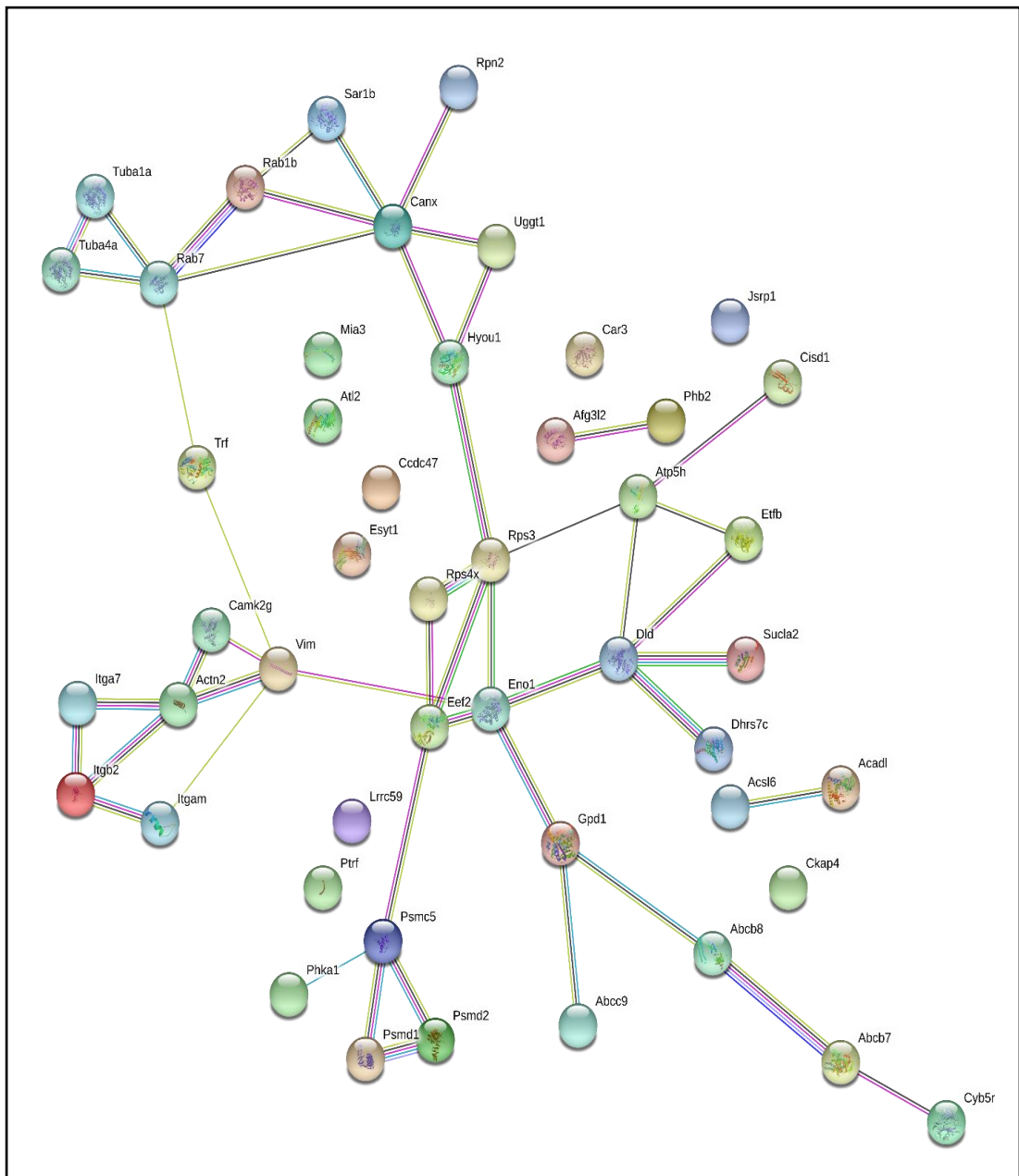


Figure 3.13: Bioinformatics analysis of proteomic changes detected in gel zone B in the microsomal fraction from dystrophic muscle

Shown are the findings from the bioinformatics analysis of protein interactions using STRING software program.

3.2.8 Mass spectrometric identification and bioinformatics analysis of altered protein interactions in muscular dystrophy in gel zone C

The comparison of proteins found exclusively in wild-type cross-linked samples in gel zone C with the proteins found exclusively in *mdx-4cv* cross-linked samples in gel zone C identified 12 proteins unique to wild-type samples, 30 proteins unique to *mdx-4cv* samples and 12 proteins in common as shown in Tables 3.9, 3.10 and 3.11 respectively. The detection of β -sarcoglycan in wild-type cross-linked samples in gel zone C suggests a potential for β -sarcoglycan to form protein complexes, especially since it is detected in both wild-type control and cross-linked samples in gel zone E. Oligomerisation is also evident for the mitochondrial proteins medium-chain specific acyl-CoA dehydrogenase, elongation factor Tu, and succinate--CoA ligase [ADP-forming] subunit beta. Detected here and in wild-type cross-linked samples in gel zone B is isoform 2 of basigin, a multi-functional transmembrane protein involved in spermatogenesis, neural network development, tumour invasion, stimulation of fibroblasts to produce matrix metalloproteinases and targeting of the monocarboxylate transporters SLC16A1, SLC16A3, SLC16A8 and SLC16A11 to the plasma membrane. STRING analysis of the 30 proteins exclusively detected in *mdx-4cv* cross-linked samples reveals a major cluster of mitochondrial proteins, which are particularly associated with the citric acid cycle and respiratory electron transport, as illustrated in Figure 3.14. These proteins include dihydrolipoyllysine-residue succinyltransferase component of 2-oxoglutarate dehydrogenase complex, fumarate hydratase, isocitrate dehydrogenase, ATP synthase subunit delta, NADH dehydrogenase [ubiquinone] 1 alpha subcomplex subunit 12 and NADH dehydrogenase [ubiquinone] iron-sulfur protein 3. Also of significance is the detection of flotillin-1 and flotillin-2, which act as scaffolding proteins within caveolar membranes.

Table 3.9: Mass spectrometric identification of proteins with a reduced gel electrophoretic mobility detected in gel zone C following chemical cross-linking of the microsomal fraction from wild-type mouse skeletal muscle

Accession	Protein Name	% Coverage	Unique peptides
P45952	Medium-chain specific acyl-CoA dehydrogenase, mitochondrial	16.63	6
Q3TVI8	Pre-B-cell leukemia transcription factor-interacting protein 1	9.22	5
P35293	Ras-related protein Rab-18	20.87	4
P60710	Actin, cytoplasmic 1	37.07	3
Q8BFR5	Elongation factor Tu, mitochondrial	10.4	3
Q61743	ATP-sensitive inward rectifier potassium channel 11	5.9	2
P82349	Beta-sarcoglycan	10	2
P16015	Carbonic anhydrase 3	8.08	2
Q8BSY0-2	Isoform 2 of Aspartyl/asparaginyl beta-hydroxylase	14.01	2
P18572-2	Isoform 2 of Basigin	8.42	2
Q9DB73-2	Isoform 2 of NADH-cytochrome b5 reductase 1	8.33	2
Q9Z2I9	Succinate--CoA ligase [ADP-forming] subunit beta, mitochondrial	4.1	2

Table 3.10: Mass spectrometric identification of proteins with a reduced gel electrophoretic mobility detected in gel zone C following chemical cross-linking of the microsomal fraction from *mdx-4cv* mouse skeletal muscle

Accession	Protein Name	% Coverage	Unique peptides
O08917	Flotillin-1	39.95	14
Q60634-3	Isoform 3 of Flotillin-2	43.27	12
Q9D2G2	Dihydrolipoyllysine-residue succinyltransferase component of 2-oxoglutarate dehydrogenase complex, mitochondrial	26.21	12
Q8R3Z5-4	Isoform 4 of Voltage-dependent L-type calcium channel subunit beta-1	27.86	10
P54071	Isocitrate dehydrogenase [NADP], mitochondrial	20.35	8
Q8C7X2-2	Isoform 2 of ER membrane protein complex subunit 1	8.55	8
Q02053	Ubiquitin-like modifier-activating enzyme 1	9.26	7
Q9DB73	NADH-cytochrome b5 reductase 1	19.02	6
P97807-2	Isoform Cytoplasmic of Fumarate hydratase, mitochondrial	16.27	6
P48678-2	Isoform C of Prelamin-A/C	10.8	5
P58281	Dynamin-like 120 kDa protein, mitochondrial	6.46	5
Q64727	Vinculin	6.1	5
P68369	Tubulin alpha-1A chain	30.6	4
Q9Z0X1	Apoptosis-inducing factor 1, mitochondrial	10.13	4
Q3U7R1-2	Isoform 2 of Extended synaptotagmin-1	5.49	4
P68372	Tubulin beta-4B chain	31.46	3
Q9DCX2	ATP synthase subunit d, mitochondrial	19.88	3
P82347	Delta-sarcoglycan	14.88	3
Q9DCT2	NADH dehydrogenase [ubiquinone] iron-sulfur protein 3, mitochondrial	14.83	3
P35564	Calnexin	8.12	3
Q6DYE8	Ectonucleotide pyrophosphatase/phosphodiesterase family member 3	6.52	3
Q921I1	Serotransferrin	6.17	3
Q9D1G1	Ras-related protein Rab-1B	29.86	2
Q91WS0	CDGSH iron-sulfur domain-containing protein 1	22.22	2
P10126	Elongation factor 1-alpha 1	20.35	2
Q7TMF3	NADH dehydrogenase [ubiquinone] 1 alpha subcomplex subunit 12	20	2
Q9D3D9	ATP synthase subunit delta, mitochondrial	13.69	2
P53994	Ras-related protein Rab-2A	11.79	2
P01868	Ig gamma-1 chain C region secreted form	6.79	2
P28650	Adenylosuccinate synthetase isozyme 1	5.69	2

Table 3.11: Mass spectrometric identification of proteins with a reduced gel electrophoretic mobility in gel zone C following chemical cross-linking of the microsomal fraction from both wild-type and *mdx-4cv* mouse skeletal muscle

Accession	Protein Name	% Coverage <i>wt</i>	Unique peptides <i>wt</i>	% Coverage <i>mdx-4cv</i>	Unique peptides <i>mdx-4cv</i>
O35129	Prohibitin-2	35.12	9	35.12	9
Q91ZJ5-2	Isoform 2 of UTP--glucose-1-phosphate uridylyltransferase	14.69	7	14.69	6
P51150	Ras-related protein Rab-7a	28.5	5	23.19	4
Q9CY27	Very-long-chain enoyl-CoA reductase	16.23	5	17.21	8
P17182	Alpha-enolase	23.04	4	49.31	14
P51174	Long-chain specific acyl-CoA dehydrogenase, mitochondrial	10.93	4	14.88	6
O54734	Dolichyl-diphosphooligosaccharide--protein glycosyltransferase 48 kDa subunit	7.03	3	7.03	3
Q9DCN2-2	Isoform 2 of NADH-cytochrome b5 reductase 3	10.43	2	13.67	5
Q6Q477-2	Isoform 2 of Plasma membrane calcium-transporting ATPase 4	9.03	2	8.31	2
Q9CRB9	MIC complex subunit Mic19	11.45	2	16.74	3
P99024	Tubulin beta-5 chain	18.02	2	33.56	3
P20152	Vimentin	9.87	2	32.83	10

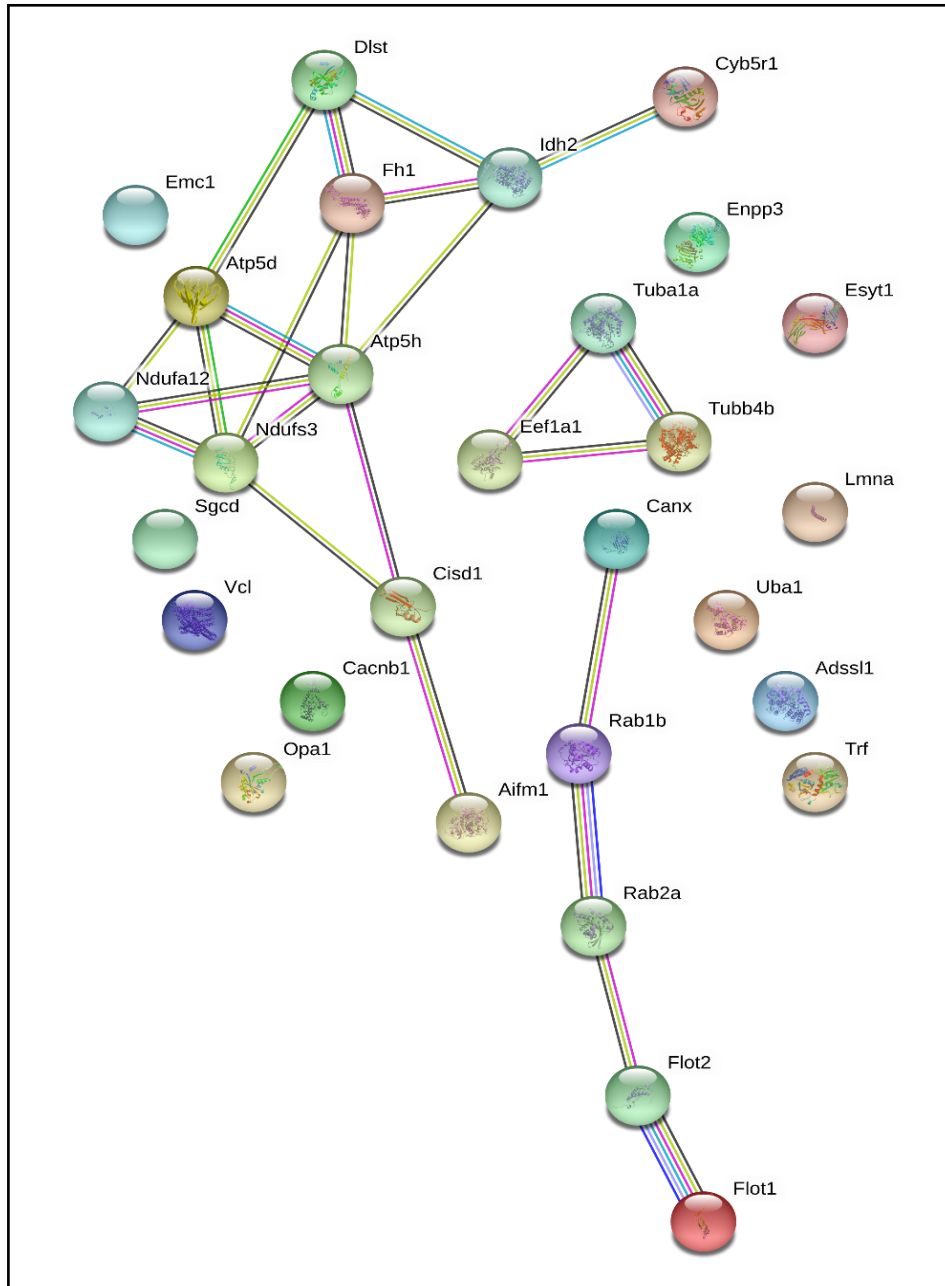


Figure 3.14: Bioinformatics analysis of proteomic changes detected in gel zone C in the microsomal fraction from dystrophic muscle

Shown are the findings from the bioinformatics analysis of protein interactions using STRING software program.

3.3 Discussion

Dystrophin is a sarcolemmal associated protein which together with a variety of other regulatory proteins forms the DGC, which acts as a stabilising bridge between intracellular actin and the extracellular matrix (Perronnet and Vaillend, 2010). DMD is characterised by mutations in the 79-exon spanning *Dmd* gene which encodes for dystrophin (Flanigan et al., 2009). Mutations in this gene result in negligible levels of dystrophin, causing destabilisation of the sarcolemma of muscle fibres, which leads to increased susceptibility to mechanical stress. Although this loss of dystrophin is the underlying pathobiochemical defect, it also triggers a number of secondary abnormalities; one of the most significant being that of myofibrosis (Zhou and Lu, 2010). A longitudinal study of 25 Duchenne patients examined over a 10-year period revealed that among all the pathological features of DMD; myofibre atrophy, necrosis and fatty deposition, only endomysial fibrosis correlated significantly with poor motor performance (Desguerre et al., 2009). Thus, alterations in the extracellular matrix surrounding degenerating fibres is a clinical characteristic of X-linked muscular dystrophy. The proteomic analysis conducted here shows a high degree of fibrosis in the hind leg of the *mdx-4cv* model, thus linking the mass spectrometric identification of decreased dystrophin expression with the infiltration of connective tissue.

The majority of previous comparative proteomic studies have failed to detect reduced expression of dystrophin in whole skeletal muscle extracts. This has been attributed to the technical difficulties associated with identifying dystrophin by proteomic means, such as its low abundance, large molecular size, close association with the sarcolemmal membrane and its existence within a heterogeneous protein complex (Brown et al., 2012). In contrast, using a careful extraction protocol and highly sensitive label-free LC-MS/MS, identification of the Dp427 isoform of dystrophin as the most reduced protein in *mdx-4cv* hind-limb has been achieved here. In addition, another member of the DGC, the adaptor protein α 1-syntrophin, was also identified as having reduced expression in dystrophic skeletal muscle. Hence the reduced density of key components of the DGC can now be unequivocally linked to the secondary abnormalities in ion homeostasis, cytoskeletal restructuring, calcium homeostasis and myofibrosis.

A number of other proteins of interest also displayed reduced abundance in dystrophic tissue. In particular, reduced levels of parvalbumin correlates the mechanical instability caused by dystrophin absence with the calcium hypothesis of

DMD pathogenesis, given that reduced expression of parvalbumin indicates impaired cytosolic buffering. Thus, calcium is a double-edged sword in the disease in that micro-rupturing of the weakened sarcolemma enables the influx of Ca^{2+} into the cytosol where they reach excessive levels given the impaired calcium buffering capacity of dystrophic fibres. Reduced densities of myoglobin, carbonic anhydrase CA3, glutathione S-transferase and fatty acid binding protein FABP-3 are also observed. Such alterations in the muscle proteome suggest altered CO_2 -removal and leakage from damaged and/or necrotic muscle fibres, modified biotransformation capacity, and reductions in oxygen transportation and fatty acid metabolism respectively.

While the mass spectrometry data correlates well with the two principal hypotheses of DMD pathobiochemistry (structural and calcium hypotheses), it also highlights the important role of myofibrosis in X-linked muscular dystrophy, evident by the large number of fibrotic proteins displaying increased abundance in dystrophic skeletal muscle. Crucial extracellular matrix proteins with an increased concentration were identified as collagen $\alpha 1(\text{VI})$ chain, collagen $\alpha 2(\text{VI})$ chain, collagen $\alpha 1(\text{I})$ chain, fibronectin, biglycan, asporin, decorin, prolargin, mimecan and lumican. This dramatic increase in components of the extracellular matrix indicates infiltration of connective tissue and the replacement of skeletal muscle with non-functional fibrotic tissue (Wynn, 2008). Thus, the simultaneous identification of reduced levels of dystrophin and elevated levels of fibrotic proteins within the same sample and same analytical run positions dystrophin in its proper pathophysiological context. Elevated abundance of the extracellular matrix protein biglycan agrees with the idea of reactive myofibrosis in response to dystrophin deficiency. However, biglycan has also been shown to influence the expression and sarcolemmal localisation of several dystrophin-associated glycoproteins including nNOS, syntrophin and dystrobrevin, with biglycan-null mice displaying a mildly dystrophic phenotype (Nastase et al., 2012). Thus, elevated abundance of this proteoglycan may represent a compensatory mechanism to help counteract alterations in the DGC in dystrophic skeletal muscle. Indeed intraperitoneal injection of recombinant human biglycan into *mdx* mice increased the levels of utrophin, γ -sarcoglycan, nNOS and $\beta 2$ -syntrophin at the sarcolemma and improved muscle function, determined by a reduction in force drop after successive eccentric contractions (Amenta et al., 2011).

The dystrophinopathy-induced elevation of collagen type VI is important given that this protein is a major filament-forming collagen of the interstitial matrix that closely interacts with a number of other fibrotic proteins; including other collagens, fibronectin, biglycan, decorin and integrins (Lieber and Ward, 2013). Elevated levels of fibrinogen as identified by this study have also been identified in dystrophic skeletal muscle from animal models and clinical samples, where it has been shown to precede the deposition of collagen (Vidal et al., 2008). Thus, fibrinogen is suggested to represent a key driver of fibrosis in dystrophic muscle, a hypothesis largely supported by the observation that fibrinogen deficient *mdx* mice display significantly reduced levels of collagen (Vidal et al., 2008). While fibrosis in animal models has been largely reported in the severely dystrophic diaphragm (Holland et al., 2015a, Ishizaki et al., 2008), this study highlights the existence of elevated levels of fibrosis-associated proteins in the more moderately affected limb muscles. This supports the concept that continuous regeneration/degeneration cycles in skeletal muscle results in chronic inflammation and infiltration of adipose and connective tissue (Mann et al., 2011). Figure 3.9 illustrates not only elevated expression of collagen VI but also a high degree of central nucleation; a hallmark of regenerated muscle fibres. At present, only palliative treatments are available for DMD patients and thus much research has focused on developing a primary treatment of DMD using strategies such as exon-skipping, stem cell transplantation and mini-dystrophin gene therapy. However, treatments aimed at diminishing the development of fibrosis may help prevent disease progression, while also increasing the success of cell- and gene-based therapies by augmenting the amount of muscle available for therapy and repair (Kharraz et al., 2014, Pessina et al., 2014).

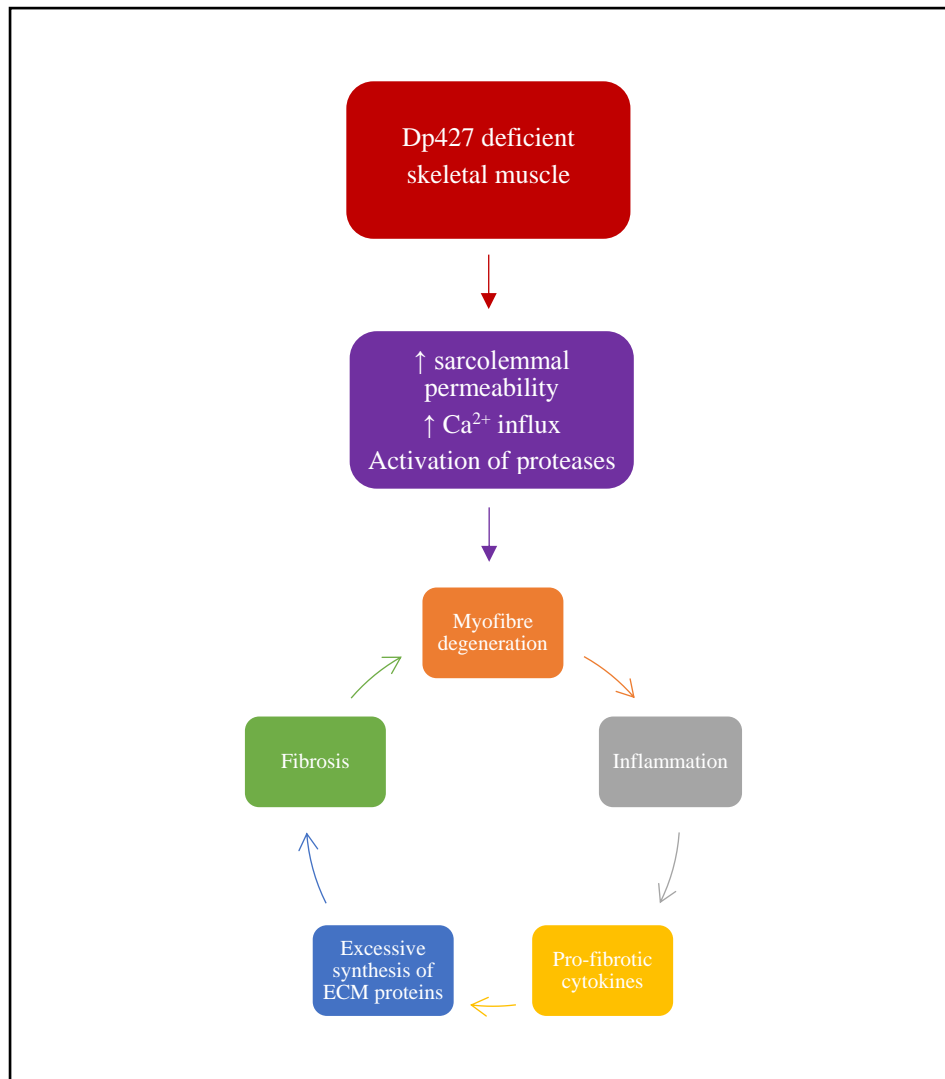


Figure 3.15: Schematic illustrating the fibrotic process in Duchenne muscular dystrophy

Dystrophin deficiency disrupts the DGC of the cell membrane. Disruption of this stabilising protein network leads to increased susceptibility of the sarcolemma to contractile and mechanical strain and excessive Ca^{2+} influx. Elevated cytosolic Ca^{2+} levels activate proteases, such as the calpains, causing myofibre degeneration. This triggers an inflammatory response characterised by the secretion of pro-fibrotic cytokines. Subsequent excessive synthesis of extracellular matrix (ECM) proteins leads to tissue fibrosis which contributes directly to progressive muscle dysfunction.

The most highly increased protein was identified as myosin-10 (non-muscle myosin type IIB), an unconventional non-muscle type of myosin with specialised roles in cytokinesis (where it localises to both meiotic and mitotic spindles) (Woolner et al., 2008), regulation of the actin cytoskeleton, cell adhesion and cell migration (Vicente-Manzanares et al., 2009). Elevated levels of myosin-9 (non-muscle myosin type IIA) were also identified in this proteomic survey. Since myosin-9 exerts similar cellular functions to that of myosin-10 (Beach et al., 2014), their coordinated augmentation suggests enhanced cellular proliferation rates in dystrophic muscle (Hawke and Garry, 2001). This excessive proliferation leads to premature senescence of satellite cells, which in turn reduces the regenerative capacity of dystrophic skeletal muscle (Decary et al., 2000). In addition to roles in cellular functions, myosin-10 has also been identified as being a key regulator of collagen I synthesis. Collagen I is synthesised as a heterotrimer of two α 1(I) chains and one α 2(I) polypeptide, for which intact non-muscle myosin filaments are required (Cai et al., 2010). Thus, enhanced levels of myosin-9 and myosin-10 in dystrophic skeletal muscle indicates increased synthesis of components of the matrisome. This result correlates well with the observed increase in a number of proteins associated with the matrisome and extracellular matrix, seen in this study and other comparative surveys of dystrophic animal models (Holland et al., 2015a).

One of the major compensatory mechanisms employed by dystrophin-deficient muscle is an increase in cytoskeletal proteins to maintain sarcolemmal integrity during contractile and mechanical strain (Law et al., 1994). This hypothesis is supported by the observed increase in various tubulin isoforms (β 6, β 5, α -1A, β 4A, β 2A, α -1B, α -4A, and α 8 chains), desmin, vinculin, talin and vimentin. Annexins also play a major role in the continued maintenance of the cytoskeletal network and in providing structural integrity to the extracellular matrix. In this capacity elevated levels of the A1, A2, A5, A6, A7 and A11 isoforms of annexin may serve to further stabilise the cytoskeletal system in the absence of the Dp427 isoform of dystrophin. In particular, elevated levels of annexins A1, A2 and A5 suggest the initiation of sarcolemmal repair mechanisms to counteract micro-rupturing of the deteriorated muscle surface membrane system (McNeil et al., 2006, Bouter et al., 2011). This is further verified by the enhanced expression of dysferlin, a known binding partner of annexins A1 and A2 involved in the membrane repair process (Lennon et al., 2003). Another highly elevated protein in dystrophic hind-limb is the major anti-protease α 1-antitrypsin.

While it represents one of the most abundant serine proteases in the circulation it also has immuno-modulatory activities, in particular the suppression of inflammation (Jonigk et al., 2013). Thus, its increase in dystrophic tissue may be a protective reaction to limit inflammatory damage to dystrophin-deficient muscle fibres (Porter et al., 2002).

In modern proteomics 2D-GE coupled to mass spectrometric identification of proteins of interest offers a highly robust and accurate system for identification of proteomic alterations between normal and pathological conditions. However, this system does have significant limitations such as poor separation of hydrophobic and highly acidic or alkaline proteins (Bunai and Yamane, 2005). In addition, it is highly sensitive to the dynamic range of the sample and thus many low abundance proteins are poorly represented on 2D gels (Rabilloud et al., 2010). LC-MS/MS aims to overcome these short-comings and has been successfully used to identify vast numbers of proteins irrespective of their molecular weight, abundance, hydrophobicity and pI (Washburn et al., 2001). This has been exemplified by this proteomic survey in which a number of proteins of high molecular weight and hydrophobic proteins were identified using an LC-MS/MS based experimental procedure. The identification of extremely large proteins included obscurin, a giant myofibrillar protein of approximately 720 kDa (Young et al., 2001), the molecular mass of which would be challenging for gel electrophoresis-based proteomic analysis. Other proteins of interest which were resolved by LC-MS/MS analysis include the sarcolemmal Na^+/K^+ -ATPase, the sarcoplasmic reticulum Ca^{2+} -ATPase, the sarcoplasmic/endoplasmic reticulum RyR and the transverse tubule associated DHP. Such membrane associated receptors are highly hydrophobic and thus would be poorly represented in 2D gel based proteomic investigations. Thus, a combination of separation techniques prior to mass spectrometric identification may provide the optimal opportunity of identifying the maximum number of proteins in complex samples. The DHP is the voltage sensor for excitation-contraction coupling. In response to sarcolemmal depolarisation the DHP sends a signal to the RyR resulting in Ca^{2+} -release from the sarcoplasmic reticulum to trigger muscle contraction (Dulhunty et al., 2002). This interaction is responsible for all voluntary movement and cardiac contraction and respiration. The fast SERCA1 type Ca^{2+} -ATPase meanwhile induces muscle relaxation through the re-uptake of Ca^{2+} ions into the sarcoplasmic reticulum, while the Na^+/K^+ -ATPase is responsible for maintaining the resting potential over the sarcolemma. The increased

abundance of these four ion-regulating proteins suggests disturbances in the regulatory pathways of *mdx-4cv* hind limb muscles. It would appear that dystrophic, degenerating muscle fibres elevate the levels of essential voltage sensors, ion release channels and ion pumps to maintain optimum excitation-contraction-relaxation cycles and stabilise the resting membrane potential over the dystrophin-deficient sarcolemma (Dunn et al., 1995).

In addition to alterations in protein abundance, muscular dystrophy induced changes may also encompass alterations in protein oligomerisation and interaction patterns. In order to investigate this possibility, chemical cross-linking of microsomal fractions from crude skeletal muscle, followed by gel electrophoretic shift analysis and mass spectrometry was employed. Proteomic analyses were particularly focused on high molecular mass ranges of approximately 100 kDa or more, which represent various supramolecular assemblies of the muscle membrane system and its associated intra- and extra- cellular structures. Comparison of proteins exclusively detected in wild-type cross-linked microsomes with proteins exclusively detected in *mdx-4cv* cross-linked microsomes was used to determine muscular dystrophy associated changes in protein interaction. In gel zone A increased tendency for oligomerisation was found for myosin-9, myosin-3, vimentin, tubulin-beta-5 chain, actin and caveolin-1, indicating potential cytoskeletal re-structuring in response to dystrophin deficiency. The presence of embryonic myosin-3 in this protein cluster is indicative of the regenerative process seen in dystrophic skeletal muscle (Fitzsimons and Hoh, 1981). Although high levels of vimentin are usually only seen during the maturation of myotubes, this intermediate filament protein has recently been proposed as a universal marker of DMD as it shows elevated abundance in a range of tissue types from the severely affected diaphragm, to the moderately affected *extensor digitorum longus* muscle and the mildly affected *interosseus* muscle in the *mdx* mouse (Holland et al., 2015b), and in crude extracts from *mdx-4cv* brain tissue (Murphy et al., 2015c). Vimentin has the capacity to act synergistically to the intermediate filament desmin, and the increased abundance of vimentin (2.42-fold increase) and desmin (2.09-fold increase) detected in the mass spectrometric analysis of crude skeletal muscle in this study (Table 3.1), coupled with the reduced gel electrophoretic mobility of vimentin in dystrophic cross-linked microsomes and its potential oligomerisation with myosin, actin and tubulin, suggests a vimentin-associated support of the structural backbone of intermediate filaments. This may help to partially restore the load-bearing function

of contractile fibres in the absence of the DGC. Myoferlin is a calcium/phospholipid binding protein which is expressed during muscle development during which it facilitates myoblast fusion. However, it also plays a role in the plasmalemma repair process which enables re-sealing of membranes disturbed by mechanical stress, and levels of both myoferlin mRNA and protein have been shown to be increased in muscular dystrophy (Demonbreun et al., 2010, Murphy et al., 2015a). Therefore, the changes in myoferlin oligomerisation evident in this XL study are likely related to the initiation of cellular repair mechanisms, a process probably supported by the augmented interactions of myoferlin with various isoforms of myosin and actin.

Caveolin-1 is a member of the caveolin family of crucial structural proteins of caveolar membranes, which are vesicular invaginations of the plasma membrane involved in vesicular trafficking and signal transduction. A study by Hernández-Deviez and co-workers examined the trafficking of dysferlin in wild-type and caveolin1^{-/-} mouse embryonic fibroblasts. This study determined that while dysferlin is not absolutely dependent on caveolin to reach the plasma membrane, it is more efficiently retained at the plasma membrane in the presence of caveolin, as in caveolin-1 deficient cells dysferlin is internalised by endocytosis (Hernández-Deviez et al., 2008). Thus, increased oligomerisation of caveolin-1 may represent a protective mechanism in muscular dystrophy to facilitate membrane repair processes at the muscle sarcolemma. This is supported by the concomitant oligomerisation of myoferlin, another member of the ferlin family of membrane repair proteins. Increased numbers of caveolae have been detected in muscle biopsies from DMD patients (Repetto et al., 1999) which agrees with the increased abundance of caveolin-3 (Repetto et al., 1999) and caveolin-1 (Murphy et al., 2015a) detected in dystrophic skeletal muscle, and with the enhanced oligomerisation of caveolin-1 identified here in cross-linked dystrophin-deficient microsomes.

Another interesting protein cluster in the uppermost region of the 1D SDS-PAGE gel is that of the mitochondrial proteins. The 2-oxoglutarate dehydrogenase complex, represented in this study by isoform 2 of 2-oxoglutarate dehydrogenase and the dihydrolipoyllysine-residue succinyltransferase component, is a multi-enzyme assembly in the mitochondrial matrix which catalyses the overall conversion of 2-oxoglutarate to succinyl-CoA and CO₂. The complex is one of three intra-mitochondrial dehydrogenases which is activated by Ca²⁺ ions in vertebrate mitochondria, along with pyruvate dehydrogenase and NAD-isocitrate dehydrogenase

(Armstrong et al., 2014). A 3.25-fold increase in the abundance of trifunctional enzyme subunit alpha was detected by proteomic analysis of crude skeletal muscle homogenates (Table A3.1), and both alpha and beta subunits of trifunctional enzyme have been shown to display enhanced oligomerisation in dystrophic microsomes. The mitochondrial trifunctional enzyme is a heterotrimeric protein which catalyses three of the four enzymatic reactions involved in the mitochondrial β -oxidation of long-chain fatty acids (Rector et al., 2008). Fatty acid oxidation represents a major source of energy for skeletal muscle and the heart, and altered functionality has severe pathological consequences relating to non-ketotic hypoglycemia, liver abnormalities, and/or skeletal and cardiac myopathy (Rector et al., 2008). Thus, the increased complex formation of the mitochondrial trifunctional enzyme and the oxoglutarate dehydrogenase complex may signify an adaptive process by dystrophic muscle to counter-act impaired lipid metabolism and insufficient ATP production that has previously been observed in muscular dystrophy (Rybalka et al., 2014). Insufficient generation of ATP is related to both an increased demand for calcium buffering and regeneration, coupled with functional abnormalities in the mitochondria and in particular a reduced capacity for oxidative phosphorylation.

A large number of proteins with reduced electrophoretic mobility in cross-linked dystrophic microsomes were detected in gel zone B. Similar to gel zone A, a variety of these proteins have roles in metabolism, which again may embody a response of dystrophic muscle fibres to elevated functional demands. In particular, increased oligomerisation of long-chain-fatty-acid-CoA ligase 6, electron transfer flavoprotein subunit beta and long-chain specific acyl-CoA dehydrogenase may be indicative of enhanced fatty acid oxidation to meet energy demands. This may be an attempt to limit the detrimental impact of the dysregulation of energy metabolism, which includes i) reduced functionality of the contractile apparatus leading to deficits in muscle strength, ii) decreased rate of protein synthesis, satellite cell activity, and ultimately muscle regeneration, and iii) impaired Ca^{2+} buffering, thus further exacerbating Ca^{2+} induced activation of proteases, protein degradation, and muscle degeneration (Timpani et al., 2015). The increased oligomerisation of succinate--CoA ligase [ADP-forming] subunit beta involved in the citric acid cycle and CDGSH iron-sulfur domain-containing protein 1 involved in the regulation of electron transport and oxidative phosphorylation also indicate compensatory mechanisms to possibly improve oxidative phosphorylation and the generation of ATP. Also of interest is a

clustering of sub-units of the 26S proteasome. The 26S proteasome is the core proteolytic powerhouse of the ubiquitin-proteasome-pathway, responsible for the removal of redundant and misfolded proteins (Gallastegui and Groll, 2010). The loss of the anchoring protein dystrophin in DMD, leads to the disarray of its associated glycoprotein complex, leaving those proteins susceptible to intracellular proteolysis, which is suggested to exacerbate the degenerative process. Indeed, proteasome inhibition using pharmaceutical agents restores α -sarcoglycan, β -dystroglycan, and α -1-syntrophin abundance and expression at the muscle sarcolemma. Dystrophin of 120 kDa, the predicted size of dystrophin based on the *mdx* mutation (premature stop codon in exon 23), was also detected by immunoblotting following proteasome inhibition (Gazzerro et al., 2010). This was accompanied by increased muscle regeneration, reduced inflammation and improved membrane integrity. Therefore, the clustering of components of the 26S proteasome as detected here by chemical cross-linking analysis may reflect one of the major molecular pathways which contributes to the disease pathophysiology.

Conversely, enhanced oligomerisation of the molecular chaperone calnexin, which has previously been shown to be increased in abundance in *mdx-4cv* crude microsomes (Murphy et al., 2015a), and its potential interactions with other proteins involved in protein re-folding such as UDP-glucose glycoprotein glucosyltransferase 1 and hypoxia up-regulated protein 1, may indicate an increase in molecular chaperoning activity to limit proteotoxic effects in the dystrophin deficient muscle. The augmented tendency for protein oligomerisation seen for the ribosomal proteins 40S ribosomal protein S3 and 40S ribosomal protein S4, along with elongation factor 2 may be indicative of an increase in protein synthesis associated with major cellular remodelling and regeneration in dystrophin-deficient tissues (Murphy et al., 2018a). Vimentin is once again detected as a protein with an enhanced capacity for protein oligomerisation in *mdx-4cv* microsomes, since it is only detected in gel zone E in wild-type control microsomes and *mdx-4cv* control microsomes, its expected location on an SDS-PAGE gel given a molecular mass of 54 kDa. The STRING analysis shown in Figure 3.13 illustrates a potential interaction of vimentin with alpha-actinin-2 and the integrins integrin beta-2, isoform alpha-7X2A of integrin alpha-7 and isoform 2 of integrin alpha-M. The integrins comprise a major family of cell surface adhesion receptors involved in both cell-cell and cell-matrix interactions (Hynes, 1992). Of special interest is integrin alpha-7 which is the main laminin receptor on skeletal

myoblasts and adult myofibers, where it plays a vital role in the maintenance of myofiber cyto-architecture, anchorage, and functional integrity. Since integrin alpha-7 is involved in linking the extracellular matrix to the intracellular cytoskeleton, and its over-expression in transgenic dystrophin/utrophin knockout mouse extends survival, reduces spinal curvature, protects against contraction-induced damage and results in functional improvements in specific force generation (Heller et al., 2015), it is likely that the clustering of various integrin isoforms in dystrophic microsomes may reflect a compensatory mechanism to limit dystrophy-induced muscle damage.

The most striking observation regarding the proteins with an augmented tendency for interactions in dystrophic microsomes in gel zone C is the enrichment of proteins associated with the citric acid cycle (dihydrolipoyllysine-residue succinyltransferase component of 2-oxoglutarate dehydrogenase complex, isocitrate dehydrogenase and fumarate hydratase) and those associated with oxidative phosphorylation (ATP synthase subunit delta, NADH dehydrogenase [ubiquinone] 1 alpha subcomplex subunit 12 and NADH dehydrogenase [ubiquinone] iron-sulfur protein 3). Chemical cross-linking followed by gel shift analysis and mass spectrometry has thus clearly established increased protein interaction patterns for a number of metabolic proteins involved in fatty acid oxidation, the citric acid cycle and oxidative phosphorylation in dystrophic skeletal muscle. This likely represents metabolic changes and bioenergetic adaptations in the face of dystrophin deficiency and ATP insufficiency. Another significant finding is the amplified oligomerisation of the scaffolding proteins flotillin-1 and flotillin-2 involved in the formation of caveolae (Bickel et al., 1997), which agrees with the detection of caveolin-1 in gel zone A and caveolae-associated protein 1 in gel zone B. Their augmented interactions in dystrophic microsomes agrees with previous observations of increased numbers of caveolae in muscular dystrophy (Repetto et al., 1999). Increased abundance of flotillin-1 and flotillin-2 has also been previously detected in crude microsomes (Murphy et al., 2015a) and sarcolemma-enriched fractions (Murphy et al., 2018a) from the *mdx-4cv* mouse model of dystrophinopathy. In analogy to the detection of tubulin beta-5 chain in gel zone A, and tubulin alpha-1A chain and tubulin alpha-4A chain in gel zone B, tubulin alpha-1A chain and tubulin beta-4B chain were detected in cross-linked dystrophic microsomes in gel zone C. This may indicate elevated interactions of tubulin proteins, which in combination with increased oligomerisation of the intermediate filament protein vimentin (gel zones A and B) and the cytoskeletal

protein vinculin (gel zone C), implies a compensatory stabilisation of the intracellular matrix in dystrophic skeletal muscle (Murphy and Ohlendieck, 2016).

3.3.1 Conclusions

DMD is a highly progressive muscle wasting disease, characterised by loss of ambulation in the early teenage years, respiratory and cardiac failure and premature death, usually in the second decade of life. While the primary genetic deficiency has long been established as mutations in the gene encoding the membrane cytoskeletal protein dystrophin, other secondary abnormalities contribute to the pathophysiological phenotype. Previous comparative proteomic studies using whole tissue have identified numerous alterations in protein expression but have largely failed to identify the primary deficiency in dystrophin and its associated glycoproteins. Organelle proteomics has been successfully used by our group to identify reduced levels of some of the key components of the DGC, and in this study reductions in dystrophin expression were identified by mass spectrometry-based proteomics in whole tissue extracts. Indeed, the full-length Dp427 isoform of dystrophin was found to be the most significantly reduced protein species in the *mdx-4cv* model of dystrophinopathy. Thus, this study enables the reduction in dystrophin to be directly related to secondary changes in dystrophic hind leg. Such secondary abnormalities were identified as being associated with Ca²⁺ buffering, the contractile apparatus, ion homeostasis, enzymatic activity, cell signalling and metabolism. Potential compensatory mechanisms to maintain cytoskeletal stability were reflected by the increased abundance of several cytoskeletal and stabilising proteins, including desmin, talin, tubulin, vimentin and vinculin. Importantly, some of the major protein increases were found for components of the ECM and the matrisome, suggesting a high degree of fibrosis in the *mdx-4cv* model. Such markers of myofibrosis include a variety of collagen isoforms, decorin, asporin, prolargin, biglycan, mimecan, lumican, fibrinogen and fibronectin. This is an important proteomic finding given that fibrotic changes in dystrophic muscle are directly correlated to motor performance in Duchenne patients. Thus, a subset of these fibrotic proteins may be suitable as potential biomarkers for monitoring disease progression. Targeting the fibrotic phenotype in muscular dystrophy may also prove crucial for enhancing the therapeutic value of cell- and gene-based treatments by increasing the amount of viable muscle for treatment. In addition to changes in protein abundances, alterations in protein interaction patterns have been established in the

mdx-4cv mouse model using a combination of chemical cross-linking, electrophoretic gel-shift analysis and mass spectrometry. A variety of muscle-associated protein species were shown to exhibit an elevated level of oligomerisation. This included proteins involved in oxidative metabolism, membrane repair, fibre regeneration, cytoskeletal stabilisation, molecular chaperoning and the ubiquitin-proteasome pathway. Many of these alterations in protein interaction patterns are probably in response to the loss of sarcolemmal integrity and represent compensatory mechanisms to rescue the dystrophic phenotype.

Chapter Four

In-depth proteomic analysis of the dystrophin-associated glycoprotein complex and the sarcolemma-enriched fraction from normal and dystrophic muscle

4.1 Introduction

The 2.4 Mb *Dmd* gene, the largest in the human genome, encodes the membrane cytoskeletal protein dystrophin. The presence of 7 promoter regions in this gene results in the production of a variety of distinct dystrophin isoforms ranging in molecular mass from 71 kDa to 427 kDa. Initial characterisation of the full length isoform of 427 kDa showed that it could be enriched by wheat germ agglutination from muscle membranes (Campbell and Kahl, 1989), despite the absence of hydrophobic regions in its primary sequence. This led to experiments demonstrating that dystrophin is anchored in the sarcolemma through tight interactions with glycoproteins (Campbell and Kahl, 1989). This dystrophin-glycoprotein complex is now known to form a supramolecular complex consisting of dystrophin, the dystroglycan complex, the sarcoglycan-sarcospan complex, α -dystrobrevin and the syntrophins (Lapidos et al., 2004). The complex serves to link intracellular actin to components of the extracellular matrix, maintain membrane integrity during muscle excitation-contraction-relaxation, and act as a scaffold for a variety of signalling proteins (Constantin, 2014, Le Rumeur et al., 2010). In DMD, primary abnormalities in the *Dmd* gene result in the almost complete absence of the full-length dystrophin isoform and cause concomitant decreases in the dystroglycans, sarcoglycans, sarcospan, dystrobrevin and syntrophins (Ohlendieck and Campbell, 1991a).

Comparative proteomics has been used extensively in recent years to study the secondary abnormalities downstream of dystrophin deficiency in skeletal muscle and cardiac tissue in both animal models and clinical samples (Bernasconi et al., 1995, Holland et al., 2013, Fröhlich et al., 2016). Such studies have enabled the identification of a range of secondary defects relating to reactive myofibrosis (Fröhlich et al., 2016), muscle regeneration and remodelling (Guevel et al., 2011), sterile inflammation and infiltration of immune cells (Murphy et al., 2017b), energy metabolism, ion homeostasis and cellular stress (Lewis et al., 2009). However, fewer studies have used proteomics to study the core DGC itself nor the muscle sarcolemma. A number of technical issues have delayed such analyses of integral membrane proteins; i) the inherently insoluble nature of integral membrane proteins makes them difficult to manipulate and leads to poor resolution on 2D SDS-PAGE gels, ii) peptide sequences derived from mass spectrometric analyses usually exclude hydrophobic amino acids which make up the transmembrane domains of integral membrane proteins, and iii)

low abundance of membrane proteins means they may be masked by higher abundance contractile and metabolic proteins in mass spectrometric analyses (Turk et al., 2016). Despite these technical difficulties the proteomic survey of the sarcolemmal proteins is imperative given that the primary pathobiochemical insult in dystrophinopathy is located in the sub-sarcolemmal cytoskeleton. Recently, immuno-precipitation (Yoon et al., 2012) and extensive gradient centrifugation (Turk et al., 2016) have been employed to characterise the dystrophin complex by mass spectrometry. Building upon these previous studies, differential centrifugation, digitonin detergent solubilisation, ion exchange chromatography, lectin affinity chromatography and density gradient centrifugation has been employed to generate a dystrophin complex enriched fraction from wild-type rabbit skeletal muscle (Ohlendieck et al., 1991). This fraction was subsequently subjected to gradient one-dimensional gel electrophoresis, on-membrane digestion and LC-MS/MS to characterise its protein components, as illustrated in Figure 4.1. Sensitive mass spectrometric analysis of the dystrophin complex enriched fraction revealed a number of potential novel interaction partners of the complex or that at least exist in close proximity to it. The identification of the cytolinkers desmoglein-1 and desmoplakin is of considerable interest, given their association with desmosomes and cellular adhesion in the skin and the heart (Hammers and Stanley, 2013, Boyer et al., 2010). Comparative analysis of desmoglein-1 abundance in normal and dystrophic mouse skeletal muscle uncovered significantly reduced levels of this cellular adhesion protein in the *mdx* mouse. This decrease is reminiscent of the fate of the other dystrophin-associated glycoproteins in dystrophin-deficient muscle (Ervasti et al., 1990).

Also of great interest is the comparative analysis of the muscle sarcolemma itself, including both the DGC and other sarcolemmal proteins. In addition to the conventional roles of a cell membrane, the sarcolemma of skeletal muscle is also involved in synaptic transmission, excitation-contraction-coupling, the propagation of action potentials towards the transverse tubular system, signalling cascades and structural support (Campbell and Stull, 2003). The importance of the sarcolemma and its two associated protein complexes, the integrin complex and the DGC, is evident by the occurrence of muscular dystrophies arising from defects in sarcolemmal and sub-sarcolemmal proteins. These include Duchenne and Becker muscular dystrophies, sarcoglycanopathies, dystroglycanopathies and dysferlinopathy, which are due to abnormalities in dystrophin, the sarcoglycans, dystroglycan and dysferlin respectively

(Nigro and Piluso, 2015). Although DMD is classified as a multi-system disorder due to secondary abnormalities including scoliosis and impairment of the cardio-respiratory system, it originates at the muscle sarcolemma whereby the almost complete loss of the membrane cytoskeletal protein dystrophin and the concomitant reduction in the DGC results in the micro-rupturing of the sarcolemma and subsequent abnormal and uncontrolled influx of Ca^{2+} .

In a similar manner to the lectin agglutination procedure used to generate the dystrophin complex enriched fraction, an enriched sarcolemmal fraction from combined hind limb muscles of wild-type and *mdx-4cv* mice was isolated, as illustrated in Figure 4.1. Mass spectrometric analysis of this sarcolemmal enriched fraction identified the core dystrophin-associated glycoproteins, along with a range of integral membrane proteins indicating successful sarcolemmal enrichment by the lectin agglutination procedure. Comparative proteomic profiling revealed altered abundance for a variety of proteins of the basement membrane-sarcolemma-cytoskeleton axis in dystrophic muscle. This includes sarcolemmal proteins, protein components of the extracellular matrix, cytoskeletal proteins, protein markers of invading immune cells and proteins associated with the motor neuron and glia cells.

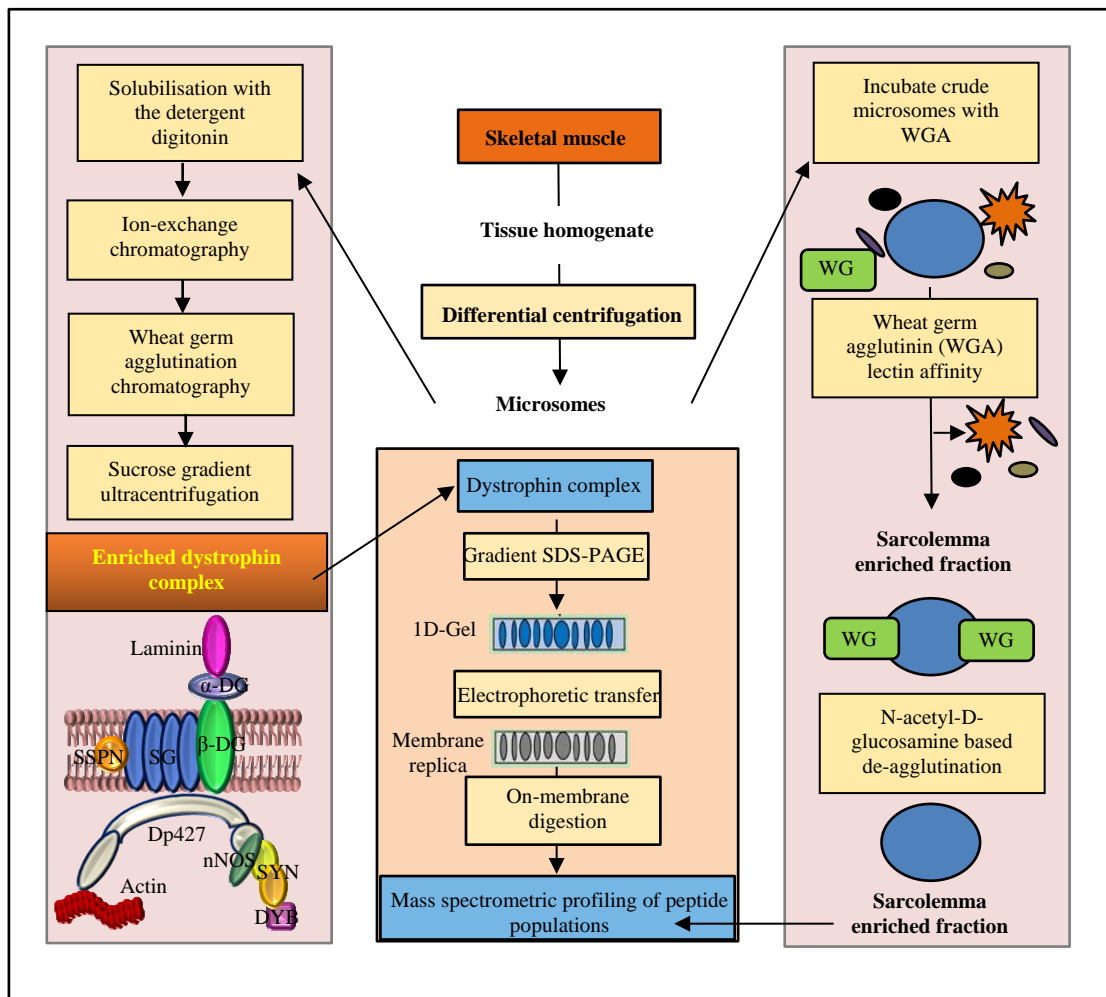


Figure 4.1: Flowchart illustrating the bio-analytical procedure for the proteomic characterisation of dystrophin and its associated glycoprotein complex and for the sarcolemma enriched fraction

Following enrichment, the dystrophin complex underwent gradient gel electrophoresis, transfer to a nitrocellulose membrane, on-membrane digestion and LC-MS/MS. Following wheat germ agglutination, enriched sarcolemma fractions were subjected to in-solution trypsin digestion and the resulting peptides were analysed by LC-MS/MS.

*Image adapted from Murphy and Ohlendieck, 2017a

4.1.1 Experimental Design

The full-length Dp427 isoform of dystrophin forms a large protein complex with dystrophin-associated glycoproteins at the muscle sarcolemma. Loss of dystrophin in DMD results in disintegration of this protein complex and renders the muscle membrane more susceptible to damage during normal muscle excitation-contraction-relaxation cycles. Proteomic investigations of the DGC are challenging as its low-abundance, large size and membrane association make conventional 2D-GE analysis more difficult and can result in suboptimal identification of components of the complex. Since, in general, proteins absorbed onto nitrocellulose sheets are more accessible to proteases, on-membrane digestion of an enriched dystrophin complex may result in improved protein identification by mass spectrometry. A dystrophin complex enriched fraction was prepared by the supervisor of this research, Professor Kay Ohlendieck, using combined hind limb and back muscle tissues from normal adult New Zealand white rabbits. Crude microsomes were prepared from muscle homogenates by differential centrifugation. Membrane proteins were solubilised with the detergent digitonin and fractionated by ion exchange chromatography and wheat germ agglutinin chromatography. A dystrophin-enriched fraction was then isolated by ultracentrifugation with a sucrose gradient (Ervasti et al., 1990). SDS-PAGE was conducted using 16 cm-long and 1.5 mm-thick one-dimensional 3-12% gradient gels. The electrophoretically separated dystrophin fraction was then transferred to nitrocellulose for 90 min at 100 V. On-membrane protein digestion was performed, and peptides analysed by mass spectrometry using an Ultimate 3000 NanoLC system (Dionex Corporation, Sunnyvale, CA, USA) coupled to a Q-Exactive mass spectrometer (Thermo Fisher Scientific). Peptides were eluted using a 65 min method over the following binary gradient: solvent A [2% (v/v) ACN and 0.1% (v/v) formic acid in LC-MS grade water] and 0-90% solvent B [80% (v/v) ACN and 0.1% (v/v) formic acid in LC-MS grade water: 3% solvent B for 5 min, 10-40% solvent B for 30 min, 40-90% solvent B for 5 min, 90% solvent B for 5 min and 3% solvent B for 10 min. Protein identification was achieved using Proteome Discoverer 1.4 (Thermo Fisher Scientific) software with Sequest HT as the search engine and the UniProtKB sequence database. Since the rabbit genome is incomplete, mass spectrometry raw files were searched against both the *Oryctolagus cuniculus* database and the *Mammalia* database. Bioinformatics analysis was performed using STRING and the

web-based gene set analysis toolkit. The status of the potential dystrophin-complex interacting partner desmoglein-1 in dystrophic skeletal muscle was investigated by immunoblot analysis of *quadriceps femoris* and *longissimus dorsi* muscle from 100-day old wild-type and age-matched *mdx* mice (n=4).

The DGC resides in the sarcolemma and the loss of the complex in dystrophinopathy renders the sarcolemma more susceptible to membrane damage and the formation of lesions. Here organelle proteomics has been performed to study proteomic perturbations in the closely associated sarcolemmal environment of the dystrophin network. Crude microsomes were prepared by ultracentrifugation of skeletal muscle homogenates from the entire hind leg of 5-month old wild-type and age-matched *mdx-4cv* mice (n=3). For each biological replicate three hind legs from three different mice were pooled. Sarcolemma vesicles were then enriched using wheat germ agglutination and ultracentrifugation. Samples were analysed by label-free LC-MS/MS using an Ultimate 3000 NanoLC system (Dionex Corporation, Sunnyvale, CA, USA) coupled to a Q-Exactive mass spectrometer (Thermo Fisher Scientific). Peptides were eluted from the column using the following binary gradient: solvent A [2% (v/v) ACN and 0.1% (v/v) formic acid in LC-MS grade water] and 0-90% solvent B [80% (v/v) ACN and 0.1% (v/v) formic acid in LCMS grade water]. The peptides were eluted as follows: 5-45% solvent B for the first 120 min, 45-90% solvent B for 2.5 min, 90% solvent B for 7 min and 3% solvent B for 43 min. Relative quantification and identification was performed with Progenesis QI for Proteomics software, using Sequest HT and MASCOT search engines and the UniProtKB-SwissProt database, where an ANOVA p value ≤ 0.01 was used to determine significant differentially abundant proteins. Bioinformatics analysis was conducted using the PANTHER database of protein families, STRING software and the DAVID bioinformatics resource (version 6.8, <https://david.ncifcrf.gov/>). A number of proteins with altered abundance in the sarcolemma enriched fraction were verified by comparative immunoblot analysis.

4.2 Results

4.2.1 Proteomic characterisation of the dystrophin complex enriched fraction

On-membrane digestion of the accessible protein constellation of the enriched DGC from rabbit skeletal muscle identified 48 proteins (44 of which were characterised and had corresponding gene names), by searching against the *Oryctolagus cuniculus* database. This enriched fraction, isolated using an established method of sequential ion exchange chromatography, lectin affinity chromatography and sucrose gradient ultra-centrifugation (Ervasti et al., 1990), was shown to contain the full-length Dp427 isoform of dystrophin and its associated glycoproteins, including β -dystroglycan, α -sarcoglycan, β -sarcoglycan, δ -sarcoglycan, γ -sarcoglycan, α 1-syntrophin, β 1-syntrophin, β 2-syntrophin and α -dystrobrevin (Table 4.1). Bioinformatics tools were used to characterise the protein components of the enriched dystrophin complex. *Oryctolagus cuniculus* uniprot identifiers for proteins identified in the dystrophin complex enriched fraction were manually converted to *Homo sapiens* uniprot identifiers to facilitate analysis using the web geneset analysis toolkit (freely available at http://www.webgestalt.org/webgestalt_2013/). Except for five proteins (the four uncharacterised proteins; G1U3Q6, G1TQ93, G1U6X0 and G1TL92, and hemoglobin subunit beta-1/2), corresponding *Homo sapiens* identifiers were found for all proteins identified in the dystrophin complex enriched fraction. An additional 8 proteins (keratin 9, keratin 19, desmoglein-1, albumin, actin gamma enteric smooth muscle, cadherin 13, dermcidin and desmocollin-1) that were identified by searching the mass spectrometry data against a mammalian database, and which had ≥ 2 unique peptides were included in the analysis, after identifying their corresponding *Homo sapiens* uniprot identifiers (proteins with ≥ 2 unique peptides but which were uncharacterised or with a high probability of being contaminants, for example bovine casein, were excluded). These proteins are listed in Table 4.1b. The analysis toolkit was used to identify enriched GO terms in our data-set with *homo sapiens_entrezgene_protein-coding* applied as the reference set for enrichment analysis. Multiple test adjustment was performed with the method of Benjamini & Hochberg. Depicted in Figure 4.2 below are the top 10 cellular components with the most significant p values (coloured red) and their non-enriched parents (coloured black). This statistical analysis verifies the enrichment of dystrophin associated glycoproteins in our dystrophin complex enriched fraction, with the identification of

sarcolemma and dystrophin-associated glycoprotein as two of the top 10 enriched cellular components (Figure 4.2).

STRING analysis was also employed to visualise and assess protein-protein interactions, as seen in Figure 4.3. This analysis was performed using the *Homo sapiens* uniprot identifiers as described above and illustrates two major clusters; clustering of the known dystrophin-associated glycoproteins and a second cluster of the cytokeratins with the desmosomal proteins desmoplakin, plakoglobin, desmoglein-1, desmocollin and plakophilin. Enrichment analysis identified the cytoskeleton (28 proteins, false discovery rate (FDR) 1.44e-14), the sarcolemma (12 proteins, FDR 1.44e-14) and the dystrophin-associated glycoprotein complex (8 proteins, FDR 1.44e-14) as enriched cellular components, agreeing with a successful dystrophin complex enrichment procedure in this study. Cellular component enrichment was also seen for the desmosome (5 proteins, FDR 8.2e-08). 6 molecular functions were enriched in the data set, mostly related to structural activity, binding (protein binding and actin binding) and cellular adhesion.

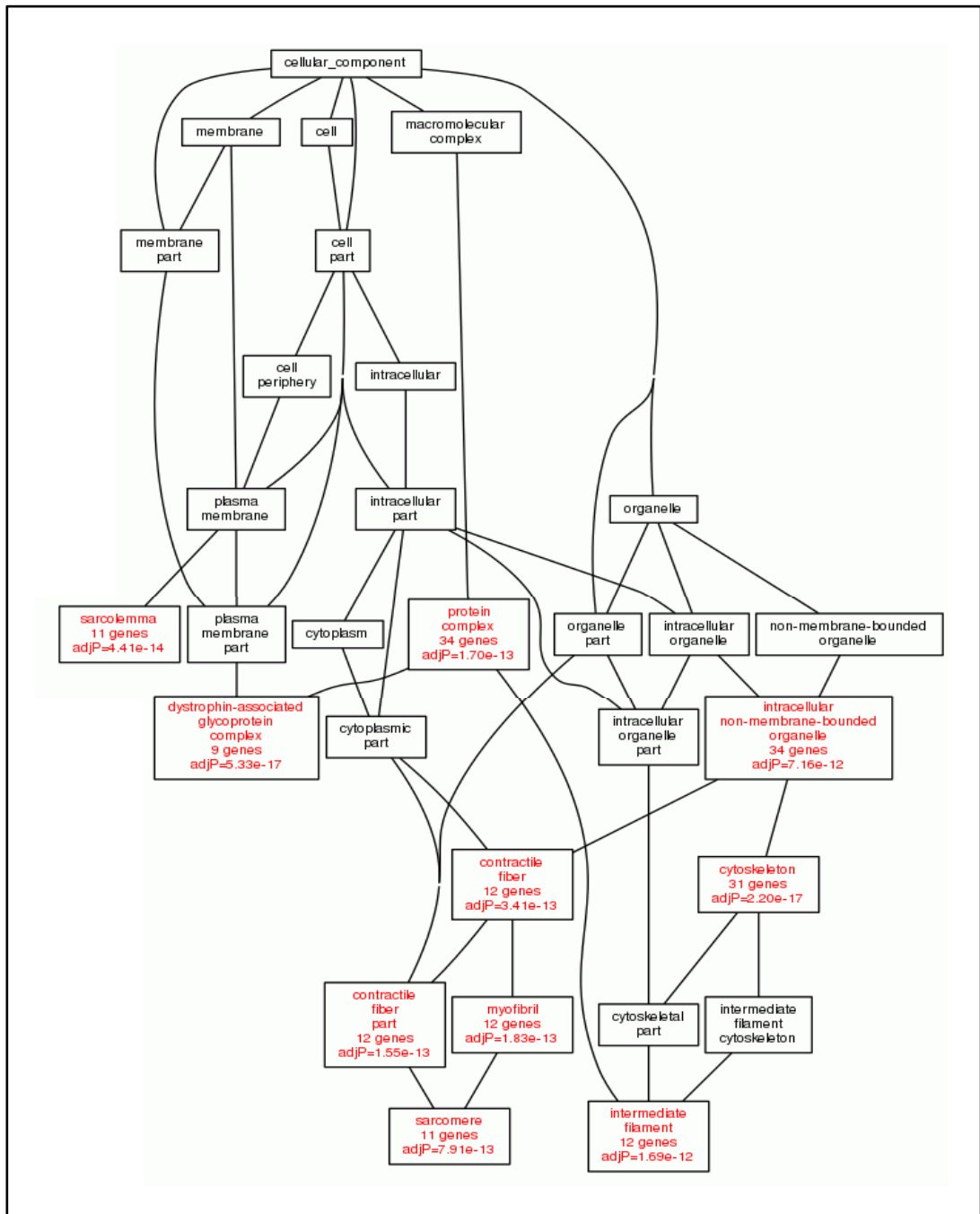


Figure 4.2: Cellular component enrichment analysis of the DGC fraction
 The web gene set analysis toolkit was used to identify enriched cellular components of the proteins identified in the DGC membrane fraction. Bioinformatics confirms the successful enrichment of the DGC in this fraction.

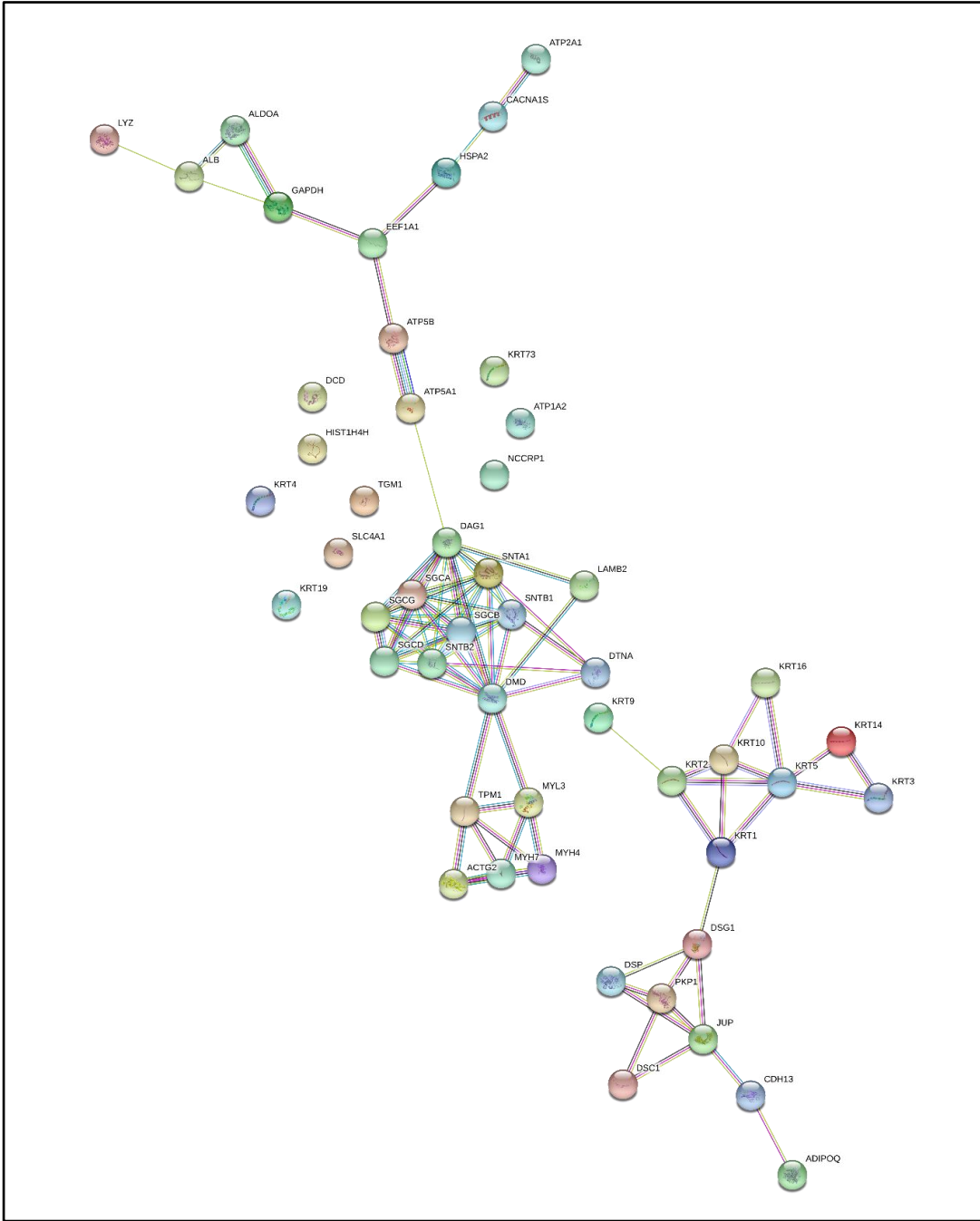


Figure 4.3: STRING analysis of DGC proteins

The freely available STRING database was used to visualise protein-protein interactions, both known and predicted. Depicted is the high confidence evidence view. Analysis reveals clustering of several protein species, particularly of the dystrophin-associated proteins and the cytokeratins.

4.2.2 Mass spectrometric identification of dystrophin co-purifying proteins

Following the confirmation of dystrophin complex enrichment, the data obtained from the dystrophin complex enriched fraction was searched for co-purifying proteins. All the 56 proteins (48 from *Oryctolagus cuniculus* database, and an additional 8 from the *Mammalia* database) identified by mass spectrometry are listed in Tables 4.1a and 4.1b. Aside from the established protein components of the DGC, various other proteins were identified in this enriched fraction. Although all these proteins may have a link with proteins of the DGC, either directly or indirectly, the anion exchange protein, cytokeratin 3 and the cytolinkers desmoglein-1 and desmoplakin are the most plausible candidates. A number of the other proteins detected possibly represent contaminating proteins from the highly abundant sarcoplasmic reticulum (fast SERCA1 Ca²⁺-ATPase) and the contractile apparatus (myosin heavy chain isoform MyHC-IIb). A number of keratins were also identified as seen in Tables 4.1a and 4.1b below, but of particular interest was the detection of keratin 19, as Stone and colleagues have previously illustrated specific interactions between the actin-binding domain of dystrophin and intermediate filaments containing keratin 19 (Stone et al., 2005). Such interactions between dystrophin and cytokeratin 19 may be particularly important in linking dystrophin to the contractile apparatus at all costameres and not just those overlaying the Z disc (Stone et al., 2005). While several filamentous proteins, including actin and desmin, are responsible for connecting the contractile apparatus to the dystrophin complex at costameres, these proteins are concentrated at the Z disc and so are unlikely to mediate connections at costameres along the M-line or those orientated longitudinally along the sarcolemma (O'Neill et al., 2002). Thus, cytokeratins may play a key role in sarcolemmal organisation in striated muscle, through mediating connections between the sarcolemma and contractile apparatus at all three costamere domains.

Desmoglein represents one of the desmosomal cadherins, which are critical for cellular motility and integrity. One segment of the desmoglein cytoplasmic tail has homology to the classical cadherins. This segment is responsible for binding to plakoglobin, which in turn binds to desmoplakin (Hammers and Stanley, 2013). On-membrane digestion of the dystrophin complex enriched fraction identified all three of these desmosomal proteins, although plakoglobin was only identified by a single unique peptide. Since desmoglein-1 is generally associated with stratified squamous epithelia cells (King et al., 1997), such as those in the skin and cornea, its mass

spectrometric identification in the skeletal muscle is of considerable interest. For this reason, it was decided to investigate this protein in skeletal muscle obtained from healthy control wild-type mice and dystrophic *mdx* mice.

Table 4.1a: Mass spectrometric identification of protein components of the dystrophin complex enriched fraction from rabbit skeletal muscle

Accession	Gene Name	Protein Name	Coverage	Unique Peptides	MW [kDa]	calc. pI
G1T1Y7	KRT14	Keratin, type I cytoskeletal 14	25.06	3	48.3	4.93
G1T4R6	KRT16	Keratin, type I cytoskeletal 16	19.15	2	49.5	5.19
G1T1V0	KRT10	Keratin, type I cytoskeletal 10	18.28	12	58.1	5.03
G1SGL0	SGCD	Delta-sarcoglycan	15.57	4	32.1	8.85
G1SI34	ATP2A1	Calcium-transporting ATPase	13.76	9	107.9	5.31
G1SKE6	SGCG	Gamma-sarcoglycan	12.37	3	32	5.25
G1T8Y6	DMD	Dystrophin	12.06	10	111.5	6.52
G1TD51	HIST1H4D	Histone H4	11.54	1	11.5	11.36
G1TB55	SNTB1	Beta-1-syntrophin	11.3	4	58.3	8.31
Q28686	SGCA	Alpha-sarcoglycan	11.11	4	42.5	6.19
Q28635	SGCB	Beta-sarcoglycan	10.06	3	34.7	8.76
G1SK59	ACTG2	Actin, gamma-enteric smooth muscle precursor	9.84	3	41.8	5.48
G1U9I8	KRT1	Keratin, type II cytoskeletal 1	9.33	3	64.2	8.47
P16973	LYZ	Lysozyme C	9.23	1	14.7	8.62
G1SKD7	DTNA	Dystrobrevin	8.01	3	63.3	8.15
G1TDN6	KRT5	Keratin, type II cytoskeletal 2 epidermal	7.14	4	62.2	7.81
G1SUH8	KRT2	Keratin, type II cytoskeletal 2 epidermal	7.12	2	63.2	8.81
G1T281	SNTA1	Alpha-1-syntrophin	6.97	2	51.8	6.64
A0A140TAV6	HBB2	Hemoglobin subunit beta-1/2	6.8	1	16.1	8.21
G1SLY0	SLC4A1	Anion exchange protein	6.31	4	102.1	5.24
G1T375	MYL3	Myosin light chain 3	6.22	1	23.1	5.19
G1TL92		Uncharacterized protein	5.9	2	48.4	5.4
G1T6S0	TPM1	Tropomyosin alpha-1 chain	4.8	1	31.3	4.81
G1T1Q1	NCCRP1	F-box only protein 50	4.53	1	29.8	5.99
G1TJG6	GAPDH	Glyceraldehyde-3-phosphate dehydrogenase	4.5	1	35.8	8.35
G1TI00	SNTB2	Beta-2-syntrophin	4.45	2	58.4	8.09
G1SPP3	KRT4	Keratin, type II cytoskeletal 4	4.36	1	63.8	7.5
G1TDN8	KRT73	Keratin, type II cytoskeletal 73	4.3	1	58.4	7.81
P00883	ALDOA	Fructose-bisphosphate aldolase A	4.12	1	39.3	8.09
G1TV17	ADIPOQ	Adiponectin	4.1	1	26.3	6.15
Q29426	KRT3	Keratin, type II cytoskeletal 3	3.82	4	64.3	7.75

Q28685	DAG1	Dystroglycan	3.58	2	97	8.27
G1U6X0		Uncharacterized protein	3.55	1	42.9	7.72
G1TQ93		Uncharacterized protein	3.11	6	253.8	6.04
G1SKT4	ATP5A1	ATP synthase subunit alpha	2.71	1	59.7	9.11
G1SQA8	ATP5B	ATP synthase subunit beta	2.47	1	60.5	5.67
G1T2J0	JUP	Junction plakoglobin	2.42	1	81.7	6.14
G1U6W1	EEF1A1	Elongation factor 1-alpha	2.38	1	50	8.62
G1T1V9	HSPA2	Heat shock-related 70 kDa protein 2	2.05	1	69.6	5.67
G1TM19	PKP1	Plakophilin-1	2	1	82.8	9.13
Q28641	MYH4	Myosin-4	1.96	2	222.9	5.81
P22758	TGM1	Protein-glutamine gamma-glutamyltransferase K	1.91	1	91.9	6.05
G1U3Q6		Uncharacterized protein	1.69	1	70.4	4.86
G1U2Z6	CACNA1S	Voltage-dependent L-type calcium channel subunit alpha-1S	1.42	2	176.5	6.44
G1TW48	MYH7	Myosin-7	1.34	1	222.9	5.74
G1U8M6	ATP1A2	Sodium/potassium-transporting ATPase subunit alpha	1.18	1	112.1	5.71
G1SN83	LAMB2	Laminin subunit beta-2	0.78	1	196	6.6
G1T4V7	DSP	Desmoplakin	0.63	1	224.5	6.93

Table 4.1b: Mass spectrometric identification of 8 additional protein components of the dystrophin complex enriched fraction from rabbit skeletal muscle, identified by a *Mammalia* database

Accession	Gene Name	Protein Name	Coverage	Unique Peptides	MW [kDa]	calc. pI
H2QCZ6	KRT9	Keratin 9	28.73	11	62.1	5.24
V8P8L1	KRT19	Keratin, type 1 cytoskeletal 19	1	2	436.1	5.14
H2QEE3	DSG1	Desmoglein-1	5.92	4	113.7	5.06
A0A140T897	ALB	Serum albumin	5.27	3	69.3	6.18
R7VT75	ACTG2	Actin, gamma-enteric smooth muscle	11.75	3	35	5.1
M1EH65	CDH13	Cadherin 13, H-cadherin	17.69	2	16.3	5.2
P81605	DCD	Dermcidin	12.73	2	11.3	6.54
G3SCF2	DSC1	Desmocollin-1	3.45	2	93.7	5.48

4.2.3 Comparative immunoblotting of desmoglein-1 in wild-type and mdx quadriceps femoris and longissimus dorsi

Leading on from the mass spectrometric identification of desmoglein-1 in the dystrophin complex enriched fraction from skeletal muscle, it was decided to investigate the status of this cytolinker protein in dystrophic skeletal muscle. Silver stain analysis and immunoblotting to the extracellular matrix protein laminin showed similar protein banding patterns and equal protein loading respectively between 100-day old wild-type and age-matched *mdx quadriceps femoris* and *longissimus dorsi* muscle. However, comparative immunoblot analysis revealed a statistically significant reduction in the abundance of desmoglein-1 in both dystrophic *quadriceps femoris* and *longissimus dorsi* skeletal muscle (Figures 4.4 and 4.5). This cytolinker suffers the same fate as a number of core dystrophin-associated glycoproteins in the absence of dystrophin.

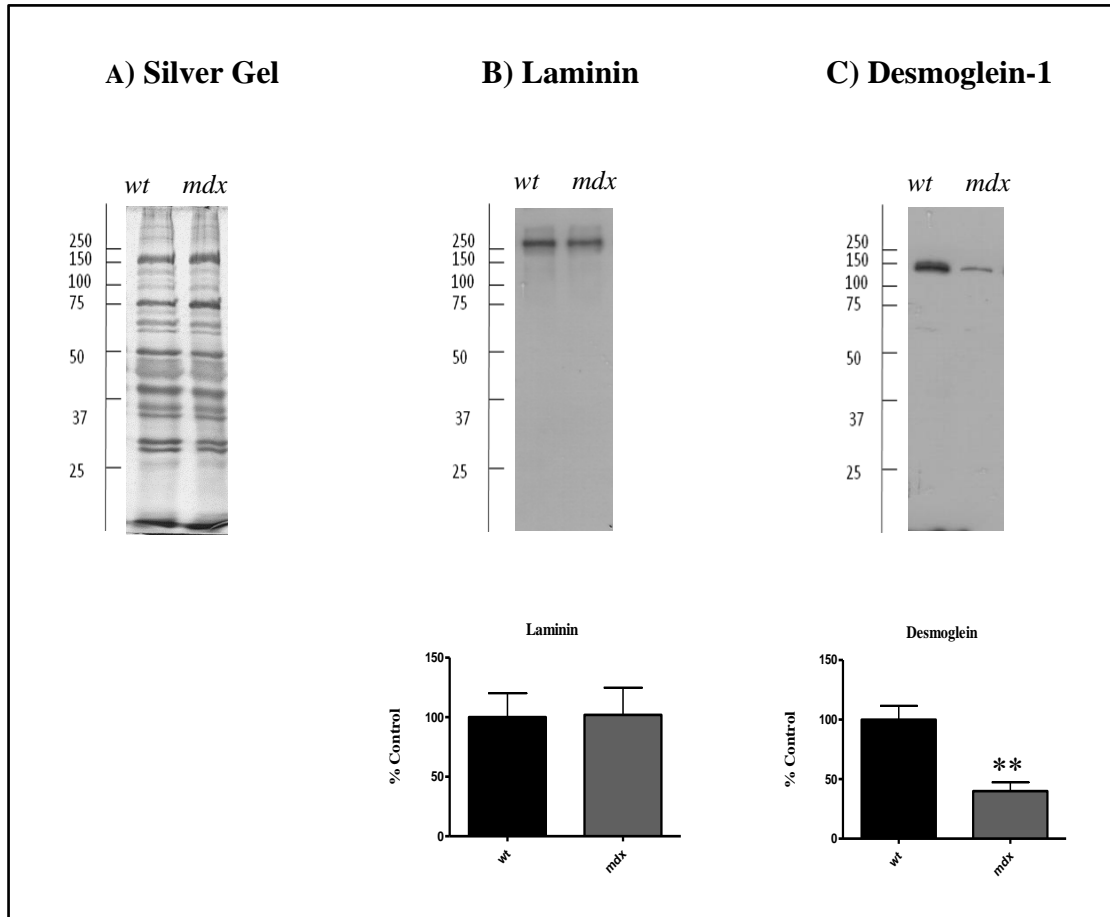


Figure 4.4: Immunoblot analysis of the cytolinker desmoglein-1 in dystrophic *quadriceps femoris* skeletal muscle

Shown is a silver stained gel (A) and immunoblot and statistical analysis of bands labelled with laminin (B). The silver stained gel shows comparable protein banding patterns for 100-day old wild-type and *mdx quadriceps femoris* muscle. Molecular weight marker is given on the left-hand-side of the image in kDa. Laminin immunoblotting did not show significant changes in concentration between wild-type and *mdx* samples and so it serves as a loading control for comparative immunoblotting. Also shown is an immunoblot to desmoglein-1 (C). Graphical representation of the immuno-decoration levels for laminin and desmoglein-1 is shown (mean values \pm SEM, Student's *t*-test; unpaired; $n=4$; $**p \leq 0.01$).

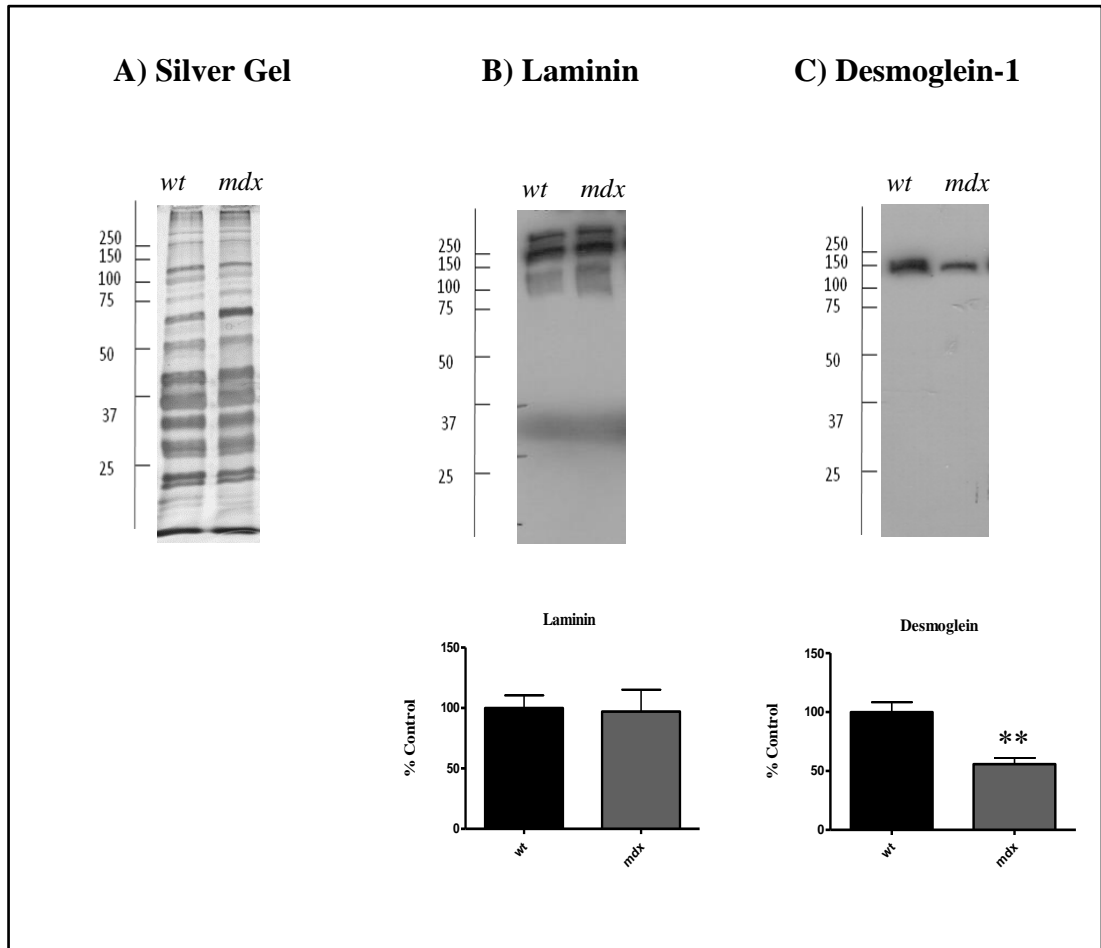


Figure 4.5: Immunoblot analysis of the cytolinker desmoglein-1 in dystrophic *longissimus dorsi* skeletal muscle

Shown is a silver stained gel (A) and immunoblot and statistical analysis of bands labelled with laminin (B). The silver stained gel shows comparable protein banding patterns for 100-day old wild-type and *mdx longissimus dorsi* muscle. Molecular weight marker is given on the left-hand-side of the image in kDa. Laminin immunoblotting did not show significant changes in concentration between wild-type and *mdx* samples and so it serves as a loading control for comparative immunoblotting. Also shown is an immunoblot to desmoglein-1 (C). Graphical representation of the immuno-decoration levels for laminin and desmoglein-1 is shown (mean values \pm SEM, Student's *t*-test; unpaired; $n=4$; $**p \leq 0.01$).

4.2.4 Qualitative analysis of wild-type versus *mdx-4cv* enriched sarcolemma

Prior to comparative analysis to identify differentially abundant proteins in wild-type versus *mdx-4cv* enriched sarcolemma, qualitative analyses were performed to confirm sarcolemmal enrichment using the wheat germ agglutination procedure. 793 proteins were identified in *mdx-4cv* preparations, of which 512 proteins had ≥ 2 unique peptides. 738 proteins were identified in wild-type samples, with 470 of those containing ≥ 2 unique peptides. The identified proteins with ≥ 2 unique peptides were loaded into the WEB-based GEne SeT AnaLysis Toolkit (WebGestalt) and searched using GO annotation to evaluate whether the lectin agglutination procedure had efficiently enriched for proteins in, and associated with, the membrane. 395 of 470 uniprot-swissprot accession numbers for wild-type sarcolemma and 429 of 512 uniprot-swissprot accession numbers for *mdx-4cv* sarcolemma were successfully mapped to unique Entrez gene IDs and were used in the analysis. Shown in Figure 4.6 is a bar chart illustrating the top 12 cellular components as identified by GO analysis in wild-type and *mdx-4cv* datasets. This analysis revealed just under two-thirds of identified proteins were associated with the membrane (64% for wild-type and 65% for *mdx-4cv*), suggesting overall enrichment of membrane proteins. More specifically, the enrichment analysis tool in the WebGestalt software identified the sarcolemma as an enriched cellular component in both wild-type and *mdx-4cv* muscle preparations (FDR 1.26e-06 for *mdx-4cv* samples and FDR 1.45e-09 for wild-type samples), indicating successful enrichment of the muscle sarcolemma. The core dystrophin complex was represented by dystrophin isoform Dp427, α/β -dystroglycan, α -sarcoglycan, β -sarcoglycan, γ -sarcoglycan, δ -sarcoglycan, and $\alpha 1$ -syntrophin. Key sarcolemmal marker proteins identified in multi-consensus qualitative data included dysferlin, the plasma membrane Ca^{2+} -transporting ATPase isoform Atp2b1, various subunits of the Na^+/K^+ -ATPase ($\alpha 1$, $\alpha 2$, $\beta 1$ and $\beta 2$ subunits), integrins (isoform $\alpha 6\text{X}1\text{A}$ of integrin $\alpha 6$, isoform $\alpha 7\text{X}2\text{A}$ of integrin $\alpha 7$, integrin $\beta 1$ and integrin $\beta 2$), annexins A1 and A2 and the sarcolemmal chloride channel protein. However, agglutinated vesicle preparations from skeletal muscle are most often contaminated by abundant membranes and protein populations from mitochondria, the sarcoplasmic reticulum, transverse tubules, the ribosome, the nucleus, serum, the Golgi apparatus, the cytosol, lysosomes and the contractile apparatus (Murphy and Ohlendieck, 2017). As seen in Figure 4.6, the sarcolemma-enriched fraction isolated here contains other

abundant cellular components including mitochondria, macromolecular complexes, the nucleus, the endoplasmic reticulum and the cytoskeleton.

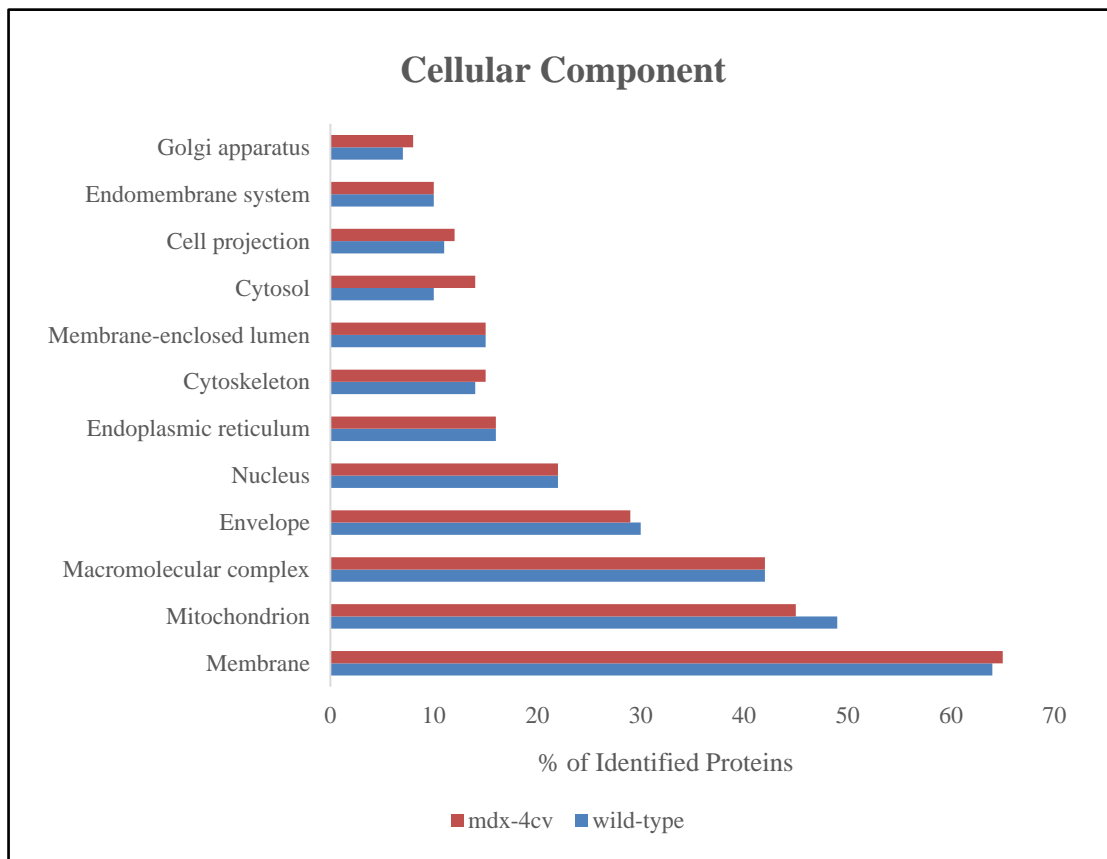


Figure 4.6: Cellular component analysis of wild-type versus *mdx-4cv* sarcolemma data

Shown are the top 12 cellular components identified by GO analysis of the identified proteins in wild-type and *mdx-4cv* enriched sarcolemma fractions.

4.2.5 Quantitative analysis of wild-type versus mdx-4cv enriched sarcolemma

The proteomic survey of two technical repeats each of three biological samples revealed altered abundance for 190 proteins. Of these proteins 163 were elevated in abundance in *mdx-4cv* samples and the remaining 27 proteins were decreased in abundance in *mdx-4cv* sarcolemma enriched fractions. The 163 increased abundance proteins and 27 decreased abundance proteins are listed in Tables 4.2, A4.1 and 4.3 respectively. A number of confirmatory proteins were identified, with reductions seen for dystrophin, β -dystroglycan, α -sarcoglycan and δ -sarcoglycan, in agreement with the known dystrophic phenotype. In addition, several previously identified proteins of increased abundance in dystrophic tissue were also verified here, including collagen α (VI), fibronectin, biglycan and the embryonic myosin isoforms myosin-4 and myosin-3. A variety of novel proteins of interest were also identified and investigated further. Of particular interest was the 21.8-fold decrease in the abundance of the scaffolding protein periaxin which functions as part of a dystrophin-related protein DRP2-dystroglycan complex in Schwann cells.

Table 4.2: List of proteins with ≥ 4 -fold increased abundance in 5-month old *mdx-4cv* enriched sarcolemma versus age-matched wild-type enriched sarcolemma as determined by label-free LC-MS/MS

Accession	Gene Name	Protein Name	Unique peptides	Confidence score	Anova (p)	Max fold change
P49290	Epx	Eosinophil peroxidase	2	3.56	1.60E-13	Infinity
P04441	Cd74	H-2 class II histocompatibility antigen gamma chain	2	3.20	1.32E-04	117.39
Q9D1I2	Card19	Caspase recruitment domain-containing protein 19	2	57.00	7.26E-04	60.65
Q5SX39	Myh4	Myosin-4	5	115.59	5.01E-03	32.91
Q9D0E1	Hnrnpm	Heterogeneous nuclear ribonucleoprotein M	2	45.79	5.08E-03	32.26
Q5SX40	Myh1	Myosin-1	15	800.40	8.51E-04	27.12
P13541	Myh3	Myosin-3	2	3.68	4.28E-03	22.75
P01901	H2-K1	H-2 class I histocompatibility antigen, K-B alpha chain	4	202.65	1.68E-07	20.09
P06800	Ptprc	Receptor-type tyrosine-protein phosphatase C	3	213.96	2.87E-07	20.03
P97457	Mylpf	Myosin regulatory light chain 2, skeletal muscle isoform	2	143.61	9.78E-04	17.18
P62918	Rpl8	60S ribosomal protein L8	3	104.98	1.05E-06	13.33
P47964	Rpl36	60S ribosomal protein L36	2	3.31	9.55E-03	12.96
Q8BMD8	Slc25a24	Calcium-binding mitochondrial carrier protein SCaMC-1	4	214.42	2.91E-05	12.72
Q62230	Siglec1	Sialoadhesin	6	302.81	6.83E-05	10.82
P62301	Rps13	40S ribosomal protein S13	2	62.73	2.35E-05	10.55
P51881	Slc25a5	ADP/ATP translocase 2	2	97.29	1.98E-05	10.32
Q8BMK4	Ckap4	Cytoskeleton-associated protein 4	7	228.98	2.47E-05	10.26
Q9D8E6	Rpl4	60S ribosomal protein L4	4	97.00	1.01E-05	9.89
P47911	Rpl6	60S ribosomal protein L6	3	162.39	4.38E-07	9.43
P43276	Hist1h1b	Histone H1.5	4	61.99	1.14E-05	8.89
P62245	Rps15a	40S ribosomal protein S15a	3	158.76	4.86E-06	8.48
P11835	Itgb2	Integrin beta-2	3	102.80	1.04E-04	7.95

Q69ZN7	Myof	Myoferlin	5	121.44	1.62E-04	7.81
P01872	Ighm	Ig mu chain C region	3	149.11	4.53E-05	7.37
Q7TPR4	Actn1	Alpha-actinin-1	2	42.54	2.98E-05	6.75
Q6ZWV7	Rpl35	60S ribosomal protein L35	2	47.05	2.17E-05	6.66
P14148	Rpl7	60S ribosomal protein L7	3	109.44	5.97E-08	6.57
Q9D8H7	Oma1	Metalloendopeptidase OMA1, mitochondrial	2	4.03	8.43E-07	6.55
P49300	Clec10a	C-type lectin domain family 10 member A	3	101.98	6.37E-05	6.49
P47963	Rpl13	60S ribosomal protein L13	2	47.63	3.83E-08	6.43
Q9WV54	Asah1	Acid ceramidase	3	105.42	1.62E-07	6.40
P28653	Bgn	Biglycan	2	116.02	3.31E-04	6.38
P62754	Rps6	40S ribosomal protein S6	2	43.95	5.97E-07	6.35
P43274	Hist1h1e	Histone H1.4	6	68.95	1.83E-06	6.32
P35979	Rpl12	60S ribosomal protein L12	2	64.42	3.07E-04	6.11
Q9CR57	Rpl14	60S ribosomal protein L14	3	190.30	1.22E-05	6.10
Q3UMR5	Mcu	Calcium uniporter protein, mitochondrial	3	130.49	1.43E-05	5.73
Q62465	Vat1	Synaptic vesicle membrane protein VAT-1 homolog	3	195.20	2.85E-05	5.66
P53026	Rpl10a	60S ribosomal protein L10a	2	55.75	2.67E-05	5.54
P97449	Anpep	Aminopeptidase N	4	118.97	3.53E-05	5.47
O88990	Actn3	Alpha-actinin-3	8	449.56	2.18E-04	5.45
P50285	Fmo1	Dimethylaniline monooxygenase [N-oxide-forming] 1	2	67.52	3.49E-04	5.41
P54116	Stom	Erythrocyte band 7 integral membrane protein	5	308.74	8.74E-05	5.34
Q923B6	Steap4	Metalloreductase STEAP4	3	79.01	1.16E-04	5.30
P29788	Vtn	Vitronectin	2	93.59	6.84E-09	5.29
Q64449	Mrc2	C-type mannose receptor 2	3	112.73	2.78E-06	5.25
P10107	Anxa1	Annexin A1	3	191.03	1.28E-05	5.25
Q8VHX6	Flnc	Filamin-C	4	62.16	3.76E-05	5.13
P62702	Rps4x	40S ribosomal protein S4, X isoform	4	68.24	9.56E-06	5.05
O08917	Flot1	Flotillin-1	3	191.19	2.01E-03	4.93

Q61738	Itga7	Integrin alpha-7	3	102.60	4.70E-05	4.83
P12970	Rpl7a	60S ribosomal protein L7a	2	88.31	9.78E-08	4.78
P27773	Pdia3	Protein disulfide-isomerase A3	4	122.02	5.40E-05	4.76
Q9DBS1	Tmem43	Transmembrane protein 43	3	97.03	2.21E-08	4.70
P08226	Apoe	Apolipoprotein E	5	200.72	2.40E-05	4.61
Q8CC88	Vwa8	von Willebrand factor A domain-containing protein 8	2	50.68	2.81E-03	4.59
Q8VDD5	Myh9	Myosin-9	3	119.65	2.12E-06	4.57
P70302	Stim1	Stromal interaction molecule 1	2	3.20	3.28E-05	4.56
P13595	Ncam1	Neural cell adhesion molecule 1	3	71.50	1.57E-05	4.48
Q9EQK5	Mvp	Major vault protein	2	57.29	7.84E-06	4.45
Q60634	Flot2	Flotillin-2	4	267.14	3.60E-07	4.41
Q61830	Mrc1	Macrophage mannose receptor 1	12	491.66	5.40E-04	4.38
Q3U7R1	Esyt1	Extended synaptotagmin-1	3	51.30	1.35E-05	4.34
Q9DCN2	Cyb5r3	NADH-cytochrome b5 reductase 3	2	103.89	4.05E-07	4.31
Q07113	Igf2r	Cation-independent mannose-6-phosphate receptor	3	50.15	8.66E-05	4.22
A2ASS6	Ttn	Titin	105	3529.12	9.91E-04	4.19
Q9DC69	Ndufa9	NADH dehydrogenase [ubiquinone] 1 alpha subcomplex subunit 9, mitochondrial	2	141.66	7.94E-04	4.05

Table 4.3: List of identified proteins with a significantly decreased abundance in 5-month old *mdx-4cv* enriched sarcolemma versus age-matched wild-type enriched sarcolemma as determined by label-free LC-MS/MS

Accession	Gene Name	Protein Name	Unique peptides	Confidence score	Anova (p)	Max fold change
P11531	Dmd	Dystrophin	8	255.88	1.26E-05	2708.22
P27573	Mpz	Myelin protein P0	2	4.58	2.84E-05	33.85
O55103	Prx	Periaxin	15	566.64	1.95E-11	21.81
Q8BKZ9	Pdhx	Pyruvate dehydrogenase protein X component, mitochondrial	2	98.21	1.76E-05	16.84
Q62165	Dag1	Dystroglycan	2	51.58	1.03E-07	14.83
P41216	Acsl1	Long-chain-fatty-acid--CoA ligase 1	3	174.03	9.99E-04	12.21
Q99LC3	Ndufa10	NADH dehydrogenase [ubiquinone] 1 alpha subcomplex subunit 10, mitochondrial	2	62.50	1.97E-04	8.21
Q8VCT4	Ces1d	Carboxylesterase 1D	2	82.19	1.64E-04	6.75
Q70IV5	Synm	Synemin	2	47.71	4.99E-06	5.30
P16330	Cnp	2',3'-cyclic-nucleotide 3'-phosphodiesterase	3	85.49	2.10E-04	4.92
P12367	Prkar2a	cAMP-dependent protein kinase type II-alpha regulatory subunit	2	3.25	6.95E-05	4.92
A2A863	Itgb4	Integrin beta-4	5	160.70	8.49E-05	4.31
P82347	Sgcd	Delta-sarcoglycan	3	57.59	3.78E-04	3.99
P82350	Sgca	Alpha-sarcoglycan	2	118.46	3.63E-06	3.74
Q8R1G2	Cmb1	Carboxymethylenbutyrolidase homolog	2	43.07	3.15E-03	3.53
P09411	Pgk1	Phosphoglycerate kinase 1	2	3.16	2.01E-06	3.32
P05064	Aldoa	Fructose-bisphosphate aldolase A	2	49.25	3.86E-05	3.28
Q64521	Gpd2	Glycerol-3-phosphate dehydrogenase, mitochondrial	2	83.59	2.75E-04	3.25
Q8BH59	Slc25a12	Calcium-binding mitochondrial carrier protein Aralar1	3	129.87	1.55E-03	3.21
Q8R3Z5	Cacnb1	Voltage-dependent L-type calcium channel subunit beta-1	2	95.19	1.25E-05	3.14
O09165	Casq1	Calsequestrin-1	2	50.25	3.30E-04	3.02

P07310	Ckm	Creatine kinase M-type	2	72.74	6.54E-03	2.89
Q03265	Atp5a1	ATP synthase subunit alpha, mitochondrial	3	107.23	2.52E-05	2.57
P61982	Ywhag	14-3-3 protein gamma	2	57.27	5.13E-06	2.44
Q61554	Fbn1	Fibrillin-1	4	183.34	2.41E-03	2.18
Q7TQ48	Srl	Sarcalumenin	3	5.57	4.52E-03	1.67
P14824	Anxa6	Annexin A6	3	216.75	1.17E-03	1.58

4.2.6 Bioinformatics of differential proteins in wild-type versus mdx-4cv enriched sarcolemma

A variety of software packages were employed to investigate the differential proteins in more detail. PANTHER analysis of the 163 proteins with elevated abundance in *mdx-4cv* dystrophic skeletal muscle revealed a huge variety of altered protein classes (Figure 4.7), with the highest proportion of increased proteins belonging to the class of nucleic acid binding proteins. The 27 proteins with decreased abundance belonged predominantly to transferase, transporter, calcium-binding and hydrolase protein classes (Figure 4.8). Figures 4.9 and 4.10 depict the medium confidence evidence view from STRING for elevated and reduced proteins respectively. STRING analysis of increased abundance proteins reveals two primary proteins clusters; that of the ribosomal proteins (the protein cluster on the left-hand-side in Figure 4.9) and that of the structural proteins titin, vimentin, biglycan, vitronectin and various isoforms of myosin, collagen, tubulin and annexin (the cluster to the bottom-right in Figure 4.9). Dystrophin deficiency is thereby suggested to result in compensatory increases in protein translation and cytoskeletal restructuring. STRING analysis of the decreased proteins identifies the well-characterised interactions of dystrophin with dystroglycan and α -sarcoglycan and δ -sarcoglycan. In turn this complex is putatively connected to the structural myelin proteins periaxin and myelin protein zero.

The DAVID bioinformatics resource was used to identify enriched protein clusters of biological significance. The 163 proteins with elevated abundance were converted to DAVID IDs and analysed using the functional annotation clustering tool, with classification stringency set to high. This identified 29 clusters of interest, of which the cluster associated with ribosomal proteins had the highest enrichment score of 21.52. Similarly STRING functional enrichment analysis also identified ribosomes as the top enriched KEGG pathway in proteins with elevated abundance in the dystrophic mouse, indicating drastic increases in ribosomal protein synthesis. Shown in Figure 4.11 are the top 5 enriched KEGG pathways for both elevated and reduced proteins.

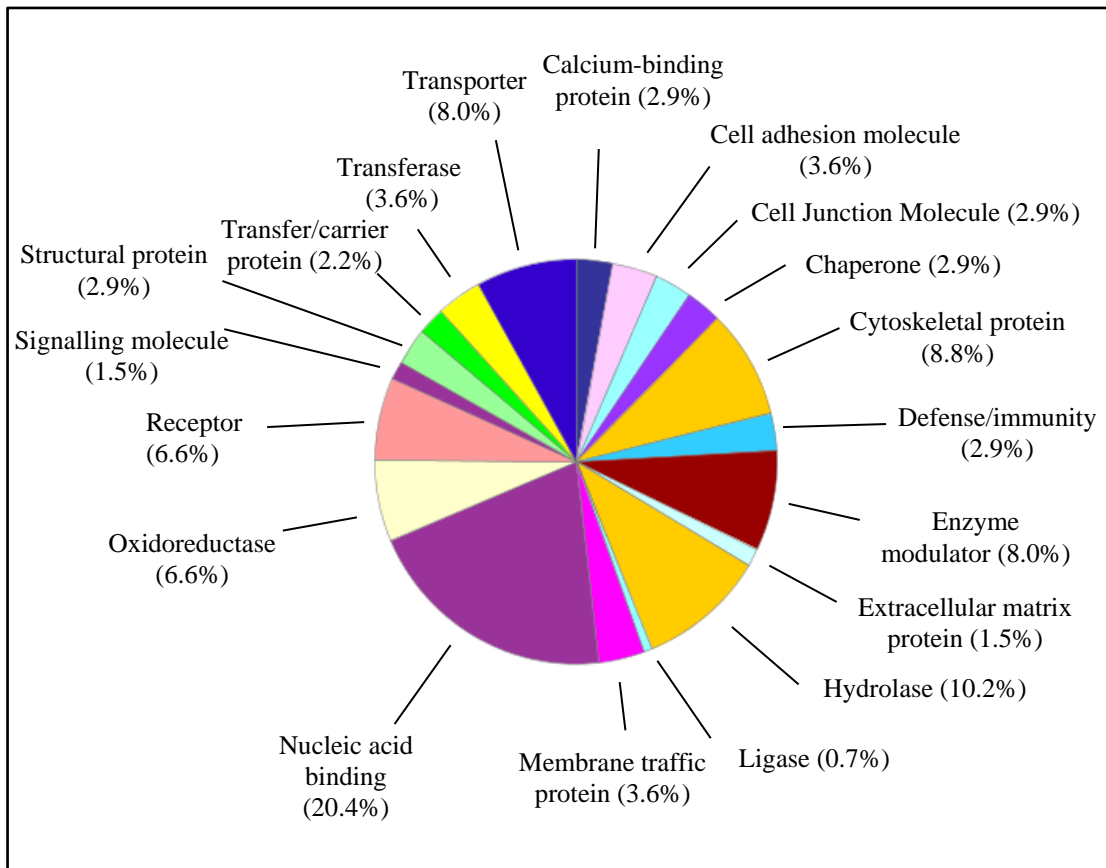


Figure 4.7: PANTHER analysis of proteins with increased abundance in *mdx-4cv* muscle sarcolemma

The 163 proteins with elevated abundance were grouped into their respective protein class using the freely available PANTHER software package.

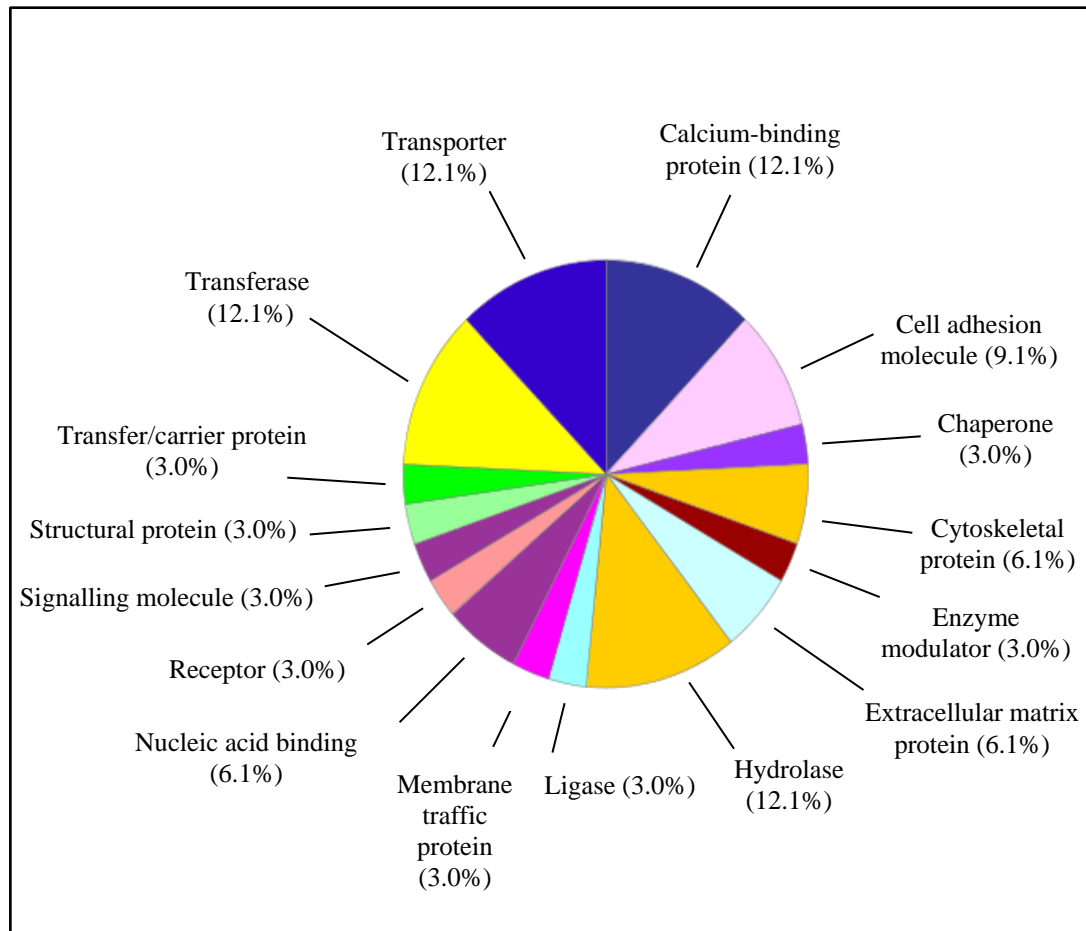


Figure 4.8: PANTHER analysis of proteins with decreased abundance in *mdx-4cv* muscle sarcolemma

The 27 proteins with reduced abundance were grouped into their respective protein class using the freely available PANTHER software package.

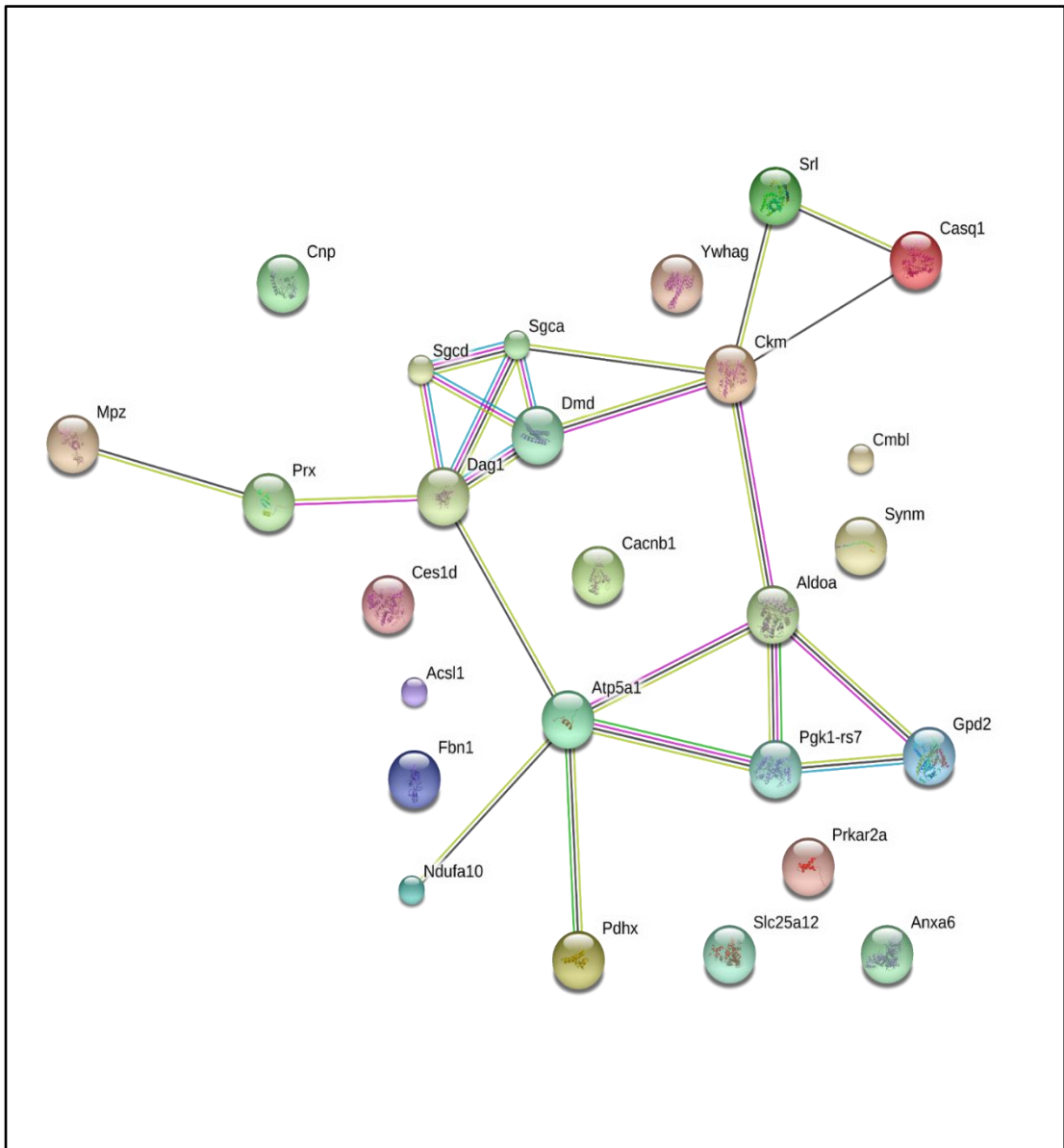


Figure 4.10: STRING analysis of proteins with decreased abundance in *mdx-4cv* muscle sarcolemma

Depicted is the STRING evidence view analysis of potential protein interactions (medium confidence) of the 27 proteins with reduced abundance in *mdx-4cv* muscle sarcolemma.

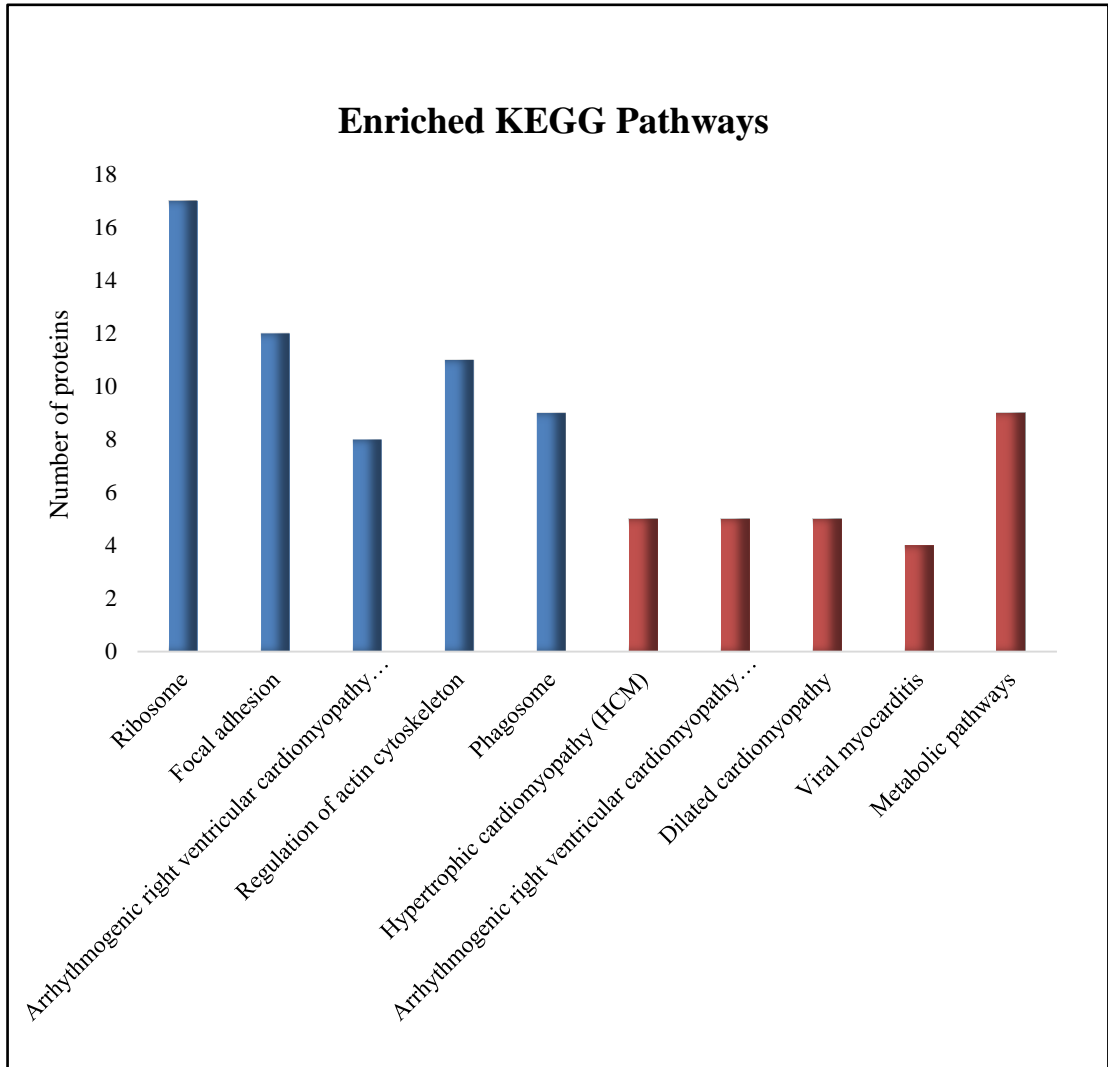


Figure 4.11: Enriched KEGG pathways of proteins with altered abundance in *mdx-4cv* muscle sarcolemma

Depicted are the top 10 enriched KEGG pathways of proteins with elevated abundance (blue columns) and reduced abundance (red columns) based on STRING functional enrichment analysis.

4.2.7 Comparative immunoblotting of differential proteins in wild-type versus *mdx-4cv* enriched sarcolemma

Comparative immunoblotting using a panel of select antibodies against crude homogenates from hind-leg skeletal muscle of 5-month old wild-type and age-matched *mdx-4cv* mice was used to independently evaluate novel protein candidates of DMD. Equal loading was confirmed by silver stain analysis along with an immunoblot against laminin, as illustrated in Figure 4.12. Decreased abundance of β -dystroglycan is a known deficit arising from the absence of its interaction partner dystrophin in muscular dystrophy and was confirmed in the *mdx-4cv* animal model here by both mass spectrometry (Table 4.3) and immunoblotting (Figure 4.13). Although not identified by mass spectrometric analysis of the sarcolemma enriched fraction, proteomic analysis of the dystrophin complex enriched fraction has identified desmoglein-1 as a potential interaction partner of the DGC and one which shows reduced abundance in skeletal muscle from the *mdx* animal model (Figures 4.4 and 4.5). This reduction in desmoglein-1 is confirmed here in crude hind limb homogenates of the *mdx-4cv* model (Figure 4.13). Dramatically reduced abundance was detected for myelin protein zero and this finding was confirmed by immunoblotting (Figure 4.14). Since the immunoblot analysis of myelin binding protein zero was only successful for membranes loaded with 50 μ g protein per lane (all other membranes contain 25 μ g protein per lane) a separate laminin equal loading immunoblot is also shown for this membrane (Figure 4.14). Although only identified by a single peptide, fibronectin (P11276, ANOVA=2.27E-07, 11.54-fold increase) is a well-established marker of reactive myofibrosis in muscular dystrophy and so its elevated abundance was evaluated by immunoblotting, where statistically significant increases of fibronectin were identified in dystrophic crude hind leg homogenates (Figure 4.15). Increased abundance was also confirmed for the proteoglycan biglycan, although this was not found to be statistically significant (Figure 4.15). Figure 4.16 depicts statistically significant increases in the abundance of annexin A2 and dysferlin, which were each detected by a single unique peptide (annexin A2; P07356, ANOVA=3.65E-06, 5.35-fold increase and dysferlin; Q9ESD7, ANOVA= 0.0028, 2.84-fold increase).

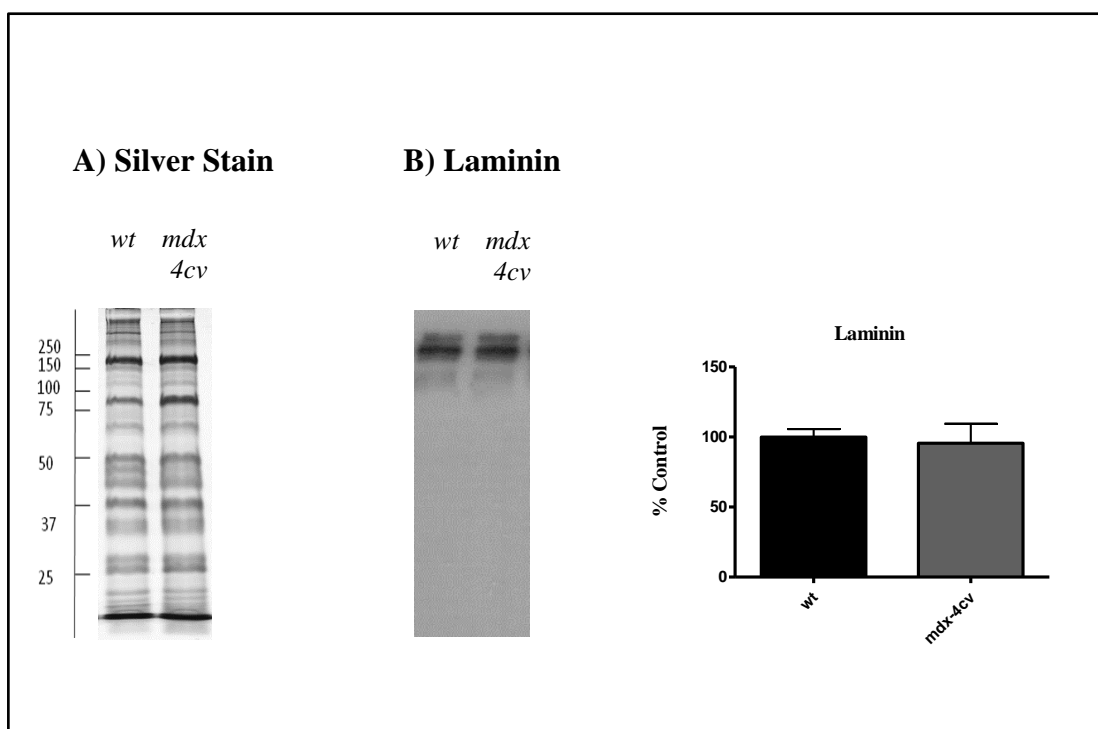


Figure 4.12: Electrophoretic and immunoblot analysis of wild-type and *mdx-4cv* muscle

Shown is a silver stained 1D gel (A) and immunoblot and statistical analysis of bands labelled with laminin (B). The silver stained gel shows comparable protein banding patterns for wild-type and *mdx-4cv* muscle preparations. Molecular weight marker is given on the left-hand-side of the image in kDa. Laminin immunoblotting did not show significant changes in concentration between wild-type and *mdx-4cv* samples and so it serves as a loading control for comparative immunoblotting. Graphical representation of the immuno-decoration level for laminin is shown (mean values \pm SEM, Student's *t*-test; unpaired; n=4).

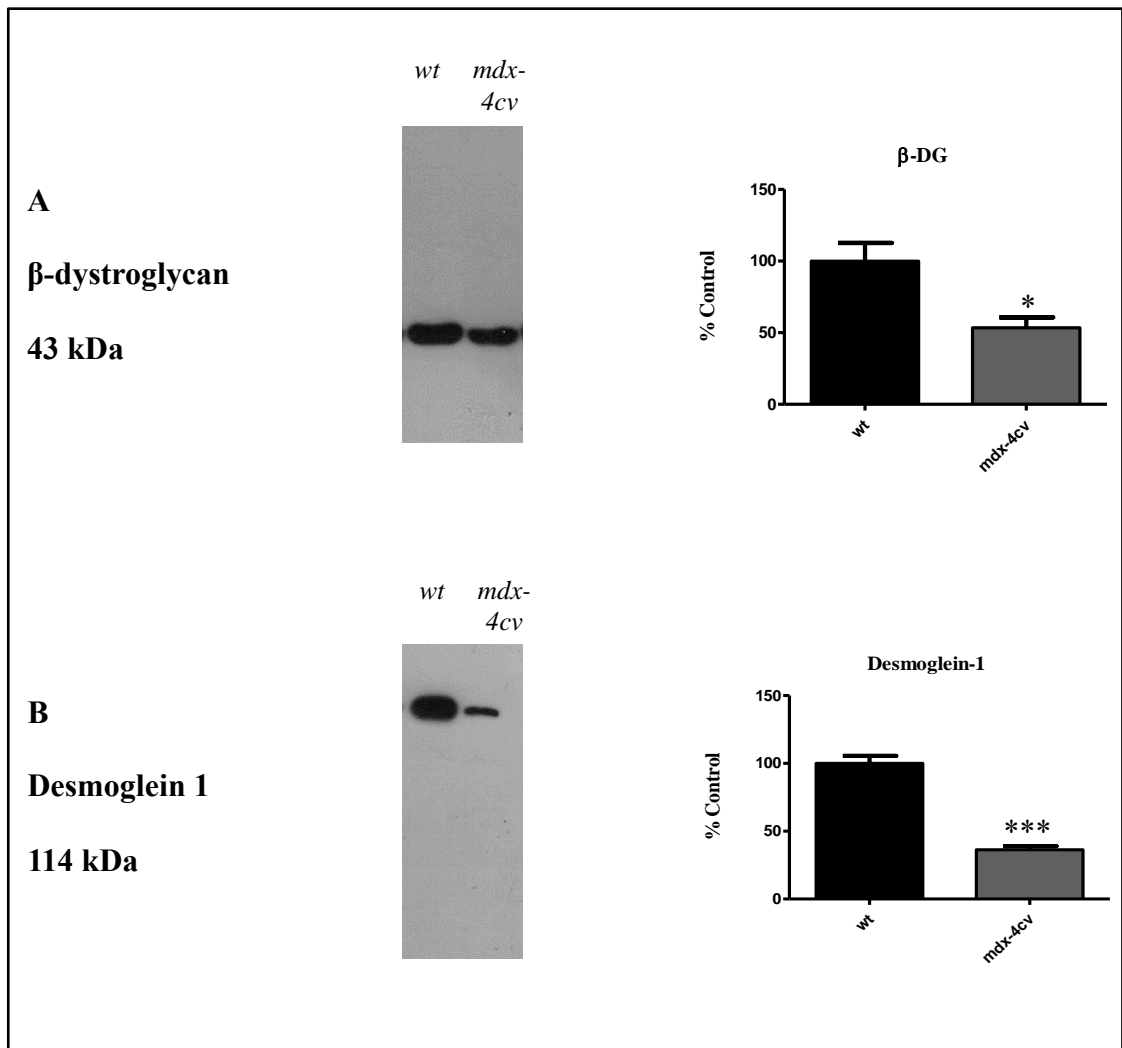


Figure 4.13: Comparative immunoblot analysis of proteins with decreased abundance in dystrophic *mdx-4cv* enriched sarcolemma

Shown are representative immunoblots with immuno-decorated bands labelled with an antibody to β -dystroglycan (A) and desmoglein-1 (B). Statistical analysis of immuno-decoration was performed with Student's *t*-test (mean values \pm SEM; unpaired; $n=4$, * $p\leq 0.05$, *** $p\leq 0.001$).

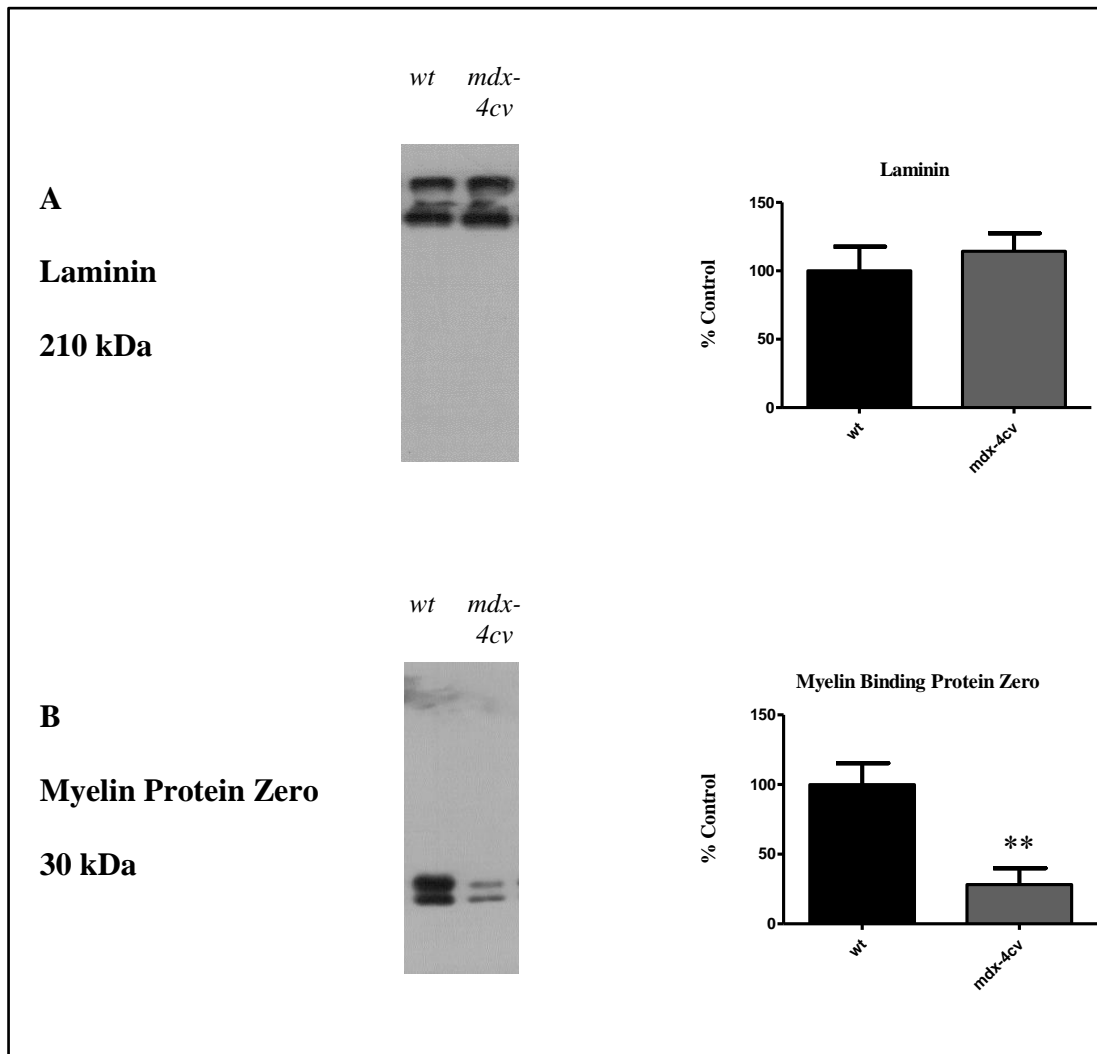


Figure 4.14: Comparative immunoblot analysis of myelin protein zero in dystrophic *mdx-4cv* enriched sarcolemma

Shown are representative immunoblots with immuno-decorated bands labelled with antibodies to laminin (A) and myelin protein zero (B). These immunoblots were performed using 50 μ g protein per lane. Statistical analysis of immuno-decoration was performed with Student's *t*-test (mean values \pm SEM; unpaired; $n=4$, ** $p\leq 0.01$).

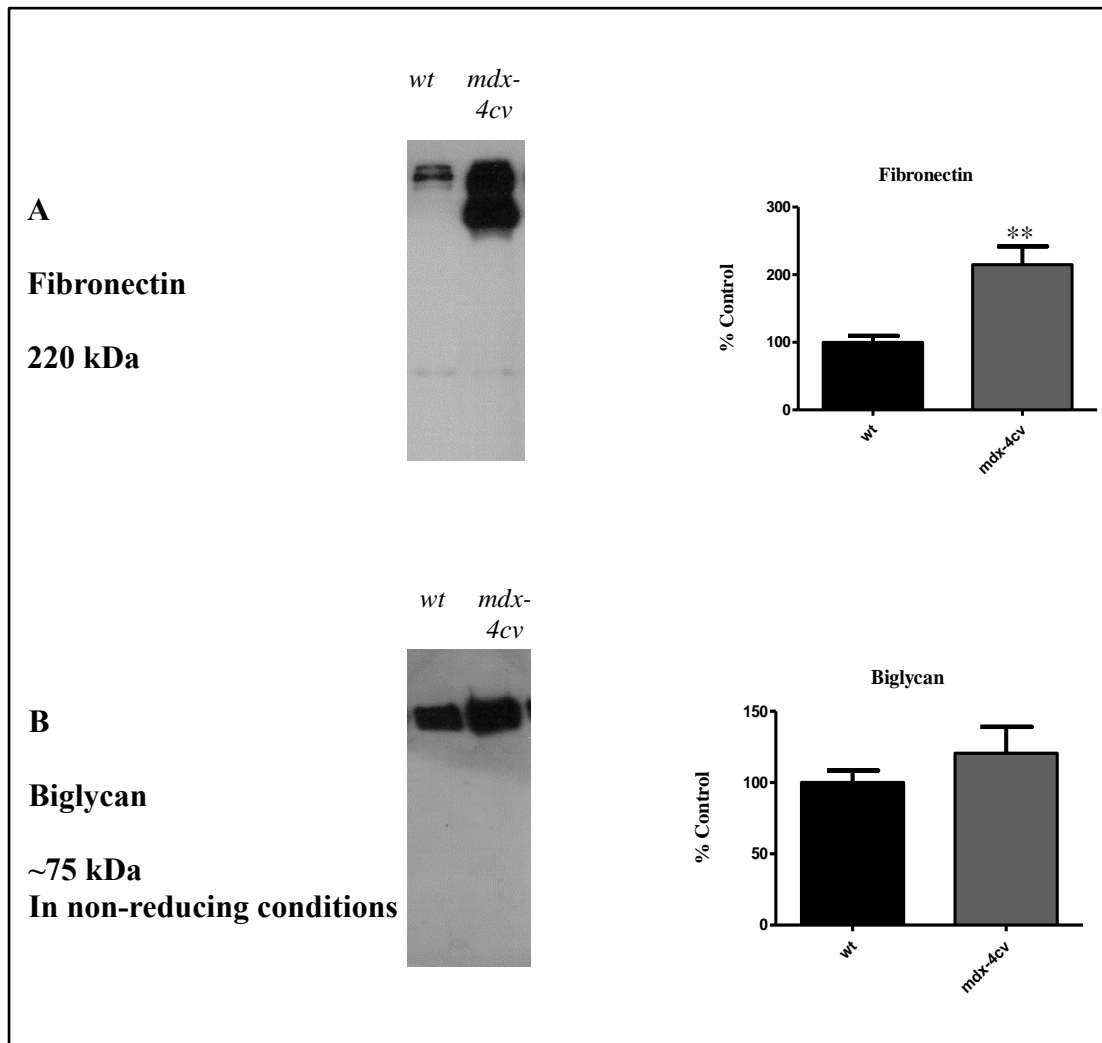


Figure 4.15: Comparative immunoblot analysis of proteins with increased abundance in dystrophic *mdx-4cv* enriched sarcolemma

Shown are representative immunoblots with immuno-decorated bands labelled with antibodies to fibronectin (A) and biglycan (B). Statistical analysis of immuno-decoration was performed with Student's *t*-test (mean values \pm SEM; unpaired; $n=4$, $**p \leq 0.01$).

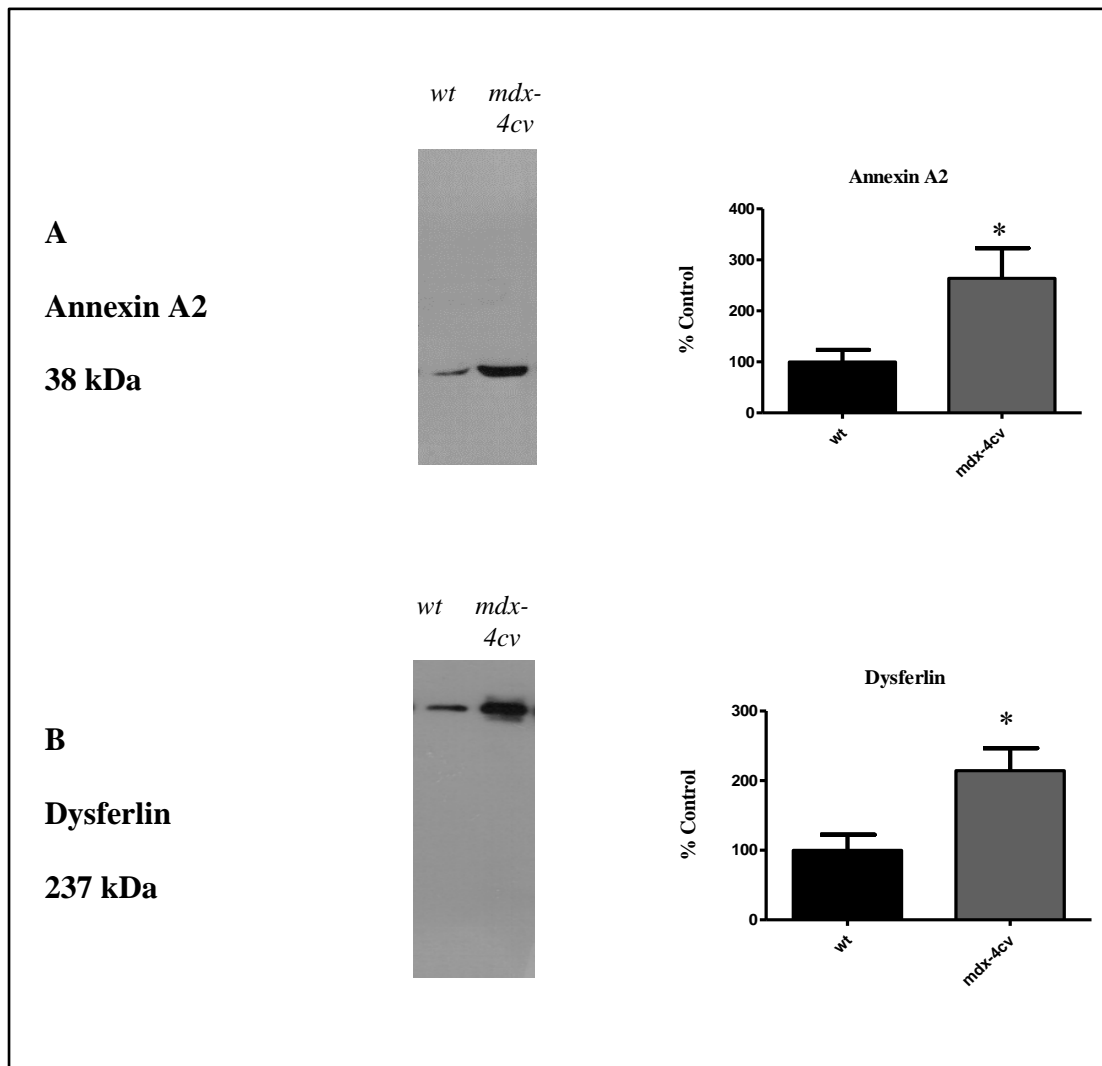


Figure 4.16: Comparative immunoblot analysis of proteins with increased abundance in dystrophic *mdx-4cv* enriched sarcolemma

Shown are representative immunoblots with immuno-decorated bands labelled with antibodies to annexin A2 (A) and dysferlin (B). Statistical analysis of immuno-decoration was performed with Student's *t*-test (mean values \pm SEM; unpaired; $n=4$, $*p \leq 0.05$).

4.3 Discussion

In the modern era of technology-driven proteomic methodologies, subcellular fractionation procedures have been crucial in reducing sample complexity, predicting protein subcellular localisation and establishing the protein constituents of a number of organelles (Gatto et al., 2010), including the nucleus (Schirmer et al., 2003, Andersen et al., 2005), mitochondria (Mootha et al., 2003), the Golgi complex (Wu et al., 2004) and the plasma membrane (Zhang et al., 2003a, Oh et al., 2004). Such subcellular fractionation procedures can greatly reduce the protein dynamic range, enabling the mass spectrometric analysis of lower abundance proteins against which there is an intrinsic bias in mass spectrometric analyses of crude homogenates. In muscular dystrophy research, few comparative proteomic studies have identified dystrophin nor its associated glycoproteins, owing to technical difficulties associated with its large size, low abundance and supramolecular assembly (Hoffman et al., 1987, Ohlendieck and Campbell, 1991b). Here, organelle separation coupled with affinity purification of distinct membrane vesicles across an optimized fractionation scheme has been used to i) enrich for the dystrophin complex to facilitate the identification of potential novel interaction partners, and ii) enrich for the muscle sarcolemma to evaluate the secondary alterations which occur at the muscle membrane in muscular dystrophy.

However, pure organelles, with the exception of the mitochondria and chloroplasts are difficult to obtain (Gatto et al., 2010), and so contaminating proteins were evident in both the dystrophin complex enriched fraction and the sarcolemma enriched fraction. In skeletal muscle, cross-contamination from the highly abundant sarcoplasmic reticulum is a particular issue. This cross-contamination from abundant membrane systems is likely due to complex changes that occur during tissue homogenisation and subcellular fractionation, including protein desorption/adsorption processes, the entrapment of proteins and smaller vesicles in larger membrane vesicles, and the formation of mixtures of membrane sheets, inside-out vesicles and right-side-out vesicles. Other contaminating proteins arise from the mitochondria, the cytosol, the ribosomes, the contractile apparatus and serum. In addition, complex pathophysiological processes, such as inflammation, necrosis and fibrosis, along with cellular adaptations in dystrophic muscle, may distort the efficient isolation of distinct organelles and subsequent comparative proteomic profiling of mutant versus wild-type membrane systems. However, independent verification experiments using

immunoblotting or immunofluorescence microscopy can usually be used to confirm key findings from mass spectrometric surveys, and thus enable the objective evaluation of the validity of pathoproteomic profiles.

Proteomic analysis of the dystrophin complex enriched fraction has enabled the identification of putative novel dystrophin interaction partners. Only a small number of proteins co-purified with the dystrophin-enriched complex. Of the 24 proteins identified when searched against the *Oryctolagus cuniculus* database and filtered for a minimum of two unique peptides, the only identified proteins apart from the known components of the dystrophin associated glycoprotein complex were a number of cytokeratins (KRT10, KRT3, KRT5, KRT1, KRT14, KRT2 and KRT16), the anion exchange protein, voltage-dependent L-type calcium channel subunit alpha-1S, myosin 4, fast SERCA calcium transporting ATPase, and two uncharacterised proteins; G1TQ93 (thought to have actin binding properties) and G1TL92 (postulated to have calcium ion binding activity). Detection of a number of cytokeratins suggests the linkage of the contractile apparatus to dystrophin at the sarcolemma as previously described (Stone et al., 2005). Detection of voltage-dependent L-type calcium channel subunit alpha_{1S}, myosin 4, and fast SERCA calcium transporting ATPase represent possible contamination from the dihydropyridine receptor (as this also binds to wheat germ lectins), the highly abundant contractile apparatus and the sarcoplasmic reticulum respectively. Additional searching of the mass spectrometric data through a *Mammalia* database identified 35 proteins with ≥ 2 unique peptides. This included mainly similar proteins to that identified by the search against the *Oryctolagus cuniculus* database, namely several cytokeratins and the core dystrophin-associated glycoproteins.

However, a number of additional proteins of interest were also identified, in particular desmoplakin, desmoglein-1 and desmocollin-1. Identification of these three proteins suggests the co-purification of a desmosome-like protein complex with the dystrophin complex. These cadherin-type proteins are found in desmosomes, and are particularly associated with cellular adhesion in epithelial cells where mutations and/or alterations in their abundance are associated with a loss of cellular adhesion and blistering of the skin (Hammers and Stanley, 2013). Aside from the skin, desmosomes have also been found to play an important role in other tissues which are subject to high levels of mechanical stress, including cardiac tissue (Lowndes et al., 2014), as illustrated in Figure 4.17. Mutations in genes encoding desmocollin 2,

desmoglein 2 and desmoplakin are all connected to cardiomyopathy, in particular dilated cardiomyopathy and arrhythmogenic right ventricular cardiomyopathy (Phelan et al., 2013). However, the potential roles of these cytolinker proteins in skeletal muscle is less well understood (Kljuic and Christiano, 2003). It is possible that these proteins may play a role in cellular adhesion in skeletal muscle, similar to the protein complexes that exist in the skin and the heart. Immunoblotting against desmoglein-1 in *quadriceps femoris* and *longissimus dorsi* muscle from 100-day old wild-type and *mdx* mice revealed i) the detection of desmoglein-1 by immunoblotting in healthy skeletal muscle and ii) significantly reduced levels of this cellular adhesion protein in dystrophic skeletal muscle. Desmoglein-1 co-purifies with the dystrophin complex and suffers a similar pathobiochemical fate as the dystrophin-associated glycoproteins (Ohlendieck and Campbell, 1991b), thus it may represent a potential dystrophin-associated protein of low abundance that is possibly involved in cellular adhesion in skeletal muscle. Its reduced abundance may have a negative impact on the dystrophic phenotype, as cellular adhesion is required for muscle regeneration. Cellular adhesion is necessary for the fusion of myoblasts to form multinucleated myotubes during muscle regeneration, and this has long thought to be primarily mediated by M-cadherin (Karalaki et al., 2009), although other studies suggest that N-cadherin can be used as a substitute (Hollnagel et al., 2002).

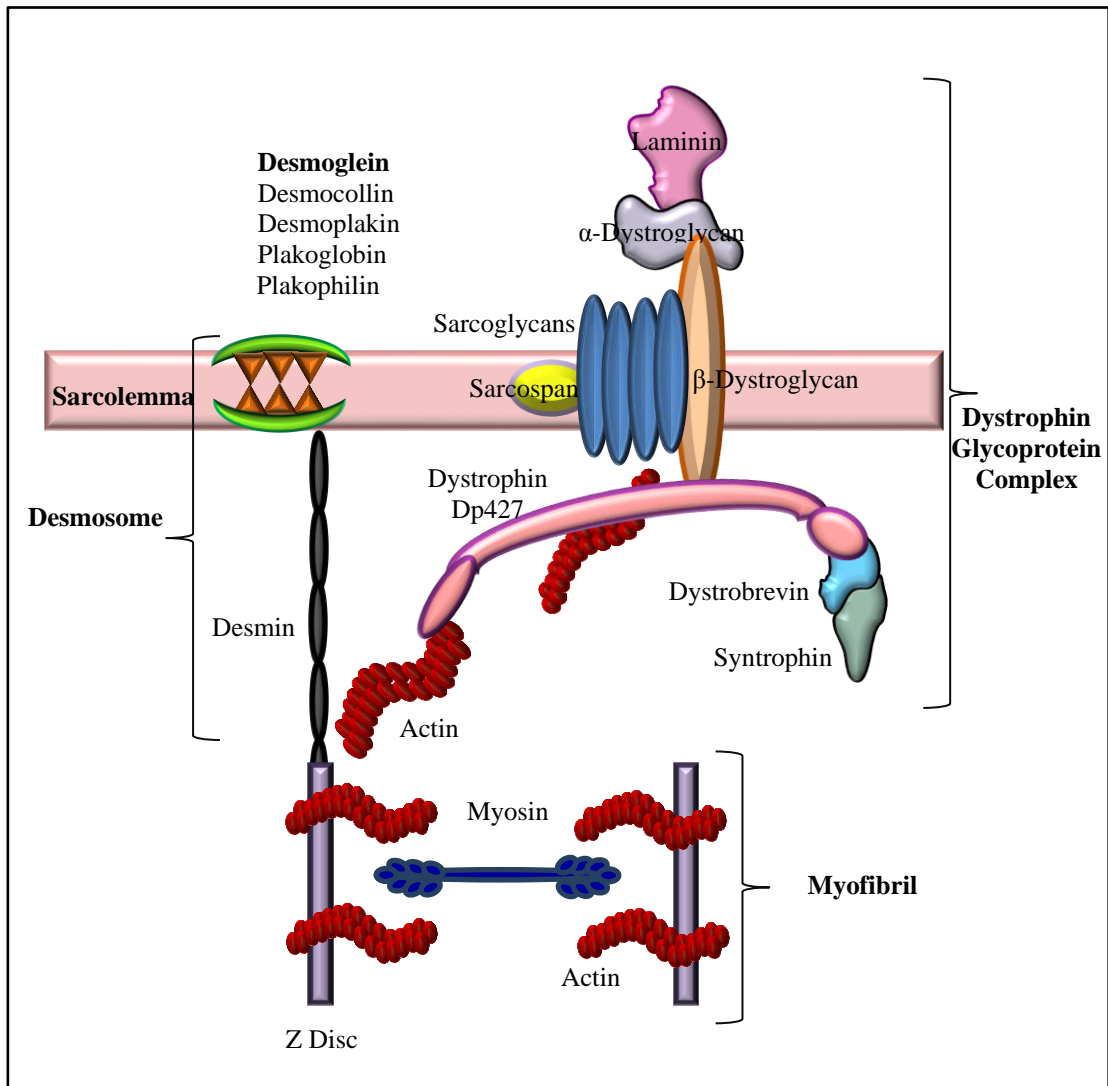


Figure 4.17: Localisation of desmosomes in cardiac tissue

In cardiac tissue, the desmosome forms a junction between adjacent cardiomyocytes and links to the cytoskeleton via the intermediate filament desmin. Several proteins form the desmosome protein complex including; desmoplakin, desmoglein, plakophilin, plakoglobin and desmocollin. With the exception of plakoglobin, mutations in the genes encoding these proteins are associated with dilated cardiomyopathy. However, the role of these proteins in skeletal muscle is less well characterised. Reduced abundance of desmoglein-1 in dystrophic skeletal muscle, as shown in immunoblot analyses, shows that desmoglein-1 suffers the same fate as members of the DGC in dystrophinopathy.

*Image modified from Phelan et al., 2013

Comparative proteomics of the enriched sarcolemma fraction from the *mdx-4cv* model of DMD revealed altered abundance for 190 distinct protein species; 163 of which were elevated in abundance and 27 of which were decreased in abundance. This analysis identified a number of distinct pathological alterations in muscle fibres; including reactive myofibrosis, compensatory up-regulation of cytoskeletal networks, perturbed Na⁺/K⁺- and Ca²⁺- pumping, shifts in bioenergetic pathways, increased protein synthesis, elevated cellular stress, impaired ion buffering, disturbed excitation-contraction coupling, activation of the innate immune response and impaired sarcolemmal integrity.

A variety of bioinformatics tools, including STRING, DAVID and KEGG all identified the ribosome as a key enriched biological category (Figures 4.9 and 4.11). Elevated abundance was detected for a considerable number of both 40S (S2, S3, S3a, S4, S6, S8, S9, S11, S13, S15a, S16, S18, S23, S25 and SA) and 60S (L4, L6, L7a, L7, L8, L10a, L12, L13, L14, L18, L35 and L36) ribosomal proteins. This is indicative of an increased rate of protein synthesis and of major regeneration occurring during muscle repair. In particular, enhanced protein synthesis of cytoskeletal and mechanical proteins may occur in order for structural remodelling to take place. This is evident in the substantial number of structural and cytoskeletal proteins with elevated abundance in *mdx-4cv* tissue, including clathrin heavy polypeptide, myosin binding protein C, myosin light chain fast skeletal muscle, tubulin alpha 4a, vimentin, actinin alpha 1, actinin alpha 2, actinin alpha 3, gelsolin and various integrin isoforms. The 22.7-fold increase in the embryonic myosin heavy chain 3 is further indicative of a regenerative process in the dystrophin-deficient skeletal muscle (Schiaffino et al., 2015).

The immune response has been recognised as a key propagator of the dystrophic phenotype, although the exact role of the immune system is still poorly understood (Villalta et al., 2015). A prominent role for the immune response is also evident here in the mass spectrometry data of enriched sarcolemma from the *mdx-4cv* mouse with the top three increased proteins; eosinophil peroxidase, H-2 class II histocompatibility antigen gamma chain and caspase recruitment domain-containing protein 19, associated with immunity (Table 4.2). Eosinophil peroxidase is the dominant component of eosinophilic granulocytes (Wang and Slungaard, 2006) and is associated with eosinophil migration, the generation of potent oxidising species (Acharya and Ackerman, 2014) and positive regulation of IL-4, a cytokine involved in the differentiation of naïve helper T cells into Th2 cells (Wehling-Henricks et al.,

2008). Initially associated with host defence through a substrate-dependent ability to kill bacteria, viruses and parasites as demonstrated by the Klebanoff group (Jong et al., 1981, Henderson et al., 1980), eosinophil peroxidase has been more recently implicated in disease pathology, for example in the pathogenesis of ulcerative colitis (Forbes et al., 2004). In the context of DMD eosinophil invasion into skeletal muscle has been previously identified (Cai et al., 2000). The associated increase in levels of eosinophil peroxidase, as seen here in the sarcolemma enriched fraction from murine hind leg, may result in elevated levels of IL-4 which may prove beneficial for the recruitment and fusion of satellite cells involved in muscle regeneration. However, the IL-4-induced shift to a prolonged Th2 immune response could potentially contribute to chronic inflammation and fibrosis (Wehling-Henricks et al., 2008). In addition, the production of the potent toxins hypohalous acids and peroxynitrate catalysed by eosinophil peroxidase may exacerbate skeletal muscle damage (Wehling-Henricks et al., 2008). The 60.7-fold increase in the caspase recruitment domain-containing protein Card19 is an interesting finding considering it has previously been shown to play a role in inhibiting the effects of BCL10-induced activation of NF- κ B (Woo et al., 2004). This increase in Card19 possibly represents a compensatory mechanism to counteract excessive activation of NF- κ B, whereby skeletal muscle-specific activation of NF- κ B occurs even prior to the onset of dystrophic damage in the *mdx* mouse (Kumar and Boriek, 2003) and inhibition of NF- κ B improves muscle function and reduces skeletal muscle degeneration in the *mdx* mouse model (Messina et al., 2006, Messina et al., 2009).

Dramatically elevated abundances were also evident for two subunits of the histocompatibility complex; 117.4-fold increase for H-2 class II histocompatibility antigen gamma chain and 20.1-fold increase for H-2 class I histocompatibility antigen, K-B alpha chain. While major histocompatibility complex I proteins are present on most nucleated cells and have previously been found at increased levels on muscle fibres from DMD patients (McDouall et al., 1989), major histocompatibility complex II proteins are normally only present on professional antigen-presenting cells and so the large increase in H-2 class II histocompatibility antigen gamma chain detected in this study likely reflects the infiltration of antigen-presenting cells into dystrophic skeletal muscle (Evans et al., 2009). Other immune proteins of interest include receptor-type tyrosine-protein phosphatase C which is positive regulator of T-cell co-activation (Mustelin and Taskén, 2003) and the macrophage-restricted marker

sialoadhesin and macrophage mannose receptor 1 which are indicative of macrophage infiltration and inflammation (O'Neill et al., 2013).

A number of proteins are associated with sarcolemmal alterations (as illustrated in Figure 4.18), an expected result given that the disease primarily affects the DGC of the sarcolemma. Decreased abundance was detected for protein components of this complex, namely dystrophin, β -dystroglycan, α -sarcoglycan and δ -sarcoglycan, as originally described in 1991 (Ohlendieck and Campbell, 1991b). The loss of dystrophin and concomitant perturbation of the DGC appears to trigger a number of secondary alterations at the sarcolemma, with a variety of proteins showing elevated abundance, including the $\alpha 1$ and $\alpha 2$ subunits of Na^+/K^+ -ATPase and the plasma membrane calcium transporting ATPase 1 (PMCA1). This indicates altered ion exchange across the muscle membrane, whereby the increase in the Na^+/K^+ -ATPase may represent a compensatory mechanism to counteract abnormal ion fluxes across the dystrophin-deficient membrane (Murphy et al., 2015a, Dunn et al., 1995). PMCA is responsible for the extrusion of Ca^{2+} out of the cell and the establishment of a Ca^{2+} gradient with low levels in the cytosol and higher levels outside of the cell, and PMCA levels have been demonstrated to increase in response to raised cytoplasmic Ca^{2+} concentrations (Abell et al., 2011). Heightened levels of PMCA have been previously identified in EDL muscle from *mdx* mice (Cully et al., 2012), where it has been proposed that PMCA activity is affected by increased Ca^{2+} leakage across the dystrophic membrane, and thus its abundance is augmented to maintain an activity similar to that seen in wild-type mice.

In addition, increased abundance was measured for integrin $\alpha 7$, the membrane repair proteins myoferlin and dysferlin and the actin-crosslinking protein filamin C. Myoferlin and dysferlin are highly related proteins of the ferlin family which are proposed to mediate membrane fusion events in response to Ca^{2+} , and thus are involved in the maintenance and repair of the plasma membrane (Bansal and Campbell, 2004). The importance of these proteins in membrane repair is evident by the fact that mutations in dysferlin are responsible for limb-girdle muscular dystrophy (type 2B) and Miyoshi myopathy and that increased abundance of myoferlin mRNA and protein have been identified in damaged myofibres from γ -sarcoglycan null mice and *mdx* mice (Demonbreun et al., 2010). Here, elevated abundance was detected for both myoferlin and dysferlin in the sarcolemma enriched fraction from *mdx-4cv* mice, indicating a potential compensatory mechanism to help repair micro-ruptures in the

dystrophin-deficient membrane. Indeed, increased abundance was also detected for annexin A1 and annexin A2 (P07356, 1 unique peptide, 5.35-fold increase), proteins previously proposed to be involved in dysferlin-mediated membrane repair (Lennon et al., 2003). The filamins are a class of actin-crosslinking proteins with three isoforms filamin A, B and C. Filamin C is a skeletal and cardiac muscle-specific isoform which localises to the myotendinous junction, sarcolemma, costameres, Z-disks and intercalated disks where it interacts with the DGC, integrins and a number of Z-disk proteins including myotilin (van der Ven et al., 2000) and myopodin (Linnemann et al., 2010). Recent results from a medaka mutant with a nonsense mutation in a filamin C homolog indicate that filamin C is involved in the maintenance of Z-disk structures, the attachment of myofibrils to the sarcolemma and the stabilisation of myofibrils at the myotendinous junction (Fujita et al., 2012). The elevated abundance of filamin C seen here may be attributable to a compensatory increase to stabilise the weakened muscle, help protect against mechanical stress and to improve actin linkage and structural stability in the absence of dystrophin. The 4.8-fold increase in the abundance of integrin alpha 7, a transmembrane link between the basal lamina and the muscle fibre, is a potential compensatory mechanism that may partially offset the negative impact of dystrophin deficiency on muscle fibre architecture. Indeed transgenic expression of rat integrin alpha 7 in severely dystrophic *mdx/utr^{-/-}* mice missing both dystrophin and its homologous protein utrophin improves lifespan, mobility and muscle function and reduces kyphosis and hindlimb joint contractures in these mice (Burkin et al., 2001).

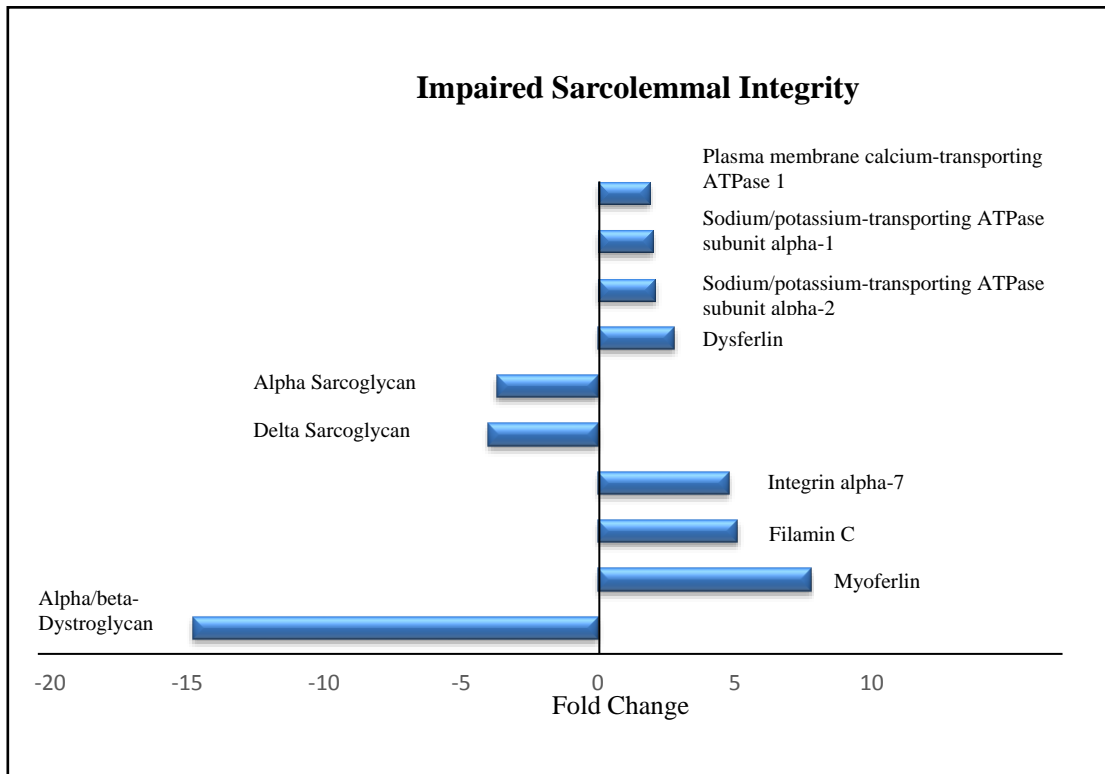


Figure 4.18: Impaired sarcolemmal integrity in the *mdx-4cv* model of Duchenne muscular dystrophy

Mass spectrometric analysis reveals alterations in abundance for 190 proteins in the *mdx-4cv* mouse model of dystrophinopathy. A number of these proteins are associated with the sarcolemma, a select panel of which are illustrated above, indicating that dystrophin deficiency in the *mdx-4cv* mouse model is accompanied by impaired sarcolemmal integrity. Proteins to the left of the y-axis line are those with decreased abundance, while proteins to the right are those with elevated abundance in the *mdx-4cv* model. Except for dysferlin all proteins were detected by a minimum of two unique peptides.

In the many types of muscular dystrophy, moderate fibre type conversions are evident, whereby fast type IIb fibres have been shown to be more susceptible to degenerative processes (Webster et al., 1988). Indeed 25% of muscle fibres in Duchenne patients only express the adult slow isoform of myosin heavy chain (Marini et al., 1991). In this study focusing on a sarcolemma-enriched fraction, co-purifying proteins from other abundant systems identified some impact on fibre speciation, with increased abundance seen for MyHC-2x (myosin-1), MyHC-2b (myosin-4) and fast myosin-binding protein C. However, no clear fibre type switching is evident, likely due to the fact that the original sample consisted of combined muscles of the hind-limb which would contain a heterogeneous mix of fibre types. Encouraging improvements in mass spectrometric analyses of muscle have recently enabled single muscle fibre proteomic analysis which has the capacity to detect fibre-type specific features of human aging, with glycolysis and glycogen metabolism increased in slow but decreased in fast muscle fibres during fibre senescence (Murgia et al., 2017). Such an approach could potentially be used to elucidate the pathophysiology of DMD in a sub-type specific manner, which could be especially interesting given the observed augmented vulnerability of fast muscle fibres to disintegration.

An interesting finding is the 5.3-fold decrease in the intermediate filament protein synemin; of which two splice variants exist in humans, α -synemin and β -synemin (also known as desmuslin), with α -synemin predominantly expressed in the brain and β -synemin predominantly expressed in skeletal muscle (Mizuno et al., 2004). β -synemin was originally shown to interact with the other major intermediate filaments desmin and vimentin to form heteropolymeric intermediate filaments where it contributes to cellular resilience (Bellin et al., 1999), with later studies also suggesting an interaction with components of the DGC; namely α -dystrobrevin (Mizuno et al., 2001), dystrophin, and utrophin (Bhosle et al., 2006). Confocal microscopy localises β -synemin mainly to the muscle Z-line, the costamere and the neuromuscular and myotendinous junctions of a myofibre, suggesting a functional role for β -synemin in maintaining muscle integrity during excitation-contraction-relaxation cycles (Mizuno et al., 2004). Thus, reduced levels of β -synemin are possibly involved in the secondary pathobiochemical changes that render dystrophin-deficient fibres more susceptible to micro-rupturing of the disintegrating sarcolemma.

This finding is particularly interesting when considered alongside the observed decrease in the abundance of the myelin specific proteins periaxin and myelin binding

protein zero. Myelin binding protein zero displayed the second highest fold decrease with a fold change of -33.8 in *mdx-4cv* sarcolemma. Reduced abundance was also detected for myelin basic protein and myelin associated glycoprotein although these proteins were only identified by a single unique peptide (myelin basic protein: accession number P04370; confidence 3.18; Anova (p) 8.9E-05; fold decrease 16.8 and myelin-associated glycoprotein: accession number P20917; confidence 2.64; Anova (p) 2.6E-03; fold decrease 33.5). Myelin basic protein belongs to the basic group of myelin proteins; proteins with a high positive charge and thus basic isoelectric point, and is one of the predominant proteins in central nervous system myelin, where it is responsible for maintaining the stability and integrity of the myelin sheath (Han et al., 2013). It also interacts with a number of proteins including the calcium sensor calmodulin (Grand and Perry, 1980), actin, tubulin (Boggs, 2006) and Src homology-3 domain containing proteins, and thus may act as a signalling molecule modulating the myelin membrane and cytoskeletal assembly (Polverini et al., 2008).

Myelin protein zero, a cell adhesion molecule of the immunoglobulin family, is the most abundant myelin protein in the peripheral nervous system (Han et al., 2013). It plays an important role in normal myelination, with mutations in the myelin protein zero gene resulting in a vast array of neuropathies, including Charcot-Marie-Tooth disease type 1, Dejerine-Sottas syndrome and congenital hypomyelination (Nelis et al., 1999). Another member of the immunoglobulin family is myelin-associated glycoprotein which is present in both central and peripheral system myelin (Han et al., 2013). It has been shown to be involved in the inhibition of neuronal regeneration in developing cerebellar and adult dorsal root ganglion neurons (Mukhopadhyay et al., 1994). The reduced abundance of a number of myelin proteins, including myelin protein zero, myelin basic protein, myelin associated glycoprotein and periaxin, likely reflects a general muscular dystrophy-induced perturbation of the motor neuron system and in particular myelination.

Interestingly, a recent study demonstrated a role for dystrophin in developmental myelination (Aranmolate et al., 2017), which may help explain the reduced levels of myelination specific proteins in the absence of dystrophin, as observed here in the dystrophin-deficient muscle sarcolemma. Indeed the study by Aranmolate identified reduced levels of total myelin basic protein in the cerebral cortex of *mdx* mice at early stages of development suggesting that myelination is developmentally delayed in this model. Periaxin was originally described in 1994 as

a novel protein of myelinating Schwann cells (Gillespie et al., 1994), and was later found by the same group to be linked to a dystroglycan complex at the Schwann cell plasma membrane through interactions with dystrophin-related protein DRP2 (Sherman et al., 2001). Given DRP2 is specifically depleted in the absence of L-periaxin, L-periaxin potentially acts as a scaffolding protein for the DRP2 dystrophin associated glycoprotein complex in Schwann cells, and its ability to homodimerise may help to cluster the complex (Sherman et al., 2001). Since dystroglycan interacts, albeit weakly, with DRP2 presumably anchoring the periaxin/DRP2 protein complex to the Schwann cell plasma membrane, the reduced abundance of β -dystroglycan in DMD may destabilise the Schwann cell dystroglycan complex thus leading to the reduced abundance of periaxin as detected here by mass spectrometry. As such a hypothesis remains to be tested experimentally, all that can be concluded with confidence is that reduced abundance of periaxin indicates muscular-dystrophy related changes in the motor neuron system, particularly related to peripheral nerve myelination whereby a periaxin/DRP2/dystroglycan complex could act as a signalling complex which regulates myelin sheath thickness and stability (Wrabetz and Feltri, 2001).

In contrast to these Schwann cell markers, elevated abundance was identified for the neural cell adhesion molecule N-CAM1 and the synaptic vesicle membrane protein VAT-1. VAT-1 is an abundant integral membrane protein of cholinergic synaptic vesicles, with early evidence for the structure and function of this protein coming from studies using VAT-1 isolated from the Torpedo electric organ (Linial et al., 1989). The VAT-1 protein is involved in vesicular transport and plays a role in neurotransmitter storage and release at cholinergic synapses. N-CAM1 is a cell adhesion glycoprotein with particularly high expression in the central nervous system where it is involved in cellular adhesion, neurite outgrowth and cell migration, proliferation and survival. N-CAM is also initially expressed at the muscle sarcolemma during skeletal muscle development, and while its levels decrease significantly following muscle fibre innervation, its abundance increases once again in both the fibre cytoplasm and sarcolemma in response to denervation and nerve crush (Moore and Walsh, 1986). Moreover, Walsh and Moore also observed increased N-CAM staining associated with regenerating myofibres in biopsies of patients with neuromuscular disease, including Becker and Duchenne muscular dystrophy, limb girdle muscular dystrophy, polymyositis and mitochondrial myopathy (Walsh and

Moore, 1985). This finding was also more recently confirmed by Prattis and colleagues where immunohistochemistry identified elevated N-CAM abundance in dystrophic *mdx* mice and GRMD dogs (Prattis et al., 1994). Thus, the occurrence of increased N-CAM1 levels detected here agrees with degeneration-regeneration cycles in the neuromuscular system.

4.3.1 Conclusions

Mass spectrometry-based proteomics has been instrumental in developing the field of muscle proteomics and in identifying proteome-wide alterations in muscle disease. In DMD, the large size, complexity, low-abundance and hydrophobicity of the DGC renders its proteomic characterisation technically challenging. In this chapter, lectin affinity chromatography has enabled the successful enrichment of the DGC and the sarcolemma from skeletal muscle. Interaction proteomics of the dystrophin complex enriched fraction has established the cytolinkers desmoglein-1 and desmoplakin as potential novel dystrophin-associated proteins. Immunoblotting of desmoglein-1 in *quadriceps femoris* and *longissimus dorsi* muscle from the *mdx* mouse and crude skeletal muscle homogenates from the *mdx-4cv* mouse has identified significantly lower levels of desmoglein-1 in these dystrophic mouse models. Thus, this desmosomal protein suffers a similar pathobiochemical fate to the known protein members of the DGC in the absence of dystrophin. The comparative proteomic profiling of the sarcolemma enriched fraction from the *mdx-4cv* mouse could furthermore establish the initiation of membrane repair involving myoferlin, dysferlin and annexins, compensatory increases in cytoskeletal proteins, infiltration of immune cells, enhanced cellular stress and an increased rate of protein synthesis suggested by increases in a large number of ribosomal protein subunits. Besides well-established decreases in dystrophin and its associated glycoproteins, reduced protein abundances were also detected for the scaffolding protein periaxin and myelin protein zero of Schwann cells, which may be indicative of altered myelination levels of motor neurons in muscular dystrophy.

Chapter Five

Proteomic profiling of the aged *mdx-4cv* heart; implications for dystrophinopathy-related cardiomyopathy

5.1 Introduction

Dystrophin, a large sub-sarcolemmal cytoskeletal protein of 427 kDa, is responsible for linking the actin cytoskeleton to components of the extracellular matrix through the DGC. Mutations affecting the *Dmd* gene encoding for dystrophin lead to dystrophinopathies including DMD, BMD and X-linked dilated cardiomyopathy (XLDCM) (Ferlini et al., 1999). Duchenne and Becker muscular dystrophies both involve progressive degeneration of the skeletal muscle with some cardiac involvement, with DMD representing the more severe form of the allelic disorder. XLDCM meanwhile is characterised by progressive cardiac dysfunction leading to heart failure in the absence of any skeletal muscle degeneration (Johnson et al., 2012). Similar to skeletal muscle, the DGC also exists in the sarcolemma of cardiomyocytes where it maintains membrane integrity and acts as a scaffold for signalling molecules such as nitric oxide. However, unlike in skeletal muscle where regeneration is facilitated by the activation of the satellite stem cell pool, there is little evidence of regeneration in the dystrophin-deficient heart despite the progressive loss of cardiomyocytes (Heydemann and McNally, 2007). Cardiac complications are usually detected later than skeletal muscle symptoms, with the earliest changes typically identified between the ages of 10 to 15 years (McNally, 2007). However, in one study, up to 25% of DMD patients with a mean age of 10.7 years already displayed abnormal left ventricle function, as indicated by a left ventricular ejection fraction $< 55\%$ (Duboc et al., 2005). This indicates that the delay in overt cardiomyopathy is not due to a later age of onset but instead it may remain undetected possibly as a result of reduced physical activity due to skeletal muscle weakness.

Cardiac complications in DMD include abnormal left ventricle function and size, reduced systolic function and cardiac arrhythmias. Angiotensin-converting enzyme inhibitors and β -adrenergic blockers are standard therapy for cardiomyopathy in general and so are typically also used in the treatment of muscular dystrophy-associated cardiomyopathy. These therapies usually improve left ventricular function and size towards normal levels (Heydemann and McNally, 2007). Other approaches are also being investigated, such as the use of the non-ionic triblock co-polymer poloxamer 188 as a membrane sealant. Pre-treatment of dystrophin-deficient cardiomyocytes with poloxamer 188 induced sufficient sealing of the membrane to prevent stretch-induced injury. In addition, *in vivo* administration of poloxamer 188 to

dystrophic *mdx* mice blocked the development of acute cardiac failure following infusion of the cardiovascular stressor dobutamine (Yasuda et al., 2005). A long-term beneficial effect has also been illustrated in the larger and more severely affected GRMD canine model using chronic infusion of poloxamer 188 (Townsend et al., 2010).

A number of studies have indicated that the survival rate of patients with DMD is increasing due to improvements in the management of the disorder. In particular, advances in respiratory care such as non-invasive ventilation and tracheostomy have led to a longer life-span (Passamano et al., 2012). However, since respiratory failure, previously the main cause of death in patients, is now more manageable progressive cardiomyopathy has become a leading cause of morbidity and mortality (Yilmaz and Sechtem, 2012). Several potential therapies for DMD are currently being trialled and some, including exon skipping and stem cell therapy, have shown promise in ameliorating the dystrophic phenotype in animal models of the disorder (Sampaolesi et al., 2006, Alter et al., 2006). However, while these treatments appear to show beneficial effects in skeletal muscle, the heart remains largely untreated (Lu et al., 2005). Caution needs to be exercised with such therapies as studies with animal models have demonstrated that treatment of the skeletal muscle alone may actually accelerate cardiac disease (Townsend et al., 2008). It is possible that increases in physical activity as a result of improvements in skeletal muscle strength may cause heightened cardiac injury in untreated dystrophin-deficient hearts, ultimately progressing to heart failure. Thus, studies investigating the pathobiochemistry of DMD-associated cardiomyopathy are required in order to best manage cardiac care in patients to further improve long-term survival.

Previous proteomic studies of dystrophic cardiomyopathy have focused on the *mdx* model of DMD. Both 2D-DIGE and label-free LC approaches coupled with mass spectrometry have been used to characterise the dystrophic heart. Such studies have identified alterations in energy metabolism, the contractile apparatus and the cellular stress response (Holland et al., 2013, Lewis et al., 2010). Building upon these comparative proteomic studies, a highly sensitive LC-MS/MS approach was used to investigate the molecular pathogenesis of cardiomyopathy in an alternative animal model; the *mdx-4cv* mouse model of DMD. This study has identified significant decreases for a variety of mitochondrial proteins, the basal membrane protein laminin,

various components of the DGC and the calcium-handling protein sarcalumenin in the aged dystrophic heart. Loss of full-length dystrophin appears to be correlated with elevated levels of fibrotic proteins such as lumican, asporin and periostin, proteins of the extracellular matrix and the cytoskeleton, and various heat shock proteins. Overall, cardiomyopathy in the senescent *mdx-4cv* heart appears to be associated with altered metabolism, calcium handling, the cellular stress response and the cytoskeletal network, similar to that seen in the *mdx* model.

5.1.1 Experimental Design

To determine the effects of dystrophin deficiency on the senescent cardiac proteome, label-free mass spectrometric analysis was performed on 20-month old cardiac tissue from the *mdx-4cv* animal model of DMD. The urea soluble protein constellation was prepared from whole hearts of age-matched wild-type and *mdx-4cv* mice (n=4). Following protein digestion and acidification, the samples were kept on ice for 30 min, centrifuged at $14,000 \times g$ at 4 °C for 20 min and the supernatant was transferred to vials for mass spectrometric analysis. Cardiac samples were analysed by label-free LC-MS/MS using an Ultimate 3000 NanoLC system (Dionex Corporation, Sunnyvale, CA, USA) coupled to a Q-Exactive mass spectrometer (Thermo Fisher Scientific). Peptides generated from cardiac proteins were eluted using the following binary gradient: solvent A [2% (v/v) ACN and 0.1% (v/v) formic acid in LC-MS grade water] and 0-90% solvent B [80% (v/v) ACN and 0.1% (v/v) formic acid in LC-MS grade water]: 2-40% solvent B for 120 min, 40-90% solvent B for 2.5 min, 90% solvent B for 9 min and 2% solvent B for 43 min. Relative quantification and identification of mass spectrometry raw files (wild-type n=4, *mdx-4cv* n=3) was performed with Progenesis QI for Proteomics software, using Sequest HT and MASCOT search engines and the UniProtKB-SwissProt database. Bioinformatics analysis was conducted using the PANTHER database of protein families and STRING software. Key proteins of interest were independently verified by comparative immunoblotting to confirm altered protein abundance levels of cardiac proteins revealed by label-free mass spectrometry.

5.2 Results

A deeper understanding of the cardiomyopathy arising from dystrophin deficiency is essential given the high proportion of cardiac complications in Duchenne patients. For this reason, proteomic profiling of wild-type versus *mdx-4cv* hearts obtained from 20-month old mice was conducted. This age group was chosen as it represents the end stage of the disease and thus may provide insights into the proteomic basis behind cardiac failure. Label-free LC-MS/MS identified alterations in the expression of 98 proteins, a number of which were subsequently verified by immunoblotting. Of these 98 proteins, 54 display increased expression in the *mdx-4cv* heart while the remaining 44 proteins are decreased in abundance in dystrophin-deficient hearts.

5.2.1 Qualitative analysis of wild-type versus *mdx-4cv* senescent heart

Advances in mass spectrometry have accelerated in recent years. While the introduction of 2D-DIGE was heralded as a major breakthrough just under 20 years ago in terms of its ability to circumvent issues of gel-to-gel variation and reproducibility (Unlü et al., 1997), the proteomic era has taken another step forward with the consistently improving resolution of LC-MS/MS. Gel-based proteomic studies have largely failed to identify very large molecular weight proteins, or have identified them but by very few peptides and little sequence coverage (Lewis and Ohlendieck, 2010a). In this proteomic survey, qualitative analysis of the aged heart identified 1,803 proteins in wild-type samples, with 1,350 of these proteins detected by at least two unique peptides. 1,660 proteins were identified in *mdx-4cv* cardiac samples of which 1,263 proteins possessed a minimum of two unique peptides. A number of components of the DGC were identified in wild-type cardiac samples including the full-length Dp427 isoform of dystrophin, α -, β -, δ - and γ -sarcoglycan, dystroglycan, isoform 7 of α -dystrobrevin and $\alpha 1$ -syntrophin. Dystrophin was identified by 24 unique peptides, a major analytical achievement given the large size, low abundance and hydrophobicity of this sarcolemmal protein.

5.2.2 Quantitative analysis of cardiac dystrophin and members of the dystrophin-glycoprotein complex

Quantitative analysis of wild-type versus *mdx-4cv* aged cardiac tissue identified reduced abundance for several components of the DGC. The full-length Dp427 isoform of dystrophin exhibits a 8.6-fold decrease in *mdx-4cv* cardiac tissue, agreeing with the dystrophic status of this animal model and its low rate of revertant fibres (Danko et al., 1992). Other members of the cardiac DGC which display reduced abundance in dystrophic cardiac preparations are α 1-syntrophin, α -sarcoglycan, β -sarcoglycan and δ -sarcoglycan (Table 5.1 and Figure 5.1). Although confident identification of proteins by LC-MS/MS typically requires the detection of a minimum of two peptides, the identification of α -, β -, and δ -sarcoglycan by a single unique peptide is shown in Table 5.1 as their small size, low abundance and highly hydrophobic nature typically results in insufficient coverage during routine proteomic screens of crude tissue homogenates. The identification of reduced expression of the cardiac DGC enabled simultaneous proteomic analysis of dystrophin deficiency and corresponding secondary abnormalities within the same animal and within a single analytical run.

Table 5.1: Components of the DGC with reduced expression in 20-month *mdx-4cv* heart

Accession Number	Protein Name	Unique Peptides	Confidence Score	ANOVA	Fold Change
P11531	Dystrophin	24	1299.27	1.79E-04	-8.56
Q61234	Alpha-1-syntrophin	2	139.43	2.37E-03	-4.36
P82349	Beta-sarcoglycan	1	81.6	5.90E-03	-4.01
P82350	Alpha-sarcoglycan	1	39.57	6.19E-03	-3.33
P82347	Delta-sarcoglycan	1	50.49	5.97E-04	-3.31

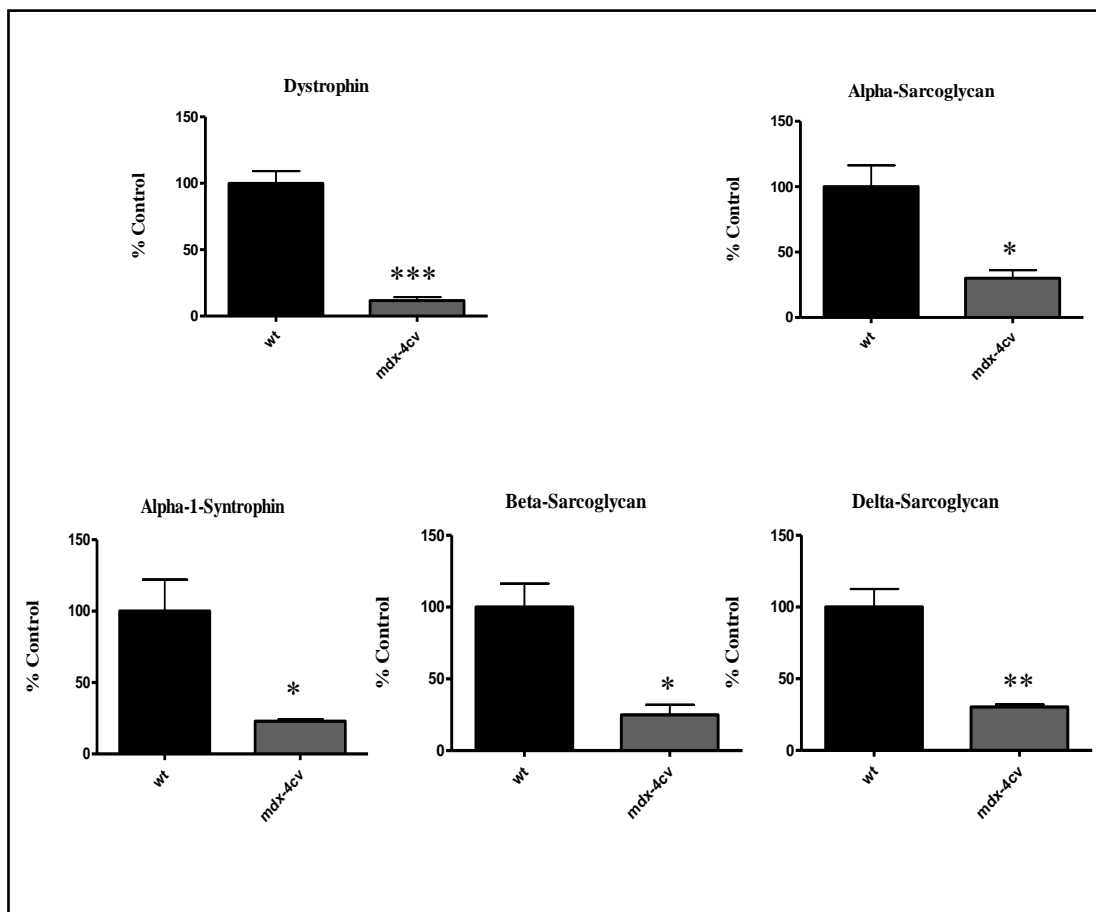


Figure 5.1: Reduction in the expression of DGC proteins as identified by LC-MS/MS

Graphical representation of the reduction in dystrophin, α -1-syntrophin, α -sarcoglycan, β -sarcoglycan and δ -sarcoglycan in 20-month old *mdx-4cv* hearts, as determined by label-free LC-MS//MS. Values are for normalised protein abundances from Progenesis QI for Proteomics software analysis, and statistical analysis was performed using an unpaired Student's *t*-test ($n \geq 3$; *wt*=4, *mdx-4cv*=3, mean \pm SEM, * $p \leq 0.05$, ** $p \leq 0.01$, *** $p \leq 0.001$).

5.2.3 Label-Free LC/MS-MS analysis of protein species with reduced expression in mdx-4cv crude heart extracts

Aside from the reduced expression of protein components of the DGC, a number of other proteins were found to be reduced in abundance indicating proteomic alterations in the absence of dystrophin. Mitochondrial metabolism in particular appears to be severely affected, given the large decreases in the expression of lipoamide acyltransferase component of branched-chain alpha-keto acid dehydrogenase complex and succinyl-CoA ligase (22-fold decrease and 10.2-fold decrease respectively). Reduced expression is seen for a variety of different protein classes including metabolic proteins (lactate dehydrogenase, adenylosuccinate synthetase, perilipin, phosphofructokinase, lipid-transfer protein, glycogen phosphorylase, hydroxysteroid dehydrogenase-like protein 2), cytoskeletal proteins (spectrin, plectin), ion-regulatory proteins (sarcalumenin, SERCA Ca²⁺-ATPase and Na⁺/K⁺-ATPase) and proteins of the extracellular matrix (laminin alpha-2 and beta-2). The 44 proteins with decreased abundance are listed in Table 5.2 below.

Table 5.2: List of identified proteins with a significantly reduced abundance in 20-month old *mdx-4cv* heart versus age-matched wild-type heart as determined by label-free LC-MS/MS

Accession	Gene Name	Protein Name	Unique peptides	Confidence score	Anova (p)	Max fold change
P53395	Dbt	Lipoamide acyltransferase component of branched-chain alpha-keto acid dehydrogenase complex, mitochondrial	2	98.81	4.51E-02	22.09
Q9Z219	Sucla2	Succinyl-CoA ligase [ADP-forming] subunit beta, mitochondrial	3	174.01	8.02E-03	10.20
P11531	Dmd	Dystrophin	24	1299.27	1.79E-04	8.56
P16125	Ldhb	L-lactate dehydrogenase B chain	2	64.80	5.83E-03	6.10
P48962	Slc25a4	ADP/ATP translocase 1	4	107.16	3.09E-02	5.59
P01869	Ighg1	Ig gamma-1 chain C region, membrane-bound form	2	51.72	4.41E-03	4.37
Q61234	Snta1	Alpha-1-syntrophin	2	139.43	2.37E-03	4.36
Q61102	Abcb7	ATP-binding cassette sub-family B member 7, mitochondrial	2	112.89	7.73E-03	3.80
P28650	Adssl1	Adenylosuccinate synthetase isozyme 1	2	115.81	1.21E-02	2.99
P07901	Hsp90aa1	Heat shock protein HSP 90-alpha	2	113.80	6.95E-03	2.67
P08032	Spta1	Spectrin alpha chain, erythrocytic 1	2	120.03	1.35E-02	2.62
O88492	Plin4	Perilipin-4	9	516.88	2.68E-04	2.55
P12382	Pfkl	ATP-dependent 6-phosphofructokinase, liver type	2	118.00	1.10E-02	2.35
Q9QXS1	Plec	Plectin	7	346.77	1.32E-02	2.23
P01872	Ighm	Ig mu chain C region	6	313.39	8.48E-03	2.21
Q7TQ48	Srl	Sarcalumenin	3	154.53	1.63E-02	2.07
Q05793	Hspg2	Basement membrane-specific heparan sulfate proteoglycan core protein	5	318.10	8.26E-03	2.03
Q60675	Lama2	Laminin subunit alpha-2	13	632.93	1.31E-03	1.98
Q9DC70	Ndufs7	NADH dehydrogenase [ubiquinone] iron-sulfur protein 7, mitochondrial	2	86.91	8.07E-03	1.87

Q02566	Myh6	Myosin-6	5	420.64	2.10E-02	1.84
P09411	Pgk1	Phosphoglycerate kinase 1	4	354.81	7.72E-03	1.83
Q9JIF9	Myot	Myotilin	3	103.24	4.45E-04	1.78
Q8VDN2	Atp1a1	Sodium/potassium-transporting ATPase subunit alpha-1	3	116.76	1.80E-02	1.75
P50544	Acadvl	Very long-chain specific acyl-CoA dehydrogenase, mitochondrial	4	258.76	1.69E-03	1.71
Q9R0P3	Esd	S-formylglutathione hydrolase	2	48.47	4.21E-02	1.70
Q60597	Ogdh	2-oxoglutarate dehydrogenase, mitochondrial	4	210.69	1.95E-03	1.70
P52825	Cpt2	Carnitine O-palmitoyltransferase 2, mitochondrial	13	760.94	3.67E-04	1.70
Q8BMS1	Hadha	Trifunctional enzyme subunit alpha, mitochondrial	9	561.61	1.67E-04	1.68
Q8R429	Atp2a1	Sarcoplasmic/endoplasmic reticulum calcium ATPase 1	2	41.78	4.22E-02	1.64
P32020	Scp2	Non-specific lipid-transfer protein	2	125.82	1.78E-02	1.63
Q9WUB3	Pygm	Glycogen phosphorylase, muscle form	4	253.34	8.33E-03	1.60
P02469	Lamb1	Laminin subunit beta-1	2	105.58	8.01E-03	1.54
Q78IK4	Apool	MIC complex subunit Mic27	3	65.98	1.04E-02	1.51
Q99JY0	Hadhb	Trifunctional enzyme subunit beta, mitochondrial	10	462.29	6.73E-03	1.48
Q8CI94	Pygb	Glycogen phosphorylase, brain form	10	492.48	3.95E-04	1.46
Q8VHX6	FlnC	Filamin-C	2	116.85	2.42E-02	1.39
P62897	CyCS	Cytochrome c, somatic	2	200.47	1.26E-02	1.38
Q8BWT1	Acaa2	3-ketoacyl-CoA thiolase, mitochondrial	3	228.54	1.73E-02	1.35
Q99MN9	Pccb	Propionyl-CoA carboxylase beta chain, mitochondrial	2	116.79	2.97E-02	1.34
Q2TPA8	Hsd12	Hydroxysteroid dehydrogenase-like protein 2	2	81.26	2.75E-02	1.32
Q9CQQ7	Atp5f1	ATP synthase F(0) complex subunit B1, mitochondrial	2	83.06	1.02E-02	1.30

Q9CQJ8	Ndufb9	NADH dehydrogenase [ubiquinone] 1 beta subcomplex subunit 9	2	56.39	1.26E-02	1.28
P47934	Crat	Carnitine O-acetyltransferase	5	270.16	1.10E-02	1.26
Q61292	Lamb2	Laminin subunit beta-2	3	166.26	1.61E-02	1.26

5.2.4 Label-Free LC/MS-MS analysis of protein species with increased expression in mdx-4cv crude heart extracts

The global picture of increased protein abundance is suggestive of fibrosis, exemplified by the increases in a number of key pro-fibrotic proteins in the *mdx-4cv* heart. Such proteins include periostin, lumican, asporin and collagen VI. Myosin light chain kinase 3 represents the protein with the highest increase in expression (413.9-fold increase), suggesting alterations in cardiac cells in relation to the regulation of force and the rate of cross-bridge recruitment. Proteins associated with metabolism again show major alterations, indicating that changes in cardiac metabolism are a consequence of dystrophinopathy. Such metabolic proteins include hypoxanthine-guanine phosphoribosyl-transferase, apolipoprotein A-I, creatine kinase, alcohol dehydrogenase, adenylate kinase, triosephosphate isomerase, enolase, glyceraldehyde-3-phosphate dehydrogenase, prostaglandin reductase and aldolase. Compensatory stabilisation of the weakened cytoskeletal network is implied by the increases in myosin-9/non-muscle myosin heavy chain A, dynactin, talin, cofilin, vinculin and tubulin. The 54 proteins with elevated abundance are listed in Table 5.3 below.

Table 5.3: List of identified proteins with a significantly increased abundance in 20-month old *mdx-4cv* heart versus age-matched wild-type heart as determined by label-free LC-MS/MS

Accession	Gene Name	Protein Name	Unique peptides	Confidence score	Anova (p)	Max fold change
Q3UIZ8	Mylk3	Myosin light chain kinase 3	4	121.10	1.56E-02	413.99
Q9D051	Pdhhb	Pyruvate dehydrogenase E1 component subunit beta, mitochondrial	2	93.71	5.45E-03	35.88
P00493	Hprt1	Hypoxanthine-guanine phosphoribosyltransferase	5	212.70	6.17E-04	4.75
O08677	Kng1	Kininogen-1	2	65.97	7.71E-03	4.73
Q62009	Postn	Periostin	3	124.97	1.19E-02	4.23
P35441	Thbs1	Thrombospondin-1	3	169.18	1.13E-02	4.22
Q8VDD5	Myh9	Myosin-9	2	147.69	3.20E-02	4.08
P51885	Lum	Lumican	2	59.86	1.72E-02	3.91
P97457	Mylpf	Myosin regulatory light chain 2, skeletal muscle isoform	4	218.82	1.86E-02	3.46
Q91Z83	Myh7	Myosin-7	5	294.66	1.21E-02	3.42
P05977;Q3USB7	Myl1	Myosin light chain 1/3, skeletal muscle isoform	2	106.65	5.33E-03	3.24
Q99MQ4	Aspn	Asporin	2	111.00	9.41E-03	3.09
P16546	Sptan1	Spectrin alpha chain, non-erythrocytic 1	2	110.55	2.03E-02	3.08
Q3TTY5	Krt2	Keratin, type II cytoskeletal 2 epidermal	2	119.19	2.76E-02	3.01
Q00898	Serpina1e	Alpha-1-antitrypsin 1-5	4	412.30	2.05E-02	2.87
Q99KJ8	Dctn2	Dynactin subunit 2	2	52.08	6.17E-03	2.87
P26039	Tln1	Talin-1	6	415.57	3.76E-02	2.29
Q00623	Apoa1	Apolipoprotein A-I	11	551.29	1.02E-02	2.25
P18760	Cfl1	Cofilin-1	3	254.02	4.63E-03	2.12
Q64727	Vcl	Vinculin	2	141.01	3.16E-02	1.93

P07310	Ckm	Creatine kinase M-type	2	148.17	2.55E-02	1.88
A2AQ07	Tubb1	Tubulin beta-1 chain	2	145.13	2.80E-02	1.85
Q61598	Gdi2	Rab GDP dissociation inhibitor beta	2	102.58	4.11E-03	1.85
O70433	Fhl2	Four and a half LIM domains protein 2	11	556.10	2.59E-03	1.81
Q9CZR8	Tsfm	Elongation factor Ts, mitochondrial	2	152.73	3.48E-03	1.77
P11983	Tcp1	T-complex protein 1 subunit alpha	2	84.52	3.70E-02	1.69
P56480	Atp5b	ATP synthase subunit beta, mitochondrial	3	208.90	2.55E-03	1.69
P07724	Alb	Serum albumin	8	495.17	5.81E-03	1.69
P28474	Adh5	Alcohol dehydrogenase class-3	2	260.69	1.91E-02	1.68
Q8VCW8	Acsf2	Acyl-CoA synthetase family member 2, mitochondrial	3	56.15	1.55E-03	1.67
P62874	Gnb1	Guanine nucleotide-binding protein G(I)/G(S)/G(T) subunit beta-1	2	227.99	1.65E-02	1.66
P46412	Gpx3	Glutathione peroxidase 3	2	114.99	1.78E-02	1.62
Q9R0Y5	Ak1	Adenylate kinase isoenzyme 1	3	130.53	1.29E-02	1.62
P14602	Hspb1	Heat shock protein beta-1	2	67.52	3.72E-03	1.60
P51174	Acadl	Long-chain specific acyl-CoA dehydrogenase, mitochondrial	2	133.23	1.86E-02	1.54
O70468	Mybpc3	Myosin-binding protein C, cardiac-type	6	411.07	4.62E-03	1.54
Q9R062	Gyg1	Glycogenin-1	2	96.89	4.30E-05	1.53
P63038	Hspd1	60 kDa heat shock protein, mitochondrial	3	175.68	7.95E-03	1.51
P17751	Tpi1	Triosephosphate isomerase	3	224.15	1.63E-02	1.51
Q60932	Vdac1	Voltage-dependent anion-selective channel protein 1	3	247.18	2.08E-03	1.51
P17182	Eno1	Alpha-enolase	2	155.79	1.07E-02	1.50
P09103	P4hb	Protein disulfide-isomerase	2	155.88	1.47E-02	1.49
Q9DBG5	Plin3	Perilipin-3	2	101.50	1.88E-02	1.48

Q9D0E1	Hnrnpm	Heterogeneous nuclear ribonucleoprotein M	2	125.83	6.89E-03	1.47
P16858	Gapdh	Glyceraldehyde-3-phosphate dehydrogenase	3	307.82	1.27E-02	1.45
P42125	Eci1	Enoyl-CoA delta isomerase 1, mitochondrial	2	189.00	1.11E-02	1.43
P60843	Eif4a1	Eukaryotic initiation factor 4A-I	2	124.47	2.63E-02	1.42
P63017	Hspa8	Heat shock cognate 71 kDa protein	3	186.17	1.59E-02	1.40
Q8VDQ1	Ptgr2	Prostaglandin reductase 2	3	172.64	1.91E-02	1.39
Q99L13	Hibadh	3-hydroxyisobutyrate dehydrogenase, mitochondrial	2	145.44	1.62E-02	1.38
Q9JKS4	Ldb3	LIM domain-binding protein 3	4	186.65	5.03E-03	1.35
P05064	Aldoa	Fructose-bisphosphate aldolase A	2	153.50	3.42E-02	1.33
P11499	Hsp90ab1	Heat shock protein HSP 90-beta	3	133.41	3.10E-04	1.33
P51667	Myl2	Myosin regulatory light chain 2, ventricular/cardiac muscle isoform	4	148.23	3.49E-02	1.28

5.2.5 Distribution of protein changes in dystrophic mdx-4cv cardiac tissue

To obtain a wider overview of the physiological roles of the proteins with altered abundance in dystrophic cardiac tissue the bioinformatics software packages PANTHER and STRING were used. PANTHER analysis was applied to group differentially expressed proteins based on their protein class (Figure 5.2). The majority of altered protein species belong to the class of cytoskeletal proteins (12.7%), which agrees with the idea of muscular dystrophy as a cytoskeletal disorder. The altered abundance of cytoskeletal proteins reflects both the reduction in key cytoskeletal proteins of the DGC and the concomitant increases in other cytoskeletal proteins such as tubulin and vimentin as a compensatory mechanism to rescue cytoskeletal stability.

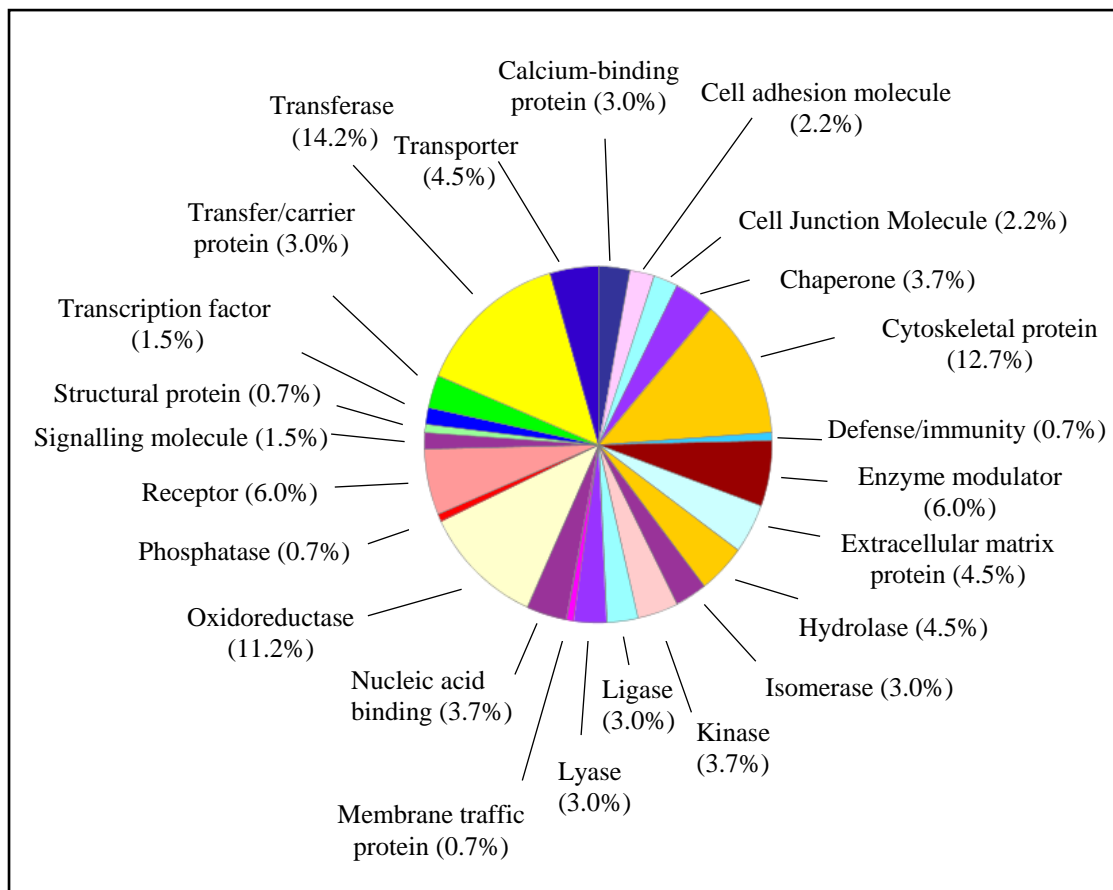


Figure 5.2: PANTHER analysis of altered protein species in dystrophic heart

The 98 differentially expressed cardiac-associated proteins were grouped into their respective protein class using the freely available PANTHER software package. This analysis identified cytoskeletal proteins as those with the greatest number of alterations in the dystrophic heart.

STRING analysis was also employed to investigate potential protein interactions (Figures 5.3 and 5.4). Differential proteins were analysed by STRING for medium confidence interactions using the evidence view. Medium confidence was used here as at high confidence the known interaction of the full-length Dp427 isoform of dystrophin with laminin was lost. This systems biology approach revealed that certain protein networks are particularly affected by dystrophin deficiency. Dystrophic cardiac tissue appears to have increased protein levels associated with metabolic pathways, fibrosis and remodelling of the extracellular matrix and cytoskeletal restructuring, as depicted in Figure 5.3. Dystrophin deficiency also appears to be tightly connected to the decrease in the laminin complex as seen in Figure 5.4. STRING analysis was also used to identify enriched gene ontology terms and KEGG pathways. The top twelve terms (based on FDR) for KEGG pathways are shown for increased abundance and decreased abundance proteins in Figures 5.5 and 5.6 respectively.

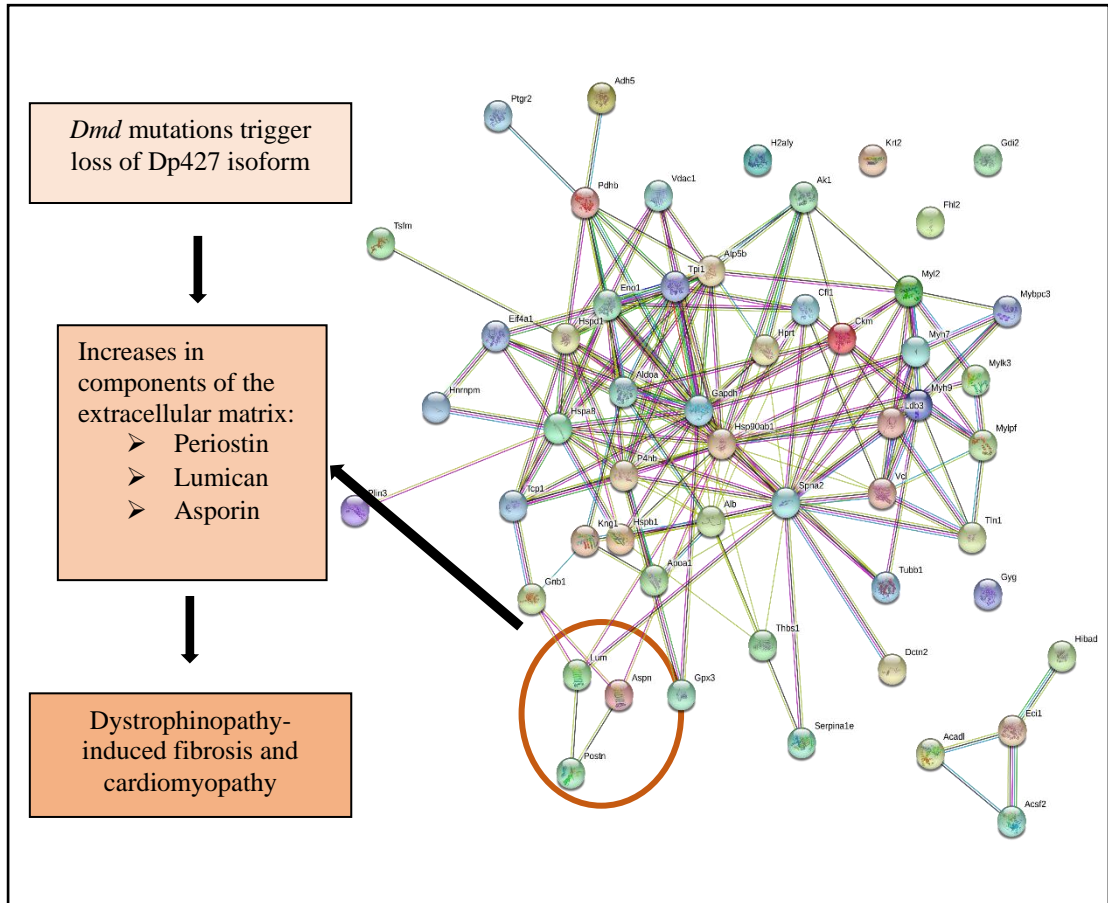


Figure 5.3: STRING analysis of the 54 proteins with increased expression in *mdx-4cv* heart

STRING analysis reveals a tightly interconnected protein network in aged dystrophic heart. Dystrophin deficiency appears to trigger compensatory up-regulation of proteins involved in the maintenance of cytoskeletal networks. Fibrosis is a defining characteristic of dystrophic tissue and is exemplified here by the increases in a number of pro-fibrotic mediators.

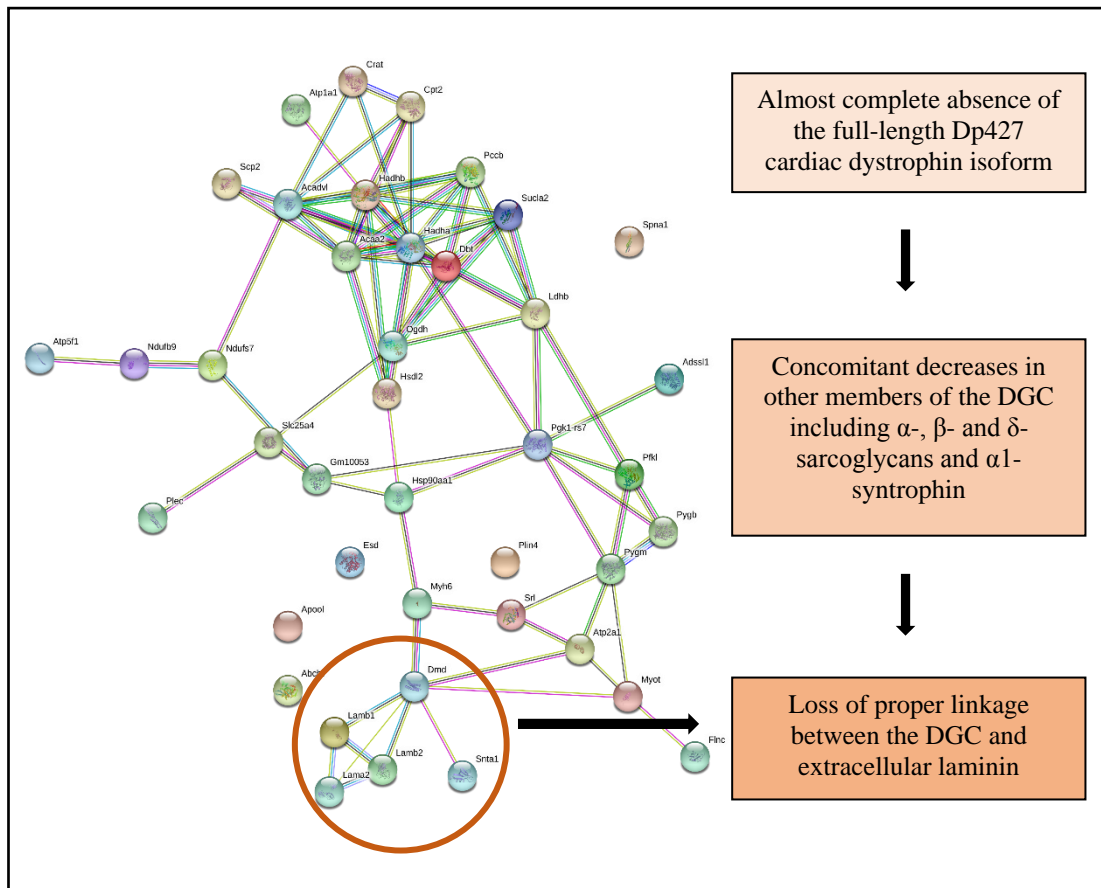


Figure 5.4: STRING analysis of the 44 proteins with diminished expression in *mdx-4cv* cardiac tissue

Bioinformatics analysis illustrates the absence in dystrophin in the heart causes a number of secondary abnormalities; in particular alterations in the expression of a number of laminin isoforms.

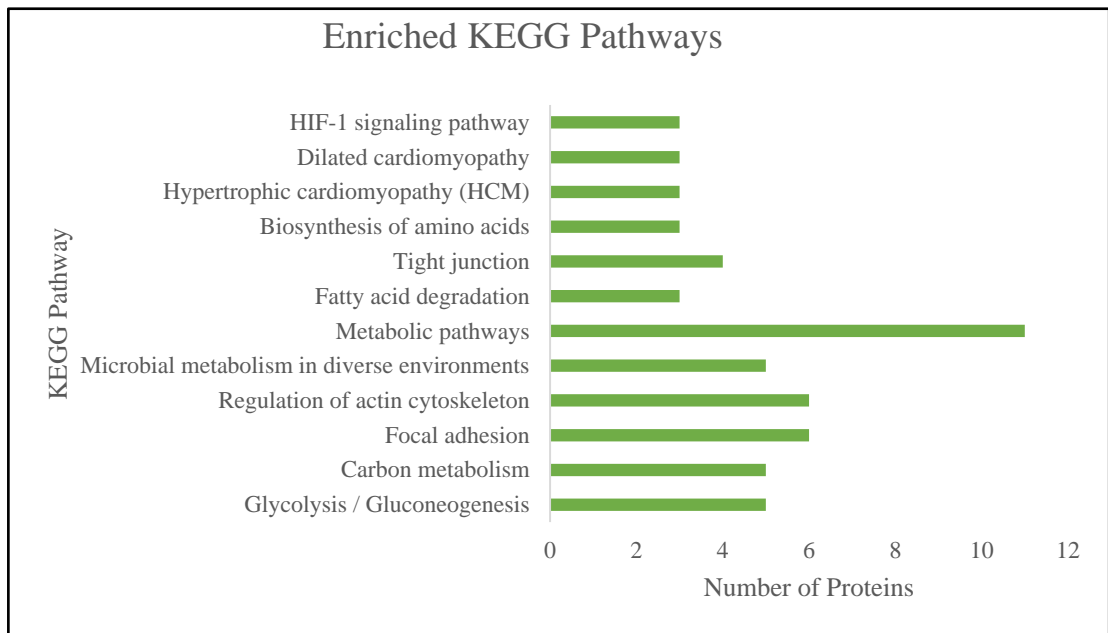


Figure 5.5: Enriched KEGG terms in proteins with increased abundance in the aged dystrophic heart

Depicted is the top twelve enriched terms for KEGG pathways, based on STRING analysis of proteins with increased abundance in the *mdx-4cv* heart.

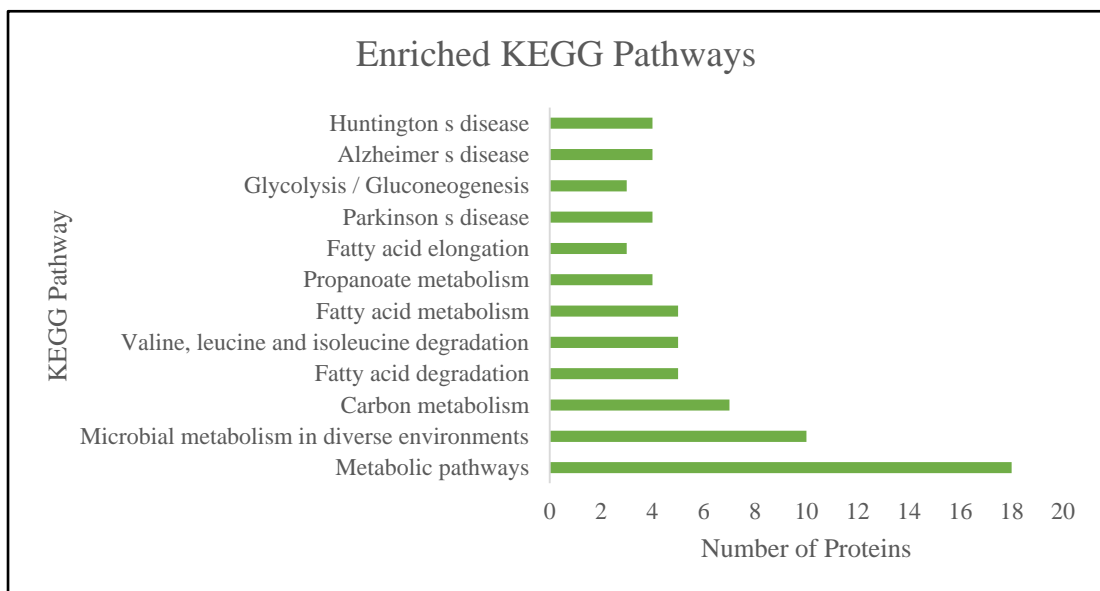


Figure 5.6: Enriched KEGG terms in proteins with decreased abundance in the aged dystrophic heart

Depicted is the top twelve enriched terms KEGG pathways, based on STRING analysis of proteins with decreased abundance in the *mdx-4cv* heart

5.2.6 Comparative immunoblot analysis of wild-type versus *mdx-4cv* 20-month heart

In order to verify the mass spectrometric data comparative immunoblotting of aged wild-type and *mdx-4cv* cardiac tissue was performed with a select panel of antibodies. The silver-stained gel depicted in Figure 5.7 shows a similar protein banding pattern between normal and dystrophic preparations. Equal loading was confirmed using this silver-stained gel and immunoblotting against the nuclear marker laminB1 whose levels do not appear to be affected by dystrophin deficiency in the aged heart (Figure 5.7). The reduced expression of laminin and lactate dehydrogenase was confirmed by immunoblotting, with decreases in laminin found to be statistically significant (Figure 5.8). The overall trend of increased expression of myosin light chain 2 (statistically significant elevation) and VDAC-1 were also confirmed by comparative immunoblot analysis (Figure 5.9). The increased levels of the fibrosis-associated proteins collagen VI, periostin, lumican and asporin (Figure 5.9 and Figure 5.10) were confirmed in the senescent dystrophic heart, for which elevations of periostin, lumican and asporin were found to be statistically significant.

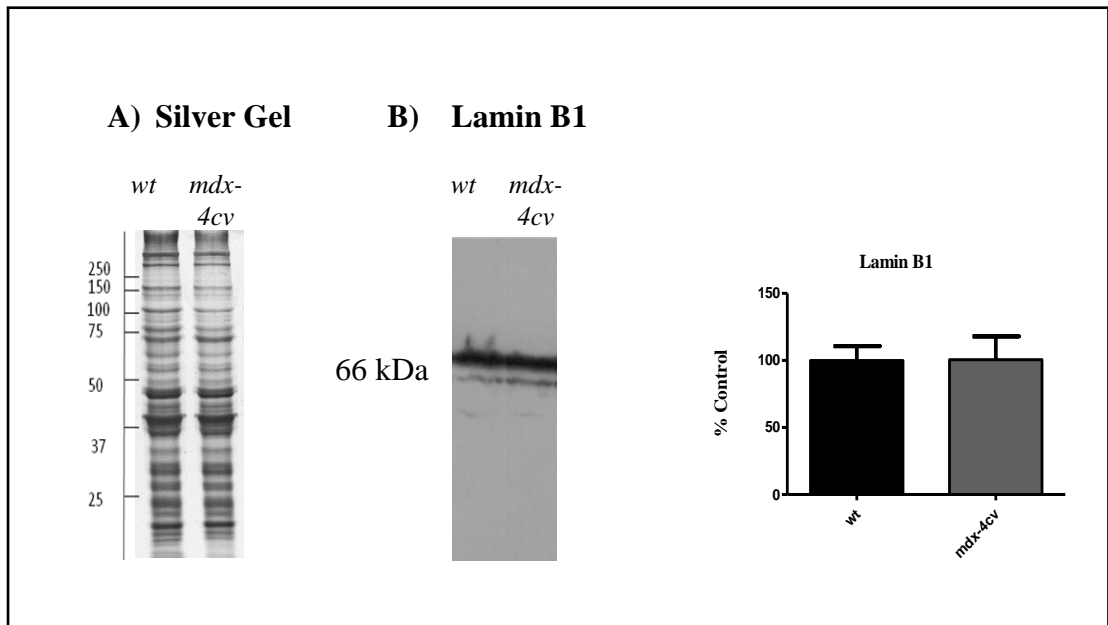


Figure 5.7: Electrophoretic and immunoblot analysis of wild-type and *mdx-4cv* heart

Shown is a silver stained 1D gel (A) and immunoblot and statistical analysis of bands labelled with lamin B1 (B). The silver stained gel shows comparable protein banding patterns for wild-type and *mdx-4cv* cardiac preparations. Molecular weight marker is given on the left-hand-side of the image in kDa. Lamin B1 immunoblotting did not show significant changes in concentration between wild-type and *mdx-4cv* samples and so it serves as a loading control for comparative immunoblotting. Graphical representation of the immuno-decoration level for lamin B1 is shown (mean values \pm SEM, Student's *t*-test; unpaired; $n=4$).

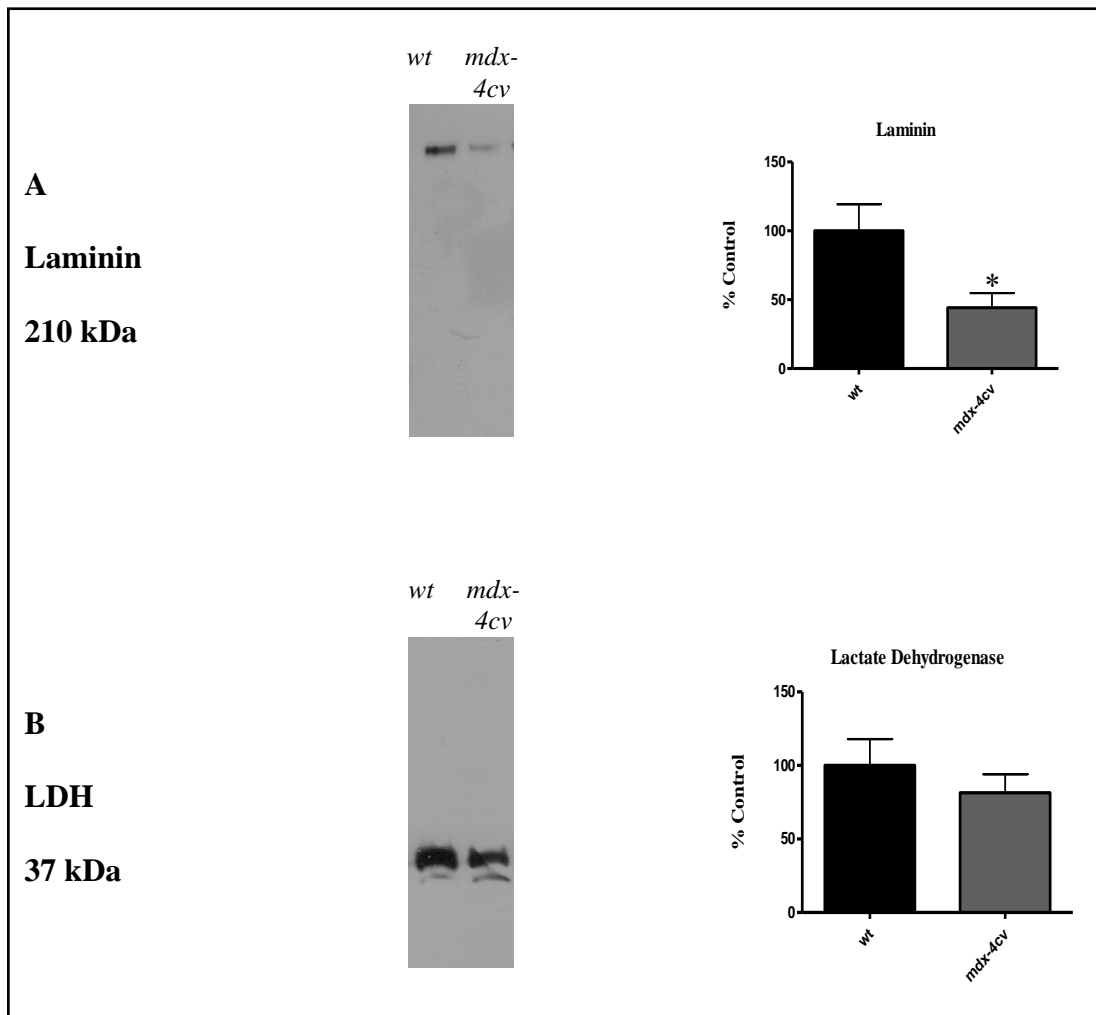


Figure 5.8: Comparative immunoblot analysis of proteins with decreased abundance in dystrophic *mdx-4cv* cardiac tissue

Shown are representative immunoblots with immuno-decorated bands labelled with antibodies to laminin (A) and lactate dehydrogenase (LDH) (B). Statistical analysis of immuno-decoration was performed with Student's *t*-test (mean values \pm SEM; unpaired; $n=4$, $*p\leq 0.05$).

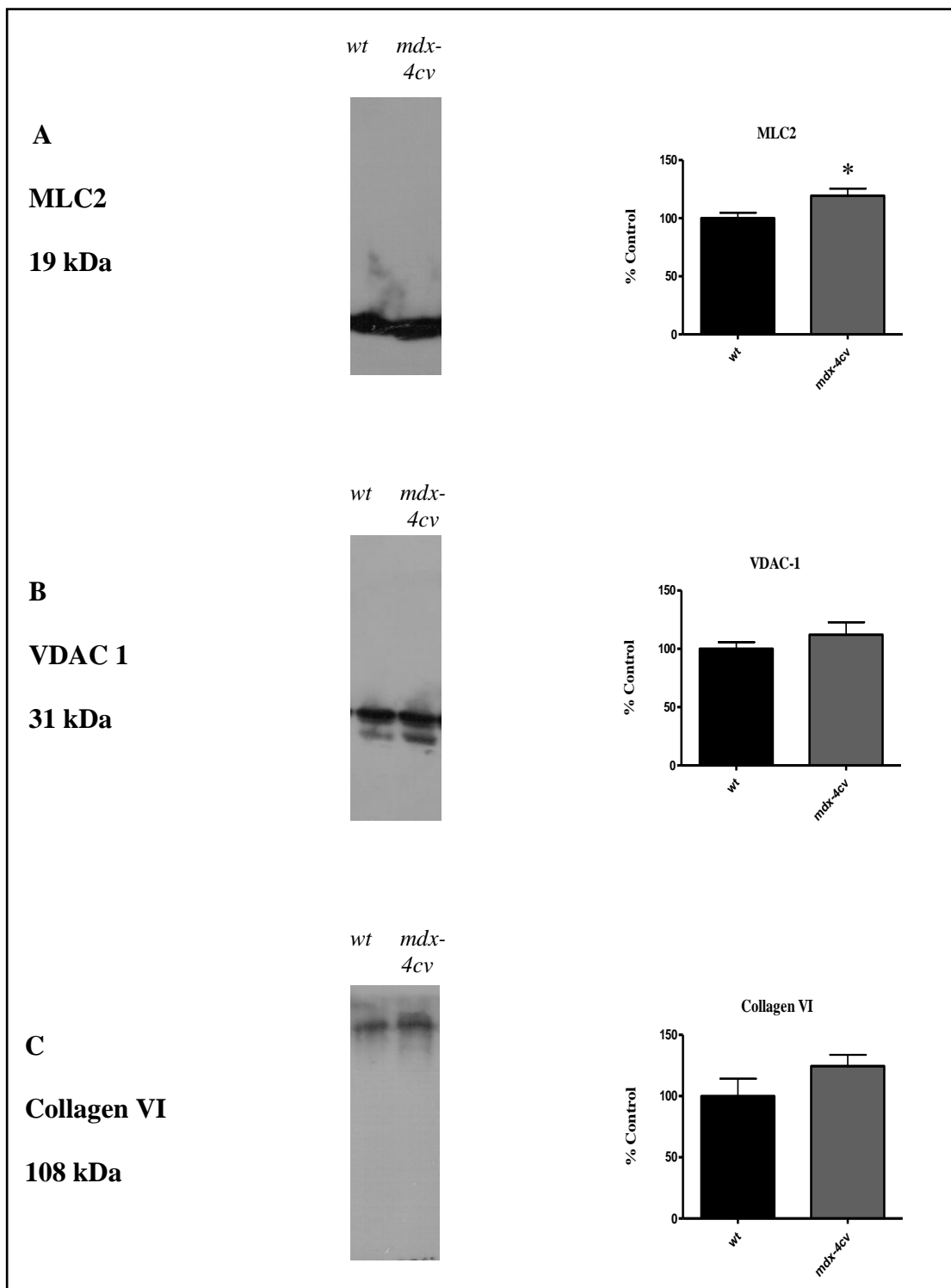


Figure 5.9: Comparative immunoblot analysis of proteins with increased abundance in dystrophic *mdx-4cv* cardiac tissue

Shown are representative immunoblots with immuno-decorated bands labelled with antibodies to myosin light chain 2 (MLC2) (A), VDAC1 (B) and collagen VI (C). Statistical analysis of immuno-decoration was performed with Student's *t*-test (mean values \pm SEM; unpaired; $n=4$, $*p \leq 0.05$).

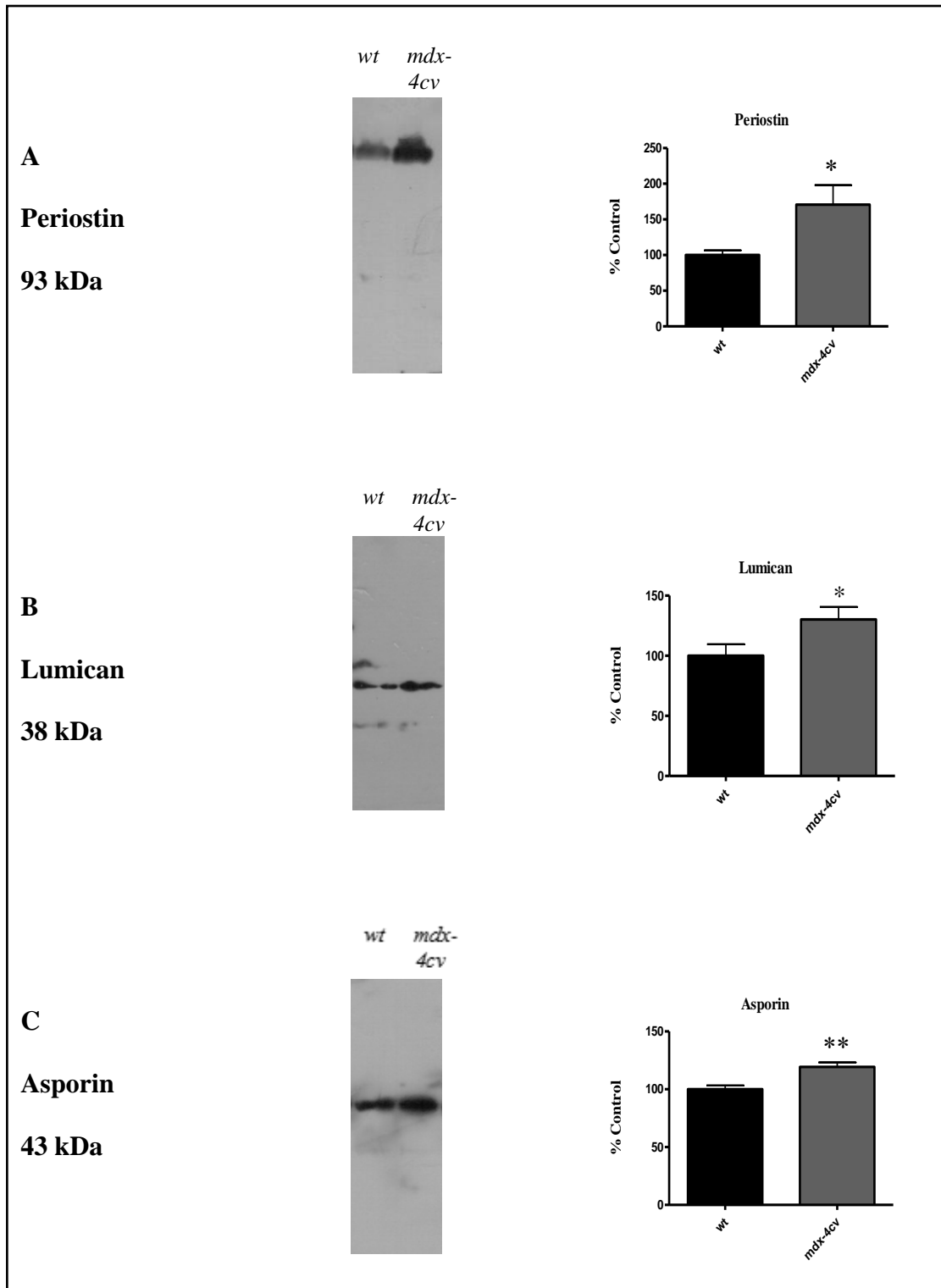


Figure 5.10: Comparative immunoblot analysis of proteins with increased abundance in dystrophic *mdx-4cv* cardiac tissue

Shown are representative immunoblots with immuno-decorated bands labelled with antibodies to periostin (A), lumican (B) and asporin (C). Statistical analysis of immuno-decoration was performed with Student's *t*-test (mean values \pm SEM; unpaired; $n=4$, * $p \leq 0.05$, ** $p \leq 0.01$).

5.3 Discussion

While advances in therapeutic options available for DMD have improved both the lifespan and quality of life of patients, cardiomyopathy still remains as a major complicating factor in the disease pathogenesis. Indeed, recent studies have suggested that targeted repair of the skeletal muscle in the absence of concomitant improvements of the cardiac dystrophic phenotype actually increases cardiac failure and dilated cardiomyopathy (Townsend et al., 2008). This highlights the importance of a need for therapies with global effects. An understanding of the molecular mechanisms underlying cardiomyopathy in dystrophin-deficient hearts is required before such therapies can be developed.

This proteomic survey of the aged dystrophic heart has revealed a general perturbation of protein expression, primarily involving the extracellular matrix, the cytoskeletal network, cycles of fibrosis and necrosis, metabolism, and the cellular stress response. Similar to that seen in dystrophic skeletal muscle, the absence of full-length dystrophin in *mdx-4cv* cardiac myocytes triggers a corresponding decrease in key components of the DGC, including $\alpha 1$ -syntrophin, β -sarcoglycan, α -sarcoglycan and δ -sarcoglycan. Decreased expression of these key cytoskeletal players was identified here by sensitive label-free mass spectrometry in the absence of any pre-fractionation steps which may introduce analytical artefacts. Dystrophin deficiency was identified by an extensive 24 unique peptides, while each of the sarcoglycan subunits was only identified by a single unique peptide, possibly owing to their highly hydrophobic nature. This establishes the *mdx-4cv* animal model and the mass spectrometric approach used in this study as a model mechanism of studying dystrophy-induced cardiomyopathy.

Fibrosis is associated with a number of chronic pathologies and it's especially noted for its contribution to severe muscle wasting in DMD. Cycles of muscle degeneration and inflammation in dystrophic muscles cause the hyper-proliferation and activation of fibrogenic cells, leading to the unwanted deposition of extracellular matrix components and eventual replacement of skeletal muscle with non-contractile fibrotic tissue (Kharraz et al., 2014). This phenomenon has also been identified in the dystrophic heart, where an age-dependent up-regulation of connective tissue growth factor (CTGF) may play a role. Elevated levels of CTGF in the dystrophic heart of *mdx* mice have been identified by micro-array analysis, immunoblotting and

immunohistochemistry, with the finding that this up-regulation is concurrent with cardiac fibrosis and precedes the onset of overt cardiomyopathy (Au et al., 2011). Such findings are consistent with the identification of elevated levels of the matricellular protein periostin, and the proteoglycans asporin and lumican in this proteomic study. Periostin has been identified in a number of dystrophic organs, including the severely affected diaphragm (Holland et al., 2015a), the moderately affected hind limb muscles (Murphy et al., 2015a) and now the aged heart, establishing it as a potential biomarker of reactive fibrosis in dystrophin-deficient tissues. Periostin is an extracellular matrix protein, which while ubiquitously expressed during embryonic development, is restricted to connective tissues exposed to mechanical stress in post-natal life (Ozdemir et al., 2014). Cycles of muscle degeneration/regeneration involving the pro-inflammatory mediator TGF- β are prevalent in dystrophic muscle (Bernasconi et al., 1995) and this process culminates in increased expression of pro-fibrotic proteins such as those identified by this proteomic survey. TGF- β signalling increases the expression of periostin, causing enhanced fibrosis and worsening of the dystrophic phenotype. This negative impact of elevated abundance of periostin has been well-documented, with studies indicating that sarcoglycan/periostin null mice display reduced tissue fibrosis and increased expression and activity of matrix metalloproteinase 9 (Lorts et al., 2012). Overall this suggests the absence of periostin reduces fibrosis and promotes beneficial remodelling of the extracellular matrix, which enhances extracellular matrix stability and reduces micro-rupturing of dystrophic sarcolemma.

In analogy to this fibrotic process identified in the heart and the skeletal muscle, the LC-MS/MS study of *mdx-4cv* brain has revealed increased levels of the glial fibrillary acidic protein GFAP (Murphy et al., 2015c). High levels of GFAP have previously been associated with astrogliosis (Eng et al., 2000), a normal physiological response to brain injury which can become pathological if the insult is not resolved, resulting in the formation of glial scars. Elevated levels of GFAP thus strongly suggest reactive astrogliosis in the dystrophin-deficient brain. As such it appears that tissue scarring and loss of elasticity is a pathophysiological hallmark of dystrophin deficient tissue and one which affects the skeletal musculature, the cardiac system and the central nervous system.

The loss of dystrophin has different effects on skeletal myocytes and cardiac myocytes. This is illustrated by the fact cardiac abnormalities, similar to those evident

in male Duchenne patients, have been observed in some female carriers of the disease, in the absence of overt skeletal muscle pathology (Hoogerwaard et al., 1999). In analogy to such findings, differences have been observed in the protein expression profile of the dystrophic heart versus the skeletal muscle. As identified in this study, laminin, a crucial component of the basal lamina, displays reduced expression in the aged *mdx-4cv* heart, similar to that seen in previous proteomic studies of the heart (Holland et al., 2013). This contrasts with the skeletal muscle, where levels of laminin remain unaffected despite the disintegration of the DGC.

Oxidative stress has been suggested to play a role in the pathogenesis of dystrophinopathies. The deficiency in dystrophin at the sarcolemma causes nNOS to be redistributed from the sarcolemma to the cytosol, where its aberrant activity can result in oxidation of free radicals (Abdel et al., 2007), which prove toxic to myocytes. Indirect evidence of a role for oxidative stress in DMD has been provided by Ragusa and colleagues. In response to hyperoxia (a known inducer of oxidative stress) control mice develop changes in the activity of superoxide dismutase and catalase, and develop levels of by-products of lipid peroxidation (thiobarbituric acid reactive substances) similar to those seen in normoxic *mdx* skeletal muscle (Ragusa et al., 1997). It thus appears that dystrophin deficiency triggers oxidative stress which culminates in an adaptive response by skeletal muscle. Alterations in the efficacy of this response may contribute to the severity of muscle damage in individual muscle types. For example extraocular muscles of the eye are largely spared in DMD (Porter et al., 1998). These muscles, involved in the fast and almost continuous eye twitch movements, experience high levels of oxidative stress even under normal conditions and thus may be better adapted to cope with the enhanced levels of free radicals seen in muscular dystrophy (Ragusa et al., 1997). Similarly, in this proteomic survey of the aged dystrophic heart elevated levels of anti-oxidants are evident. For example the increased levels of glutathione peroxidase 3, an enzyme responsible for catalyzing the reduction of hydrogen peroxide, lipid peroxides and organic hydroperoxide, may represent a compensatory mechanism by the dystrophin-deficient heart to counteract oxidative-stress-induced cellular damage (Khouzami et al., 2010). Chaperone-mediated autophagy is a constitutive process only found in mammalian cells which serves to maintain cellular homeostasis, which has been shown to be further activated by oxidative stress (Kiffin et al., 2004). Since this type of autophagy relies on the

interaction between HSP70, lysosome-associated membrane protein 2A and HSP90 (Linton et al., 2015), the elevated levels of HSP90- β and heat shock cognate 71kDa protein identified here in dystrophic cardiac tissue may indicate increased oxidative stress in the aged, dystrophin-deficient heart.

Age-related cardiac dysfunction is well-discussed in the literature with hypertrophy, fibrosis and alterations in autophagy appearing as factors involved in aged-associated cardiomyopathy in both murine and human hearts (Linton et al., 2015, Boyle et al., 2011, Olivetti et al., 1991). Fibrosis in the aged murine heart has been associated with increased levels of collagen and cardiac hypertrophy, indicating that even in otherwise healthy mice, aging alone induces expansion of the extracellular matrix, with impairment of left ventricular systolic function evident by 18 months of age (Boyle et al., 2011). The fact that numerous fibrotic proteins, including lumican, asporin, periostin and collagen isoform $\alpha 1$ (VI), display elevated expression in the aged dystrophic heart as compared to the control aged heart (20 months) indicates that dystrophin absence in cardiac tissue induces a degree of fibrosis worse than that caused by aging alone. Thus, cardiomyopathy and subsequent cardiac failure remain as major risk factors for Duchenne boys during aging.

While the primary role of the full-length dystrophin protein is the maintenance of structural stability, its absence affects not only cytoskeletal structure but also cellular metabolism. Indeed, it has been reported that the dystrophic heart displays changes in energy metabolism prior to the onset of overt cardiomyopathy (Khairallah et al., 2007). On a proteomic level, the reduction in the expression of a number of key mitochondrial proteins of lipid metabolism seen here agree with both a previous gel-based study (Lewis et al., 2010) and with Khairallah and colleagues observation of a shift away from the utilisation of fatty acids as a fuel source in dystrophin-deficient hearts (Khairallah et al., 2007). Decreased expression of acyl-CoA dehydrogenase, an enzyme involved in the mitochondrial fatty acid beta-oxidation pathway (Kurtz et al., 1998), is indicative of an impaired lipid metabolism in the dystrophic heart. Reduced levels of this enzyme may worsen the cardiac phenotype in dystrophic mice, given that long-chain acyl-CoA dehydrogenase knockout mice display myocardial degeneration and cardiac lipidoses in response to fasting (Kurtz et al., 1998). Pyruvate dehydrogenase, an enzyme responsible for the conversion of pyruvate (the end product of glycolysis) to acetyl-CoA (a component of the tricarboxylic acid cycle)

(Ohlendieck, 2010) displays elevated expression in the aged dystrophin-deficient cardiac tissue. In analogy a large number of glycolytic enzymes were also revealed to be increased in expression, suggesting a possible compensatory up-regulation of an anaerobic pathway to counteract the alterations seen in mitochondrial metabolism. Such glycolytic enzymes include triosephosphate isomerase, enolase, glyceraldehyde-3-phosphate dehydrogenase and aldolase. However, levels of lactate dehydrogenase are slightly decreased, indicating that the pyruvate produced by glycolysis is not converted to lactate at an increased rate in the *mdx-4cv* heart.

A whole host of other proteins display altered expression levels in dystrophic tissues. Cofilin, a small protein of 19 kDa, regulates actin polymerisation and depolymerisation, and thus is involved in cell motility (Bravo-Cordero et al., 2013). Cofilin plays a role in foetal muscle development, where it is associated with the fusion of embryonic myoblasts to form myotubes (Bamburg and Wiggan, 2002), but is normally expressed at low levels during postnatal skeletal muscle development. The expression of cofilin-1, as detected here by label-free LC-MS/MS, is higher in the dystrophic heart tissue. Given that cofilin is normally associated with foetal muscle development, its elevated abundance may indicate the presence of regenerating muscle fibres in dystrophic cardiac tissue. The increased expression of predominantly prenatal/perinatal proteins has also been identified by previous proteomic work in dystrophic leg tissue, where elevated levels of perinatal myosin 8 suggest the recruitment of newly differentiated myofibres. Other studies have also identified cofilin expression in regenerating muscle fibres as well as pre-existing muscle fibres in the chicken and mouse models of muscular dystrophy (Hayakawa et al., 1993). Overall, increased cofilin expression appears to suggest remodelling in dystrophic muscle fibres.

Voltage-dependent anion selective channel (VDAC) is associated with the outer mitochondrial membrane, where it interacts with the adenine nucleotide translocator located in the inner mitochondrial membrane (Crompton et al., 1998), to maintain the movement of ADP/ATP in and out of the mitochondria (Rostovtseva and Colombini, 1997). Viola and colleagues have found that the deficiency in dystrophin and concurrent disruption of cytoskeletal networks in *mdx* cardiac myocytes leads to impaired communication between the L-type calcium channel and VDAC, which in turn appears to at least partially account for the reduction seen in metabolic activity in

the dystrophic heart (Viola et al., 2014). This proteomic survey has identified a slight increase in the expression of VDAC1 (1.5-fold) in the *mdx-4cv* heart. Such an increase may represent a compensatory mechanism in dystrophin-deficient cardiomyocytes to maintain metabolism and meet the heart's energy demands in the face of impaired communication between some of the key players of mitochondrial metabolism.

Many proposed therapies for DMD, such as exon skipping, have primarily shown restoration of dystrophin expression in the skeletal muscle while failing to target the heart (Lu et al., 2005). However, the emerging CRISPR-Cas9 technology has shown promise in rescuing dystrophin expression in both skeletal muscle and cardiomyocytes in postnatal *mdx* mice (Long et al., 2016). Such studies have validated the therapeutic benefit by measuring dystrophin expression, by analysing the histopathological hallmarks of muscular dystrophy and by using the grip-strength test to examine muscle function (Long et al., 2014). However, it may be interesting to examine whether such therapies also ameliorate the secondary abnormalities associated with the disease. A label-free LC-MS/MS approach, similar to that used in this investigation, may be of benefit in identifying protein biomarkers associated with an improvement in disease pathogenesis following treatment. Similar types of studies have been performed for examining the efficacy of exon skipping. For example Doran and colleagues demonstrated, using a 2D-DIGE approach, that exon skipping of exon 23 in the *mdx* mouse reversed some of the downstream secondary abnormalities in the treated dystrophic diaphragm (Doran et al., 2009b).

5.3.1 Conclusion

Improvements in respiratory care for Duchenne patients such as mechanical ventilation have dramatically increased survival. However, cardiac complications remain as critical issues affecting a large majority of patients and which have severe impacts on quality of life and survival. In this chapter, proteomic profiling of the aged dystrophic heart is described and used to elucidate potential molecular mechanisms responsible for cardiac impairment. Mass spectrometric analysis revealed reduced abundance of core proteins of the DGC; dystrophin, α 1-syntrophin, α -sarcoglycan, β -sarcoglycan and δ -sarcoglycan, in senescent *mdx-4cv* cardiac tissue. Reductions in this stabilising protein complex of the sarcolemma is accompanied by a range of secondary abnormalities, particularly related to metabolic alterations, cytoskeletal remodelling,

cellular stress and altered ion homeostasis. A number of proteins associated with fibrosis were found to be increased in abundance in dystrophic hearts, as shown by mass spectrometry and immunoblot analysis. Such protein species include collagen, asporin, lumican and periostin. This reveals fibrosis as a major contributor to cardiomyopathy in which excessive deposition of matricellular and extracellular matrix proteins and subsequent tissue scarring may negatively impact normal cardiac function. Thus, these proteins may serve as both potential protein markers of cardiac dysfunction and therapeutic targets to counteract cardiomyopathy.

Chapter Six

Glial fibrillary acidic protein as a marker of neurotoxicity in the *mdx-4cv* model of dystrophinopathy

6.1 Introduction

DMD is a paediatric disorder of the skeletal musculature which is characterised by a variety of alterations in muscle fibres, including changes in myofibre size, fibre branching, necrosis, central nucleation, regeneration, immune cell invasion and the infiltration of fatty and connective tissue. A number of secondary complications are also associated with the disorder, including cardiomyopathy, respiratory insufficiency, orthopaedic issues linked to muscle contractures and the development of scoliosis, cognitive impairments, and endocrinological issues related to growth and weight gain (Murphy et al., 2015b).

Investigations into the pathogenesis of DMD are complicated by the presence of multiple promoters that facilitate the expression of various dystrophin isoforms ranging in size from 71 to 427 kDa. While all genetic mutations in the *Dmd* gene result in the loss of the full-length isoform of dystrophin, the loss of the other dystrophin isoforms depends on the location of the genetic mutation in relation to the location of the promoters. Three full-length isoforms of dystrophin exist; Dp427-M expressed in muscles, Dp427-B expressed in the brain and Dp427-P expressed in cerebellar Purkinje cells (Perronnet and Vaillend, 2010). In addition, four shorter isoforms which arise from transcription from different promoters in the *Dmd* gene also exist. These are Dp260-R found in the retina, Dp140-B/K expressed in the brain and kidney, Dp116-S in Schwann cells and Dp71-B/U in brain and non-muscle tissue (Culligan et al., 2001). These alternative isoforms of dystrophin differ not only in their cellular location, but also in their size and composition, with only Dp427 expressing an actin-binding domain. The absence of this domain from the remaining dystrophin isoforms suggest that dystrophin may have roles other than linkage of intracellular actin to the extracellular matrix. While the impacts of dystrophin deficiency on skeletal muscle, cardiac muscle and the diaphragm have been studied extensively (Holland et al., 2013, Holland et al., 2015a, Wang et al., 2015), its effect on cognition is largely unresolved. This is in spite of the fact that non-progressive cognitive defects are a clinical symptom of DMD, originally observed by Duchenne in some of his patients. Cognitive deficits affect approximately one-third of all patients, are non-progressive and have been shown to affect verbal more than non-verbal intelligence (Cotton et al., 2001). Moderate memory and attention impairments are seen in almost all DMD sufferers, suggesting a role for full-length Dp427 in its pathogenesis. However, mutations

affecting the Dp140 and Dp71 isoforms are correlated with a higher incidence and severity of cognitive impacts (Culligan et al., 2001).

Full-length isoforms of brain dystrophin are present in the neurons of the cerebellar cortex and the hippocampus along with cerebellar Purkinje cells (Snow et al., 2013). The Dp140 isoform is most highly expressed during brain development (Lidov et al., 1995), while the most abundant brain isoform, Dp71, is present in neurons and glia cells of the *dentate gyrus* and the olfactory bulb (Culligan et al., 2001). Transcriptomic analysis of the developing human brain revealed that Dp427 expression is low during foetal development, shows a slight increase at two years of age and remains low during middle adulthood. Dp140 is highly expressed in mid-foetal stages and is expressed throughout middle adulthood. Dp71 expression is high during foetal stages and remains high after birth and throughout life (Doorenweerd et al., 2017). Dystrophin and the brain DGC (including α - and β -dystroglycan, β 2-syntrophin and dystrobrevin but not the sarcoglycan complex) may play a role in neuronal development, and thus, abnormalities seen in the brain may arise as a result of altered calcium-mediated signalling and/or disruption of cellular proteins which normally would interact with the DGC (Mehler, 2000). Loss of dystrophin in *mdx* mouse models is associated with a large reduction in the size and number of GABA_A (gamma-aminobutyric acid) receptor clusters in the hippocampus cerebellum and amygdalon (Sekiguchi et al., 2009, Knuesel et al., 1999) and increases in choline-containing compounds. Thus, dystrophin and its associated glycoproteins likely play a role in the stability of receptors and in synaptic function in the brain. It has been suggested that compensatory mechanisms to maintain functional stability may actually contribute to disruption of neuronal function through continuous perturbations (Cohen et al., 2015).

Animal models have been especially useful in determining the downstream abnormalities induced by dystrophin absence. In particular, the *mdx* mouse model has been used to illustrate the cognitive deficits induced by dystrophin deficiency. Such studies have revealed slower learning in bar-pressing tasks and reduced performance at long time delays in tests measuring recognition and spatial memories (Muntoni et al., 1991). Dystrophin deficiency has also been shown to impair long-term object recognition memory and long-term spatial memory in dystrophic mice (Vaillend et al., 2004). Since the *mdx-4cv* animal model has been studied less extensively, despite representing an improved pathobiochemical phenotype, label-free LC-MS/MS has

been performed here on brain tissue obtained from 12-month old wild-type and *mdx-4cv* mice to investigate the secondary abnormalities in dystrophin-deficient brain. This study was undertaken with the aim of improving understanding of the impact of dystrophin deficiency on proteostasis in the brain and to elucidate the pathophysiological mechanisms that facilitate impaired brain function in muscular dystrophy. The unbiased, technology-driven proteomics approach used in this study has identified a number of altered proteins of interest, including the intermediate filament protein vimentin, the membrane repair protein annexin A5, glial fibrillary acidic protein, the calcium binding protein calretinin and the plasma membrane Ca^{2+} -ATPase. In analogy to the effects on cardiac and skeletal muscle, the loss of dystrophin in brain tissue would appear to trigger cytoskeletal remodelling, membrane repair and altered Ca^{2+} handling. In addition, proteins more specific to the nervous system were also found to be differentially abundant, including the dendritic spine protein drebrin suggested to participate in neuronal growth, protein bassoon involved in the organisation of the cytomatrix at the active zone of nerve terminals, and syntaxin-1B and syntaxin-binding protein 1 involved in synaptic vesicle docking. These disturbed neuronal proteins illustrate the complexity of the molecular pathogenesis in the central nervous system of dystrophic *mdx-4cv* mice.

6.1.1 Experimental Design

Since approximately one-third of patients with dystrophinopathy also present with mild cognitive impairments it was of interest to investigate potential proteomic alterations in the dystrophin-deficient brain. Whole brain samples from 12-month old wild-type and age-matched *mdx-4cv* mice (n=4) were prepared for this proteomic study. Crude brain homogenates were analysed by label-free LC-MS/MS using an Ultimate 3000 nanoLC system (Dionex) coupled to an LTQ Orbitrap XL mass spectrometer (Thermo Fisher Scientific) in the Proteomics Facility of the National Institute for Cellular Biotechnology, Dublin City University. Brain-tissue derived peptides were eluted with the following binary gradients: solvent A [2 % (v/v) ACN and 0.1 % (v/v) formic acid in LC-MS grade water] and 0–25 % solvent B [80 % ACN and 0.08 % (v/v) formic acid in LC-MS grade water] for 240 min and 25–50 % solvent B for a further 60 min. Relative quantification and identification was performed with Progenesis QI for Proteomics software, using Sequest HT and MASCOT search engines and the UniProtKB-SwissProt database. Bioinformatics analysis was

conducted using the PANTHER database of protein families and STRING software. Comparative immunoblot analysis was used as an orthogonal method to verify altered protein abundance. Immunoblotting was also used to confirm the tissue specificity of GFAP, and for this analysis protein extracts from the liver, diaphragm, heart and skeletal muscle of wild-type mice were used.

6.2 Results

In order to investigate the potential effect of muscular dystrophy on the brain, as suggested by cognitive defects in a sub-group of patients with DMD, proteomic profiling of 12-month old wild-type versus age-matched *mdx-4cv* brain was conducted. A label-free LC-MS/MS approach was used to identify protein alterations in the dystrophin-deficient brain. Consequently, key proteins of interest were verified by comparative immunoblotting.

6.2.1 Label-Free LC/MS-MS analysis of altered protein species in total *mdx-4cv* brain extracts

In contrast to proteomic profiling of skeletal muscle from *mdx-4cv* animal models of dystrophinopathy, in which large alterations in protein expression have been identified (Murphy et al., 2015a), relatively few alterations were identified in dystrophin-deficient brain tissue. LC-MS/MS analysis of brain-derived proteins identified alterations in the abundance of 46 proteins; 7 of which were decreased in expression (Table 6.1) and 39 of which displayed increased abundance (Table 6.2). In addition, the majority of these proteins showed only minor differences in their abundance, with only plasma membrane calcium-transporting ATPase 2 displaying a reduction in expression by more than two-fold (-2.77) in dystrophin-deficient brain tissue. Meanwhile 11 proteins depicted increases in expression by more than two-fold in *mdx-4cv* preparations, with hemopexin showing the highest increase at a fold increase of 5.64. While these results may seem surprising given that up to one-third of DMD boys suffer from some degree of mental impairment (Bresolin et al., 1994), it may be partly contributed to the animal model used in this study. The *mdx-4cv* mouse model carries a non-sense mutation in exon 53 of the *Dmd* gene, which renders it highly attractive for studying the efficacy of novel therapeutic strategies such as exon skipping, given that this exon is a major mutation hotspot in the human disorder (Mitrpant et al., 2009). In analogy to the human condition this model fails to express the Dp427 isoform of dystrophin, which is the major muscle isoform involved in stabilisation of the sarcolemma through interactions with other membrane associated glycoproteins to form the DGC. However, Im et al., have shown that this model does express the Dp71 dystrophin isoform which is predominantly found in the brain and other non-muscle tissues (Im et al., 1996). The expression of the Dp71 isoform of dystrophin may prove protective for the maintenance of brain function given that a study by Moizard et al.,

has indicated that mutations in the Dp71 isoform of dystrophin, leading to premature termination of translation, are more closely correlated with severe mental retardation (Moizard et al., 2000). Hence proteomic profiling of mouse models lacking this brain-specific dystrophin isoform (such as the *mdx-3cv* model) may show a higher degree of differential protein expression. Proteomic profiling of the *mdx-4cv* model used in this study is still useful given that this model closely represents the human disorder.

Table 6.1: List of identified proteins with a significantly reduced abundance in 12-month old *mdx-4cv* brain versus age-matched wild-type brain as determined by label-free LC-MS/MS

Accession	Gene Name	Protein Name	Unique peptides	Confidence score	Anova (p)	Max fold change
Q9R0K7	Stx1b	Plasma membrane calcium-transporting ATPase 2	2	108.25	1.78E-02	2.77
Q9WV92	Stxbp1	Band 4.1-like protein 3	3	218.67	8.93E-03	1.90
O08599	Epb4113	Syntaxin-binding protein 1	4	315.93	1.97E-02	1.54
P07901	Rab7a	Heat shock protein HSP 90-alpha	2	109.14	3.84E-02	1.54
P51150	Atp2b2	Ras-related protein Rab-7a	3	106.89	1.10E-02	1.51
Q02053	Hsp90aa1	Ubiquitin-like modifier-activating enzyme 1	2	131.59	4.44E-02	1.41
P61264	Uba1	Syntaxin-1B	4	356.83	1.22E-03	1.28

Table 6.2: List of identified proteins with a significantly increased abundance in 12-month old *mdx-4cv* brain versus age-matched wild-type brain as determined by label-free LC-MS/MS

Accession	Gene Name	Protein Name	Unique peptides	Confidence score	Anova (p)	Max fold change
Q91X72	Hpx	Hemopexin	3	131.20	1.16E-03	5.64
P29699	Ahsg	Alpha-2-HS-glycoprotein	2	125.19	1.72E-03	3.47
P22599	Serpina1b	Alpha-1-antitrypsin 1-2	2	114.76	1.45E-02	3.29
P02088	Hbb-b1	Hemoglobin subunit beta-1	3	260.19	1.05E-03	3.24
P01942	Hba	Hemoglobin subunit alpha	5	370.80	2.13E-04	3.22
Q00623	Apoa1	Apolipoprotein A-I	8	316.97	5.23E-03	2.88
P07758	Serpina1a	Alpha-1-antitrypsin 1-1	4	108.28	1.74E-02	2.52
P07724	Alb	Serum albumin	16	1174.48	4.94E-04	2.51
Q923D2	Blvrb	Flavin reductase (NADPH)	3	203.95	1.72E-03	2.51
Q921I1	Tf	Serotransferrin	8	374.59	1.66E-02	2.18
P03995	Gfap	Glial fibrillary acidic protein	8	491.51	3.53E-02	2.00
Q08331	Calb2	Calretinin	2	94.24	4.02E-02	1.93
P48036	Anxa5	Annexin A5	2	132.70	3.20E-02	1.56
P20152	Vim	Vimentin	2	213.31	4.40E-03	1.55
Q9R0P9	Uchl1	Ubiquitin carboxyl-terminal hydrolase isozyme L1	3	165.79	2.31E-02	1.51
P46460	Nsf	Vesicle-fusing ATPase	2	134.05	1.10E-03	1.44
Q9D0E1	Hnrnpm	Heterogeneous nuclear ribonucleoprotein M	3	63.46	1.49E-02	1.44
O08788	Dctn1	Dynactin subunit 1	2	126.53	1.03E-02	1.44
P38647	Hspa9	Stress-70 protein, mitochondrial	6	476.79	1.76E-03	1.42
P48758	Cbr1	Carbonyl reductase [NADPH] 1	2	119.09	1.33E-02	1.42
P00920	Ca2	Carbonic anhydrase 2	2	135.96	2.81E-02	1.42
P14733	Lmnb1	Lamin-B1	2	150.58	2.92E-02	1.41
Q6IRU5	Cltb	Clathrin light chain B	2	125.00	4.20E-02	1.40
Q8R3V5	Sh3glb2	Endophilin-B2	4	201.90	2.06E-02	1.39

Q8QZT1	Acat1	Acetyl-CoA acetyltransferase, mitochondrial	4	215.23	6.81E-03	1.36
P27773	Pdia3	Protein disulfide-isomerase A3	5	295.10	1.30E-02	1.35
Q91VR2	Atp5c1	ATP synthase subunit gamma, mitochondrial	4	251.82	2.56E-03	1.35
Q6ZWY9	Hist1h2bc	Histone H2B type 1-C/E/G	2	121.60	4.21E-02	1.34
Q61171	Prdx2	Peroxiredoxin-2	2	141.40	1.28E-02	1.33
Q9D051	Pdhb	Pyruvate dehydrogenase E1 component subunit beta, mitochondrial	4	262.12	4.09E-03	1.32
O35737	Hnrnp1	Heterogeneous nuclear ribonucleoprotein H	2	100.27	1.67E-02	1.31
Q03265	Atp5a1	ATP synthase subunit alpha, mitochondrial	6	480.06	5.82E-03	1.30
P20029	Hspa5	78 kDa glucose-regulated protein	2	150.07	2.51E-02	1.29
Q9QXS6	Dbn1	Drebrin	3	142.39	1.93E-02	1.28
P62259	Ywhae	14-3-3 protein epsilon	2	103.44	2.86E-02	1.27
O88737	Bsn	Protein bassoon	3	215.46	1.33E-02	1.25
Q811D0	Dlg1	Disks large homolog 1	2	110.76	6.40E-03	1.25
P14873	Map1b	Microtubule-associated protein 1B	2	126.07	5.00E-03	1.24
P16546	Sptan1	Spectrin alpha chain, non-erythrocytic 1	3	197.38	1.49E-02	1.24

6.2.2 Distribution of protein changes in dystrophic mdx-4cv brain tissue

To more closely examine the role of these alterations in the expression of brain-derived proteins, standard bioinformatics software was employed. PANTHER analysis was conducted to investigate the distribution and molecular function of the affected proteins. This analysis revealed alterations in anti-oxidant activity (2.0%), binding (25.5%), catalytic activity (37.3%), enzyme regulator activity (7.8%), receptor activity (2.0%), structural molecule activity (15.7%) and transporter activity (9.8%). Of the 15.7% proteins involved in structural molecule activity, 87.5% of these were associated with the cytoskeleton, with the remaining proteins connected to ribosomal structure. The PANTHER database was also applied to illustrate the protein class of identified proteins with altered abundance (Figure 6.1). The majority of altered protein species again belong to the class of cytoskeletal proteins, suggesting that dystrophin deficiency causes restructuring of the cytoskeleton in the brain. These cytoskeletal proteins include drebrin, microtubule associated protein 1B, vimentin, endophilin B2, glial fibrillary acidic protein, spectrin α 1 chain, dynactin and lamin-B1. All of these proteins display increased abundance in dystrophic samples, indicating compensatory up-regulation of cytoskeletal and stabilising components in order to counter-act dystrophin deficiency. This agrees with the classification of X-linked muscular dystrophy as a primary disorder of the membrane cytoskeleton. STRING analysis was also performed to examine potential interaction networks between the altered proteins. Figure 6.2 shows the overall interaction patterns amongst altered protein species.

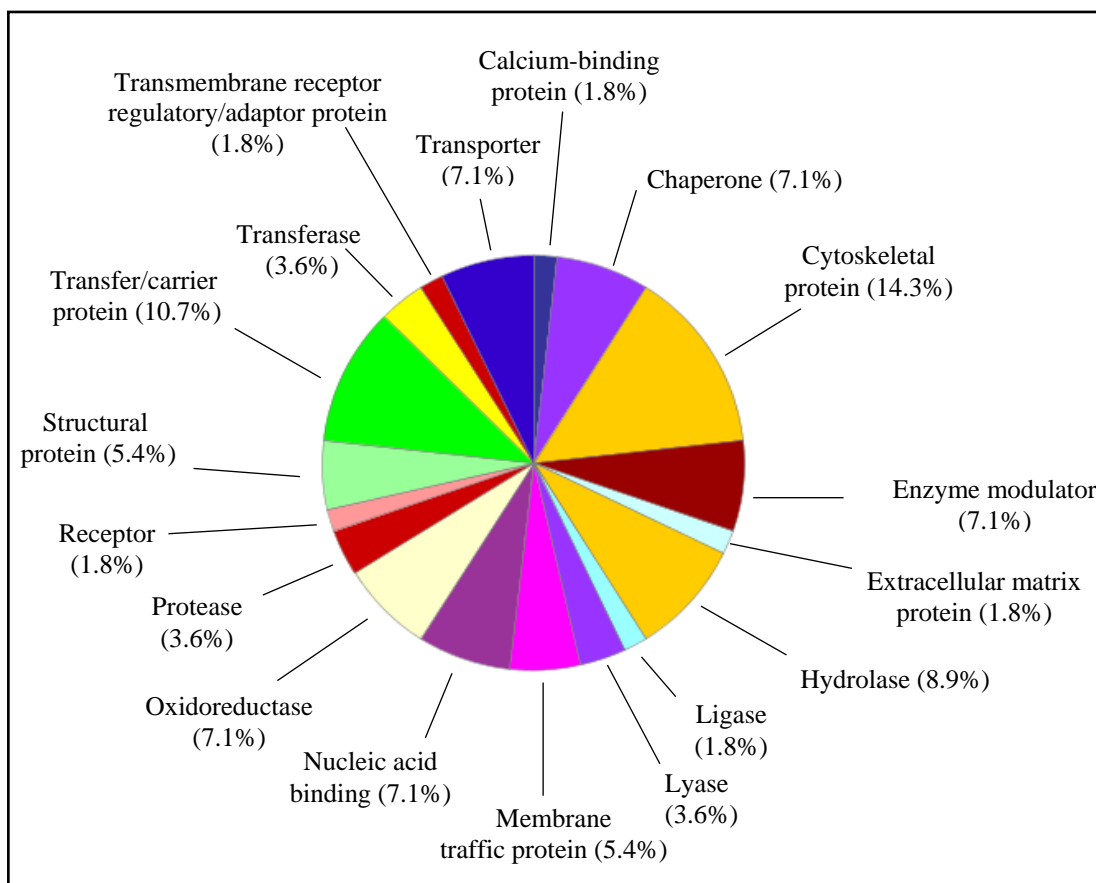


Figure 6.1: Graphical representation of changed protein classes with altered abundance in *mdx-4cv* brain tissue

The bioinformatics software programme PANTHER was applied to identify the clustering of protein classes based on the mass spectrometric identification of altered protein species in control versus dystrophin-deficient brain preparations.

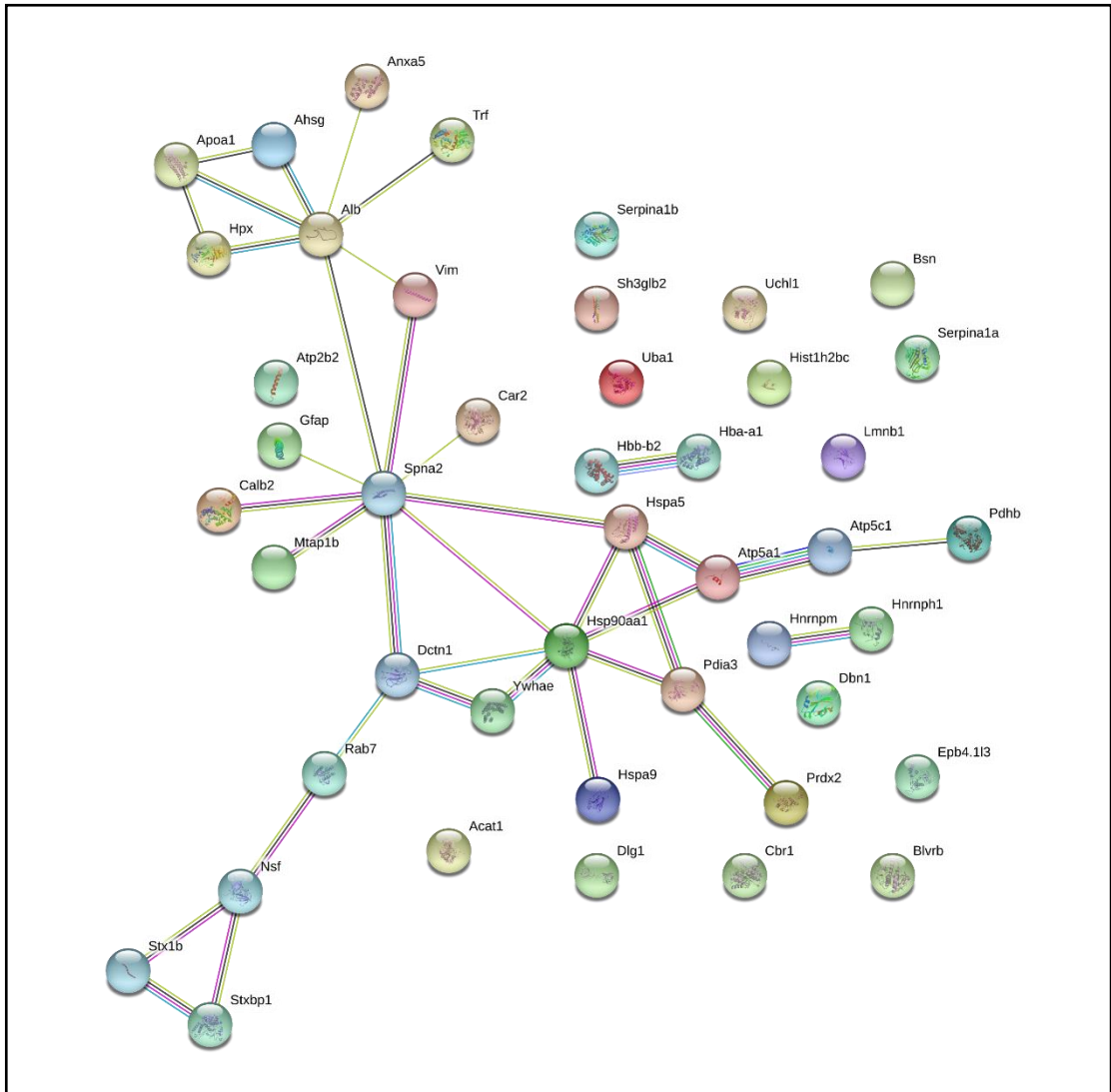


Figure 6.2: Interaction map of altered proteins from *mdx-4cv* brain tissue
 The bioinformatics STRING database was applied to generate a protein interaction map with known and predicted protein associations, based on both direct physical and indirect functional protein interactions

6.2.3 Verification of proteomic alterations in dystrophin-deficient brain tissue by immunoblotting

In order to verify some of the key proteomic findings from the comparative analysis of wild-type versus *mdx-4cv* brain tissue, immunoblotting against select protein hits (listed in Tables 6.1 and 6.2) was carried out. For loading controls, a silver-stained protein gel and the unchanged abundance of lactate dehydrogenase was used and is presented in Figure 6.3. The trend of increased abundance of lamin-B1 was confirmed by immunoblotting (Figure 6.4). Increased abundance of both annexin A5 and vimentin and reduction in the expression of the plasma membrane calcium-transporting ATPase 2 were also verified by immunoblotting (Figure 6.4 and Figure 6.5 respectively) and their altered abundance was found to be statistically significant. These findings are in agreement with the proteomic data in this report and suggests an overall restructuring of the cytoskeleton and alterations in ion homeostasis in dystrophin-deficient conditions.

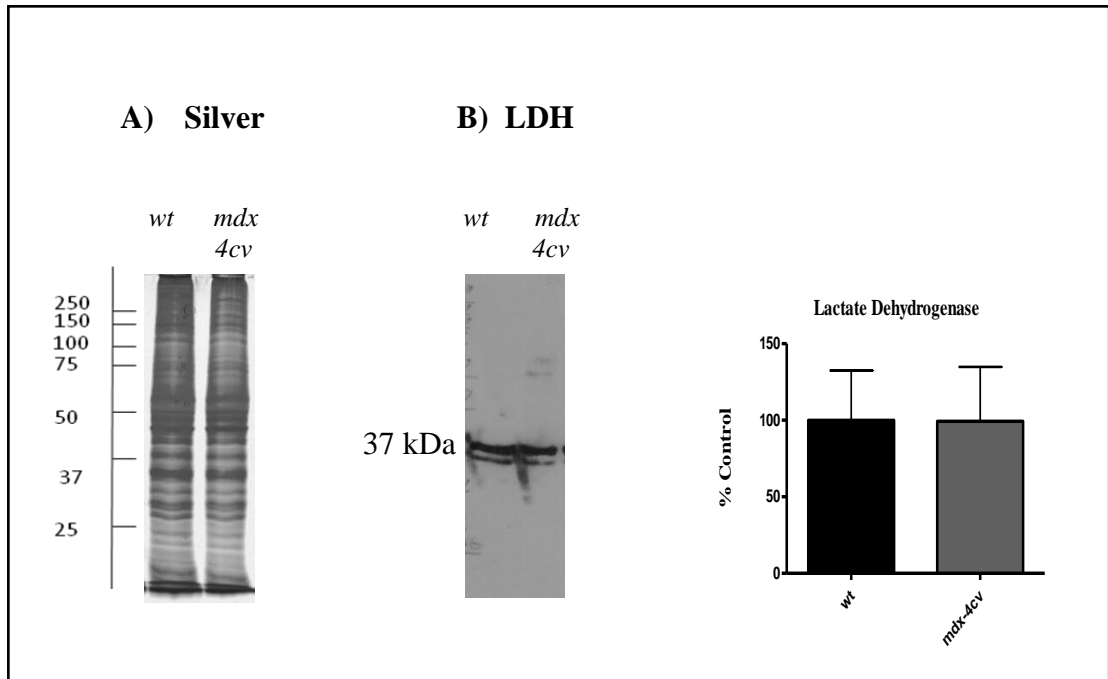


Figure 6.3: Electrophoretic and immunoblot analysis of wild-type and *mdx-4cv* brain

Shown is a silver stained 1D gel (A) and immunoblot and statistical analysis of bands labelled with lactate dehydrogenase (B). The silver stained gel shows comparable protein banding patterns for wild-type and *mdx-4cv* brain preparations. Molecular weight marker is given on the left-hand-side of the image in kDa. Lactate dehydrogenase immunoblotting did not show significant changes in concentration between wild-type and *mdx-4cv* samples and so it serves as a loading control for comparative immunoblotting. Graphical representation of the immuno-decoration level for lactate dehydrogenase is shown (mean values \pm SEM, Student's *t*-test; unpaired; $n=4$).

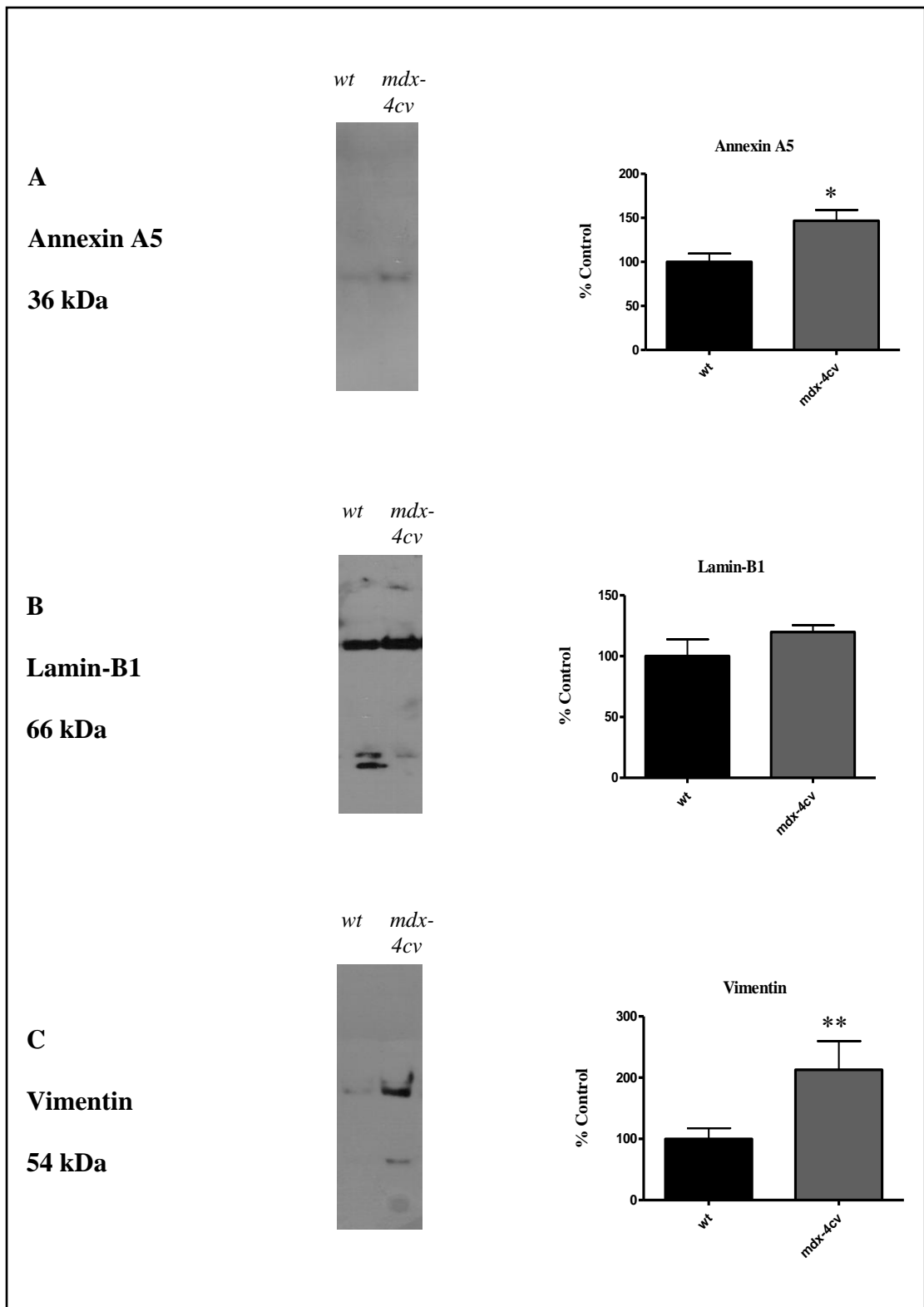


Figure 6.4: Comparative immunoblot analysis of proteins with increased abundance in dystrophic *mdx-4cv* brain tissue

Shown are representative immunoblots with immuno-decorated bands labelled with antibodies to annexin A5 (A), lamin-B1 (B) and vimentin (C). Statistical analysis of immuno-decoration was performed with Student's *t*-test (mean values \pm SEM; unpaired; $n=4$, * $p \leq 0.05$, ** $p \leq 0.01$).

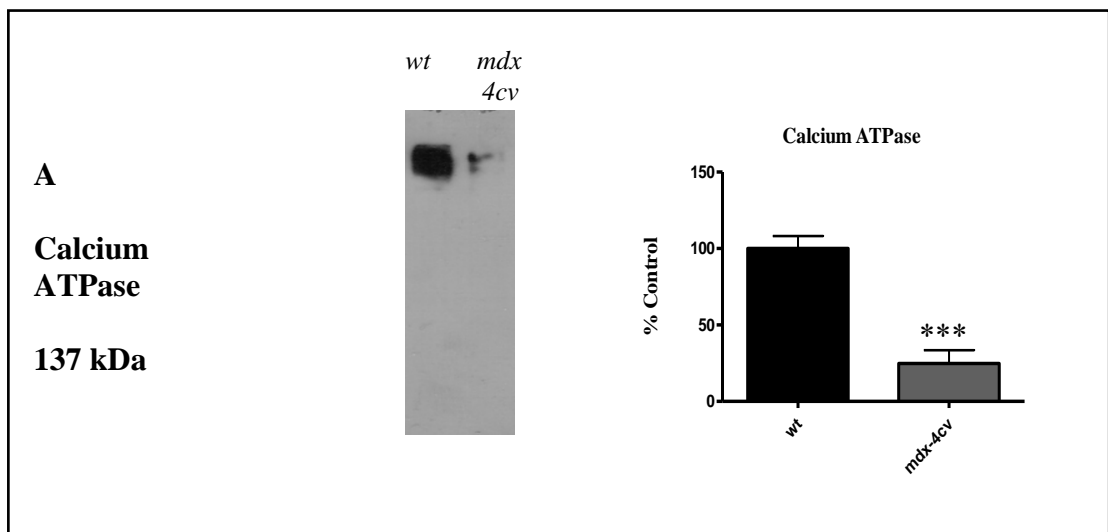


Figure 6.5: Comparative immunoblot analysis of proteins with decreased abundance in dystrophic *mdx-4cv* brain tissue

Shown is a representative immunoblot with immuno-decorated bands labelled with an antibody to the plasma membrane calcium-transporting ATPase 2 (Calcium ATPase, A). Statistical analysis of immuno-decoration was performed with Student's *t*-test (mean values \pm SEM; unpaired; $n=4$, *** $p \leq 0.001$).

6.2.4 Immunoblot and immunofluorescence microscopy analysis of GFAP as a marker of reactive gliosis

The 2-fold increase in the expression of GFAP in the dystrophin-deficient brain as identified by label-free mass spectrometry is an important proteomic finding given its elevated expression is an indicator of astrogliosis. To further investigate the potential induction of astrogliosis in the *mdx-4cv* brain in the absence of dystrophin, immunoblot analysis and immunofluorescence microscopy was performed. Figure 6.6 illustrates the specificity of the GFAP antibody used in this proteomic analysis. While the cytosolic enzyme lactate dehydrogenase and the nuclear envelope marker laminB1 are present in crude extracts from wild-type mouse liver, diaphragm, skeletal muscle, cardiac tissue and the brain, GFAP is only detected in the brain extracts (Figure 6.6). A silver-stained gel depicting different protein banding patterns for the different tissues is also depicted. Previous immunoblot analyses of GFAP protein have shown a tight banding pattern with two to three protein bands with slightly different electrophoretic mobility (Singh et al., 2009). Similarly, as shown in Figure 6.7, higher levels of brain protein per lane result in a broader banding pattern for GFAP. Based on these results, an intermediate level of brain protein was used for comparative immunoblot analysis.

Immunoblot analysis of 12-month old wild-type versus *mdx-4cv* brain preparations confirmed the elevation of this protein and was found to be statistically significant (Figure 6.8). To examine whether this increase is stage-specific, immunoblotting was conducted with wild-type and *mdx-4cv* brain samples at 2-months-old, 8-months-old and 12-months-old (Figure 6.9). At all ages tested, levels of GFAP were found to be higher in the dystrophic preparations, suggesting that this process of astrogliosis occurs throughout the disease.

In order to determine whether increased abundance of GFAP may serve as a marker of neurodegeneration, GFAP expression in the wobbler mouse model of amyotrophic lateral sclerosis (ALS) was investigated by immunoblotting. ALS is characterised by the progressive degeneration of motor neurons, which affects signalling cascades and culminates in progressive muscle paralysis (Rowland and Shneider, 2001). Immunoblotting confirmed the increased abundance of GFAP in brain tissue extracted from 2-month old wobbler mice compared to age-matched control mice (n=4) (Figure 6.10). This suggests that elevated levels of GFAP are associated with reactive gliosis in response to damage to the brain. This supports the

hypothesis that dystrophin deficiency in the *mdx-4cv* brain may trigger astrogliosis and glial scar formation.

Analysis of GFAP expression in the brain by immunofluorescence microscopy also confirmed the results obtained by proteomic analysis and immunoblotting. As shown in Figure 6.11, dystrophin-deficient brain sections display substantially higher levels of GFAP labelling than wild-type brain sections. This data agrees with the idea of astrogliosis as a consequence of progressive central nervous system damage in the dystrophin-deficient brain.

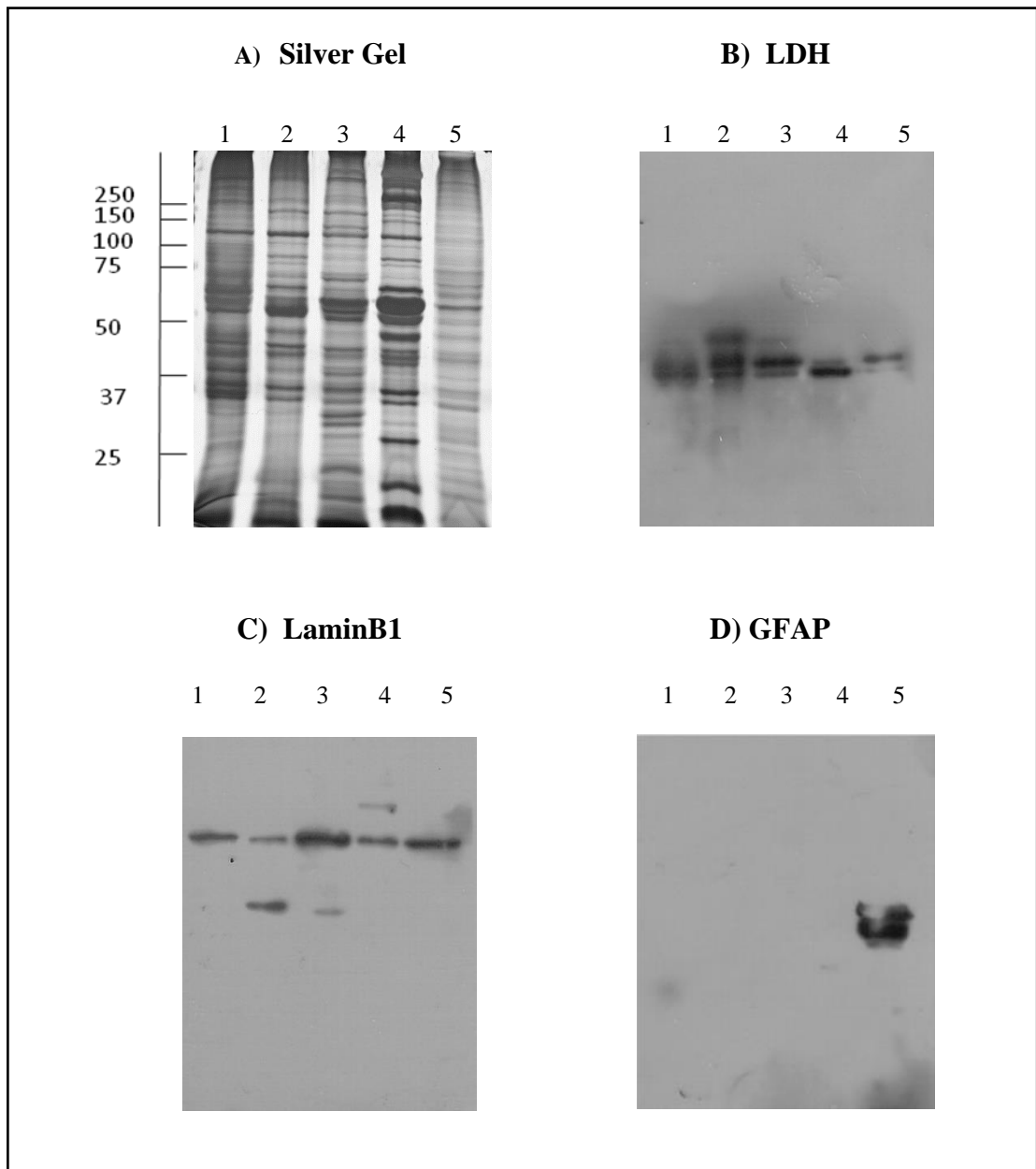


Figure 6.6: Immunoblot analysis of the specificity of the GFAP antibody

Depicted is a silver-stained gel (A) and corresponding immunoblots to the cytoplasmic enzyme lactate dehydrogenase (B), the nuclear marker lamin B1 (C) and the glial fibrillary acidic protein GFAP (D). Lanes 1 to 5 correspond to crude extracts from wild-type mouse liver, diaphragm, cardiac tissue, skeletal muscle and the brain respectively. While lactate dehydrogenase and lamin B1 were detected in all tissue extracts, GFAP was only detected by the brain tissue, illustrating the specificity of the ab7260 antibody to GFAP; a brain-specific protein.

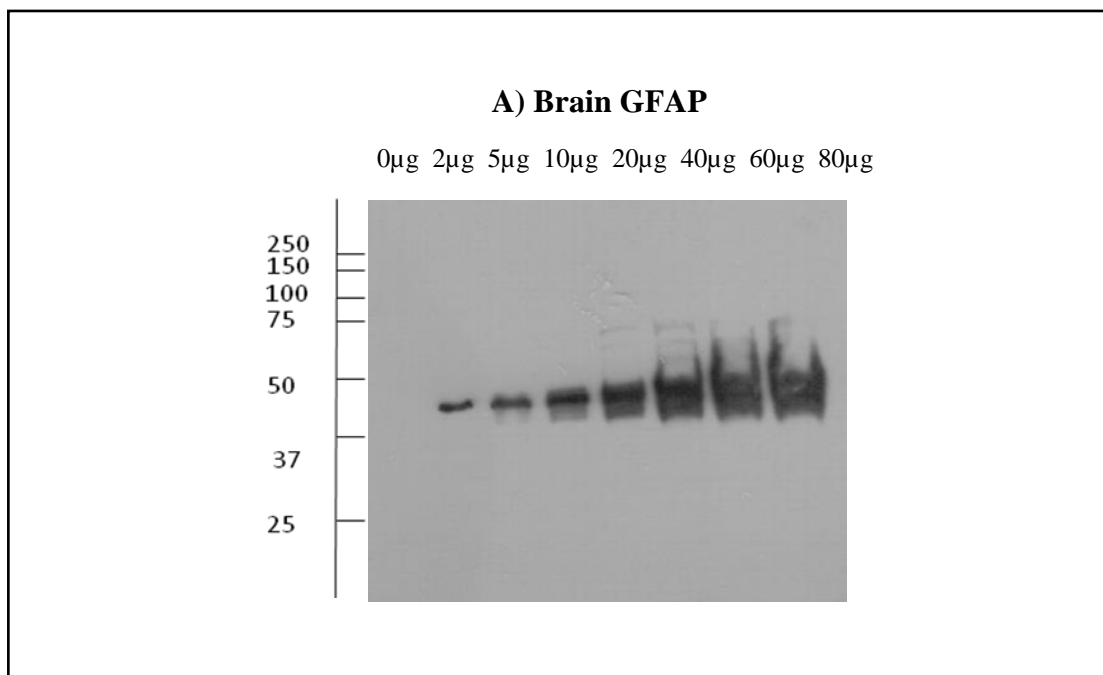


Figure 6.7: Dilution series of the GFAP antibody

Shown is an immunoblot depicting an increase in signal of the GFAP protein in a dilution series. Increasing amounts of mouse brain protein per lane (from 0 μ g to 80 μ g) results in a broader immuno-labelled GFAP pattern at higher concentrations.

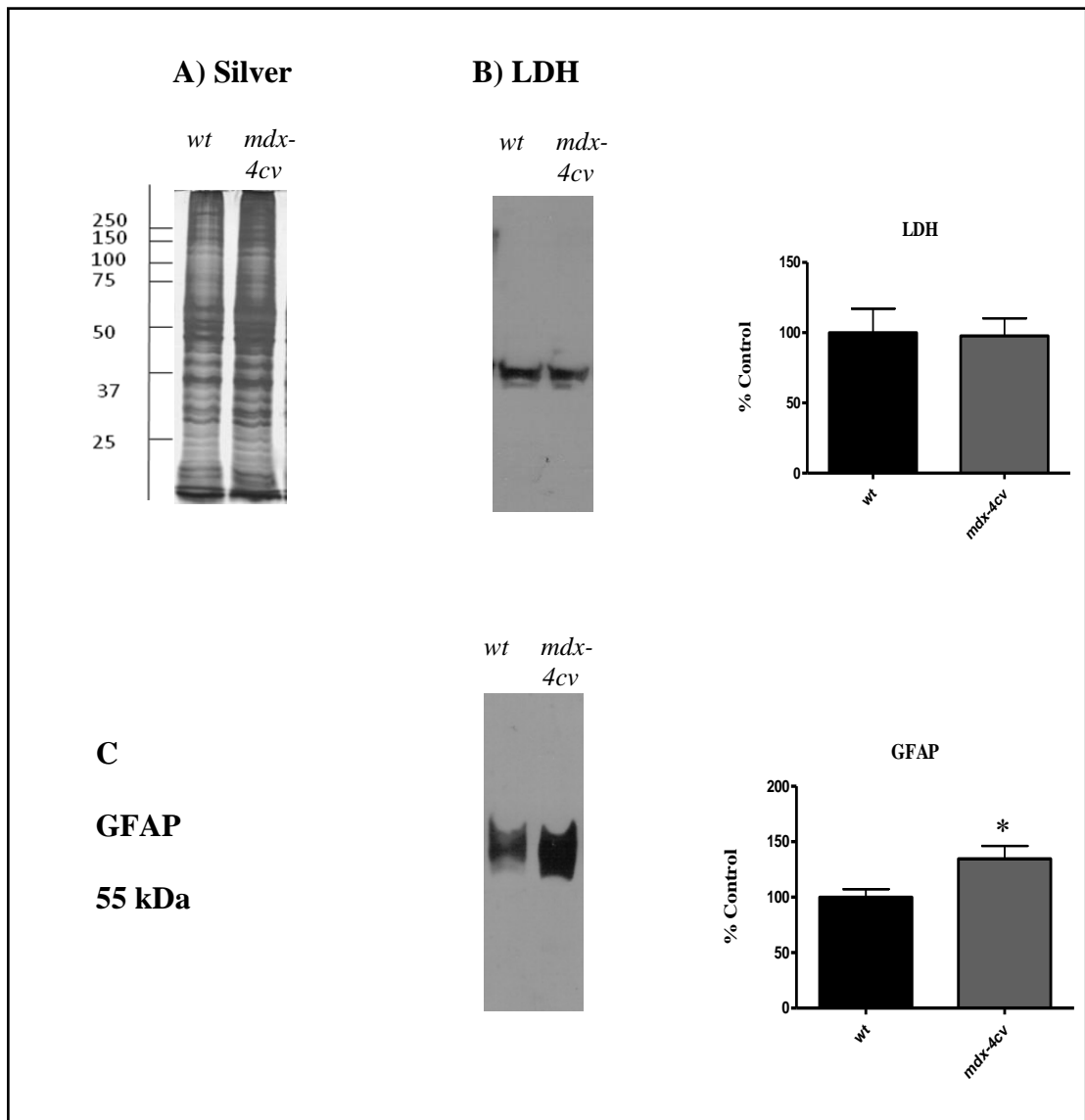


Figure 6.8: Comparative immunoblot analysis of the glial fibrillary acidic protein GFAP in wild-type versus *mdx-4cv* brain specimens

Shown is a representative silver-stained gel (A) and immunoblot (B) and statistical analysis of bands labelled with lactate dehydrogenase. The silver stained gel shows comparable protein banding patterns for wild-type and *mdx-4cv* 12-month old brain. Molecular weight marker is given on the left-hand-side of the image in kDa. Lactate dehydrogenase immunoblotting did not show significant changes in concentration between wild-type and *mdx-4cv* samples and so it serves as a loading control for comparative immunoblotting. Also shown is an immunoblot to GFAP (C). Graphical representation of the immuno-decoration levels for lactate dehydrogenase and GFAP is shown (mean values \pm SEM, Student's *t*-test; unpaired; $n=4$; $*p \leq 0.05$).

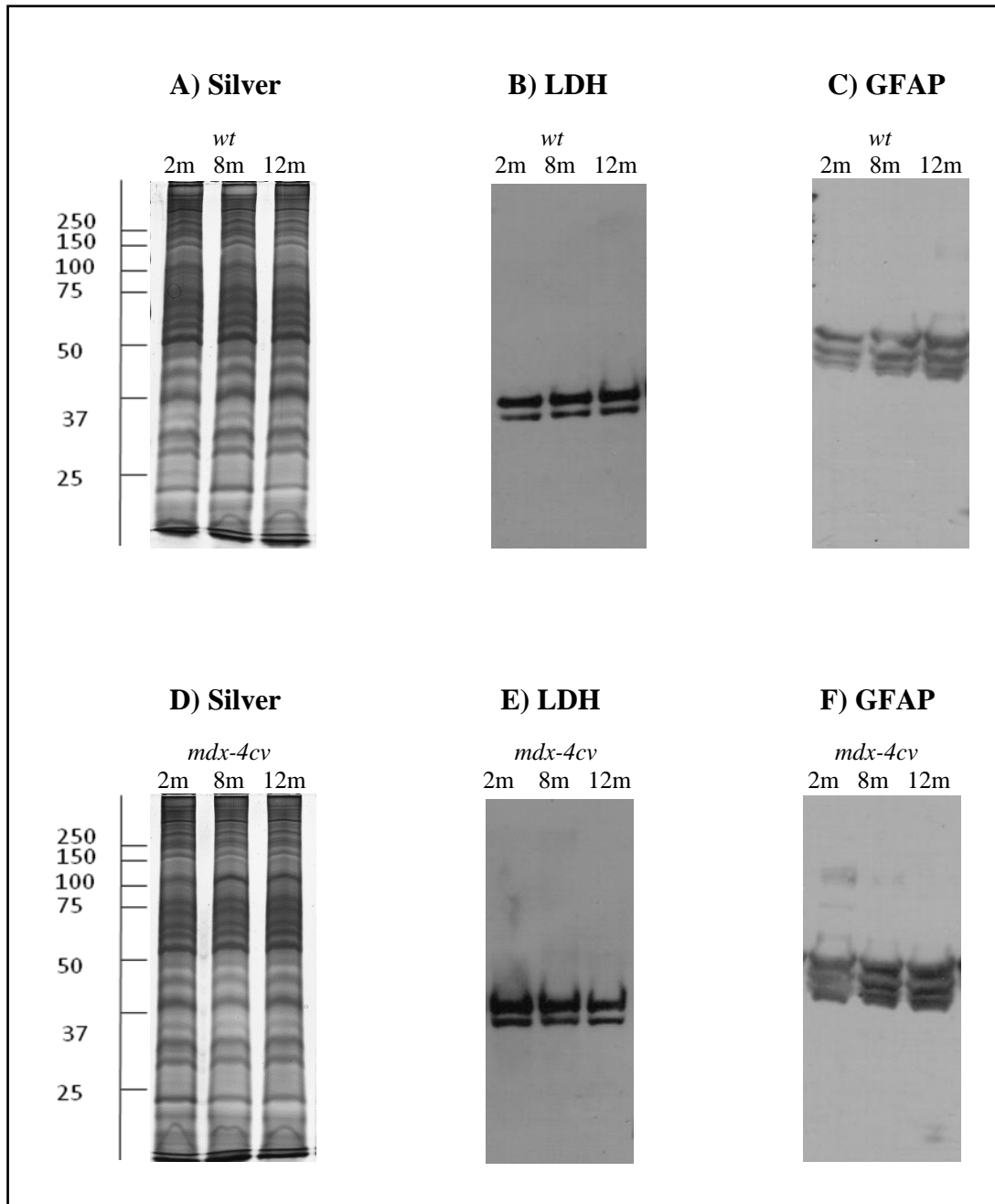


Figure 6.9: Comparative immunoblot analysis of the glial fibrillary acidic protein GFAP in wild-type versus *mdx-4cv* brain specimens from 2-12 months

Shown are representative silver-stained gels (A, D) and immunoblot analysis of bands labelled with lactate dehydrogenase (B, E). Images A, B and C correspond to 2-month old, 8-month old and 12-month old brain samples from wild-type mice while images D, E and F depict 2-month old, 8-month old and 12-month old brain specimens from *mdx-4cv* mice. The silver stained gels show comparable protein banding patterns for wild-type and *mdx-4cv* brain. Molecular weight marker is given on the left-hand-side of the image in kDa. Lactate dehydrogenase immunoblotting did not show significant changes in concentration between wild-type and *mdx-4cv* samples and so it serves as a loading control for comparative immunoblotting. Also shown is an immunoblot to GFAP (C, F).

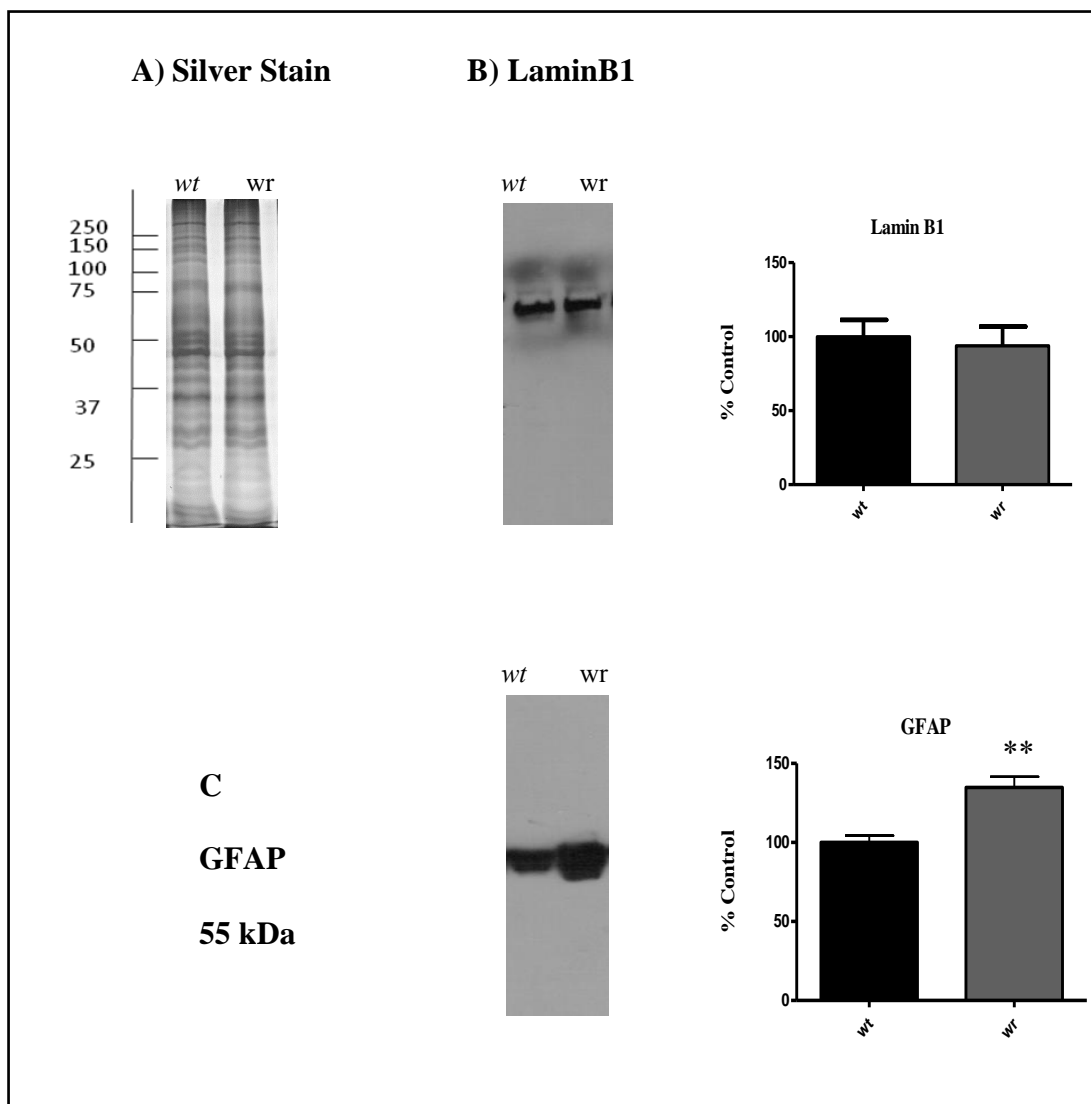


Figure 6.10: Comparative immunoblot analysis of the glial fibrillary acidic protein GFAP in wild-type versus wobbler brain specimens

Shown is a representative silver-stained gel (A) and immunoblot (B) and statistical analysis of bands labelled with lamin B1. The silver stained gel shows comparable protein banding patterns for wild-type and wobbler 2-month old brain. Molecular weight marker is given on the left-hand-side of the image in kDa. Lamin B1 immunoblotting did not show significant changes in concentration between wild-type and wobbler samples and so it serves as a loading control for comparative immunoblotting. Also shown is an immunoblot to GFAP (C). Graphical representation of the immuno-decoration levels for lamin B1 and GFAP is shown (mean values \pm SEM, Student's *t*-test; unpaired; $n=4$; $**p \leq 0.01$).

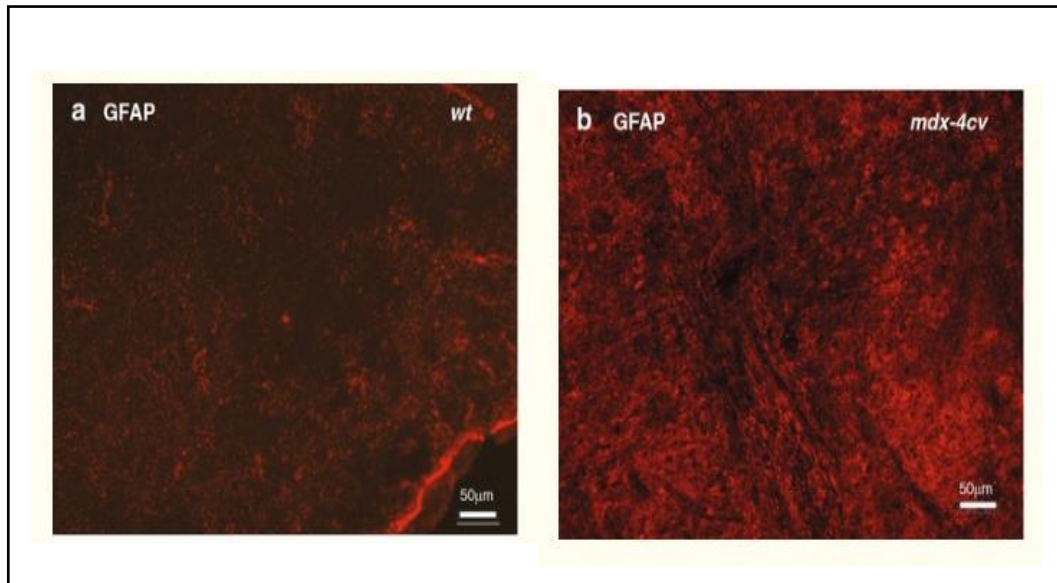


Figure 6.11: Immunofluorescence microscopy of GFAP in wild-type versus *mdx-4cv* brain sections

Shown is the immunofluorescence staining of brain sections with GFAP (a, b). The *mdx-4cv* brain tissue exhibits an increased level of GFAP labelling (b) as compared to wild-type brain sections (a). This agrees with the mass spectrometry data and immunoblot analysis presented in this report.

* Image from Murphy et al., 2015c

6.3 Discussion

Despite a relatively large proportion of DMD patients expressing some degree of cognitive impairment, most comparative proteomic surveys have focused on the severely fibrotic diaphragm and heart, the moderately affected limb muscles, and protected muscles such as extraocular muscle (Carberry et al., 2013, Holland et al., 2015a, Ge et al., 2003). This proteomic survey aimed to identify alterations in protein expression in the *mdx-4cv* brain through a combination of mass spectrometry and western blotting. This methodology has uncovered alterations in proteins involved in calcium homeostasis, structural re-organisation, the cellular stress response, iron homeostasis and neurotransmission. These changes in the dystrophin-deficient brain may represent contributing factors to mental impairment in X-linked dystrophinopathies.

The observed elevation in the levels of hemopexin (5.64-fold increase), haemoglobin subunit $\beta 1$ (3.24-fold increase), haemoglobin subunit α (3.22-fold increase) and serotransferrin (2.18-fold increase) suggests altered blood-flow and disturbed iron homeostasis in muscular dystrophy. While it could be argued that the increased abundance of haemoglobin may be an artefact, given the brain samples were not perfused, the fact that increased abundance is seen for both the α and $\beta 1$ subunits, and that their fold changes are closely correlated may indicate higher vascularisation and hence increased blood-flow to dystrophin-deficient brains (Holland et al., 2014). Serotransferrin is an essential iron transporter serving a number of important roles. It is the main distributor of iron to tissue, and it also acts as a sink to sequester extracellular iron and thus prevents cytotoxic stress from excess free iron in plasma (Szöke and Panteghini, 2012). Its increased abundance could be linked to altered iron homeostasis in the dystrophin-deficient brain. In this proteomic survey the protein with the largest increase in abundance was the heme-binding plasma glycoprotein hemopexin. Serum hemopexin levels have been observed to be increased in response to elevated levels of free heme, in which case it may serve to scavenge free heme and thus provide antioxidant protection (Delanghe and Langlois, 2001). In DMD, the dystrophin-deficient sarcolemma is weakened, enabling the leakage of muscle-associated proteins, such as myoglobin into plasma. This has the potential to lead to the production of myoglobin-derived heme in plasma, which may explain the increased levels of hemopexin seen in neuromuscular disease (Adornato et al., 1978). The increased abundance of these two iron-regulating proteins suggests a protective

role against potential iron overload in the dystrophin-deficient brain, which may otherwise prove cytotoxic. Elevated levels of the important anti-inflammatory agent anti-trypsin suggest the induction of a protective mechanism in response to potential brain inflammation (Miravittles, 2012). The classification of mental impairments as a clinical hallmark of DMD is supported by the proteomic identification of increased levels of fetuin-A, a previously identified biomarker of general neuro-degeneration (Mori et al., 2011).

A large proportion of the altered protein species in dystrophin-deficient brain samples belong to the class of cytoskeletal proteins (14.3%). Similar to other tissue types such as skeletal muscle, the deficit in dystrophin expression in the *mdx-4cv* brain appears to induce compensatory up-regulation of cytoskeletal proteins as a means of counteracting dystrophin deficiency-induced weakness and susceptibility to mechanical stress (Law et al., 1994). In the absence of the actin-binding Dp427 isoform of dystrophin, levels of the actin-regulatory protein drebrin may be increased, as seen in this proteomic survey. Drebrin, through its co-localisation with actin filaments, has been proposed to be integral to synaptic plasticity (Shim and Lubec, 2002), and hence reduced levels of drebrin have been associated with neurodegenerative conditions (Harigaya et al., 1996). Drebrin is also involved in regulating the assembly of actin filaments and in this regard its elevated levels in the dystrophin-deficient brain may suggest compensatory stabilisation of the actin cytoskeleton in order to maintain an internal scaffold capable of absorbing mechanical stress. Recent reports have also suggested a role for nuclear structural integrity in resistance against mechanical stress (Houben et al., 2007), with potential roles established for the nuclear membrane, the nuclear lamina and lamina-associated proteins such as A- and B-type lamins. B-type lamins appear to have particular importance given that they are expressed in virtually all cell types, and thus may represent the essential component of the nuclear lamina (Broers et al., 2006). Increased abundance of lamin-B1 has been identified by both mass spectrometry and immunoblotting in this proteomic survey, agreeing with the role of lamina-associated proteins in maintaining nuclear integrity which is essential for cell survival. This role of lamin-B1 is further validated by the observed increase in histone H2B type 1-C/E/G. Histones serve as components of the nucleosome and play roles in DNA repair and replication and in chromosomal stability. Thus, the increase in histone H2B may represent an attempt by the *mdx-4cv* brain to maintain nuclear and thus cellular

integrity in the absence of Dp427. The increased expression of these two proteins may be responsible for safeguarding the nuclear structure, thus increasing the “mechanical stiffness” of the cell. This may enhance the ability of cells to endure the mechanical stress prevalent in weakened, dystrophin-deficient cells.

Glial fibrillary acidic protein (GFAP) is an intermediate filament III protein unique to astrocytes, enteric glial cells and non-myelinating Schwann cells in the peripheral nervous system (Eng, 1985). This brain-specific protein plays key structural roles in provision of the cytoskeletal structure of glial cells and maintenance of glial cell mechanical strength (Yang and Wang, 2015), along with maintaining the blood-brain barrier, regulating ion and fluid homeostasis and controlling central nervous system blood-flow (Sofroniew and Vinters, 2010). Thus, in this role as a supporting intermediate filament its elevated abundance in the *mdx-4cv* brain is consistent with the hypothesis of structural re-organisation in dystrophic tissue to counteract dystrophin-deficiency. This claim is further substantiated by the increased abundance of vimentin, a closely related intermediate filament protein. Together, the increased abundance of these structural proteins may partially restore mechanical strength to cells made fragile by the absence of the large structural protein dystrophin. Increases in the expression of GFAP may also be indicative of astrogliosis (Eng et al., 2000), in which either the genetic deficiency in dystrophin and/or the secondary abnormalities which ensue may cause the activation of astrocytes. Reactive astrocytes, characterised by hypertrophy of their cellular processes and increased expression of GFAP, are essential for reducing the spread and persistence of inflammatory cells, repairing the blood brain barrier, and isolating affecting regions from neighbouring healthy tissue to limit the lesion size and subsequent tissue damage (Pekny et al., 2014). GFAP induction and associated gliosis are also associated with neuro-regeneration (Yang and Wang, 2015). While neuro-regeneration may initially be a positive, reparative response, in cases where the triggering factor for astrogliosis is unresolved it has the potential to lead to tissue scarring and inhibition of axon regeneration. Similarly in dystrophic skeletal muscle, excess connective tissue is produced in response to muscle damage (Holland et al., 2015a). Over time this fibrosis becomes pathological and contributes to the worsening phenotype seen in DMD. Perhaps the gliosis, induced neuro-regeneration and potential tissue scarring in the dystrophin-deficient brain is the equivalent to the severe fibrosis seen in skeletal muscle. Interestingly, TGF- β has been shown to induce GFAP gene transcription, resulting in elevated levels of GFAP

protein (Reilly et al., 1998). In skeletal muscle fibrosis is also modulated by TGF- β , since it stimulates the secretion of pro-fibrotic proteins such as collagen and periostin (Lorts et al., 2012, Vidal et al., 2008). Thus, this inflammatory mediator may contribute to tissue scarring in both dystrophin-deficient brain tissue and skeletal muscle. Astrogliosis and concomitant increases in GFAP have also been identified in brain tissue from individuals with Alzheimer's disease, in cerebral freeze-injury and in the experimental autoimmune encephalomyelitis model of multiple sclerosis (Eng et al., 2000, Rodríguez et al., 2009). In addition, in this study immunoblotting of brain tissue from the wobbler mouse model of ALS revealed elevated levels of GFAP. Therefore, GFAP appears to represent a potential biomarker of neurotoxicity. In the absence of dystrophin, constant neuronal loss and alterations in calcium homeostasis may trigger non-specific reactive gliosis which may represent the underlying mechanism that triggers developmental cognitive defects in DMD. Indeed a previous case report of a Duchenne patient with severe mental retardation described multifocal glial nodules in the cerebellar cortex with proliferating glial cells showing an intense immunoreactivity for GFAP (Itoh et al., 1999).

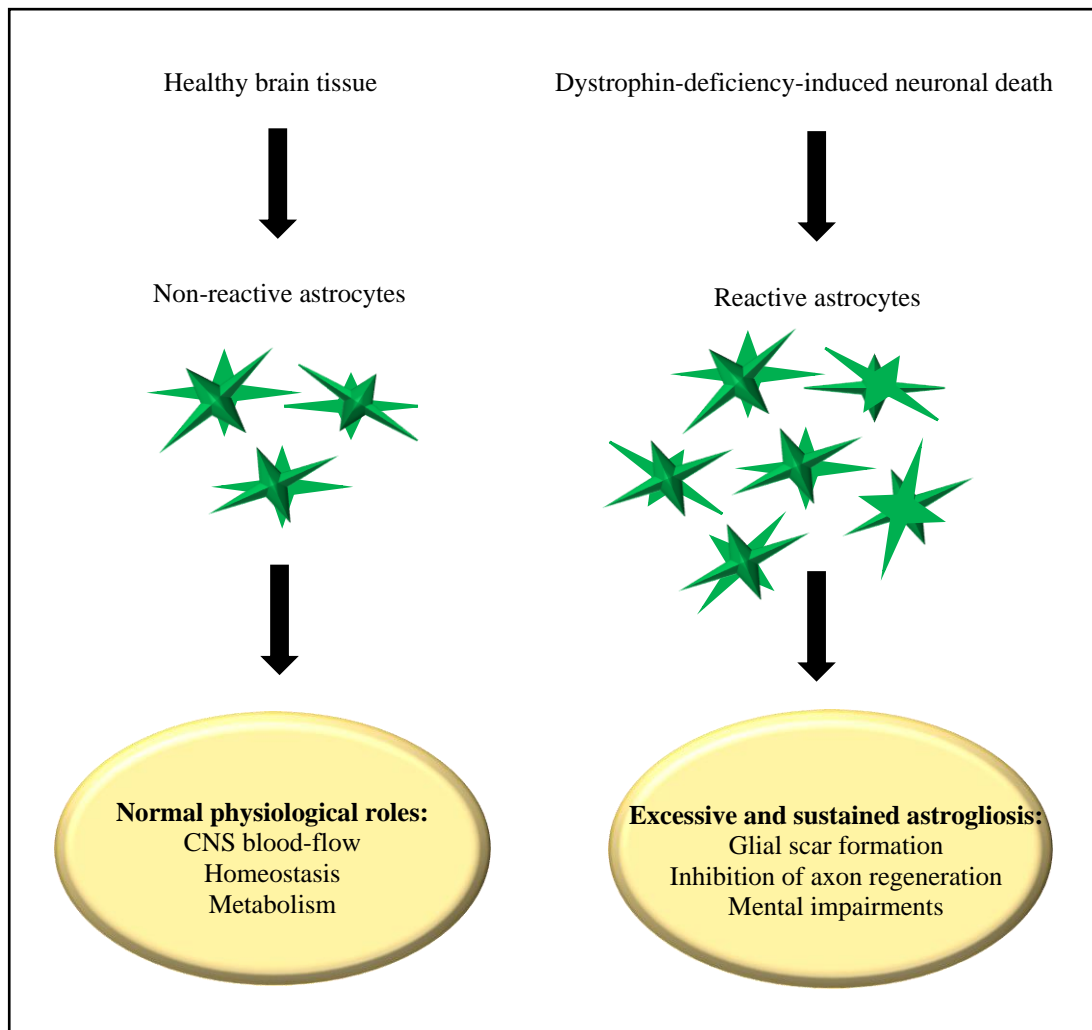


Figure 6.12: A potential role for astrogliosis in the pathophysiology of mental impairment in the dystrophin-deficient brain

In healthy tissue astrocytes are involved in maintaining homeostasis. In DMD the absence of dystrophin may lead to neuronal death which in turn may trigger astrogliosis. Unresolved astrogliosis may lead to the formation of glial scars and this process may represent the underlying mechanism responsible for cognitive deficiencies in DMD.

The abnormal expression of syntaxin-binding protein 1, syntaxin-1B and protein bassoon are indicative of variations in neurotransmission. Neurotransmission is a key biological process tightly regulated by a multitude of proteins that form the exocytosis release machinery, of which syntaxin-1 is a member (Yang et al., 2015). Syntaxin-binding protein 1, the binding partner of syntaxin, is also involved in neurotransmitter release via regulation of the protein receptor syntaxin. Both syntaxin-binding protein 1 and syntaxin-1B display reduced abundance in *mdx-4cv* brain preparations, indicating a potential reduction in neurotransmission in the dystrophin-deficient brain. Such reductions in glutamate neurotransmission have been identified in Alzheimer's disease patients, where it has been suggested to contribute to cognitive impairment (Lin et al., 2003). Thus, a similar process may be responsible for cognitive deficits in X-linked muscular dystrophy. However, a slight increase in the expression of protein bassoon was also observed in dystrophin-deficient brain tissue. This protein is involved in the organisation of the cytomatrix at the nerve terminals active zone (Dick et al., 2003), where it regulates neurotransmitter release from brain glutamatergic synapses. Its increased expression may represent an attempt to promote neurotransmission in the face of reduced levels of other regulatory proteins. Alternatively, taken together the altered expression of syntaxin-binding protein 1, syntaxin-1B and protein bassoon may indicate a global disturbance of neurotransmission in dystrophin-deficient brain tissue.

The calcium hypothesis of DMD remains a key player in investigations of the disorder's pathobiochemistry. This model postulates that the absence of functional dystrophin and concomitant ablation of the DGC weakens the sarcolemma enabling micro-rupturing and excess influx of Ca^{2+} into the sarcoplasm (Millay et al., 2009). Elevated levels of cytosolic calcium are thought to alter ion homeostasis, cellular signalling and activate protein degradation in affected muscle fibres. Absence of the DGC from the brain may affect neuronal membranes in the same fashion as the sarcolemma of muscle fibres. This hypothesis is supported by the observation that cerebellar granule-cell neurones from *mdx* mice have 24% more free calcium than normal wild-type mice (Hopf and Steinhardt, 1992). This may explain the observed increase in the calcium-binding protein calretinin in dystrophin-deficient brain evident in this proteomic survey (1.93-fold increase). Excessively high levels of intracellular calcium can induce cell death and thus the apparent up-regulation of calretinin may act as a compensatory mechanism in which calretinin acts as a calcium-buffering

protein to protect against calcium influx (Carretta et al., 2003). This may be particularly beneficial in emerging neurons where alterations in calcium ion homeostasis initiates cell death during development.

It has been recently proposed that the calcium-binding membrane repair proteins, the annexins, represent universal biomarkers of dystrophinopathy. Elevated levels of this protein class have been identified in the severely dystrophic *mdx* diaphragm, the moderately affected *soleus* and *extensor digitorum longus mdx* muscles and the relatively mildly affected *interosseus* and *flexor digitorum brevis mdx* muscles (Holland et al., 2015b). Elevated cytoplasmic calcium triggers the translocation of annexins to the membrane, with each annexin isoform having a particular calcium threshold (Draeger et al., 2011). While annexins 1 and 2 are widely known to be involved in membrane repair (McNeil et al., 2006, Lennon et al., 2003), a novel role for annexin A5 in this essential biological process has recently been suggested. Upon calcium activation annexin A5 has been shown to self-assemble into 2D arrays on membranes with the aim of re-sealing membrane tears. Both annexin A5-null cells and cells expressing mutant annexin A5 which cannot form 2D arrays exhibit a severe membrane repair defect (Bouter et al., 2011). Hence, the elevated levels of annexin A5 in dystrophin-deficient brain may represent a marker of neuronal membrane damage, which is consistent with the hypothesis that dystrophin-deficient membrane is highly susceptible to injury.

Alterations in calcium homeostasis are also suggested by the drastic reduction in the expression of the plasma membrane calcium transporting ATPase 2 (PMCA), an essential component for maintaining cellular calcium homeostasis. PMCA is the protein product of a multigene family with PMCA 1 and 4 expressed almost ubiquitously while PMCA 2 and 3 are restricted to neurons (Stauffer et al., 1995). In neuronal cells calcium homeostasis is maintained predominantly by a combination of sarcoplasmic/endoplasmic reticulum calcium ATPases, responsible for calcium uptake into the organelles, and the PMCA, responsible for calcium extrusion (Fresu et al., 1999). The absence of dystrophin isoforms (Dp71, Dp116, Dp140, Dp260, Dp427, one or more of which may be absent depending on the genetic mutation) at the neuronal membrane induces susceptibility to membrane micro-injury, as suggested by elevated levels of the membrane repair protein annexin A5. Such injuries have been shown to facilitate the entry of Ca^{2+} , which in the absence of efficient calcium pumping proteins such as PMCA 2 may build up to cytotoxic levels. Excessive

cytosolic calcium may be partially responsible for the neurotoxicity of these neuronal cells in dystrophin-deficient brain, which ultimately may contribute to impaired cognitive ability in some DMD patients.

The issue of a link between cognitive impairment and DMD is a highly debated and contentious one. While some argue that mental deficits represent an artefact, others suggest that brain function may be impaired by the extent of physical disability in Duchenne patients. On the other hand, mental impairment may represent a true clinical feature of X-linked dystrophinopathy. Meta-analysis of recorded intelligence quotients (IQ) in 721 DMD patients by Emery and Muntoni indicated that the overall mean IQ was approximately one standard deviation below the population mean. Of those patients, 19% demonstrated an IQ below 70 (the generally accepted cut-off value for a diagnosis of mental retardation) while 3% presented with an IQ less than 50, indicating moderate to severe mental retardation. A number of studies have focused their attention on investigating the contribution of physical disability to mental acuity. Some have questioned the suitability of complete Wechsler tests to measure IQ in patients with DMD, given that this type of assessment includes a physical aspect, in which the IQ measured may not be a true reflection of the subject's intelligence but may instead reflect the motor handicap. However, a study by Ogasawara identified significantly lower total IQ in 44 DMD adolescents (IQ 83.4) compared to 10 patients with spinal muscular atrophy (SMA) (IQ 95.1). Since patients with SMA have a similar degree of motor impairment to DMD patients, the lower IQ in DMD patients may not be attributed to physical disability (Ogasawara, 1989). Other studies have shown that older children and adolescents with SMA perform significantly better on the verbal IQ scale than non-affected peers (von Gontard et al., 2002), with the suggestion that these disabled children may compensate for their physical handicap through attaining cognitive skills and knowledge. Taken together these reports suggest that the mental impairment seen in approximately one-third of DMD patients is a clinical manifestation of the disease, due to mutations in the gene encoding dystrophin. The proteomic data presented in this report also point to this hypothesis. PANTHER analysis of altered protein species identified that the largest class of affected proteins was that of cytoskeletal proteins, which correlates well with proteomic alterations seen in dystrophic skeletal muscle. The observed increase in cytoskeletal elements may serve as a compensatory mechanism to counteract dystrophin absence at the neuronal membrane. In particular, the increased abundance of annexin A5 is indicative of

membrane perturbations, suggesting that the loss of dystrophin at neuronal membranes results in membrane fragility and increased susceptibility to micro-rupturing (Bouter et al., 2011). The proteomic data also provides evidence of astrogliosis, which may be indicative of neurotoxicity (Brahmachari et al., 2006). Thus, the absence of the full-length Dp427 isoform of dystrophin appears to have significant neurological effects which may be responsible for impaired cognitive function in a subset of DMD patients. The non-progressive nature of mental retardation may perhaps reflect the success of compensatory mechanisms in halting further damage and stabilising brain functionality.

6.3.1 Conclusions

DMD is primarily a disorder of the skeletal muscle triggering severe muscle necrosis and the replacement of skeletal muscle with adipose and connective tissue. Muscle degeneration causes loss of ambulation, respiratory and cardiac failure, and premature death. However, mild non-progressive cognitive impairments also represent a clinical characteristic of X-linked dystrophinopathy in subset of patients. In this chapter label-free LC-MS/MS has been used to illustrate that dystrophin deficiency causes similar secondary abnormalities in the dystrophin-deficient brain to those commonly seen in dystrophic skeletal and cardiac muscle. Such abnormalities include altered calcium and iron homeostasis, compensatory up-regulation of components of the cytoskeletal lattice and membrane alterations. However, brain-specific defects were also observed; in particular elevated levels of GFAP were identified by mass spectrometry, immunoblotting and immunofluorescence microscopy. This intermediate filament protein has been previously suggested as a marker of neurotoxicity and has been shown here to also be increased in brain samples from the wobbler mouse model of ALS. Overall this proteomic survey of brain tissue from the *mdx-4cv* mouse indicates that dystrophin deficiency has consequences for the central nervous system, and this may contribute to non-progressive cognitive deficits.

Chapter Seven

Proteomic profiling of serum and saliva in the *mdx-4cv* model of dystrophinopathy

7.1 Introduction

DMD is a devastating, life-limiting neuromuscular disease. The disorder is due to primary abnormalities on the *Dmd* gene encoding the cytoskeletal protein dystrophin (Koenig et al., 1989), it predominantly affects males, and is characterised by severe and progressive skeletal muscle wasting. On a histopathological level, dystrophic muscles are identified by alterations in fibre size, infiltration of adipose and connective tissue, sterile inflammation, and central nucleation which is indicative of cycles of muscle fibre degeneration/regeneration.

Currently disease progression and response to therapeutic intervention are largely monitored by physiological tests, mainly the six-minute walk test and the North Star Ambulatory Assessment (NSAA). The six-minute walk test records the distance covered by a participant walking for six minutes (Enright, 2003). The NSAA covers a range of physical movement including standing, standing on one leg, jumping, rising from a lying position to a sitting position and a standing position, climbing and descending from a box step and running for 10 meters (Mazzone et al., 2010). While useful, these methods have disadvantages in that they can only be used on patients who are still ambulatory and the results can be affected by the motivation of the participant to complete the tasks (Geiger et al., 2007). For this reason, molecular measurements reflective of the severity of the disease and responsiveness to therapy are required. At present, creatine kinase is used in the diagnosis of the disease (Okinaka et al., 1961, Cacchiarelli et al., 2011). However, it suffers a number of downfalls in that i) its levels can vary from day to day, ii) it is indicative of muscular damage but is not specific to DMD, iii) its levels can be easily influenced by exercise and iv) its levels decrease with age rendering it impractical for monitoring disease progression or therapeutic benefit (Hathout et al., 2016). Thus, a panel of biomarkers holds the most promise for the specific and sensitive diagnosis, prognosis and therapy monitoring of patients afflicted with DMD.

While tissue proteomics has greatly aided the search for protein biomarkers representative of dystrophinopathy (Holland et al., 2015b, Carberry et al., 2012, Murphy et al., 2015b, Lorts et al., 2012, Ge et al., 2003), tissue biopsy is highly invasive. Thus, circulating biomarkers may be advantageous for translation to the clinic. A plethora of different fluids exist in the human body, including blood, saliva, urine, cerebrospinal fluid and tears, and with advances in proteomic profiling alterations in the proteomes of these biofluids in health and disease have been

extensively characterised (Jung et al., 2017, Finehout et al., 2007, Doeckke et al., 2012, Dowling et al., 2008, Rouillon et al., 2014). These biofluids could potentially be mined for the presence of protein markers which may reflect the health status of an individual. Indeed a number of biofluids have already gained momentum in this regard, including bronchoalveolar fluid as a proximal biofluid for the discovery of lung cancer biomarkers (Himmier et al., 2017), cerebrospinal fluid as a source of markers of Alzheimer's disease (Andreasen and Blennow, 2005) and urine as a non-invasive starting point for the detection of prostate cancer indicators (Dijkstra et al., 2014). Mass spectrometry-based proteomic methodologies offer an unbiased approach for the identification of global alterations in protein abundance and can identify hundreds to thousands of differentially expressed proteins. Such protein biomarkers could be easily integrated into current biochemical assays, such as enzyme-linked immunosorbent assays, in a clinical setting (Coenen-Stass et al., 2015). One of the major challenges facing the mass spectrometric profiling of biofluids, particularly blood, serum and urine, is the huge dynamic range that exists between the proteins of highest and lowest abundance. In blood/serum the top twenty most abundant proteins (including albumin, immunoglobulins, transferrin, and fibrinogen) account for more than 90% of total protein (Hortin et al., 2008). The large dynamic range, estimated to span 10-12 orders of magnitude (Hortin and Sviridov, 2010), far exceeds the maximum dynamic range capacity of modern mass spectrometers. This can result in ion suppression whereby peptides from higher abundance proteins are repeatedly selected for fragmentation, resulting in limited identification of peptides arising from lower abundance proteins (Qian et al., 2006), which are more likely to represent clinically relevant protein biomarkers (Zolotarjova et al., 2008).

Multiple strategies exist for simplifying the serum proteome (Whiteaker et al., 2007), including enrichment of a specific sub-proteome (Zhang et al., 2003b, Gao et al., 2015), biophysical fractionation (Tirumalai et al., 2003) and immuno-depletion of the most highly abundant proteins (Smith et al., 2011). The immuno-depletion method typically removes one or more of the following proteins depending on the specific immuno-depletion resin used; albumin, immunoglobulins, haptoglobin, fibrinogen, transferrin and antitrypsin. Since albumin alone accounts for approximately 50% of the total protein content of serum (Tirumalai et al., 2003) it is frequently targeted for removal by immuno-depletion. Given its physiological role as a carrier and transport protein in the blood, albumin binds to a multitude of molecules including hormones,

lipids, proteins, peptides, cytokines and chemokines and thus its depletion from serum samples may result in the concomitant depletion of any molecules bound to it (Zhou et al., 2004, Gundry et al., 2007). Immuno-depletion of serum prior to mass spectrometric analysis is therefore a compromise, in which sample complexity is reduced enabling for an enriched pool of low-abundance proteins and the prevention of ion suppression by high abundance proteins, at the expense of losing some potentially important protein species which may be co-eluted with the intended targets of immuno-depletion. Thus, analysis of serum samples is highly complex and ideally multiple methodologies should be used in tandem to provide the optimum in-depth coverage of the serum proteome.

Saliva is composed of secretions from the salivary glands (the three paired major salivary glands; parotid, submandibular and sublingual glands, and the hundreds of minor salivary glands), food deposits, blood-derived compounds, desquamated epithelial cells and micro-organisms (Loo et al., 2010). Saliva also contains fluids originating from upper airways secretions, gastrointestinal reflux and the gingival crevice (Chiappin et al., 2007). Despite having a composition of almost 99% water, saliva also contains a wide range of proteins, many of which with either a salivary gland (α -amylase, cystatins, lysozymes, lactotransferrin and mucins) or serum (albumin) origin (Lima et al., 2010). Recent ultra-deep salivary proteome analysis has identified more than 5,500 proteins (Grassl et al., 2016) and this depth of information provided by salivary proteomics along with low-cost and non-invasive saliva collection methods suggests that salivary proteomics may become a useful addition to the range of diagnostic and prognostic tools currently available. As a result, saliva is currently under investigation as a source of biomarkers in a variety of disorders ranging from infectious disease such as hepatitis and HIV, to head and neck cancer to autoimmune disorders such as Sjogren's Syndrome (Lima et al., 2010). Although not currently used in clinical practice, salivary proteomics for the diagnosis and therapy monitoring of DMD represents an attractive option, particularly for paediatric patients.

With the explosion of mass-spectrometry- and proteomics-driven biomarker research, several potential biomarkers of DMD have been identified. Such potential biomarkers include miRNA in serum of both animal models and human patients (Cacchiarelli et al., 2011), titin fragments in clinical urine samples (Rouillon et al., 2014) and circulating protein biomarkers, particularly fibronectin (Cynthia Martin et al., 2014), myoglobin (Hathout et al., 2014, Hathout et al., 2015) and carbonic

anhydrase 3 (Ayoglu et al., 2014). In this study, label-free LC-MS/MS has been used to identify potential protein biomarkers in serum and saliva samples from 6-month old *mdx-4cv* mice. In the serum proteome 371 differentially abundant proteins (greater than two-fold change) were identified. Similar to previous studies, elevated abundance was identified for myoglobin, carbonic anhydrase 3, parvalbumin, lactate dehydrogenase, fatty acid binding protein and titin (Hathout et al., 2014). Interestingly, a dramatic increase in abundance was observed for haptoglobin. Elevations in serum haptoglobin was identified by gel electrophoretic analyses of serum obtained from DMD patients in the late 1980s (John and Purdom, 1989), but has remained largely unexplored as a potential biomarker. In addition, 14 proteins with altered abundance were characterised in the saliva proteome, with perturbations evident for proteins associated with inflammation, extracellular matrix remodelling and protease activity.

7.1.1 Experimental Design

Since there is an urgent need for improved protein biomarkers for the diagnosis, prognosis and therapy-monitoring of dystrophinopathy, a proteomic survey of two distinct biofluids (serum and saliva) from 6-month old wild-type and age-matched *mdx-4cv* mice was conducted. Given the large dynamic range and complexity of the serum proteome, serum samples were immuno-depleted prior to mass spectrometric analysis. Serum samples were prepared for mass spectrometry as described in the methods section 2.2.12, whereas filter-aided sample preparation (FASP) was used to prepare saliva samples for mass spectrometry. Both serum and saliva samples were analysed by label-free LC-MS/MS, using an Ultimate 3000 NanoLC system (Dionex Corporation, Sunnyvale, CA, USA) coupled to a Q-Exactive mass spectrometer (Thermo Fisher Scientific). Peptides from serum samples were eluted over 180 min using the following binary gradient solvent A [2% (v/v) ACN and 0.1% (v/v) formic acid in LC-MS grade water] and 0-90% solvent B [80% (v/v) ACN and 0.1% (v/v) formic acid in LC-MS grade water]: 5-45% solvent B for 120 min, 45-90% solvent B for 2.5 min, 90% solvent B for 9 min and 2% solvent B for 43 min. Peptides from saliva samples were eluted over 65 min using the following binary gradient [solvent A: (2% (v/v) ACN and 0.1% (v/v) formic acid in LC-MS grade water and solvent B: 80% (v/v) ACN and 0.1% (v/v) formic acid in LC-MS grade water]: 3-10% solvent B for 5 min, 10-40% solvent B for 30 min, 40-90% solvent B for 5 min, 90% solvent B for 5 min and 3% solvent B for 10 min. For the quantitative analysis of the serum

proteome Progenesis QI for Proteomics software using Sequest HT and MASCOT search engines and the UniProtKB-SwissProt database was employed. The analysis of alterations in the saliva proteome was performed using MaxQuant with the Andromeda search engine and the UniProtKB-SwissProt database, and Perseus software. Bioinformatics analysis was conducted using Cytoscape and the PANTHER database of protein families. Comparative immunoblot analysis and enzyme-linked immunosorbent assays were used to confirm some of the major protein hits from the serum data.

7.2 Results

Serum represents a major source of potential biomarkers given it contains both circulatory proteins and tissue-derived proteins that may leak into circulation following tissue damage. In DMD a number of circulating biomarkers; creatine kinase, lactate dehydrogenase, parvalbumin and myoglobin have been described, but such markers are generally indicative of muscular damage in general and not DMD specifically. Thus, a larger panel of biomarkers is required for the effective diagnosis, prognosis and therapeutic monitoring of dystrophinopathies. One of the major issues hindering the proteomic profiling of serum samples is the enormous dynamic range of proteins, with highly abundant proteins masking the lower abundance proteins. To overcome this issue an immuno-depletion protocol was used to reduce sample complexity prior to label-free LC-MS/MS. This comparative proteomic profiling approach compared serum samples from 6-month old wild-type and *mdx-4cv* mice. In addition to profiling of the serum proteome, mass spectrometry-based proteomics was used to identify potential protein markers of dystrophinopathy in saliva samples from *mdx-4cv* mice.

7.2.1 *Gel electrophoretic and immunoblot analysis of immuno-depleted serum samples*

To confirm the removal of the highly abundant proteins immunoglobulin and albumin from immuno-depleted serum samples, gel electrophoresis and immunoblotting was employed. Gel electrophoresis indicated the large reduction in a protein band at approximately 60-70 kDa, suggesting the removal of albumin. Immunoblotting using antibodies against albumin and immunoglobulin confirmed the removal of the vast majority of albumin and the heavy and light chains of immunoglobulin by immuno-depletion. Immuno-depleted samples were then used for mass spectrometric analyses.

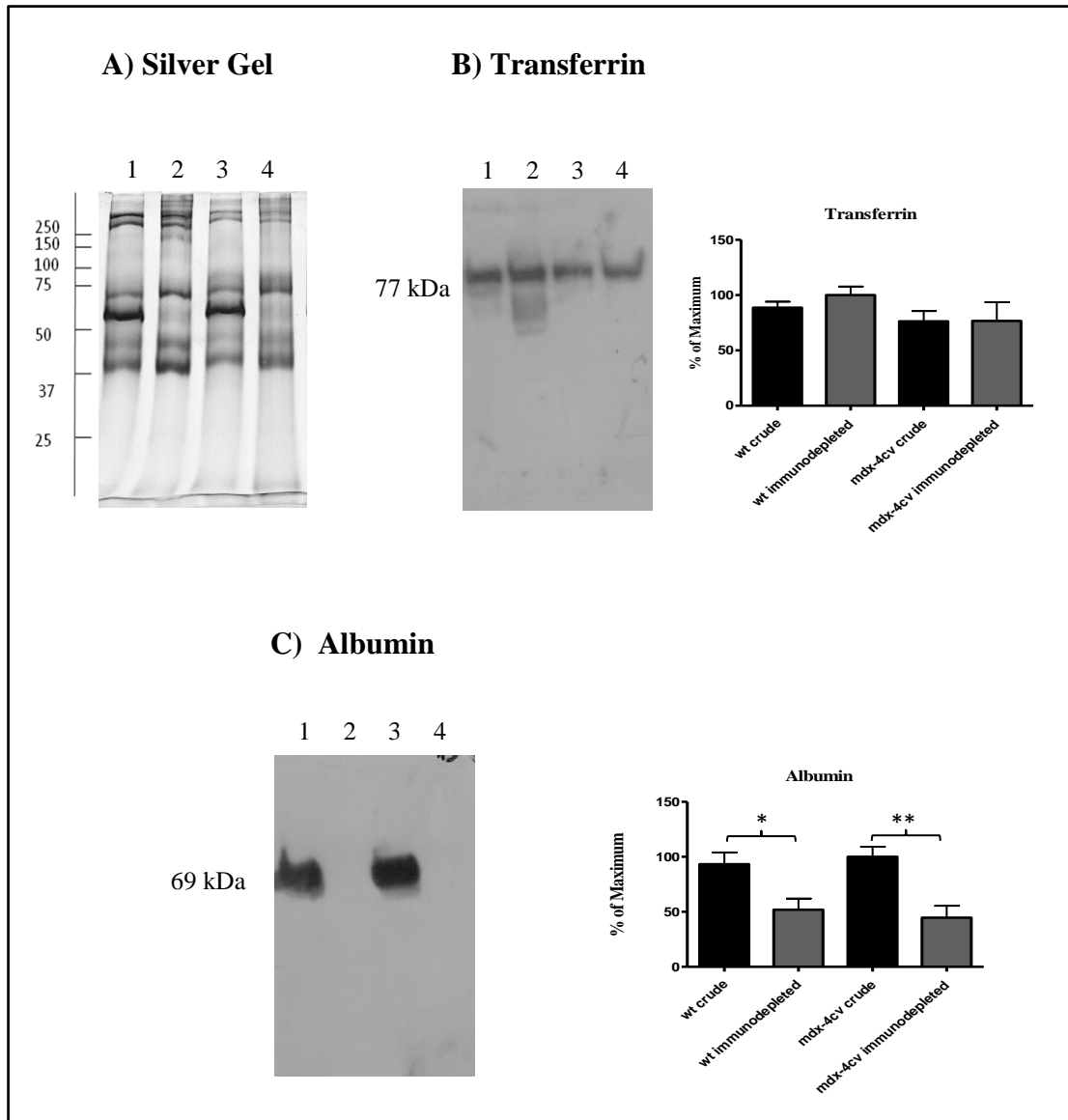


Figure 7.1: Gel electrophoretic and immunoblot analysis of albumin depletion in wild-type and *mdx-4cv* serum

Shown is a representative silver-stained gel (A) and immunoblot and statistical analysis of bands labelled with transferrin (B). The silver stained gel shows reduced levels of albumin in immuno-depleted serum. Molecular weight marker is given on the left-hand-side of the image in kDa. Transferrin immunoblotting did not show significant changes in concentration between wild-type and *mdx-4cv* crude and immuno-depleted samples and so it serves as a loading control for comparative immunoblotting. Also shown is an immunoblot to albumin (C), which shows greatly reduced levels in immuno-depleted serum. Lanes 1, 2, 3 and 4 refer to wild-type crude serum, wild-type immuno-depleted serum, *mdx-4cv* crude serum and *mdx-4cv* immuno-depleted serum respectively. Graphical representation of the immunodecoration levels for transferrin and albumin is shown (mean values \pm SEM, Student's *t*-test; unpaired; $n=4$; * $p \leq 0.05$, ** $p \leq 0.01$).

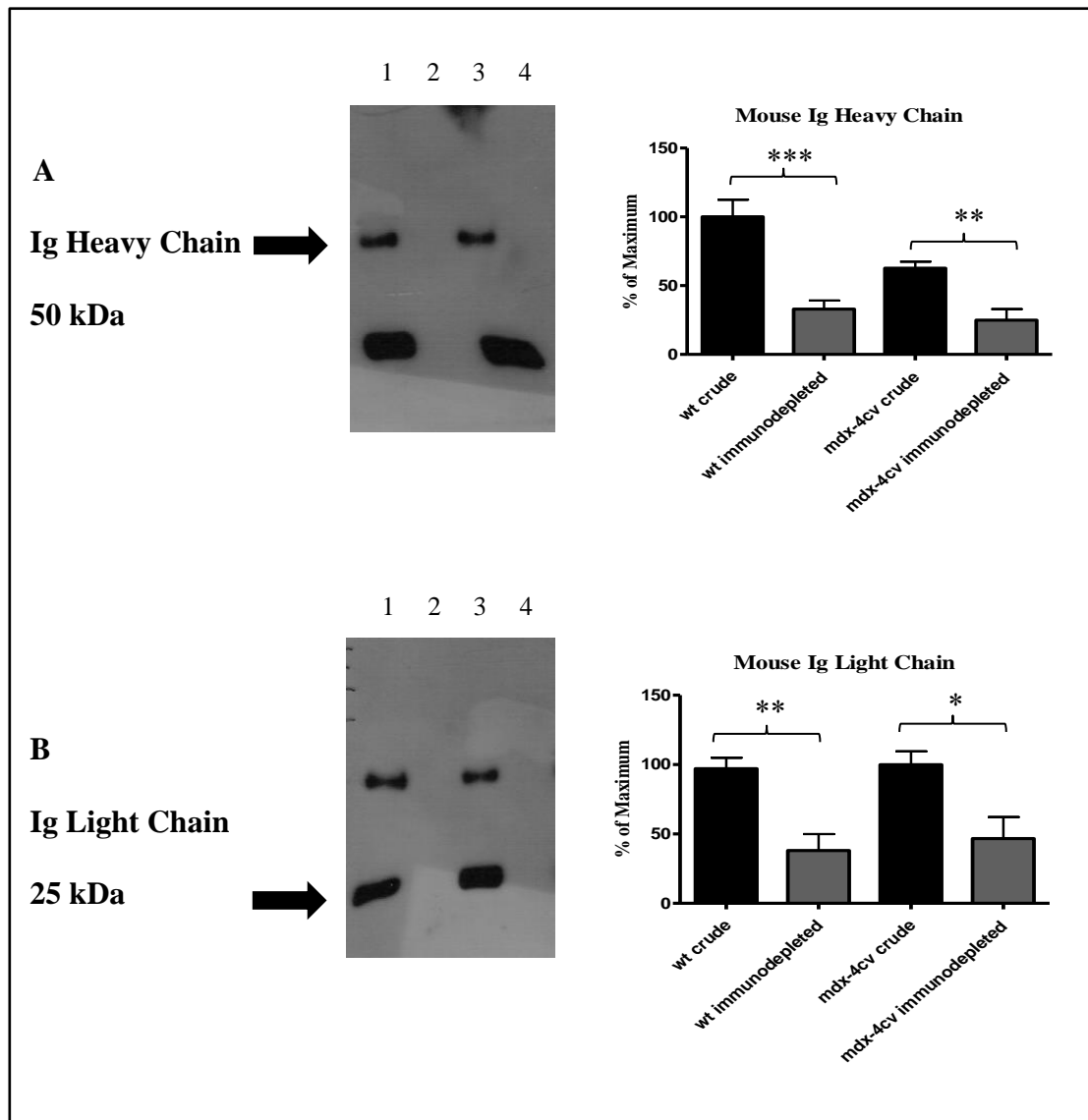


Figure 7.2: Immunoblot analysis of immunoglobulin depletion in wild-type and *mdx-4cv* serum

Shown are representative immunoblots and statistical analysis of mouse immunoglobulins (A, B). Both immunoblots illustrate the reduced abundance of immunoglobulin heavy chain (50 kDa bands) and immunoglobulin light chain (25 kDa bands) in immuno-depleted serum samples. Lanes 1, 2, 3 and 4 refer to wild-type crude serum, wild-type immuno-depleted serum, *mdx-4cv* crude serum and *mdx-4cv* immuno-depleted serum respectively. Graphical representation of the immunodecoration levels for immunoglobulin heavy and light chains is shown (mean values \pm SEM, Student's *t*-test; unpaired; $n=4$; * $p \leq 0.05$, ** $p \leq 0.01$, *** $p \leq 0.001$).

7.2.2 Qualitative analysis of the serum proteome

Qualitative analysis of immuno-depleted serum samples identified a total of 1,030 proteins in wild-type serum and 1,278 proteins in *mdx-4cv* serum. 12.5% of wild-type proteins and 16.1% of *mdx-4cv* proteins had a percentage sequence coverage greater than 50%. The proteins with highest percentage coverages in wild-type and *mdx-4cv* serum include haemoglobin subunit alpha (100% coverage), carbonic anhydrase 3 (89.62% in wild-type and 92.69% in *mdx-4cv*), carbonic anhydrase 1 (88.12% in wild-type and 87.74% in *mdx-4cv*), complement C3 (86.71% in wild-type and 85.87% in *mdx-4cv*) and fructose-bisphosphate aldolase A (81.59% in wild-type and 83.79% in *mdx-4cv*).

7.2.3 Quantitative label-free LC-MS/MS analysis of wild-type versus *mdx-4cv* serum

The removal of the vast majority of the highly abundant serum proteins albumin and immunoglobulins sufficiently reduced sample complexity to allow a relatively in-depth comparative proteomic analysis of serum obtained from wild-type and dystrophic mice. Overall, mass spectrometry identified a total of 371 differentially expressed proteins based on a p-value ≤ 0.05 , at least two unique peptides and a minimum fold change of 2. Of these proteins 334 were increased in abundance in *mdx-4cv* serum while the remaining 37 proteins displayed reduced abundance. 26.6% of all proteins (increased and decreased) displayed a fold change ≥ 10 . Greater fold changes were seen for the proteins with elevated abundance; maximum fold change of 384.81 and 54% of increased abundance proteins displaying a fold change ≥ 5 . All proteins with decreased abundance had a fold change < 4 , with the highest fold change seen for angiotensin-converting enzyme (-3.48-fold decrease). The mass spectrometric data indicates a severely disturbed serum proteome, with inflammation (increased abundance of inflammatory markers haptoglobin and serum amyloid A), alterations in enzymatic activity and calcium homeostasis, and muscle degeneration (presence of muscle-specific proteins, such as titin fragments, in serum) evident.

Table 7.1: List of identified proteins with ≥ 12.7 -fold increased abundance in 6-month old *mdx-4cv* serum versus age-matched wild-type serum as determined by label-free LC-MS/MS

Accession	Gene Name	Protein Name	Unique peptides	Confidence score	Anova (p)	Max fold change
P70441	Slc9a3r1	Na(+)/H(+) exchange regulatory cofactor NHERF1	2	128.77	3.47E-05	384.81
Q9D5J6	Shpk	Sedoheptulokinase	3	181.59	4.21E-03	213.06
Q19L12	A1bg	Alpha-1B-glycoprotein	3	201.11	2.07E-03	199.86
Q99020	Hnrnpab	Heterogeneous nuclear ribonucleoprotein A/B	2	120.87	2.40E-04	131.39
P09405	Ncl	Nucleolin	2	66.85	2.14E-04	104.30
Q62446	Fkbp3	Peptidyl-prolyl cis-trans isomerase FKBP3	2	69.16	3.01E-04	89.12
Q8BG05	Hnrnpa3	Heterogeneous nuclear ribonucleoprotein A3	2	132.17	2.62E-05	72.76
Q08331	Calb2	Calretinin	5	174.30	5.09E-04	59.85
P07361	Orm2	Alpha-1-acid glycoprotein 2	2	101.47	9.48E-09	56.75
P00493	Hprt1	Hypoxanthine-guanine phosphoribosyltransferase	2	73.54	1.28E-03	53.30
Q61646	Hp	Haptoglobin	14	826.52	4.25E-07	50.28
Q9D0R2	Tars	Threonine--tRNA ligase, cytoplasmic	5	187.79	5.00E-03	48.44
P48428	Tbca	Tubulin-specific chaperone A	2	59.15	1.78E-03	46.75
Q99KP3	Cry11	Lambda-crystallin homolog	3	173.73	3.22E-02	43.29
A2ABU4	Myom3	Myomesin-3	9	588.37	6.71E-12	38.64
Q99KC8	Vwa5a	von Willebrand factor A domain-containing protein 5A	2	41.66	4.64E-05	37.21
P05366	Saa1	Serum amyloid A-1 protein	2	135.98	2.54E-08	36.98
Q8VC12	Uroc1	Urocanate hydratase	10	751.33	9.91E-04	36.87
P47199	Cryz	Quinone oxidoreductase	4	206.42	1.61E-04	36.77
Q91X52	Dcxr	L-xylulose reductase	2	99.38	1.76E-05	32.75
Q8VCX1	Akr1d1	3-oxo-5-beta-steroid 4-dehydrogenase	5	177.09	1.74E-04	31.24
Q9WTP6	Ak2	Adenylate kinase 2, mitochondrial	2	67.03	4.27E-03	31.23
A3KMP2	Ttc38	Tetratricopeptide repeat protein 38	4	177.89	5.40E-04	30.60
Q5SX40	Myh1	Myosin-1	62	4670.12	3.89E-13	30.35

A2ASS6	Ttn	Titin	88	4357.28	6.29E-13	30.22
P99027	Rplp2	60S acidic ribosomal protein P2	2	162.50	3.75E-03	30.11
Q8VCT4	Ces1d	Carboxylesterase 1D	5	114.10	9.04E-05	26.83
P53026	Rpl10a	60S ribosomal protein L10a	2	97.35	3.71E-03	26.48
P68040	Gnb211	Guanine nucleotide-binding protein subunit beta-2-like 1	2	48.55	8.01E-05	25.64
Q9QXE0	Hac11	2-hydroxyacyl-CoA lyase 1	4	252.90	6.70E-03	24.50
Q9D8Y0	Efhd2	EF-hand domain-containing protein D2	3	162.57	2.00E-04	23.88
Q9CXN7	Pbld2	Phenazine biosynthesis-like domain-containing protein 2	5	346.95	1.25E-03	23.72
P61458	Pcbd1	Pterin-4-alpha-carbinolamine dehydratase	5	239.45	5.34E-03	23.22
Q60866	Pter	Phosphotriesterase-related protein	3	145.96	3.01E-02	21.53
Q9QUR6	Prep	Prolyl endopeptidase	5	266.66	6.31E-03	20.99
P35492	Hal	Histidine ammonia-lyase	13	939.85	2.36E-03	20.94
Q8CHR6	Dpyd	Dihydropyrimidine dehydrogenase [NADP(+)]	4	219.69	3.46E-03	20.71
Q8VCN5	Cth	Cystathionine gamma-lyase	9	552.72	3.10E-03	19.52
Q9DCT1	Akr1e2	1,5-anhydro-D-fructose reductase	2	84.60	1.09E-02	19.07
P12246	Apcs	Serum amyloid P-component	7	427.15	3.61E-11	18.85
Q05816	Fabp5	Fatty acid-binding protein, epidermal	8	385.47	1.66E-05	18.32
P13412	Tnni2	Troponin I, fast skeletal muscle	3	131.21	9.00E-08	18.23
Q99L47	St13	Hsc70-interacting protein	2	81.37	5.54E-03	18.01
Q00915	Rbp1	Retinol-binding protein 1	3	212.04	5.19E-05	17.83
P12658	Calb1	Calbindin	4	280.34	1.54E-03	17.82
Q8VC28	Akr1c13	Aldo-keto reductase family 1 member C13	6	353.98	6.05E-04	17.47
Q9DCG6	Pbld1	Phenazine biosynthesis-like domain-containing protein 1	9	531.49	1.04E-03	17.19
P97328	Khk	Ketohexokinase	4	336.94	9.67E-04	16.98
Q9DBF1	Aldh7a1	Alpha-amino adipic semialdehyde dehydrogenase	8	432.11	1.52E-04	16.74
P50431	Shmt1	Serine hydroxymethyltransferase cytosolic	16	811.20	5.67E-03	16.48

Q9EQF5	Dpys	Dihydropyrimidinase	10	449.94	1.01E-02	16.48
Q9CWS0	Ddah1	N(G),N(G)-dimethylarginine dimethylaminohydrolase 1	4	138.62	2.81E-04	16.39
Q8VVK1	Nit1	Nitrilase homolog 1	2	125.41	1.20E-04	16.35
Q91V76	N/A	Ester hydrolase C11orf54 homolog	8	449.50	1.05E-03	15.78
O08997	Atox1	Copper transport protein ATOX1	2	71.42	1.84E-05	15.57
Q8CAY6	Acat2	Acetyl-CoA acetyltransferase, cytosolic	8	542.64	3.46E-03	15.57
P08074	Cbr2	Carbonyl reductase [NADPH] 2	2	86.35	9.01E-03	15.47
Q8BTY1	Ccb1l	Kynurenine--oxoglutarate transaminase 1	6	252.66	1.59E-04	15.29
P62897	Cyca	Cytochrome c, somatic	5	543.08	9.05E-12	15.24
Q5SX39	Myh4	Myosin-4	23	1562.66	2.27E-11	14.90
P05063	Aldoc	Fructose-bisphosphate aldolase C	9	679.32	3.04E-04	14.82
Q8R1G2	Cmb1	Carboxymethylenebutenolidase homolog	6	242.97	1.07E-04	14.68
Q91X91	Qprt	Nicotinate-nucleotide pyrophosphorylase [carboxylating]	7	359.79	4.04E-04	14.61
Q64374	Rgn	Regucalcin	16	1310.14	9.81E-04	14.34
P29391	Ftl1	Ferritin light chain 1	9	768.17	4.80E-05	14.09
P30115	Gsta3	Glutathione S-transferase A3	8	498.65	6.05E-04	13.72
Q9JHW2	Nit2	Omega-amidase NIT2	12	604.83	8.05E-04	13.56
P47857	Pfkm	ATP-dependent 6-phosphofructokinase, muscle type	22	1691.19	2.42E-13	13.49
P97457	Mylpf	Myosin regulatory light chain 2, skeletal muscle isoform	8	505.80	2.55E-10	13.28
Q8VHX6	Flnc	Filamin-C	7	418.63	7.68E-09	13.27
P58044	Idi1	Isopentenyl-diphosphate Delta-isomerase 1	2	91.15	6.85E-08	13.25
O09173	Hgd	Homogentisate 1,2-dioxygenase	20	1081.44	1.69E-03	13.11
P62204	Calml	Calmodulin	2	103.84	8.39E-06	12.91
P28271	Aco1	Cytoplasmic aconitate hydratase	7	318.28	1.73E-04	12.87
P35505	Fah	Fumarylacetoacetase	18	1386.08	7.13E-04	12.73

Table 7.2: List of identified proteins with a significantly decreased abundance in 6-month old *mdx-4cv* serum versus age-matched wild-type serum as determined by label-free LC-MS/MS

Accession	Gene Name	Protein Name	Unique peptides	Confidence score	Anova (p)	Max fold change
P09470	Ace	Angiotensin-converting enzyme	2	97.76	1.75E-03	3.48
O35930	Gp1ba	Platelet glycoprotein Ib alpha chain	11	865.35	9.65E-07	3.40
Q07456	Ambp	Protein AMBP	4	362.51	1.26E-02	3.06
P28665	Mug1	Murinoglobulin-1	116	12973.81	2.62E-06	2.91
B5X0G2	Mup17	Major urinary protein 17	5	231.60	1.04E-03	2.77
Q00898	Serpina1e	Alpha-1-antitrypsin 1-5	14	1024.28	3.78E-03	2.69
P05208	Cela2a	Chymotrypsin-like elastase family member 2A	3	230.49	1.16E-07	2.69
O08742	Gp5	Platelet glycoprotein V	5	601.56	7.52E-04	2.62
Q03311	Bche	Cholinesterase	7	362.36	4.76E-06	2.61
P01942	Hba	Hemoglobin subunit alpha	7	448.81	1.14E-02	2.61
P42703	Lifr	Leukemia inhibitory factor receptor	28	2444.33	1.78E-07	2.49
Q62351	Tfrc	Transferrin receptor protein 1	5	278.54	9.37E-06	2.48
Q9DBB9	Cpn2	Carboxypeptidase N subunit 2	15	1509.87	1.77E-07	2.43
Q8QZR3	Ces2a	Pyrethroid hydrolase Ces2a	2	114.66	6.44E-03	2.42
Q8BPB5	Efemp1	EGF-containing fibulin-like extracellular matrix protein 1	4	182.66	7.38E-04	2.41
O88968	Tcn2	Transcobalamin-2	9	577.32	5.17E-05	2.40
Q61704	Itih3	Inter-alpha-trypsin inhibitor heavy chain H3	7	627.52	5.34E-03	2.40
Q03734	Serpina3m	Serine protease inhibitor A3M	9	788.27	3.49E-03	2.39
E9Q414	Apob	Apolipoprotein B-100	35	1947.84	1.90E-03	2.38
Q07235	Serpine2	Glia-derived nexin	5	234.21	1.91E-03	2.37
P07758	Serpina1a	Alpha-1-antitrypsin 1-1	11	1371.40	5.81E-03	2.37
Q61247	Serpinf2	Alpha-2-antiplasmin	3	294.61	4.79E-04	2.36

P06683	C9	Complement component C9	21	1327.94	3.07E-03	2.28
P32261	Serpinc1	Antithrombin-III	5	669.57	5.00E-03	2.24
O70165	Fcn1	Ficolin-1	8	539.88	6.24E-06	2.22
P35917	Flt4	Vascular endothelial growth factor receptor 3	4	201.55	2.09E-08	2.18
Q61703	Itih2	Inter-alpha-trypsin inhibitor heavy chain H2	18	1687.48	4.61E-04	2.18
P28666	Mug2	Murinoglobulin-2	3	214.49	5.86E-05	2.17
P22599	Serpina1b	Alpha-1-antitrypsin 1-2	11	1257.05	9.64E-04	2.15
O09159	Man2b1	Lysosomal alpha-mannosidase	3	205.08	2.05E-05	2.14
Q8BH35	C8b	Complement component C8 beta chain	24	2136.71	2.76E-03	2.12
Q08879	Fbln1	Fibulin-1	3	124.02	1.84E-03	2.11
Q8CIZ8	Vwf	von Willebrand factor	2	104.40	3.34E-05	2.08
Q8K182	C8a	Complement component C8 alpha chain	27	2579.27	5.51E-04	2.08
Q01279	Egfr	Epidermal growth factor receptor	21	1995.68	1.38E-05	2.07
Q61702	Itih1	Inter-alpha-trypsin inhibitor heavy chain H1	18	1267.61	7.88E-04	2.02
Q9JJN5	Cpn1	Carboxypeptidase N catalytic chain	13	1198.91	1.97E-06	2.00

7.2.4 Distribution of protein alterations in dystrophic serum

Standard bioinformatics analysis was used to visualise the proteomic changes in serum from dystrophic *mdx-4cv* mice. As depicted in the PANTHER analysis in Figure 7.3 and Figure 7.4, the proteomic analysis revealed the highest number of increased abundance proteins belong to the hydrolase protein class (21.2%), while the largest number of decreased abundance proteins belong to the enzyme modulator protein class (48.1%). This suggests that *mdx-4cv* serum reflects several changes in enzymatic activity in the *mdx-4cv* model of dystrophinopathy. It is postulated the degeneration of necrotic muscle fibres results in the release of muscle-derived proteins into the circulatory system. To investigate this phenomenon, the ClueGO plug-in of the Cytoscape bioinformatics package was used to identify enriched cellular components associated with proteins that display an increased abundance in *mdx-4cv* serum. As seen in Figure 7.5, several enriched cellular component categories were those associated with skeletal muscle, including myofibril, I, M and A bands, myosin complex, actin cytoskeleton and actomyosin, indicating the leakage of muscle proteins into the serum.

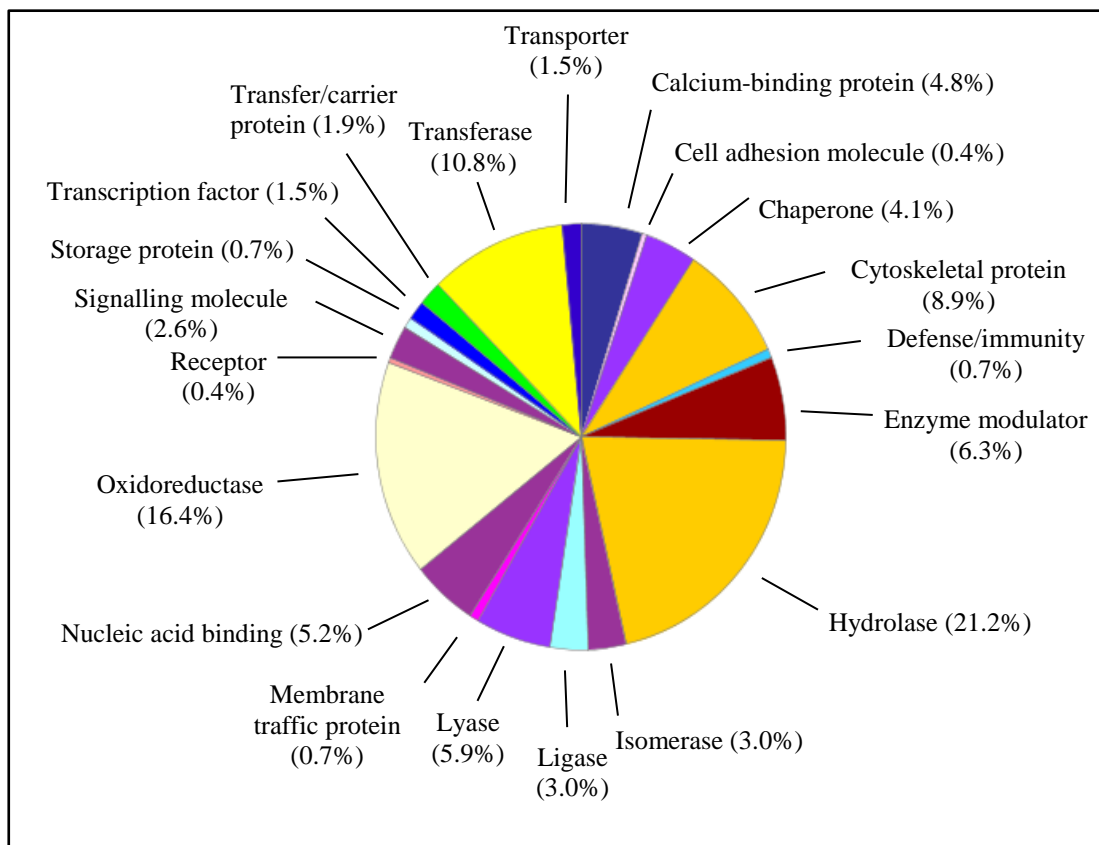


Figure 7.3: PANTHER analysis of proteins with increased abundance in *mdx-4cv* serum

The 334 proteins with elevated abundance were grouped into their respective protein class using the freely available PANTHER software package. This analysis identified the class of hydrolase as containing the most altered protein species in *mdx-4cv* serum.

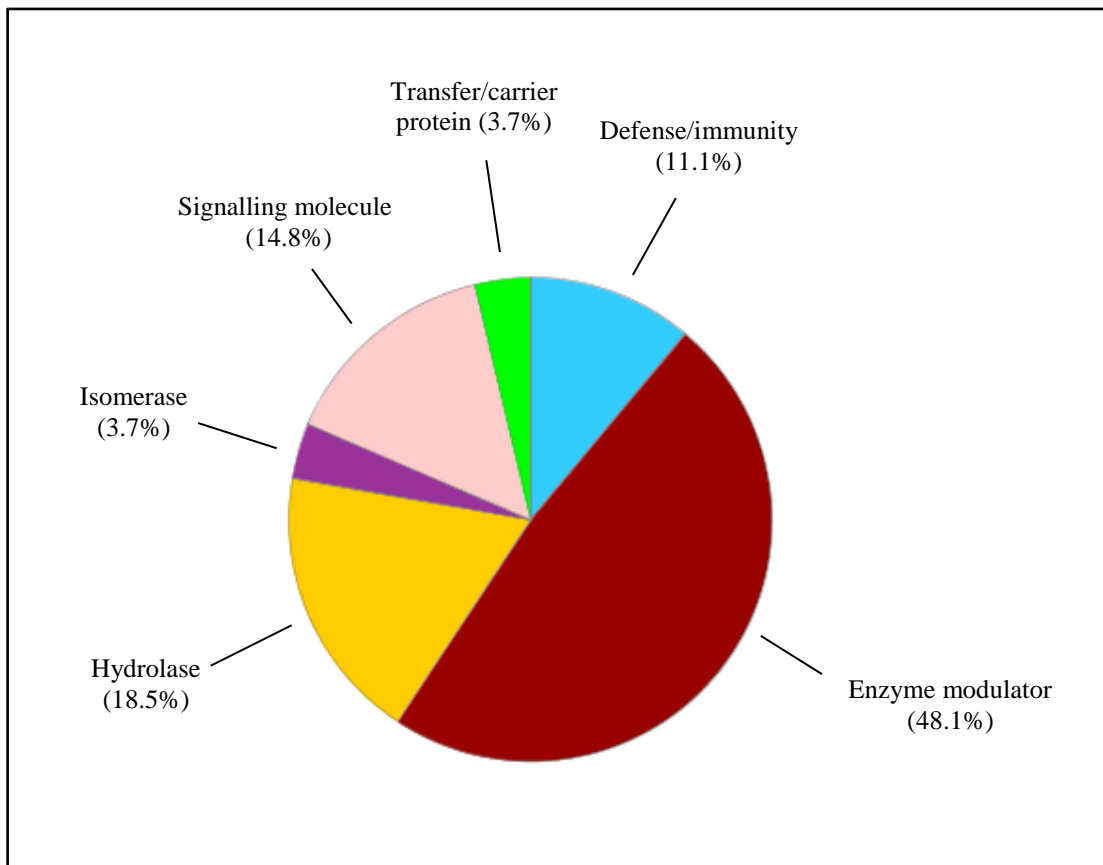


Figure 7.4: PANTHER analysis of proteins with decreased abundance in *mdx-4cv* serum

The 37 proteins with reduced abundance were grouped into their respective protein class using the freely available PANTHER software package. This analysis identified the class of enzyme modulator as containing the most altered protein species in *mdx-4cv* serum.

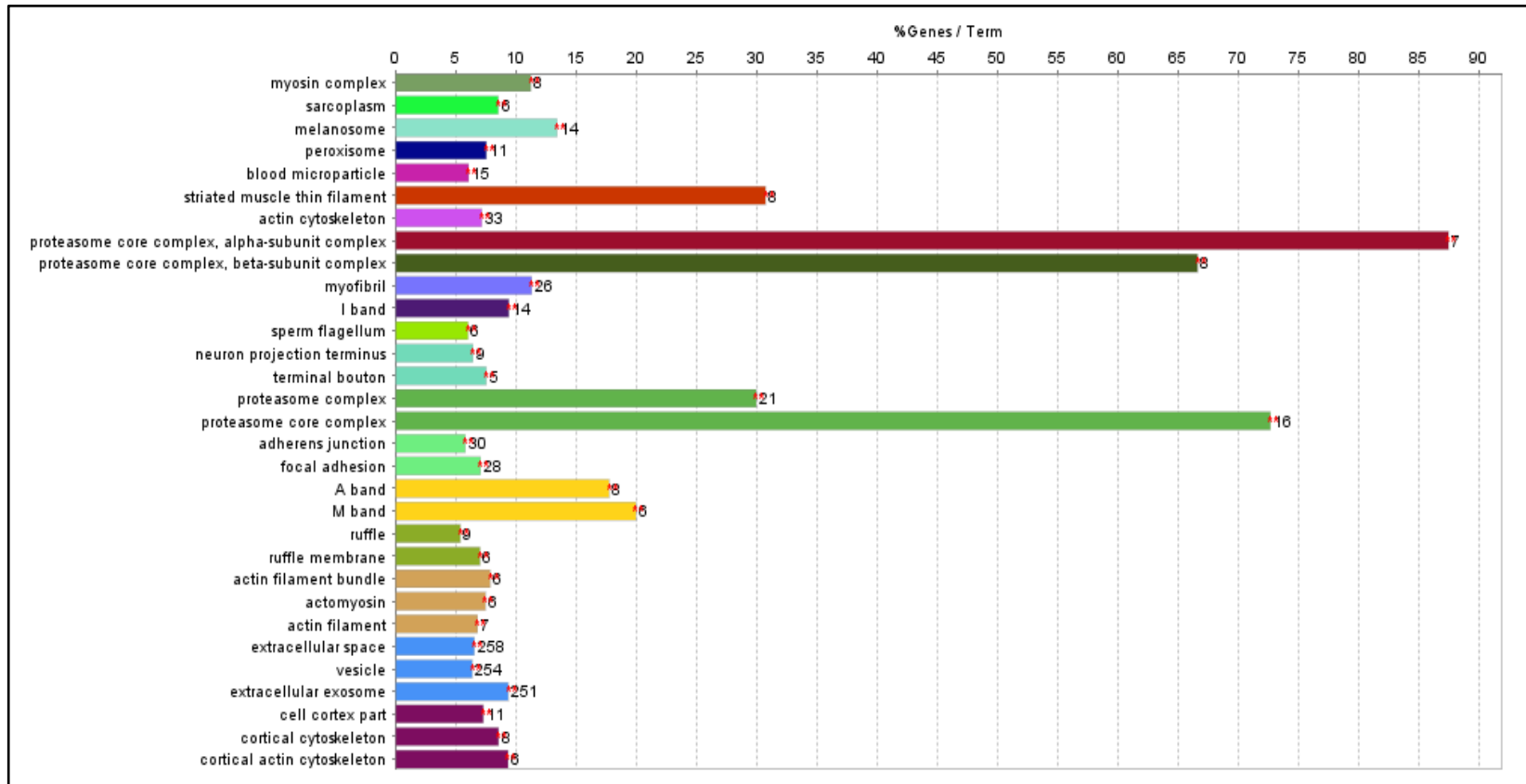


Figure 7.5: ClueGO analysis of proteins with increased abundance in *mdx-4cv* serum

The ClueGO plug-in app in Cytoscape was used to identify significantly enriched cellular component GO terms of the proteins with elevated abundance in *mdx-4cv* serum samples.

7.2.5 Independent verification of differentially abundant proteins by immunoblotting

Immunoblotting using a panel of select antibodies was used to verify some of the differentially abundant proteins identified by label-free LC-MS/MS. Equal loading was confirmed by a combination of silver-stained gels and immunoblots to transferrin, a loading control used for serum, as shown in Figure 7.6. Lactate dehydrogenase, parvalbumin and fatty-acid binding protein 1 (FABP-1) were identified as having increased levels in serum from *mdx-4cv* mice by LC-MS/MS, and this was confirmed by immunoblotting, for which only the increases in lactate dehydrogenase and FABP-1 were found to be statistically significant (Figure 7.7). In contrast to other studies (Hathout et al., 2014), myoglobin (accession P04247; 3 unique peptides; confidence score 258.55) was found to be slightly decreased in *mdx-4cv* serum (-1.88-fold decrease) although immunoblot analysis shows little difference in myoglobin abundance between wild-type and *mdx-4cv* serum (Figure 7.8).

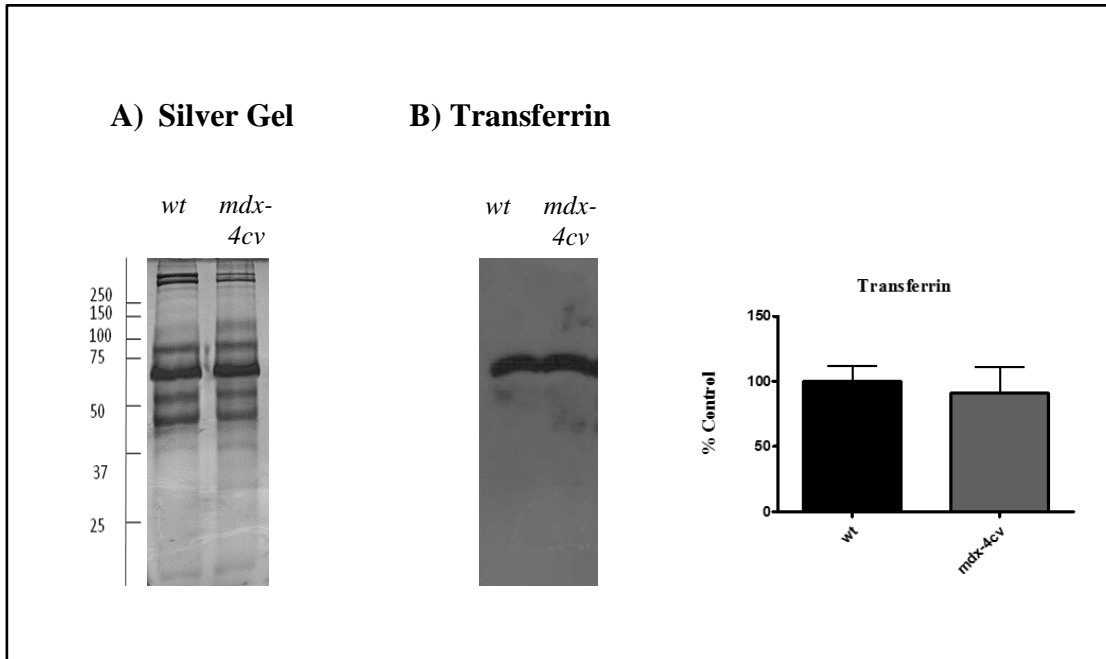


Figure 7.6: Electrophoretic and immunoblot analysis of wild-type and *mdx-4cv* serum

Shown is a silver stained 1D gel (A) and immunoblot and statistical analysis of bands labelled with transferrin (B). The silver stained gel shows comparable protein banding patterns for wild-type and *mdx-4cv* serum. Molecular weight marker is given on the left-hand-side of the image in kDa. Transferrin immunoblotting did not show significant changes in concentration between wild-type and *mdx-4cv* samples and so it serves as a loading control for comparative immunoblotting. Graphical representation of the immuno-decoration level for transferrin is shown (mean values \pm SEM, Student's *t*-test; unpaired; $n=4$).

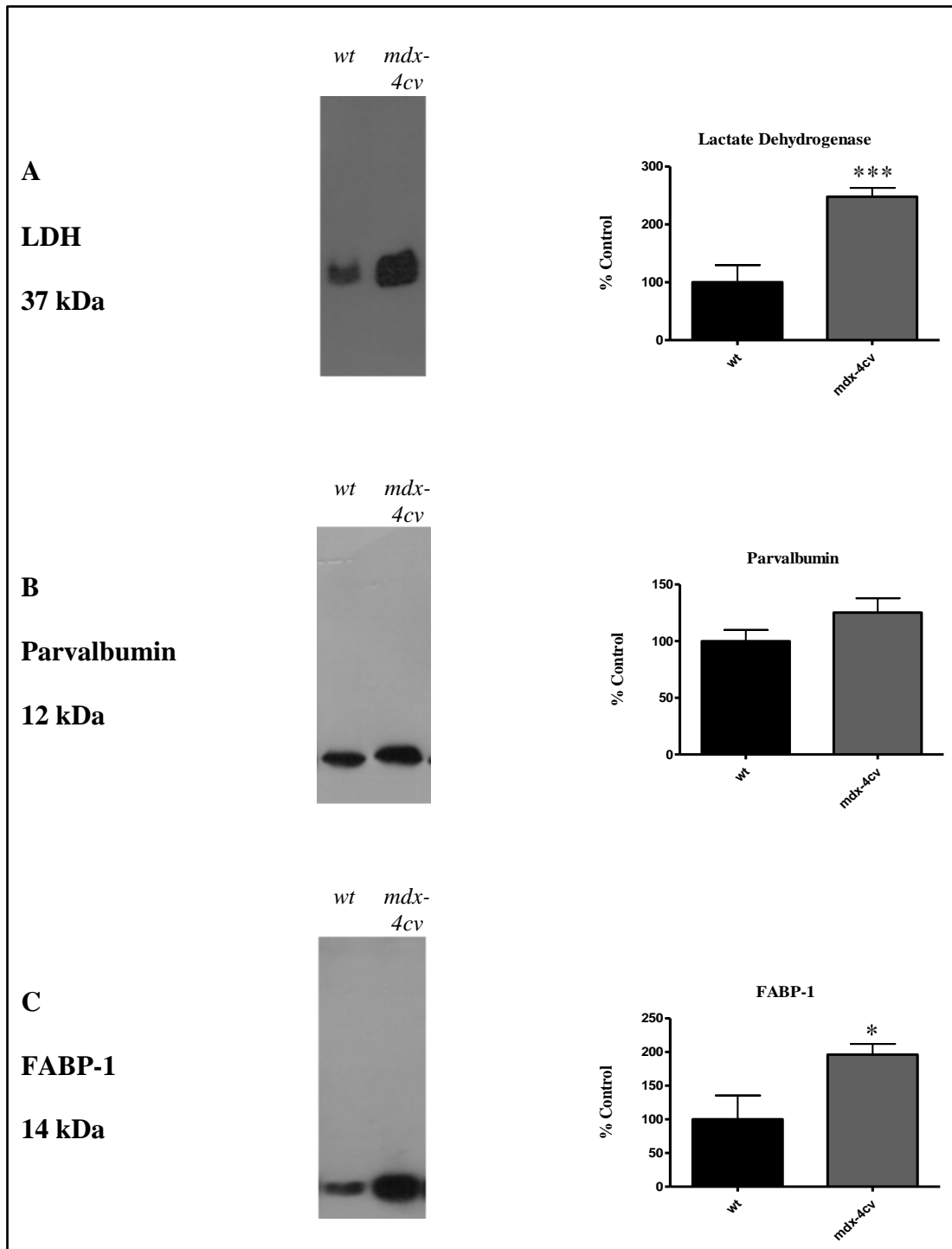


Figure 7.7: Comparative immunoblot analysis of proteins with increased abundance in dystrophic *mdx-4cv* serum

Shown are representative immunoblots with immuno-decorated bands labelled with antibodies to lactate dehydrogenase (A), parvalbumin (B) and FABP-1 (C). Statistical analysis of immuno-decoration was performed with Student's *t*-test (mean values \pm SEM; unpaired; $n=4$, $*p \leq 0.05$, $***p \leq 0.001$).

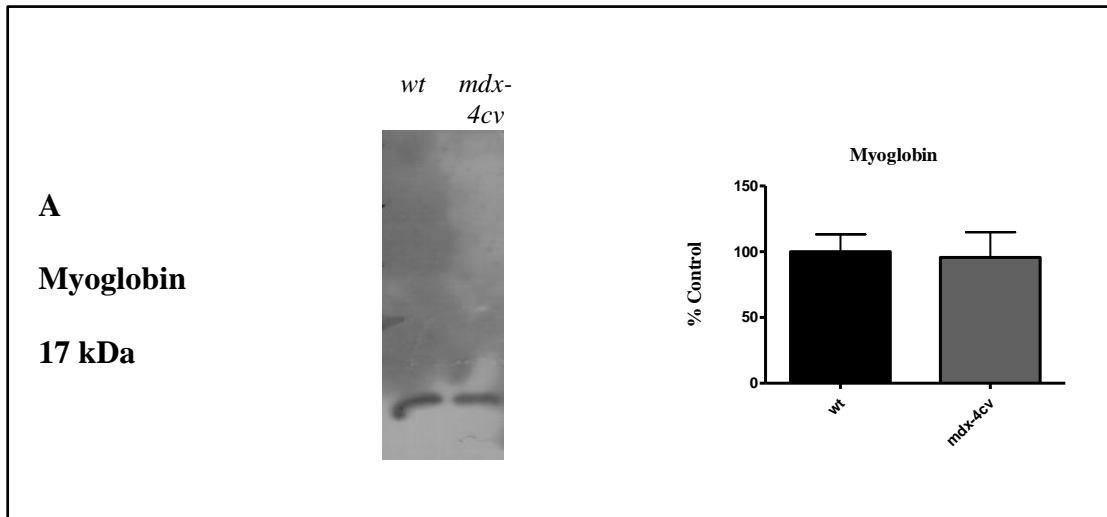


Figure 7.8: Comparative immunoblot analysis of proteins with decreased abundance in dystrophic *mdx-4cv* serum

Shown is a representative immunoblot with immuno-decorated bands labelled with an antibody to myoglobin (A). Statistical evaluation of immuno-decoration was performed with Student's *t*-test (mean values \pm SEM; unpaired; $n=4$).

7.2.6 Immunoblot analysis of the increased abundance of haptoglobin in *mdx-4cv* serum

Despite the observed increase in haptoglobin levels in plasma from patients with DMD by gel electrophoresis in 1989, there have been few other reports of this phenomenon. We have here identified a very large increase (50.28-fold) in the abundance of haptoglobin in serum isolated from the *mdx-4cv* animal model of dystrophinopathy by LC-MS/MS. The LC-MS/MS analysis identified 14 unique peptides belonging to the haptoglobin protein, providing excellent coverage of the whole protein (Figure 7.9). Increased abundance of haptoglobin was confirmed by immunoblot analysis using two distinct haptoglobin antibodies; ab131236 and ab157714 (Figure 7.10). To further investigate this protein as a potential serum biomarker of DMD, its abundance in serum from 12-month old wild-type and *mdx-4cv* mice was also analysed by comparative immunoblotting (Figure 7.12). Immunoblotting confirmed the trend of increased abundance of haptoglobin in *mdx-4cv* serum, although this was not found to be statistically significant. The abundance of FABP-1 in serum from 12-month old wild-type and *mdx-4cv* mice was also investigated by comparative immunoblotting and was found to be significantly increased in *mdx-4cv* serum as illustrated in Figure 7.13.

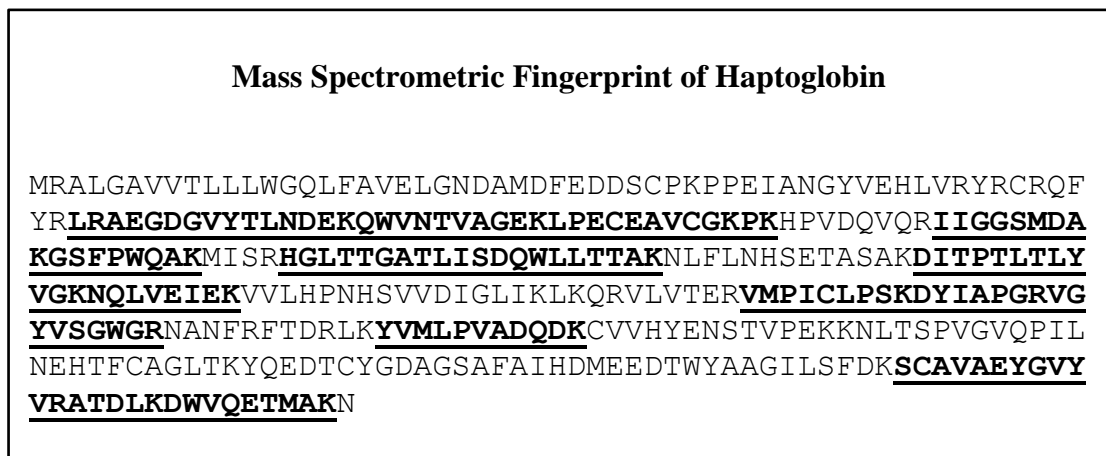


Figure 7.9: Mass spectrometric fingerprint of haptoglobin

The 14 peptides used in the identification of haptoglobin are highlighted in bold and underlined, showing good coverage of the entire haptoglobin protein by LC-MS/MS.

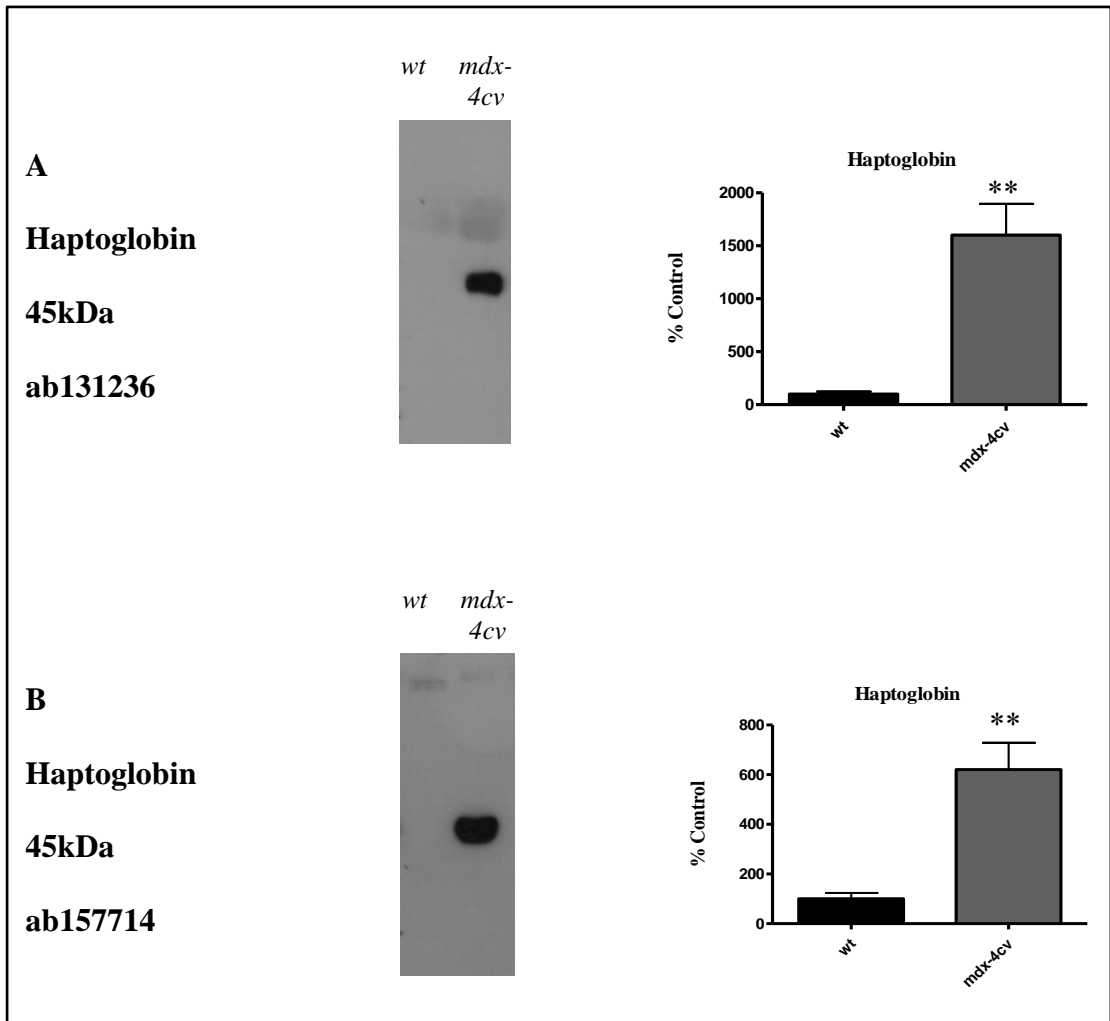


Figure 7.10: Comparative immunoblot analysis of haptoglobin in dystrophic 6-month *mdx-4cv* serum

Shown are representative immunoblots with immuno-decorated bands labelled with two separate antibodies to haptoglobin; ab131236 (A) and ab157714 (B). Statistical analysis of immuno-decoration was performed with Student's *t*-test (mean values \pm SEM; unpaired; $n \geq 5$; $wt=5$, $mdx-4cv=8$; ** $p \leq 0.01$).

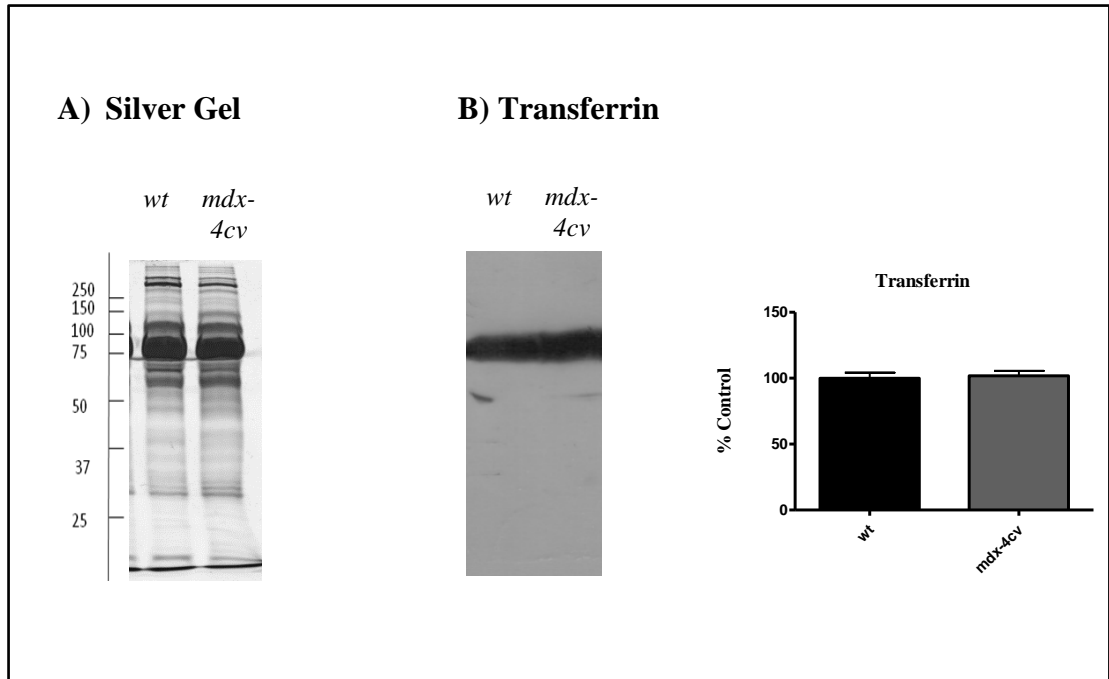


Figure 7.11: Electrophoretic and immunoblot analysis of wild-type and *mdx-4cv* 12-month old serum

Shown is a silver stained 1D gel (A) and immunoblot and statistical analysis of bands labelled with transferrin (B). The silver stained gel shows comparable protein banding patterns for wild-type and *mdx-4cv* serum. Molecular weight marker is given on the left-hand-side of the image in kDa. Transferrin immunoblotting did not show significant changes in concentration between wild-type and *mdx-4cv* samples and so it serves as a loading control for comparative immunoblotting. Graphical representation of the immuno-decoration level for transferrin is shown (mean values \pm SEM, Student's *t*-test; unpaired; $n=4$).

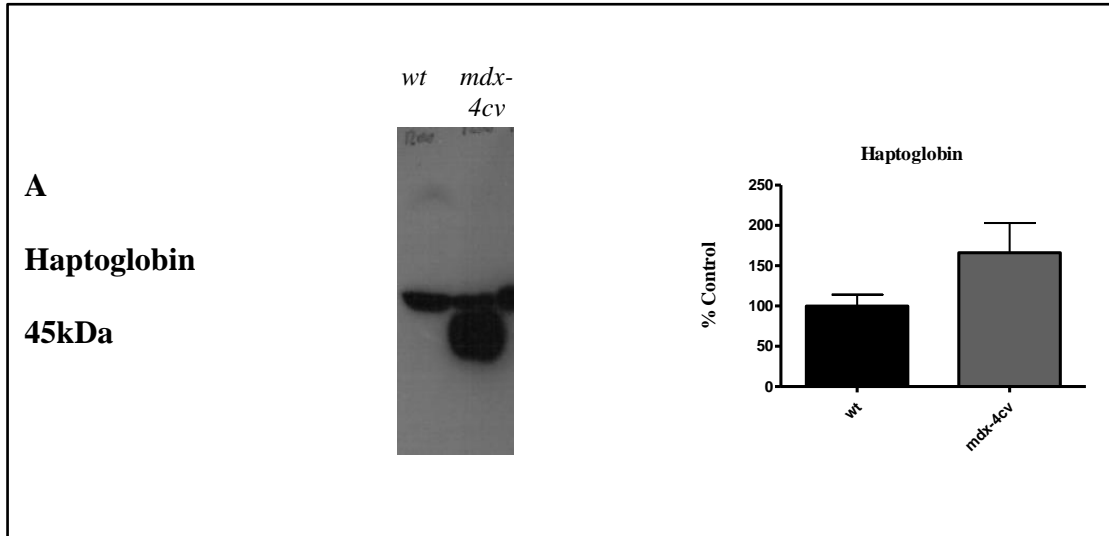


Figure 7.12: Comparative immunoblot analysis of haptoglobin in dystrophic 12-month *mdx-4cv* serum

Shown is a representative immunoblot with immuno-decorated bands labelled with an antibody to haptoglobin (A). Statistical analysis of immuno-decoration was performed with Student's *t*-test (mean values \pm SEM; unpaired; n=4).

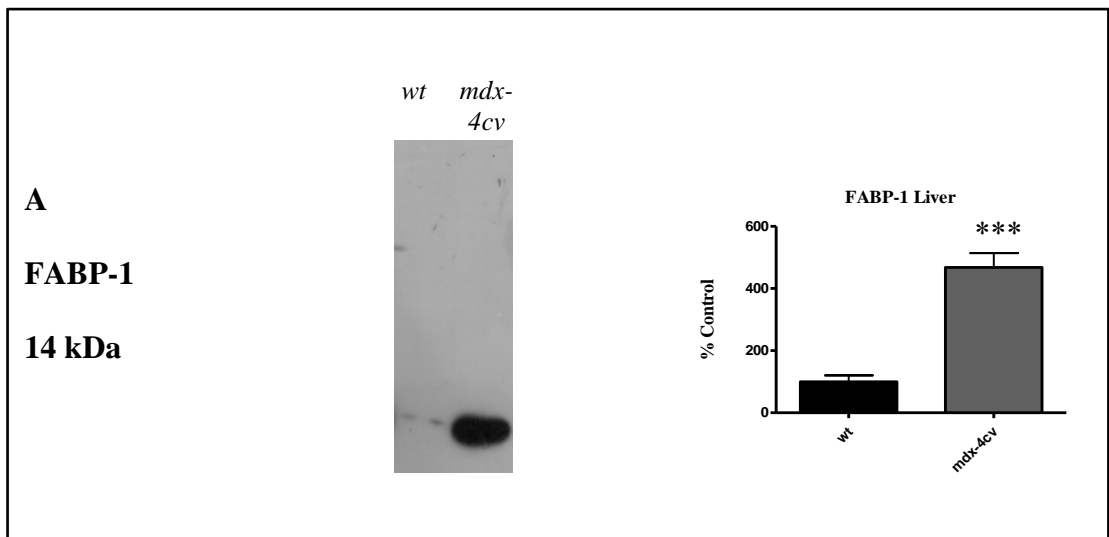


Figure 7.13: Comparative immunoblot analysis of FABP-1 in dystrophic 12-month *mdx-4cv* serum

Shown is a representative immunoblot with immuno-decorated bands labelled with an antibody to FABP-1 (A). Statistical analysis of immuno-decoration was performed with Student's *t*-test (mean values \pm SEM; unpaired; n=4, *** $p \leq 0.001$).

7.2.7 ELISA analysis of the increased abundance of FABP-1 and haptoglobin in mdx-4cv serum

Box and whisker plots were constructed based on the findings from the ELISA assays and illustrate information regarding the range, the median and the quartiles for FABP-1 (6-month serum samples) and haptoglobin (6 and 12-month serum samples). Levels of FABP-1 increased from an average of 1.64 $\mu\text{g/ml}$ in wild-type samples to 3.13 $\mu\text{g/ml}$ in *mdx-4cv* samples, and this increase was found to be statistically significant by the Mann Whitney U Test (Figure 7.14). Haptoglobin levels in 6-month serum increased from an average of 0.54 $\mu\text{g/ml}$ in wild-type serum to 29.82 $\mu\text{g/ml}$ in *mdx-4cv* serum, which was found to be statistically significant (Figure 7.15). Haptoglobin levels in 12-month serum rose from an average of 0.15 $\mu\text{g/ml}$ in wild-type serum to 15.34 $\mu\text{g/ml}$ in *mdx-4cv* serum, although this was not found to be statistically significant ($p=0.0571$) (Figure 7.16).

Receiver operating characteristic (ROC) curves were also constructed and the area under the ROC curve (AUC) was calculated to indicate the discriminating power of FABP-1 and haptoglobin to distinguish wild-type samples from *mdx-4cv* samples. FABP-1 shows a sensitivity of 100%, a specificity of 80% and an AUC of 0.95 (Figure 7.14). At both 6-months and 12-months haptoglobin displays a sensitivity of 100%, a specificity of 100% and an AUC of 1.000 (Figures 7.15 and 7.16). AUC values were also calculated for the combination of FABP-1 and haptoglobin using logistic regression analysis and was found to be equal to 1.000.

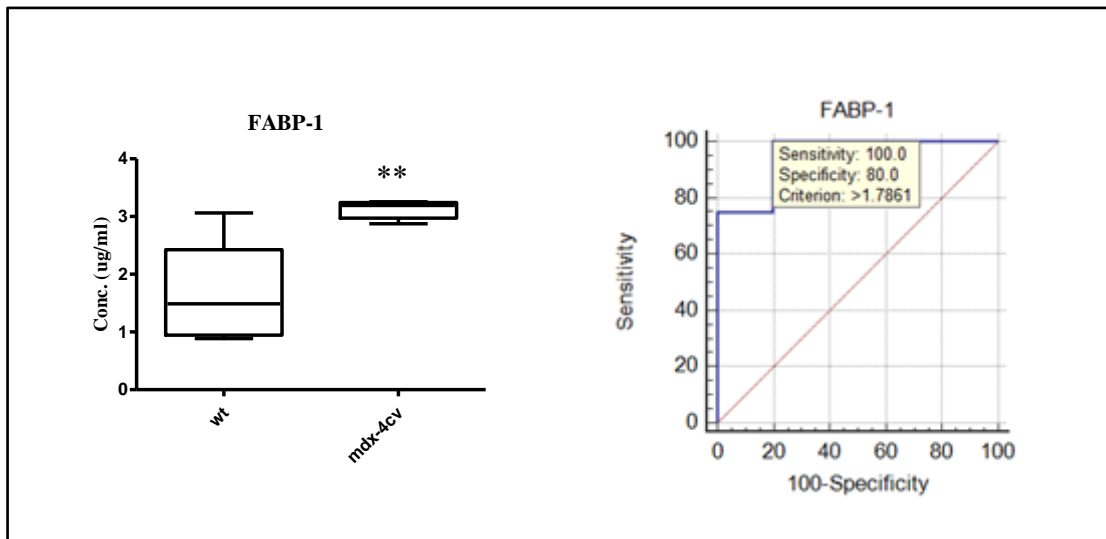


Figure 7.14: Box and whisker plots and ROC curve for FABP-1

Shown is the box and whisker plot and the ROC curve calculated from ELISA analysis conducted on 5 wild-type mice and 8 *mdx-4cv* mice. Statistical evaluation was performed using the Mann Whitney U test (** $p \leq 0.01$)

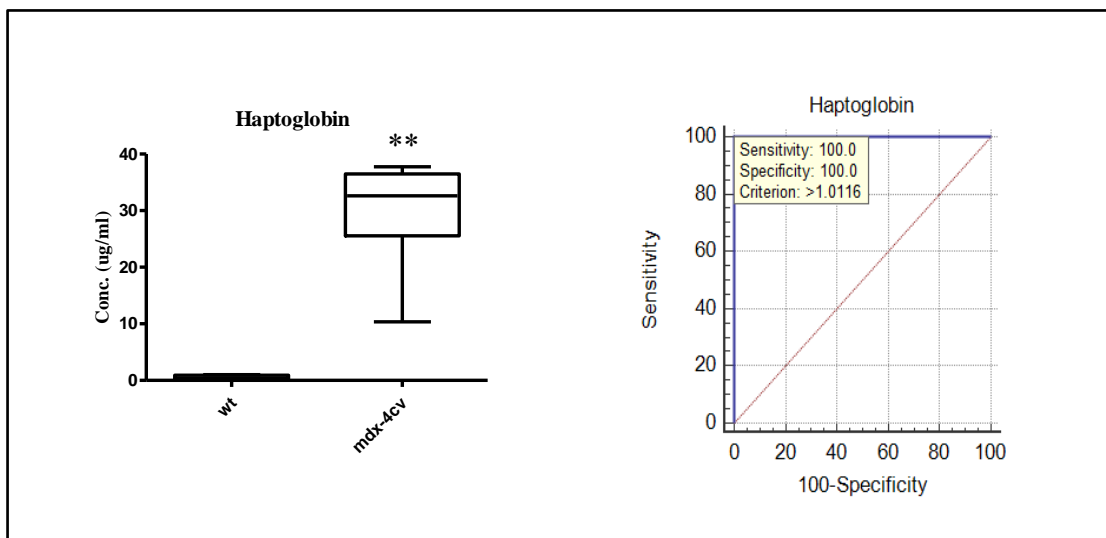


Figure 7.15: Box and whisker plots and ROC curve for haptoglobin in 6-month serum

Shown is the box and whisker plot and the ROC curve calculated from ELISA analysis conducted on 5 wild-type mice and 7 *mdx-4cv* mice. Statistical evaluation was performed using the Mann Whitney U test (** $p \leq 0.01$)

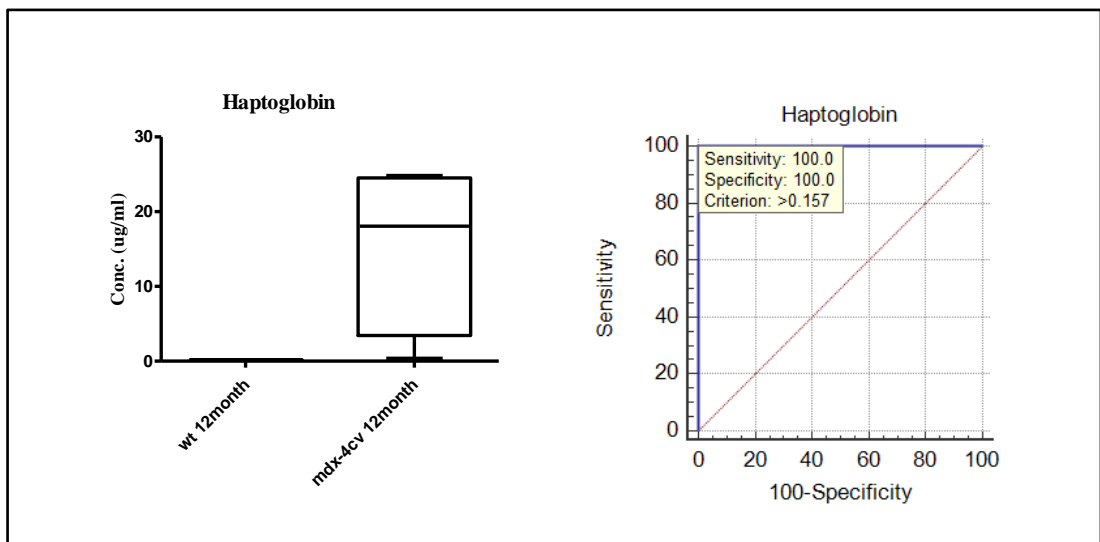


Figure 7.16: Box and whisker plots and ROC curve for haptoglobin in 12-month serum

Shown is the box and whisker plot and the ROC curve calculated from ELISA analysis conducted on 5 wild-type mice and 7 *mdx-4cv* mice. Statistical evaluation was performed using the Mann Whitney U test.

7.2.8 Protein identification in wild-type and *mdx-4cv* saliva

Qualitative analysis of the proteomics data using Proteome Discoverer 1.4 revealed the core saliva proteome for wild-type and *mdx-4cv* mice, which consisted of 137 proteins for wild-type and 112 proteins for *mdx-4cv* saliva samples. PANTHER analysis of the identified proteins revealed they belonged to a variety of protein classes, most notably hydrolases, enzyme modulators, transfer/carrier proteins, isomerases and signalling molecules, as illustrated in Figure 7.17. In both wild-type and *mdx-4cv* saliva proteomes, nine of the top 10 proteins ranked by sequence coverage were isoforms of the kallikrein 1-related peptidases, a sub-group of serine proteases which participate in normal physiological processes.

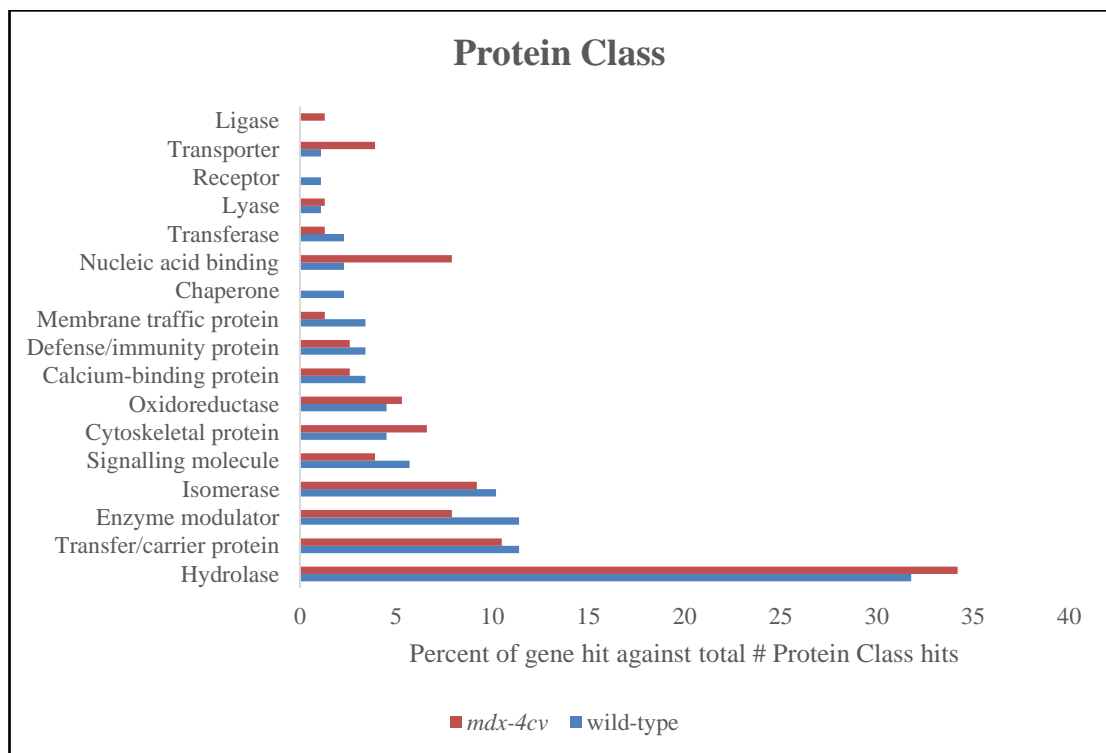


Figure 7.17: Protein class of salivary proteins

Illustrated is the PANTHER analysis of the 137 and 112 identified proteins in the saliva proteome from wild-type and *mdx-4cv* mice respectively.

7.2.9 Comparison of the wild-type saliva core proteome with the wild-type serum proteome

Comparison of the 137 proteins identified in wild-type saliva with the 1,030 proteins identified in wild-type immuno-depleted serum reveals 78 proteins in common. Thus 56.9% of the identified salivary proteins are also identified in serum, suggesting that serum proteins are reflected in saliva. The webgestalt analysis software was used to compare the salivary and serum proteomes from wild-type mice based on their gene ontology (GO) in relation to biological function, cellular component and molecular function as illustrated in Figures 7.18, 7.19 and 7.20 respectively. The GO data is based on the 750 (of 1,030) and 108 (of 137) proteins which were unambiguously mapped to unique Entrez Gene IDs in serum and saliva respectively. Both biofluids show similar protein distributions in terms of biological process (Figure 7.18). In terms of cellular component, both biofluids show the highest proportion of proteins belonging to vesicle, membrane, extracellular space and macromolecular complex, but with higher levels of proteins associated with the nucleus and cytoskeletal in the salivary proteome than the serum proteome (Figure 7.19). In addition, the distributions of salivary proteins are enhanced in hydrolase activity while serum proteins are increased in ion binding in relation to molecular function (Figure 7.20).

Thus, while serum and saliva clearly have their unique properties, the high proportion of salivary proteins which are also reflected in serum, and the significant similarities across GO categories suggests that saliva may represent a potential source of disease markers which could be used for non-invasive disease diagnosis and monitoring. Indeed, kallikrein 1-related peptidases, several members of which have already been proposed as cancer markers (Schmitt et al., 2013), which were detected with high sequence coverage in wild-type and *mdx-4cv* saliva, have also been detected in serum samples. 14 of the 78 proteins shared by wild-type serum and salivary proteomes belong to the kallikrein 1 serine protease family, as depicted in Table 7.3.

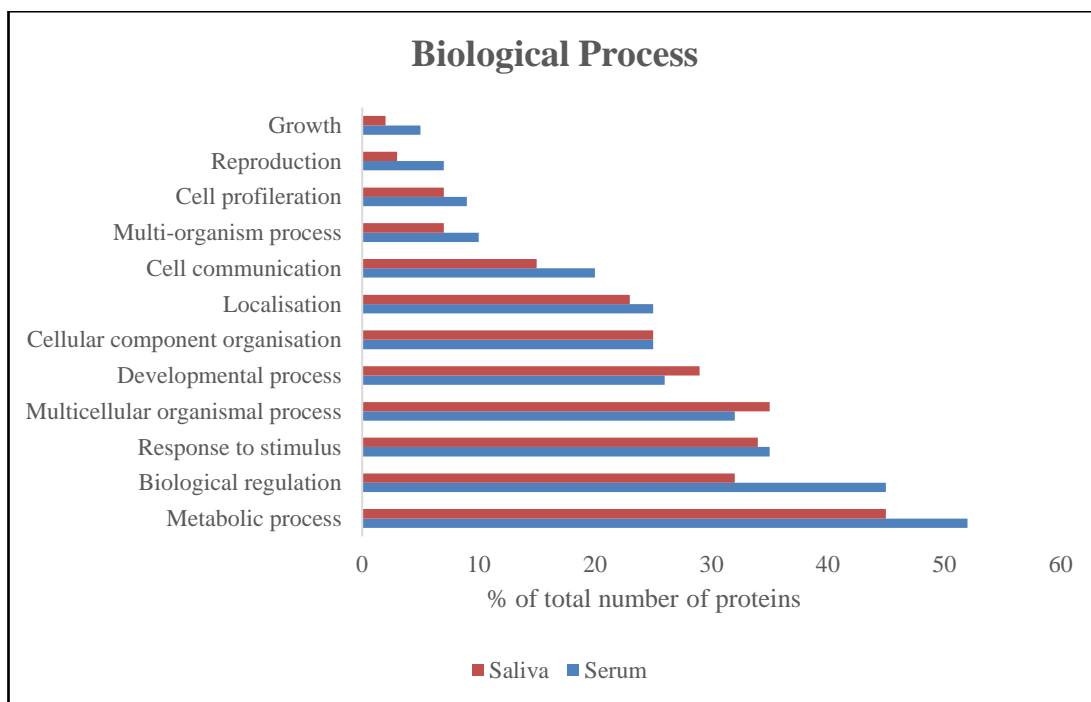


Figure 7.18: Biological process analysis of the serum versus saliva proteome
 Depicted is the GO category biological process for wild-type saliva and serum proteomes, based on results from the webgestalt software.

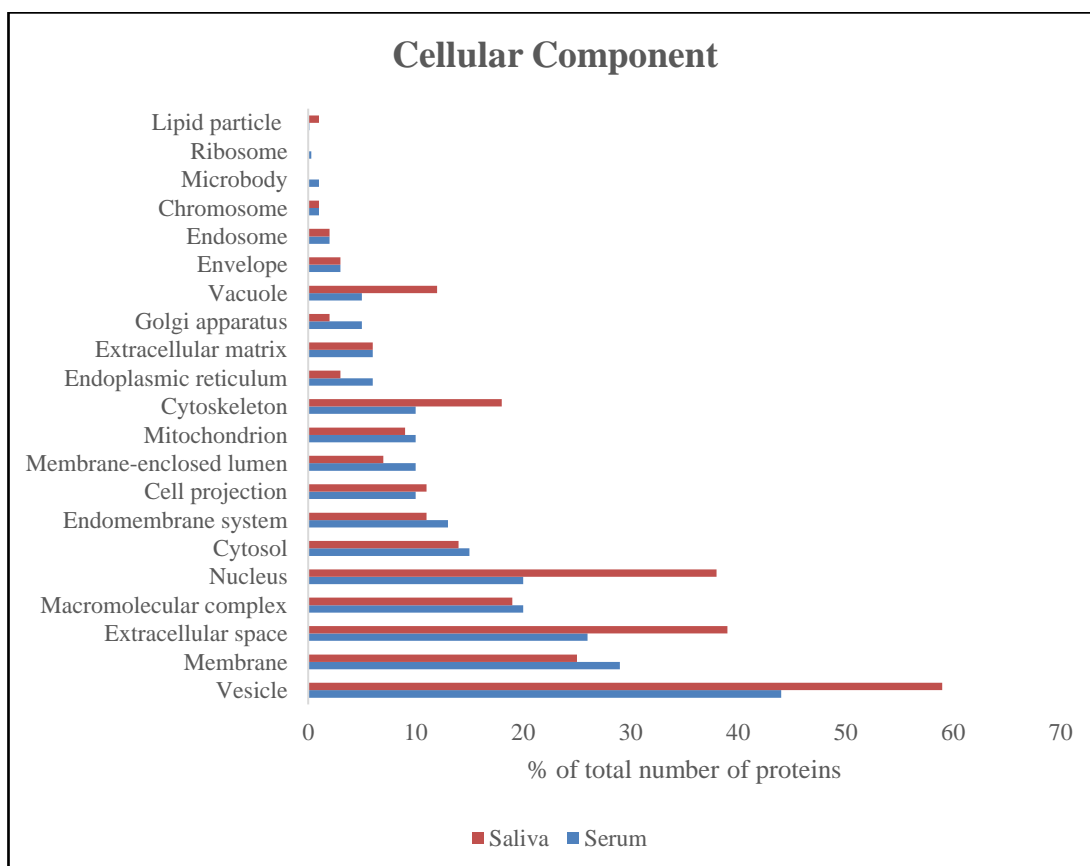


Figure 7.19: Cellular component analysis of the serum versus saliva proteome
 Depicted is the GO category cellular component for wild-type saliva and serum proteomes, based on results from the webgestalt software.

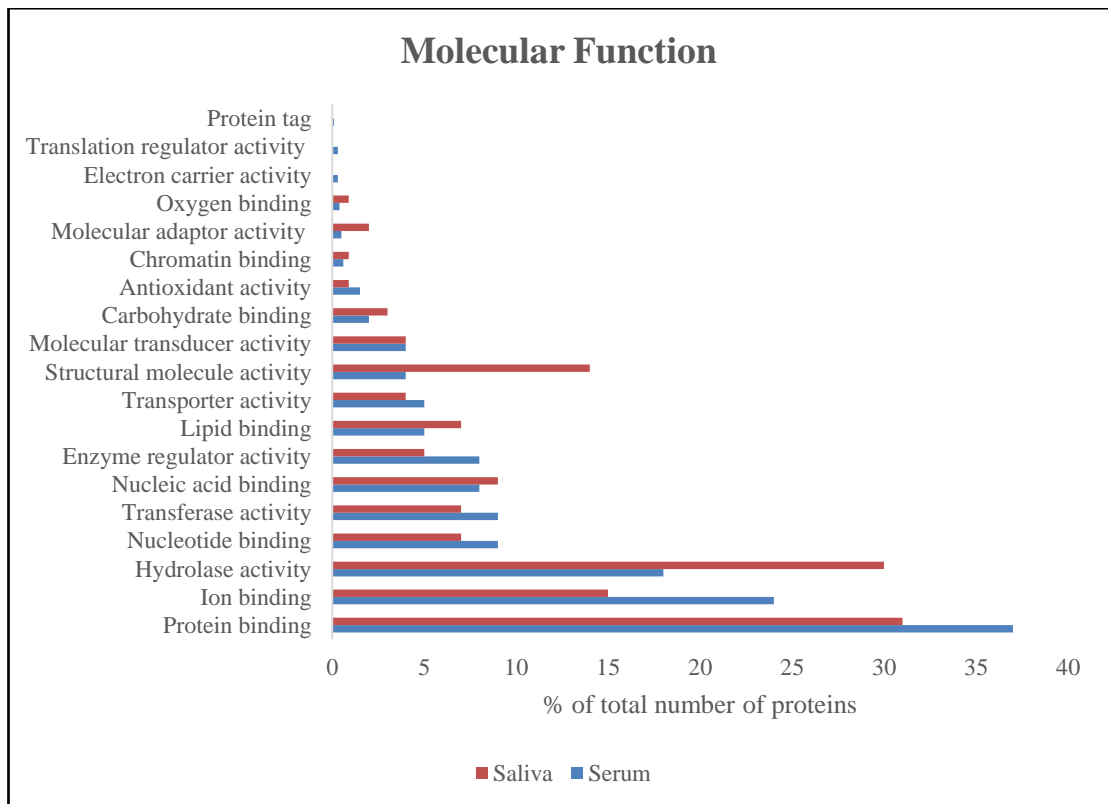


Figure 7.20: Molecular function analysis of the serum versus saliva proteome
 Depicted is the GO category molecular function for wild-type saliva and serum proteomes, based on results from the webgestalt software.

Table 7.3: Identification of kallikrein 1 and kallikrein 1-related peptidases in wild-type serum and saliva

Accession	Protein Name	Unique peptides in saliva	% Coverage in saliva	Unique peptides in serum	% Coverage in serum
P00756	Kallikrein 1-related peptidase b3	4	39.46	8	77.01
P15946	Kallikrein 1-related peptidase b11	5	44.83	13	73.56
P00755	Kallikrein 1-related peptidase b1	4	41.76	10	72.8
P15948	Kallikrein 1-related peptidase b22	5	27.03	13	71.81
P07628	Kallikrein 1-related peptidase b8	7	49.43	8	70.5
P15949	Kallikrein 1-related peptidase b9	5	45.98	10	68.97
P04071	Kallikrein 1-related peptidase b16	7	44.83	9	60.92
Q9JM71	Kallikrein 1-related peptidase b27	3	41.83	6	58.17
P36369	Kallikrein 1-related peptidase b26	3	42.53	5	57.47
Q61759	Kallikrein 1-related peptidase b21	2	37.55	2	49.43
P15945	Kallikrein 1-related peptidase b5	4	30.27	6	47.51
P00757	Kallikrein 1-related peptidase-like b4	6	33.98	10	43.75
Q61754	Kallikrein 1-related peptidase b24	3	38.4	4	42.59
P15947	Kallikrein-1	2	27.59	3	38.7

7.2.10 Quantitative analysis of wild-type versus *mdx-4cv* saliva

Quantitative analysis of saliva-derived protein samples using the MaxQuant and Perseus workflow identified 14 proteins with statistically significant differential abundance between wild-type and *mdx-4cv* samples. 7 proteins were found to be elevated in abundance while 7 were decreased, as listed in Tables 7.4 and 7.5 respectively. This comparative analysis identified kallikrein-1 and three kallikrein 1-related peptidases (b1, b5 and b22) as having elevated abundance in *mdx-4cv* saliva. Interestingly, elevated abundance for kallikrein-1 was also detected in *mdx-4cv* serum, where a 6.4-fold increase was identified (Table 7A.1). Illustrated in Figure 7.21 is a silver stained protein gel showing the typical banding pattern for wild-type and *mdx-4cv* saliva, along with the mass spectrometric identification of elevated levels of kallikrein-1 in *mdx-4cv* serum and saliva. Shown is the kallikrein-1 sequence with the three unique peptides identified in serum shown in bold and the three unique peptides detected in saliva shown as underlined. Two of the identified peptides were detected in both saliva and serum, with one additional unique peptide identified each in serum and saliva. Representative MS/MS scans for the three unique peptides for kallikrein-1 identified in wild-type and *mdx-4cv* saliva samples are shown in Figure 7.22. Higher peak intensities are evident for all three peptides in *mdx-4cv* saliva compared to wild-type saliva.

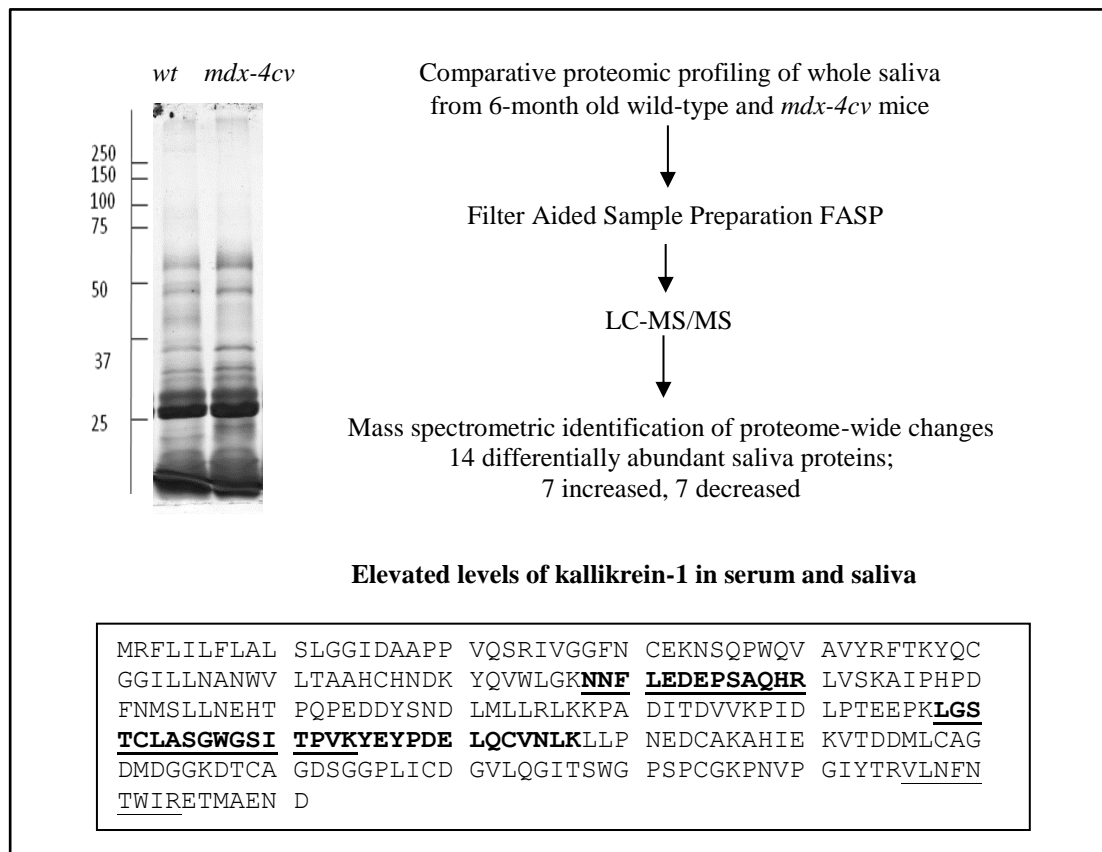


Figure 7.21: Mass spectrometric fingerprint of kallikrein-1

Shown in bold are the three unique peptides identified as having elevated abundance in serum from 6-month old *mdx-4cv* mice, while shown as underlined are the 3 unique peptides detected with increased levels in saliva samples from 6-month old *mdx-4cv* mice.

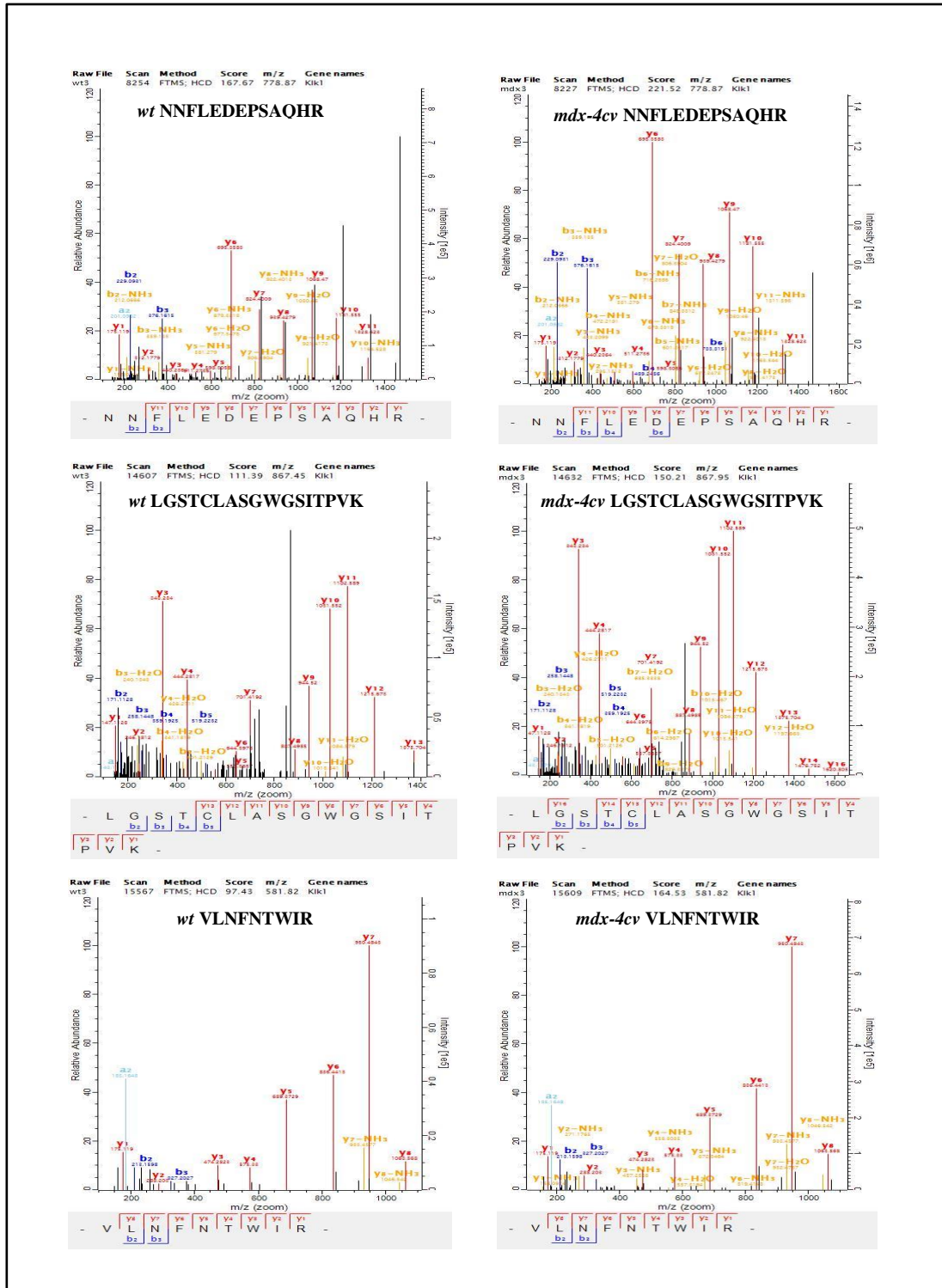


Figure 7.22: Proteomic identification of kallikrein isoform Klk1 in saliva from the *mdx-4cv* mouse model of Duchenne muscular dystrophy
 Shown are representative MS/MS scans of the three unique Klk-1 peptides NNFLEDEPSAQHR, LGSTCLASGWGSITPVK and VLNFNTWIR which were identified and compared in wild-type versus *mdx-4cv* saliva, respectively.

Table 7.4: List of identified proteins with a significantly increased abundance in 6-month old *mdx-4cv* saliva versus age-matched wild-type saliva as determined by label-free LC-MS/MS

Accession	Gene Name	Protein Name	Unique peptides	Score	Anova (p)	Fold Change
P15947	Klk1	Kallikrein-1	3	189.70	8.23E-03	4.16
Q07797	Lgals3bp	Galectin-3-binding protein	4	33.37	7.88E-04	3.54
O09159	Man2b1	Lysosomal alpha-mannosidase	21	323.31	1.93E-03	3.36
P15948	Klk1b22	Kallikrein 1-related peptidase b22	9	323.31	1.02E-02	1.97
P00755	Klk1b1	Kallikrein 1-related peptidase b1	6	215.37	6.03E-03	1.96
P15945	Klk1b5	Kallikrein 1-related peptidase b5	5	323.31	3.20E-02	1.49
P01139	Ngf	Beta-nerve growth factor	4	323.31	1.88E-02	1.34

Table 7.5: List of identified proteins with a significantly decreased abundance in 6-month old *mdx-4cv* saliva versus age-matched wild-type saliva as determined by label-free LC-MS/MS

Accession	Gene Name	Protein Name	Unique peptides	Score	Anova (p)	Fold Change
P07743	Bpifa2	BPI fold-containing family A member 2	6	289.80	7.21E-03	0.11
Q91Z98	Chi14	Chitinase-like protein 4	7	95.18	3.15E-03	0.15
Q3UU35	Ovos	Ovostatin homolog	6	323.31	3.47E-04	0.34
P04104	Krt1	Keratin, type II cytoskeletal 1	5	323.31	3.98E-02	0.37
P10126; P62631	Eef1a1 Eef1a2	Elongation factor 1-alpha 1; Elongation factor 1-alpha 2	7	100.44	1.31E-02	0.41
Q8K1H9	Obp2a	Odorant-binding protein 2a	3	75.90	4.57E-02	0.42
P03958	Ada	Adenosine deaminase	4	56.58	1.78E-02	0.44

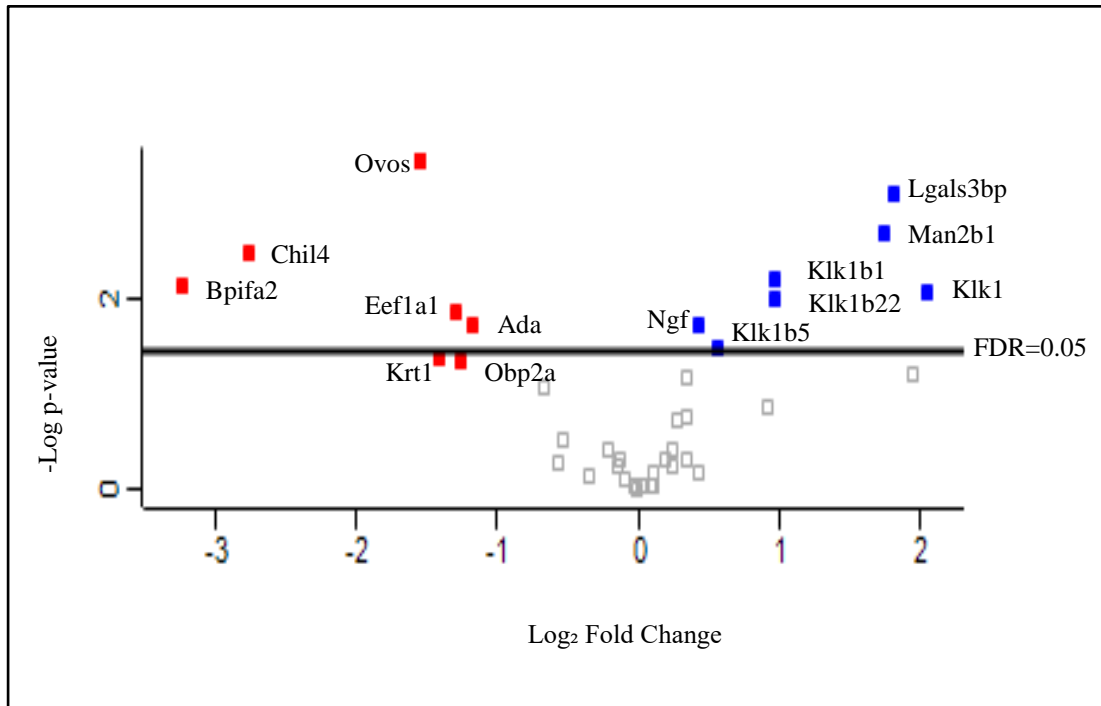


Figure 7.23 Volcano plots of all identified proteins based on relative abundance differences between wild-type and *mdx-4cv* saliva

Volcano plot illustrating the distribution of quantified proteins according to p value ($-\log_{10}$ p-value) and fold change (\log_2 mean LFQ intensity difference). Boxes represent proteins where boxes coloured red are those with decreased abundance in *mdx-4cv* saliva, and blue boxes are proteins with increased abundance in *mdx-4cv* saliva. All coloured boxes are statistically significant ($p\text{-value} \leq 0.05$), and coloured boxes above the line are those which also pass an FDR criterion of 0.05.

7.3 Discussion

While the primary deficiency in DMD is the loss of the full-length isoform of dystrophin, chronic inflammation represents a major secondary pathology and one which contributes to disease progression. Dystrophinopathy-induced secondary abnormalities of sarcolemmal instability and micro-rupturing, altered ion homeostasis, abnormal calcium ion fluxes, elevated extracellular ATP and increased proteolysis may serve as damage-associated molecular patterns which initiate a non-infectious inflammatory response. The initial immune response is a typical Th1 inflammatory response mediated by neutrophils and classically activated M1 macrophages with a pro-inflammatory phenotype (Tidball and Villalta, 2010). The recruitment of these M1 macrophages serves to phagocytose myofibre debris (Madaro and Bouché, 2014), but they also release pro-inflammatory cytokines, such as tumour necrosis factor alpha (TNF- α), the blockade of which has been shown to reduce muscle necrosis, contractile dysfunction and fibrosis and improve muscle function in the *mdx* mouse model (Hodgetts et al., 2006, Grounds and Torrisi, 2004). There is a subsequent invasion of alternatively activated M2 macrophages, which are associated with tissue repair and regeneration (Kharraz et al., 2013). M1 macrophages contain inducible nitric oxide synthase (iNOS) with M2 macrophages possessing arginase. Arginase and iNOS compete for arginine and thus increased numbers of M2 macrophages reduces the amount of arginine available to iNOS (Chang et al., 1998) and thus reduces the nitric-oxide mediated lysis of muscle cells.

In addition, M2 macrophages secrete IL-10 and IL-4; IL-10 is an anti-inflammatory cytokine and helps to dampen the immune response, and along with IL-4 it promotes satellite cell activation and muscle regeneration (Villalta et al., 2009). M1 macrophages are hypothesised to represent the primary macrophage phenotype during peak muscle necrosis (4 weeks) in *mdx* mice with a transition to a higher proportion of M2 macrophages during muscle regeneration (Villalta et al., 2009). Our mass spectrometric data supports this hypothesis given elevated serum concentrations of arginase-1 (6.8-fold increase), expressed by M2 macrophages, in *mdx-4cv* mice. These elevated levels of arginase-1 may have detrimental effects on the pathogenesis of the disease given that it has been shown recently that arginase metabolism by macrophages of the M2 phenotype promotes fibrosis in the *mdx* mouse model (Wehling-Henricks et al., 2010). Indeed, arginase 1 produces the amino acid proline

which is a prerequisite for collagen synthesis (Wynn, 2004), with excessive collagen deposition associated with the onset of fibrosis.

Haptoglobin is an acute phase plasma protein which is largely known for its role in binding to free haemoglobin with high affinity (Lim et al., 1998). This plasma glycoprotein also has anti-oxidant properties with its main site of synthesis occurring in the liver (Alper et al., 1965). In this chapter, substantial elevations in the abundance of serum haptoglobin in the *mdx-4cv* animal model of dystrophinopathy has been identified by three orthogonal methods; label-free LC-MS/MS, comparative immunoblotting and ELISA. Haptoglobin has been shown to be transcriptionally activated by pro-inflammatory cytokines such as IL-6 (Oliviero and Cortese, 1989) and so it is possible that the pro-inflammatory environment in dystrophic muscle may result in increased transcription of the haptoglobin gene thus resulting in the elevated abundance of serum haptoglobin as identified in this study, as outlined in Figure 7.24. Since serum haptoglobin is induced by pro-inflammatory cytokines it has potential to serve as a biomarker candidate of sterile inflammation in DMD. Its advantages are numerous in that it is detectable by three independent methodologies, it displays a significant elevation in its abundance (50.3-fold by mass spectrometry), ROC curve analysis showed promising specificity and sensitivity values (although this would need to be verified using a large cohort of clinical samples) and it is easily accessible and thus represents a non-invasive biomarker. Although activated by pro-inflammatory cytokines, haptoglobin itself has anti-inflammatory activity. It is a potent anti-oxidant agent and inhibits the biosynthesis of the prostaglandin pro-inflammatory mediators. It also specifically inhibits the tissue protease cathepsin B (Snellman and Sylvén, 1967) (which was found in elevated abundance in *mdx-4cv* serum) and thus may play a regulatory role in tissue proteolysis associated with inflammation. The elevated abundance of serum haptoglobin as identified here by comparative proteomics agrees with an earlier pre-proteomic study in which 2D gel electrophoresis and densitometric scanning identified elevated levels of haptoglobin in Duchenne patients (John and Purdom, 1989). Thus, haptoglobin represents a potential non-invasive serum biomarker candidate of sterile inflammation in dystrophinopathy.

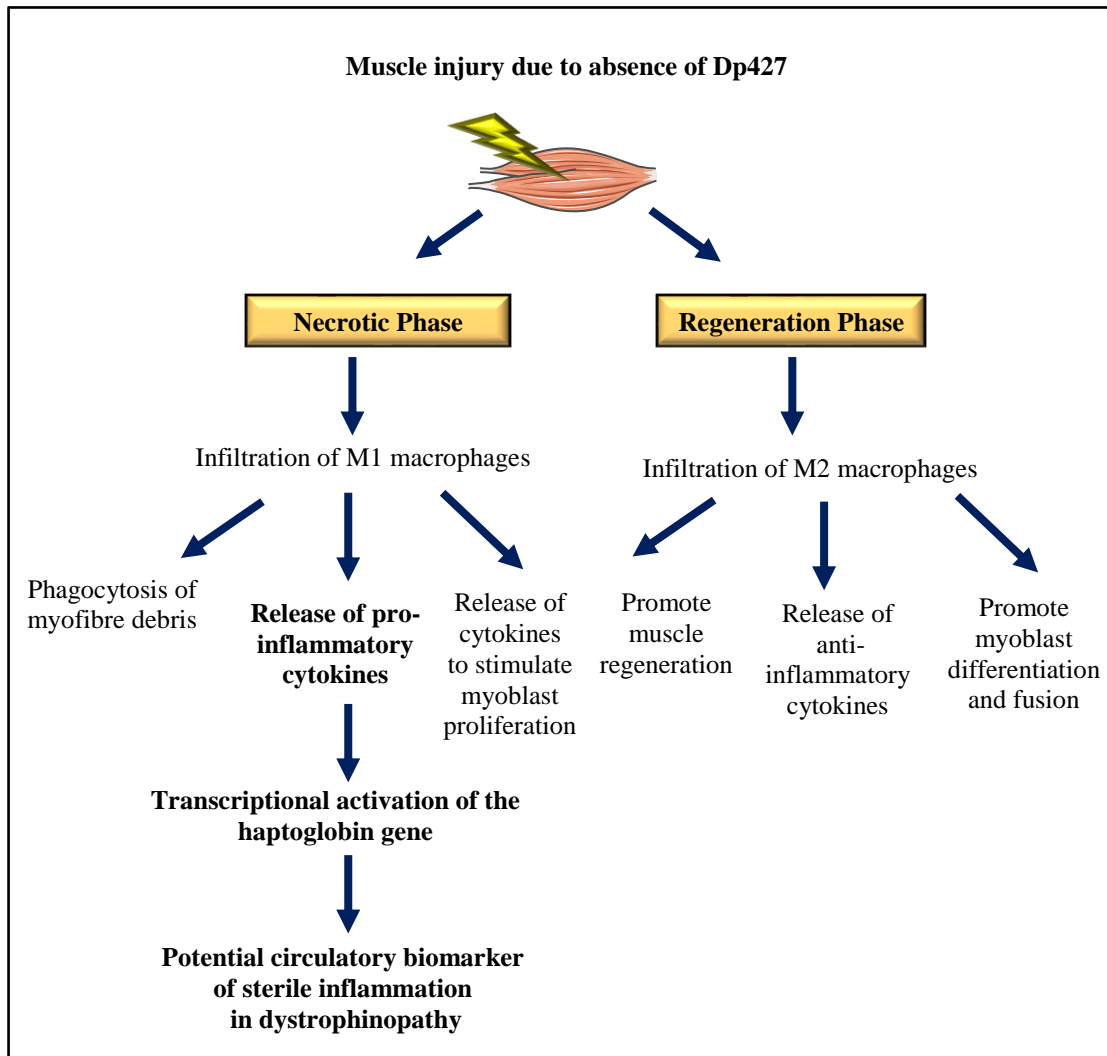


Figure 7.24: The role of the immune system in dystrophinopathy

Two main phases exist in DMD; the necrotic phase and the regeneration phase. During the necrotic phase there is an infiltration of M1 macrophages with a pro-inflammatory phenotype. M2 macrophages dampen the immune response and promote muscle growth and repair during the regeneration phase. The pro-inflammatory environment in dystrophic muscle may act as the stimulus for the transcriptional activation of haptoglobin, resulting in elevated serum haptoglobin which could serve as a biomarker candidate of sterile inflammation in DMD.

High levels of other acute phase proteins, such as the 36.98-fold increase in the abundance of serum amyloid A-1 protein, further substantiates a role for inflammation in the disease aetiology. Serum concentrations of serum amyloid A have been shown to increase by up to 1,000-fold following infection/inflammation and more modest elevations have been identified in chronic inflammatory diseases such as rheumatoid arthritis (O'Hara et al., 2000). Unlike haptoglobin, which has anti-inflammatory activity and which may serve to bind to heme proteins released from injured and degenerating muscle fibres, serum amyloid A propagates the immune response. This effect is thought to be mediated by its ability to stimulate cytokine production, with research by Patel and colleagues showing an ability of serum amyloid A to induce IL-1 β release *in vitro* (Patel et al., 1998), and through its chemoattractant effects on monocytes and neutrophils (Badolato et al., 1994, Su et al., 1999).

Muscle-derived proteins represent an important class of potential biomarkers of dystrophinopathy given their elevated levels in serum are typically representative of muscle fibre degeneration and the release of muscle-associated proteins into the circulatory system. Here, elevated abundance of the FABP-1 isoform of fatty acid binding protein was identified in serum from dystrophic *mdx-4cv* mice. This result is concurrent with the observation of reduced levels of FABP-1 in muscle specimens as identified by LC-MS/MS of *mdx* quadriceps muscle (-8.54-fold decrease in dystrophic quadriceps) (Murphy et al., 2017a). Several structural components of the muscle have also been identified as having an increased abundance in *mdx-4cv* serum, perhaps indicating the disintegration of muscle fibres. Such protein components include myomesin-3, a key component of the M-band in striated muscle (Schoenauer et al., 2008), which has previously been identified as having elevated abundance in dystrophinopathy (Hathout et al., 2014), and titin, fragments of which have been detected in the urine of patients with DMD (Rouillon et al., 2014).

A number of “typical” markers of DMD as identified by a large cohort of investigations have also been identified by this LC-MS/MS approach, as listed in Table 7.6. These circulatory biomarkers include in particular myofibrillar proteins (titin and myomesin 3), muscle-derived proteins (fatty acid binding protein, carbonic anhydrase III) and metabolic enzymes (lactate dehydrogenase, creatine kinase, pyruvate kinase, triosephosphate isomerase, alanine aminotransferase). The appearance of myofibrillar proteins in *mdx-4cv* serum and in patient samples (Rouillon et al., 2015, Rouillon et al., 2014) indicates muscle necrosis and the remodelling of

damaged muscle fibres. This is further substantiated by the observed increased abundance of structural and cytoskeletal proteins in dystrophic skeletal muscle samples, reflecting a potential compensatory mechanism to help counterbalance the loss of dystrophin and the DGC (Murphy et al., 2015a). The presence of muscle-derived proteins in *mdx-4cv* serum likely reflects leakage from degenerating muscle fibres. However, previous studies have also identified elevated levels of muscle-derived proteins such as FABP-3, aldolase A and actin in serum of *mdx* mice at 7 days, prior to the onset of muscle necrosis (Hathout et al., 2014). Such pre-necrosis markers were hypothesised to possibly reflect exosomal shedding and/or sarcolemmal permeability. The increase in metabolic enzymes in serum from the dystrophic mouse model possibly indicates an impairment of muscle energy metabolism which has previously been reviewed in detail (Dowling et al., 2014b).

Table 7.6: Major circulating protein biomarkers of dystrophinopathy common to our LC-MS/MS data and the literature

*Adiponectin was detected as having a fold decrease of 1.46 in our analysis (accession number Q60994; 3 unique peptides; confidence score 197.1)

Protein Marker	Abundance in dystrophinopathy	References
Creatine Kinase	Increased	(Mokuno et al., 1987)
Lactate dehydrogenase	Increased	(Yasmineh et al., 1978)
Fibronectin	Increased	(Cynthia Martin et al., 2014)
Pyruvate Kinase	Increased	(Zatz et al., 1991)
Carbonic Anhydrase III	Increased	(Ohta et al., 1991)
Titin	Increased	(Rouillon et al., 2014) (Hathout et al., 2015)
Troponin I fast skeletal	Increased	(Hathout et al., 2015)
Myomesin 3	Increased	(Rouillon et al., 2015)
Triosephosphate isomerase	Increased	(Rouillon et al., 2015, Coenen-Stass et al., 2015)
Alanine aminotransferase	Increased	(Zhu et al., 2015)
Adiponectin*	Decreased	(Hathout et al., 2014)

Large elevations in abundance were detected for the neuronal calcium binding protein calretinin (59.8-fold) and for GFAP, a protein specifically associated with astrocytes in the central nervous system, in *mdx-4cv* serum. GFAP was only identified by a single unique peptide (accession number: P03995, confidence score: 57.48, p value: 2.50E-02) but was detected to have a 1,289.8-fold increase in *mdx-4cv* serum. Increased abundance of calretinin and GFAP has been previously reported in *mdx-4cv* brain tissue (Murphy et al., 2015c). In the dystrophin-deficient brain, elevated abundance of GFAP may represent a reactive astrogliosis response (Yang and Wang, 2015) to dystrophin deficiency in the central nervous system, similar to the fibrotic response evident in dystrophin-deficient skeletal muscle, diaphragm and cardiac tissue (Holland et al., 2015a, Murphy et al., 2016b, Mann et al., 2011). Calretinin belongs to the family of EF-hand calcium binding proteins (Palczewska et al., 2003), and contains a well-conserved helix-loop-helix motif, responsible for binding to calcium ions with high affinity (Schwaller et al., 2002). Its elevated abundance in the *mdx-4cv* brain may represent a possible compensatory mechanism to counterbalance abnormal calcium fluxes within the central nervous system. The presence of these glial and neuronal proteins in serum may reflect damage occurring in the dystrophin-deficient brain, as previously shown by Vos and colleagues, in which levels of GFAP, S100b and neuron specific enolase in serum significantly correlated with the severity of traumatic brain injury and with poorer prognosis (Vos et al., 2004). The presence of brain-derived proteins in serum possibly has the potential to serve as surrogate biomarkers for monitoring dystrophinopathy in the brain. This is an important consideration given that approximately one-third of Duchenne patients display some degree of non-progressive cognitive impairments (Chamova et al., 2013).

Although fewer in number (37 proteins) and with more modest fold changes (largest fold decrease being 3.5 for angiotensin-converting enzyme), the class of proteins displaying reduced abundance in *mdx-4cv* serum is of interest. Their reduced abundance cannot be as easily explained as those proteins with elevated abundance whereby in a large proportion of cases their increased levels in *mdx-4cv* serum likely reflects release from necrotic and degenerating muscle fibres. KEGG pathway analysis of the 37 proteins with decreased abundance illustrates that they are predominantly involved in complement and coagulation cascades (9 proteins were identified as being involved in these cascades), as depicted in Figure 7.25. These proteins include von Willebrand factor, complement component C9, complement component C8 alpha

chain, complement component C8 beta chain, anti-thrombin III, and the serine protease inhibitors alpha-2-antiplasmin, alpha-1-antitrypsin 1-1, alpha-1-antitrypsin 1-2 and alpha-1-antitrypsin 1-5. Overall this suggests a dysregulation of the complement and coagulation cascades. This is in contrast to a number of other studies which have generally reported elevated levels of proteins associated with coagulation and fibrinolysis in patients with DMD, particularly those patients with cardiac involvement (Saito et al., 2005). This elevation appears to be in response to factors released from degenerating and necrotic muscle fibres. This disparity in results may be due to the animal model used, as there may not always be a direct correlation between animal models of disease and human counterparts. In addition, the serum samples used in this study were obtained from 6-month old *mdx-4cv* mice, a stage in which cardiac involvement may not be as apparent. Alternatively, the difference seen could potentially be because different markers of coagulation and fibrinolysis were used.

Previous studies have generally utilised levels of fibrin and fibrinogen degradation products as markers of coagulation and fibrinolysis, for which elevated levels have been identified in dystrophinopathy (Saito et al., 2001, Saito et al., 2005). These molecules were not found to be differentially expressed in our mass spectrometric data of *mdx-4cv* serum. However, decreased plasminogen, as identified in this study (accession number: P20918, confidence score: 3881.77, p value: 2.49E-05, fold decrease: 1.74) is associated with early fibrinolytic events following severe trauma (Amara et al., 2008), and thus its reduced abundance in *mdx-4cv* serum may represent fibrinolysis following muscle degeneration. Decreased levels of von Willebrand have also been identified in other forms of muscular dystrophy (Bertin et al., 1989). The reduced abundance of several components of the complement cascade in *mdx-4cv* serum possibly reflects its recruitment to necrotic muscle fibres. This recruitment to muscle fibres may contribute to the disease pathophysiology by forming a membrane attack complex (Sewry et al., 1987). The activation of the complement cascade can trigger the assembly of a membrane attack complex, usually responsible for inserting into and lysing host pathogens, particularly gram-negative bacteria (Serna et al., 2016). However, these membrane attack complexes have also been associated with neuromuscular diseases, such as dysferlinopathy (Brunn et al., 2006), amyotrophic lateral sclerosis (Bahia El Idrissi et al., 2016), dermatomyositis (Dalakas, 1991) and DMD (Engel and Biesecker, 1982). While Engel and Biesecker illustrated

that necrotic fibres in DMD biopsy specimens were reactive for membrane attack complex antigens, the presence of a membrane attack complex in DMD is controversial. Spuler and Engel were only able to identify sarcolemmal membrane attack complex deposits in samples of inflammatory myopathy but their study focused on the presence of such a complex on non-necrotic fibres, of which they were unable to find any in the BMD and DMD samples (Spuler and Engel, 1998). Similar to the study by Engel and Biesecker, Louboutin and colleagues demonstrated immunostaining of necrotic fibres in DMD specimens using antibodies against membrane attack complex (Louboutin et al., 2003). Thus, while the presence and potential role of such a complex requires further investigation, the difference in results obtained may be due to the type of muscle fibre studied. Indeed CD59, a membrane attack complex inhibitor glycoprotein (Meri et al., 1990), was immunolocalised to the sarcolemma of non-necrotic fibres, but not necrotic muscle fibres (Louboutin et al., 2003).

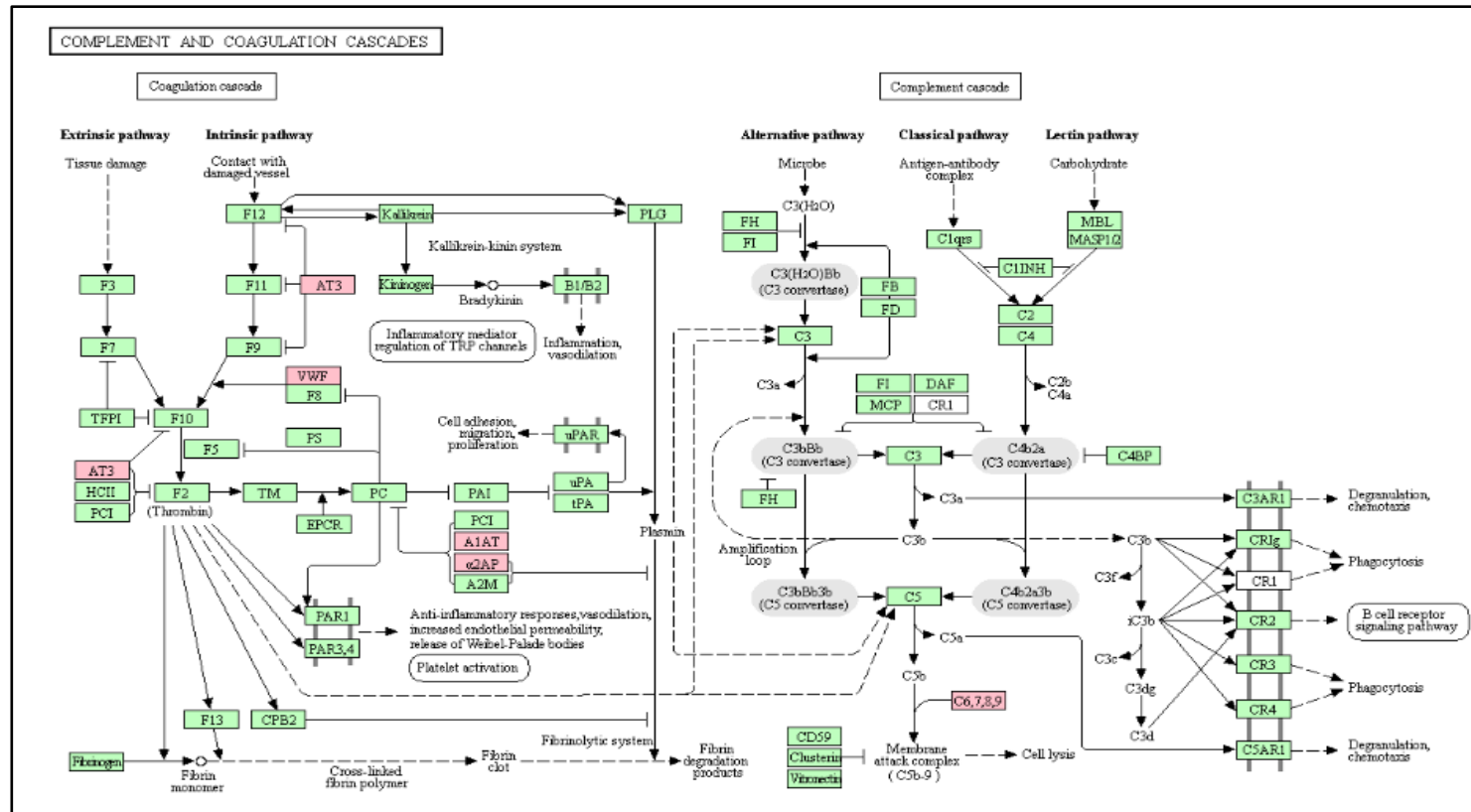


Figure 7.25: Complement and coagulation cascades in *Mus musculus*

Shown are the complement and coagulation cascades in *Mus musculus*. Proteins highlighted in pink are those with reduced abundance in *mdx-4cv* serum. The image was generated using KEGG search and colour pathway.

Proteomic profiling of serum samples has revealed potential novel protein markers of muscular dystrophy and these could potentially be translated to clinical applications. In the field of muscle pathology, clinical biofluid analyses are typically restricted to simple blood tests with a focus on muscle-derived serum proteins that are indicative of skeletal muscle damage, including creatine kinase and myoglobin. However, the more evenly distributed concentration of the saliva proteome as compared to the serum/plasma proteome negates the necessity for pre-fractionation and so may establish the salivary proteome as an alternative clinical biofluid which is non-invasive and amenable to systemic sampling even in paediatric patients. Importantly, salivary glands also exhibit a high permeability for their surrounding capillaries, which enables the infiltration of circulating peptides and proteins from blood, and saliva may be representative of the serum/plasma proteome. In a proof-of-concept study, label-free LC-MS/MS was used to identify alterations in protein abundance in *mdx-4cv* saliva samples. Preliminary findings suggest that with further research saliva could serve as a non-invasive surrogate for serum samples.

Serine proteases comprise approximately one-third of proteolytic enzymes and are involved in a variety of biological processes related to immunity, blood coagulation, development and digestion. Their catalytic activity is determined by the presence of a nucleophilic serine amino acid residue in their active site which attacks the carbonyl moiety in the substrate peptide bond (Page and Di Cera, 2008). Given their potentially devastating protease activity, as seen in auto-immune disease and tumour metastasis, the activity of the serine proteases is tightly regulated, for example by the presence of a superfamily of serine protease inhibitors known as serpins (Heutinck et al., 2010, Law et al., 2006). Kallikrein-related peptidases (KLKs) comprise a family of 15 highly conserved chymotrypsin- or trypsin-like serine proteases (KLKs 1-15), encoded by genes which are tightly clustered on the 19q13.33–13.41 chromosome region (Stefanini et al., 2015). They are involved in numerous physiological processes including innate immunity, semen liquefaction, remodelling of the extra-cellular matrix and skin desquamation (Sotiropoulou et al., 2009). Mass spectrometric analysis of saliva has here identified increased abundance for kallikrein-1 and three kallikrein 1-related peptidases (KLKs b1, b5 and b22) in *mdx-4cv* saliva samples. Kallikrein-1 is functionally conserved in its ability to cleave the circulating protein kininogen to release the vasoactive peptide bradykinin. This kallikrein/kinin and bradykinin signalling axis of vasoactive peptides is involved in blood pressure

regulation, tissue homeostasis and renal function. Bradykinin has two receptors; a constitutive B2 receptor and an inducible B1 receptor. Blockade of these receptors using antagonists resulted in increased muscle damage, fibrosis and immune cell infiltration in the *mdx* mouse, suggesting that the kallikrein kinin system may play a protective role in muscular dystrophy (Acuña et al., 2017). In support of this hypothesis, over-expression of tissue kallikrein and kinin restored cardiac function in rats post myocardial infarction by inhibiting fibrosis and promoting angiogenesis. (Yao et al., 2007). The increased abundance of kallikrein-1 and kallikrein 1-related peptidases identified in *mdx-4v* saliva may be reflective of an attempt to limit fibrosis.

Quantitative transcriptomics analysis of 27 different human organs and tissues identified highest expression of kallikrein-1 in the pancreas and salivary glands, with very low levels of expression evident in the other tested tissues (Fagerberg et al., 2014). The kallikrein-related peptidases have a well-established role in the degradation of extracellular matrix components, and kallikrein-1 can activate latent matrix metalloprotease 9 (MMP-9) (Sotiropoulou and Pampalakis, 2010). Increased serum levels of MMP-9 has been previously identified in Duchenne patients, where it was suggested as a potential biomarker to monitor disease progression (Nadarajah et al., 2011). Augmented abundance of MMP-9 in muscular dystrophy is suggested to contribute to the muscle pathogenesis through excessive remodelling of the extracellular matrix and basement membrane leading to fibrosis, the recruitment of macrophages, and the activation of TGF- β , a predominant mediator of fibrosis (Ogura et al., 2014). Indeed both genetic ablation and pharmacological inhibition of MMP-9 in *mdx* mice reduces muscle fibrosis, improves muscle structure and significantly increases muscle regeneration (Li et al., 2009). Therefore, elevated levels of kallikrein-1 in serum and saliva as detected here in *mdx-4cv* mice, may contribute to extracellular matrix remodelling and inflammation, key drivers of the disease pathophysiology. However, expression of MMP-9 is also modulated by NF- κ B and activator protein 1 transcription factors. Given their role in extracellular matrix remodelling, members of the kallikrein family of serine proteases have been suggested to be involved in tissue remodelling, angiogenesis, and/or metastasis in cancer, particularly in hormone-dependent malignancies, and represent both cancer biomarkers and therapeutic targets (Borgoño and Diamandis, 2004). Indeed, prostate specific antigen/kallikrein-3 represents the most valuable clinical biomarker for prostate cancer diagnosis. Kallikrein-1 and its related peptidases have limited utility in diagnosis of DMD given

this lack of specificity but may still prove useful for monitoring disease progression and response to therapy.

Increased abundance was also detected for galectin-3-binding protein, a 60-90 kDa protein which interacts with its ligand galectin-3 to mediate cell-to-cell adhesion. Galectin-3 is also proposed to play a role in the inflammatory process through leukocyte recruitment, chemotaxis of monocytes and macrophages, and the induction of IL-1 production in macrophages (Almkvist and Karlsson, 2002). Galectin-3 and galectin-3 binding protein are also involved in tissue fibrosis (Li et al., 2014), with elevated abundance of galectin-3 binding protein correlated to fibrosis and cirrhosis in both hepatitis C related- and alcohol related- liver disease (Cheung et al., 2010). In addition, increased abundance of galectin-3 has been previously identified in crude microsomes from skeletal muscle of the *mdx-4cv* animal model of DMD (Murphy et al., 2015a). The augmented levels of galectin-3 binding protein identified here in saliva of *mdx-4cv* mice may be reflective of the fibrotic and inflammatory processes occurring in response to dystrophin deficiency. Other proteins with increased abundance in *mdx-4cv* saliva include lysosomal alpha-mannosidase and beta-nerve growth factor. Elevated abundance of lysosomal alpha-mannosidase is in agreement with previous studies which demonstrated its increased activity in muscle biopsy samples from Duchenne patients, where it was suggested to reflect the infiltration of leukocytes into dystrophic muscle (Kawai et al., 1995). Nerve growth factor is a neurotrophin produced during muscle development, and which has been found at elevated levels in regenerating muscle fibres in muscular dystrophy (Toti et al., 2003).

Reduced abundance for a variety of proteins was also detected in saliva samples from *mdx-4cv* mice. Overall these proteins appear to be involved in catalytic activity but are not especially associated with muscular dystrophy. BPI fold-containing family A member 2 is an abundantly expressed protein in salivary secretions where, as a member of the bactericidal/permeability-increasing protein family, it is involved in host defence against bacteria. Chitinase-like protein 4 is a member of the chitinase-like protein family which are lectins that combine the properties of cytokines and growth factors. While expressed in rodents it is absent in humans (Kzhyshkowska et al., 2016). Other members of the chitinase-like protein family are however expressed in humans and some, particularly chitinase-3-like protein 1, have been associated with inflammation, cancer, diabetes and cardiovascular disease. Chitinase-3-like protein 1 is also involved in extracellular

matrix remodelling and can stimulate the proliferation of human connective tissue cells such as fibroblasts and chondrocytes (Rathcke and Vestergaard, 2009). Indeed transcriptomic analysis of cranial *sartorius* muscle from the GRMD dog model of DMD identified increased levels of chitinase-3-like protein 1, where it was suggested to participate in disease progression through promotion of fibrosis (Brinkmeyer-Langford et al., 2018). The decreased abundance of chitinase-like protein 4 identified in saliva samples of the *mdx-4cv* mouse here contrasts with these previous studies where increased abundance of the chitinase-like proteins is associated with inflammation and fibrosis, classical hallmarks of dystrophinopathy. Given that the chitinase-like protein 4 detected here is only expressed in rodents it is possible that it may play an undiscovered alternative role to that of its associated chitinase-like proteins which are expressed in both rodents and humans.

Ovostatin homolog belongs to the proteinase inhibitor I39 (alpha-macroglobulin) family; a group of protease inhibitors with the ability to inhibit proteases from all catalytic classes. Reduced abundance of alpha-2-macroglobulin has been previously identified in plasma samples from *mdx* mice (Colussi et al., 2010), and in a muscle proteomic analysis of 2-day old dystrophic pigs, an uncharacterised protein with homology to alpha-2-macroglobulin was detected only in wild-type muscle samples (Fröhlich et al., 2016). The reduced abundance of ovostatin homolog identified here by mass spectrometric analysis of saliva may be reflective of alterations in the serum and muscle proteomes of dystrophic animal models. Reduced abundance of the alpha-macroglobulin proteases may exacerbate the dystrophic phenotype by increasing protease activity.

Elongation factors regulate muscle protein synthesis by facilitating the delivery of aminoacyl-tRNA to the ribosome. Increased abundance of elongation factor 1-alpha 1 and elongation factor 1-alpha 2 may therefore be associated with increased protein synthesis associated with muscle regeneration and their elevated expression has been identified in dystrophic *mdx* diaphragm, *soleus*, *extensor digitorum longus* and *interosseus* muscle (Holland et al., 2015b), and increased abundance of elongation factor 1-alpha 1 was detected in *mdx-4cv* serum samples (Table A7.1). However, decreased abundance of elongation factor 1-alpha 1 and elongation factor 1-alpha 2 was found in aged *mdx* cardiac tissue (Holland et al., 2013), indicating a potential effect of age and/or tissue type on the abundance of the

elongation factors. Overall the altered levels of these proteins in dystrophic tissue and biofluids may reflect perturbed protein synthesis.

7.3.1 Conclusions

There is an urgent requirement for novel biofluid-derived protein markers for DMD which are i) highly sensitive and specific and can be used for disease diagnosis, prognosis and therapy-monitoring, and ii) minimally invasive or non-invasive to facilitate repeated sampling, particularly for monitoring prognosis and therapy outcomes. Mass spectrometry-based proteomics offers an unbiased technology-driven approach for the global analysis of alterations in protein abundance. Label-free LC-MS/MS has been performed on serum and saliva samples from the *mdx-4cv* animal model of DMD. A vast number of potential protein markers were identified in the immuno-depleted serum proteome, with 90% of the differentially abundant proteins showing elevated levels in *mdx-4cv* serum. This high proportion of increased abundance as opposed to decreased abundance proteins, and the bioinformatics analysis showing enrichment of muscle-derived proteins indicates that many of these are muscle proteins that are leaked into the serum upon muscle necrosis and degeneration. Of particular interest is the inflammation-inducible plasma protein haptoglobin which shows a 50.28-fold increase, and which was verified by both comparative immunoblotting and ELISA analyses. A smaller number of differentially abundant proteins were detected in the saliva proteome, with the identified proteins largely related to inflammation, extracellular matrix remodelling and protease activity. Kallikrein-1 and a number of kallikrein-1 related peptidases demonstrated elevated abundance in saliva samples from dystrophic mice. Interestingly, augmented levels of kallikrein-1 were also identified in *mdx-4cv* serum samples, suggesting that this protein represents a potential circulatory biomarker of inflammation in dystrophinopathy. Since the serum and saliva proteome are modified by stress, exercise, diet, inflammation, trauma, and drug use, these confounding factors would need to be taken into consideration when transferred to a Duchenne patient population. However, the proteomic studies described here offer proof-of-principle that easily accessible biofluids such as serum and saliva may have clinical utility in serving as important sources of novel disease biomarkers of progressive muscular dystrophy.

Chapter Eight

General Discussion

8.1 Discussion

The application of 2D-GE to skeletal muscle has played an essential role in the development of skeletal muscle proteomics and the characterisation of the muscle proteome in both health and disease. Publications relating to gel electrophoretic analysis of skeletal muscle have increased dramatically since 1976, with a spiked increase evident following the incorporation of mass spectrometry-based proteomics for the routine analysis of skeletal muscle tissues since 2004 (Murphy et al., 2016a). Such studies have also been instrumental in identifying some of the secondary abnormalities associated with dystrophin deficiency in DMD. However, given the large size, hydrophobicity and low-abundance of the DGC, the majority of previous proteomic surveys have failed to detect or could only partially detect the main members of the complex. Alternative strategies have employed immuno-precipitation (Yoon et al., 2012) and gradient centrifugation (Turk et al., 2016). In Chapter 3, an in-solution digestion protocol coupled to mass spectrometry analysis using an improved Q-Exactive mass spectrometer enabled the identification of reduced abundance of dystrophin and $\alpha 1$ -sytrophin in crude homogenates from hind-limb samples from wild-type versus *mdx-4cv* mice. This mass spectrometric detection of dystrophin within a highly complex crude muscle homogenate represents a technological achievement and one with implications for future mass spectrometry-based quantification of dystrophin in muscle.

At present, several clinical trials aimed at restoring dystrophin expression are in progress and a key biochemical outcome measure for these trials is the accurate quantification of dystrophin. Immunoblotting and immunofluorescence microscopy are typically used to evaluate dystrophin expression in clinical trials, however these methods are challenging for the detection of the very large and low abundance dystrophin, are only semi-quantitative (Aartsma-Rus, 2014) and in the absence of standard operating procedures significant levels of intra- and inter-laboratory variability have been reported (Anthony et al., 2014). Thus, mass spectrometry may offer an alternative for the more robust absolute quantification of dystrophin in human muscle biopsies (Brown et al., 2012). Given that mass spectrometry would only give an indication of total dystrophin levels, it may be prudent to combine such an analysis with immunofluorescence microscopy which has the capacity to also examine dystrophin localisation to the sarcolemma which has functional implications. The identification of reduced dystrophin abundance in dystrophic skeletal muscle in

Chapter 3 enabled a direct correlation between dystrophin deficiency and secondary abnormalities. These secondary effects were found to be especially related to myofibrosis, cytoskeletal remodelling, muscle regeneration, membrane repair, ion homeostasis, and impaired calcium buffering. Large increases in protein abundance were particularly evident for fibrotic proteins, including fibronectin, biglycan, collagen, fibrinogen, asporin and decorin. These proteins represent potential biomarkers for DMD, particularly as some, including fibronectin, have also been identified in serum samples from the *mdx-4cv* mouse (Murphy et al., 2017b) and from Duchenne patients (Cynthia Martin et al., 2014). These proteins may also act as novel therapeutic targets, as treatments aimed at reducing fibrosis may improve the disease phenotype while also increasing the amount of muscle available for treatment by novel therapeutic agents. Dystrophin deficiency and the simultaneous disintegration of the DGC results in severe perturbations of the muscle proteome in terms of both protein abundance and protein oligomerisation. In Chapter 3, chemical cross-linking of a membrane-enriched fraction from wild-type and dystrophic skeletal muscle was coupled to gel electrophoretic shift analysis and mass spectrometry to evaluate alterations in protein interaction patterns. Augmented oligomerisation was evident for proteins related to membrane repair, cytoskeletal remodelling, fatty acid oxidation, metabolism, and chaperoning. These enhanced protein networks likely occur as compensatory mechanisms to rescue the dystrophic phenotype and offer novel insights into the disease pathophysiology.

While the proteomic profiling approach illustrated in Chapter 3 provides a global overview of proteomic alterations in dystrophic skeletal muscle, in Chapter 4 a combination of organelle proteomics, on-membrane digestion and label-free mass spectrometric analyses were used to i) characterise the DGC and ii) give a detailed map of proteomic alterations at the dystrophin-deficient sarcolemma. Standard 2D gels are typically incapable of resolving large molecular weight proteins, whereas 1D gradient gels can resolve very large proteins of up to 2,000 kDa (Ohlendieck, 2011c). Indeed, recent proteomic analysis of a myofibrillar fraction from a dried and long-term stored 1D polyacrylamide gel identified a large number of proteins including titin of approximately 3,400 kDa (Murphy and Ohlendieck, 2018). Thus, differential centrifugation, digitonin detergent solubilisation, ion exchange chromatography, lectin affinity chromatography and density gradient centrifugation were used to generate a dystrophin-complex enriched fraction from wild-type skeletal muscle

which was separated on a 1D 3-12% gradient gel and transferred to a nitrocellulose membrane. Muscle proteins absorbed onto nitrocellulose sheets appear to be more accessible to proteases, resulting in improved digestion efficiency and the superior detection of large membrane proteins (Ohlendieck, 2011c). This study identified both the core members of the DGC and proteins which potentially interact with or exist in close proximity to the complex. Of particular interest was the identification of the desmosomal cadherins desmoglein-1 and desmoplakin. Comparative immunoblotting identified greatly reduced abundance for desmoglein-1 in both *mdx* and *mdx-4cv* skeletal muscle preparations, indicating that it suffers the same pathobiochemical fate as components of the core DGC. Thus, this protein may warrant further attention to fully elucidate its role in normal muscle and in X-linked muscular dystrophy. An organelle proteomics approach was used to specifically focus on the fate of proteins closely linked to the muscle sarcolemma in the absence of dystrophin. This proteomic profiling of the dystrophic sarcolemma confirmed a number of perturbations previously identified, including structural remodelling, molecular chaperoning, elevated cellular stress, increased protein synthesis, altered ion handling, inflammation and membrane repair. Importantly, this study also offered novel insights, especially in relation to the identification of reduced levels of the intermediate filament protein synemin which has previously been suggested to interact with components of the DGC, and decreased abundance of the myelin specific proteins periaxin and myelin binding protein zero, indicating a potential perturbation of motor neuron myelination in dystrophic tissue.

Chapters 3 and 4 give insights into proteomic alterations in skeletal muscle, which is severely and progressively impaired in DMD. However, cardiorespiratory difficulties are a major complication for Duchenne patients, and in a subset of patients mild and non-progressive cognitive impairments are also evident. To ascertain a proteomic basis for these observations, label-free LC-MS/MS proteomic profiling was extended to dystrophin-deficient cardiac and brain tissue in Chapters 5 and 6. Cardiomyopathy is a serious complication in muscular dystrophy, and further research in this area is crucial as i) it is a clinical manifestation in approximately 90% of patients, ii) heart failure is responsible for an estimated 20% of deaths, iii) there is no cure, and iv) emerging potential therapies not only fail to treat the heart but treatment of skeletal muscle alone may actually accelerate heart disease (Faysoil et al., 2010). The DGC in cardiomyocytes has a costameric distribution, and is present in the

sarcolemma, T-tubules and in intercalated discs, where it is involved in transduction of mechanical force to the extracellular matrix. Similar to skeletal muscle, the loss of dystrophin and its associated glycoprotein complex in cardiac tissue culminates in increased vulnerability to mechanical stress, micro-rupturing of the sarcolemma, and dysregulated ion influx and efflux resulting in elevated Ca^{2+} concentration. Increased intracellular Ca^{2+} results in the activation of calpains which degrade muscle proteins leading to necrosis, and mitochondrial-mediated cell death (Tsuda and Fitzgerald, 2017). Death of cardiomyocytes is then followed by immune cell infiltration and myofibrosis where fibroblasts invade damaged cardiac tissue and contribute to the deposition of extracellular matrix proteins and scar formation. This process of cardiomyopathy first affects the posterobasal and lateral walls of the left ventricle (LV), which is later accompanied by an increase in wall stress. Over time, systolic LV function decreases and myocardial oxygen consumption increases, resulting in LV dilation and dysfunction (Fayssol et al., 2010). Since cardiac dysfunction progresses slowly before an abrupt onset of acute cardiomyopathy at later stages of the disease, pharmacological treatment is given before the commencement of cardiac symptoms to delay the onset of heart failure. Corticosteroids and angiotensin-converting-enzyme inhibitors are typically used to prevent/delay LV dysfunction (D'Amario et al., 2017). In Chapter 5 proteomic profiling of senescent *mdx-4cv* cardiac tissue was performed to identify proteomic alterations in the aged heart which may give insights into the pathology of cardiomyopathy. This approach identified 98 proteins with an altered abundance in the dystrophic heart, 54 of which were increased in abundance and 44 of which showed decreased levels.

In analogy to the profiling of dystrophic skeletal muscle in Chapter 3, reduced abundance was detected for dystrophin, $\alpha 1$ -syntrophin, α -sarcoglycan, β -sarcoglycan and δ -sarcoglycan in dystrophic hearts, enabling the simultaneous evaluation of dystrophin deficiency and downstream secondary abnormalities. One of the major alterations identified in the aged heart is that of myofibrosis, evident by elevated abundance of the matricellular protein periostin, the proteoglycans asporin and lumican, and the extracellular matrix protein collagen. Comparative proteomics also revealed augmented levels of molecular chaperones, anti-proteases and anti-inflammation factors, suggesting a compensatory mechanism to limit proteotoxic effects. In conjunction with elevated abundance of a range of cytoskeletal proteins, these alterations represent an attempt to rescue the dystrophic phenotype. A potentially

useful new heart-associated marker of cardiomyopathy is myosin light chain kinase 3, which showed the largest elevation in dystrophic hearts with a 414-fold increase. Myosin light chain kinase 3 is a key enzyme that is responsible for the phosphorylation of specific light and heavy chains of cardiac myosin, involved in potentiating the force and rate of cross-bridge recruitment in cardiac fibres (Murphy et al., 2016b). The drastically elevated levels of myosin light chain kinase 3 indicate considerable changes in the regulation of myosin interactions in the *mdx-4cv* heart.

Approximately one-third of patients with DMD display cognitive impairments which are usually mild and non-progressive, although there is large variation in cognitive function amongst Duchenne patients. A neuropsychological study performed on DMD children and a matched control group of children with SMA found that the SMA group showed no signs of cognitive dysfunction, despite progressive muscle wasting and premature death. This suggests that the cognitive deficits seen in Duchenne patients are specific to the loss of dystrophin and not the psychological consequence of a degenerative disease (Billard et al., 1992). General intellect has been reported to be relatively comparable between DMD patients and healthy age-matched controls, and between DMD patients and controls with a different neuromuscular disorder, and so cognitive impairments appear to affect only specific functions, with major deficits specifically seen in short-term memory which may contribute to impaired intellectual development (Wicksell et al., 2004). While the muscle isoform Dp427m is the principal dystrophin isoform in skeletal muscle, a plethora of dystrophin isoforms exist in the brain, including the cortical Dp427c isoform in neurons of the cortex and in the *cornu ammonis* of the hippocampus, the Purkinje isoform Dp427p expressed in cerebellar Purkinje cells, Dp140 predominantly expressed in the foetal brain, and Dp71 which is ubiquitously expressed but with highest levels in the central nervous system (Doorenweerd et al., 2017). Recent studies have suggested that a correlation exists between cognitive defects and the location of the dystrophin gene mutation. More distal mutations affect increasing numbers of dystrophin isoforms, and the severity of cognitive impairment is proposed to be linked to the cumulative loss of distal central nervous system expressed dystrophin isoforms, particularly Dp140 and Dp71 (Taylor et al., 2010).

To facilitate a molecular understanding of the effect of dystrophin deficiency on brain tissue, a label-free LC-MS/MS study was performed on brain tissue from 12-month old wild-type and age-matched *mdx-4cv* mice, which due to a premature stop

codon in exon 53 expresses neither Dp427, Dp260 nor Dp140, but stably expresses Dp71 (Im et al., 1996). As described in Chapter 6, proteomic profiling revealed altered abundance for 46 proteins, 39 of which were increased in abundance and 7 of which were decreased. Overall, proteomic perturbations in the brain proteome are similar to those seen in skeletal muscle and the heart, where increased abundance of cytoskeletal components such as vimentin, spectrin and drebrin may represent a compensatory mechanism to partially restore mechanical strength to dystrophin-deficient cells. Elevated abundance of annexin A5 is indicative of membrane repair whilst reduced abundance of plasma membrane calcium transporting ATPase 2 suggests altered calcium ion homeostasis (Murphy et al., 2015b). The largest fold increase was seen for the heme-binding serum glycoprotein hemopexin, whose increased abundance may be linked to altered iron metabolism in the *mdx-4cv* brain, which has previously been described in the *mdx* heart (Holland et al., 2013). One finding of particular interest was the 2.00-fold increase in the abundance of GFAP, an intermediate filament protein of the central nervous system, the abundance of which was further investigated by immunoblotting and immunofluorescence microscopy. Augmented levels of GFAP are indicative of cellular hypertrophy and/or proliferation of astrocytes usually in response to a central nervous system insult (Eng et al., 2000). Prolonged astrocyte activation can lead to glial scar formation and tissue scarring. Similar to infiltration of myofibroblasts and the deposition of extracellular matrix proteins leading to fibrosis in dystrophic skeletal muscle and the heart, dystrophin deficiency in the central nervous system may lead to the activation of astrocytes, non-specific reactive astrogliosis and tissue scar formation. Thus, GFAP represents a protein marker with great potential to be exploited to further improve understanding of muscular dystrophy-associated cognitive impairments. This is particularly relevant given a previous case report of a Duchenne patient with severe mental retardation who possessed multifocal glial nodules with intense immunoreactivity for GFAP in the cerebral cortex (Itoh et al., 1999). Astrogliosis may also represent a therapeutic target. There is growing evidence for a pathogenic role of glia cells (microglia and astrocytes) in several neurodegenerative disorders, such as Alzheimer's disease, ALS and Parkinson's disease, where glia-induced inflammation can amplify the disease pathology and contribute to disease progression (Colangelo et al., 2012). Inhibition of neuro-inflammation may reduce the production of factors that contribute to neurotoxicity and thus have clinical benefit.

There is an urgent need for a superior biomarker panel for DMD, ideally based on quantifiable molecules which are easily accessible (Hathout et al., 2015). Unlike protein markers identified in tissue samples, the detection of biomarkers in biofluids such as blood, urine and saliva is minimally invasive and thus is amenable to repeated sampling. An improved biofluid-based protein biomarker panel could be used i) in disease diagnosis, ii) in pharmacodynamics to monitor therapy safety and efficacy, and iii) to improve understanding of disease pathophysiology and identify novel therapeutic targets (Hathout et al., 2016). To address this issue comparative proteomic profiling was performed on serum and saliva samples from 6-month old wild-type and *mdx-4cv* mice in Chapter 7. Serum proteomics identified 371 differentially abundant proteins; 334 of which were increased in abundance and 37 of which displayed reduced abundance. Cellular component analysis of the augmented proteins revealed that a large majority of them were muscle-derived proteins, thus their increased levels in serum reflects leakage from muscle through the damaged sarcolemma, and muscle necrosis and degeneration. Two proteins of particular interest were haptoglobin and FABP-1, whose elevated abundance as detected by label-free LC-MS/MS was verified by immunoblotting and ELISA analysis. Increased abundance of the inflammation-inducible plasma protein haptoglobin suggests sterile inflammation, and thus haptoglobin may serve as a potential biomarker candidate of inflammation in dystrophinopathy. Elevated abundance of FABP-1 in serum agrees with its reduced levels in *mdx* muscle samples (Murphy et al., 2017a). Its increased abundance in serum may therefore reflect skeletal muscle degeneration and the release of muscle proteins into the circulatory system. Both biomarker candidates offer potential for their use in developing a superior biomarker panel of X-linked muscular dystrophy, however they would need to be first validated in a large cohort of clinical samples.

Saliva proteomics uncovered 14 proteins with differential abundance; 7 of which were increased in abundance and 7 of which were found to be decreased in abundance. Overall, this pilot study of saliva proteomics identified altered proteins associated with protein signalling, extracellular matrix remodelling and inflammation. Of particular importance was the detection of increased abundance of kallikrein-1, kallikrein 1-related peptidase b1, kallikrein 1-related peptidase b5 and kallikrein 1-related peptidase b22 in *mdx-4cv* saliva. The kallikrein family play diverse roles in extracellular matrix remodelling, inflammation and in the vasoactive peptide system. Kallikrein-1 is especially interesting given it was also found to be increased by 6.28-

fold in *mdx-4cv* serum, indicating that it is a potentially useful circulatory marker for muscular dystrophy. Together, these studies of serum and saliva establish liquid biopsy procedures as a suitable bioanalytical tool for the survey of potential biomarker candidates of DMD. These initial proteomic surveys have identified a number of possible biomarker candidates, including haptoglobin, FABP-1 and kallikrein-1. However, further studies are required to investigate the influence of age, gender, ethnicity, diet, general lifestyle, physical activity, stress, co-morbidities and pharmacological side effects on the levels of these protein markers.

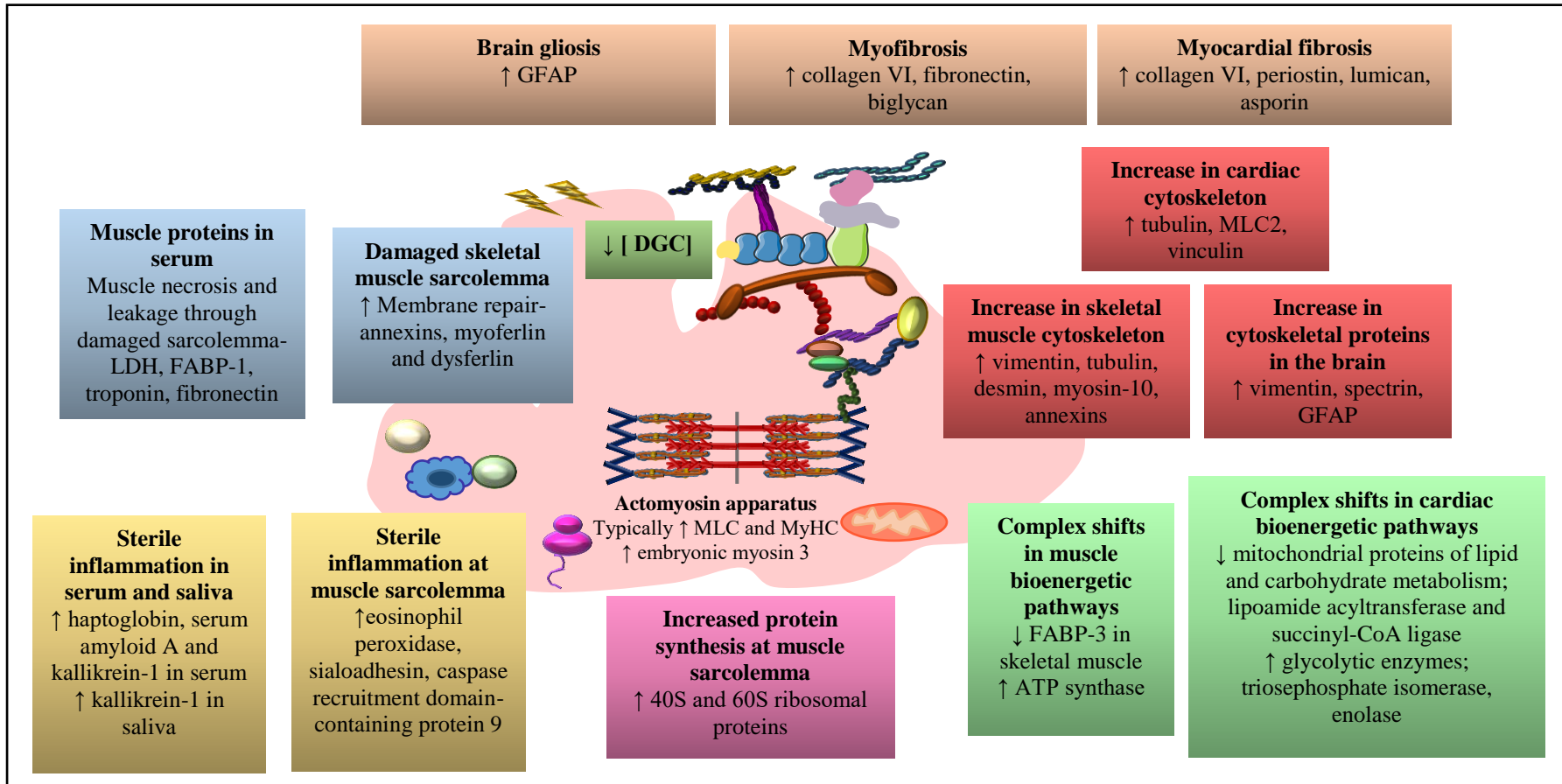


Figure 8.1 Overview of muscular dystrophy-induced changes in skeletal muscle, the heart, brain, serum and saliva
 Illustrated is an overview of the principal secondary abnormalities downstream of dystrophin deficiency, as identified by the mass spectrometric analysis of dystrophin-deficient tissues and biofluids described in this work.

Tissue proteomics has identified statistically significant altered abundance for 199 proteins in 6-month old crude skeletal muscle (Chapter 3), 190 proteins in 5-month old sarcolemma-enriched muscle homogenates (Chapter 4), 98 proteins in senescent 20-month old cardiac tissue (Chapter 5) and 46 proteins in 12-month old brain tissue (Chapter 6). To investigate whether any of these proteins could represent global protein markers of dystrophinopathy, irrespective of age and/or tissue type, a cross-comparison of all altered proteins from each tissue proteomics study was performed, as illustrated in Figure 8.2. While no single protein was identified to be differentially abundant in all four tissues, 69 proteins were found in two of the four tissues and 12 proteins were found to be differentially abundant in three of the four tissue proteomes. These 12 proteins are listed in Table 8.1. While the majority of these proteins show the same trend of increased versus decreased abundance, in some cases proteins elevated in skeletal muscle and sarcolemma were found to be decreased in cardiac tissue (Na⁺/K⁺-ATPase subunit alpha-1, Ig mu chain C region, and filamin C). This may reflect differences in the response of cardiac tissue versus skeletal muscle to dystrophin deficiency and/or may be age-related given that in this work only the cardiac tissue is representative of the end stage of the disease. Importantly, reduced levels of dystrophin were detected in skeletal muscle, the sarcolemma and the heart, thus verifying the mutant status of the *mdx-4cv* mouse model used in this research.

Myosin 9, a cellular myosin involved in cytokinesis and cytoskeletal reorganisation was found to be increased in abundance in skeletal muscle, the sarcolemma and the heart. Elevated levels of myosin 9 have also been previously reported in the severely dystrophic diaphragm of *mdx-4cv* mice, further establishing myosin 9 as a potential biomarker candidate of X-linked muscular dystrophy (Holland et al., 2015a). Its augmented levels in dystrophin-deficient tissue likely reflect cytoskeletal remodelling, enhanced cellular proliferation and increased synthesis of components of the matrisome (Murphy et al., 2015b).

Increased abundance was also detected for the alpha-1 subunit of the integral membrane protein Na⁺/K⁺-ATPase in skeletal muscle and the sarcolemma. This suggests that damaged skeletal muscle fibres attempt to compensate abnormal ion fluxes by increasing the availability of this ion pump to stabilise the membrane potential (Dunn et al., 1995). However, slightly decreased abundance of this ion pump was detected in aged cardiac tissue, indicating that either this compensatory mechanism is restricted to skeletal muscle and/or that this attempt to stabilise the

membrane potential is lost during senescence. Age-dependant decreases in Na⁺/K⁺-ATPase activity have previously been reported in humans (Maurya and Prakash, 2013) and in mouse brain (Tanaka and Ando, 1990). While these studies reported only the activity of Na⁺/K⁺-ATPase and not its abundance, the potential effect of aging on both the abundance and activity of Na⁺/K⁺-ATPase would need to be considered should it be considered as a potential marker of dystrophinopathy.

Raised levels of Ig mu chain C region identified in the skeletal muscle and sarcolemma may be reflective of autoimmunity. It has been speculated that instability of the DGC and the chronic inflammatory environment in dystrophic tissue may contribute to an autoimmune response to proteins of the DGC or other muscle-derived proteins (Villalta et al., 2015). Such auto-antibodies may be present in skeletal muscle through infiltration of the leaky dystrophin-deficient sarcolemma (Holland et al., 2013). This appears to affect skeletal muscle more than cardiac muscle, given reduced levels of Ig mu chain were detected in the heart.

Filamin C is a muscle-specific, actin-crosslinking protein which localises at Z-discs, myotendinous junctions, costameres, and intercalated disks in mammalian skeletal and cardiac muscle. Filamin C interacts with the DGC, integrin, and the Z-disc proteins myopodin and myotilin, indicating a role in the maintenance of muscle integrity (Fujita et al., 2012). Localised myofibrillar damage of live cardiomyocytes resulted in the rapid recruitment of filamin C to damaged areas indicating that in contrast to previous understanding of filamin C as a static structural protein, filamin C may also be involved in myofibrillar remodelling (Leber et al., 2016). Elevated abundance of filamin C, as seen in dystrophic skeletal muscle and the sarcolemma may therefore be indicative of myofibrillar damage, probably as a result of Ca²⁺ overload, protease activation, protein degradation and muscle necrosis. It also suggests a repair response by dystrophic skeletal muscle to mend damaged muscle. The reduction of filamin C in 20-month old dystrophin-deficient heart likely represents a decrease in the ability of dystrophic muscle to mediate repair mechanisms with age.

A variety of heat shock proteins have been shown to be elevated in abundance in dystrophic muscle, including cardiovascular heat shock protein/HSPB7 in the *mdx* diaphragm (Doran et al., 2006b), HSP90-beta in *mdx soleus*, *extensor digitorum longus* and *flexor digitorum brevis* (Holland et al., 2015b) and HSP90-beta, heat shock cognate 71 kDa protein and 60 kDa heat shock protein in *mdx gastrocnemius* (Gardan-Salmon et al., 2011). In analogy to these previous studies of the *mdx* mouse model,

increased abundance of HSP90-beta1 has been identified in crude skeletal muscle homogenates, the sarcolemma and the aged heart from the *mdx-4cv* mouse, as indicated in Table 8.1. In skeletal muscle, HSPs play key roles in cellular signalling, modulation of the immune response, myogenesis, myofibril assembly, and the stabilisation of misfolded and denatured proteins following exposure to stress (Brinkmeier and Ohlendieck, 2014). Therefore, the increased abundance of HSP90-beta1 seen in Chapters 3, 4 and 5 suggests elevated cytoprotection of vulnerable skeletal and cardiac muscle fibres to limit proteotoxic effects. HSP90-beta1 may represent a potential biomarker candidate for the superior diagnosis, prognosis and therapy-monitoring of DMD. A partial reversal of muscular dystrophy-induced increased abundance of cardiovascular HSP/HSPB7 has been previously described following exon-23 skipping in the *mdx* mouse (Doran et al., 2009b). Thus, HSPs may represent a class of protein markers useful for the evaluation of the ability of emerging therapies to reverse secondary changes, such as cellular stress, in dystrophinopathy.

Heterogeneous nuclear ribonucleoproteins (hnRNPs) are a large family of multi-functional RNA-binding proteins, which are involved in cellular nucleic acid metabolism, particularly in relation to alternative splicing, mRNA stabilization, and transcriptional and translational regulation. In human cells, hnRNP complexes are composed of at least 20 core hnRNP proteins and other less abundant minor hnRNP proteins. The core proteins termed hnRNP A1 through to hnRNP U are reported to differ in their preferred binding site and in their function, with functional roles ranging from splicing to stability to translation (Chaudhury et al., 2010). The reported purpose of hnRNP M, shown to have elevated abundance in dystrophin-deficient sarcolemma, cardiac and brain tissue, is splicing (Hovhannisyanyan and Carstens, 2007). Many proteins which are essential for striated muscle development exist in multiple isoforms which are generated by alternative splicing. This includes transcription factors, components of the myofibril, and metabolic enzymes (Pistoni et al., 2010). The elevated abundance of hnRNP in dystrophin-deficient sarcolemma, cardiac and brain tissue may therefore be necessary for alternative splicing of an increased number of muscle proteins. Enhanced protein synthesis is a feature of dystrophic tissue to provide enough protein for muscle regeneration, cytoskeletal remodelling and metabolic homeostasis.

Apolipoprotein A-I is the major protein component of high density lipoprotein in plasma, which interacts with apolipoprotein A-I binding protein, and is involved in

cholesterol efflux. A 5-6 fold increase in the relative rate of apolipoprotein A-I synthesis in mature dystrophic fast-twitch breast muscle has previously been described in dystrophic chickens, where this increase was associated with elevated levels of apolipoprotein A-I mRNA (Shackelford and Lebherz, 1985). Increased abundance of apolipoprotein A-I in *mdx-4cv* skeletal muscle, heart and brain may indicate a compensatory mechanism to counter-act impaired lipid metabolism in dystrophin-deficient fibres and support the altered metabolic needs of dystrophic tissues.

Spectrins are large, actin-crosslinking, membrane cytoskeletal proteins, of which both non-erythroid and erythroid isoforms exist in skeletal and cardiac muscle. Erythroid spectrin has been suggested to localise at the costameric junction between the Z-line and the sarcolemma, while non-erythroid spectrin has been shown to localise at Z-line striations and at the neuromuscular junction (Vybiral et al., 1992). Spectrin forms heterodimers and through its interactions with actin filaments and membrane-bound cytoskeletal proteins, it forms a membrane-cytoskeletal scaffolding complex. This complex confers cellular flexibility to erythrocytes and structural integrity to non-erythroid cells (Isayama et al., 1993). Given the role of spectrin in forming a scaffolding protein complex and providing plasmalemmal integrity (Murphy et al., 2016b), its elevated abundance in dystrophin-deficient skeletal muscle, cardiac and brain tissue may reflect a compensatory mechanism to maintain structural integrity in the absence of the DGC. This would appear to be a conserved response across the skeletal, circulatory and central nervous systems in response to dystrophin deficiency.

Metabolic disturbances are a key hallmark of DMD, with perturbations in the cytosolic proteins of glycolysis and the mitochondrial enzymes of the tricarboxylic acid cycle and electron transport chain consistently reported in Duchenne patients and animal models of the disease (Timpani et al., 2015). This results in reduced ATP synthesis which has negative implications for Ca^{2+} -buffering, contractile apparatus function, protein synthesis, and muscle regeneration. ATP synthase is a mitochondrial complex V enzyme which plays a critical role in the generation of ATP (Holland et al., 2013). This protein shows an altered abundance profile, whereby increased abundance is detected in crude skeletal muscle homogenates and brain (Chapters 3 and 6), but reduced abundance is seen in sarcolemma-enriched skeletal muscle (Chapter 4). Reduced abundance of ATP synthase in the sarcolemma possibly represents an artefact from the extensive subcellular fractionation procedure, or may

be in line with previous studies of aged *mdx* cardiac tissue in which reduced abundance of ATP synthase was linked to impaired mitochondrial metabolism and an inability of dystrophic cardiac mitochondria to meet ATP demands (Holland et al., 2013). On the other hand, elevated levels of various subunits of ATP synthase in crude skeletal muscle (ATP synthase F₀ complex subunit B1, ATP synthase subunit O, and ATP synthase subunit alpha) and brain (ATP synthase subunit gamma and ATP synthase subunit alpha) possibly indicates a compensatory mechanism to counteract ATP insufficiency in dystrophic tissue.

The Ca²⁺-regulated phospholipid- and membrane- binding family of annexin proteins and the type III intermediate filament protein vimentin have been previously suggested as universal biomarkers of DMD, given their increased abundance in both mildly and severely affected mouse skeletal muscle (Holland et al., 2015b). Both annexin A5 and vimentin were shown here to be increased in skeletal muscle, the sarcolemma and the brain, where their increased abundance likely reflects membrane repair processes and structural remodelling respectively.

Overall, the 12 proteins listed in Table 8.1 offer unique insights into the pathophysiology of DMD and the effect of tissue type and age on the disease process. They reveal enhanced cellular stress, cytoskeletal remodelling, ion homeostasis, membrane repair, and metabolism as key altered processes within dystrophin-deficient tissue. These proteins offer huge potential to be exploited as possible protein biomarkers for the improved diagnosis, prognosis and therapy-monitoring of dystrophinopathy. Future work should evaluate such biomarker candidates in a large cohort of clinical samples and attempt to link their status to disease progression and/or response to therapy.

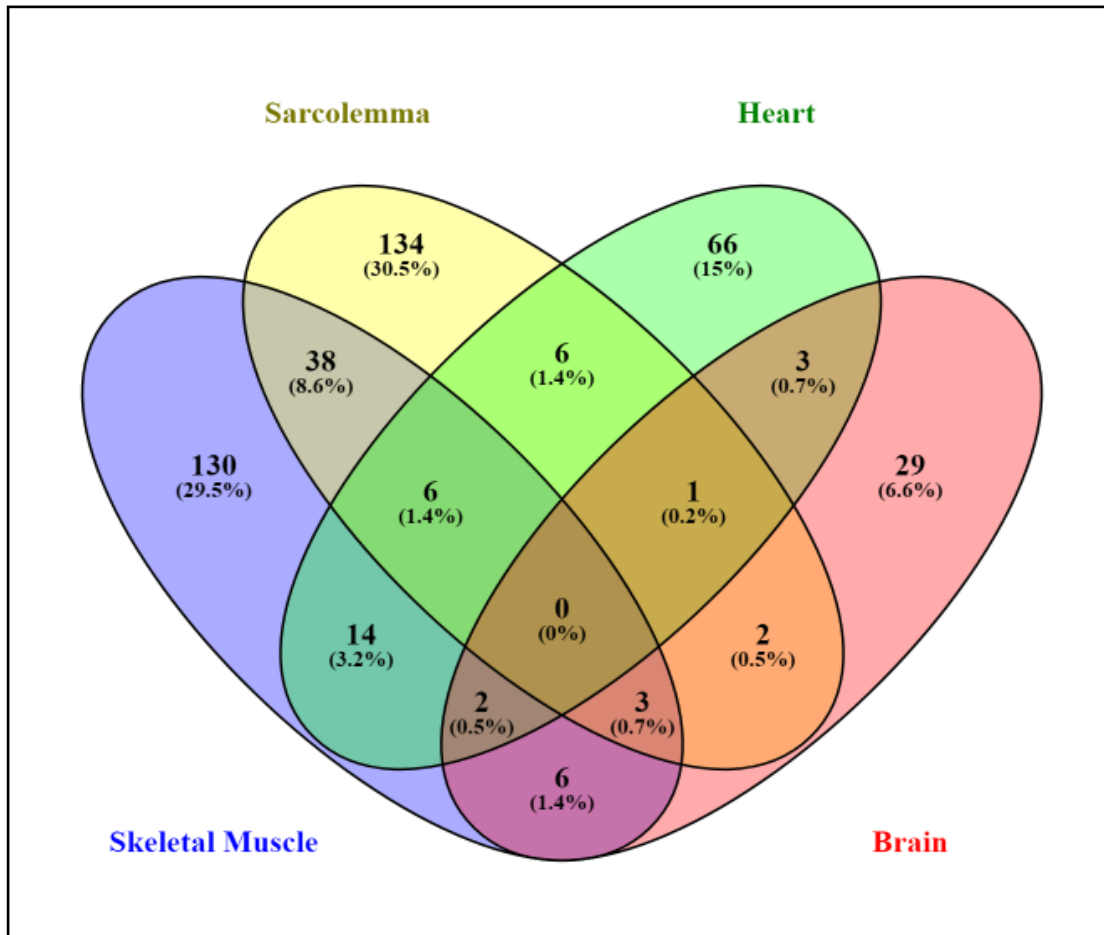


Figure 8.2 Cross-comparison of differentially abundant proteins in tissue proteomic studies

Venn diagram analysis was used to determine which differentially abundant proteins from the skeletal muscle, sarcolemma-enriched, cardiac and brain tissue proteomes described in Chapters 3, 4, 5 and 6 are shared by more than one dystrophic proteome.

*Image was generated using Oliveros, J.C. (2007-2015) Venny. An interactive tool for comparing lists with Venn's diagrams.

<http://bioinfogp.cnb.csic.es/tools/venny/index.html>

Table 8.1: Shown are the 12 proteins detected by label-free mass spectrometric analysis to have altered abundance in three of four dystrophic proteomes; 6-month old crude skeletal muscle, 5-month old sarcolemma, 20-month old heart, and 12-month old brain

Accession	Protein Name	Skeletal Muscle	Sarcolemma	Heart	Brain
P11531	Dystrophin	14.6-fold decrease	2,708.2-fold decrease	8.6-fold decrease	-
Q8VDD5	Myosin-9	15.8-fold increase	4.6-fold increase	4.1-fold increase	-
Q8VDN2	Sodium/potassium-transporting ATPase subunit alpha-1	6.1-fold increase	2.0-fold increase	1.7-fold decrease	-
P01872	Ig mu chain C region	3.7-fold increase	7.4-fold increase	2.2-fold decrease	-
Q8VHX6	Filamin-C	2.1-fold increase	5.1-fold increase	1.4-fold decrease	-
P14602	Heat shock protein beta-1	2.0-fold increase	2.2-fold increase	1.6-fold increase	-
Q9D0E1	Heterogeneous nuclear ribonucleoprotein M	-	32.3-fold increase	1.5-fold increase	1.44-fold increase
Q00623	Apolipoprotein A-I	4.6-fold increase	-	2.3-fold increase	2.9-fold increase
P16546	Spectrin alpha chain, non-erythrocytic 1	3.7-fold increase	-	3.1-fold increase	1.2-fold increase
Q03265	ATP synthase subunit alpha, mitochondrial	2.1-fold increase	2.6-fold decrease	-	1.3-fold increase
P20152	Vimentin	2.4-fold increase	2.5-fold increase	-	1.6-fold increase
P48036	Annexin A5	2.7-fold increase	2.5-fold increase	-	1.6-fold increase

Proteomics is an evolving field, with major advances including the emergence of 2D-DIGE which greatly reduced issues of reproducibility and gel-to-gel variability, and LC-MS/MS which offers an alternative to gel-based approaches which have limited resolving power for large proteins, hydrophobic proteins and those with extreme *pI* values. Thus, the integration of gel-based and liquid chromatography-based mass spectrometry can provide complementary information in the quest to characterise complete proteomes. Discovery proteomics is frequently employed as an initial tool to identify and quantify the protein components of a biological system, and such analyses typically use data-dependent acquisition (DDA), where only the most abundant precursor ions are selected for fragmentation (Collins et al., 2017). As a result, precursor ion selection is stochastic, and this can lead to issues with irreproducibility and missing values in proteomics datasets, whereby a peptide may be detected in some but not all the samples analysed. An alternative emerging approach is that of data-independent acquisition (DIA), of which SWATH (sequential window acquisition of all theoretical fragment ion spectra) mass spectrometry is one of the most widely used. In this method all precursor ions within a user defined *m/z* window are fragmented, thus eliminating the stochastic nature of DDA. Protein identification is achieved using targeted data extraction to query the acquired fragment ion maps for the presence and quantity of specific peptides, using *a priori* information contained in spectral libraries (Gillet et al., 2012). This type of DIA mass spectrometry may be particularly suited to the analysis of skeletal muscle proteomes, where the extensive dynamic range between the most highly abundant proteins such as the contractile proteins and low abundance proteins such as signalling molecules, limits the detection of lower abundance proteins in DDA mass spectrometry (Ohlendieck, 2011c).

Ebhardt and co-workers have recently applied SWATH mass spectrometry to skeletal muscle proteomics of cancer-induced muscle wasting (cancer cachexia) and found the cancer cachexia proteome to be distinct from all other investigated control groups (weight-stable cancer, healthy non-sarcopenic and age-related sarcopenia). Three distinct protein networks were found to distinguish cancer cachexia from all other groups; the Fo complex, electron transport chain and contractile fibre (Ebhardt et al., 2017). Given the success of this pilot study, SWATH mass spectrometry could now be applied in the analysis of other neuromuscular disorders, including DMD. Such an approach may give unprecedented depth of coverage of alterations in the skeletal muscle proteome in health and disease and may offer new insights into the

disease mechanisms and identify possible therapeutic targets. SWATH mass spectrometry could also be used for the analysis of serum/plasma samples in biomarker-based studies as it may circumvent the issue of high dynamic range of proteins in serum/plasma which is a current limiting factor in their analysis by mass spectrometry.

The proteomic characterisation of the *mdx-4v* animal model of DMD described here has identified numerous biomarker candidates with potential applications for the improved diagnosis, prognosis and therapy monitoring of dystrophinopathy. However, despite an increasing number of proteomic studies identifying novel protein biomarker candidates, few of these discovered biomarkers have been incorporated into routine clinical care. One of the major bottlenecks in the biomarker pipeline is the verification of candidates generated in discovery-phase studies. Currently, verification of potential biomarkers is performed with established immunoassay such as ELISA, however such assays are dependent on the availability of antibodies, and development of a new ELISA is time-consuming and expensive (Makawita and Diamandis, 2010). An alternative approach which can simultaneously quantify numerous proteins in parallel and which can be developed for all novel candidates of interest is multiple reaction monitoring (MRM) mass spectrometry. In MRM typically 3-5 proteotypic peptides are picked to serve as representations of the intact protein of interest. For each peptide the mass-to-charge ratio (m/z) of the precursor ion and its optimum product ions is known, is referred to as a “transition” and is used to select for the target peptide. In a typical MRM mass spectrometry analysis, the sample of interest, for example serum, is added to the LC-MS/MS system and only the precursor ions of the target protein are selected and subjected to fragmentation. The optimum product ions are then selected and quantified. Peptide intensities can subsequently be compared between two experimental conditions for relative quantification or to reference intensities generated by standards of known concentration for absolute quantification (Meng and Veenstra, 2011). MRM is currently being investigated for its use in clinical proteomics as a means of biomarker verification in a number of diseases. Kim and co-workers used MRM to evaluate 12 biomarker candidates for diabetic retinopathy that they had previously identified in a discovery study (Kim et al., 2010). In oncology studies, a similar approach to MRM known as parallel reaction monitoring (PRM) has been used to verify differential abundance of the activation peptide of the coagulation factor XIII in serum samples of colorectal cancer. PRM analysis revealed statistically significant

differences in the abundance of this peptide between control and colorectal samples and showed a diagnostic accuracy of 0.93 in a cohort of 73 samples (27 cancer patients and 46 controls), confirming the potential use of this peptide as a serum biomarker of colorectal cancer (Peltier et al., 2018). Future studies in muscular dystrophy research could harness the potential of MRM and PRM mass spectrometry for the relatively high-throughput verification of previously identified serum/plasma and tissue candidate biomarkers. The most promising candidates could then be further verified by immunoassays and potentially be translated for clinical use. Such an approach may help overcome the bottleneck in the biomarker pipeline and result in tangible health benefits for muscular dystrophy patients.

Proteomic analysis of skeletal muscle, aged heart tissue, serum and saliva samples from the *mdx-4cv* mouse model of DMD has revealed increased abundance of numerous proteins associated with extracellular matrix remodelling and fibrosis. Thus, tackling fibrosis represents a clear therapeutic target to help improve muscle function. Anti-fibrotic research has been mainly conducted with *mdx* mice, where studies have largely focused on i) blocking fibrotic cytokine signalling to reduce gene expression and protein synthesis of extracellular matrix proteins, ii) suppressing inflammation to reduce the production of pro-fibrotic cytokines and iii) promoting muscle regeneration (Zhou and Lu, 2010). An interesting new area of fibrosis research which may be applicable to DMD is the use of *in vitro* models of fibrosis. Engineered tissues can serve as excellent models to mimic tissue fibrosis, to give insights into the response of cells and the extracellular matrix to individual stimuli, and to facilitate the screening of new therapeutics (van Spreeuwel et al., 2017). A cardiac micro-tissue platform consisting of an extracellular matrix containing hydrogel with a mixture of cardiomyocytes and fibroblasts was used to recapitulate cardiac fibrosis, where altering either the number of fibroblasts or the amount of collagen was performed to mimic the different features of fibrosis. Measuring the dynamic contraction force of the micro-tissues revealed that while increasing collagen accumulation had no effect on contraction, contraction force was significantly decreased in response to increased numbers of fibroblasts. The average beating frequency also decreased significantly in micro-tissues containing more than 50% fibroblasts (van Spreeuwel et al., 2017). Liver fibrosis and cirrhosis are major risk factors for liver failure and the development of liver cancer. Currently, one of the most popular *in vitro* models of liver fibrosis is the culture of hepatic stellate cells (HSC) on plastic tissue culture dishes in the presence

of serum which induces trans-differentiation to myofibroblasts (van Grunsven, 2017). However, while HSC activation can be achieved through culture, the mechanisms by which it is mediated is thought to differ substantially from *in vivo* HSC activation. Therefore, intense research has aimed to produce 3D tissue models. While further optimisation is still required, hepatocyte damage-induced HSC activation and fibrosis has been reported in precision-cut liver slice cultures, bio-printed liver tissue cultures, and co-cultured spheroids (van Grunsven, 2017). The engineering of skeletal muscle for *in vitro* screening is likely to be highly complex given that engineered skeletal muscle tissue will require the generation of a microenvironment that provides anisotropic cues to promote uniaxial alignment, 3D matrices to provide a biomimetic microenvironment, mechanical and electrical stimuli, and interaction with support cells and tissues such as endothelial cells and motor neurons of the peripheral nervous system (Smith et al., 2016).

However, given that a large number of different mutations in the dystrophin gene have been discovered so far in patients with DMD (Bladen et al., 2015), and this heterogeneity cannot be currently modelled by animal models, patient-specific dystrophic myotubes derived from human induced pluripotent stem cells (iPSCs) could revolutionise the field of muscular dystrophy research. iPSCs are an extremely useful research tool as they can provide a limitless supply of cells that can be differentiated into a range of cell types and retain the genotype and phenotype of the donor. Gaun and co-workers have successfully created beating cardiomyocytes using iPSCs generated from urine-derived stem cells from healthy volunteers and a Duchenne patient (Guan et al., 2014). Dystrophin expression was undetectable in DMD iPSC cardiomyocytes by immunofluorescence and by immunoblotting demonstrating that these cells retained their dystrophic phenotype. In addition, DMD iPSC cardiomyocytes showed abnormal Ca^{2+} handling and increased susceptibility to mechanical stress compared to iPSC cardiomyocytes derived from healthy controls (Guan et al., 2014). A model for cardiomyopathy was chosen as experimental protocols to differentiate stem cells to cardiomyocytes are more advanced than similar approaches available for the generation of skeletal muscle. However, Chal and colleagues could differentiate striated, contractile fibres supporting a niche of Pax7⁺ cells that resemble satellite cells from embryonic stem cells and human iPSCs (Chal et al., 2015). Muscle fibres derived from embryonic stem cells of the *mdx* mouse

showed an abnormal branched phenotype typical of that described *in vivo*. Advances in tissue-engineering strategies coupled with emerging iPSC-related technologies suggests the ability to generate *in vitro* disease models of human muscle tissue. While still in its infancy, such an approach has the potential to revolutionise mechanistic studies, drug discovery and personalised medicine. Given recent successes in generating models of cardiac and liver fibrosis, this may also be extended to modelling cardiac and skeletal muscle fibrosis associated with DMD.

8.1.1 Concluding Remarks

Mass spectrometry-based proteomics has been used extensively throughout this work to characterise the *mdx-4cv* mouse model of DMD. This approach has helped to improve understanding of the molecular mechanisms underlying the disease pathogenesis in skeletal muscle, the sarcolemma, the aged heart and the brain. The differentially abundant proteins identified in these tissue proteomic studies give insights into the disease pathophysiology, identify potential therapeutic targets and may also be useful as biomarker candidates for the superior diagnosis, prognosis and therapy-monitoring of DMD. Since minimally invasive and non-invasive biomarkers are preferable to those obtained through invasive muscle biopsy, proteomic profiling was also performed on serum and saliva samples from the *mdx-4cv* mouse. These studies particularly identified certain muscle-derived proteins, haptoglobin, and kallikrein-1 as potential biomarker candidates of interest. To further progress this work, validation is required in a large cohort of clinical samples. In addition, ideally a multi-omics approach should be undertaken, integrating genomics, transcriptomics, proteomics and metabolomics to give a full picture of the dystrophic phenotype (Hasin et al., 2017).

In the future, advances in mass spectrometry analyses such as SWATH and MRM mass spectrometry may expand the field of muscle proteomics and enable near-to-complete proteome characterisation. In addition, novel strategies such as the use of engineered muscle tissue and iPSCs may drive muscular dystrophy research forward towards an improved understanding of dystrophic disease mechanisms and facilitate *in vitro* drug screening and personalised medicine. The ultimate aim of muscular dystrophy research is to improve the quality of life of patients with Duchenne muscular dystrophy and ultimately provide a therapy or cure. The research presented here is a first step in reaching that goal.

Chapter Nine

Bibliography

9 Bibliography

- AAGAARD, P., SUETTA, C., CASEROTTI, P., MAGNUSSON, S. P. & KJAER, M. 2010. Role of the nervous system in sarcopenia and muscle atrophy with aging: strength training as a countermeasure. *Scand J Med Sci Sports*, 20, 49-64.
- AARTSMA-RUS, A. 2014. Dystrophin Analysis in Clinical Trials. *J Neuromuscul Dis*, 1, 41-53.
- AARTSMA-RUS, A. & VAN OMMEN, G. J. 2007. Antisense-mediated exon skipping: a versatile tool with therapeutic and research applications. *RNA*, 13, 1609-24.
- ABDEL, S. E., ABDEL-MEGUID, I. & KORRAA, S. 2007. Markers of oxidative stress and aging in Duchene muscular dystrophy patients and the possible ameliorating effect of He:Ne laser. *Acta Myol*, 26, 14-21.
- ABELL, E., AHRENDTS, R., BANDARA, S., PARK, B. O. & TERUEL, M. N. 2011. Parallel adaptive feedback enhances reliability of the Ca²⁺ signaling system. *Proc Natl Acad Sci USA*, 108, 14485-90.
- ACHARYA, K. R. & ACKERMAN, S. J. 2014. Eosinophil granule proteins: form and function. *J Biol Chem*, 289, 17406-15.
- ACUÑA, M. J., SALAS, D., CORDOVA-CASANOVA, A., CRUZ-SOCA, M., CÉSPEDES, C., VIO, C. P. & BRANDAN, E. 2017. Blockade of Bradykinin receptors worsens the dystrophic phenotype of mdx mice: differential effects for B1 and B2 receptors. *J Cell Commun Signal*. <https://doi.org/10.1007/s12079-017-0439-x>
- ADAMS, M. E., BUTLER, M. H., DWYER, T. M., PETERS, M. F., MURNANE, A. A. & FROEHLER, S. C. 1993. Two forms of mouse syntrophin, a 58 kd dystrophin-associated protein, differ in primary structure and tissue distribution. *Neuron*, 11, 531-40.
- ADAMS, M. E., MUELLER, H. A. & FROEHLER, S. C. 2001. In vivo requirement of the alpha-syntrophin PDZ domain for the sarcolemmal localization of nNOS and aquaporin-4. *J Cell Biol*, 155, 113-22.
- ADORNATO, B. T., ENGEL, W. K. & FOIDART-DESALLE, M. 1978. Elevations of hemopexin levels in neuromuscular disease. *Arch Neurol*, 35, 577-80.
- AHN, A. H. & KUNKEL, L. M. 1995. Syntrophin binds to an alternatively spliced exon of dystrophin. *J Cell Biol*, 128, 363-71.
- ALDERTON, J. M. & STEINHARDT, R. A. 2000. Calcium influx through calcium leak channels is responsible for the elevated levels of calcium-dependent proteolysis in dystrophic myotubes. *J Biol Chem*, 275, 9452-60.
- ALLSOPP, R. C., VAZIRI, H., PATTERSON, C., GOLDSTEIN, S., YOUNGLAI, E. V., FUTCHER, A. B., GREIDER, C. W. & HARLEY, C. B. 1992. Telomere length predicts replicative capacity of human fibroblasts. *Proc Natl Acad Sci USA*, 89, 10114-8.
- ALMKVIST, J. & KARLSSON, A. 2002. Galectins as inflammatory mediators. *Glycoconj J*, 19, 575-81.
- ALPER, C. A., PETERS, J. H., BIRTCH, A. G. & GARDNER, F. H. 1965. Haptoglobin synthesis. I. In vivo studies of the production of haptoglobin, fibrinogen, and gamma-globulin by the canine liver. *J Clin Invest*, 44, 574-81.
- ALTER, J., LOU, F., RABINOWITZ, A., YIN, H., ROSENFELD, J., WILTON, S. D., PARTRIDGE, T. A. & LU, Q. L. 2006. Systemic delivery of morpholino oligonucleotide restores dystrophin expression bodywide and improves dystrophic pathology. *Nat Med*, 12, 175-7.
- AMARA, U., RITTIRSCH, D., FLIERL, M., BRUCKNER, U., KLOS, A., GEBHARD, F., LAMBRIS, J. D. & HUBER-LANG, M. 2008. Interaction between the coagulation and complement system. *Adv Exp Med Biol*, 632, 71-9.

- AMENTA, A. R., YILMAZ, A., BOGDANOVICH, S., MCKECHNIE, B. A., ABEDI, M., KHURANA, T. S. & FALLON, J. R. 2011. Biglycan recruits utrophin to the sarcolemma and counters dystrophic pathology in mdx mice. *Proc Natl Acad Sci USA*, 108, 762-7.
- ANDERSEN, J. S., LAM, Y. W., LEUNG, A. K., ONG, S. E., LYON, C. E., LAMOND, A. I. & MANN, M. 2005. Nucleolar proteome dynamics. *Nature*, 433, 77-83.
- ANDERSON, J. E. & VARGAS, C. 2003. Correlated NOS-Imu and myf5 expression by satellite cells in mdx mouse muscle regeneration during NOS manipulation and deflazacort treatment. *Neuromuscul Disord*, 13, 388-96.
- ANDERSON, J. E., MCINTOSH, L. M. & POETTCKER, R. 1996. Deflazacort but not prednisone improves both muscle repair and fiber growth in diaphragm and limb muscle in vivo in the mdx dystrophic mouse. *Muscle Nerve*, 19, 1576-85.
- ANDERSON, N. L. & ANDERSON, N. G. 2002. The human plasma proteome: history, character, and diagnostic prospects. *Mol Cell Proteomics*, 1, 845-67.
- ANDREASEN, N. & BLENNOW, K. 2005. CSF biomarkers for mild cognitive impairment and early Alzheimer's disease. *Clin Neurol Neurosurg*, 107, 165-73.
- ANGELINI, C. & PETERLE, E. 2012. Old and new therapeutic developments in steroid treatment in Duchenne muscular dystrophy. *Acta Myol*, 31, 9-15.
- ANTHONY, K., ARECHAVALA-GOMEZA, V., TAYLOR, L. E., VULIN, A., KAMINOH, Y., TORELLI, S., FENG, L., JANGHRA, N., BONNE, G., BEUVIN, M., BARRESI, R., HENDERSON, M., LAVAL, S., LOURBAKOS, A., CAMPION, G., STRAUB, V., VOIT, T., SEWRY, C. A., MORGAN, J. E., FLANIGAN, K. M. & MUNTONI, F. 2014. Dystrophin quantification: Biological and translational research implications. *Neurology*, 83, 2062-9.
- AOKI, Y., NAKAMURA, A., YOKOTA, T., SAITO, T., OKAZAWA, H., NAGATA, T. & TAKEDA, S. 2010. In-frame dystrophin following exon 51-skipping improves muscle pathology and function in the exon 52-deficient mdx mouse. *Mol Ther*, 18, 1995-2005.
- ARANMOLATE, A., TSE, N. & COLOGNATO, H. 2017. Myelination is delayed during postnatal brain development in the mdx mouse model of Duchenne muscular dystrophy. *BMC Neurosci*, 18, 63.
- ARMSTRONG, C. T., ANDERSON, J. L. & DENTON, R. M. 2014. Studies on the regulation of the human E1 subunit of the 2-oxoglutarate dehydrogenase complex, including the identification of a novel calcium-binding site. *Biochem J*, 459, 369-81.
- AU, C. G., BUTLER, T. L., SHERWOOD, M. C., EGAN, J. R., NORTH, K. N. & WINLAW, D. S. 2011. Increased connective tissue growth factor associated with cardiac fibrosis in the mdx mouse model of dystrophic cardiomyopathy. *Int J Exp Pathol*, 92, 57-65.
- AYOGLU, B., CHAOUCH, A., LOCHMÜLLER, H., POLITANO, L., BERTINI, E., SPITALI, P., HILLER, M., NIKS, E. H., GUALANDI, F., PONTÉN, F., BUSHBY, K., AARTSMA-RUS, A., SCHWARTZ, E., LE PRIOL, Y., STRAUB, V., UHLÉN, M., CIRAK, S., THOEN, P. A., MUNTONI, F., FERLINI, A., SCHWENK, J. M., NILSSON, P. & AL-KHALILI SZIGYARTO, C. 2014. Affinity proteomics within rare diseases: a BIO-NMD study for blood biomarkers of muscular dystrophies. *EMBO Mol Med*, 6, 918-36.
- BADALAMENTE, M. A. & STRACHER, A. 2000. Delay of muscle degeneration and necrosis in mdx mice by calpain inhibition. *Muscle Nerve*, 23, 106-11.
- BADOLATO, R., WANG, J. M., MURPHY, W. J., LLOYD, A. R., MICHIEL, D. F., BAUSSERMAN, L. L., KELVIN, D. J. & OPPENHEIM, J. J. 1994. Serum amyloid A is a chemoattractant: induction of migration, adhesion, and tissue infiltration of monocytes and polymorphonuclear leukocytes. *J Exp Med*, 180, 203-9.

- BAHIA EL IDRISSE, N., BOSCH, S., RAMAGLIA, V., ARONICA, E., BAAS, F. & TROOST, D. 2016. Complement activation at the motor end-plates in amyotrophic lateral sclerosis. *J Neuroinflammation*, 13, 72.
- BAKKAR, N., WANG, J., LADNER, K. J., WANG, H., DAHLMAN, J. M., CARATHERS, M., ACHARYYA, S., RUDNICKI, M. A., HOLLENBACH, A. D. & GUTTRIDGE, D. C. 2008. IKK/NF-kappaB regulates skeletal myogenesis via a signaling switch to inhibit differentiation and promote mitochondrial biogenesis. *J Cell Biol*, 180, 787-802.
- BALABAN, B., MATTHEWS, D. J., CLAYTON, G. H. & CARRY, T. 2005. Corticosteroid treatment and functional improvement in Duchenne muscular dystrophy: long-term effect. *Am J Phys Med Rehabil*, 84, 843-50.
- BAMBURG, J. R. & WIGGAN, O. P. 2002. ADF/cofilin and actin dynamics in disease. *Trends Cell Biol*, 12, 598-605.
- BANSAL, D. & CAMPBELL, K. P. 2004. Dysferlin and the plasma membrane repair in muscular dystrophy. *Trends Cell Biol*, 14, 206-13.
- BARTLETT, R. J., STOCKINGER, S., DENIS, M. M., BARTLETT, W. T., INVERARDI, L., LE, T. T., THI MAN, N., MORRIS, G. E., BOGAN, D. J., METCALF-BOGAN, J. & KORNEGAY, J. N. 2000. In vivo targeted repair of a point mutation in the canine dystrophin gene by a chimeric RNA/DNA oligonucleotide. *Nat Biotechnol*, 18, 615-22.
- BATCHELOR, C. L. & WINDER, S. J. 2006. Sparks, signals and shock absorbers: how dystrophin loss causes muscular dystrophy. *Trends Cell Biol*, 16, 198-205.
- BEACH, J. R., SHAO, L., REMMERT, K., LI, D., BETZIG, E. & HAMMER, J. A. 2014. Nonmuscle myosin II isoforms coassemble in living cells. *Curr Biol*, 24, 1160-6.
- BEENAKKER, E. A., FOCK, J. M., VAN TOL, M. J., MAURITS, N. M., KOOPMAN, H. M., BROUWER, O. F. & VAN DER HOEVEN, J. H. 2005. Intermittent prednisone therapy in Duchenne muscular dystrophy: a randomized controlled trial. *Arch Neurol*, 62, 128-32.
- BELLIN, R. M., SERNETT, S. W., BECKER, B., IP, W., HUIATT, T. W. & ROBSON, R. M. 1999. Molecular characteristics and interactions of the intermediate filament protein synemin. Interactions with alpha-actinin may anchor synemin-containing heterofilaments. *J Biol Chem*, 274, 29493-9.
- BENGTSSON, N. E., HALL, J. K., ODOM, G. L., PHELPS, M. P., ANDRUS, C. R., HAWKINS, R. D., HAUSCHKA, S. D., CHAMBERLAIN, J. R. & CHAMBERLAIN, J. S. 2017. Muscle-specific CRISPR/Cas9 dystrophin gene editing ameliorates pathophysiology in a mouse model for Duchenne muscular dystrophy. *Nat Commun*, 8, 14454.
- BENSON, M. A., NEWEY, S. E., MARTIN-RENDON, E., HAWKES, R. & BLAKE, D. J. 2001. Dysbindin, a novel coiled-coil-containing protein that interacts with the dystrobrevins in muscle and brain. *J Biol Chem*, 276, 24232-41.
- BERNASCONI, P., TORCHIANA, E., CONFALONIERI, P., BRUGNONI, R., BARRESI, R., MORA, M., CORNELIO, F., MORANDI, L. & MANTEGAZZA, R. 1995. Expression of transforming growth factor-beta 1 in dystrophic patient muscles correlates with fibrosis. Pathogenetic role of a fibrogenic cytokine. *J Clin Invest*, 96, 1137-44.
- BERTIN, P., TREVES, R., JULIA, A., GAILLARD, S. & DESPROGES-GOTTERON, R. 1989. Ehlers-Danlos syndrome, clotting disorders and muscular dystrophy. *Ann Rheum Dis*, 48, 953-6.
- BHOSLE, R. C., MICHELE, D. E., CAMPBELL, K. P., LI, Z. & ROBSON, R. M. 2006. Interactions of intermediate filament protein synemin with dystrophin and utrophin. *Biochem Biophys Res Commun*, 346, 768-77.

- BICKEL, P. E., SCHERER, P. E., SCHNITZER, J. E., OH, P., LISANTI, M. P. & LODISH, H. F. 1997. Flotillin and epidermal surface antigen define a new family of caveolae-associated integral membrane proteins. *J Biol Chem*, 272, 13793-802.
- BILLARD, C., GILLET, P., SIGNORET, J. L., UICAUT, E., BERTRAND, P., FARDEAU, M., BARTHEZ-CARPENTIER, M. A. & SANTINI, J. J. 1992. Cognitive functions in Duchenne muscular dystrophy: a reappraisal and comparison with spinal muscular atrophy. *Neuromuscul Disord*, 2, 371-8.
- BLADEN, C. L., SALGADO, D., MONGES, S., FONCUBERTA, M. E., KEKOU, K., KOSMA, K., DAWKINS, H., LAMONT, L., ROY, A. J., CHAMOVA, T., GUERGUELTCHEVA, V., CHAN, S., KORNGUT, L., CAMPBELL, C., DAI, Y., WANG, J., BARIŠIĆ, N., BRABEC, P., LAHDETIE, J., WALTER, M. C., SCHREIBER-KATZ, O., KARCAGI, V., GARAMI, M., VISWANATHAN, V., BAYAT, F., BUCCELLA, F., KIMURA, E., KOEKS, Z., VAN DEN BERGEN, J. C., RODRIGUES, M., ROXBURGH, R., LUSAKOWSKA, A., KOSTERA-PRUSZCZYK, A., ZIMOWSKI, J., SANTOS, R., NEAGU, E., ARTEMIEVA, S., RASIC, V. M., VOJINOVIC, D., POSADA, M., BLOETZER, C., JEANNET, P. Y., JONCOURT, F., DÍAZ-MANERA, J., GALLARDO, E., KARADUMAN, A. A., TOPALOĞLU, H., EL SHERIF, R., STRINGER, A., SHATILLO, A. V., MARTIN, A. S., PEAY, H. L., BELLGARD, M. I., KIRSCHNER, J., FLANIGAN, K. M., STRAUB, V., BUSHBY, K., VERSCHUUREN, J., AARTSMA-RUS, A., BÉROUD, C. & LOCHMÜLLER, H. 2015. The TREAT-NMD DMD Global Database: analysis of more than 7,000 Duchenne muscular dystrophy mutations. *Hum Mutat*, 36, 395-402.
- BLAKE, D. J., WEIR, A., NEWHEY, S. E. & DAVIES, K. E. 2002. Function and genetics of dystrophin and dystrophin-related proteins in muscle. *Physiol Rev*, 82, 291-329.
- BODENSTEINER, J. B. & ENGEL, A. G. 1978. Intracellular calcium accumulation in Duchenne dystrophy and other myopathies: a study of 567,000 muscle fibers in 114 biopsies. *Neurology*, 28, 439-46.
- BOGDANOVICH, S., KRAG, T. O., BARTON, E. R., MORRIS, L. D., WHITTEMORE, L. A., AHIMA, R. S. & KHURANA, T. S. 2002. Functional improvement of dystrophic muscle by myostatin blockade. *Nature*, 420, 418-21.
- BOGGS, J. M. 2006. Myelin basic protein: a multifunctional protein. *Cell Mol Life Sci*, 63, 1945-61.
- BONIFATI, M. D., RUZZA, G., BONOMETTO, P., BERARDINELLI, A., GORNI, K., ORCESI, S., LANZI, G. & ANGELINI, C. 2000. A multicenter, double-blind, randomized trial of deflazacort versus prednisone in Duchenne muscular dystrophy. *Muscle Nerve*, 23, 1344-7.
- BORGOÑO, C. A. & DIAMANDIS, E. P. 2004. The emerging roles of human tissue kallikreins in cancer. *Nat Rev Cancer*, 4, 876-90.
- BOUTER, A., GOUNOU, C., BÉRAT, R., TAN, S., GALLOIS, B., GRANIER, T., D'ESTAINTOT, B. L., PÖSCHL, E., BRACHVOGEL, B. & BRISSON, A. R. 2011. Annexin-A5 assembled into two-dimensional arrays promotes cell membrane repair. *Nat Commun*, 2, 270.
- BOYD, Y., BUCKLE, V., HOLT, S., MUNRO, E., HUNTER, D. & CRAIG, I. 1986. Muscular dystrophy in girls with X;autosomal translocations. *J Med Genet*, 23, 484-90.
- BOYER, J. G., BERNSTEIN, M. A. & BOUDREAU-LARIVIÈRE, C. 2010. Plakins in striated muscle. *Muscle Nerve*, 41, 299-308.
- BOYLE, A. J., SHIH, H., HWANG, J., YE, J., LEE, B., ZHANG, Y., KWON, D., JUN, K., ZHENG, D., SIEVERS, R., ANGELI, F., YEGHIAZARIANS, Y. & LEE, R. 2011. Cardiomyopathy of aging in the mammalian heart is characterized by myocardial hypertrophy, fibrosis and a predisposition towards cardiomyocyte apoptosis and autophagy. *Exp Gerontol*, 46, 549-59.
- BRADFORD, M. M. 1976. A rapid and sensitive method for the quantitation of microgram quantities of protein utilizing the principle of protein-dye binding. *Anal Biochem*, 72, 248-54.

- BRAHMACHARI, S., FUNG, Y. K. & PAHAN, K. 2006. Induction of glial fibrillary acidic protein expression in astrocytes by nitric oxide. *J Neurosci*, 26, 4930-9.
- BRAVO-CORDERO, J. J., MAGALHAES, M. A., EDDY, R. J., HODGSON, L. & CONDEELIS, J. 2013. Functions of cofilin in cell locomotion and invasion. *Nat Rev Mol Cell Biol*, 14, 405-15.
- BRESOLIN, N., CASTELLI, E., COMI, G. P., FELISARI, G., BARDONI, A., PERANI, D., GRASSI, F., TURCONI, A., MAZZUCHELLI, F. & GALLOTTI, D. 1994. Cognitive impairment in Duchenne muscular dystrophy. *Neuromuscul Disord*, 4, 359-69.
- BRIGUET, A., ERB, M., COURDIER-FRUH, I., BARZAGHI, P., SANTOS, G., HERZNER, H., LESCOPE, C., SIENDT, H., HENNEBOEHLE, M., WEYERMANN, P., MAGYAR, J. P., DUBACH-POWELL, J., METZ, G. & MEIER, T. 2008. Effect of calpain and proteasome inhibition on Ca²⁺-dependent proteolysis and muscle histopathology in the mdx mouse. *FASEB J*, 22, 4190-200.
- BRINKMEIER, H. & OHLENDIECK, K. 2014. Chaperoning heat shock proteins: proteomic analysis and relevance for normal and dystrophin-deficient muscle. *Proteomics Clin Appl*, 8, 875-95.
- BRINKMEYER-LANGFORD, C., CHU, C., BALOG-ALVAREZ, C., YU, X., CAI, J. J., NABITY, M. & KORNEGAY, J. N. 2018. Expression profiling of disease progression in canine model of Duchenne muscular dystrophy. *PLoS One*, 13, e0194485.
<https://doi.org/10.1371/journal.pone.0194485>
- BROERS, J. L., RAMAEKERS, F. C., BONNE, G., YAOU, R. B. & HUTCHISON, C. J. 2006. Nuclear lamins: laminopathies and their role in premature ageing. *Physiol Rev*, 86, 967-1008.
- BROWN, K. J., MARATHI, R., FIORILLO, A. A., CICCIMARO, E. F., SHARMA, S., ROWLANDS, D. S., RAYAVARAPU, S., NAGARAJU, K., HOFFMAN, E. P. & HATHOUT, Y. 2012. Accurate Quantitation of Dystrophin Protein in Human Skeletal Muscle Using Mass Spectrometry. *J Bioanal Biomed*, Suppl 7.
- BRUNN, A., SCHRÖDER, R. & DECKERT, M. 2006. The inflammatory reaction pattern distinguishes primary dysferlinopathies from idiopathic inflammatory myopathies: an important role for the membrane attack complex. *Acta Neuropathol*, 112, 325-32.
- BULFIELD, G., SILLER, W. G., WIGHT, P. A. & MOORE, K. J. 1984. X chromosome-linked muscular dystrophy (mdx) in the mouse. *Proc Natl Acad Sci USA*, 81, 1189-92.
- BUNAI, K. & YAMANE, K. 2005. Effectiveness and limitation of two-dimensional gel electrophoresis in bacterial membrane protein proteomics and perspectives. *J Chromatogr B Analyt Technol Biomed Life Sci*, 815, 227-36.
- BURKIN, D. J., WALLACE, G. Q., NICOL, K. J., KAUFMAN, D. J. & KAUFMAN, S. J. 2001. Enhanced expression of the alpha 7 beta 1 integrin reduces muscular dystrophy and restores viability in dystrophic mice. *J Cell Biol*, 152, 1207-18.
- BUSHBY, K., FINKEL, R., BIRNKRANT, D. J., CASE, L. E., CLEMENS, P. R., CRIPE, L., KAUL, A., KINNETT, K., MCDONALD, C., PANDYA, S., POYSKY, J., SHAPIRO, F., TOMEZSKO, J., CONSTANTIN, C. & GROUP, D. C. C. W. 2010. Diagnosis and management of Duchenne muscular dystrophy, part 1: diagnosis, and pharmacological and psychosocial management. *Lancet Neurol*, 9, 77-93.
- BUSHBY, K., FINKEL, R., WONG, B., BAROHN, R., CAMPBELL, C., COMI, G. P., CONNOLLY, A. M., DAY, J. W., FLANIGAN, K. M., GOEMANS, N., JONES, K. J., MERCURI, E., QUINLIVAN, R., RENFROE, J. B., RUSSMAN, B., RYAN, M. M., TULINIUS, M., VOIT, T., MOORE, S. A., LEE SWEENEY, H., ABRESCH, R. T., COLEMAN, K. L., EAGLE, M., FLORENCE, J., GAPPMAIER, E., GLANZMAN, A. M., HENRICSON, E., BARTH, J., ELFRING, G. L., REHA, A., SPIEGEL, R. J., O'DONNELL, M. W., PELTZ, S. W., MCDONALD, C. M. & GROUP, P.-G.-D. S. 2014. Ataluren treatment of patients with nonsense mutation dystrophinopathy. *Muscle Nerve*, 50, 477-87.

- CACCHIARELLI, D., LEGNINI, I., MARTONE, J., CAZZELLA, V., D'AMICO, A., BERTINI, E. & BOZZONI, I. 2011. miRNAs as serum biomarkers for Duchenne muscular dystrophy. *EMBO Mol Med*, 3, 258-65.
- CAI, B., SPENCER, M. J., NAKAMURA, G., TSENG-ONG, L. & TIDBALL, J. G. 2000. Eosinophilia of dystrophin-deficient muscle is promoted by perforin-mediated cytotoxicity by T cell effectors. *Am J Pathol*, 156, 1789-96.
- CAI, L., FRITZ, D., STEFANOVIC, L. & STEFANOVIC, B. 2010. Nonmuscle myosin-dependent synthesis of type I collagen. *J Mol Biol*, 401, 564-78.
- CALDERÓN, J. C., BOLAÑOS, P. & CAPUTO, C. 2014. The excitation-contraction coupling mechanism in skeletal muscle. *Biophys Rev*, 6, 133-160.
- CAMPBELL, K. P. & KAHL, S. D. 1989. Association of dystrophin and an integral membrane glycoprotein. *Nature*, 338, 259-62.
- CAMPBELL, K. P. & STULL, J. T. 2003. Skeletal muscle basement membrane-sarcolemma-cytoskeleton interaction minireview series. *J Biol Chem*, 278, 12599-600.
- CARBERRY, S., BRINKMEIER, H., ZHANG, Y., WINKLER, C. K. & OHLENDIECK, K. 2013. Comparative proteomic profiling of soleus, extensor digitorum longus, flexor digitorum brevis and interosseus muscles from the mdx mouse model of Duchenne muscular dystrophy. *Int J Mol Med*, 32, 544-56.
- CARBERRY, S., ZWEYER, M., SWANDULLA, D. & OHLENDIECK, K. 2014. Comparative proteomic analysis of the contractile-protein-depleted fraction from normal versus dystrophic skeletal muscle. *Anal Biochem*, 446, 108-15.
- CARBERRY, S., ZWEYER, M., SWANDULLA, D. & OHLENDIECK, K. 2012. Proteomics reveals drastic increase of extracellular matrix proteins collagen and dermatopontin in the aged mdx diaphragm model of Duchenne muscular dystrophy. *Int J Mol Med*, 30, 229-34.
- CARRETTA, D., SANTARELLI, M., VANNI, D., CIABATTI, S., SBRICCOLI, A., PINTO, F. & MINCIACCHI, D. 2003. Cortical and brainstem neurons containing calcium-binding proteins in a murine model of Duchenne's muscular dystrophy: selective changes in the sensorimotor cortex. *J Comp Neurol*, 456, 48-59.
- CASAR, J. C., MCKECHNIE, B. A., FALLON, J. R., YOUNG, M. F. & BRANDAN, E. 2004. Transient up-regulation of biglycan during skeletal muscle regeneration: delayed fiber growth along with decorin increase in biglycan-deficient mice. *Dev Biol*, 268, 358-71.
- CATHERMAN, A. D., SKINNER, O. S. & KELLEHER, N. L. 2014. Top Down proteomics: facts and perspectives. *Biochem Biophys Res Commun*, 445, 683-93.
- CERLETTI, M., NEGRI, T., COZZI, F., COLPO, R., ANDREETTA, F., CROCI, D., DAVIES, K. E., CORNELIO, F., POZZA, O., KARPATI, G., GILBERT, R. & MORA, M. 2003. Dystrophic phenotype of canine X-linked muscular dystrophy is mitigated by adenovirus-mediated utrophin gene transfer. *Gene Ther*, 10, 750-7.
- CHAL, J., OGINUMA, M., AL TANOURY, Z., GOBERT, B., SUMARA, O., HICK, A., BOUSSON, F., ZIDOUNI, Y., MURSCH, C., MONCUQUET, P., TASSY, O., VINCENT, S., MIYANARI, A., BERA, A., GARNIER, J. M., GUEVARA, G., HESTIN, M., KENNEDY, L., HAYASHI, S., DRAYTON, B., CHERRIER, T., GAYRAUD-MOREL, B., GUSSONI, E., RELAIX, F., TAJBAKSH, S. & POURQUIÉ, O. 2015. Differentiation of pluripotent stem cells to muscle fiber to model Duchenne muscular dystrophy. *Nat Biotechnol*, 33, 962-9.
- CHAMBERLAIN, J. S., METZGER, J., REYES, M., TOWNSEND, D. & FAULKNER, J. A. 2007. Dystrophin-deficient mdx mice display a reduced life span and are susceptible to spontaneous rhabdomyosarcoma. *FASEB J*, 21, 2195-204.

- CHAMOVA, T., GUERGUELTCHEVA, V., RAYCHEVA, M., TODOROV, T., GENOVA, J., BICHEV, S., BOJINOVA, V., MITEV, V., TOURNEV, I. & TODOROVA, A. 2013. Association between loss of dp140 and cognitive impairment in duchenne and becker dystrophies. *Balkan J Med Genet*, 16, 21-30.
- CHANG, C. I., LIAO, J. C. & KUO, L. 1998. Arginase modulates nitric oxide production in activated macrophages. *Am J Physiol*, 274, H342-8.
- CHANG, N. C., CHEVALIER, F. P. & RUDNICKI, M. A. 2016. Satellite Cells in Muscular Dystrophy - Lost in Polarity. *Trends Mol Med*, 22, 479-496.
- CHAPMAN, V. M., MILLER, D. R., ARMSTRONG, D. & CASKEY, C. T. 1989. Recovery of induced mutations for X chromosome-linked muscular dystrophy in mice. *Proc Natl Acad Sci USA*, 86, 1292-6.
- CHAUDHURY, A., CHANDER, P. & HOWE, P. H. 2010. Heterogeneous nuclear ribonucleoproteins (hnRNPs) in cellular processes: Focus on hnRNP E1's multifunctional regulatory roles. *RNA*, 16, 1449-62.
- CHEN, Z., HAGUE, C., HALL, R. A. & MINNEMAN, K. P. 2006. Syntrophins regulate alpha1D-adrenergic receptors through a PDZ domain-mediated interaction. *J Biol Chem*, 281, 12414-20.
- CHEUNG, K. J., LIBBRECHT, L., TILLEMANN, K., DEFORCE, D., COLLE, I. & VAN VLIERBERGHE, H. 2010. Galectin-3-binding protein: a serological and histological assessment in accordance with hepatitis C-related liver fibrosis. *Eur J Gastroenterol Hepatol*, 22, 1066-73.
- CHEVALLET, M., LUCHE, S. & RABILLOUD, T. 2006. Silver staining of proteins in polyacrylamide gels. *Nat Protoc*, 1, 1852-8.
- CHIAPPIN, S., ANTONELLI, G., GATTI, R. & DE PALO, E. F. 2007. Saliva specimen: a new laboratory tool for diagnostic and basic investigation. *Clin Chim Acta*, 383, 30-40.
- CHOCKALINGAM, P. S., GEE, S. H. & JARRETT, H. W. 1999. Pleckstrin homology domain 1 of mouse alpha 1-syntrophin binds phosphatidylinositol 4,5-bisphosphate. *Biochemistry*, 38, 5596-602.
- CHRISTOFOROU, A., MULVEY, C. M., BRECKELS, L. M., GELADAKI, A., HURRELL, T., HAYWARD, P. C., NAAKE, T., GATTO, L., VINER, R., MARTINEZ ARIAS, A. & LILLEY, K. S. 2016. A draft map of the mouse pluripotent stem cell spatial proteome. *Nat Commun*, 7, 8992.
- CLARK, K. A., MCELHINNY, A. S., BECKERLE, M. C. & GREGORIO, C. C. 2002. Striated muscle cytoarchitecture: an intricate web of form and function. *Annu Rev Cell Dev Biol*, 18, 637-706.
- CLARKE, J. L. & GOWERS, W. R. 1874. On a Case of Pseudo-hypertrophic Muscular Paralysis. *Med Chir Trans*, 57, 247-260.5.
- COENEN-STASS, A. M., MCCLOREY, G., MANZANO, R., BETTS, C. A., BLAIN, A., SALEH, A. F., GAIT, M. J., LOCHMÜLLER, H., WOOD, M. J. & ROBERTS, T. C. 2015. Identification of novel, therapy-responsive protein biomarkers in a mouse model of Duchenne muscular dystrophy by aptamer-based serum proteomics. *Sci Rep*, 5, 17014.
- COHEN, E. J., QUARTA, E., FULGENZI, G. & MINCIACCHI, D. 2015. Acetylcholine, GABA and neuronal networks: a working hypothesis for compensations in the dystrophic brain. *Brain Res Bull*, 110, 1-13.
- COLANGELO, A. M., CIRILLO, G., LAVITRANO, M. L., ALBERGHINA, L. & PAPA, M. 2012. Targeting reactive astrogliosis by novel biotechnological strategies. *Biotechnol Adv*, 30, 261-71.
- COLLINS, B. C., HUNTER, C. L., LIU, Y., SCHILLING, B., ROSENBERGER, G., BADER, S. L., CHAN, D. W., GIBSON, B. W., GINGRAS, A. C., HELD, J. M., HIRAYAMA-KUROGI, M., HOU, G., KRISP, C., LARSEN, B., LIN, L., LIU, S., MOLLOY, M. P., MORITZ, R. L., OHTSUKI, S., SCHLAPBACH, R., SELEVSEK, N., THOMAS, S. N., TZENG, S. C., ZHANG, H. & AEBERSOLD,

- R. 2017. Multi-laboratory assessment of reproducibility, qualitative and quantitative performance of SWATH-mass spectrometry. *Nat Commun*, 8, 291.
- COLUSSI, C., BANFI, C., BRIOSCHI, M., TREMOLI, E., STRAINO, S., SPALLOTTA, F., MAI, A., ROTILI, D., CAPOGROSSI, M. C. & GAETANO, C. 2010. Proteomic profile of differentially expressed plasma proteins from dystrophic mice and following suberoylanilide hydroxamic acid treatment. *Proteomics Clin Appl*, 4, 71-83.
- CONSTANTIN, B. 2014. Dystrophin complex functions as a scaffold for signalling proteins. *Biochim Biophys Acta*, 1838, 635-42.
- COTTON, S., VOUDOURIS, N. J. & GREENWOOD, K. M. 2001. Intelligence and Duchenne muscular dystrophy: full-scale, verbal, and performance intelligence quotients. *Dev Med Child Neurol*, 43, 497-501.
- COX, G. A., PHELPS, S. F., CHAPMAN, V. M. & CHAMBERLAIN, J. S. 1993a. New mdx mutation disrupts expression of muscle and nonmuscle isoforms of dystrophin. *Nat Genet*, 4, 87-93.
- COX, G. A., COLE, N. M., MATSUMURA, K., PHELPS, S. F., HAUSCHKA, S. D., CAMPBELL, K. P., FAULKNER, J. A. & CHAMBERLAIN, J. S. 1993b. Overexpression of dystrophin in transgenic mdx mice eliminates dystrophic symptoms without toxicity. *Nature*, 364, 725-9.
- COX, J., HEIN, M. Y., LUBER, C. A., PARON, I., NAGARAJ, N. & MANN, M. 2014. Accurate proteome-wide label-free quantification by delayed normalization and maximal peptide ratio extraction, termed MaxLFQ. *Mol Cell Proteomics*, 13, 2513-26.
- CROMPTON, M., VIRJI, S. & WARD, J. M. 1998. Cyclophilin-D binds strongly to complexes of the voltage-dependent anion channel and the adenine nucleotide translocase to form the permeability transition pore. *Eur J Biochem*, 258, 729-35.
- CROSBIE, R. H., HEIGHWAY, J., VENZKE, D. P., LEE, J. C. & CAMPBELL, K. P. 1997. Sarcospan, the 25-kDa transmembrane component of the dystrophin-glycoprotein complex. *J Biol Chem*, 272, 31221-4.
- CULLIGAN, K., BANVILLE, N., DOWLING, P. & OHLENDIECK, K. 2002. Drastic reduction of calsequestrin-like proteins and impaired calcium binding in dystrophic mdx muscle. *J Appl Physiol* (1985), 92, 435-45.
- CULLIGAN, K., GLOVER, L., DOWLING, P. & OHLENDIECK, K. 2001. Brain dystrophin-glycoprotein complex: persistent expression of beta-dystroglycan, impaired oligomerization of Dp71 and up-regulation of utrophins in animal models of muscular dystrophy. *BMC Cell Biol*, 2, 2.
- CULLY, T. R., EDWARDS, J. N., FRIEDRICH, O., STEPHENSON, D. G., MURPHY, R. M. & LAUNIKONIS, B. S. 2012. Changes in plasma membrane Ca-ATPase and stromal interacting molecule 1 expression levels for Ca(2+) signaling in dystrophic mdx mouse muscle. *Am J Physiol Cell Physiol*, 303, C567-76.
- CYNTHIA MARTIN, F., HILLER, M., SPITALI, P., OONK, S., DALEBOUT, H., PALMBLAD, M., CHAOUCH, A., GUGLIERI, M., STRAUB, V., LOCHMÜLLER, H., NIKS, E. H., VERSCHUUREN, J. J., AARTSMA-RUS, A., DEELDER, A. M., VAN DER BURGT, Y. E. & 'T HOEN, P. A. 2014. Fibronectin is a serum biomarker for Duchenne muscular dystrophy. *Proteomics Clin Appl*, 8, 269-78.
- DALAKAS, M. C. 1991. Polymyositis, dermatomyositis and inclusion-body myositis. *N Engl J Med*, 325, 1487-98.
- D'AMARIO, D., AMODEO, A., ADORISIO, R., TIZIANO, F. D., LEONE, A. M., PERRI, G., BRUNO, P., MASSETTI, M., FERLINI, A., PANE, M., NICCOLI, G., PORTO, I., D'ANGELO, G. A., BOROVAC, J. A., MERCURI, E. & CREA, F. 2017. A current approach to heart failure in Duchenne muscular dystrophy. *Heart*, 103, 1770-1779.

- D'ANGELO, M. G., LORUSSO, M. L., CIVATI, F., COMI, G. P., MAGRI, F., DEL BO, R., GUGLIERI, M., MOLteni, M., TURCONI, A. C. & BRESOLIN, N. 2011. Neurocognitive profiles in Duchenne muscular dystrophy and gene mutation site. *Pediatr Neurol*, 45, 292-9.
- DANKO, I., CHAPMAN, V. & WOLFF, J. A. 1992. The frequency of revertants in mdx mouse genetic models for Duchenne muscular dystrophy. *Pediatr Res*, 32, 128-31.
- DANOWSKI, B. A., IMANAKA-YOSHIDA, K., SANGER, J. M. & SANGER, J. W. 1992. Costameres are sites of force transmission to the substratum in adult rat cardiomyocytes. *J Cell Biol*, 118, 1411-20.
- DAOUD, F., ANGEARD, N., DEMERRE, B., MARTIE, I., BENYAOU, R., LETURCQ, F., COSSÉE, M., DEBURGRAVE, N., SAILLOUR, Y., TUFFERY, S., URTIZBEREA, A., TOUTAIN, A., ECHENNE, B., FRISCHMAN, M., MAYER, M., DESGUERRE, I., ESTOURNET, B., RÉVEILLÈRE, C., PENISSON-BESNIER, CUISSET, J. M., KAPLAN, J. C., HÉRON, D., RIVIER, F. & CHELLY, J. 2009. Analysis of Dp71 contribution in the severity of mental retardation through comparison of Duchenne and Becker patients differing by mutation consequences on Dp71 expression. *Hum Mol Genet*, 18, 3779-94.
- DAVIES, K. E., PEARSON, P. L., HARPER, P. S., MURRAY, J. M., O'BRIEN, T., SARFARAZI, M. & WILLIAMSON, R. 1983. Linkage analysis of two cloned DNA sequences flanking the Duchenne muscular dystrophy locus on the short arm of the human X chromosome. *Nucleic Acids Res*, 11, 2303-12.
- DECARY, S., HAMIDA, C. B., MOULY, V., BARBET, J. P., HENTATI, F. & BUTLER-BROWNE, G. S. 2000. Shorter telomeres in dystrophic muscle consistent with extensive regeneration in young children. *Neuromuscul Disord*, 10, 113-20.
- DECONINCK, A. E., RAFAEL, J. A., SKINNER, J. A., BROWN, S. C., POTTER, A. C., METZINGER, L., WATT, D. J., DICKSON, J. G., TINSLEY, J. M. & DAVIES, K. E. 1997. Utrophin-dystrophin-deficient mice as a model for Duchenne muscular dystrophy. *Cell*, 90, 717-27.
- DECONINCK, N. & DAN, B. 2007. Pathophysiology of duchenne muscular dystrophy: current hypotheses. *Pediatr Neurol*, 36, 1-7.
- DELANGHE, J. R. & LANGLOIS, M. R. 2001. Hemopexin: a review of biological aspects and the role in laboratory medicine. *Clin Chim Acta*, 312, 13-23.
- DEMONBREUN, A. R., LAPIDOS, K. A., HERETIS, K., LEVIN, S., DALE, R., PYTEL, P., SVENSSON, E. C. & MCNALLY, E. M. 2010. Myoferlin regulation by NFAT in muscle injury, regeneration and repair. *J Cell Sci*, 123, 2413-22.
- DESGUERRE, I., MAYER, M., LETURCQ, F., BARBET, J. P., GHERARDI, R. K. & CHRISTOV, C. 2009. Endomysial fibrosis in Duchenne muscular dystrophy: a marker of poor outcome associated with macrophage alternative activation. *J Neuropathol Exp Neurol*, 68, 762-73.
- DESHMUKH, A. S. 2016. Proteomics of Skeletal Muscle: Focus on Insulin Resistance and Exercise Biology. *Proteomes*, 4.
- DESHMUKH, A. S., MURGIA, M., NAGARAJ, N., TREEBAK, J. T., COX, J. & MANN, M. 2015. Deep proteomics of mouse skeletal muscle enables quantitation of protein isoforms, metabolic pathways, and transcription factors. *Mol Cell Proteomics*, 14, 841-53.
- DESLYPER, G., COLGAN, T. J., COOPER, A. J., HOLLAND, C. V. & CAROLAN, J. C. 2016. A Proteomic Investigation of Hepatic Resistance to *Ascaris* in a Murine Model. *PLoS Negl Trop Dis*, 10, e0004837.
- DICK, O., TOM DIECK, S., ALTROCK, W. D., AMMERMÜLLER, J., WEILER, R., GARNER, C. C., GUNDELFINGER, E. D. & BRANDSTÄTTER, J. H. 2003. The presynaptic active zone protein bassoon is essential for photoreceptor ribbon synapse formation in the retina. *Neuron*, 37, 775-86.

- DIJKSTRA, S., MULDER, P. F. & SCHALKEN, J. A. 2014. Clinical use of novel urine and blood based prostate cancer biomarkers: a review. *Clin Biochem*, 47, 889-96.
- DOECKE, J. D., LAWS, S. M., FAUX, N. G., WILSON, W., BURNHAM, S. C., LAM, C. P., MONDAL, A., BEDO, J., BUSH, A. I., BROWN, B., DE RUYCK, K., ELLIS, K. A., FOWLER, C., GUPTA, V. B., HEAD, R., MACAULAY, S. L., PERTILE, K., ROWE, C. C., REMBACH, A., RODRIGUES, M., RUMBLE, R., SZOEKE, C., TADDEI, K., TADDEI, T., TROUNSON, B., AMES, D., MASTERS, C. L., MARTINS, R. N., INITIATIVE, A. S. D. N. & GROUP, A. I. B. A. L. R. 2012. Blood-based protein biomarkers for diagnosis of Alzheimer disease. *Arch Neurol*, 69, 1318-25.
- DOLL, S., DREßEN, M., GEYER, P. E., ITZHAK, D. N., BRAUN, C., DOPPLER, S. A., MEIER, F., DEUTSCH, M. A., LAHM, H., LANGE, R., KRANE, M. & MANN, M. 2017. Region and cell-type resolved quantitative proteomic map of the human heart. *Nat Commun*, 8, 1469.
- DOORENWEERD, N., MAHFOUZ, A., VAN PUTTEN, M., KALIYAPERUMAL, R., T' HOEN, P. A. C., HENDRIKSEN, J. G. M., AARTSMA-RUS, A. M., VERSCHUUREN, J. J. G. M., NIKS, E. H., REINDERS, M. J. T., KAN, H. E. & LELIEVELDT, B. P. F. 2017. Timing and localization of human dystrophin isoform expression provide insights into the cognitive phenotype of Duchenne muscular dystrophy. *Sci Rep*, 7, 12575.
- DORAN, P., DONOGHUE, P., O'CONNELL, K., GANNON, J. & OHLENDIECK, K. 2009a. Proteomics of skeletal muscle aging. *Proteomics*, 9, 989-1003.
- DORAN, P., DOWLING, P., DONOGHUE, P., BUFFINI, M. & OHLENDIECK, K. 2006a. Reduced expression of regucalcin in young and aged mdx diaphragm indicates abnormal cytosolic calcium handling in dystrophin-deficient muscle. *Biochim Biophys Acta*, 1764, 773-85.
- DORAN, P., GANNON, J., O'CONNELL, K. & OHLENDIECK, K. 2007. Aging skeletal muscle shows a drastic increase in the small heat shock proteins alphaB-crystallin/HspB5 and cvHsp/HspB7. *Eur J Cell Biol*, 86, 629-40.
- DORAN, P., MARTIN, G., DOWLING, P., JOCKUSCH, H. & OHLENDIECK, K. 2006b. Proteome analysis of the dystrophin-deficient MDX diaphragm reveals a drastic increase in the heat shock protein cvHSP. *Proteomics*, 6, 4610-21.
- DORAN, P., WILTON, S. D., FLETCHER, S. & OHLENDIECK, K. 2009b. Proteomic profiling of antisense-induced exon skipping reveals reversal of pathobiochemical abnormalities in dystrophic mdx diaphragm. *Proteomics*, 9, 671-85.
- DORN, G. W. 2013. Mitochondrial dynamics in heart disease. *Biochim Biophys Acta*, 1833, 233-41.
- DOWLING, P., DORAN, P. & OHLENDIECK, K. 2004. Drastic reduction of sarcalumenin in Dp427 (dystrophin of 427 kDa)-deficient fibres indicates that abnormal calcium handling plays a key role in muscular dystrophy. *Biochem J*, 379, 479-88.
- DOWLING, P., HAYES, C., TING, K. R., HAMEED, A., MEILLER, J., MITSIADES, C., ANDERSON, K. C., CLYNES, M., CLARKE, C., RICHARDSON, P. & O'GORMAN, P. 2014a. Identification of proteins found to be significantly altered when comparing the serum proteome from Multiple Myeloma patients with varying degrees of bone disease. *BMC Genomics*, 15, 904.
- DOWLING, P., HOLLAND, A. & OHLENDIECK, K. 2014b. Mass Spectrometry-Based Identification of Muscle-Associated and Muscle-Derived Proteomic Biomarkers of Dystrophinopathies. *J Neuromuscul Dis*, 1, 15-40.
- DOWLING, P., LOHAN, J. & OHLENDIECK, K. 2003. Comparative analysis of Dp427-deficient mdx tissues shows that the milder dystrophic phenotype of extraocular and toe muscle fibres is associated with a persistent expression of beta-dystroglycan. *Eur J Cell Biol*, 82, 222-30.
- DOWLING, P., MORAN, B., MCAULEY, E., MELEADY, P., HENRY, M., CLYNES, M., MCMENAMIN, M., LEONARD, N., MONKS, M., WYNNE, B., ORMOND, P. & LARKIN, A.

- 2016a. Quantitative label-free mass spectrometry analysis of formalin-fixed, paraffin-embedded tissue representing the invasive cutaneous malignant melanoma proteome. *Oncol Lett*, 12, 3296-3304.
- DOWLING, P., MURPHY, S. & OHLENDIECK, K. 2016b. Proteomic profiling of muscle fibre type shifting in neuromuscular diseases. *Expert Rev Proteomics*, 13, 783-99.
- DOWLING, P., WORMALD, R., MELEADY, P., HENRY, M., CURRAN, A. & CLYNES, M. 2008. Analysis of the saliva proteome from patients with head and neck squamous cell carcinoma reveals differences in abundance levels of proteins associated with tumour progression and metastasis. *J Proteomics*, 71, 168-75.
- DRACHMAN, D. B., TOYKA, K. V. & MYER, E. 1974. Prednisone in Duchenne muscular dystrophy. *Lancet*, 2, 1409-12.
- DRAEGER, A., MONASTYRSKAYA, K. & BABIYCHUK, E. B. 2011. Plasma membrane repair and cellular damage control: the annexin survival kit. *Biochem Pharmacol*, 81, 703-12.
- DUBOC, D., MEUNE, C., LEREBOURS, G., DEVAUX, J. Y., VAKSMANN, G. & BÉCANE, H. M. 2005. Effect of perindopril on the onset and progression of left ventricular dysfunction in Duchenne muscular dystrophy. *J Am Coll Cardiol*, 45, 855-7.
- DUCHENNE 1867. The Pathology of Paralysis with Muscular Degeneration (Paralysie Myosclerotique), or Paralysis with Apparent Hypertrophy. *Br Med J*, 2, 541-2.
- DULHUNTY, A. F., HAARMANN, C. S., GREEN, D., LAVER, D. R., BOARD, P. G. & CASAROTTO, M. G. 2002. Interactions between dihydropyridine receptors and ryanodine receptors in striated muscle. *Prog Biophys Mol Biol*, 79, 45-75.
- DUMONT, N. A. & RUDNICKI, M. A. 2016. Targeting muscle stem cell intrinsic defects to treat Duchenne muscular dystrophy. *NPJ Regen Med*, 1.
- DUMONT, N. A., BENTZINGER, C. F., SINCENNES, M. C. & RUDNICKI, M. A. 2015. Satellite Cells and Skeletal Muscle Regeneration. *Compr Physiol*, 5, 1027-59.
- DUNN, J. F., BURTON, K. A. & DAUNCEY, M. J. 1995. Ouabain sensitive Na⁺/K⁺-ATPase content is elevated in mdx mice: implications for the regulation of ions in dystrophic muscle. *J Neurol Sci*, 133, 11-5.
- DURBEEJ, M. & CAMPBELL, K. P. 2002. Muscular dystrophies involving the dystrophin-glycoprotein complex: an overview of current mouse models. *Curr Opin Genet Dev*, 12, 349-61.
- EBHARDT, H. A., DEGEN, S., TADINI, V., SCHILB, A., JOHNS, N., GREIG, C. A., FEARON, K. C. H., AEBERSOLD, R. & JACOBI, C. 2017. Comprehensive proteome analysis of human skeletal muscle in cachexia and sarcopenia: a pilot study. *J Cachexia Sarcopenia Muscle*, 8, 567-582.
- EDSTRÖM, E., ALTUN, M., BERGMAN, E., JOHNSON, H., KULLBERG, S., RAMÍREZ-LEÓN, V. & ULFHAKE, B. 2007. Factors contributing to neuromuscular impairment and sarcopenia during aging. *Physiol Behav*, 92, 129-35.
- EMERY, A. E. 2002. The muscular dystrophies. *Lancet*, 359, 687-95.
- EMERY, A. & MUNTONI, F. 2003. Duchenne muscular dystrophy. *Oxford University Press, Oxford* (3rd edition).
- ENDO, T. 2015. Molecular mechanisms of skeletal muscle development, regeneration, and osteogenic conversion. *Bone*, 80, 2-13.
- ENG, L. F. 1985. Glial fibrillary acidic protein (GFAP): the major protein of glial intermediate filaments in differentiated astrocytes. *J Neuroimmunol*, 8, 203-14.
- ENG, L. F., GHIRNIKAR, R. S. & LEE, Y. L. 2000. Glial fibrillary acidic protein: GFAP-thirty-one years (1969-2000). *Neurochem Res*, 25, 1439-51.

- ENGEL, A. G. & BIESECKER, G. 1982. Complement activation in muscle fiber necrosis: demonstration of the membrane attack complex of complement in necrotic fibers. *Ann Neurol*, 12, 289-96.
- ENRIGHT, P. L. 2003. The six-minute walk test. *Respir Care*, 48, 783-5.
- ERVASTI, J. M. 2007. Dystrophin, its interactions with other proteins, and implications for muscular dystrophy. *Biochim Biophys Acta*, 1772, 108-17.
- ERVASTI, J. M. & CAMPBELL, K. P. 1993. A role for the dystrophin-glycoprotein complex as a transmembrane linker between laminin and actin. *J Cell Biol*, 122, 809-23.
- ERVASTI, J. M., OHLENDIECK, K., KAHL, S. D., GAVER, M. G. & CAMPBELL, K. P. 1990. Deficiency of a glycoprotein component of the dystrophin complex in dystrophic muscle. *Nature*, 345, 315-9.
- EVANS, N. P., MISYAK, S. A., ROBERTSON, J. L., BASSAGANYA-RIERA, J. & GRANGE, R. W. 2009. Immune-mediated mechanisms potentially regulate the disease time-course of duchenne muscular dystrophy and provide targets for therapeutic intervention. *PM R*, 1, 755-68.
- FAGERBERG, L., HALLSTRÖM, B. M., OKSVOLD, P., KAMPF, C., DJUREINOVIC, D., ODEBERG, J., HABUKA, M., TAHMASEBPOOR, S., DANIELSSON, A., EDLUND, K., ASPLUND, A., SJÖSTEDT, E., LUNDBERG, E., SZIGYARTO, C. A., SKOGS, M., TAKANEN, J. O., BERLING, H., TEGEL, H., MULDER, J., NILSSON, P., SCHWENK, J. M., LINDSKOG, C., DANIELSSON, F., MARDINOGLU, A., SIVERTSSON, A., VON FEILITZEN, K., FORSBERG, M., ZWAHLEN, M., OLSSON, I., NAVANI, S., HUSS, M., NIELSEN, J., PONTEN, F. & UHLÉN, M. 2014. Analysis of the human tissue-specific expression by genome-wide integration of transcriptomics and antibody-based proteomics. *Mol Cell Proteomics*, 13, 397-406.
- FAIRCLOUGH, R. J., WOOD, M. J. & DAVIES, K. E. 2013. Therapy for Duchenne muscular dystrophy: renewed optimism from genetic approaches. *Nat Rev Genet*, 14, 373-8.
- FALZARANO, M. S., SCOTTON, C., PASSARELLI, C. & FERLINI, A. 2015. Duchenne Muscular Dystrophy: From Diagnosis to Therapy. *Molecules*, 20, 18168-84.
- FARRAH, T., DEUTSCH, E. W., OMENN, G. S., SUN, Z., WATTS, J. D., YAMAMOTO, T., SHTEYNBERG, D., HARRIS, M. M. & MORITZ, R. L. 2014. State of the human proteome in 2013 as viewed through PeptideAtlas: comparing the kidney, urine, and plasma proteomes for the biology- and disease-driven Human Proteome Project. *J Proteome Res*, 13, 60-75.
- FAYSSOIL, A., NARDI, O., ORLIKOWSKI, D. & ANNANE, D. 2010. Cardiomyopathy in Duchenne muscular dystrophy: pathogenesis and therapeutics. *Heart Fail Rev*, 15, 103-7.
- FERLINI, A., NERI, M. & GUALANDI, F. 2013. The medical genetics of dystrophinopathies: molecular genetic diagnosis and its impact on clinical practice. *Neuromuscul Disord*, 23, 4-14.
- FERLINI, A., SEWRY, C., MELIS, M. A., MATEDDU, A. & MUNTONI, F. 1999. X-linked dilated cardiomyopathy and the dystrophin gene. *Neuromuscul Disord*, 9, 339-46.
- FINEHOUT, E. J., FRANCK, Z., CHOE, L. H., RELKIN, N. & LEE, K. H. 2007. Cerebrospinal fluid proteomic biomarkers for Alzheimer's disease. *Ann Neurol*, 61, 120-9.
- FITZSIMONS, R. B. & HOH, J. F. 1981. Embryonic and foetal myosins in human skeletal muscle. The presence of foetal myosins in duchenne muscular dystrophy and infantile spinal muscular atrophy. *J Neurol Sci*, 52, 367-84.
- FLANIGAN, K. M., DUNN, D. M., VON NIEDERHAUSERN, A., SOLTANZADEH, P., GAPPMAIER, E., HOWARD, M. T., SAMPSON, J. B., MENDELL, J. R., WALL, C., KING, W. M., PESTRONK, A., FLORENCE, J. M., CONNOLLY, A. M., MATHEWS, K. D., STEPHAN, C. M., LAUBENTHAL, K. S., WONG, B. L., MOREHART, P. J., MEYER, A., FINKEL, R. S., BONNEMANN, C. G., MEDNE, L., DAY, J. W., DALTON, J. C., MARGOLIS, M. K., HINTON, V.

- J., WEISS, R. B. & CONSORTIUM, U. D. P. 2009. Mutational spectrum of DMD mutations in dystrophinopathy patients: application of modern diagnostic techniques to a large cohort. *Hum Mutat*, 30, 1657-66.
- FONG, P. Y., TURNER, P. R., DENETCLAW, W. F. & STEINHARDT, R. A. 1990. Increased activity of calcium leak channels in myotubes of Duchenne human and mdx mouse origin. *Science*, 250, 673-6.
- FORBES, E., MURASE, T., YANG, M., MATTHAEI, K. I., LEE, J. J., LEE, N. A., FOSTER, P. S. & HOGAN, S. P. 2004. Immunopathogenesis of experimental ulcerative colitis is mediated by eosinophil peroxidase. *J Immunol*, 172, 5664-75.
- FOSTER, H., SHARP, P. S., ATHANASOPOULOS, T., TROLLET, C., GRAHAM, I. R., FOSTER, K., WELLS, D. J. & DICKSON, G. 2008. Codon and mRNA sequence optimization of microdystrophin transgenes improves expression and physiological outcome in dystrophic mdx mice following AAV2/8 gene transfer. *Mol Ther*, 16, 1825-32.
- FRANCKE, U., OCHS, H. D., DE MARTINVILLE, B., GIACALONE, J., LINDGREN, V., DISTÈCHE, C., PAGON, R. A., HOFKER, M. H., VAN OMMEN, G. J. & PEARSON, P. L. 1985. Minor Xp21 chromosome deletion in a male associated with expression of Duchenne muscular dystrophy, chronic granulomatous disease, retinitis pigmentosa, and McLeod syndrome. *Am J Hum Genet*, 37, 250-67.
- FRESU, L., DEHPUR, A., GENAZZANI, A. A., CARAFOLI, E. & GUERINI, D. 1999. Plasma membrane calcium ATPase isoforms in astrocytes. *Glia*, 28, 150-5.
- FROEMMING, G. R. & OHLENDIECK, K. 2001. The role of ion-regulatory membrane proteins of excitation-contraction coupling and relaxation in inherited muscle diseases. *Front Biosci*, 6, D65-74.
- FRÖHLICH, T., KEMTER, E., FLENKENTHALER, F., KLYMIUK, N., OTTE, K. A., BLUTKE, A., KRAUSE, S., WALTER, M. C., WANKE, R., WOLF, E. & ARNOLD, G. J. 2016. Progressive muscle proteome changes in a clinically relevant pig model of Duchenne muscular dystrophy. *Sci Rep*, 6, 33362.
- FRONTERA, W. R. & OCHALA, J. 2015. Skeletal muscle: a brief review of structure and function. *Calcif Tissue Int*, 96, 183-95.
- FUJITA, M., MITSUHASHI, H., ISOGAI, S., NAKATA, T., KAWAKAMI, A., NONAKA, I., NOGUCHI, S., HAYASHI, Y. K., NISHINO, I. & KUDO, A. 2012. Filamin C plays an essential role in the maintenance of the structural integrity of cardiac and skeletal muscles, revealed by the medaka mutant zacro. *Dev Biol*, 361, 79-89.
- FUKUDA, N., GRANZIER, H. L., ISHIWATA, S. & KURIHARA, S. 2008. Physiological functions of the giant elastic protein titin in mammalian striated muscle. *J Physiol Sci*, 58, 151-9.
- FULLER, H. R., GRAHAM, L. C., LLAVERO HURTADO, M. & WISHART, T. M. 2016. Understanding the molecular consequences of inherited muscular dystrophies: advancements through proteomic experimentation. *Expert Rev Proteomics*, 13, 659-71.
- GALLASTEGUI, N. & GROLL, M. 2010. The 26S proteasome: assembly and function of a destructive machine. *Trends Biochem Sci*, 35, 634-642.
- GANNON, J., DORAN, P., KIRWAN, A. & OHLENDIECK, K. 2009. Drastic increase of myosin light chain MLC-2 in senescent skeletal muscle indicates fast-to-slow fibre transition in sarcopenia of old age. *Eur J Cell Biol*, 88, 685-700.
- GAO, H. J., CHEN, Y. J., ZUO, D., XIAO, M. M., LI, Y., GUO, H., ZHANG, N. & CHEN, R. B. 2015. Quantitative proteomic analysis for high-throughput screening of differential glycoproteins in hepatocellular carcinoma serum. *Cancer Biol Med*, 12, 246-54.

- GARCIA-TOVAR, C. G., PEREZ, A., LUNA, J., MENA, R., OSORIO, B., ALEMAN, V., MONDRAGON, R., MORNET, D., RENDÓN, A. & HERNANDEZ, J. M. 2001. Biochemical and histochemical analysis of 71 kDa dystrophin isoform (Dp71f) in rat brain. *Acta Histochem*, 103, 209-24.
- GARDAN-SALMON, D., DIXON, J. M., LONERGAN, S. M. & SELSBY, J. T. 2011. Proteomic assessment of the acute phase of dystrophin deficiency in mdx mice. *Eur J Appl Physiol*, 111, 2763-73.
- GATTO, L., VIZCAÍNO, J. A., HERMJAKOB, H., HUBER, W. & LILLEY, K. S. 2010. Organelle proteomics experimental designs and analysis. *Proteomics*, 10, 3957-69.
- GAZZERRO, E., ASSERETO, S., BONETTO, A., SOTGIA, F., SCARFÌ, S., PISTORIO, A., BONUCCELLI, G., CILLI, M., BRUNO, C., ZARA, F., LISANTI, M. P. & MINETTI, C. 2010. Therapeutic potential of proteasome inhibition in Duchenne and Becker muscular dystrophies. *Am J Pathol*, 176, 1863-77.
- GE, Y., MOLLOY, M. P., CHAMBERLAIN, J. S. & ANDREWS, P. C. 2003. Proteomic analysis of mdx skeletal muscle: Great reduction of adenylate kinase 1 expression and enzymatic activity. *Proteomics*, 3, 1895-903.
- GEIGER, R., STRASAK, A., TREML, B., GASSER, K., KLEINSASSER, A., FISCHER, V., GEIGER, H., LOECKINGER, A. & STEIN, J. I. 2007. Six-minute walk test in children and adolescents. *J Pediatr*, 150, 395-9, 399.e1-2.
- GELFI, C., VIGANO, A., RIPAMONTI, M., PONTOGLIO, A., BEGUM, S., PELLEGRINO, M. A., GRASSI, B., BOTTINELLI, R., WAIT, R. & CERRETELLI, P. 2006. The human muscle proteome in aging. *J Proteome Res*, 5, 1344-53.
- GILLESPIE, C. S., SHERMAN, D. L., BLAIR, G. E. & BROPHY, P. J. 1994. Periaxin, a novel protein of myelinating Schwann cells with a possible role in axonal ensheathment. *Neuron*, 12, 497-508.
- GILLET, L. C., NAVARRO, P., TATE, S., RÖST, H., SELEVSEK, N., REITER, L., BONNER, R. & AEBERSOLD, R. 2012. Targeted data extraction of the MS/MS spectra generated by data-independent acquisition: a new concept for consistent and accurate proteome analysis. *Mol Cell Proteomics*, 11, O111.016717.
- GILLIES, A. R. & LIEBER, R. L. 2011. Structure and function of the skeletal muscle extracellular matrix. *Muscle Nerve*, 44, 318-31.
- GOMES, A. V., POTTER, J. D. & SZCZESNA-CORDARY, D. 2002. The role of troponins in muscle contraction. *IUBMB Life*, 54, 323-33.
- GRADY, R. M., TENG, H., NICHOL, M. C., CUNNINGHAM, J. C., WILKINSON, R. S. & SANES, J. R. 1997. Skeletal and cardiac myopathies in mice lacking utrophin and dystrophin: a model for Duchenne muscular dystrophy. *Cell*, 90, 729-38.
- GRAND, R. J. & PERRY, S. V. 1980. The binding of calmodulin to myelin basic protein and histone H2B. *Biochem J*, 189, 227-40.
- GRASSL, N., KULAK, N. A., PICHLER, G., GEYER, P. E., JUNG, J., SCHUBERT, S., SINITYCYN, P., COX, J. & MANN, M. 2016. Ultra-deep and quantitative saliva proteome reveals dynamics of the oral microbiome. *Genome Med*, 8, 44.
- GREFTE, S., KUIJPERS-JAGTMAN, A. M., TORENSMA, R. & VON DEN HOFF, J. W. 2007. Skeletal muscle development and regeneration. *Stem Cells Dev*, 16, 857-68.
- GRIFFIN, M. A., FENG, H., TEWARI, M., ACOSTA, P., KAWANA, M., SWEENEY, H. L. & DISCHER, D. E. 2005. gamma-Sarcoglycan deficiency increases cell contractility, apoptosis and MAPK pathway activation but does not affect adhesion. *J Cell Sci*, 118, 1405-16.

GROUNDS, M. D. & TORRISI, J. 2004. Anti-TNFalpha (Remicade) therapy protects dystrophic skeletal muscle from necrosis. *FASEB J*, 18, 676-82.

GROZDANOVIC, Z. & BAUMGARTEN, H. G. 1999. Nitric oxide synthase in skeletal muscle fibers: a signaling component of the dystrophin-glycoprotein complex. *Histol Histopathol*, 14, 243-56.

GUAN, X., MACK, D. L., MORENO, C. M., STRANDE, J. L., MATHIEU, J., SHI, Y., MARKERT, C. D., WANG, Z., LIU, G., LAWLOR, M. W., MOOREFIELD, E. C., JONES, T. N., FUGATE, J. A., FURTH, M. E., MURRY, C. E., RUOHOLA-BAKER, H., ZHANG, Y., SANTANA, L. F. & CHILDERS, M. K. 2014. Dystrophin-deficient cardiomyocytes derived from human urine: new biologic reagents for drug discovery. *Stem Cell Res*, 12, 467-80.

GUEVEL, L., LAVOIE, J. R., PEREZ-IRATXETA, C., ROUGER, K., DUBREIL, L., FERON, M., TALON, S., BRAND, M. & MEGENEY, L. A. 2011. Quantitative proteomic analysis of dystrophic dog muscle. *J Proteome Res*, 10, 2465-78.

GUIRAUD, S., AARTSMA-RUS, A., VIEIRA, N. M., DAVIES, K. E., VAN OMMEN, G. J. & KUNKEL, L. M. 2015. The Pathogenesis and Therapy of Muscular Dystrophies. *Annu Rev Genomics Hum Genet*, 16, 281-308.

GUIRAUD, S., EDWARDS, B., SQUIRE, S. E., BABBS, A., SHAH, N., BERG, A., CHEN, H. & DAVIES, K. E. 2017. Identification of serum protein biomarkers for utrophin based DMD therapy. *Sci Rep*, 7, 43697.

GUNDRY, R. L., FU, Q., JELINEK, C. A., VAN EYK, J. E. & COTTER, R. J. 2007. Investigation of an albumin-enriched fraction of human serum and its albuminome. *Proteomics Clin Appl*, 1, 73-88.

HAMMERS, C. M. & STANLEY, J. R. 2013. Desmoglein-1, differentiation, and disease. *J Clin Invest*, 123, 1419-22.

HAN, H., MYLLYKOSKI, M., RUSKAMO, S., WANG, C. & KURSULA, P. 2013. Myelin-specific proteins: a structurally diverse group of membrane-interacting molecules. *Biofactors*, 39, 233-41.

HARIGAYA, Y., SHOJI, M., SHIRAO, T. & HIRAI, S. 1996. Disappearance of actin-binding protein, drebrin, from hippocampal synapses in Alzheimer's disease. *J Neurosci Res*, 43, 87-92.

HARPER, S. Q., HAUSER, M. A., DELLORUSSO, C., DUAN, D., CRAWFORD, R. W., PHELPS, S. F., HARPER, H. A., ROBINSON, A. S., ENGELHARDT, J. F., BROOKS, S. V. & CHAMBERLAIN, J. S. 2002. Modular flexibility of dystrophin: implications for gene therapy of Duchenne muscular dystrophy. *Nat Med*, 8, 253-61.

HASEGAWA, M., CUENDA, A., SPILLANTINI, M. G., THOMAS, G. M., BUÉE-SCHERRER, V., COHEN, P. & GOEDERT, M. 1999. Stress-activated protein kinase-3 interacts with the PDZ domain of alpha1-syntrophin. A mechanism for specific substrate recognition. *J Biol Chem*, 274, 12626-31.

HASIN, Y., SELDIN, M. & LUSIS, A. 2017. Multi-omics approaches to disease. *Genome Biol*, 18, 83.

HASLETT, J. N., SANODOU, D., KHO, A. T., BENNETT, R. R., GREENBERG, S. A., KOHANE, I. S., BEGGS, A. H. & KUNKEL, L. M. 2002. Gene expression comparison of biopsies from Duchenne muscular dystrophy (DMD) and normal skeletal muscle. *Proc Natl Acad Sci USA*, 99, 15000-5.

HATHOUT, Y., BRODY, E., CLEMENS, P. R., CRIPE, L., DELISLE, R. K., FURLONG, P., GORDISH-DRESSMAN, H., HACHE, L., HENRICSON, E., HOFFMAN, E. P., KOBAYASHI, Y. M., LORTS, A., MAH, J. K., MCDONALD, C., MEHLER, B., NELSON, S., NIKRAD, M., SINGER, B., STEELE, F., STERLING, D., SWEENEY, H. L., WILLIAMS, S. & GOLD, L. 2015. Large-scale serum protein biomarker discovery in Duchenne muscular dystrophy. *Proc Natl Acad Sci USA*, 112, 7153-8.

HATHOUT, Y., MARATHI, R. L., RAYAVARAPU, S., ZHANG, A., BROWN, K. J., SEOL, H., GORDISH-DRESSMAN, H., CIRAK, S., BELLO, L., NAGARAJU, K., PARTRIDGE, T.,

- HOFFMAN, E. P., TAKEDA, S., MAH, J. K., HENRICSON, E. & MCDONALD, C. 2014. Discovery of serum protein biomarkers in the mdx mouse model and cross-species comparison to Duchenne muscular dystrophy patients. *Hum Mol Genet*, 23, 6458-69.
- HATHOUT, Y., SEOL, H., HAN, M. H., ZHANG, A., BROWN, K. J. & HOFFMAN, E. P. 2016. Clinical utility of serum biomarkers in Duchenne muscular dystrophy. *Clin Proteomics*, 13, 9.
- HAWKE, T. J. & GARRY, D. J. 2001. Myogenic satellite cells: physiology to molecular biology. *J Appl Physiol* (1985), 91, 534-51.
- HAYAKAWA, K., MINAMI, N., ONO, S., OGASAWARA, Y., TOTSUKA, T., ABE, H., TANAKA, T. & OBINATA, T. 1993. Increased expression of cofilin in dystrophic chicken and mouse skeletal muscles. *J Biochem*, 114, 582-7.
- HELLER, K. N., MONTGOMERY, C. L., SHONTZ, K. M., CLARK, K. R., MENDELL, J. R. & RODINO-KLAPAC, L. R. 2015. Human $\alpha 7$ Integrin Gene (ITGA7) Delivered by Adeno-Associated Virus Extends Survival of Severely Affected Dystrophin/Utrophin-Deficient Mice. *Hum Gene Ther*, 26, 647-56.
- HENDERSON, W. R., JONG, E. C. & KLEBANOFF, S. J. 1980. Binding of eosinophil peroxidase to mast cell granules with retention of peroxidatic activity. *J Immunol*, 124, 1383-8.
- HERNÁNDEZ-DEVIEZ, D. J., HOWES, M. T., LAVAL, S. H., BUSHBY, K., HANCOCK, J. F. & PARTON, R. G. 2008. Caveolin regulates endocytosis of the muscle repair protein, dysferlin. *J Biol Chem*, 283, 6476-88.
- HEUTINCK, K. M., TEN BERGE, I. J., HACK, C. E., HAMANN, J. & ROWSHANI, A. T. 2010. Serine proteases of the human immune system in health and disease. *Mol Immunol*, 47, 1943-55.
- HEYDEMANN, A. & MCNALLY, E. M. 2007. Consequences of disrupting the dystrophin-sarcoglycan complex in cardiac and skeletal myopathy. *Trends Cardiovasc Med*, 17, 55-9.
- HEYDEMANN, A., HUBER, J. M., KAKKAR, R., WHEELER, M. T. & MCNALLY, E. M. 2004. Functional nitric oxide synthase mislocalization in cardiomyopathy. *J Mol Cell Cardiol*, 36, 213-23.
- HMMIER, A., O'BRIEN, M. E., LYNCH, V., CLYNES, M., MORGAN, R. & DOWLING, P. 2017. Proteomic analysis of bronchoalveolar lavage fluid (BALF) from lung cancer patients using label-free mass spectrometry. *BBA Clin*, 7, 97-104.
- HODGETTS, S., RADLEY, H., DAVIES, M. & GROUNDS, M. D. 2006. Reduced necrosis of dystrophic muscle by depletion of host neutrophils, or blocking TNF α function with Etanercept in mdx mice. *Neuromuscul Disord*, 16, 591-602.
- HOFFMAN, E. P., BROWN, R. H. & KUNKEL, L. M. 1987. Dystrophin: the protein product of the Duchenne muscular dystrophy locus. *Cell*, 51, 919-28.
- HOGAN, A., SHEPHERD, L., CHABOT, J., QUENNEVILLE, S., PRESCOTT, S. M., TOPHAM, M. K. & GEE, S. H. 2001. Interaction of gamma 1-syntrophin with diacylglycerol kinase-zeta. Regulation of nuclear localization by PDZ interactions. *J Biol Chem*, 276, 26526-33.
- HOLLAND, A. & OHLENDIECK, K. 2013. Proteomic profiling of the contractile apparatus from skeletal muscle. *Expert Rev Proteomics*, 10, 239-57.
- HOLLAND, A., DOWLING, P., MELEADY, P., HENRY, M., ZWEYER, M., MUNDEGAR, R. R., SWANDULLA, D. & OHLENDIECK, K. 2015a. Label-free mass spectrometric analysis of the mdx-4cv diaphragm identifies the matricellular protein periostin as a potential factor involved in dystrophinopathy-related fibrosis. *Proteomics*, 15, 2,318-2,331.
- HOLLAND, A., HENRY, M., MELEADY, P., WINKLER, C. K., KRAUTWALD, M., BRINKMEIER, H. & OHLENDIECK, K. 2015b. Comparative Label-Free Mass Spectrometric

Analysis of Mildly versus Severely Affected mdx Mouse Skeletal Muscles Identifies Annexin, Laminin, and Vimentin as Universal Dystrophic Markers. *Molecules*, 20, 11317-44.

HOLLAND, A., DOWLING, P., ZWEYER, M., SWANDULLA, D., HENRY, M., CLYNES, M. & OHLENDIECK, K. 2013. Proteomic profiling of cardiomyopathic tissue from the aged mdx model of Duchenne muscular dystrophy reveals a drastic decrease in laminin, nidogen and annexin. *Proteomics*, 13, 2312-23.

HOLLAND, A., SCHMITT-JOHN, T., DOWLING, P., MELEADY, P., HENRY, M., CLYNES, M. & OHLENDIECK, K. 2014. Intricate effects of primary motor neuronopathy on contractile proteins and metabolic muscle enzymes as revealed by label-free mass spectrometry. *Biosci Rep*, 34.

HOLLNAGEL, A., GRUND, C., FRANKE, W. W. & ARNOLD, H. H. 2002. The cell adhesion molecule M-cadherin is not essential for muscle development and regeneration. *Mol Cell Biol*, 22, 4760-70.

HOLLOWAY, K. V., O'GORMAN, M., WOODS, P., MORTON, J. P., EVANS, L., CABLE, N. T., GOLDSPINK, D. F. & BURNISTON, J. G. 2009. Proteomic investigation of changes in human vastus lateralis muscle in response to interval-exercise training. *Proteomics*, 9, 5155-74.

HOOGERWAARD, E. M., VAN DER WOUW, P. A., WILDE, A. A., BAKKER, E., IPPEL, P. F., OOSTERWIJK, J. C., MAJOUR-KRAKAUER, D. F., VAN ESSEN, A. J., LESCHOT, N. J. & DE VISSER, M. 1999. Cardiac involvement in carriers of Duchenne and Becker muscular dystrophy. *Neuromuscul Disord*, 9, 347-51.

HOPF, F. W. & STEINHARDT, R. A. 1992. Regulation of intracellular free calcium in normal and dystrophic mouse cerebellar neurons. *Brain Res*, 578, 49-54.

HORTIN, G. L. & SVIRIDOV, D. 2010. The dynamic range problem in the analysis of the plasma proteome. *J Proteomics*, 73, 629-36.

HORTIN, G. L., SVIRIDOV, D. & ANDERSON, N. L. 2008. High-abundance polypeptides of the human plasma proteome comprising the top 4 logs of polypeptide abundance. *Clin Chem*, 54, 1608-16.

HOUBEN, F., RAMAEKERS, F. C., SNOECKX, L. H. & BROERS, J. L. 2007. Role of nuclear lamina-cytoskeleton interactions in the maintenance of cellular strength. *Biochim Biophys Acta*, 1773, 675-86.

HOVHANNISYAN, R. H. & CARSTENS, R. P. 2007. Heterogeneous ribonucleoprotein m is a splicing regulatory protein that can enhance or silence splicing of alternatively spliced exons. *J Biol Chem*, 282, 36265-74.

HUANG, X., POY, F., ZHANG, R., JOACHIMIAK, A., SUDOL, M. & ECK, M. J. 2000. Structure of a WW domain containing fragment of dystrophin in complex with beta-dystroglycan. *Nat Struct Biol*, 7, 634-8.

HUSSEIN, M. R., HAMED, S. A., MOSTAFA, M. G., ABU-DIEF, E. E., KAMEL, N. F. & KANDIL, M. R. 2006. The effects of glucocorticoid therapy on the inflammatory and dendritic cells in muscular dystrophies. *Int J Exp Pathol*, 87, 451-61.

HYNES, R. O. 1992. Integrins: versatility, modulation, and signaling in cell adhesion. *Cell*, 69, 11-25.

IBRAGHIMOV-BESKROVNAYA, O., ERVASTI, J. M., LEVEILLE, C. J., SLAUGHTER, C. A., SERNETT, S. W. & CAMPBELL, K. P. 1992. Primary structure of dystrophin-associated glycoproteins linking dystrophin to the extracellular matrix. *Nature*, 355, 696-702.

IM, W. B., PHELPS, S. F., COPEN, E. H., ADAMS, E. G., SLIGHTOM, J. L. & CHAMBERLAIN, J. S. 1996. Differential expression of dystrophin isoforms in strains of mdx mice with different mutations. *Hum Mol Genet*, 5, 1149-53.

- ISAYAMA, T., GOODMAN, S. R. & ZAGON, I. S. 1993. Localization of spectrin isoforms in the adult mouse heart. *Cell Tissue Res*, 274, 127-33.
- ISHIZAKI, M., SUGA, T., KIMURA, E., SHIOTA, T., KAWANO, R., UCHIDA, Y., UCHINO, K., YAMASHITA, S., MAEDA, Y. & UCHINO, M. 2008. Mdx respiratory impairment following fibrosis of the diaphragm. *Neuromuscul Disord*, 18, 342-8.
- ISSAQ, H. & VEENSTRA, T. 2008. Two-dimensional polyacrylamide gel electrophoresis (2D-PAGE): advances and perspectives. *Biotechniques*, 44, 697-8, 700.
- ITOH, K., JINNAI, K., TADA, K., HARA, K., ITOH, H. & TAKAHASHI, K. 1999. Multifocal glial nodules in a case of Duchenne muscular dystrophy with severe mental retardation. *Neuropathology*, 19, 322-327.
- JOHN, H. A. & PURDOM, I. F. 1989. Elevated plasma levels of haptoglobin in Duchenne muscular dystrophy: electrophoretic variants in patients with a severe form of the disease. *Electrophoresis*, 10, 489-93.
- JOHNSON, E. K., ZHANG, L., ADAMS, M. E., PHILLIPS, A., FREITAS, M. A., FROEHNER, S. C., GREEN-CHURCH, K. B. & MONTANARO, F. 2012. Proteomic analysis reveals new cardiac-specific dystrophin-associated proteins. *PLoS One*, 7, e43515.
- JONG, E. C., MAHMOUD, A. A. & KLEBANOFF, S. J. 1981. Peroxidase-mediated toxicity to schistosomula of *Schistosoma mansoni*. *J Immunol*, 126, 468-71.
- JONIGK, D., AL-OMARI, M., MAEGEL, L., MÜLLER, M., IZYKOWSKI, N., HONG, J., HONG, K., KIM, S. H., DORSCH, M., MAHADEVA, R., LAENGER, F., KREIPE, H., BRAUN, A., SHAHAF, G., LEWIS, E. C., WELTE, T., DINARELLO, C. A. & JANCIAUSKIENE, S. 2013. Anti-inflammatory and immunomodulatory properties of α 1-antitrypsin without inhibition of elastase. *Proc Natl Acad Sci USA*, 110, 15007-12.
- JUNG, J. H., JI, Y. W., HWANG, H. S., OH, J. W., KIM, H. C., LEE, H. K. & KIM, K. P. 2017. Proteomic analysis of human lacrimal and tear fluid in dry eye disease. *Sci Rep*, 7, 13363.
- KARALAKI, M., FILI, S., PHILIPPOU, A. & KOUTSILIERIS, M. 2009. Muscle regeneration: cellular and molecular events. *In Vivo*, 23, 779-96.
- KAWAI, H., YONEDA, K., NARUO, T., NISHIDA, Y., KASHIWAGI, S., KUNISHIGE, M. & SAITO, S. 1995. Lysosomal enzyme activities in skeletal muscle of patients with neuromuscular diseases. *Muscle Nerve*, 18, 1009-15.
- KHAIRALLAH, M., KHAIRALLAH, R., YOUNG, M. E., DYCK, J. R., PETROF, B. J. & DES ROSIERS, C. 2007. Metabolic and signaling alterations in dystrophin-deficient hearts precede overt cardiomyopathy. *J Mol Cell Cardiol*, 43, 119-29.
- KHARRAZ, Y., GUERRA, J., MANN, C. J., SERRANO, A. L. & MUÑOZ-CÁNOVES, P. 2013. Macrophage plasticity and the role of inflammation in skeletal muscle repair. *Mediators Inflamm*, 2013, 491497.
- KHARRAZ, Y., GUERRA, J., PESSINA, P., SERRANO, A. L. & MUÑOZ-CÁNOVES, P. 2014. Understanding the process of fibrosis in Duchenne muscular dystrophy. *Biomed Res Int*, 2014, 965631.
- KHOUZAMI, L., BOURIN, M. C., CHRISTOV, C., DAMY, T., ESCOUBET, B., CARMELLE, P., PERIER, M., WAHBI, K., MEUNE, C., PAVOINE, C. & PECKER, F. 2010. Delayed cardiomyopathy in dystrophin deficient mdx mice relies on intrinsic glutathione resource. *Am J Pathol*, 177, 1356-64.
- KHURANA, T. S., WATKINS, S. C., CHAFEY, P., CHELLY, J., TOMÉ, F. M., FARDEAU, M., KAPLAN, J. C. & KUNKEL, L. M. 1991. Immunolocalization and developmental expression of dystrophin related protein in skeletal muscle. *Neuromuscul Disord*, 1, 185-94.

- KIFFIN, R., CHRISTIAN, C., KNECHT, E. & CUERVO, A. M. 2004. Activation of chaperone-mediated autophagy during oxidative stress. *Mol Biol Cell*, 15, 4829-40.
- KIM, K., KIM, S. J., YU, H. G., YU, J., PARK, K. S., JANG, I. J. & KIM, Y. 2010. Verification of biomarkers for diabetic retinopathy by multiple reaction monitoring. *J Proteome Res*, 9, 689-99.
- KINALI, M., ARECHAVALA-GOMEZA, V., CIRAK, S., GLOVER, A., GUGLIERI, M., FENG, L., HOLLINGSWORTH, K. G., HUNT, D., JUNGBLUTH, H., ROPER, H. P., QUINLIVAN, R. M., GOSALAKKAL, J. A., JAYAWANT, S., NADEAU, A., HUGHES-CARRE, L., MANZUR, A. Y., MERCURI, E., MORGAN, J. E., STRAUB, V., BUSHBY, K., SEWRY, C., RUTHERFORD, M. & MUNTONI, F. 2011. Muscle histology vs MRI in Duchenne muscular dystrophy. *Neurology*, 76, 346-53.
- KING, I. A., ANGST, B. D., HUNT, D. M., KRUGER, M., ARNEMANN, J. & BUXTON, R. S. 1997. Hierarchical expression of desmosomal cadherins during stratified epithelial morphogenesis in the mouse. *Differentiation*, 62, 83-96.
- KIPLING, D. & COOKE, H. J. 1990. Hypervariable ultra-long telomeres in mice. *Nature*, 347, 400-2.
- KLIETSCH, R., ERVASTI, J. M., ARNOLD, W., CAMPBELL, K. P. & JORGENSEN, A. O. 1993. Dystrophin-glycoprotein complex and laminin colocalize to the sarcolemma and transverse tubules of cardiac muscle. *Circ Res*, 72, 349-60.
- KLJUIC, A. & CHRISTIANO, A. M. 2003. A novel mouse desmosomal cadherin family member, desmoglein 1 gamma. *Exp Dermatol*, 12, 20-9.
- KLYMIUK, N., BLUTKE, A., GRAF, A., KRAUSE, S., BURKHARDT, K., WUENSCH, A., KREBS, S., KESSLER, B., ZAKHARTCHENKO, V., KUROME, M., KEMTER, E., NAGASHIMA, H., SCHOSER, B., HERBACH, N., BLUM, H., WANKE, R., AARTSMA-RUS, A., THIRION, C., LOCHMÜLLER, H., WALTER, M. C. & WOLF, E. 2013. Dystrophin-deficient pigs provide new insights into the hierarchy of physiological derangements of dystrophic muscle. *Hum Mol Genet*, 22, 4368-82.
- KNUESEL, I., MASTROCOLA, M., ZUELLIG, R. A., BORNHAUSER, B., SCHAUB, M. C. & FRITSCHY, J. M. 1999. Short communication: altered synaptic clustering of GABAA receptors in mice lacking dystrophin (mdx mice). *Eur J Neurosci*, 11, 4457-62.
- KOENIG, M. & KUNKEL, L. M. 1990. Detailed analysis of the repeat domain of dystrophin reveals four potential hinge segments that may confer flexibility. *J Biol Chem*, 265, 4560-6.
- KOENIG, M., BEGGS, A. H., MOYER, M., SCHERPF, S., HEINDRICH, K., BETTECKEN, T., MENG, G., MÜLLER, C. R., LINDLÖF, M. & KAARIAINEN, H. 1989. The molecular basis for Duchenne versus Becker muscular dystrophy: correlation of severity with type of deletion. *Am J Hum Genet*, 45, 498-506.
- KOENIG, M., HOFFMAN, E. P., BERTELSON, C. J., MONACO, A. P., FEENER, C. & KUNKEL, L. M. 1987. Complete cloning of the Duchenne muscular dystrophy (DMD) cDNA and preliminary genomic organization of the DMD gene in normal and affected individuals. *Cell*, 50, 509-17.
- KOENIG, M., MONACO, A. P. & KUNKEL, L. M. 1988. The complete sequence of dystrophin predicts a rod-shaped cytoskeletal protein. *Cell*, 53, 219-28.
- KORNEGAY, J. N., PETERSON, J. M., BOGAN, D. J., KLINE, W., BOGAN, J. R., DOW, J. L., FAN, Z., WANG, J., AHN, M., ZHU, H., STYNER, M. & GUTTRIDGE, D. C. 2014. NBD delivery improves the disease phenotype of the golden retriever model of Duchenne muscular dystrophy. *Skelet Muscle*, 4, 18.
- KOSTETSKII, I., LI, J., XIONG, Y., ZHOU, R., FERRARI, V. A., PATEL, V. V., MOLKENTIN, J. D. & RADICE, G. L. 2005. Induced deletion of the N-cadherin gene in the heart leads to dissolution of the intercalated disc structure. *Circ Res*, 96, 346-54.

- KRUGER, M., WRIGHT, J. & WANG, K. 1991. Nebulin as a length regulator of thin filaments of vertebrate skeletal muscles: correlation of thin filament length, nebulin size, and epitope profile. *J Cell Biol*, 115, 97-107.
- KUMAR, A. & BORIEK, A. M. 2003. Mechanical stress activates the nuclear factor-kappaB pathway in skeletal muscle fibers: a possible role in Duchenne muscular dystrophy. *FASEB J*, 17, 386-96.
- KURTZ, D. M., RINALDO, P., RHEAD, W. J., TIAN, L., MILLINGTON, D. S., VOCKLEY, J., HAMM, D. A., BRIX, A. E., LINDSEY, J. R., PINKERT, C. A., O'BRIEN, W. E. & WOOD, P. A. 1998. Targeted disruption of mouse long-chain acyl-CoA dehydrogenase gene reveals crucial roles for fatty acid oxidation. *Proc Natl Acad Sci USA*, 95, 15592-7.
- KZHYSHKOWSKA, J., YIN, S., LIU, T., RIABOV, V. & MITROFANOVA, I. 2016. Role of chitinase-like proteins in cancer. *Biol Chem*, 397, 231-47.
- LAEMMLI, U. K. 1970. Cleavage of structural proteins during the assembly of the head of bacteriophage T4. *Nature*, 227, 680-5.
- LAI, Y., ZHAO, J., YUE, Y., WASALA, N. B. & DUAN, D. 2014. Partial restoration of cardiac function with Δ PDZ nNOS in aged mdx model of Duchenne cardiomyopathy. *Hum Mol Genet*, 23, 3189-99.
- LANDER, E. S. 2011. Initial impact of the sequencing of the human genome. *Nature*, 470, 187-97.
- LAPIDOS, K. A., KAKKAR, R. & MCNALLY, E. M. 2004. The dystrophin glycoprotein complex: signaling strength and integrity for the sarcolemma. *Circ Res*, 94, 1023-31.
- LAW, D. J., ALLEN, D. L. & TIDBALL, J. G. 1994. Talin, vinculin and DRP (utrophin) concentrations are increased at mdx myotendinous junctions following onset of necrosis. *J Cell Sci*, 107 (Pt 6), 1477-83.
- LAW, R. H., ZHANG, Q., MCGOWAN, S., BUCKLE, A. M., SILVERMAN, G. A., WONG, W., ROSADO, C. J., LANGENDORF, C. G., PIKE, R. N., BIRD, P. I. & WHISSTOCK, J. C. 2006. An overview of the serpin superfamily. *Genome Biol*, 7, 216.
- LE RUMEUR, E., WINDER, S. J. & HUBERT, J. F. 2010. Dystrophin: more than just the sum of its parts. *Biochim Biophys Acta*, 1804, 1713-22.
- LEBER, Y., RUPARELIA, A. A., KIRFEL, G., VAN DER VEN, P. F., HOFFMANN, B., MERKEL, R., BRYSON-RICHARDSON, R. J. & FÜRST, D. O. 2016. Filamin C is a highly dynamic protein associated with fast repair of myofibrillar microdamage. *Hum Mol Genet*, 25, 2776-2788.
- LENNON, N. J., KHO, A., BACSKAI, B. J., PERLMUTTER, S. L., HYMAN, B. T. & BROWN, R. H. 2003. Dysferlin interacts with annexins A1 and A2 and mediates sarcolemmal wound-healing. *J Biol Chem*, 278, 50466-73.
- LEVINE, B. A., MOIR, A. J., PATCHELL, V. B. & PERRY, S. V. 1992. Binding sites involved in the interaction of actin with the N-terminal region of dystrophin. *FEBS Lett*, 298, 44-8.
- LEWIS, C. & OHLENDIECK, K. 2010a. Mass spectrometric identification of dystrophin isoform Dp427 by on-membrane digestion of sarcolemma from skeletal muscle. *Anal Biochem*, 404, 197-203.
- LEWIS, C. & OHLENDIECK, K. 2010b. Proteomic profiling of naturally protected extraocular muscles from the dystrophin-deficient mdx mouse. *Biochem Biophys Res Commun*, 396, 1024-9.
- LEWIS, C., CARBERRY, S. & OHLENDIECK, K. 2009. Proteomic profiling of x-linked muscular dystrophy. *J Muscle Res Cell Motil*, 30, 267-9.
- LEWIS, C., JOCKUSCH, H. & OHLENDIECK, K. 2010. Proteomic Profiling of the Dystrophin-Deficient MDX Heart Reveals Drastically Altered Levels of Key Metabolic and Contractile Proteins. *J Biomed Biotechnol*, 2010, 648501.

- LI, H., MITTAL, A., MAKONCHUK, D. Y., BHATNAGAR, S. & KUMAR, A. 2009. Matrix metalloproteinase-9 inhibition ameliorates pathogenesis and improves skeletal muscle regeneration in muscular dystrophy. *Hum Mol Genet*, 18, 2584-98.
- LI, L. C., LI, J. & GAO, J. 2014. Functions of galectin-3 and its role in fibrotic diseases. *J Pharmacol Exp Ther*, 351, 336-43.
- LIDOV, H. G., SELIG, S. & KUNKEL, L. M. 1995. Dp140: a novel 140 kDa CNS transcript from the dystrophin locus. *Hum Mol Genet*, 4, 329-35.
- LIEBER, R. L. & WARD, S. R. 2013. Cellular mechanisms of tissue fibrosis. 4. Structural and functional consequences of skeletal muscle fibrosis. *Am J Physiol Cell Physiol*, 305, C241-52.
- LIM, K. R., MARUYAMA, R. & YOKOTA, T. 2017. Eteplirsen in the treatment of Duchenne muscular dystrophy. *Drug Des Devel Ther*, 11, 533-545.
- LIM, S. K., KIM, H., BIN ALI, A., LIM, Y. K., WANG, Y., CHONG, S. M., COSTANTINI, F. & BAUMMAN, H. 1998. Increased susceptibility in Hp knockout mice during acute hemolysis. *Blood*, 92, 1870-7.
- LIMA, D. P., DINIZ, D. G., MOIMAZ, S. A., SUMIDA, D. H. & OKAMOTO, A. C. 2010. Saliva: reflection of the body. *Int J Infect Dis*, 14, e184-8.
- LIN, A. P., SHIC, F., ENRIQUEZ, C. & ROSS, B. D. 2003. Reduced glutamate neurotransmission in patients with Alzheimer's disease -- an in vivo (13)C magnetic resonance spectroscopy study. *MAGMA*, 16, 29-42.
- LINGE, A., KENNEDY, S., O'FLYNN, D., BEATTY, S., MORIARTY, P., HENRY, M., CLYNES, M., LARKIN, A. & MELEADY, P. 2012. Differential expression of fourteen proteins between uveal melanoma from patients who subsequently developed distant metastases versus those who did not. *Invest Ophthalmol Vis Sci*, 53, 4634-43.
- LINIAL, M., MILLER, K. & SCHELLER, R. H. 1989. VAT-1: an abundant membrane protein from Torpedo cholinergic synaptic vesicles. *Neuron*, 2, 1265-73.
- LINNEMANN, A., VAN DER VEN, P. F., VAKEEL, P., ALBINUS, B., SIMONIS, D., BENDAS, G., SCHENK, J. A., MICHEEL, B., KLEY, R. A. & FÜRST, D. O. 2010. The sarcomeric Z-disc component myopodin is a multiadapter protein that interacts with filamin and alpha-actinin. *Eur J Cell Biol*, 89, 681-92.
- LINTON, P. J., GURNEY, M., SENGSTOCK, D., MENTZER, R. M. & GOTTLIEB, R. A. 2015. This old heart: Cardiac aging and autophagy. *J Mol Cell Cardiol*, 83, 44-54.
- LIU, C. W., BRAMER, L., WEBB-ROBERTSON, B. J., WAUGH, K., REWERS, M. J. & ZHANG, Q. 2017. Temporal profiles of plasma proteome during childhood development. *J Proteomics*, 152, 321-328.
- LIU, Y., BOUHENNI, R. A., DUFRESNE, C. P., SEMBA, R. D. & EDWARD, D. P. 2016. Differential Expression of Vitreous Proteins in Young and Mature New Zealand White Rabbits. *PLoS One*, 11, e0153560.
- LOLMEDE, K., CAMPANA, L., VEZZOLI, M., BOSURGI, L., TONLORENZI, R., CLEMENTI, E., BIANCHI, M. E., COSSU, G., MANFREDI, A. A., BRUNELLI, S. & ROVERE-QUERINI, P. 2009. Inflammatory and alternatively activated human macrophages attract vessel-associated stem cells, relying on separate HMGB1- and MMP-9-dependent pathways. *J Leukoc Biol*, 85, 779-87.
- LONG, C., AMOASII, L., MIREAULT, A. A., MCANALLY, J. R., LI, H., SANCHEZ-ORTIZ, E., BHATTACHARYYA, S., SHELTON, J. M., BASSEL-DUBY, R. & OLSON, E. N. 2016. Postnatal genome editing partially restores dystrophin expression in a mouse model of muscular dystrophy. *Science*, 351, 400-3.

- LONG, C., MCANALLY, J. R., SHELTON, J. M., MIREAULT, A. A., BASSEL-DUBY, R. & OLSON, E. N. 2014. Prevention of muscular dystrophy in mice by CRISPR/Cas9-mediated editing of germline DNA. *Science*, 345, 1184-8.
- LOO, J. A., YAN, W., RAMACHANDRAN, P. & WONG, D. T. 2010. Comparative human salivary and plasma proteomes. *J Dent Res*, 89, 1016-23.
- LORTS, A., SCHWANERKAMP, J. A., BAUDINO, T. A., MCNALLY, E. M. & MOLKENTIN, J. D. 2012. Deletion of periostin reduces muscular dystrophy and fibrosis in mice by modulating the transforming growth factor- β pathway. *Proc Natl Acad Sci USA*, 109, 10978-83.
- LOUBOUTIN, J. P., NAVENOT, J. M., ROUGER, K. & BLANCHARD, D. 2003. S-protein is expressed in necrotic fibers in Duchenne muscular dystrophy and polymyositis. *Muscle Nerve*, 27, 575-81.
- LOWNDES, M., RAKSHIT, S., SHAFRAZ, O., BORGHI, N., HARMON, R. M., GREEN, K. J., SIVASANKAR, S. & NELSON, W. J. 2014. Different roles of cadherins in the assembly and structural integrity of the desmosome complex. *J Cell Sci*, 127, 2339-50.
- LU, Q. L., MANN, C. J., LOU, F., BOU-GHARIOS, G., MORRIS, G. E., XUE, S. A., FLETCHER, S., PARTRIDGE, T. A. & WILTON, S. D. 2003. Functional amounts of dystrophin produced by skipping the mutated exon in the mdx dystrophic mouse. *Nat Med*, 9, 1009-14.
- LU, Q. L., RABINOWITZ, A., CHEN, Y. C., YOKOTA, T., YIN, H., ALTER, J., JADOON, A., BOU-GHARIOS, G. & PARTRIDGE, T. 2005. Systemic delivery of antisense oligoribonucleotide restores dystrophin expression in body-wide skeletal muscles. *Proc Natl Acad Sci USA*, 102, 198-203.
- LUMENG, C., PHELPS, S., CRAWFORD, G. E., WALDEN, P. D., BARALD, K. & CHAMBERLAIN, J. S. 1999. Interactions between beta 2-syntrophin and a family of microtubule-associated serine/threonine kinases. *Nat Neurosci*, 2, 611-7.
- LUQUE-GARCIA, J. L. & NEUBERT, T. A. 2009. On-membrane tryptic digestion of proteins for mass spectrometry analysis. *Methods Mol Biol*, 536, 331-41.
- LYSSAND, J. S., DEFINO, M. C., TANG, X. B., HERTZ, A. L., FELLER, D. B., WACKER, J. L., ADAMS, M. E. & HAGUE, C. 2008. Blood pressure is regulated by an alpha1D-adrenergic receptor/dystrophin signalosome. *J Biol Chem*, 283, 18792-800.
- MADARO, L. & BOUCHÉ, M. 2014. From innate to adaptive immune response in muscular dystrophies and skeletal muscle regeneration: the role of lymphocytes. *Biomed Res Int*, 2014, 438675.
- MAH, J. K. 2016. Current and emerging treatment strategies for Duchenne muscular dystrophy. *Neuropsychiatr Dis Treat*, 12, 1795-807.
- MAKAWITA, S. & DIAMANDIS, E. P. 2010. The bottleneck in the cancer biomarker pipeline and protein quantification through mass spectrometry-based approaches: current strategies for candidate verification. *Clin Chem*, 56, 212-22.
- MALI, P., ESVELT, K. M. & CHURCH, G. M. 2013. Cas9 as a versatile tool for engineering biology. *Nat Methods*, 10, 957-63.
- MALIK, V., RODINO-KLAPAC, L. R., VIOLLET, L., WALL, C., KING, W., AL-DAHAK, R., LEWIS, S., SHILLING, C. J., KOTA, J., SERRANO-MUNUERA, C., HAYES, J., MAHAN, J. D., CAMPBELL, K. J., BANWELL, B., DASOUKI, M., WATTS, V., SIVAKUMAR, K., BIENWILLNER, R., FLANIGAN, K. M., SAHENK, Z., BAROHN, R. J., WALKER, C. M. & MENDELL, J. R. 2010. Gentamicin-induced readthrough of stop codons in Duchenne muscular dystrophy. *Ann Neurol*, 67, 771-80.
- MANN, C. J., PERDIGUERO, E., KHARRAZ, Y., AGUILAR, S., PESSINA, P., SERRANO, A. L. & MUÑOZ-CÁNOVES, P. 2011. Aberrant repair and fibrosis development in skeletal muscle. *Skelet Muscle*, 1, 21.

- MARINI, J. F., PONS, F., LEGER, J., LOFFREDA, N., ANOAL, M., CHEVALLAY, M., FARDEAU, M. & LEGER, J. J. 1991. Expression of myosin heavy chain isoforms in Duchenne muscular dystrophy patients and carriers. *Neuromuscul Disord*, 1, 397-409.
- MARKHAM, L. W., SPICER, R. L., KHOURY, P. R., WONG, B. L., MATHEWS, K. D. & CRIFE, L. H. 2005. Steroid therapy and cardiac function in Duchenne muscular dystrophy. *Pediatr Cardiol*, 26, 768-71.
- MAROUGA, R., DAVID, S. & HAWKINS, E. 2005. The development of the DIGE system: 2D fluorescence difference gel analysis technology. *Anal Bioanal Chem*, 382, 669-78.
- MARQUES, M. J., FERRETTI, R., VOMERO, V. U., MINATEL, E. & NETO, H. S. 2007. Intrinsic laryngeal muscles are spared from myonecrosis in the mdx mouse model of Duchenne muscular dystrophy. *Muscle Nerve*, 35, 349-53.
- MARSH, G. G. & MUNSAT, T. L. 1974. Evidence of early impairment of verbal intelligence in Duchenne muscular dystrophy. *Arch Dis Child*, 49, 118-22.
- MARSHALL, J. L., HOLMBERG, J., CHOU, E., OCAMPO, A. C., OH, J., LEE, J., PETER, A. K., MARTIN, P. T. & CROSBIE-WATSON, R. H. 2012. Sarcospan-dependent Akt activation is required for utrophin expression and muscle regeneration. *J Cell Biol*, 197, 1009-27.
- MAURYA, P. K. & PRAKASH, S. 2013. Decreased activity of Ca(++)-ATPase and Na(+)/K(+)-ATPase during aging in humans. *Appl Biochem Biotechnol*, 170, 131-7.
- MAZZONE, E., MARTINELLI, D., BERARDINELLI, A., MESSINA, S., D'AMICO, A., VASCO, G., MAIN, M., DOGLIO, L., POLITANO, L., CAVALLARO, F., FROSINI, S., BELLO, L., CARLESI, A., BONETTI, A. M., ZUCCHINI, E., DE SANCTIS, R., SCUTIFERO, M., BIANCO, F., ROSSI, F., MOTTA, M. C., SACCO, A., DONATI, M. A., MONGINI, T., PINI, A., BATTINI, R., PEGORARO, E., PANE, M., PASQUINI, E., BRUNO, C., VITA, G., DE WAURE, C., BERTINI, E. & MERCURI, E. 2010. North Star Ambulatory Assessment, 6-minute walk test and timed items in ambulant boys with Duchenne muscular dystrophy. *Neuromuscul Disord*, 20, 712-6.
- MCARDLE, A., DILLMANN, W. H., MESTRIL, R., FAULKNER, J. A. & JACKSON, M. J. 2004. Overexpression of HSP70 in mouse skeletal muscle protects against muscle damage and age-related muscle dysfunction. *FASEB J*, 18, 355-7.
- MCDOUALL, R. M., DUNN, M. J. & DUBOWITZ, V. 1989. Expression of class I and class II MHC antigens in neuromuscular diseases. *J Neurol Sci*, 89, 213-26.
- MCGOUGH, A. 1999. How to build a molecular shock absorber. *Curr Biol*, 9, R887-9.
- MCGREEVY, J. W., HAKIM, C. H., MCINTOSH, M. A. & DUAN, D. 2015. Animal models of Duchenne muscular dystrophy: from basic mechanisms to gene therapy. *Dis Model Mech*, 8, 195-213.
- MCNALLY, E. M. 2007. New approaches in the therapy of cardiomyopathy in muscular dystrophy. *Annu Rev Med*, 58, 75-88.
- MCNEIL, A. K., RESCHER, U., GERKE, V. & MCNEIL, P. L. 2006. Requirement for annexin A1 in plasma membrane repair. *J Biol Chem*, 281, 35202-7.
- MCNEIL, C. J., DOHERTY, T. J., STASHUK, D. W. & RICE, C. L. 2005. Motor unit number estimates in the tibialis anterior muscle of young, old, and very old men. *Muscle Nerve*, 31, 461-7.
- MEGENEY, L. A., KABLAR, B., GARRETT, K., ANDERSON, J. E. & RUDNICKI, M. A. 1996. MyoD is required for myogenic stem cell function in adult skeletal muscle. *Genes Dev*, 10, 1173-83.
- MEGENEY, L. A., KABLAR, B., PERRY, R. L., YING, C., MAY, L. & RUDNICKI, M. A. 1999. Severe cardiomyopathy in mice lacking dystrophin and MyoD. *Proc Natl Acad Sci USA*, 96, 220-5.
- MEHLER, M. F. 2000. Brain dystrophin, neurogenetics and mental retardation. *Brain Res Brain Res Rev*, 32, 277-307.

- MELEADY, P., DOOLAN, P., HENRY, M., BARRON, N., KEENAN, J., O'SULLIVAN, F., CLARKE, C., GAMMELL, P., MELVILLE, M. W., LEONARD, M. & CLYNES, M. 2011. Sustained productivity in recombinant Chinese hamster ovary (CHO) cell lines: proteome analysis of the molecular basis for a process-related phenotype. *BMC Biotechnol*, 11, 78.
- MELEADY, P., GALLAGHER, M., CLARKE, C., HENRY, M., SANCHEZ, N., BARRON, N. & CLYNES, M. 2012a. Impact of miR-7 over-expression on the proteome of Chinese hamster ovary cells. *J Biotechnol*, 160, 251-62.
- MELEADY, P., HOFFFROGGE, R., HENRY, M., RUPP, O., BORT, J. H., CLARKE, C., BRINKROLF, K., KELLY, S., MÜLLER, B., DOOLAN, P., HACKL, M., BECKMANN, T. F., NOLL, T., GRILLARI, J., BARRON, N., PÜHLER, A., CLYNES, M. & BORTH, N. 2012b. Utilization and evaluation of CHO-specific sequence databases for mass spectrometry based proteomics. *Biotechnol Bioeng*, 109, 1386-94.
- MENDELL, J. R., RODINO-KLAPAC, L. R., SAHENK, Z., ROUSH, K., BIRD, L., LOWES, L. P., ALFANO, L., GOMEZ, A. M., LEWIS, S., KOTA, J., MALIK, V., SHONTZ, K., WALKER, C. M., FLANIGAN, K. M., CORRIDORE, M., KEAN, J. R., ALLEN, H. D., SHILLING, C., MELIA, K. R., SAZANI, P., SAOUD, J. B., KAYE, E. M. & GROUP, E. S. 2013. Eteplirsen for the treatment of Duchenne muscular dystrophy. *Ann Neurol*, 74, 637-47.
- MENG, Z. & VEENSTRA, T. D. 2011. Targeted mass spectrometry approaches for protein biomarker verification. *J Proteomics*, 74, 2650-9.
- MERI, S., MORGAN, B. P., DAVIES, A., DANIELS, R. H., OLAVESSEN, M. G., WALDMANN, H. & LACHMANN, P. J. 1990. Human protectin (CD59), an 18,000-20,000 MW complement lysis restricting factor, inhibits C5b-8 catalysed insertion of C9 into lipid bilayers. *Immunology*, 71, 1-9.
- MERLINI, L., CICOGNANI, A., MALASPINA, E., GENNARI, M., GNUDI, S., TALIM, B. & FRANZONI, E. 2003. Early prednisone treatment in Duchenne muscular dystrophy. *Muscle Nerve*, 27, 222-7.
- MERYON, E. 1852. On Granular and Fatty Degeneration of the Voluntary Muscles. *Med Chir Trans*, 35, 73-84.1.
- MESSINA, S., BITTO, A., AGUENNOUZ, M., MAZZEO, A., MIGLIORATO, A., POLITO, F., IRRERA, N., ALTAVILLA, D., VITA, G. L., RUSSO, M., NARO, A., DE PASQUALE, M. G., RIZZUTO, E., MUSARÒ, A., SQUADRITO, F. & VITA, G. 2009. Flavocoxid counteracts muscle necrosis and improves functional properties in mdx mice: a comparison study with methylprednisolone. *Exp Neurol*, 220, 349-58.
- MESSINA, S., BITTO, A., AGUENNOUZ, M., MINUTOLI, L., MONICI, M. C., ALTAVILLA, D., SQUADRITO, F. & VITA, G. 2006. Nuclear factor kappa-B blockade reduces skeletal muscle degeneration and enhances muscle function in Mdx mice. *Exp Neurol*, 198, 234-41.
- MI, H., MURUGANUJAN, A. & THOMAS, P. D. 2013. PANTHER in 2013: modeling the evolution of gene function, and other gene attributes, in the context of phylogenetic trees. *Nucleic Acids Res*, 41, D377-86.
- MILLAY, D. P., GOONASEKERA, S. A., SARGENT, M. A., MAILLET, M., ARONOW, B. J. & MOKKENTIN, J. D. 2009. Calcium influx is sufficient to induce muscular dystrophy through a TRPC-dependent mechanism. *Proc Natl Acad Sci USA*, 106, 19023-8.
- MIN, K. W., LEE, S. H. & BAEK, S. J. 2016. Moonlighting proteins in cancer. *Cancer Lett*, 370, 108-16.
- MIRAVITLLES, M. 2012. Alpha-1-antitrypsin and other proteinase inhibitors. *Curr Opin Pharmacol*, 12, 309-14.

- MITCHELL, K. J., PANNÉREC, A., CADOT, B., PARLAKIAN, A., BESSON, V., GOMES, E. R., MARAZZI, G. & SASSOON, D. A. 2010. Identification and characterization of a non-satellite cell muscle resident progenitor during postnatal development. *Nat Cell Biol*, 12, 257-66.
- MITRPANT, C., FLETCHER, S., IVERSEN, P. L. & WILTON, S. D. 2009. By-passing the nonsense mutation in the 4 CV mouse model of muscular dystrophy by induced exon skipping. *J Gene Med*, 11, 46-56.
- MIZUNO, Y., GUYON, J. R., WATKINS, S. C., MIZUSHIMA, K., SASAOKA, T., IMAMURA, M., KUNKEL, L. M. & OKAMOTO, K. 2004. Beta-synemin localizes to regions of high stress in human skeletal myofibers. *Muscle Nerve*, 30, 337-46.
- MIZUNO, Y., THOMPSON, T. G., GUYON, J. R., LIDOV, H. G., BROSIUS, M., IMAMURA, M., OZAWA, E., WATKINS, S. C. & KUNKEL, L. M. 2001. Desmuslin, an intermediate filament protein that interacts with alpha -dystrobrevin and desmin. *Proc Natl Acad Sci USA*, 98, 6156-61.
- MOENS, P., BAATSEN, P. H. & MARÉCHAL, G. 1993. Increased susceptibility of EDL muscles from mdx mice to damage induced by contractions with stretch. *J Muscle Res Cell Motil*, 14, 446-51.
- MOIZARD, M. P., TOUTAIN, A., FOURNIER, D., BERRET, F., RAYNAUD, M., BILLARD, C., ANDRES, C. & MORAINÉ, C. 2000. Severe cognitive impairment in DMD: obvious clinical indication for Dp71 isoform point mutation screening. *Eur J Hum Genet*, 8, 552-6.
- MOKHTARIAN, A., LEFAUCHEUR, J. P., EVEN, P. C. & SEBILLE, A. 1999. Hindlimb immobilization applied to 21-day-old mdx mice prevents the occurrence of muscle degeneration. *J Appl Physiol* (1985), 86, 924-31.
- MOKUNO, K., RIKU, S., SUGIMURA, K., TAKAHASHI, A., KATO, K. & OSUGI, S. 1987. Serum creatine kinase isoenzymes in Duchenne muscular dystrophy determined by sensitive enzyme immunoassay methods. *Muscle Nerve*, 10, 459-63.
- MONTI, R. J., ROY, R. R. & EDGERTON, V. R. 2001. Role of motor unit structure in defining function. *Muscle Nerve*, 24, 848-66.
- MOORE, S. E. & WALSH, F. S. 1986. Nerve dependent regulation of neural cell adhesion molecule expression in skeletal muscle. *Neuroscience*, 18, 499-505.
- MOOTHA, V. K., BUNKENBORG, J., OLSEN, J. V., HJERRILD, M., WISNIEWSKI, J. R., STAHL, E., BOLOURI, M. S., RAY, H. N., SIHAG, S., KAMAL, M., PATTERSON, N., LANDER, E. S. & MANN, M. 2003. Integrated analysis of protein composition, tissue diversity, and gene regulation in mouse mitochondria. *Cell*, 115, 629-40.
- MORI, K., EMOTO, M. & INABA, M. 2011. Fetuin-A: a multifunctional protein. *Recent Pat Endocr Metab Immune Drug Discov*, 5, 124-46.
- MORRISON, J., LU, Q. L., PASTORET, C., PARTRIDGE, T. & BOU-GHARIOS, G. 2000. T-cell-dependent fibrosis in the mdx dystrophic mouse. *Lab Invest*, 80, 881-91.
- MOSS, F. P. & LEBLOND, C. P. 1971. Satellite cells as the source of nuclei in muscles of growing rats. *Anat Rec*, 170, 421-35.
- MOURKIOTI, F., KUSTAN, J., KRAFT, P., DAY, J. W., ZHAO, M. M., KOST-ALIMOVA, M., PROTOPOPOV, A., DEPINHO, R. A., BERNSTEIN, D., MEEKER, A. K. & BLAU, H. M. 2013. Role of telomere dysfunction in cardiac failure in Duchenne muscular dystrophy. *Nat Cell Biol*, 15, 895-904.
- MUKHOPADHYAY, G., DOHERTY, P., WALSH, F. S., CROCKER, P. R. & FILBIN, M. T. 1994. A novel role for myelin-associated glycoprotein as an inhibitor of axonal regeneration. *Neuron*, 13, 757-67.

- MUNTONI, F., MATEDDU, A. & SERRA, G. 1991. Passive avoidance behaviour deficit in the mdx mouse. *Neuromuscul Disord*, 1, 121-3.
- MUNTONI, F., TORELLI, S. & FERLINI, A. 2003. Dystrophin and mutations: one gene, several proteins, multiple phenotypes. *Lancet Neurol*, 2, 731-40.
- MURGIA, M., TONIOLO, L., NAGARAJ, N., CICILIOT, S., VINDIGNI, V., SCHIAFFINO, S., REGGIANI, C. & MANN, M. 2017. Single Muscle Fiber Proteomics Reveals Fiber-Type-Specific Features of Human Muscle Aging. *Cell Rep*, 19, 2396-2409.
- MURPHY, S. & OHLENDIECK, K. 2016. The biochemical and mass spectrometric profiling of the dystrophin complexome from skeletal muscle. *Comput Struct Biotechnol J*, 14, 20-7.
- MURPHY, S. & OHLENDIECK, K. 2017. Mass spectrometric identification of dystrophin, the protein product of the Duchenne muscular dystrophy gene, in distinct muscle surface membranes. *Int J Mol Med*, 40(4), 1078-1088.
- MURPHY, S. & OHLENDIECK, K. 2018. Proteomic profiling of large myofibrillar proteins from dried and long-term stored polyacrylamide gels. *Anal Biochem*, 543, 8-11.
- MURPHY, S., BRINKMEIER, H., KRAUTWALD, M., HENRY, M., MELEADY, P. & OHLENDIECK, K. 2017a. Proteomic profiling of the dystrophin complex and membrane fraction from dystrophic mdx muscle reveals decreases in the cytolinker desmoglein and increases in the extracellular matrix stabilizers biglycan and fibronectin. *J Muscle Res Cell Motil*, 38, 251-268.
- MURPHY, S., DOWLING, P., ZWEYER, M., HENRY, M., MELEADY, P., MUNDEGAR, R. R., SWANDULLA, D. & OHLENDIECK, K. 2017b. Proteomic profiling of mdx-4cv serum reveals highly elevated levels of the inflammation-induced plasma marker haptoglobin in muscular dystrophy. *Int J Mol Med*, 39, 1,357-1,370.
- MURPHY, S., DOWLING, P. & OHLENDIECK, K. 2016a. Comparative Skeletal Muscle Proteomics Using Two-Dimensional Gel Electrophoresis. *Proteomes*, 4.
- MURPHY, S., DOWLING, P., ZWEYER, M., MUNDEGAR, R. R., HENRY, M., MELEADY, P., SWANDULLA, D. & OHLENDIECK, K. 2016b. Proteomic analysis of dystrophin deficiency and associated changes in the aged mdx-4cv heart model of dystrophinopathy-related cardiomyopathy. *J Proteomics*, 145, 24-36.
- MURPHY, S., HENRY, M., MELEADY, P., ZWEYER, M., MUNDEGAR, R. R., SWANDULLA, D. & OHLENDIECK, K. 2015a. Simultaneous Pathoproteomic Evaluation of the Dystrophin-Glycoprotein Complex and Secondary Changes in the mdx-4cv Mouse Model of Duchenne Muscular Dystrophy. *Biology (Basel)*, 4, 397-423.
- MURPHY, S., ZWEYER, M., MUNDEGAR, R. R., HENRY, M., MELEADY, P., SWANDULLA, D. & OHLENDIECK, K. 2015b. Concurrent Label-Free Mass Spectrometric Analysis of Dystrophin Isoform Dp427 and the Myofibrosis Marker Collagen in Crude Extracts from. *Proteomes*, 3, 298-327.
- MURPHY, S., ZWEYER, M., HENRY, M., MELEADY, P., MUNDEGAR, R. R., SWANDULLA, D. & OHLENDIECK, K. 2015c. Label-free mass spectrometric analysis reveals complex changes in the brain proteome from the mdx-4cv mouse model of Duchenne muscular dystrophy. *Clin Proteomics*, 12, 27.
- MURPHY, S., ZWEYER, M., HENRY, M., MELEADY, P., MUNDEGAR, R. R., SWANDULLA, D. & OHLENDIECK, K. 2018a. Proteomic analysis of the sarcolemma-enriched fraction from dystrophic mdx-4cv skeletal muscle. *J Proteomics*.
- MURPHY, S., ZWEYER, M., MUNDEGAR, R. R., SWANDULLA, D. & OHLENDIECK, K. 2018b. Proteomic serum biomarkers for neuromuscular diseases. *Expert Rev Proteomics*, 1-15.
- MURRAY, B. E. & OHLENDIECK, K. 1997. Cross-linking analysis of the ryanodine receptor and alpha1-dihydropyridine receptor in rabbit skeletal muscle triads. *Biochem J*, 324 (Pt 2), 689-96.

- MURRAY, B. E. & OHLENDIECK, K. 2000. Chemical cross-linking analysis of Ca(2+-)ATPase from rabbit skeletal muscle. *Biochem Educ*, 28, 41-46.
- MUSTELIN, T. & TASKÉN, K. 2003. Positive and negative regulation of T-cell activation through kinases and phosphatases. *Biochem J*, 371, 15-27.
- NADARAJAH, V. D., VAN PUTTEN, M., CHAOUCH, A., GARROOD, P., STRAUB, V., LOCHMÜLLER, H., GINJAAR, H. B., AARTSMA-RUS, A. M., VAN OMMEN, G. J., DEN DUNNEN, J. T. & 'T HOEN, P. A. 2011. Serum matrix metalloproteinase-9 (MMP-9) as a biomarker for monitoring disease progression in Duchenne muscular dystrophy (DMD). *Neuromuscul Disord*, 21, 569-78.
- NALLAMILLI, B. R., ANKALA, A. & HEGDE, M. 2014. Molecular diagnosis of duchenne muscular dystrophy. *Curr Protoc Hum Genet*, 83, 9.25.1-9.25.29.
- NASTASE, M. V., YOUNG, M. F. & SCHAEFER, L. 2012. Biglycan: a multivalent proteoglycan providing structure and signals. *J Histochem Cytochem*, 60, 963-75.
- NELIS, E., HAITES, N. & VAN BROECKHOVEN, C. 1999. Mutations in the peripheral myelin genes and associated genes in inherited peripheral neuropathies. *Hum Mutat*, 13, 11-28.
- NEUHOFF, V., AROLD, N., TAUBE, D. & EHRHARDT, W. 1988. Improved staining of proteins in polyacrylamide gels including isoelectric focusing gels with clear background at nanogram sensitivity using Coomassie Brilliant Blue G-250 and R-250. *Electrophoresis*, 9, 255-62.
- NEWHEY, S. E., HOWMAN, E. V., PONTING, C. P., BENSON, M. A., NAWROTZKI, R., LOH, N. Y., DAVIES, K. E. & BLAKE, D. J. 2001. Syncoilin, a novel member of the intermediate filament superfamily that interacts with alpha-dystrobrevin in skeletal muscle. *J Biol Chem*, 276, 6645-55.
- NGUYEN, H. X. & TIDBALL, J. G. 2003. Interactions between neutrophils and macrophages promote macrophage killing of rat muscle cells in vitro. *J Physiol*, 547, 125-32.
- NIGRO, V. & PILUSO, G. 2015. Spectrum of muscular dystrophies associated with sarcolemmal-protein genetic defects. *Biochim Biophys Acta*, 1852, 585-93.
- NORWOOD, F. L., SUTHERLAND-SMITH, A. J., KEEP, N. H. & KENDRICK-JONES, J. 2000. The structure of the N-terminal actin-binding domain of human dystrophin and how mutations in this domain may cause Duchenne or Becker muscular dystrophy. *Structure*, 8, 481-91.
- OAK, S. A., ZHOU, Y. W. & JARRETT, H. W. 2003. Skeletal muscle signaling pathway through the dystrophin glycoprotein complex and Rac1. *J Biol Chem*, 278, 39287-95.
- O'CONNELL, K. & OHLENDIECK, K. 2009. Proteomic DIGE analysis of the mitochondria-enriched fraction from aged rat skeletal muscle. *Proteomics*, 9, 5509-24.
- O'CONNELL, K., GANNON, J., DORAN, P. & OHLENDIECK, K. 2007. Proteomic profiling reveals a severely perturbed protein expression pattern in aged skeletal muscle. *Int J Mol Med*, 20, 145-53.
- O'FARRELL, P. H. 1975. High resolution two-dimensional electrophoresis of proteins. *J Biol Chem*, 250, 4007-21.
- OGASAWARA, A. 1989. Downward shift in IQ in persons with Duchenne muscular dystrophy compared to those with spinal muscular atrophy. *Am J Ment Retard*, 93, 544-547.
- OGURA, Y., TAJRISHI, M. M., SATO, S., HINDI, S. M. & KUMAR, A. 2014. Therapeutic potential of matrix metalloproteinases in Duchenne muscular dystrophy. *Front Cell Dev Biol*, 2, 11.
- OH, P., LI, Y., YU, J., DURR, E., KRASINSKA, K. M., CARVER, L. A., TESTA, J. E. & SCHNITZER, J. E. 2004. Subtractive proteomic mapping of the endothelial surface in lung and solid tumours for tissue-specific therapy. *Nature*, 429, 629-35.

- O'HARA, R., MURPHY, E. P., WHITEHEAD, A. S., FITZGERALD, O. & BRESNIHAN, B. 2000. Acute-phase serum amyloid A production by rheumatoid arthritis synovial tissue. *Arthritis Res*, 2, 142-4.
- OHLENDIECK, K. & CAMPBELL, K. P. 1991a. Dystrophin-associated proteins are greatly reduced in skeletal muscle from mdx mice. *J Cell Biol*, 115, 1685-94.
- OHLENDIECK, K. & CAMPBELL, K. P. 1991b. Dystrophin constitutes 5% of membrane cytoskeleton in skeletal muscle. *FEBS Lett*, 283, 230-4.
- OHLENDIECK, K. 2013. Proteomic identification of biomarkers of skeletal muscle disorders. *Biomark Med*, 7, 169-86.
- OHLENDIECK, K. 2011a. Proteomic Profiling of Fast-To-Slow Muscle Transitions during Aging. *Front Physiol*, 2, 105.
- OHLENDIECK, K. 2011b. Proteomic profiling of skeletal muscle plasticity. *Muscles Ligaments Tendons J*, 1, 119-26.
- OHLENDIECK, K. 2011c. Skeletal muscle proteomics: current approaches, technical challenges and emerging techniques. *Skelet Muscle*, 1, 6.
- OHLENDIECK, K. 2010. Proteomics of skeletal muscle glycolysis. *Biochim Biophys Acta*, 1804, 2089-101.
- OHLENDIECK, K., ERVASTI, J. M., SNOOK, J. B. & CAMPBELL, K. P. 1991. Dystrophin-glycoprotein complex is highly enriched in isolated skeletal muscle sarcolemma. *J Cell Biol*, 112, 135-48.
- OHLENDIECK, K., MATSUMURA, K., IONASESCU, V. V., TOWBIN, J. A., BOSCH, E. P., WEINSTEIN, S. L., SERNETT, S. W. & CAMPBELL, K. P. 1993. Duchenne muscular dystrophy: deficiency of dystrophin-associated proteins in the sarcolemma. *Neurology*, 43, 795-800.
- OHTA, M., ITAGAKI, Y., ITOH, N., HAYASHI, K., NISHITANI, H. & OHTA, K. 1991. Carbonic anhydrase III in serum in muscular dystrophy and other neurological disorders: relationship with creatine kinase. *Clin Chem*, 37, 36-9.
- OKINAKA, S., KUMAGAI, H., EBASHI, S., SUGITA, H., MOMOI, H., TOYOKURA, Y. & FUJIE, Y. 1961. Serum creatine phosphokinase. Activity in progressive muscular dystrophy and neuromuscular diseases. *Arch Neurol*, 4, 520-5.
- OKUMURA, A., NAGAI, K. & OKUMURA, N. 2008. Interaction of alpha1-syntrophin with multiple isoforms of heterotrimeric G protein alpha subunits. *FEBS J*, 275, 22-33.
- OLIVETTI, G., MELISSARI, M., CAPASSO, J. M. & ANVERSA, P. 1991. Cardiomyopathy of the aging human heart. Myocyte loss and reactive cellular hypertrophy. *Circ Res*, 68, 1560-8.
- OLIVIERO, S. & CORTESE, R. 1989. The human haptoglobin gene promoter: interleukin-6-responsive elements interact with a DNA-binding protein induced by interleukin-6. *EMBO J*, 8, 1145-51.
- O'NEILL, A. S., VAN DEN BERG, T. K. & MULLEN, G. E. 2013. Sialoadhesin - a macrophage-restricted marker of immunoregulation and inflammation. *Immunology*, 138, 198-207.
- O'NEILL, A., WILLIAMS, M. W., RESNECK, W. G., MILNER, D. J., CAPETANAKI, Y. & BLOCH, R. J. 2002. Sarcolemmal organization in skeletal muscle lacking desmin: evidence for cytokeratins associated with the membrane skeleton at costameres. *Mol Biol Cell*, 13, 2347-59.
- OZDEMIR, C., AKPULAT, U., SHARAFI, P., YILDIZ, Y., ONBAŞILAR, I. & KOCAEFE, C. 2014. Periostin is temporally expressed as an extracellular matrix component in skeletal muscle regeneration and differentiation. *Gene*, 553, 130-9.

- PAGE, M. J. & DI CERA, E. 2008. Serine peptidases: classification, structure and function. *Cell Mol Life Sci*, 65, 1220-36.
- PALCZEWSKA, M., GROVES, P., BATTÀ, G., HEISE, B. & KUŹNICKI, J. 2003. Calretinin and calbindin D28k have different domain organizations. *Protein Sci*, 12, 180-4.
- PASSAMANO, L., TAGLIA, A., PALLADINO, A., VIGGIANO, E., D'AMBROSIO, P., SCUTIFERO, M., ROSARIA CECIO, M., TORRE, V., DE LUCA, F., PICILLO, E., PACIELLO, O., PILUSO, G., NIGRO, G. & POLITANO, L. 2012. Improvement of survival in Duchenne Muscular Dystrophy: retrospective analysis of 835 patients. *Acta Myol*, 31, 121-5.
- PASTORET, C. & SEBILLE, A. 1995. mdx mice show progressive weakness and muscle deterioration with age. *J Neurol Sci*, 129, 97-105.
- PATEL, H., FELLOWES, R., COADE, S. & WOO, P. 1998. Human serum amyloid A has cytokine-like properties. *Scand J Immunol*, 48, 410-8.
- PAULOVICH, A. G., WHITEAKER, J. R., HOOFNAGLE, A. N. & WANG, P. 2008. The interface between biomarker discovery and clinical validation: The tar pit of the protein biomarker pipeline. *Proteomics Clin Appl*, 2, 1386-1402.
- PEKNY, M., WILHELMSSON, U. & PEKNA, M. 2014. The dual role of astrocyte activation and reactive gliosis. *Neurosci Lett*, 565, 30-8.
- PELTIER, J., ROPERCH, J. P., AUDEBERT, S., BORG, J. P. & CAMOIN, L. 2018. Activation peptide of the coagulation factor XIII (AP-F13A1) as a new biomarker for the screening of colorectal cancer. *Clin Proteomics*, 15, 15.
- PERKINS, K. J. & DAVIES, K. E. 2002. The role of utrophin in the potential therapy of Duchenne muscular dystrophy. *Neuromuscul Disord*, 12 Suppl 1, S78-89.
- PERRONNET, C. & VAILLEND, C. 2010. Dystrophins, utrophins, and associated scaffolding complexes: role in mammalian brain and implications for therapeutic strategies. *J Biomed Biotechnol*, 2010, 849426.
- PESSINA, P., CABRERA, D., MORALES, M. G., RIQUELME, C. A., GUTIÉRREZ, J., SERRANO, A. L., BRANDAN, E. & MUÑOZ-CÁNOVES, P. 2014. Novel and optimized strategies for inducing fibrosis in vivo: focus on Duchenne Muscular Dystrophy. *Skelet Muscle*, 4, 7.
- PETER, A. K., MARSHALL, J. L. & CROSBIE, R. H. 2008. Sarcospan reduces dystrophic pathology: stabilization of the utrophin-glycoprotein complex. *J Cell Biol*, 183, 419-27.
- PETERSON, J. M., KLINE, W., CANAN, B. D., RICCA, D. J., KASPAR, B., DELFÍN, D. A., DIRIENZO, K., CLEMENS, P. R., ROBBINS, P. D., BALDWIN, A. S., FLOOD, P., KAUMAYA, P., FREITAS, M., KORNEGAY, J. N., MENDELL, J. R., RAFAEL-FORTNEY, J. A., GUTTRIDGE, D. C. & JANSSEN, P. M. 2011. Peptide-based inhibition of NF- κ B rescues diaphragm muscle contractile dysfunction in a murine model of Duchenne muscular dystrophy. *Mol Med*, 17, 508-15.
- PETROF, B. J., SHRAGER, J. B., STEDMAN, H. H., KELLY, A. M. & SWEENEY, H. L. 1993. Dystrophin protects the sarcolemma from stresses developed during muscle contraction. *Proc Natl Acad Sci USA*, 90, 3710-4.
- PHELAN D, WILSON GR, JAMES PA, LOCKHART PJ. 2013. The genetics of cardiomyopathy, new technologies and the path to personalised medicine. *OA Genetics*, 1(1):9.
- PILLERS, D. A., BULMAN, D. E., WELEBER, R. G., SIGESMUND, D. A., MUSARELLA, M. A., POWELL, B. R., MURPHEY, W. H., WESTALL, C., PANTON, C. & BECKER, L. E. 1993. Dystrophin expression in the human retina is required for normal function as defined by electroretinography. *Nat Genet*, 4, 82-6.

- PISTONI, M., GHIGNA, C. & GABELLINI, D. 2010. Alternative splicing and muscular dystrophy. *RNA Biol*, 7, 441-52.
- POLVERINI, E., RANGARAJ, G., LIBICH, D. S., BOGGS, J. M. & HARAUZ, G. 2008. Binding of the proline-rich segment of myelin basic protein to SH3 domains: spectroscopic, microarray, and modeling studies of ligand conformation and effects of posttranslational modifications. *Biochemistry*, 47, 267-82.
- PORTER, J. D., KHANNA, S., KAMINSKI, H. J., RAO, J. S., MERRIAM, A. P., RICHMONDS, C. R., LEAHY, P., LI, J., GUO, W. & ANDRADE, F. H. 2002. A chronic inflammatory response dominates the skeletal muscle molecular signature in dystrophin-deficient mdx mice. *Hum Mol Genet*, 11, 263-72.
- PORTER, J. D., RAFAEL, J. A., RAGUSA, R. J., BRUECKNER, J. K., TRICKETT, J. I. & DAVIES, K. E. 1998. The sparing of extraocular muscle in dystrophinopathy is lost in mice lacking utrophin and dystrophin. *J Cell Sci*, 111 (Pt 13), 1801-11.
- POURTEYMOUR, S., LEE, S., LANGLEITE, T. M., ECKARDT, K., HJORTH, M., BINDESBØLL, C., DALEN, K. T., BIRKELAND, K. I., DREVON, C. A., HOLEN, T. & NORHEIM, F. 2015. Perilipin 4 in human skeletal muscle: localization and effect of physical activity. *Physiol Rep*, 3.
- PRATTIS, S. M., HORTON, S. B., VAN CAMP, S. D. & KORNEGAY, J. N. 1994. Immunohistochemical detection of neural cell adhesion molecule and laminin in X-linked dystrophic dogs and mdx mice. *J Comp Pathol*, 110, 253-66.
- PROC, J. L., KUZYK, M. A., HARDIE, D. B., YANG, J., SMITH, D. S., JACKSON, A. M., PARKER, C. E. & BORCHERS, C. H. 2010. A quantitative study of the effects of chaotropic agents, surfactants, and solvents on the digestion efficiency of human plasma proteins by trypsin. *J Proteome Res*, 9, 5422-37.
- QIAN, W. J., JACOBS, J. M., LIU, T., CAMP, D. G. & SMITH, R. D. 2006. Advances and challenges in liquid chromatography-mass spectrometry-based proteomics profiling for clinical applications. *Mol Cell Proteomics*, 5, 1727-44.
- RABILLOUD, T. & LELONG, C. 2011. Two-dimensional gel electrophoresis in proteomics: a tutorial. *J Proteomics*, 74, 1829-41.
- RABILLOUD, T., CHEVALLET, M., LUCHE, S. & LELONG, C. 2010. Two-dimensional gel electrophoresis in proteomics: Past, present and future. *J Proteomics*, 73, 2064-77.
- RAFAEL, J. A., COX, G. A., CORRADO, K., JUNG, D., CAMPBELL, K. P. & CHAMBERLAIN, J. S. 1996. Forced expression of dystrophin deletion constructs reveals structure-function correlations. *J Cell Biol*, 134, 93-102.
- RAFII, M. S., HAGIWARA, H., MERCADO, M. L., SEO, N. S., XU, T., DUGAN, T., OWENS, R. T., HOOK, M., MCQUILLAN, D. J., YOUNG, M. F. & FALLON, J. R. 2006. Biglycan binds to alpha- and gamma-sarcoglycan and regulates their expression during development. *J Cell Physiol*, 209, 439-47.
- RAGUSA, R. J., CHOW, C. K. & PORTER, J. D. 1997. Oxidative stress as a potential pathogenic mechanism in an animal model of Duchenne muscular dystrophy. *Neuromuscul Disord*, 7, 379-86.
- RAHIMOV, F. & KUNKEL, L. M. 2013. The cell biology of disease: cellular and molecular mechanisms underlying muscular dystrophy. *J Cell Biol*, 201, 499-510.
- RAMACHANDRAN, J., SCHNEIDER, J. S., CRASSOUS, P. A., ZHENG, R., GONZALEZ, J. P., XIE, L. H., BEUVE, A., FRAIDENRAICH, D. & PELUFFO, R. D. 2013. Nitric oxide signalling pathway in Duchenne muscular dystrophy mice: up-regulation of L-arginine transporters. *Biochem J*, 449, 133-42.

- RAMASAMY, P., MURPHY, C. C., CLYNES, M., HORGAN, N., MORIARTY, P., TIERNAN, D., BEATTY, S., KENNEDY, S. & MELEADY, P. 2014. Proteomics in uveal melanoma. *Exp Eye Res*, 118, 1-12.
- RATHCKE, C. N. & VESTERGAARD, H. 2009. YKL-40--an emerging biomarker in cardiovascular disease and diabetes. *Cardiovasc Diabetol*, 8, 61.
- RECTOR, R. S., PAYNE, R. M. & IBDAH, J. A. 2008. Mitochondrial trifunctional protein defects: clinical implications and therapeutic approaches. *Adv Drug Deliv Rev*, 60, 1488-96.
- REILLY, J. F., MAHER, P. A. & KUMARI, V. G. 1998. Regulation of astrocyte GFAP expression by TGF-beta1 and FGF-2. *Glia*, 22, 202-10.
- RELAIX, F. & ZAMMIT, P. S. 2012. Satellite cells are essential for skeletal muscle regeneration: the cell on the edge returns centre stage. *Development*, 139, 2845-56.
- RENTSCHLER, S., LINN, H., DEININGER, K., BEDFORD, M. T., ESPANEL, X. & SUDOL, M. 1999. The WW domain of dystrophin requires EF-hands region to interact with beta-dystroglycan. *Biol Chem*, 380, 431-42.
- REPETTO, S., BADO, M., BRODA, P., LUCANIA, G., MASETTI, E., SOTGIA, F., CARBONE, I., PAVAN, A., BONILLA, E., CORDONE, G., LISANTI, M. P. & MINETTI, C. 1999. Increased number of caveolae and caveolin-3 overexpression in Duchenne muscular dystrophy. *Biochem Biophys Res Commun*, 261, 547-50.
- RICOTTI, V., SPINTY, S., ROPER, H., HUGHES, I., TEJURA, B., ROBINSON, N., LAYTON, G., DAVIES, K., MUNTONI, F. & TINSLEY, J. 2016. Safety, Tolerability, and Pharmacokinetics of SMT C1100, a 2-Arylbenzoxazole Utrophin Modulator, following Single- and Multiple-Dose Administration to Pediatric Patients with Duchenne Muscular Dystrophy. *PLoS One*, 11, e0152840.
- RIFAI, N., GILLETTE, M. A. & CARR, S. A. 2006. Protein biomarker discovery and validation: the long and uncertain path to clinical utility. *Nat Biotechnol*, 24, 971-83.
- RODRÍGUEZ, J. J., OLABARRIA, M., CHVATAL, A. & VERKHRATSKY, A. 2009. Astroglia in dementia and Alzheimer's disease. *Cell Death Differ*, 16, 378-85.
- ROONEY, J. E., GURPUR, P. B. & BURKIN, D. J. 2009. Laminin-111 protein therapy prevents muscle disease in the mdx mouse model for Duchenne muscular dystrophy. *Proc Natl Acad Sci USA*, 106, 7991-6.
- ROSTOVTSEVA, T. & COLOMBINI, M. 1997. VDAC channels mediate and gate the flow of ATP: implications for the regulation of mitochondrial function. *Biophys J*, 72, 1954-62.
- ROUILLON, J., POUPIOT, J., ZOCEVIC, A., AMOR, F., LÉGER, T., GARCIA, C., CAMADRO, J. M., WONG, B., PINILLA, R., COSETTE, J., COENEN-STASS, A. M., MCCLOREY, G., ROBERTS, T. C., WOOD, M. J., SERVAIS, L., UDD, B., VOIT, T., RICHARD, I. & SVINARTCHOUK, F. 2015. Serum proteomic profiling reveals fragments of MYOM3 as potential biomarkers for monitoring the outcome of therapeutic interventions in muscular dystrophies. *Hum Mol Genet*, 24, 4916-32.
- ROUILLON, J., ZOCEVIC, A., LEGER, T., GARCIA, C., CAMADRO, J. M., UDD, B., WONG, B., SERVAIS, L., VOIT, T. & SVINARTCHOUK, F. 2014. Proteomics profiling of urine reveals specific titin fragments as biomarkers of Duchenne muscular dystrophy. *Neuromuscul Disord*, 24, 563-73.
- ROWLAND, L. P. & SHNEIDER, N. A. 2001. Amyotrophic lateral sclerosis. *N Engl J Med*, 344, 1688-700.
- RYBAKOVA, I. N., PATEL, J. R. & ERVASTI, J. M. 2000. The dystrophin complex forms a mechanically strong link between the sarcolemma and costameric actin. *J Cell Biol*, 150, 1209-14.

- RYBALKA, E., TIMPANI, C. A., COOKE, M. B., WILLIAMS, A. D. & HAYES, A. 2014. Defects in mitochondrial ATP synthesis in dystrophin-deficient mdx skeletal muscles may be caused by complex I insufficiency. *PLoS One*, 9, e115763.
- SACCO, A., MOURKIOTI, F., TRAN, R., CHOI, J., LLEWELLYN, M., KRAFT, P., SHKRELI, M., DELP, S., POMERANTZ, J. H., ARTANDI, S. E. & BLAU, H. M. 2010. Short telomeres and stem cell exhaustion model Duchenne muscular dystrophy in mdx/mTR mice. *Cell*, 143, 1059-71.
- SADOLET-PUCCIO, H. M., RAJALA, M. & KUNKEL, L. M. 1997. Dystrobrevin and dystrophin: an interaction through coiled-coil motifs. *Proc Natl Acad Sci USA*, 94, 12413-8.
- SAITO, F., MASAKI, T., KAMAKURA, K., ANDERSON, L. V., FUJITA, S., FUKUTA-OHI, H., SUNADA, Y., SHIMIZU, T. & MATSUMURA, K. 1999. Characterization of the transmembrane molecular architecture of the dystroglycan complex in schwann cells. *J Biol Chem*, 274, 8240-6.
- SAITO, T., TAKENAKA, M., MIYAI, I., YAMAMOTO, Y., MATSUMURA, T., NOZAKI, S. & KANG, J. 2001. Coagulation and fibrinolysis disorder in muscular dystrophy. *Muscle Nerve*, 24, 399-402.
- SAITO, T., YAMAMOTO, Y., MATSUMURA, T., NOZAKI, S., FUJIMURA, H. & SHINNO, S. 2005. Coagulation system activated in Duchenne muscular dystrophy patients with cardiac dysfunction. *Brain Dev*, 27, 415-8.
- SAMPAOLESI, M., BLOT, S., D'ANTONA, G., GRANGER, N., TONLORENZI, R., INNOCENZI, A., MOGNOL, P., THIBAUD, J. L., GALVEZ, B. G., BARTHÉLÉMY, I., PERANI, L., MANTERO, S., GUTTINGER, M., PANSARASA, O., RINALDI, C., CUSELLA DE ANGELIS, M. G., TORRENTE, Y., BORDIGNON, C., BOTTINELLI, R. & COSSU, G. 2006. Mesoangioblast stem cells ameliorate muscle function in dystrophic dogs. *Nature*, 444, 574-9.
- SCHIAFFINO, S. & REGGIANI, C. 2011. Fiber types in mammalian skeletal muscles. *Physiol Rev*, 91, 1447-531.
- SCHIAFFINO, S., ROSSI, A. C., SMERDU, V., LEINWAND, L. A. & REGGIANI, C. 2015. Developmental myosins: expression patterns and functional significance. *Skelet Muscle*, 5, 22.
- SCHIRMER, E. C., FLORENS, L., GUAN, T., YATES, J. R. & GERACE, L. 2003. Nuclear membrane proteins with potential disease links found by subtractive proteomics. *Science*, 301, 1380-2.
- SCHMITT, M., MAGDOLEN, V., YANG, F., KIECHLE, M., BAYANI, J., YOUSEF, G. M., SCORILAS, A., DIAMANDIS, E. P. & DORN, J. 2013. Emerging clinical importance of the cancer biomarkers kallikrein-related peptidases (KLK) in female and male reproductive organ malignancies. *Radiol Oncol*, 47, 319-29.
- SCHMITT-JOHN, T. 2015. VPS54 and the wobbler mouse. *Front Neurosci*, 9, 381.
- SCHOENAUER, R., LANGE, S., HIRSCHY, A., EHLER, E., PERRIARD, J. C. & AGARKOVA, I. 2008. Myomesin 3, a novel structural component of the M-band in striated muscle. *J Mol Biol*, 376, 338-51.
- SCHWALLER, B., MEYER, M. & SCHIFFMANN, S. 2002. 'New' functions for 'old' proteins: the role of the calcium-binding proteins calbindin D-28k, calretinin and parvalbumin, in cerebellar physiology. Studies with knockout mice. *Cerebellum*, 1, 241-58.
- SCOTTING, P., MCDERMOTT, H. & MAYER, R. J. 1991. Ubiquitin-protein conjugates and alpha B crystallin are selectively present in cells undergoing major cytomorphological reorganisation in early chicken embryos. *FEBS Lett*, 285, 75-9.
- SCOTTON, C., PASSARELLI, C., NERI, M. & FERLINI, A. 2014. Biomarkers in rare neuromuscular diseases. *Exp Cell Res*, 325, 44-9.

- SEKIGUCHI, M., ZUSHIDA, K., YOSHIDA, M., MAEKAWA, M., KAMICHI, S., SAHARA, Y., YUASA, S., TAKEDA, S. & WADA, K. 2009. A deficit of brain dystrophin impairs specific amygdala GABAergic transmission and enhances defensive behaviour in mice. *Brain*, 132, 124-35.
- SELSBY, J. T., ROSS, J. W., NONNEMAN, D. & HOLLINGER, K. 2015. Porcine models of muscular dystrophy. *ILAR J*, 56, 116-26.
- SELSBY, J., PENDRAK, K., ZADEL, M., TIAN, Z., PHAM, J., CARVER, T., ACOSTA, P., BARTON, E. & SWEENEY, H. L. 2010. Leupeptin-based inhibitors do not improve the mdx phenotype. *Am J Physiol Regul Integr Comp Physiol*, 299, R1192-201.
- SERNA, M., GILES, J. L., MORGAN, B. P. & BUBECK, D. 2016. Structural basis of complement membrane attack complex formation. *Nat Commun*, 7, 10587.
- SEWRY, C. A., DUBOWITZ, V., ABRAHA, A., LUZIO, J. P. & CAMPBELL, A. K. 1987. Immunocytochemical localisation of complement components C8 and C9 in human diseased muscle. The role of complement in muscle fibre damage. *J Neurol Sci*, 81, 141-53.
- SHACKELFORD, J. E. & LEBHERZ, H. G. 1985. Synthesis of apolipoprotein A1 in skeletal muscles of normal and dystrophic chickens. *J Biol Chem*, 260, 288-91.
- SHARP, N. J., KORNEGAY, J. N., VAN CAMP, S. D., HERBSTREITH, M. H., SECORE, S. L., KETTLE, S., HUNG, W. Y., CONSTANTINOU, C. D., DYKSTRA, M. J. & ROSES, A. D. 1992. An error in dystrophin mRNA processing in golden retriever muscular dystrophy, an animal homologue of Duchenne muscular dystrophy. *Genomics*, 13, 115-21.
- SHERMAN, D. L., FABRIZI, C., GILLESPIE, C. S. & BROPHY, P. J. 2001. Specific disruption of a schwann cell dystrophin-related protein complex in a demyelinating neuropathy. *Neuron*, 30, 677-87.
- SHEVCHENKO, A., TOMAS, H., HAVLIS, J., OLSEN, J. V. & MANN, M. 2006. In-gel digestion for mass spectrometric characterization of proteins and proteomes. *Nat Protoc*, 1, 2856-60.
- SHIM, K. S. & LUBEC, G. 2002. Drebrin, a dendritic spine protein, is manifold decreased in brains of patients with Alzheimer's disease and Down syndrome. *Neurosci Lett*, 324, 209-12.
- SICINSKI, P., GENG, Y., RYDER-COOK, A. S., BARNARD, E. A., DARLISON, M. G. & BARNARD, P. J. 1989. The molecular basis of muscular dystrophy in the mdx mouse: a point mutation. *Science*, 244, 1578-80.
- SIMONDS, A. K., MUNTONI, F., HEATHER, S. & FIELDING, S. 1998. Impact of nasal ventilation on survival in hypercapnic Duchenne muscular dystrophy. *Thorax*, 53, 949-52.
- SINGH, A., ISAAC, A. O., LUO, X., MOHAN, M. L., COHEN, M. L., CHEN, F., KONG, Q., BARTZ, J. & SINGH, N. 2009. Abnormal brain iron homeostasis in human and animal prion disorders. *PLoS Pathog*, 5, e1000336.
- SINZ, A. 2006. Chemical cross-linking and mass spectrometry to map three-dimensional protein structures and protein-protein interactions. *Mass Spectrom Rev*, 25, 663-82.
- SMITH, A. S. T., DAVIS, J., LEE, G., MACK, D. L. & KIM, D. H. 2016. Muscular dystrophy in a dish: engineered human skeletal muscle mimetics for disease modeling and drug discovery. *Drug Discov Today*, 21, 1387-1398.
- SMITH, M. P., WOOD, S. L., ZOUGMAN, A., HO, J. T., PENG, J., JACKSON, D., CAIRNS, D. A., LEWINGTON, A. J., SELBY, P. J. & BANKS, R. E. 2011. A systematic analysis of the effects of increasing degrees of serum immunodepletion in terms of depth of coverage and other key aspects in top-down and bottom-up proteomic analyses. *Proteomics*, 11, 2222-35.
- SNELLMAN, O. & SYLVÉN, B. 1967. Haptoglobin acting as a natural inhibitor of cathepsin B activity. *Nature*, 216, 1033.

- SNOW, W. M., FRY, M. & ANDERSON, J. E. 2013. Increased density of dystrophin protein in the lateral versus the vermal mouse cerebellum. *Cell Mol Neurobiol*, 33, 513-20.
- SOFRONIEW, M. V. & VINTERS, H. V. 2010. Astrocytes: biology and pathology. *Acta Neuropathol*, 119, 7-35.
- SOTGIA, F., LEE, H., BEDFORD, M. T., PETRUCCI, T., SUDOL, M. & LISANTI, M. P. 2001. Tyrosine phosphorylation of beta-dystroglycan at its WW domain binding motif, PPxY, recruits SH2 domain containing proteins. *Biochemistry*, 40, 14585-92.
- SOTIROPOULOU, G. & PAMPALAKIS, G. 2010. Kallikrein-related peptidases: bridges between immune functions and extracellular matrix degradation. *Biol Chem*, 391, 321-31.
- SOTIROPOULOU, G., PAMPALAKIS, G. & DIAMANDIS, E. P. 2009. Functional roles of human kallikrein-related peptidases. *J Biol Chem*, 284, 32989-94.
- SPENCE, H. J., DHILLON, A. S., JAMES, M. & WINDER, S. J. 2004. Dystroglycan, a scaffold for the ERK-MAP kinase cascade. *EMBO Rep*, 5, 484-9.
- SPENCER, M. J. & MELLGREN, R. L. 2002. Overexpression of a calpastatin transgene in mdx muscle reduces dystrophic pathology. *Hum Mol Genet*, 11, 2645-55.
- SPENCER, M. J. & TIDBALL, J. G. 2001. Do immune cells promote the pathology of dystrophin-deficient myopathies? *Neuromuscul Disord*, 11, 556-64.
- SPENCER, M. J., CROALL, D. E. & TIDBALL, J. G. 1995. Calpains are activated in necrotic fibers from mdx dystrophic mice. *J Biol Chem*, 270, 10909-14.
- SPENCER, M. J., MONTECINO-RODRIGUEZ, E., DORSHKIND, K. & TIDBALL, J. G. 2001. Helper (CD4(+)) and cytotoxic (CD8(+)) T cells promote the pathology of dystrophin-deficient muscle. *Clin Immunol*, 98, 235-43.
- SPULER, S. & ENGEL, A. G. 1998. Unexpected sarcolemmal complement membrane attack complex deposits on nonnecrotic muscle fibers in muscular dystrophies. *Neurology*, 50, 41-6.
- SPURNEY, C. F. 2011. Cardiomyopathy of Duchenne muscular dystrophy: current understanding and future directions. *Muscle Nerve*, 44, 8-19.
- STAUFFER, T. P., GUERINI, D. & CARAFOLI, E. 1995. Tissue distribution of the four gene products of the plasma membrane Ca²⁺ pump. A study using specific antibodies. *J Biol Chem*, 270, 12184-90.
- STAUNTON, L., ZWEYER, M., SWANDULLA, D. & OHLENDIECK, K. 2012. Mass spectrometry-based proteomic analysis of middle-aged vs. aged vastus lateralis reveals increased levels of carbonic anhydrase isoform 3 in senescent human skeletal muscle. *Int J Mol Med*, 30, 723-33.
- STEDMAN, H. H., SWEENEY, H. L., SHRAGER, J. B., MAGUIRE, H. C., PANETTIERI, R. A., PETROF, B., NARUSAWA, M., LEFEROVICH, J. M., SLADKY, J. T. & KELLY, A. M. 1991. The mdx mouse diaphragm reproduces the degenerative changes of Duchenne muscular dystrophy. *Nature*, 352, 536-9.
- STEFANINI, A. C., DA CUNHA, B. R., HENRIQUE, T. & TAJARA, E. H. 2015. Involvement of Kallikrein-Related Peptidases in Normal and Pathologic Processes. *Dis Markers*, 2015, 946572.
- STEPHENSON, D. G., LAMB, G. D. & STEPHENSON, G. M. 1998. Events of the excitation-contraction-relaxation (E-C-R) cycle in fast- and slow-twitch mammalian muscle fibres relevant to muscle fatigue. *Acta Physiol Scand*, 162, 229-45.
- STONE, M. R., O'NEILL, A., CATINO, D. & BLOCH, R. J. 2005. Specific interaction of the actin-binding domain of dystrophin with intermediate filaments containing keratin 19. *Mol Biol Cell*, 16, 4280-93.
- STRIMBU, K. & TAVEL, J. A. 2010. What are biomarkers? *Curr Opin HIV AIDS*, 5, 463-6.

- SU, S. B., GONG, W., GAO, J. L., SHEN, W., MURPHY, P. M., OPPENHEIM, J. J. & WANG, J. M. 1999. A seven-transmembrane, G protein-coupled receptor, FPRL1, mediates the chemotactic activity of serum amyloid A for human phagocytic cells. *J Exp Med*, 189, 395-402.
- SZKLARCZYK, D., MORRIS, J. H., COOK, H., KUHN, M., WYDER, S., SIMONOVIC, M., SANTOS, A., DONCHEVA, N. T., ROTH, A., BORK, P., JENSEN, L. J. & VON MERING, C. 2017. The STRING database in 2017: quality-controlled protein-protein association networks, made broadly accessible. *Nucleic Acids Res*, 45, D362-D368.
- SZŐKE, D. & PANTEGHINI, M. 2012. Diagnostic value of transferrin. *Clin Chim Acta*, 413, 1184-9.
- TANAKA, Y. & ANDO, S. 1990. Synaptic aging as revealed by changes in membrane potential and decreased activity of Na⁺,K⁽⁺⁾-ATPase. *Brain Res*, 506, 46-52.
- TANNU, N. S. & HEMBY, S. E. 2006. Two-dimensional fluorescence difference gel electrophoresis for comparative proteomics profiling. *Nat Protoc*, 1, 1732-42.
- TANOUE, T., ADACHI, M., MORIGUCHI, T. & NISHIDA, E. 2000. A conserved docking motif in MAP kinases common to substrates, activators and regulators. *Nat Cell Biol*, 2, 110-6.
- TAYLOR, P. J., BETTS, G. A., MAROULIS, S., GILISSEN, C., PEDERSEN, R. L., MOWAT, D. R., JOHNSTON, H. M. & BUCKLEY, M. F. 2010. Dystrophin gene mutation location and the risk of cognitive impairment in Duchenne muscular dystrophy. *PLoS One*, 5, e8803.
- TENG, P. N., BATEMAN, N. W., HOOD, B. L. & CONRADS, T. P. 2010. Advances in proximal fluid proteomics for disease biomarker discovery. *J Proteome Res*, 9, 6091-100.
- THUL, P. J., ÅKESSON, L., WIKING, M., MAHDESSIAN, D., GELADAKI, A., AIT BLAL, H., ALM, T., ASPLUND, A., BJÖRK, L., BRECKELS, L. M., BÄCKSTRÖM, A., DANIELSSON, F., FAGERBERG, L., FALL, J., GATTO, L., GNANN, C., HOBER, S., HJELMARE, M., JOHANSSON, F., LEE, S., LINDSKOG, C., MULDER, J., MULVEY, C. M., NILSSON, P., OKSVOLD, P., ROCKBERG, J., SCHUTTEN, R., SCHWENK, J. M., SIVERTSSON, Å., SJÖSTEDT, E., SKOGS, M., STADLER, C., SULLIVAN, D. P., TEGEL, H., WINSNES, C., ZHANG, C., ZWAHLEN, M., MARDINOGLU, A., PONTÉN, F., VON FEILITZEN, K., LILLEY, K. S., UHLÉN, M. & LUNDBERG, E. 2017. A subcellular map of the human proteome. *Science*, 356.
- TIDBALL, J. G. & SPENCER, M. J. 2000. Calpains and muscular dystrophies. *Int J Biochem Cell Biol*, 32, 1-5.
- TIDBALL, J. G. & VILLALTA, S. A. 2010. Regulatory interactions between muscle and the immune system during muscle regeneration. *Am J Physiol Regul Integr Comp Physiol*, 298, R1173-87.
- TIDBALL, J. G. & WEHLING-HENRICKS, M. 2004. Evolving therapeutic strategies for Duchenne muscular dystrophy: targeting downstream events. *Pediatr Res*, 56, 831-41.
- TIMPANI, C. A., HAYES, A. & RYBALKA, E. 2015. Revisiting the dystrophin-ATP connection: How half a century of research still implicates mitochondrial dysfunction in Duchenne Muscular Dystrophy aetiology. *Med Hypotheses*, 85, 1021-33.
- TINSLEY, J. M., POTTER, A. C., PHELPS, S. R., FISHER, R., TRICKETT, J. I. & DAVIES, K. E. 1996. Amelioration of the dystrophic phenotype of mdx mice using a truncated utrophin transgene. *Nature*, 384, 349-53.
- TINSLEY, J., DECONINCK, N., FISHER, R., KAHN, D., PHELPS, S., GILLIS, J. M. & DAVIES, K. 1998. Expression of full-length utrophin prevents muscular dystrophy in mdx mice. *Nat Med*, 4, 1441-4.
- TIRUMALAI, R. S., CHAN, K. C., PRIETO, D. A., ISSAQ, H. J., CONRADS, T. P. & VEENSTRA, T. D. 2003. Characterization of the low molecular weight human serum proteome. *Mol Cell Proteomics*, 2, 1096-103.

- TOTI, P., VILLANOVA, M., VATTI, R., SCHUERFELD, K., STUMPO, M., BARBAGLI, L., MALANDRINI, A. & COSTANTINI, M. 2003. Nerve growth factor expression in human dystrophic muscles. *Muscle Nerve*, 27, 370-3.
- TOWBIN, H., STAEBELIN, T. & GORDON, J. 1979. Electrophoretic transfer of proteins from polyacrylamide gels to nitrocellulose sheets: procedure and some applications. *Proc Natl Acad Sci USA*, 76, 4350-4.
- TOWNSEND, D., TURNER, I., YASUDA, S., MARTINDALE, J., DAVIS, J., SHILLINGFORD, M., KORNEGAY, J. N. & METZGER, J. M. 2010. Chronic administration of membrane sealant prevents severe cardiac injury and ventricular dilatation in dystrophic dogs. *J Clin Invest*, 120, 1140-50.
- TOWNSEND, D., YASUDA, S., LI, S., CHAMBERLAIN, J. S. & METZGER, J. M. 2008. Emergent dilated cardiomyopathy caused by targeted repair of dystrophic skeletal muscle. *Mol Ther*, 16, 832-5.
- TRAN, J. C., ZAMDBORG, L., AHLF, D. R., LEE, J. E., CATHERMAN, A. D., DURBIN, K. R., TIPTON, J. D., VELLAICHAMY, A., KELLIE, J. F., LI, M., WU, C., SWEET, S. M., EARLY, B. P., SIUTI, N., LEDUC, R. D., COMPTON, P. D., THOMAS, P. M. & KELLEHER, N. L. 2011. Mapping intact protein isoforms in discovery mode using top-down proteomics. *Nature*, 480, 254-8.
- TSUDA, T. & FITZGERALD, K. K. 2017. Dystrophic Cardiomyopathy: Complex Pathobiological Processes to Generate Clinical Phenotype. *J Cardiovasc Dev Dis*, 4, 14.
- TUFVESSON, E. & WESTERGREN-THORSSON, G. 2003. Biglycan and decorin induce morphological and cytoskeletal changes involving signalling by the small GTPases RhoA and Rac1 resulting in lung fibroblast migration. *J Cell Sci*, 116, 4857-64.
- TURK, R., HSIAO, J. J., SMITS, M. M., NG, B. H., POSPISIL, T. C., JONES, K. S., CAMPBELL, K. P. & WRIGHT, M. E. 2016. Molecular Signatures of Membrane Protein Complexes Underlying Muscular Dystrophy. *Mol Cell Proteomics*, 15, 2169-85.
- TURK, R., STERRENBURG, E., DE MEIJER, E. J., VAN OMMEN, G. J., DEN DUNNEN, J. T. & 'T HOEN, P. A. 2005. Muscle regeneration in dystrophin-deficient mdx mice studied by gene expression profiling. *BMC Genomics*, 6, 98.
- TUTDIBI, O., BRINKMEIER, H., RÜDEL, R. & FÖHR, K. J. 1999. Increased calcium entry into dystrophin-deficient muscle fibres of MDX and ADR-MDX mice is reduced by ion channel blockers. *J Physiol*, 515 (Pt 3), 859-68.
- TYLER, K. L. 2003. Origins and early descriptions of "Duchenne muscular dystrophy". *Muscle Nerve*, 28, 402-22.
- UNLÜ, M., MORGAN, M. E. & MINDEN, J. S. 1997. Difference gel electrophoresis: a single gel method for detecting changes in protein extracts. *Electrophoresis*, 18, 2071-7.
- VAILLEND, C., BILLARD, J. M. & LAROCHE, S. 2004. Impaired long-term spatial and recognition memory and enhanced CA1 hippocampal LTP in the dystrophin-deficient Dmd(mdx) mouse. *Neurobiol Dis*, 17, 10-20.
- VALENTINE, B. A., WINAND, N. J., PRADHAN, D., MOISE, N. S., DE LAHUNTA, A., KORNEGAY, J. N. & COOPER, B. J. 1992. Canine X-linked muscular dystrophy as an animal model of Duchenne muscular dystrophy: a review. *Am J Med Genet*, 42, 352-6.
- VAN DER VEN, P. F., WIESNER, S., SALMIKANGAS, P., AUERBACH, D., HIMMEL, M., KEMPA, S., HAYESS, K., PACHOLSKY, D., TAIVAINEN, A., SCHRÖDER, R., CARPÉN, O. & FÜRST, D. O. 2000. Indications for a novel muscular dystrophy pathway. gamma-filamin, the muscle-specific filamin isoform, interacts with myotilin. *J Cell Biol*, 151, 235-48.
- VAN ERP, C., LOCH, D., LAWS, N., TREBBIN, A. & HOEY, A. J. 2010. Timeline of cardiac dystrophy in 3-18-month-old MDX mice. *Muscle Nerve*, 42, 504-13.

- VAN GRUNSVEN, L. A. 2017. 3D in vitro models of liver fibrosis. *Adv Drug Deliv Rev*, 121, 133-146.
- VAN SPREEUWEL, A. C. C., BAX, N. A. M., VAN NIEROP, B. J., AARTSMA-RUS, A., GOUMANS, M. T. H. & BOUTEN, C. V. C. 2017. Mimicking Cardiac Fibrosis in a Dish: Fibroblast Density Rather than Collagen Density Weakens Cardiomyocyte Function. *J Cardiovasc Transl Res*, 10, 116-127.
- VAN WESTERING, T. L., BETTS, C. A. & WOOD, M. J. 2015. Current understanding of molecular pathology and treatment of cardiomyopathy in duchenne muscular dystrophy. *Molecules*, 20, 8823-55.
- VANDEBROUCK, C., MARTIN, D., COLSON-VAN SCHOOR, M., DEBAIX, H. & GAILLY, P. 2002. Involvement of TRPC in the abnormal calcium influx observed in dystrophic (mdx) mouse skeletal muscle fibers. *J Cell Biol*, 158, 1089-96.
- VASILAKI, A., JACKSON, M. J. & MCARDLE, A. 2002. Attenuated HSP70 response in skeletal muscle of aged rats following contractile activity. *Muscle Nerve*, 25, 902-5.
- VÉLEZ, P., IZQUIERDO, I., ROSA, I. & GARCÍA, Á. 2015. A 2D-DIGE-based proteomic analysis reveals differences in the platelet releasate composition when comparing thrombin and collagen stimulations. *Sci Rep*, 5, 8198.
- VENEMA, V. J., JU, H., ZOU, R. & VENEMA, R. C. 1997. Interaction of neuronal nitric-oxide synthase with caveolin-3 in skeletal muscle. Identification of a novel caveolin scaffolding/inhibitory domain. *J Biol Chem*, 272, 28187-90.
- VERELLEN-DUMOULIN, C., FREUND, M., DE MEYER, R., LATERRE, C., FRÉDÉRIC, J., THOMPSON, M. W., MARKOVIC, V. D. & WORTON, R. G. 1984. Expression of an X-linked muscular dystrophy in a female due to translocation involving Xp21 and non-random inactivation of the normal X chromosome. *Hum Genet*, 67, 115-9.
- VICENTE-MANZANARES, M., MA, X., ADELSTEIN, R. S. & HORWITZ, A. R. 2009. Non-muscle myosin II takes centre stage in cell adhesion and migration. *Nat Rev Mol Cell Biol*, 10, 778-90.
- VIDAL, B., SERRANO, A. L., TJWA, M., SUELVE, M., ARDITE, E., DE MORI, R., BAEZARAJA, B., MARTÍNEZ DE LAGRÁN, M., LAFUSTE, P., RUIZ-BONILLA, V., JARDÍ, M., GHERARDI, R., CHRISTOV, C., DIERSSEN, M., CARMELIET, P., DEGEN, J. L., DEWERCHIN, M. & MUÑOZ-CÁNOVES, P. 2008. Fibrinogen drives dystrophic muscle fibrosis via a TGFbeta/alternative macrophage activation pathway. *Genes Dev*, 22, 1747-52.
- VILLALTA, S. A., NGUYEN, H. X., DENG, B., GOTOH, T. & TIDBALL, J. G. 2009. Shifts in macrophage phenotypes and macrophage competition for arginine metabolism affect the severity of muscle pathology in muscular dystrophy. *Hum Mol Genet*, 18, 482-96.
- VILLALTA, S. A., ROSENBERG, A. S. & BLUESTONE, J. A. 2015. The immune system in Duchenne muscular dystrophy: Friend or foe. *Rare Dis*, 3, e1010966.
- VILQUIN, J. T., BRUSSEE, V., ASSELIN, I., KINOSHITA, I., GINGRAS, M. & TREMBLAY, J. P. 1998. Evidence of mdx mouse skeletal muscle fragility in vivo by eccentric running exercise. *Muscle Nerve*, 21, 567-76.
- VIOLA, H. M., ADAMS, A. M., DAVIES, S. M., FLETCHER, S., FILIPOVSKA, A. & HOOL, L. C. 2014. Impaired functional communication between the L-type calcium channel and mitochondria contributes to metabolic inhibition in the mdx heart. *Proc Natl Acad Sci USA*, 111, E2905-14.
- VOERMANS, N. C., LAAN, A. E., OOSTERHOF, A., VAN KUPPEVELT, T. H., DROST, G., LAMMENS, M., KAMSTEEG, E. J., SCOTTON, C., GUALANDI, F., GUGLIELMI, V., VAN DEN HEUVEL, L., VATTEMI, G. & VAN ENGELEN, B. G. 2012. Brody syndrome: a clinically heterogeneous entity distinct from Brody disease: a review of literature and a cross-sectional clinical study in 17 patients. *Neuromuscul Disord*, 22, 944-54.

- VOIT, T., TOPALOGLU, H., STRAUB, V., MUNTONI, F., DECONINCK, N., CAMPION, G., DE KIMPE, S. J., EAGLE, M., GUGLIERI, M., HOOD, S., LIEFAARD, L., LOURBAKOS, A., MORGAN, A., NAKIELNY, J., QUARCOO, N., RICOTTI, V., ROLFE, K., SERVAIS, L., WARDELL, C., WILSON, R., WRIGHT, P. & KRAUS, J. E. 2014. Safety and efficacy of drisapersen for the treatment of Duchenne muscular dystrophy (DEMAND II): an exploratory, randomised, placebo-controlled phase 2 study. *Lancet Neurol*, 13, 987-96.
- VON GONTARD, A., ZERRES, K., BACKES, M., LAUFERSWEILER-PLOSS, C., WENDLAND, C., MELCHERS, P., LEHMKUHL, G. & RUDNIK-SCHÖNEBORN, S. 2002. Intelligence and cognitive function in children and adolescents with spinal muscular atrophy. *Neuromuscul Disord*, 12, 130-6.
- VOS, P. E., LAMERS, K. J., HENDRIKS, J. C., VAN HAAREN, M., BEEMS, T., ZIMMERMAN, C., VAN GEEL, W., DE REUS, H., BIERT, J. & VERBEEK, M. M. 2004. Glial and neuronal proteins in serum predict outcome after severe traumatic brain injury. *Neurology*, 62, 1303-10.
- VULIN, A., BARTHÉLÉMY, I., GOYENVALLE, A., THIBAUD, J. L., BELEY, C., GRIFFITH, G., BENCHAOUIR, R., LE HIR, M., UNTERFINGER, Y., LORAIN, S., DREYFUS, P., VOIT, T., CARLIER, P., BLOT, S. & GARCIA, L. 2012. Muscle function recovery in golden retriever muscular dystrophy after AAV1-U7 exon skipping. *Mol Ther*, 20, 2120-33.
- VULIN, A., WEIN, N., STRANDJORD, D. M., JOHNSON, E. K., FINDLAY, A. R., MAITI, B., HOWARD, M. T., KAMINOH, Y. J., TAYLOR, L. E., SIMMONS, T. R., RAY, W. C., MONTANARO, F., ERVASTI, J. M. & FLANIGAN, K. M. 2014. The ZZ domain of dystrophin in DMD: making sense of missense mutations. *Hum Mutat*, 35, 257-64.
- VYBIRAL, T., WINKELMANN, J. C., ROBERTS, R., JOE, E., CASEY, D. L., WILLIAMS, J. K. & EPSTEIN, H. F. 1992. Human cardiac and skeletal muscle spectrins: differential expression and localization. *Cell Motil Cytoskeleton*, 21, 293-304.
- WALSH, F. S. & MOORE, S. E. 1985. Expression of cell adhesion molecule, N-CAM, in diseases of adult human skeletal muscle. *Neurosci Lett*, 59, 73-8.
- WANG, J. & SLUNGAARD, A. 2006. Role of eosinophil peroxidase in host defense and disease pathology. *Arch Biochem Biophys*, 445, 256-60.
- WANG, Y., ZHANG, K., WASALA, N. B., DUAN, D. & YAO, G. 2015. Optical polarization tractography revealed significant fiber disarray in skeletal muscles of a mouse model for Duchenne muscular dystrophy. *Biomed Opt Express*, 6, 347-52.
- WASHBURN, M. P., WOLTERS, D. & YATES, J. R. 2001. Large-scale analysis of the yeast proteome by multidimensional protein identification technology. *Nat Biotechnol*, 19, 242-7.
- WEBSTER, C., SILBERSTEIN, L., HAYS, A. P. & BLAU, H. M. 1988. Fast muscle fibers are preferentially affected in Duchenne muscular dystrophy. *Cell*, 52, 503-13.
- WEHLING-HENRICKS, M., JORDAN, M. C., GOTOH, T., GRODY, W. W., ROOS, K. P. & TIDBALL, J. G. 2010. Arginine metabolism by macrophages promotes cardiac and muscle fibrosis in mdx muscular dystrophy. *PLoS One*, 5, e10763.
- WEHLING-HENRICKS, M., LEE, J. J. & TIDBALL, J. G. 2004. Prednisolone decreases cellular adhesion molecules required for inflammatory cell infiltration in dystrophin-deficient skeletal muscle. *Neuromuscul Disord*, 14, 483-90.
- WEHLING-HENRICKS, M., SOKOLOW, S., LEE, J. J., MYUNG, K. H., VILLALTA, S. A. & TIDBALL, J. G. 2008. Major basic protein-1 promotes fibrosis of dystrophic muscle and attenuates the cellular immune response in muscular dystrophy. *Hum Mol Genet*, 17, 2280-92.
- WHITEAKER, J. R., ZHANG, H., ENG, J. K., FANG, R., PIENING, B. D., FENG, L. C., LORENTZEN, T. D., SCHOENHERR, R. M., KEANE, J. F., HOLZMAN, T., FITZGIBBON, M., LIN, C., COOKE, K., LIU, T., CAMP, D. G., ANDERSON, L., WATTS, J., SMITH, R. D.,

- MCINTOSH, M. W. & PAULOVICH, A. G. 2007. Head-to-head comparison of serum fractionation techniques. *J Proteome Res*, 6, 828-36.
- WICKSELL, R. K., KIHLGREN, M., MELIN, L. & EEG-OLOFSSON, O. 2004. Specific cognitive deficits are common in children with Duchenne muscular dystrophy. *Dev Med Child Neurol*, 46, 154-9.
- WIŚNIEWSKI, J. R., ZOUGMAN, A., NAGARAJ, N. & MANN, M. 2009. Universal sample preparation method for proteome analysis. *Nat Methods*, 6, 359-62.
- WOLFE, R. R. 2006. The underappreciated role of muscle in health and disease. *Am J Clin Nutr*, 84, 475-82.
- WOO, H. N., HONG, G. S., JUN, J. I., CHO, D. H., CHOI, H. W., LEE, H. J., CHUNG, C. W., KIM, I. K., JO, D. G., PYO, J. O., BERTIN, J. & JUNG, Y. K. 2004. Inhibition of Bcl10-mediated activation of NF-kappa B by BinCARD, a Bcl10-interacting CARD protein. *FEBS Lett*, 578, 239-44.
- WOOLF, P. J., LU, S., CORNFORD-NAIRN, R., WATSON, M., XIAO, X. H., HOLROYD, S. M., BROWN, L. & HOEY, A. J. 2006. Alterations in dihydropyridine receptors in dystrophin-deficient cardiac muscle. *Am J Physiol Heart Circ Physiol*, 290, H2439-45.
- WOOLNER, S., O'BRIEN, L. L., WIESE, C. & BEMENT, W. M. 2008. Myosin-10 and actin filaments are essential for mitotic spindle function. *J Cell Biol*, 182, 77-88.
- WRABETZ, L. & FELTRI, M. L. 2001. Do Schwann cells stop, DR(o)P2, and roll? *Neuron*, 30, 642-4.
- WU, C. C., MACCOSS, M. J., MARDONES, G., FINNIGAN, C., MOGELSVANG, S., YATES, J. R. & HOWELL, K. E. 2004. Organellar proteomics reveals Golgi arginine dimethylation. *Mol Biol Cell*, 15, 2907-19.
- WYNN, T. A. 2004. Fibrotic disease and the T(H)1/T(H)2 paradigm. *Nat Rev Immunol*, 4, 583-94.
- WYNN, T. A. 2008. Cellular and molecular mechanisms of fibrosis. *J Pathol*, 214, 199-210.
- XIE, F., LIU, T., QIAN, W. J., PETYUK, V. A. & SMITH, R. D. 2011. Liquid chromatography-mass spectrometry-based quantitative proteomics. *J Biol Chem*, 286, 25443-9.
- YANG, B., JUNG, D., MOTTO, D., MEYER, J., KORETZKY, G. & CAMPBELL, K. P. 1995. SH3 domain-mediated interaction of dystroglycan and Grb2. *J Biol Chem*, 270, 11711-4.
- YANG, X., WANG, S., SHENG, Y., ZHANG, M., ZOU, W., WU, L., KANG, L., RIZO, J., ZHANG, R., XU, T. & MA, C. 2015. Syntaxin opening by the MUN domain underlies the function of Munc13 in synaptic-vesicle priming. *Nat Struct Mol Biol*, 22, 547-554.
- YANG, Z. & WANG, K. K. 2015. Glial fibrillary acidic protein: from intermediate filament assembly and gliosis to neurobiomarker. *Trends Neurosci*, 38, 364-374.
- YAO, Y. Y., YIN, H., SHEN, B., CHAO, L. & CHAO, J. 2007. Tissue kallikrein and kinin infusion rescues failing myocardium after myocardial infarction. *J Card Fail*, 13, 588-96.
- YASMINEH, W. G., IBRAHIM, G. A., ABBASNEZHAD, M. & AWAD, E. A. 1978. Isoenzyme distribution of creatine kinase and lactate dehydrogenase in serum and skeletal muscle in Duchenne muscular dystrophy, collagen disease, and other muscular disorders. *Clin Chem*, 24, 1985-9.
- YASUDA, S., TOWNSEND, D., MICHELE, D. E., FAVRE, E. G., DAY, S. M. & METZGER, J. M. 2005. Dystrophic heart failure blocked by membrane sealant poloxamer. *Nature*, 436, 1025-9.
- YILMAZ, A. & SECHTEM, U. 2012. Cardiac involvement in muscular dystrophy: advances in diagnosis and therapy. *Heart*, 98, 420-9.

- YOON, J. H., JOHNSON, E., XU, R., MARTIN, L. T., MARTIN, P. T. & MONTANARO, F. 2012. Comparative proteomic profiling of dystroglycan-associated proteins in wild-type, mdx, and Galgt2 transgenic mouse skeletal muscle. *J Proteome Res*, 11, 4413-24.
- YOSHIDA, M., SUZUKI, A., YAMAMOTO, H., NOGUCHI, S., MIZUNO, Y. & OZAWA, E. 1994. Dissociation of the complex of dystrophin and its associated proteins into several unique groups by n-octyl beta-D-glucoside. *Eur J Biochem*, 222, 1055-61.
- YOUNG, P., EHLER, E. & GAUTEL, M. 2001. Obscurin, a giant sarcomeric Rho guanine nucleotide exchange factor protein involved in sarcomere assembly. *J Cell Biol*, 154, 123-36.
- ZATZ, M., RAPAPORT, D., VAINZOF, M., PASSOS-BUENO, M. R., BORTOLINI, E. R., PAVANELLO, R. E. C. & PERES, C. A. 1991. Serum creatine-kinase (CK) and pyruvate-kinase (PK) activities in Duchenne (DMD) as compared with Becker (BMD) muscular dystrophy. *J Neurol Sci*, 102, 190-6.
- ZATZ, M., VIANNA-MORGANTE, A. M., CAMPOS, P. & DIAMENT, A. J. 1981. Translocation (X;6) in a female with Duchenne muscular dystrophy: implications for the localisation of the DMD locus. *J Med Genet*, 18, 442-7.
- ZHANG, W., ZHOU, G., ZHAO, Y. & WHITE, M. A. 2003a. Affinity enrichment of plasma membrane for proteomics analysis. *Electrophoresis*, 24, 2855-63.
- ZHANG, H., LI, X. J., MARTIN, D. B. & AEBERSOLD, R. 2003b. Identification and quantification of N-linked glycoproteins using hydrazide chemistry, stable isotope labeling and mass spectrometry. *Nat Biotechnol*, 21, 660-6.
- ZHANG, Y., FONSLow, B. R., SHAN, B., BAEK, M. C. & YATES, J. R. 2013. Protein analysis by shotgun/bottom-up proteomics. *Chem Rev*, 113, 2343-94.
- ZHOU, L. & LU, H. 2010. Targeting fibrosis in Duchenne muscular dystrophy. *J Neuropathol Exp Neurol*, 69, 771-6.
- ZHOU, M., LUCAS, D. A., CHAN, K. C., ISSAQ, H. J., PETRICOIN, E. F., LIOTTA, L. A., VEENSTRA, T. D. & CONRADS, T. P. 2004. An investigation into the human serum "interactome". *Electrophoresis*, 25, 1289-98.
- ZHU, Y., ZHANG, H., SUN, Y., LI, Y., DENG, L., WEN, X., WANG, H. & ZHANG, C. 2015. Serum Enzyme Profiles Differentiate Five Types of Muscular Dystrophy. *Dis Markers*, 2015, 543282.
- ZOLOTOARJOVA, N., MROZINSKI, P., CHEN, H. & MARTOSELLA, J. 2008. Combination of affinity depletion of abundant proteins and reversed-phase fractionation in proteomic analysis of human plasma/serum. *J Chromatogr A*, 1189, 332-8.

Appendix

Appendix: List of tables

Table A3.1	List of identified proteins with a significantly increased abundance ≤ 3.5 -fold in <i>mdx-4cv</i> hind-limb as determined by label-free LC-MS/MS	368
Table A4.1	List of identified proteins with a significantly increased abundance ≤ 4 -fold in <i>mdx-4cv</i> enriched sarcolemma as determined by label-free LC-MS/MS	372
Table A7.1	List of identified proteins with a significantly increased abundance ≤ 12.7 -fold in <i>mdx-4cv</i> serum as determined by label-free LC-MS/MS	376

Table A3.1: List of identified proteins with a significantly increased abundance ≤ 3.5 -fold in *mdx-4cv* hind-limb as determined by label-free LC-MS/MS

Accession	Gene Name	Protein Name	Unique peptides	Confidence score	Anova (p)	Max fold change
P22599	Serpina1b	Alpha-1-antitrypsin 1-2	3	186.18	4.00E-03	3.47
Q6ZWY9	Hist1h2bc	Histone H2B type 1-C/E/G	3	310.51	6.48E-03	3.46
P26039	Tln1	Talin-1	3	199.15	1.18E-03	3.37
P18826	Phka1	Phosphorylase b kinase regulatory subunit alpha, skeletal muscle isoform	3	235.73	8.09E-03	3.35
P15864	Hist1h1c	Histone H1.2	2	94.98	1.11E-02	3.28
P62806	Hist1h4a	Histone H4	5	312.46	1.07E-02	3.28
Q8BMS1	Hadha	Trifunctional enzyme subunit alpha, mitochondrial	9	762.37	1.15E-02	3.25
P26041	Msn	Moesin	5	180.37	5.63E-04	3.23
P14148	Rpl7	60S ribosomal protein L7	3	181.65	1.33E-02	3.23
Q8VEM8	Slc25a3	Phosphate carrier protein, mitochondrial	5	264.80	1.49E-02	3.22
Q61207	Psap	Sulfated glycoprotein 1	3	122.35	3.19E-03	3.14
Q04857	Col6a1	Collagen alpha-1(VI) chain	3	87.73	1.80E-02	3.12
P61027; O35963; P61294; Q8K386	Rab10	Ras-related protein Rab-10	3	118.38	1.58E-03	3.12
P28654	Dcn	Decorin	5	350.61	1.65E-02	3.10
Q9D783	Klhl40	Kelch-like protein 40	6	330.13	1.03E-03	3.10
P97927	Lama4	Laminin subunit alpha-4	3	144.02	2.28E-03	3.03
O08532	Cacna2d1	Voltage-dependent calcium channel subunit alpha-2/delta-1	5	289.94	1.17E-02	3.03
Q8BTM8	Flna	Filamin-A	3	123.04	6.68E-03	2.98
A2AUC9	Klhl41	Kelch-like protein 41	12	774.92	8.24E-03	2.97
P07758	Serpina1a	Alpha-1-antitrypsin 1-1	9	691.92	1.43E-02	2.94
Q9CVB6	Arpc2	Actin-related protein 2/3 complex subunit 2	3	154.12	3.07E-04	2.92

P18760	Cfl1	Cofilin-1	5	305.01	4.51E-03	2.90
Q8CI43	Myl6b	Myosin light chain 6B	2	66.66	7.58E-03	2.89
P48962	Slc25a4	ADP/ATP translocase 1	9	579.28	1.72E-02	2.86
Q9D6F9	Tubb4a	Tubulin beta-4A chain	5	478.95	3.73E-03	2.79
Q8R429; O55143; Q64518	Atp2a1	Sarcoplasmic/endoplasmic reticulum calcium ATPase 1	39	3489.26	1.99E-02	2.78
P09405	Ncl	Nucleolin	2	4.54	5.11E-03	2.75
P24369	Ppib	Peptidyl-prolyl cis-trans isomerase B	2	132.93	5.97E-04	2.73
P13541	Myh3	Myosin-3	5	425.08	1.80E-02	2.71
P48036	Anxa5	Annexin A5	8	459.76	3.11E-03	2.71
P29391	Ftl1	Ferritin light chain 1	9	652.00	5.57E-03	2.68
P62874	Gnb1	Guanine nucleotide-binding protein G(I)/G(S)/G(T) subunit beta-1	3	178.56	1.34E-03	2.68
P32261	Serpinc1	Antithrombin-III	3	178.10	4.70E-03	2.66
P07759	Serpina3k	Serine protease inhibitor A3K	9	716.84	2.93E-03	2.65
Q7TMM9	Tubb2a	Tubulin beta-2A chain	10	632.26	1.38E-03	2.64
P47911	Rpl6	60S ribosomal protein L6	2	145.75	1.12E-02	2.59
Q91X72	Hpx	Hemopexin	13	636.31	1.69E-02	2.58
P14869	Rplp0	60S acidic ribosomal protein P0	3	86.01	5.00E-03	2.57
Q9JK53	Prelp	Prolargin	5	227.25	5.28E-03	2.57
P48678	Lmna	Prelamin-A/C	25	1641.09	3.50E-04	2.56
Q9CQQ7	Atp5f1	ATP synthase F(0) complex subunit B1, mitochondrial	5	211.76	3.67E-03	2.55
Q9CZM2	Rpl15	60S ribosomal protein L15	2	104.98	2.48E-02	2.52
P62962	Pfn1	Profilin-1	4	270.97	1.55E-02	2.49
Q91VI7	Rnh1	Ribonuclease inhibitor	7	339.14	1.34E-02	2.49
Q07076	Anxa7	Annexin A7	2	120.89	1.60E-03	2.47
Q8R4E4	Myoz3	Myozenin-3	2	100.52	1.18E-03	2.45

P62141	Ppp1cb	Serine/threonine-protein phosphatase PP1-beta catalytic subunit	2	177.19	1.51E-03	2.45
Q70IV5	Synm	Synemin	2	104.43	1.86E-04	2.44
P20152	Vim	Vimentin	15	1088.58	2.26E-03	2.42
P35980	Rpl18	60S ribosomal protein L18	3	154.74	1.82E-02	2.42
Q62000	Ogn	Mimecan	7	497.76	1.61E-02	2.42
Q60930	Vdac2	Voltage-dependent anion-selective channel protein 2	9	649.61	4.09E-02	2.37
Q8BFR5	Tufm	Elongation factor Tu, mitochondrial	9	509.16	4.82E-03	2.37
Q9WTR5	Cdh13	Cadherin-13	3	245.57	6.04E-03	2.37
P47757	Capzb	F-actin-capping protein subunit beta	2	143.11	3.43E-03	2.34
Q9Z1E4	Gys1	Glycogen [starch] synthase, muscle	4	199.63	1.94E-02	2.33
P97384; O35639	Anxa11	Annexin A11	5	201.61	4.23E-04	2.32
P68040	Gnb211	Guanine nucleotide-binding protein subunit beta-2-like 1	6	311.81	6.94E-04	2.32
Q91WD5	Ndufs2	NADH dehydrogenase [ubiquinone] iron-sulfur protein 2, mitochondrial	8	305.45	1.41E-03	2.32
P47963	Rpl13	60S ribosomal protein L13	2	109.22	2.31E-02	2.31
P50543	S100a11	Protein S100-A11	2	136.84	3.35E-03	2.30
Q61425	Hadh	Hydroxyacyl-coenzyme A dehydrogenase, mitochondrial	2	115.44	1.28E-02	2.30
P05213	Tuba1b	Tubulin alpha-1B chain	2	209.92	1.60E-02	2.30
P68368	Tuba4a	Tubulin alpha-4A chain	3	305.20	6.36E-03	2.28
Q8BG05	Hnrnpa3	Heterogeneous nuclear ribonucleoprotein A3	2	82.45	4.02E-02	2.28
Q6ZWX6	Eif2s1	Eukaryotic translation initiation factor 2 subunit 1	2	73.19	1.86E-02	2.28
A2AAJ9	Obscn	Obscurin	9	474.23	4.43E-03	2.27
P62889	Rpl30	60S ribosomal protein L30	4	279.47	1.89E-03	2.26
Q9DC69	Ndufa9	NADH dehydrogenase [ubiquinone] 1 alpha subcomplex subunit 9, mitochondrial	3	184.74	1.44E-02	2.26

P50544	Acadvl	Very long-chain specific acyl-CoA dehydrogenase, mitochondrial	3	148.79	2.72E-03	2.25
P63101	Ywhaz	14-3-3 protein zeta/delta	4	390.88	6.99E-03	2.23
Q8BK84	Dupd1	Dual specificity phosphatase DUPD1	2	146.83	4.76E-03	2.21
Q9DB20	Atp5o	ATP synthase subunit O, mitochondrial	4	277.86	1.02E-02	2.19
Q3MI48	Jsrp1	Junctional sarcoplasmic reticulum protein 1	3	145.69	2.10E-02	2.18
P14824	Anxa6	Annexin A6	5	539.07	3.05E-03	2.15
Q03265	Atp5a1	ATP synthase subunit alpha, mitochondrial	11	778.39	1.16E-03	2.10
Q9JJZ2	Tuba8	Tubulin alpha-8 chain	2	68.22	2.36E-02	2.10
Q60605	Myl6	Myosin light polypeptide 6	4	300.27	1.04E-02	2.10
Q99JB8	Pacsin3	Protein kinase C and casein kinase II substrate protein 3	8	439.70	1.20E-05	2.10
P31001	Des	Desmin	18	1622.83	1.45E-03	2.09
Q61292	Lamb2	Laminin subunit beta-2	5	233.63	1.34E-02	2.08
P40124	Cap1	Adenylyl cyclase-associated protein 1	2	52.13	1.47E-03	2.08
Q8VHX6	Flnc	Filamin-C	20	1257.45	3.83E-02	2.07
P51885	Lum	Lumican	5	346.14	2.11E-02	2.07
Q9CZU6	Cs	Citrate synthase, mitochondrial	5	373.29	1.48E-02	2.07
O35129	Phb2	Prohibitin-2	3	122.36	4.05E-03	2.07
Q9DB60	Fam213b	Prostamide/prostaglandin F synthase	2	48.58	1.14E-03	2.06
O88342	Wdr1	WD repeat-containing protein 1	3	205.65	4.63E-03	2.05
P14602	Hspb1	Heat shock protein beta-1	6	349.70	2.02E-03	2.05
P14733	Lmnb1	Lamin-B1	5	244.43	1.90E-03	2.03
Q60936	Adck3	Chaperone activity of bc1 complex-like, mitochondrial	2	98.44	2.83E-02	2.02
P35979	Rpl12	60S ribosomal protein L12	3	172.68	2.01E-02	2.02
Q02053	Uba1	Ubiquitin-like modifier-activating enzyme 1	2	170.90	3.08E-02	2.01

Table A4.1: List of identified proteins with a significantly increased abundance ≤ 4 -fold in *mdx-4cv* enriched sarcolemma as determined by label-free LC-MS/MS

Accession	Gene Name	Protein Name	Unique peptides	Confidence score	Anova (p)	Max fold change
Q5XKE0	Mybpc2	Myosin-binding protein C, fast-type	3	238.99	5.42E-04	3.95
P14131	Rps16	40S ribosomal protein S16	3	137.60	3.60E-07	3.93
P19324	Serpinh1	Serpin H1	3	80.53	2.01E-05	3.89
Q8BY89	Slc44a2	Choline transporter-like protein 2	2	54.46	7.41E-04	3.84
P47740	Aldh3a2	Fatty aldehyde dehydrogenase	2	101.65	2.89E-05	3.82
P22315	Fech	Ferrochelatase, mitochondrial	2	3.62	2.79E-03	3.80
P80318	Cct3	T-complex protein 1 subunit gamma	2	65.56	4.94E-05	3.72
Q04857	Col6a1	Collagen alpha-1(VI) chain	2	5.45	2.88E-05	3.68
Q61941	Nnt	NAD(P) transhydrogenase, mitochondrial	2	62.95	1.25E-03	3.67
Q62159	Rhoc	Rho-related GTP-binding protein RhoC	2	60.96	1.22E-08	3.66
P35980	Rpl18	60S ribosomal protein L18	2	53.04	3.20E-03	3.62
P09055	Itgb1	Integrin beta-1	3	5.45	2.28E-04	3.60
P25444	Rps2	40S ribosomal protein S2	3	108.83	4.15E-06	3.58
Q91ZX7	Lrp1	Prolow-density lipoprotein receptor-related protein 1	4	184.28	4.03E-04	3.55
P48678	Lmna	Prelamin-A/C	5	166.15	1.51E-06	3.46
O55143	Atp2a2	Sarcoplasmic/endoplasmic reticulum calcium ATPase 2	7	370.13	1.16E-06	3.41
P51863	Atp6v0d1	V-type proton ATPase subunit d 1	3	116.14	6.71E-05	3.40
Q6ZWN5	Rps9	40S ribosomal protein S9	6	212.10	4.32E-08	3.35
Q8BFR5	Tufm	Elongation factor Tu, mitochondrial	2	4.43	2.80E-03	3.34
Q9JI91	Actn2	Alpha-actinin-2	7	251.46	1.86E-04	3.32
Q61475	Cd55	Complement decay-accelerating factor, GPI-anchored	2	83.81	5.51E-05	3.31
Q64133	Maoa	Amine oxidase [flavin-containing] A	4	196.24	8.22E-06	3.31
Q9JHU4	Dync1h1	Cytoplasmic dynein 1 heavy chain 1	2	53.59	2.27E-08	3.22
Q60936	Coq8a	Atypical kinase COQ8A, mitochondrial	2	117.46	1.61E-03	3.21

Q9D517	Agpat3	1-acyl-sn-glycerol-3-phosphate acyltransferase gamma	3	139.69	5.17E-05	3.20
Q8JZQ2	Afg3l2	AFG3-like protein 2	4	94.76	9.47E-06	3.08
Q9CXR1	Dhrs7	Dehydrogenase/reductase SDR family member 7	2	3.62	4.11E-04	3.06
O09161	Casq2	Calsequestrin-2	4	74.31	9.36E-04	3.06
Q68FD5	Cltc	Clathrin heavy chain 1	5	191.31	2.18E-04	3.02
Q02788	Col6a2	Collagen alpha-2(VI) chain	3	88.66	1.26E-06	3.02
P14206	Rpsa	40S ribosomal protein SA	2	135.04	4.63E-04	3.01
Q8BIJ6	Iars2	Isoleucine--tRNA ligase, mitochondrial	3	108.15	1.13E-04	3.01
Q9CZR2	Naalad2	N-acetylated-alpha-linked acidic dipeptidase 2	3	139.01	1.20E-06	3.00
P62852	Rps25	40S ribosomal protein S25	2	102.21	5.17E-04	2.99
P62270	Rps18	40S ribosomal protein S18	4	248.81	4.28E-04	2.98
Q9D0L4	Adck1	Uncharacterized aarF domain-containing protein kinase 1	2	102.89	2.46E-03	2.98
Q8VCM8	Ncln	Nicalin	2	51.22	2.21E-04	2.92
P62281	Rps11	40S ribosomal protein S11	2	97.27	2.85E-05	2.91
P97429	Anxa4	Annexin A4	2	94.33	4.42E-05	2.91
P42932	Cct8	T-complex protein 1 subunit theta	2	105.73	2.84E-05	2.87
Q61838	Pzp	Pregnancy zone protein	3	143.08	1.04E-04	2.83
Q9Z1E4	Gys1	Glycogen [starch] synthase, muscle	4	72.84	1.36E-06	2.81
Q91V79	Fitm1	Fat storage-inducing transmembrane protein 1	3	222.11	1.85E-04	2.76
Q9ET30	Tm9sf3	Transmembrane 9 superfamily member 3	2	51.28	1.94E-05	2.72
P62267	Rps23	40S ribosomal protein S23	2	124.94	2.66E-04	2.71
Q8C129	Lnpep	Leucyl-cystinyl aminopeptidase	2	90.89	8.18E-06	2.71
Q8BW75	Maob	Amine oxidase [flavin-containing] B	5	172.46	5.15E-07	2.67
P97351	Rps3a	40S ribosomal protein S3a	3	63.48	4.12E-06	2.63
Q8VDM4	Psm2	26S proteasome non-ATPase regulatory subunit 2	2	113.58	1.94E-03	2.61

Q61543	Glg1	Golgi apparatus protein 1	2	57.80	3.74E-05	2.58
P47738	Aldh2	Aldehyde dehydrogenase, mitochondrial	2	69.34	2.25E-04	2.58
Q8CI59	Steap3	Metalloreductase STEAP3	3	137.05	6.01E-05	2.58
P10852	Slc3a2	4F2 cell-surface antigen heavy chain	2	56.76	6.48E-05	2.57
O70251	Eef1b	Elongation factor 1-beta	2	108.59	3.45E-03	2.56
P43406	Itgav	Integrin alpha-V	3	146.70	1.68E-04	2.55
P80317	Cct6a	T-complex protein 1 subunit zeta	2	104.89	2.08E-03	2.54
P13020	Gsn	Gelsolin	2	42.35	1.30E-03	2.54
Q811U4	Mfn1	Mitofusin-1	2	112.72	2.31E-06	2.51
P48036	Anxa5	Annexin A5	2	121.80	3.13E-03	2.48
P20152	Vim	Vimentin	4	141.90	1.82E-04	2.46
Q91WC9	Daglb	Sn1-specific diacylglycerol lipase beta	2	60.78	8.23E-03	2.42
Q8R127	Sccpdh	Saccharopine dehydrogenase-like oxidoreductase	3	119.61	4.02E-05	2.42
E9PZQ0	Ryr1	Ryanodine receptor 1	3	173.44	4.78E-03	2.41
P62242	Rps8	40S ribosomal protein S8	3	122.17	2.16E-04	2.40
Q61334	Bcap29	B-cell receptor-associated protein 29	3	54.56	6.40E-04	2.40
Q99P72	Rtn4	Reticulon-4	3	48.54	4.66E-07	2.31
Q921I1	Tf	Serotransferrin	2	96.97	6.81E-04	2.30
Q9WTR5	Cdh13	Cadherin-13	2	66.32	9.61E-04	2.29
Q9WUQ2	Preb	Prolactin regulatory element-binding protein	3	165.29	3.41E-05	2.28
Q9WV91	Ptgfrn	Prostaglandin F2 receptor negative regulator	2	118.63	1.62E-04	2.27
Q9D379	Ephx1	Epoxide hydrolase 1	3	52.48	4.69E-04	2.26
Q9Z2I0	Letm1	LETM1 and EF-hand domain-containing protein 1, mitochondrial	3	63.22	2.36E-03	2.23
Q924X2	Cpt1b	Carnitine O-palmitoyltransferase 1, muscle isoform	3	187.01	1.92E-03	2.22
Q8C7X2	Emc1	ER membrane protein complex subunit 1	3	132.59	8.08E-04	2.22

P14602	Hspb1	Heat shock protein beta-1	2	83.78	1.21E-05	2.18
P35293	Rab18	Ras-related protein Rab-18	3	74.22	1.55E-04	2.15
Q6PIE5	Atp1a2	Sodium/potassium-transporting ATPase subunit alpha-2	4	96.25	6.76E-04	2.15
O35114	Scarb2	Lysosome membrane protein 2	3	185.98	3.26E-04	2.13
Q9D6U8	Fam162a	Protein FAM162A	2	4.01	5.57E-04	2.12
Q9DBH5	Lman2	Vesicular integral-membrane protein VIP36	7	188.62	9.85E-06	2.12
Q05144	Rac2	Ras-related C3 botulinum toxin substrate 2	2	49.74	1.72E-04	2.12
Q91YQ5	Rpn1	Dolichyl-diphosphooligosaccharide--protein glycosyltransferase subunit 1	5	237.36	2.92E-03	2.10
Q6PD26	Pigs	GPI transamidase component PIG-S	2	101.18	1.32E-04	2.09
P68040	Rack1	Receptor of activated protein C kinase 1	3	143.91	5.88E-03	2.07
P58252	Eef2	Elongation factor 2	2	43.37	1.97E-03	2.05
Q01339	ApoH	Beta-2-glycoprotein 1	2	102.53	1.16E-05	2.04
P47758	Srprb	Signal recognition particle receptor subunit beta	2	88.21	4.38E-04	2.01
P62908	Rps3	40S ribosomal protein S3	2	118.03	7.18E-05	2.00
Q8VDN2	Atp1a1	Sodium/potassium-transporting ATPase subunit alpha-1	5	225.57	3.96E-05	1.97
Q8VEE1	Lmcd1	LIM and cysteine-rich domains protein 1	2	68.63	1.60E-05	1.95
G5E829	Atp2b1	Plasma membrane calcium-transporting ATPase 1	3	148.47	5.71E-04	1.90
Q9Z2I9	Sucla2	Succinate--CoA ligase [ADP-forming] subunit beta, mitochondrial	2	93.87	3.30E-03	1.87
P68368	Tuba4a	Tubulin alpha-4A chain	3	99.25	3.01E-03	1.85
P09470	Ace	Angiotensin-converting enzyme	3	54.45	2.47E-04	1.80
A2AUC9	Klhl41	Kelch-like protein 41	3	45.52	2.74E-04	1.70
Q9ERI6	Rdh14	Retinol dehydrogenase 14	2	95.91	7.16E-05	1.63

Table A7.1: List of identified proteins with a significantly increased abundance ≤ 12.7 -fold in *mdx-4cv* serum as determined by label-free LC-MS/MS

Accession	Gene Name	Protein Name	Unique peptides	Confidence score	Anova (p)	Max fold change
Q8R0Y6	Aldh1l1	Cytosolic 10-formyltetrahydrofolate dehydrogenase	40	2619.27	9.28E-04	12.66
P58771	Tpm1	Tropomyosin alpha-1 chain	6	325.91	6.97E-06	12.62
Q9D6Y7	Msra	Mitochondrial peptide methionine sulfoxide reductase	6	228.52	1.56E-03	12.47
P05977	Myl1	Myosin light chain 1/3, skeletal muscle isoform	9	561.43	7.93E-09	12.01
O08553	Dpysl2	Dihydropyrimidine-related protein 2	14	885.02	3.79E-06	11.83
Q8BH00	Aldh8a1	Aldehyde dehydrogenase family 8 member A1	5	250.25	2.17E-02	11.82
Q99KK7	Dpp3	Dipeptidyl peptidase 3	6	322.74	2.99E-02	11.57
Q9JI75	Nqo2	Ribosyldihydroinicotinamide dehydrogenase [quinone]	6	262.85	7.40E-05	11.51
O88844	Idh1	Isocitrate dehydrogenase [NADP] cytoplasmic	17	1420.19	1.90E-04	11.45
O35490	Bhmt	Betaine--homocysteine S-methyltransferase 1	20	1756.08	3.42E-03	11.27
P00329	Adh1	Alcohol dehydrogenase 1	11	771.25	5.93E-04	10.70
P52480	Pkm	Pyruvate kinase PKM	46	4564.30	2.03E-12	10.39
Q9Z2Y8	Prosc	Proline synthase co-transcribed bacterial homolog protein	2	88.56	1.55E-02	10.14
Q9QXD6	Fbp1	Fructose-1,6-bisphosphatase 1	19	1633.89	3.53E-03	10.01
Q5XKE0	Mybpc2	Myosin-binding protein C, fast-type	12	688.24	1.56E-08	9.90
Q9R0P9	Uchl1	Ubiquitin carboxyl-terminal hydrolase isozyme L1	6	349.78	1.27E-03	9.76
Q3THE2	Myl12b	Myosin regulatory light chain 12B	2	147.06	2.42E-02	9.67
Q9JLJ2	Aldh9a1	4-trimethylaminobutyraldehyde dehydrogenase	2	66.79	1.09E-02	9.65
Q9ET01	Pygl	Glycogen phosphorylase, liver form	36	2184.82	9.16E-08	9.65

P52760	Hrsp12	Ribonuclease UK114	8	633.43	1.77E-03	9.65
P16546	Sptan1	Spectrin alpha chain, non-erythrocytic 1	2	92.39	9.98E-03	9.32
G3X982	Aox3	Aldehyde oxidase 3	11	598.26	1.28E-03	9.31
P06801	Me1	NADP-dependent malic enzyme	20	1095.95	1.98E-04	9.21
Q91Z53	Grhpr	Glyoxylate reductase/hydroxypruvate reductase	9	414.87	2.50E-04	9.13
Q78JT3	Haa0	3-hydroxyanthranilate 3,4-dioxygenase	15	902.31	4.31E-03	9.02
Q9QXF8	Gnmt	Glycine N-methyltransferase	11	854.76	5.01E-03	8.98
P54728	Rad23b	UV excision repair protein RAD23 homolog B	3	113.01	1.45E-05	8.94
Q9DBA8	Amdhd1	Probable imidazolonepropionase	5	227.18	2.09E-03	8.82
P10518	Alad	Delta-aminolevulinic acid dehydratase	6	340.77	2.29E-03	8.81
Q8K183	Pdxk	Pyridoxal kinase	4	344.80	5.29E-05	8.79
Q8K157	Galm	Aldose 1-epimerase	5	192.81	9.04E-03	8.75
Q9DBB8	Dhdh	Trans-1,2-dihydrobenzene-1,2-diol dehydrogenase	7	392.04	1.04E-03	8.74
P49429	Hpd	4-hydroxyphenylpyruvate dioxygenase	21	1181.72	2.62E-03	8.65
P99025	Gchfr	GTP cyclohydrolase 1 feedback regulatory protein	2	129.86	2.95E-02	8.60
P24472	Gsta4	Glutathione S-transferase A4	6	295.90	1.81E-04	8.58
Q9CRB3	Urah	5-hydroxyisourate hydrolase	2	110.41	1.03E-02	8.50
O35215	Ddt	D-dopachrome decarboxylase	8	595.48	1.83E-04	8.50
P14824	Anxa6	Annexin A6	14	567.16	3.24E-06	8.49
P12710	Fabp1	Fatty acid-binding protein, liver	11	928.62	6.11E-04	8.43
P57776	Eef1d	Elongation factor 1-delta	2	159.07	4.32E-06	8.42
P68134	Acta1	Actin, alpha skeletal muscle	9	1086.68	5.87E-09	8.41
Q04447	Ckb	Creatine kinase B-type	17	1492.20	1.47E-04	8.15
Q9JJU8	Sh3bgr1	SH3 domain-binding glutamic acid-rich-like protein	3	202.84	1.87E-06	7.88

P51855	Gss	Glutathione synthetase	3	187.20	4.46E-04	7.82
Q02053	Uba1	Ubiquitin-like modifier-activating enzyme 1	3	135.72	2.75E-04	7.75
P55264	Adk	Adenosine kinase	13	870.80	6.13E-04	7.71
P63158	Hmgb1	High mobility group protein B1	4	220.94	5.05E-04	7.69
Q9CQM5	Txndc17	Thioredoxin domain-containing protein 17	3	170.56	5.62E-06	7.61
P11499	Hsp90ab1	Heat shock protein HSP 90-beta	4	202.62	2.66E-05	7.56
Q9Z2V4	Pck1	Phosphoenolpyruvate carboxykinase, cytosolic [GTP]	3	149.38	5.46E-03	7.55
P09528	Fth1	Ferritin heavy chain	8	503.24	2.02E-04	7.53
P61979	Hnrnpk	Heterogeneous nuclear ribonucleoprotein K	2	126.56	1.60E-05	7.42
P10649	Gstm1	Glutathione S-transferase Mu 1	21	1827.86	3.30E-04	7.33
Q91XD4	Ftcd	Formimidoyltransferase-cyclodeaminase	4	228.30	4.06E-03	7.30
Q64442	Sord	Sorbitol dehydrogenase	17	1504.41	4.76E-03	7.15
Q9WVL0	Gstz1	Maleylacetoacetate isomerase	4	200.18	7.76E-03	7.09
O88569	Hnrnpa2b1	Heterogeneous nuclear ribonucleoproteins A2/B1	4	271.37	6.18E-07	7.04
Q9WUB3	Pygm	Glycogen phosphorylase, muscle form	48	4290.78	6.10E-10	7.01
Q9JII6	Akr1a1	Alcohol dehydrogenase [NADP(+)]	16	893.69	2.28E-04	6.97
P40936	Inmt	Indolethylamine N-methyltransferase	9	621.80	2.08E-04	6.87
Q8BVI4	Qdpr	Dihydropteridine reductase	11	711.78	6.14E-04	6.81
Q61176	Arg1	Arginase-1	13	862.80	1.29E-03	6.81
O35381	Anp32a	Acidic leucine-rich nuclear phosphoprotein 32 family member A	3	173.99	5.36E-04	6.79
P28474	Adh5	Alcohol dehydrogenase class-3	13	829.45	9.68E-04	6.75
P26041	Msn	Moesin	4	116.72	9.54E-03	6.73
O88587	Comt	Catechol O-methyltransferase	5	189.20	5.21E-05	6.73
Q9D819	Ppa1	Inorganic pyrophosphatase	3	209.39	1.27E-03	6.73

P15626	Gstm2	Glutathione S-transferase Mu 2	6	316.36	7.01E-05	6.71
Q00519	Xdh	Xanthine dehydrogenase/oxidase	7	408.00	5.65E-04	6.64
P16045	Lgals1	Galectin-1	4	288.16	2.39E-07	6.59
P09103	P4hb	Protein disulfide-isomerase	13	624.22	9.79E-05	6.59
Q91X83	Mat1a	S-adenosylmethionine synthase isoform type-1	5	206.43	6.77E-04	6.55
P31786	Dbi	Acyl-CoA-binding protein	7	642.62	1.19E-04	6.51
O88990	Actn3	Alpha-actinin-3	4	223.00	2.76E-03	6.51
P15105	Glul	Glutamine synthetase	18	1100.96	4.68E-04	6.39
P68254	Ywhaq	14-3-3 protein theta	6	296.68	5.28E-08	6.38
P15947	Klk1	Kallikrein-1	3	139.32	3.16E-02	6.38
P70694	Akr1c6	Estradiol 17 beta-dehydrogenase 5	16	903.05	1.26E-03	6.37
Q91Y97	Aldob	Fructose-bisphosphate aldolase B	20	1745.78	2.47E-04	6.36
Q9R257	Hebp1	Heme-binding protein 1	3	214.37	8.84E-05	6.35
Q9CQV8	Ywhab	14-3-3 protein beta/alpha	5	277.42	3.17E-05	6.25
P58774	Tpm2	Tropomyosin beta chain	11	671.83	1.80E-05	6.18
P07724	Alb	Serum albumin	29	2066.14	1.05E-02	6.16
P19639	Gstm3	Glutathione S-transferase Mu 3	2	134.13	4.55E-05	6.15
P97807	Fh	Fumarate hydratase, mitochondrial	9	650.71	5.19E-05	6.07
P61982	Ywhag	14-3-3 protein gamma	10	586.96	4.31E-08	5.88
Q61599	Arhgdib	Rho GDP-dissociation inhibitor 2	2	44.20	6.92E-05	5.77
Q62422	Ostf1	Osteoclast-stimulating factor 1	2	86.08	3.30E-05	5.75
P45591	Cfl2	Cofilin-2	6	292.55	2.73E-08	5.74
P17183	Eno2	Gamma-enolase	6	437.74	1.44E-03	5.71
P08249	Mdh2	Malate dehydrogenase, mitochondrial	6	274.29	3.87E-08	5.66
Q11136	Pepd	Xaa-Pro dipeptidase	2	83.29	2.77E-06	5.63
P20801	Tnnc2	Troponin C, skeletal muscle	3	192.78	3.63E-05	5.59

P50247	Ahcy	Adenosylhomocysteinase	25	1596.15	2.31E-03	5.55
Q8VDQ1	Ptgr2	Prostaglandin reductase 2	3	153.65	3.65E-04	5.54
Q91VH6	Memo1	Protein MEMO1	2	57.62	2.99E-05	5.53
P24527	Lta4h	Leukotriene A-4 hydrolase	2	81.66	5.06E-03	5.46
P26043	Rdx	Radixin	7	325.80	6.19E-03	5.43
Q9D154	Serpinb1a	Leukocyte elastase inhibitor A	2	72.78	9.42E-03	5.24
Q8QZR5	Gpt	Alanine aminotransferase 1	13	555.35	9.66E-03	5.24
Q60864	Stip1	Stress-induced-phosphoprotein 1	3	114.47	8.05E-04	5.16
Q9JMH6	Txnrd1	Thioredoxin reductase 1, cytoplasmic	6	340.28	8.13E-04	5.15
P18760	Cfl1	Cofilin-1	5	406.91	2.94E-05	5.11
Q9D8N0	Eef1g	Elongation factor 1-gamma	3	98.33	6.70E-03	5.10
P20152	Vim	Vimentin	4	186.80	2.72E-06	5.06
P08228	Sod1	Superoxide dismutase [Cu-Zn]	4	325.78	2.55E-02	5.02
Q9CPY7	Lap3	Cytosol aminopeptidase	12	627.46	4.46E-04	4.99
P48036	Anxa5	Annexin A5	2	90.78	6.62E-03	4.95
Q9DAK9	Phpt1	14 kDa phosphohistidine phosphatase	3	104.93	1.19E-05	4.94
P56565	S100a1	Protein S100-A1	2	127.11	2.24E-02	4.92
Q9R0P5	Dstn	Destrin	6	290.59	2.82E-04	4.83
P05202	Got2	Aspartate aminotransferase, mitochondrial	7	361.26	8.32E-06	4.78
P48758	Cbr1	Carbonyl reductase [NADPH] 1	8	368.65	5.26E-04	4.75
Q9CZY3	Ube2v1	Ubiquitin-conjugating enzyme E2 variant 1	2	107.01	2.33E-08	4.67
P47791	Gsr	Glutathione reductase, mitochondrial	4	238.51	2.46E-06	4.65
P26443	Glud1	Glutamate dehydrogenase 1, mitochondrial	6	207.62	3.38E-06	4.62
Q9Z1Q5	Clic1	Chloride intracellular channel protein 1	4	190.37	2.43E-06	4.59
P62715	Ppp2cb	Serine/threonine-protein phosphatase 2A catalytic subunit beta isoform	2	149.69	1.52E-05	4.53

P16460	Ass1	Argininosuccinate synthase	10	575.46	1.19E-02	4.48
P62259	Ywhae	14-3-3 protein epsilon	12	717.43	2.08E-07	4.47
P59325	Eif5	Eukaryotic translation initiation factor 5	2	108.88	7.98E-05	4.42
Q9WV35	Apobec2	C->U-editing enzyme APOBEC-2	2	75.39	2.13E-03	4.38
Q9CRB6	Tppp3	Tubulin polymerization-promoting protein family member 3	2	98.02	1.19E-05	4.38
Q93092	Taldo1	Transaldolase	10	511.02	9.00E-06	4.38
Q9R0Q7	Ptges3	Prostaglandin E synthase 3	3	134.11	3.06E-04	4.35
P28063	Psmb8	Proteasome subunit beta type-8	2	112.96	2.07E-03	4.31
Q91ZZ3	Sncb	Beta-synuclein	3	49.72	3.41E-05	4.16
Q91YI0	Asl	Argininosuccinate lyase	12	754.47	1.31E-03	4.12
Q99KI0	Aco2	Aconitate hydratase, mitochondrial	5	337.46	4.22E-08	4.11
P05201	Got1	Aspartate aminotransferase, cytoplasmic	22	1513.62	1.06E-06	4.08
Q9DCS2	1 SV	UPF0585 protein C16orf13 homolog	2	74.67	1.11E-03	4.08
P68369	Tuba1a	Tubulin alpha-1A chain	7	691.16	1.79E-04	4.05
P28650	Adss11	Adenylosuccinate synthetase isozyme 1	8	490.67	4.31E-06	4.05
Q8R429	Atp2a1	Sarcoplasmic/endoplasmic reticulum calcium ATPase 1	8	425.26	1.30E-02	4.04
Q9R0P3	Esd	S-formylglutathione hydrolase	10	629.82	3.49E-04	4.04
Q91ZJ5	Ugp2	UTP--glucose-1-phosphate uridylyltransferase	2	108.32	1.33E-04	4.00
Q99J08	Sec14l2	SEC14-like protein 2	4	161.48	9.69E-04	3.96
Q9D0F9	Pgm1	Phosphoglucomutase-1	22	1318.77	9.21E-06	3.96
Q9DBP5	Cmpk1	UMP-CMP kinase	5	276.57	7.84E-03	3.90
Q61316	Hspa4	Heat shock 70 kDa protein 4	20	1146.72	2.76E-06	3.89
P99029	Prdx5	Peroxiredoxin-5, mitochondrial	10	599.57	1.07E-04	3.87
P10126	Eef1a1	Elongation factor 1-alpha 1	7	328.86	1.31E-04	3.86
P50396	Gdi1	Rab GDP dissociation inhibitor alpha	14	910.39	5.90E-07	3.83

Q62426	Cstb	Cystatin-B	2	109.40	1.42E-04	3.80
Q9CQI6	Cotl1	Coactosin-like protein	3	155.14	8.91E-04	3.76
P14211	Calr	Calreticulin	7	390.91	3.82E-04	3.73
P53657	Pklr	Pyruvate kinase PKLR	3	119.98	5.29E-04	3.71
P63028	Tpt1	Translationally-controlled tumor protein	2	165.71	1.88E-06	3.71
P97447	Fhl1	Four and a half LIM domains protein 1	8	346.65	4.55E-06	3.71
Q924M7	Mpi	Mannose-6-phosphate isomerase	3	44.41	1.05E-05	3.70
Q6P8J7	Ckmt2	Creatine kinase S-type, mitochondrial	10	596.62	8.29E-07	3.68
Q7TMM9	Tubb2a	Tubulin beta-2A chain	6	375.91	5.68E-03	3.66
P23927	Cryab	Alpha-crystallin B chain	4	258.84	5.43E-04	3.61
P63101	Ywhaz	14-3-3 protein zeta/delta	11	876.80	6.15E-06	3.61
Q99KB8	Hagh	Hydroxyacylglutathione hydrolase, mitochondrial	4	278.74	2.09E-04	3.60
P68510	Ywhah	14-3-3 protein eta	11	613.82	6.22E-07	3.57
Q8VCT3	Rnpep	Aminopeptidase B	2	79.91	1.53E-03	3.53
Q9QYG0	Ndrp2	Protein NDRG2	8	456.40	5.59E-05	3.48
Q9DBJ1	Pgam1	Phosphoglycerate mutase 1	8	360.93	2.50E-06	3.42
P40142	Tkt	Transketolase	23	1526.70	2.60E-04	3.40
P19096	Fasn	Fatty acid synthase	9	437.49	4.70E-04	3.36
P21107	Tpm3	Tropomyosin alpha-3 chain	2	43.67	1.70E-04	3.32
P14602	Hspb1	Heat shock protein beta-1	3	150.33	3.19E-05	3.31
O09131	Gsto1	Glutathione S-transferase omega-1	6	244.05	2.28E-03	3.31
O55234	Psmb5	Proteasome subunit beta type-5	4	225.11	1.46E-08	3.30
P27773	Pdia3	Protein disulfide-isomerase A3	11	474.25	4.62E-04	3.29
P14152	Mdh1	Malate dehydrogenase, cytoplasmic	13	1108.02	8.77E-06	3.28
Q9R1P1	Psmb3	Proteasome subunit beta type-3	5	234.40	8.96E-07	3.27
P10605	Ctsb	Cathepsin B	6	304.18	3.09E-04	3.26
Q63880	Ces3a	Carboxylesterase 3A	2	130.69	1.69E-03	3.25
Q9CPU0	Glo1	Lactoylglutathione lyase	9	504.21	5.25E-04	3.23

Q01853	Vcp	Transitional endoplasmic reticulum ATPase	12	690.82	5.52E-03	3.22
P56376	Acyp1	Acylphosphatase-1	2	111.56	9.44E-05	3.17
Q9JMD3	Stard10	PCTP-like protein	2	106.89	1.38E-02	3.17
Q8CDN6	Txn1	Thioredoxin-like protein 1	2	69.34	1.56E-07	3.15
Q9R1P3	Psmb2	Proteasome subunit beta type-2	6	433.52	1.59E-06	3.15
Q99LX0	Park7	Protein deglycase DJ-1	12	994.45	4.32E-07	3.14
P61939	Serpina7	Thyroxine-binding globulin	9	398.42	1.86E-05	3.13
P05064	Aldoa	Fructose-bisphosphate aldolase A	30	3015.50	8.77E-06	3.11
Q61598	Gdi2	Rab GDP dissociation inhibitor beta	8	375.33	4.83E-05	3.11
P70296	Pebp1	Phosphatidylethanol amine-binding protein 1	8	514.05	6.84E-07	3.10
Q91VI7	Rnh1	Ribonuclease inhibitor	7	325.40	4.83E-06	3.10
Q3UGR5	Hdhd2	Haloacid dehalogenase-like hydrolase domain-containing protein 2	2	79.10	2.08E-04	3.08
P26928	Mst1	Hepatocyte growth factor-like protein	2	76.95	7.95E-03	3.06
Q9R1P4	Psma1	Proteasome subunit alpha type-1	6	308.27	5.81E-07	3.05
P17742	Ppia	Peptidyl-prolyl cis-trans isomerase A	11	1015.27	1.27E-05	2.99
Q60605	Myl6	Myosin light polypeptide 6	3	134.99	1.14E-03	2.97
Q9JKB1	Uchl3	Ubiquitin carboxyl-terminal hydrolase isozyme L3	2	97.98	1.27E-05	2.95
Q9Z2U1	Psma5	Proteasome subunit alpha type-5	6	423.30	3.20E-07	2.94
P20029	Hspa5	78 kDa glucose-regulated protein	12	810.94	2.07E-06	2.94
P16125	Ldhb	L-lactate dehydrogenase B chain	12	1000.89	1.25E-06	2.92
Q9Z2U0	Psma7	Proteasome subunit alpha type-7	6	382.97	4.30E-07	2.90
Q9QUM9	Psma6	Proteasome subunit alpha type-6	9	649.65	9.76E-07	2.88
P06151	Ldha	L-lactate dehydrogenase A chain	24	1813.38	5.30E-08	2.86
Q9Z1T2	Thbs4	Thrombospondin-4	7	412.56	1.81E-05	2.85
P56395	Cyb5a	Cytochrome b5	4	212.78	1.42E-04	2.85

P58252	Eef2	Elongation factor 2	11	549.58	4.43E-05	2.81
P28654	Dcn	Decorin	3	105.99	1.48E-07	2.80
Q9DBE0	Csad	Cysteine sulfinic acid decarboxylase	4	192.16	7.43E-03	2.79
Q9Z2W0	Dnpep	Aspartyl aminopeptidase	5	266.59	1.37E-04	2.79
P13707	Gpd1	Glycerol-3-phosphate dehydrogenase [NAD(+)], cytoplasmic	12	629.16	8.02E-06	2.77
P07901	Hsp90aa1	Heat shock protein HSP 90-alpha	4	172.93	7.56E-04	2.77
Q9R1P0	Psma4	Proteasome subunit alpha type-4	8	418.89	5.97E-07	2.77
Q8BWT1	Acaa2	3-ketoacyl-CoA thiolase, mitochondrial	3	128.96	5.92E-03	2.76
Q01768	Nme2	Nucleoside diphosphate kinase B	12	824.20	6.65E-07	2.75
P63242	Eif5a	Eukaryotic translation initiation factor 5A-1	7	617.89	3.10E-04	2.73
Q8K4Z3	Apoa1bp	NAD(P)H-hydrate epimerase	2	93.42	3.60E-03	2.73
Q9D1A2	Cndp2	Cytosolic non-specific dipeptidase	4	161.45	4.89E-03	2.69
P49722	Psma2	Proteasome subunit alpha type-2	5	375.45	4.49E-06	2.69
O88342	Wdr1	WD repeat-containing protein 1	13	697.04	5.85E-05	2.67
P17182	Eno1	Alpha-enolase	25	1951.59	2.86E-10	2.65
P06745	Gpi	Glucose-6-phosphate isomerase	18	1312.49	2.56E-07	2.65
P17751	Tpi1	Triosephosphate isomerase	14	1281.99	3.22E-06	2.64
P61971	Nutf2	Nuclear transport factor 2	3	141.02	1.42E-05	2.63
Q9DCD0	Pgd	6-phosphogluconate dehydrogenase, decarboxylating	9	543.35	2.71E-03	2.62
Q60854	Serpinb6	Serpin B6	5	223.18	7.99E-04	2.62
Q11011	Npepps	Puromycin-sensitive aminopeptidase	7	290.64	1.87E-05	2.61
P32848	Pvalb	Parvalbumin alpha	16	1096.30	1.40E-05	2.61
P99026	Psmb4	Proteasome subunit beta type-4	7	375.80	1.31E-06	2.60
O70435	Psma3	Proteasome subunit alpha type-3	5	390.64	9.53E-07	2.56
P63017	Hspa8	Heat shock cognate 71 kDa protein	18	1479.96	5.30E-08	2.55

P16858	Gapdh	Glyceraldehyde-3-phosphate dehydrogenase	12	1069.11	1.72E-07	2.50
P15532	Nme1	Nucleoside diphosphate kinase A	2	55.33	1.41E-05	2.48
P17563	Selenbp1	Selenium-binding protein 1	20	1412.15	1.53E-03	2.47
P16015	Ca3	Carbonic anhydrase 3	15	830.57	4.43E-03	2.44
P70349	Hint1	Histidine triad nucleotide-binding protein 1	5	237.49	5.30E-06	2.43
Q9D6F9	Tubb4a	Tubulin beta-4A chain	4	186.13	1.95E-03	2.42
P97494	Gclc	Glutamate--cysteine ligase catalytic subunit	3	175.08	3.21E-04	2.42
O09061	Psmbl	Proteasome subunit beta type-1	4	304.86	1.01E-07	2.41
P10639	Txn	Thioredoxin	2	106.36	9.73E-04	2.40
P09411	Pgk1	Phosphoglycerate kinase 1	19	1311.93	1.65E-05	2.38
P07310	Ckm	Creatine kinase M-type	30	2895.13	5.69E-06	2.38
Q61233	Lcp1	Plastin-2	2	88.51	1.17E-02	2.38
P11276	<td>Fibronectin</td> <td>6</td> <td>298.37</td> <td>1.04E-03</td> <td>2.37</td>	Fibronectin	6	298.37	1.04E-03	2.37
O08709	Prdx6	Peroxiredoxin-6	7	432.41	3.13E-05	2.36
Q8CHP8	Pgp	Phosphoglycolate phosphatase	2	188.24	1.43E-05	2.36
P19157	Gstp1	Glutathione S-transferase P 1	9	598.62	5.70E-03	2.36
Q99PT1	Arhgdia	Rho GDP-dissociation inhibitor 1	3	216.58	1.22E-05	2.33
Q91XR9	Gpx4	Phospholipid hydroperoxide glutathione peroxidase, nuclear	2	90.93	1.02E-03	2.31
Q8R016	Blmh	Bleomycin hydrolase	11	645.79	6.54E-07	2.30
P04117	Fabp4	Fatty acid-binding protein, adipocyte	9	800.82	3.83E-03	2.30
Q9R0Y5	Ak1	Adenylate kinase isoenzyme 1	3	247.30	5.37E-03	2.28
Q60692	Psmbl6	Proteasome subunit beta type-6	6	274.09	2.66E-03	2.28
P35700	Prdx1	Peroxiredoxin-1	10	493.83	2.82E-05	2.27
P11352	Gpx1	Glutathione peroxidase 1	7	402.38	1.78E-02	2.24
Q4KML4	Abrac1	Costars family protein ABRACL	2	139.64	1.47E-03	2.22

P62983	Rps27a	Ubiquitin-40S ribosomal protein S27a	3	166.25	6.36E-03	2.22
Q8CG14	C1sa	Complement C1s-A subcomponent	3	195.25	1.20E-03	2.21
O70250	Pgam2	Phosphoglycerate mutase 2	10	714.82	1.19E-02	2.20
P45376	Akr1b1	Aldose reductase	11	505.47	1.24E-04	2.20
P60710	Actb	Actin, cytoplasmic 1	10	939.87	6.62E-06	2.18
Q9CWJ9	Atic	Bifunctional purine biosynthesis protein PURH	14	783.17	7.17E-05	2.17
P21550	Eno3	Beta-enolase	23	2090.28	1.67E-04	2.16
P97371	Psmel	Proteasome activator complex subunit 1	2	96.03	2.95E-03	2.14
O35945	Aldh1a7	Aldehyde dehydrogenase, cytosolic 1	5	288.72	3.19E-03	2.11
O55042	Snca	Alpha-synuclein	2	183.14	4.09E-02	2.08
Q3TMH2	Scrn3	Secernin-3	3	170.80	1.62E-03	2.08
O35350	Capn1	Calpain-1 catalytic subunit	2	111.43	1.68E-03	2.02
P70195	Psmb7	Proteasome subunit beta type-7	4	172.92	1.07E-03	2.00